FABAD

JOURNAL of PHARMACEUTICAL SCIENCES

ISSN 1300-4182
e-ISSN: 2651-4648
www.fabad.org.tr

Volume: 51 • Issue: 1 • March 2026

An Official Journal of The Society of Pharmaceutical Sciences of Ankara (FABAD)

The Society of Pharmaceutical Sciences of Ankara (FABAD)
FABAD Journal of Pharmaceutical Sciences
Volume: 51 Issue: 1 March 2026

Publisher

Sevgi AKAYDIN (Gazi University, Department of Biochemistry, Ankara, Turkey)

Editor in Chief

Nesrin Gökhan KELEKÇİ (Hacettepe University, Department of Pharmaceutical Chemistry, Ankara, Turkey)

Co-Editors

Hayriye Eda ŞATANA (Gazi University, Department of Analytical Chemistry, Ankara, Turkey)
Selin Seda TİMUR (Hacettepe University, Department of Pharmaceutical Technology, Ankara, Turkey)
Hasya Nazlı GÖK (Gazi University, Department of Pharmacognosy, Ankara, Turkey)

Technical Editors

Gökçen TELLİ (Hacettepe University, Department of Pharmacology, Ankara, Turkey)
Aylin ELKAMA (Gazi University, Department of Pharmaceutical Toxicology, Ankara, Turkey)

Biostatistics Editor

Hatice Yağmur ZENGİN Hacettepe University, Faculty of Medicine, Department of Biostatistics, Ankara, Turkey

Editorial Board

Almira RAMANAVİČİENĖ Vilnius University, Nanotechnology and Material Sciences Center, Vilnius, Latvia
Alper GÖKBULUT Ankara University, Department of Pharmacognosy, Ankara, Turkey
Ashok K. SHAKYA Al Ahliyya Amman University, Department of Pharmaceutical Chemistry, Amman, Jordan
Aygin EKİNCİOĞLU Hacettepe University, Department of Clinical Pharmacy, Ankara, Turkey
Ayşe KURUÜZÜM UZ Hacettepe University, Department of Pharmacognosy, Ankara, Turkey
Bharat JHNAWAR Lovely Professional University, Pharmaceutical Sciences, Punjap, India
Bülent KIRAN Ege University, Department of Pharmacy Management, İzmir, Turkey
Ceyda Tuba ŞENGEL TÜRK Ankara University, Department of Pharmaceutical Technology, Ankara, Turkey
Chia-Yi TSENG Chung Yuan Christian University, Biomedical Engineering, Taoyuan, Taiwan
Didem DELİORMAN ORHAN Gazi University, Department of Pharmacognosy, Ankara, Turkey
Emel Öykü ÇETİN UYANIKGİL Ege University, Department of Pharmaceutical Technology, Izmir, Turkey
Filiz BAKAR ATEŞ Ankara University, Department of Biochemistry, Ankara, Turkey
Francesco EPIFANO G. D'Annunzio" University, Department of Pharmaceutical Chemistry, Chieti-Pescara, Italy
Gerard LIZARD University of Burgundy, French Institute for Medical and Health Research, Dijon, France
Gökçe CİHAN ÜSTÜNDAĞ Istanbul University, Department of Pharmaceutical Chemistry, Ankara, Turkey
Gökçen EREN Gazi University, Department of Pharmaceutical Chemistry, Ankara, Turkey
Hande GÜRER ORHAN Ege University, Department of Pharmaceutical Toxicology, Izmir, Turkey
Hasan Abougazar YUSUFOĞLU King Saud University, Department of Pharmacognosy, Riyadh, Saudi Arabia
Hasan KIRMIZIBEKMEZ Yeditepe University, Department of Pharmacognosy, Istanbul, Turkey
Ikhlas KHAN University of Missipsippi, National Center for Natural Product Research, USA.
Işıl ÖZAKCA GÜNDÜZ Ankara University, Department of Pharmacology, Ankara, Turkey
İnci Selin DOĞAN Karadeniz Technical University, Department of Pharmaceutical Chemistry, Trabzon, Turkey
Leyla YURTTAŞ Anadolu University, Department of Pharmaceutical Chemistry, Eskisehir, Turkey
Melike H. ÖZKAN Hacettepe University, Department of Pharmacology, Ankara, Turkey
Meltem ÜNLÜSOY Ankara University, Department of Pharmaceutical Chemistry, Ankara, Turkey
Merve BACANLI University of Health Sciences, Department of Pharmaceutical Toxicology, Ankara, Turkey
Merve BECİT Afyonkarahisar University of Health Sciences, Department of Pharmaceutical Toxicology, Afyonkarahisar, Turkey
Mesut SANCAR Marmara University, Department of Clinical Pharmacy, Istanbul, Turkey
Ming-Wei CHAO Chung Yuan Christian University, Department of Bioscience Technology, Taoyuan, Taiwan
Muharrem ÖLÇER Afyonkarahisar University of Health Sciences, Department of Pharmaceutical Technology, Afyonkarahisar, Turkey
Natalizia MICELI University of Messina, Department of Chemistry and Biology, Messina, Italy
Özlem Nazan ERDOĞAN Istanbul University, Department of Pharmacy Management, Ankara, Turkey
Sevda ŞENEL Hacettepe University, Department of Pharmaceutical Technology, Ankara, Turkey
Sevtap AYDIN DİLSİZ Hacettepe University, Department of Pharmaceutical Toxicology, Ankara, Turkey
Suryakanta SWAIN The Assam Kaziranga University, Department of Pharmaceutical Sciences, Assam, India
Şükrü BEYDEMİR Anadolu University, Department of Pharmaceutical Microbiology, Ankara, Turkey
Tuba İNCEÇAYIR Gazi University, Department of Pharmaceutical Technology, Ankara, Turkey
Tuğba TÜYLÜ KÜÇÜKKILINÇ Hacettepe University, Department of Biochemistry, Ankara, Turkey
Tuğçe YEŞİL Marmara University, Department of Pharmaceutical Toxicology, Istanbul, Turkey
Uğur TAMER Gazi University, Department of Analytical Chemistry, Eskisehir, Turkey
Vu Dang HOANG Hanoi University of Pharmacy, Department of Analytical Chemistry and Toxicology, Hanoi, Vietnam
Wolfgang SCHUHLY University of Graz Institute of Pharmaceutical Sciences, Department of Pharmacognosy, Graz, Austria

The FABAD Journal of Pharmaceutical Sciences is published three times a year by the
Society of Pharmaceutical Sciences of Ankara (FABAD)

All expressions of opinion and statements of supposed facts appearing in articles and / or advertisiments carried in this journal are published on the responsibility of the author and / or advertiser, and are not to be regarded those of the Society of Pharmaceutical Sciences of Ankara. The manuscript submitted to the Journal has the requirement of not being published previously and has not been submitted elsewhere. Manuscript should bu prepared in accordance with the requirements specified as in the back cover. The submission of the manuscript to the Journal is not a condition for acceptance; articles are accepted or rejected on merit alone. This Journal is published electronically and it is an open-access journal without publication fee. All rights reserved. Neither this work nor any part may be reproduced or transmitted in any form or by any means, electronic or mechanical, microfilming and recording, or by any information storage and retrieval systems without written permission from FABAD Journal of Pharmaceutical Sciences.

The FABAD Journal of Pharmaceutical Sciences is indexed in Chemical Abstracts,
Analytical Abstracts, International Pharmaceutical Abstracts, Excerpta Medica (EMBASE), Scopus and TR Index

CONTENTS

Research Articles

1 Investigation of Benzothiazole-Schiff Bases for Antimicrobial Activities Through ADMET, Molecular Docking, and DFT Analysis
Augustine Onuche SULE[*], Olatunde ABIMBOLA MODUPE[**], Banjo SEMIRE[*°]**

23 Development and Validation of RP-HPLC for Determination Bedaquiline Fumarate in Nanostructured Lipid Carriers, Tablets, and Human Plasma Using Design of Experiment Method
Asti RAHAYU[*], SATRIALDI[**], Neng Fisheri KURNIATI[***], Rachmat MAULUDIN[**°]**

41 Unveiling The Therapeutic Potential of *Nyctanthes arbor-tristis* Linn. In Breast Cancer: A Network Pharmacology and Molecular Docking Approach
Omkar TIPUGADE[*], Jyotiram SAWALE[°], Namdeo JADHAV[***]**

53 Intranasal Delivery of Nicotine Via Thermoresponsive Hydrogel Systems: Design, Characterization, and *In Vitro* Evaluation
Sema ARISOY[*°], Özlem YAPAR[**], Betül KARAKURT[***], Ramazan BAKAL[****], Dilara ÖRGÜL[*****]

67 Analgesic and Anti-Inflammatory Activity of Ethanolic Extract of *Ipomoea Hederifolia* Linn
Kailas Krishnat MALI[*°], Nitin Hindurao SALUNKHE[**], Suraj Ashok SUTAR[***], Remeth Jacky DIAS[****], Balaji Dattatray JADHAV[*****]

89 Evaluation for Dissolution Profile Similarity of Multisource Generic Products Containing Favipiravir in the Treatment of COVID-19: Model-independent Bootstrap f_2 and Model-dependent Approaches
Duygu YILMAZ USTA[*°]

105 Rethinking Oral Infection Control: Antimicrobial Peptides and Essential Oils as Alternative Antibacterial Agents
Murat Sefa KARAASLAN[*], Nurten ALTANLAR[°], Sinem ASLAN ERDEM[***]**

115 Investigation of Synthesis, X-Ray Characterization and Biological Activities of Copper(II) Imidazole Complexes
Sevda ER[*°], Hakan ÜNVER[**], Banu BARUTCA[***]

129 Mucoadhesive Delivery of Alfuzosin HCl Using Hupu Gum: Insights from *In Silico* Docking and *Ex Vivo - In Vivo* Adhesion Studies
Rajeswari ALETI[*°], Monika NIJHAWAN[**], Pavan KUMAR THOTA[***], Bhavana JIDIGE[****]

147 Investigation of Maillard-Type Drug–Excipient Interaction Between Rivaroxaban and Lactose: Implications for Stability and *In Vitro* Anticoagulant Activity
Kunal BACHCHHAO[*°], Ajaygiri GOSWAMI[**], Chandragauda PATIL[***], Dipak PATIL[****]

163 Anticancer Potential of Piperidine-Substituted Mannich Bases: Evidence of Cytotoxic Activity and Apoptotic Effects on Various Cancer Cells
Gülşah KARAKAYA[*], Canan SEVİMLİ GÜR[**], Mutlu AYTEMİR[*°]**

175 Dornase Alfa as a Potential Treatment Option for SARSCoV- 2: *In Vitro* Insights
Derya DİLEK KANÇAĞI[*°], Cihan TAŞTAN[**], Kevser Buse KARADENİZ[***], Selen ABANUZ[****], Didem ÇAKIRSOY[*****], Yaren BÜYÜKÇOLAK[******], Sezer AKYÖNEY[*******], Gözde SIR KARAKUŞ[********], Bulut YURTSEVER[*********], Koray YALÇIN[**********], İsmail Tuncer DEĞİM[**********], Ercüment OVALI[***********]

189 Smoking Behavior, Nicotine Dependence, and Awareness of Cessation Methods Among Pharmacy Students: A Cross-Sectional Analysis
Nesligül ÖZDEMİR AYDURAN[*°], Nida AÇAR[**], Zeynep Ülkü GÜN[***]

207 A Cross-Sectional Survey on the Attitudes of Future Pharmacists Towards Phytotherapeutic Product Use and Safety
Suheda Rumeysa OSMANLIOGLU DAG[*°], Ceyhan CERAN SERDAR[**], Seyma YIGITBASI[***], Iffet Irem TATLI CANKAYA[****]

223 The Effects of Garlic (*Allium sativum L.*) and Allicin on Heart Rate: A Systematic Review and Meta-Analysis of Experimental and Clinical Studies
Rita RAKHMAWATI[*°], Rasmaya NIRURI[**]

239 An Integrated Taguchi Design and Response Surface Methodological Approach for Development of Bedaquiline-Loaded Nanostructured Lipid Carriers
Rachmat MAULUDIN[*°], Asti RAHAYU[**], SATRIALDI[***], Neng Fisheri KURNIATI[****]

257 Anti-Aging Activity of Ethanol Extract of the Oil Palm Mesocarp (Elaeis guineensis Jacq.): *In Vitro* and *In Silico* Studies
Retno WIDYOWATI[*°], Anisa Yustikka PUTRI[**], SUKARDIMAN[***], Irawati SHOLOKHAH[****], Rosita HANDAYANI[*****], Katsuyoshi MATSUNAMI[******], Hsin-I CHANG[*******]

275 Total Phenolic and Flavonoid Contents of Ethanol Extract of *Manilkara kauki* Leaves and Antibiofilm Activity Test Against Biofilms of *Pseudomonas aeruginosa*
Lilik FARKHIYAH[*], Tukiran TUKIRAN[°]**

Review Articles

291 *Cimicifuga racemosa* (L.) Nutt.: Pharmacological Effects, Using Areas and Current Clinical Data
Ecenur BAYIR[*°], Gözde ELGİN CEBE[**]

305 Therapeutic Applications of Garlic (*Allium sativum L.*) Essential Oil: A Review on Different Extraction Methods and Characterization on Its Bioactive Compound
Nastiti Nur INDRIYANI[*°], Dwi Ayu Lutfiani AMALIA[**], Maulana Nur ARDIAN[***], Didi RAMADANI[****]

327 Tailored Polymers in Therapeutics: Bridging Drug Delivery and Biomedical Engineering
Manjeet KAUR[*], Lakhvir KAUR[°], Gurjeet SINGH[***], Lovepreet SINGH[****], RK DHAWAN[*****], Navdeep KAUR[******], Manbir KAUR[*******], Peeyush SHARMA[********]**

351 Medicinal Chemistry Approaches for Combatting SARS-CoV-2 and COVID-19 Therapeutics
Neelottama KUSHWAHA[*°], Swatantra K.S. KUSHWAHA[**], Anmol KUMAR[***]

383 Repurposing Antidiabetic Agents as Potential Therapeutics in Neurodegenerative Diseases: Current Status and Future Perspectives
Ahmet Hüsamettin BARAN[*°]

403 Asbestos Exposure in Occupational and Environmental Settings Following the 2023 Earthquake in Türkiye: A Focused Review
Hürü DİKEÇ[*], Aysun ÖKÇESİZ HACISEYİTOĞLU[°]**

419 The Role of Glucocorticoids in Hepatic Gluconeogenesis, Associated Pathologies, and Novel Therapeutic Approaches
Yusuf Anil AY[*], Elif CADIRCI[°]**

FABAD J. Pharm. Sci., 51, 1, 1-22, 2026
Doi: 10.55262/fabadeczacilik.1792162
RESEARCH ARTICLE

Investigation of Benzothiazole-Schiff Bases for Antimicrobial Activities Through ADMET, Molecular Docking, and DFT Analysis

Augustine Onuche SULE*, Olatunde ABIMBOLA MODUPE**, Banjo SEMIRE***°

Investigation of Benzothiazole-Schiff Bases for Antimicrobial Activities Through ADMET, Molecular Docking, and DFT Analysis

SUMMARY

Antimicrobial resistance is a critical global health issue, driving the urgent need for novel antimicrobial agents. This study employs an integrated computational framework combining Density Functional Theory (DFT), molecular docking, and ADMET profiling to evaluate the antibacterial potential of four benzothiazole-Schiff base hybrids (S08, S13, S15, S19). DFT calculations revealed that the hybrids possess lower HOMO-LUMO energy gaps (4.05-4.11 eV) and higher electrophilicity indices (2.669-3.156 eV) than ciprofloxacin, indicating enhanced chemical reactivity that correlates with their potent experimental Minimum Inhibitory Concentrations (MICs: 3.91-15.6 µg/mL). Molecular docking demonstrated strong binding affinities to bacterial DNA gyrase targets (Staphylococcus aureus Gyrase B and Escherichia coli Gyrase B), with key interactions identified at the atomic level. Crucially, ADMET profiling designated S19 as the lead candidate, exhibiting a favorable drug-likeness profile, high gastrointestinal absorption, and a superior safety profile, being non-mutagenic and devoid of hERG cardiotoxicity risks. This comprehensive in silico investigation provides profound insights into the structure-activity-toxicity relationships of these hybrids and firmly nominates S19 as a promising lead compound for subsequent synthesis and experimental development as a novel antimicrobial agent.

Keywords: *Schiff bases, MIC, DFT, molecular docking, and ADMET.*

ADMET, Moleküler Yerleştirme ve DFT Analizi ile Benzotiyazol-Schiff Bazlarının Antimikrobiyal Aktivitelerinin İncelenmesi

ÖZ

Antimikrobiyal direnç, yeni antimikrobiyal ajanlara olan acil ihtiyacı artıran kritik bir küresel sağlık sorunudur. Bu çalışma, dört benzotiyazol-Schiff baz hibritinin (S08, S13, S15, S19) antibakteriyel potansiyelini değerlendirmek için Yoğunluk Fonksiyonel Teorisi (DFT), moleküler yerleştirme ve ADMET profillemesini birleştiren entegre bir hesaplamalı çerçeve kullanmaktadır. DFT hesaplamaları, hibritlerin siprofloksasinden daha düşük HOMO-LUMO enerji aralıklarına (4,05 - 4,11 eV) ve daha yüksek elektrofilisite indekslerine (2,669 - 3,156 eV) sahip olduğunu ortaya koymuştur; bu da, güçlü deneysel Minimum İnhibitör Konsantrasyonları (MİK: 3,91 - 15,6 µg/mL) ile korelasyon gösteren artan kimyasal reaktiviteye işaret etmektedir. Moleküler yerleştirme, bakteriyel DNA giraz hedeflerine (Staphylococcus aureus Giraz B ve Escherichia coli Giraz B) karşı güçlü bağlanma afiniteleri gösterdi ve atomik düzeyde anahtar etkileşimler tanımlandı. En önemlisi, ADMET profillemesi, uygun bir ilaç-benzeri profil, yüksek gastrointestinal emilim ve üstün bir güvenlik profili sergileyen (mutajenik olmaması ve hERG kardiyotoksisite risklerinden arınmış olması nedeniyle) S19'u öncü aday olarak belirledi. Bu kapsamlı in siliko araştırma, bu hibritlerin yapı-aktivite-toksisite ilişkilerine dair derin içgörüler sağlamakta ve S19'u, yeni bir antimikrobiyal ajan olarak sonraki sentez ve deneysel geliştirme için umut verici bir öncü bileşik olarak kesin bir şekilde önermektedir.

Anahtar Kelimeler: *Schiff bazları, MİK, DFT, moleküler yerleştirme, ADMET.*

Recieved: 27.09.2025
Revised: 31.10.2025
Accepted: 4.11.2025

* ORCID: 0009-0006-3953-209X, Department of Chemistry, Federal University, Lokoja, Nigeria
** ORCID: 0000-0002-6253-8645, Department of Chemistry, University of Ibadan, Ibadan, Oyo State, Nigeria
*** ORCID: 0000-0002-4173-9165, Computational Chemistry Research Laboratory, Department of Pure and Applied Chemistry, Ladoke Akintola University of Technology, Ogbomoso, Nigeria

° Corresponding Author; Banjo SEMIRE
E-mail: bsemire@latech.edu.ng

INTRODUCTION

Current resistance to antibiotics hinders the efficacy of therapeutics, leading to further spread of infectious diseases. This underscores the pressing necessity for the development of an innovative class of antimicrobial compounds (Singh et al., 2017). Modern pharmacological design is heavily dependent on heterocyclic compounds, which can mimic biomolecules and engage in selective interactions with biological receptor complexes (Pibiri, 2024). These features provide a potent framework for adjusting physicochemical characteristics such as polarity and solubility, pharmacokinetic (ADME) profile, and toxicity of the drug candidate (Hahn, 2024).

By combining aldehydes or ketones with amines in a condensation reaction, an imine (-C=N-) bond is formed, replacing the carbonyl (–C=O) group and creating a major subclass of Schiff bases (Abdel Aziz, Ramadan, Sidqi, & Sayed, 2023; Babaei, Rezvan, Gilani, & Mansour, 2024). The presence of an imine linkage in the Schiff base molecules is essential for exhibiting this compound's wide spectrum of biological applications, like analgesic (Yassen & AL-Azzawi, 2023), anticancer (Alasadi, Jumaa, & Mukhlif, 2023; Aroua et al., 2023), antimicrobial (Alfonso-Herrera et al., 2022; Awolope, Ejidike, & Clayton, 2022), antitumor (Rezaei et al., 2023), antioxidant (Abd El-Hamid, Sadeek, Mohammed, Ahmed, & El-Gedamy, 2023; Aytac, Gundogdu, Bingol, & Gulcin, 2023), antiviral (Pore et al., 2023) and anti-inflammatory activity (Krishna, Dhanya, Shanty, Raghu, & Mohanan, 2023). Furthermore, Schiff bases can be used as chemosensors in analytical chemistry, among other areas (Ejiah, Rofiu, Oloba-Whenu, & Fasina, 2023), corrosion inhibitors (Boulechfar et al., 2023), dyes (Rajimon, Elangovan, Amir Khairbek, & Thomas, 2023; Wu, Bhamidipati, Coles, & Rao, 2004), optical data storage systems and NLO materials (Hadigheh Rezvan & Aminivand, 2024), and phases in the synthesis of organic compounds (Babaei et al., 2024; Sule, Obiyenwa, Salawu, & Semire, 2025).

Interest in the benzothiazole moiety's biological importance has persisted. In 2015, Singh et al. synthesized a series of benzothiazole-Schiff bases, which were evaluated for possible antibacterial action (Singh, Kumar Singh, Thakur, Ray, & Singh, 2015). Previous studies have investigated the antimicrobial properties, quantitative structure-activity relationships, and potential mechanisms for the efficacy of benzothiazole Schiff base hybrids (Singh et al., 2017). Additionally, the antimicrobial inhibitory properties by examining their binding to lipopolysaccharides (LPS) and the depolarization of both the outer and cytoplasmic membranes were also investigated. The antimicrobial study of the compounds of interest against bacteria revealed that nine out of twenty of the benzothiazole-Schiff hybrids showed a certain degree of antimicrobial activity, as represented in Table 1. The inhibition of the growth of bacteria with good to excellent MIC values ranging between 1 and 100 μg/mL (Singh et al., 2017).

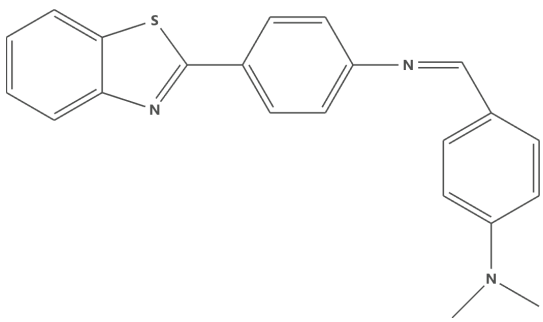
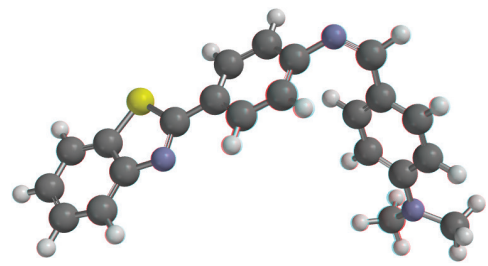
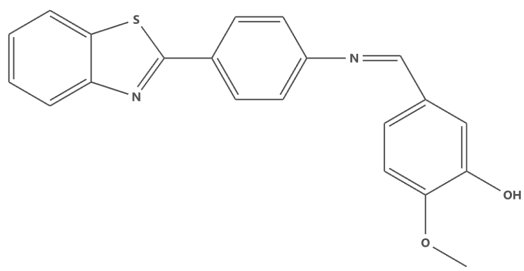
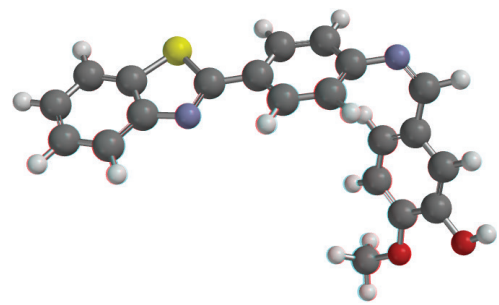
Table 1. MIC (μg/mL) of benzothiazole-Schiff bases against tested bacteria (Singh et al., 2017)

Cpd code	*S. aureus*	*E. coli*
S01	31.2	15.6
S02	31.2	15.6
S05	31.2	62.5
S08	15.6	3.91
S13	7.81	15.6
S15	3.91	7.81
S17	31.2	62.5
S19	7.81	15.6
S20	15.6	15.6
Ciprofloxacin	≥ 6.25	≥ 6.25

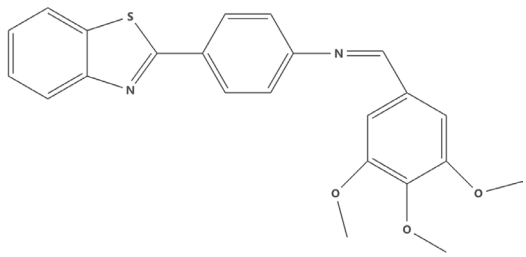
A deeper comprehension of molecular characteristics and interaction mechanisms at the atomic level is made possible by computational tools, which are a potent complement to experimental approaches that offer priceless insights into the antibacterial efficacy of new drugs. Calculations using Density Functional Theory (DFT) are essential for forecasting and clarifying molecules' electronic structures and global reactivity indices, which are essential for comprehending

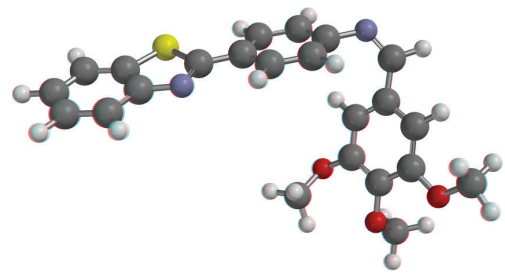
their stability and chemical behavior (Semire, Mutiu, & Oyebamiji, 2017). Additionally, possible drug candidates' binding affinities and modes of interaction with certain biological targets, including bacterial enzymes, can be accurately predicted using a molecular docking simulation, which helps to guide rational drug design (Meng, Zhang, Mezei, & Cui, 2011). The pharmacokinetic and toxicological profiles of compounds are predicted by Absorption, Distribution, Metabolism, Excretion, and Toxicity (ADMET) studies, which are also crucial *in silico* evaluations that help eliminate inappropriate drug candidates early in the discovery pipeline and cut down on the time and expense of drug development (El-Shamy et al., 2022).

In this study, *in silico* analysis of benzothiazole Schiff base hybrids (S08, S13, S15, and S19) taken from Singh et al., (2017) As shown in Table 1, were carried out by comparing the empirically derived Minimum Inhibitory Concentrations (MICs) against a variety of microbial strains (*S. aureus* and *E. coli*) with their theoretically derived electronic characteristics utilizing DFT, forecasted binding affinities through molecular docking methodologies, and ADMET profiles. These synergistic computational and experimental methodologies aspire to furnish a profound understanding of their structure-activity relationships, elucidate prospective molecular mechanisms, and ultimately inform the rational design and advancement of more efficacious antimicrobial agents. The 2-D and optimized 3-D structures of the benzothiazole Schiff base hybrids are illustrated in Figure 1 and Supplementary Figure S1.

Cpd code	2-D Structure	Optimized 3-D Structure
S08		
	4-(((4-(benzo[d]thiazol-2-yl)phenyl)imino)methyl)-N, N-dimethylaniline	
S13		
	5-(((4-(benzo[d]thiazol-2-yl)phenyl)imino)methyl)-2-methoxyphenol	

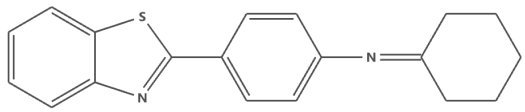
S15

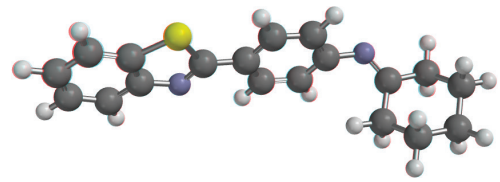




4-(benzo[d]thiazol-2-yl)-N-(3,4,5-trimethoxybenzylidene)aniline

S19





4-(benzo[d]thiazol-2-yl)-N-cyclohexylideneaniline

Figure 1. Chemical structures of the selected benzothiazole-Schiff base hybrids (S08, S13, S15, S19) investigated in this study. The complete set of 2D and optimized 3D structures for all synthesized hybrids (S01-S20) is provided in **Supplementary Figure S1**.

MATERIALS AND METHODS

DFT calculations

Using Spartan v2014 software, selected benzothiazole Schiff base hybrids and standard drug (ciprofloxacin) were optimized using the DFT approach, which is represented in the Becke-3 Parameter-Lee-Yang-Parr (B3LYP) model and the 6-31G** basis set (El-Shamy et al., 2022). The compounds S08, S13, S15, and S19 show excellent to excellent results with the MIC of these agents from 3.91 to 15.6 μg/mL (Singh et al., 2017), indicating they have strong antimicrobial potential. Ciprofloxacin was chosen as the reference because it is well-known for its effectiveness and because it specifically stops bacteria by targeting DNA gyrase, which is the main focus of our docking studies (Hooper, 2001; Singh et al., 2017).

Preliminary conformational searches of all compounds utilizing the Monte Carlo search technique and the MMFF method served as the foundation for the DFT calculations (Paul, Dilipkumar Singh, Bedamani Singh, & Sarkar, 2015). The default parameters utilized in the Spartan 14 software served as the convergence criteria for the energy calculations and geometry optimizations employed in the computations (Semire et al., 2017). The molecular parameters such as the frontier orbital energies, LOMO energy (E_{LUMO}), HOMO energy (E_{HOMO}) and energy gap ($\Delta E = (E_{LUMO} - E_{HOMO})$) and reactivity indicators, like chemical hardness ($\eta = (\Delta E)/2$), chemical potential ($\mu = (E_{LUMO} + E_{HOMO})/2$), chemical softness ($S = 1/2\eta$), overall electrophilicity ($\omega = \mu^2/2\eta$), and electronegativity ($\chi = -\mu$) are evaluated to determine the stable characteristics of these in a biological environment (Ouhazza et al., 2025; Semire et al., 2017).

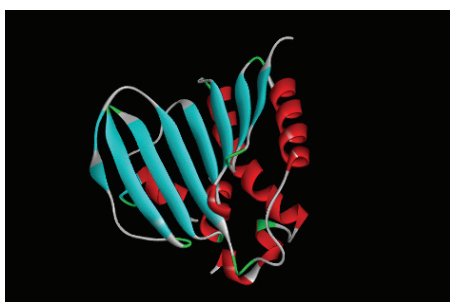
Molecular docking simulations

The use of PyRx version 0.8 facilitated the assessment of the binding affinity and interactions between the benzothiazole Schiff base hybrids (S08, S13, S15, and S19) and the standard antibiotic ciprofloxacin, targeting two bacterial proteins (**4URO** and **6F86**). The three-dimensional structures of *Staphylococcus aureus* (Crystal Structure of Staphylococcus GyraseB 24kDa in complex with Novobiocin, PDB ID: **4URO**),

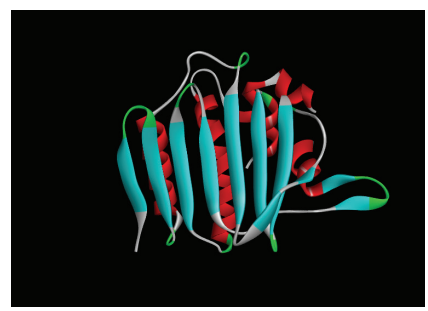
and *Escherichia coli* (Crystal Structure of *E. coli* GyraseB 24kDa in complex with 4-(4-bromo-1H-pyrazol-1-yl)-6-[(ethylcarbamoyl)amino]-N-(pyridin-3-yl)pyridine-3-carboxamide, PDB ID: **6F86**), with respective resolutions of 2.40 Å, and 1.90 Å were procured from the RCSB Protein Data Bank website (http://www.rcsb.org/pdb). The missing hydrogen atoms, secondary structures assigned, and Ramachandran plots were carried out to repair the proteins using the online protein repair server (Nnyigide, Nnyigide, Lee, & Hyun, 2022), as shown in Figure 2 and Supplementary Figure S2. The Autodock tool version 1.5.7 was utilized to prepare the protein receptors, removing water molecules, incorporating polar hydrogen atoms, and allocating Gasteiger charges to the receptor atoms. Subsequently, the rigid protein PDBQT files were archived (El-Shamy et al., 2022).

The ligand structures were prepared using the Molecular Operating Environment (MOE) version 2015 software. The protonation state was determined based on a physiological pH of 7.4, and energy minimization was performed using the MMFF94x force field to achieve a stable three-dimensional conformation. The final ligand structures were then exported for the docking process.

In PyRx, the grid box established by the Vina wizard grid was delineated manually to encompass the complete ligand binding site, and the correct active site was confirmed by redocking the co-ligand. The total quantity of generated binding conformations was constrained to 10 solutions. The binding conformations of each ligand in conjunction with the receptor were scrutinized utilizing Discovery Studio software 2019 (Ouhazza et al., 2025; Trott & Olson, 2010).



4URO



6F86

Figure 2: Three-dimensional structures of the repaired bacterial enzyme targets used for molecular docking: *S. aureus* **Gyrase B (4URO)** and *E. coli* **Gyrase B (6F86)**. The complete set of validation data, including Ramachandran plots and secondary structure assignments, is available in **Supplementary Figure S2**.

Drug-likeness and ADMET evaluation

Drug-likeness is a way to match a drug's physicochemical properties with the biological properties that the human body requires (El-Shamy et al., 2022). Lipinski's five rules state that a drug's likeness is a criterion for evaluating an active medication as a potential therapeutic candidate (Benet, Hosey, Ursu, & Oprea, 2016; Erol, Celik, & Kuyucuklu, 2021). Oral drugs should not break more than one of Lipinski's rules: the molecular weight (MW) should not be greater than 500 g/mol, the octanol/water partition coefficient (log P) value should not be greater than 5, and the chemical structures should not contain more than ten hydrogen bond acceptors (HBA) and five hydrogen bond donors (HBD) (Daina, Michielin, & Zoete, 2017).

The drug-likeness properties of the compounds were analyzed using the SwissADME tool (Listyarini, 2021; Macabeo et al., 2020). The SwissADME tool and pkCSM web server were used to estimate the drugs' ADMET profile, toxicity evaluation, and cardiotoxicity prediction (Lipinski, Lombardo, Dominy, & Feeney, 1997; Macabeo et al., 2020).

RESULTS AND DISCUSSION

DFT calculations

In DFT calculations, examining electronic energies has become crucial for understanding molecular stability and reactivity (El-Shamy et al., 2022). Koopmans' theorem provides a theoretical framework to relate the chemical behavior of molecules to their electronic properties (Tsuneda, Song, Suzuki, & Hirao, 2010).

Quantum chemical descriptors based on Koopmans' theorem can analyze a molecule's reactivity, including parameters like hardness (η), softness (S), chemical potential (μ), electronegativity (χ), and electrophilicity (ω), as shown in Table 2. Electron transfer between chemical entities occurs via molecular frontier orbitals, analyzed at the B3LYP/6–31** theoretical level (Ejalonibu et al., 2020). The Lowest Unoccupied Molecular Orbital (LUMO) and the Highest Occupied Molecular Orbital (HOMO), respectively, indicate a molecule's ability to accept and donate electrons, as displayed in Table 2 (Akbari et al., 2024).

The energy gap (ΔE) is a key quantum property of the benzothiazole-Schiff base hybrids, providing important insights into these molecules (Elangovan et al., 2024). Molecules with a smaller ΔE require less excitation energy, classifying them as chemically soft. The ΔE was calculated for each molecule; a large ΔE suggests lower chemical reactivity because it is energetically unfavorable to add an electron to the high LUMO or remove one from the low HOMO (Manolopoulos, May, & Down, 1991; Ruiz-Morales, 2002). The ΔE values of the Schiff base compounds S08 (4.08 eV), S13 (4.07 eV), S15 (4.05 eV), and S19 (4.11 eV) are markedly lower than that of ciprofloxacin (4.36 eV). This observation implies that S13, S15, and S19 may exhibit a greater propensity to participate in charge transfer interactions with biological targets in comparison to the reference drug, which correlates with their remarkable Minimum Inhibitory Concentrations (MICs) ranging from 3.91 to 15.6 μg/mL (Singh et al., 2017).

Chemically soft molecules are defined by their enhanced bioactivity (Miar, Shiroudi, Pourshamsian, Oliaey, & Hatamjafari, 2021). The biological efficacy is also dependent on the electrophilicity descriptors. Biological reactivity escalates with an increase in the electrophilicity index and chemical softness (Maria Julie et al., 2021). Electrophilicity (ω) functions as a metric of the electrophilic nature of a chemical species; it quantifies the propensity of a molecule to accept an electron, with higher values indicating pronounced electrophilicity within a molecule. The following categorization ranks organic molecules according to their electrophilicity; weak electrophiles are designated as having values below 0.8 eV, moderate electrophiles fall within the range of 0.8 to 1.5 eV, and strong electrophiles exceed 1.5 eV (Edim et al., 2021). In this investigation, all the Schiff base compounds exhibited greater electrophilicity than ciprofloxacin (ω = 2.667 eV). S15 emerged as the strongest electrophile (ω = 3.156 eV), succeeded by S19 (ω = 2.972 eV), followed by S13 (ω = 2.933 eV), and finally S08 (ω = 2.669 eV).

Chemical hardness (η) and softness (S) serve as critical parameters for elucidating stability (Domingo, Ríos-Gutiérrez, & Pérez, 2016). Ciprofloxacin, characterized by the highest hardness and the lowest softness, emerges as the most stable and least reactive entity within the studied molecular set. Conversely, the remaining compounds exhibit comparatively greater chemical softness. Compound S15 manifests the highest softness (S = 0.247 eV-1) among the hybrids, which correlates with its pronounced electrophilicity, thereby aligning with its impressive MIC values, which range from 3.91 to 7.81 μg/mL against various bacterial targets (Singh et al., 2017). Molecules exhibiting softness are generally more polarizable and are associated with enhanced bioactivity due to their capacity to readily deform their electron clouds for effective interaction with biological receptors (Miar et al., 2021).

The chemical potential (μ) serves as an indicator of the propensity for a chemical reaction; a heightened value (less negative) signifies an augmented likelihood of electron donation (acting as an electron donor), whereas a diminished value (more negative) indicates a stronger inclination towards electron acceptance (functioning as an electron acceptor) (Domingo et al., 2016). Electronegativity (χ) quantitatively assesses a molecule's capacity to attract electrons (Karton & Spackman, 2021). Density functional theory calculations elucidate significant interrelations between electronic structure and biological activity. The values for electronegativity (χ) and chemical potential (μ) remain invariant across the compounds (χ = -μ) (Hosny, Samir, & Abdel-Rhman, 2024), with S15 demonstrating the most pronounced electron-withdrawing capacity (χ = -3.575 eV, μ = 3.575 eV). The elevated electronegativity of S15 amplifies its biological activity, resulting in broad-spectrum efficacy (MICs = 3.91 to 7.81 μg/mL) (Domingo et al., 2016). S19 presents intermediate parameters (χ = -3.495 eV, μ = 3.495 eV), leading to favorable experimental MIC results (7.81 to 15.6 μg/mL). The well-balanced electronic characteristics of S08 (χ = -3.300 eV, μ = 3.300 eV) correspond with its outstanding experimental MIC values of 3.91 to 7.81 μg/mL against bacterial strains (Singh et al., 2017). These findings underscore the significance of electronegativity and chemical potential as robust predictors of antimicrobial efficacy within benzothiazole-Schiff base hybrids, positing that optimal electron-withdrawing properties enhance target-specific interactions while ensuring sufficient bioavailability (Domingo et al., 2016).

The dipole moment values elucidate a molecule's intrinsic polarity. Ciprofloxacin demonstrates a high polarity (8.2 Debye), thereby promoting solubility in aqueous environments. S19 and S15 exhibit moderate dipole moment values (3.07 and 2.86 Debye, respectively). This balanced polarity is advantageous, suggesting a favorable equilibrium in which the molecules possess adequate solubility for transport within bodily fluids, while maintaining sufficient non-polar characteristics to facilitate interaction with and penetration of the hydrophobic barriers of cellular membranes (Arnott & Planey, 2012). The HOMO and LUMO overlay S08, S13, S15, S19, and ciprofloxacin display in Figure 3.

Table 2. Global reactivity indices for the S08, S13, S15, S19 and Ciprofloxacin

Cpd Code	HOMO (eV)	LUMO (eV)	ΔE (eV)	η (eV)	μ (eV)	χ (eV)	S (eV^{-1})	ω (eV)	Dipole moment (Debye)
S08	-5.34	-1.26	4.08	2.04	-3.300	3.300	0.245	2.669	6.72
S13	-5.49	-1.42	4.07	2.035	-3.455	3.455	0.246	2.933	5.21
S15	-5.6	-1.55	4.05	2.025	-3.575	3.575	0.247	3.156	2.86
S19	-5.55	-1.44	4.11	2.055	-3.495	3.495	0.243	2.972	3.07
Ciprofloxacin	-5.59	-1.23	4.36	2.18	-3.41	3.41	0.229	2.667	8.2

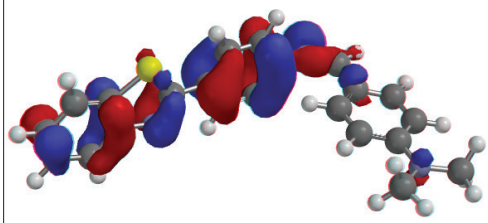
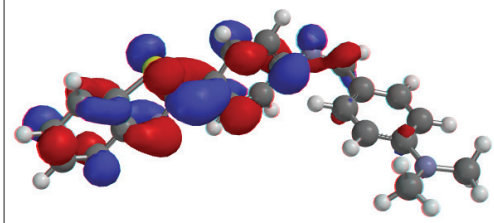
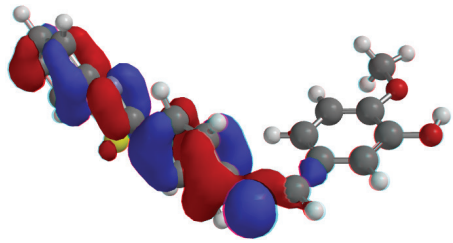
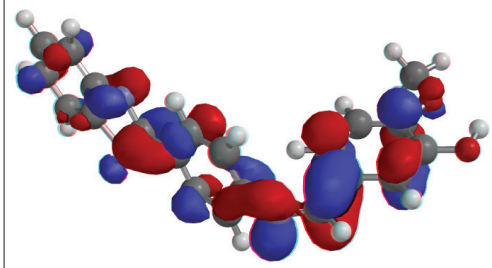
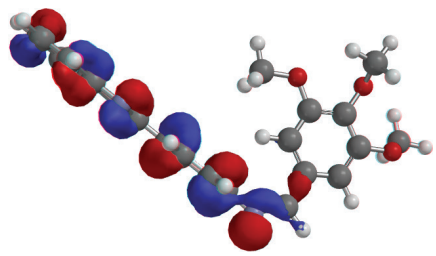
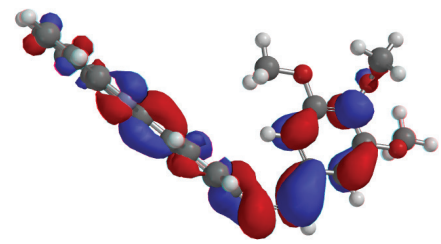
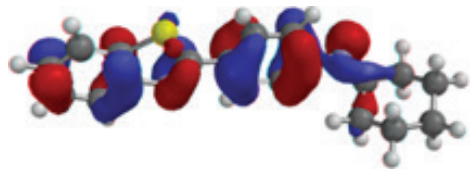
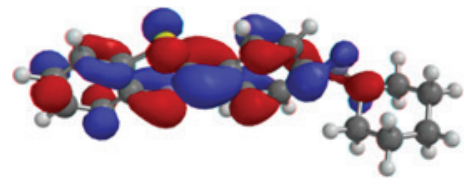
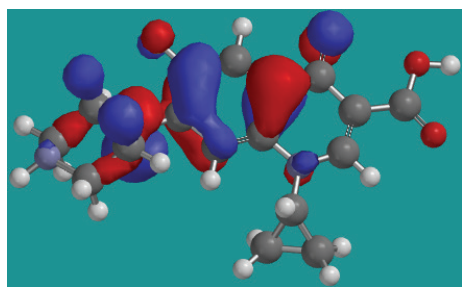
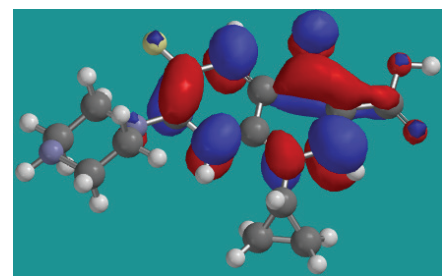
Cpd code	HOMO	LUMO
S08		
S13		
S15		
S19		
Ciprofloxacin		

Figure 3: Frontier molecular orbitals: HOMO and LUMO of S08, S13, S15, S19, and Ciprofloxacin.

Charge distribution analysis

One of the most efficacious methodologies for determining the charge population distributions within a molecular entity in the realm of quantum chemistry is the Mulliken charge analysis (Semire et al., 2017). The distribution of electronic charges (electron density) on selected heteroatoms can provide insights into variations in the vibrational spectrum, which subsequently influences numerous additional characteristics of the system, including atomic bond lengths, dipole moments, electronic architectures, molecular polarizability, and acid-base properties (Preethi, Vijukumar, AnilaRaj, & Vidya, 2024). Furthermore, various chemical reactions, along with the physicochemical

attributes of substances, are contingent upon the electron densities. (Semire et al., 2017; Sule et al., 2025).

Various arrangements of electrons in benzothiazole-Schiff base hybrids are depicted in Table 3 through Mulliken charge analysis, which is associated with their ability to combat bacteria. Between -0.518 and the negative charge of N1, the nitrogen atom in its imine group has. This facilitates the formation of hydrogen bonds between the bacteria's targets (Domingo et al., 2016). The finding is consistent with previous research that has shown that nitrogen atoms with higher electron numbers in Schiff bases are more effective at killing bacteria because they have greater connectivity with their targets (Singh et al., 2017). S08, S13, and S15, along with their respective positive charges of 0.200 to 0.205, all have a minor positive charge in the thiazole ring (S1). The sulfur is responsible for binding the molecule to bacteria by creating weak interactions, like hydrophobic or van der Waals forces, in the region where it binds. This finding indicates this (Meng et al., 2011).

Table 3. Mulliken Charge for S08, S13, S15, S19 and Ciprofloxacin at B3LYP/6-31** basis set

Mulliken Charge								
	O1	O2	O3	N1	N2	N3	S1	F1
S08	----	----	----	-0.598	-0.456	-0.507	0.2	---
S13	0.565	-0.555	----	-0.519	-0.448	-0.519	0.202	---
S15	-0.535	-0.531	-0.526	-0.518	-0.448	----	0.204	---
S19	----	----	----	-0.518	-0.488	----	0.205	---
Ciprofloxacin	-0.511	-0.515	-0.466	-0.565	-0.536	-0.503		---

Molecular electrostatic potential (MEP)

The Molecular Electrostatic Potential (MEP) functions as an advanced quantum computational mechanism that delineates the charge distribution within a molecular entity, thereby offering valuable insights into its chemical reactivity (Aljameel, 2022; Arulaabaranam, Muthu, Mani, & Ben Geoffrey, 2021). The zones characterized as nucleophilic, electrophilic, and neutral are represented through distinct blue, red, and green color gradients, respectively (Pal et al., 2021). The MEP surfaces are illustrated in Figure 4. The spatial distribution of charge across the molecular surface imparts comprehensive information regarding its responsiveness, specifically concerning how it reacts and interacts with incoming molecular species (Maria Julie et al., 2021).

In this analytical framework, elevated negative values of MEP indicate the attraction of hydrogen ions or lighter cations within the red regions, where electron density is more concentrated at the molecular interface. Conversely, positive values of MEP denote a repulsive interaction towards protons or lighter cations in the blue regions, characterized by a diminished concentration of electron density (Miar et al., 2021). In the analyzed Schiff base compounds (S08, S13, S15, and S19), the negatively charged zones are predominantly located on the nitrogen atoms of the imine functionalities, as well as on the oxygen atoms and thiazolyl nitrogen atoms.

Consequently, these specific atoms and sites exhibit a heightened propensity to undergo electrophilic attack and engage in bond formation, such as hydrogen bonding interactions with the active sites of target proteins. Simultaneously, the positively charged zones of the compound are distributed along the hydrogen atoms of the benzothiazolyl moiety and the carbon atoms within the same group. The atoms or functional groups situated in the blue regions are susceptible to nucleophilic attack and are capable of participating in hydrophobic interactions (Abedin, Pal, Chanmiya Sheikh, & Alam, 2024).

In contrast, the chemical structure of ciprofloxacin causes its charge distribution to be dissimilar on an MEP surface. In the carboxylic acid and ketone group,

the carbonyl oxygens have the most negative potential, while the positive potential is concentrated over the protonated nitrogen in the piperazine ring and the C-H bond (Arulaabaranam et al., 2021). Its unique binding mode is accounted for by its distinct MEP map, which relies on the ionic and hydrogen bond interactions of its charged functional group (Meng et al., 2011).

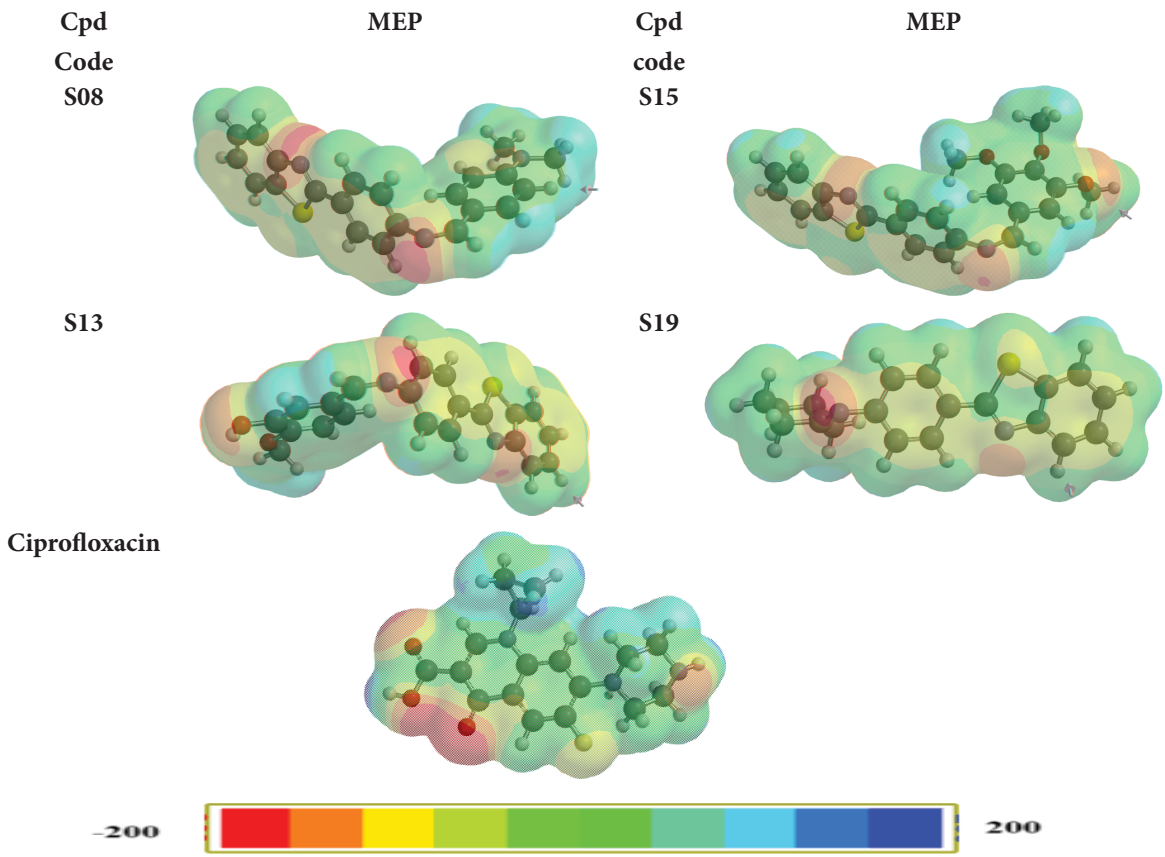


Figure 4. The Molecular Electrostatic Potential surface for S08, S13, S15, S19, and Ciprofloxacin at B3LYP/6-31** basis set

Validation of molecular docking protocol

The reliability of the molecular methodology was validated by redocking of the native co-crystallized ligands into their respective binding sites. For *S. aureus* Gyrase B (4URO), the ligand **novobicin** was extracted and subsequently redocked, yielding a root mean square deviation (RMSD) of 1.03 Å between the docked conformation and the original crystallographic pose. Similarly, for *E. coli* Gyrase B (6F86), the native ligand **4-(4-bromo-1H-pyrazol-1-yl)-6-[(ethylcarbamoyl)amino]-N-(pyridin-3-yl)pyridine-3-carboxamide** was redocked, resulting in an RMSD of 2.04 Å.

An RMSD value below 2.5 Å is considered to be a reliable indicator for a successful reproduction of the experimental binding mode (Castro-Alvarez, Costa, & Vilarrasa, 2017; Trott & Olson, 2010). The obtained values confirmed that the docking protocol employed in this investigation is both valid and proficient in accurately replicating the observed binding mode for these targets (Figure 5.).

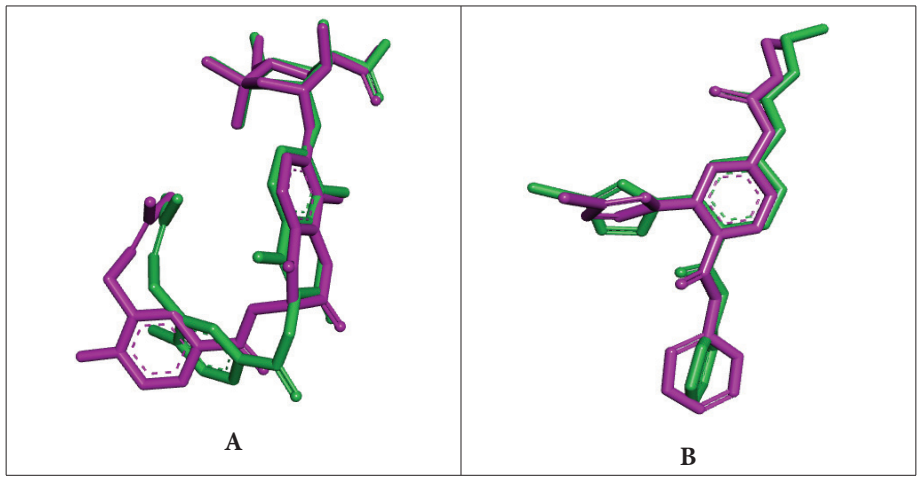


Figure 5. Validation of molecular docking protocol by superposition of crystallographic and re-docked ligand poses. **(A)** Novobiocin in the active site of *S. aureus* Gyrase B (4URO). **(B)** 4-(4-bromopyrazol-1-yl)-6-[(ethylcarbamoyl)amino]-N-(pyridin-3-yl)pyridine-3-carboxamide in the active site of *E. coli* Gyrase B (6F86). The crystallographic (native) pose is shown in green, and the re-docked pose is shown in purple.

Molecular docking

The benzothiazole Schiff base hybrids (S08, S13, S15, and S19), along with the reference antibiotic ciprofloxacin, were tested using docking simulations in the active sites of proteins from three bacteria: *S. aureus* (4URO), and *E. coli* (6F86). The results of the binding energy for these compounds are shown in Table 4. The binding energies vary from moderate to strong across the two targets (Meng et al., 2011).

S19 showed the best binding affinity against 6F86 with a value of -7.9 Kcal/mol, which is better than ciprofloxacin. This explains why S19 had good experimental MIC values (7.81 to 15.6 µg/mL) as listed in Table 1 (Singh et al., 2017). This strong binding isn't a coincidence. It's supported by S19 having a good balance of ΔE (4.11eV) and electrophilicity (ω=2.972 eV), which means it can react well with the target but still stay stable, making it a good inhibitor (Domingo et al., 2016).

S15, which had the best MIC values (3.91 to 7.81 µg/mL), also showed a strong binding energy of -6.9 Kcal/mol against 6F86. This strong activity is because of its high electrophilicity (ω = 3.156 eV) and low softness (S = 0.247 eV^{-1}), which means it can accept electrons and adjust its electron cloud to fit tightly in the enzyme's binding pocket (Miar et al., 2021). S13 had the strongest binding energy against 4URO and matched its good MIC value of 7.81 µg/mL against S. aureus (Trott & Olson, 2010).

Table 4. Binding energy of the docked benzothiazole Schiff base hybrids (S08, S13, S15, and S19) and standard drug (Ciprofloxacin) with different bacterial receptors

Cpd Code	*S.aureus* (4URO) (Kcal/mol)	*E.coli* (6F86) (Kcal/mol)
S08	-5.7	-6.7
S13	-6.9	-6.7
S15	-5.5	-6.9
S19	-5.9	-7.9
Ciprofloxacin	-5.7	-7.0

Molecular interactions

Figures 6 and 7 present the two-dimensional and three-dimensional interaction diagrams pertinent to compounds S08, S13, S15, and S19 alongside the standard antibiotic ciprofloxacin, in association with *S. aureus* (4URO), and *E. coli* (6F86), respectively.

The analyses of interactions with *S. aureus* Gyrase B (4URO), presented in Figure 6, elucidate the varying binding modalities attributable to the specificities

of this enzyme's active site. Structural studies have clearly shown that the active site of *S.aureus* Gyrase B (4URO) has a typical ATP-binding pocket, with key residues such as ASP57 and GLU58 involved in attaching natural inhibitors like novobiocin (Lu et al., 2014). Encouragingly, our docking results match this pattern exactly. The interactions associated with S19 encompass a combination of attractive charge interaction with GLU 58, a conventional hydrogen bond with ASP 57, and stabilization via hydrophobic interactions (Pi-Cation, Pi-Anion, and Pi-Alkyl) with residues ASP 67, ARG 84, GLU 58, ALA 61, and PRO 87 (Pinzi & Rastelli, 2019).

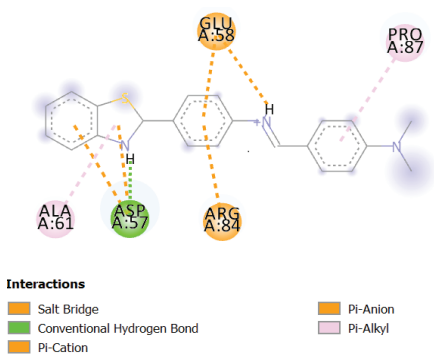
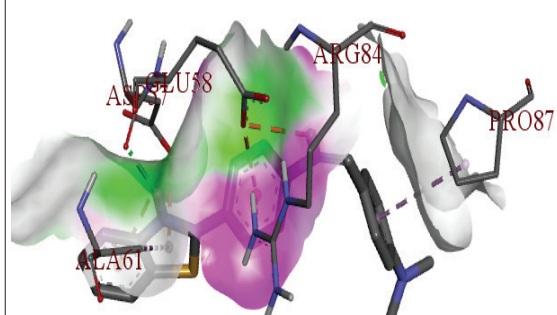
Compound S08 exhibits a conventional hydrogen bond interaction with ASP 57 and a salt bridge formation with GLU 58. It is further stabilized by a series of hydrophobic interactions, including Pi-Cation, Pi-Anion, and Pi-Alkyl interactions with residues such as ALA 61, GLU 58, PRO 87, and ARG 84.

The way S13 binds is because of hydrogen bonds with ASP 57, ARG 84, and GLU 58, a carbon-hydrogen bond with GLY 85, and Pi-Alkyl bonds with PRO 87, ALA 61, and LEU 60. These multiple hydrogen bonds and hydrophobic contacts help S13 stick strongly to *S. aureus*. Hydrogen bonds help guide the binding, while the hydrophobic interactions make the overall binding stronger (Fischer, Smieško, Sellner, & Lill, 2021; Meng et al., 2011).

Compound S15 demonstrates an attractive charge interaction with GLU 58; however, it is predominantly reliant on hydrophobic interactions (Pi-Anion, Pi-Sigma, and Pi-Alkyl) with residues including ILE 102, GLU 58, and ALA 61.

The notable abundance of hydrogen bonding interactions endows the compounds with considerable pharmacological significance, as the presence of hydrogen bonds markedly affects the pharmacological efficacy of ligands (Meng et al., 2011). This underlines the rationale for the compounds exhibiting excellent to good activity against *S. aureus*, as evidenced by their experimental MICs, which span from 3.91 to 15.6 µg/mL (Singh et al., 2017).

Conventional hydrogen bond interactions with ARG 58 and GLN 91 are responsible for the interaction between ciprofloxacin and the *S.aureus* protein. It also forms hydrophobic interactions like Pi-cation and alkyl interactions with residues like PRO 87, ILE 86, and ARG 84. This diverse array of interactions highlights the drug's effective anchoring within the active site of the *S.aureus* protein (Trott & Olson, 2010).

Cpd Code	2-D	3-D
S08		

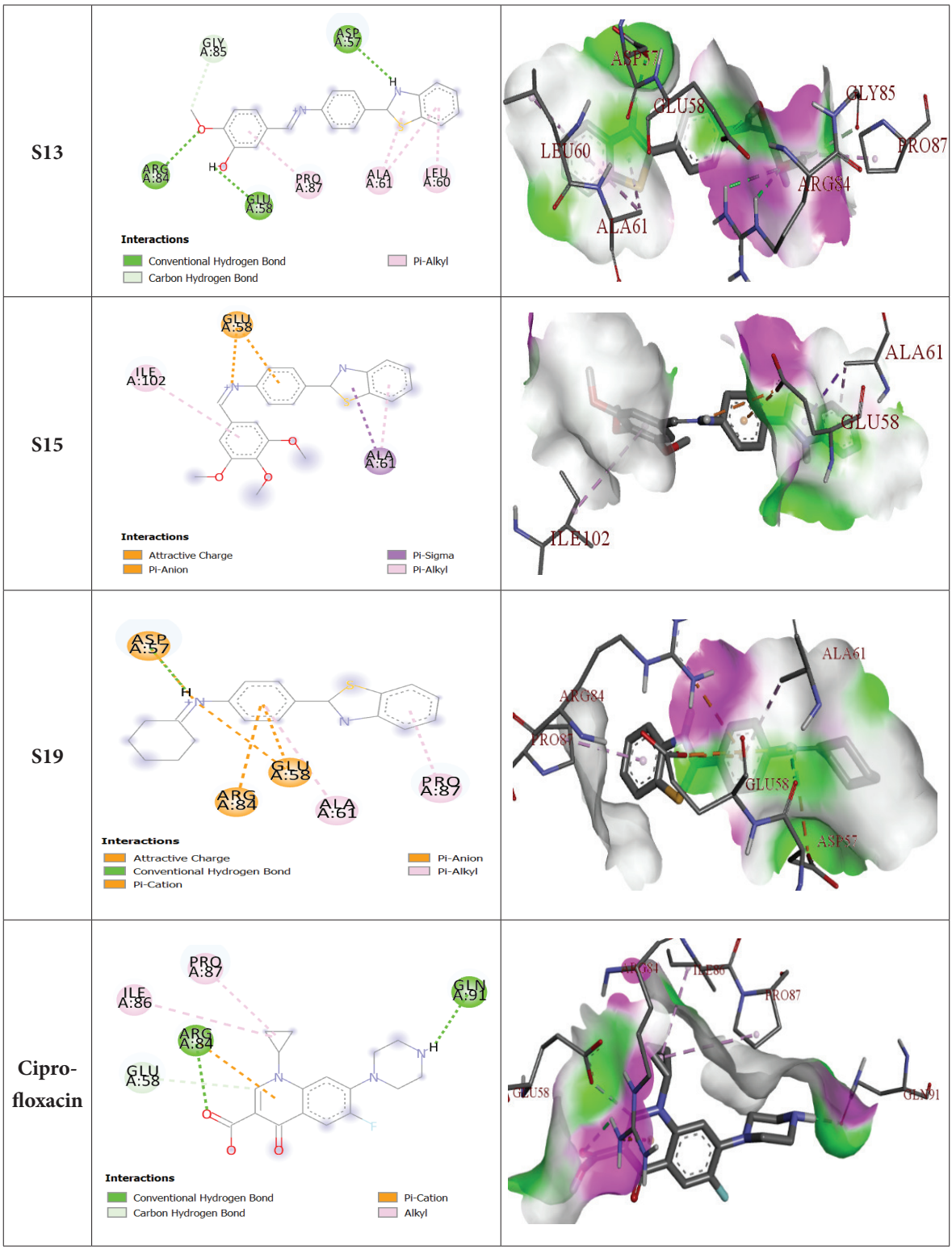


Figure 6. Two and three-dimensional interactions of S08, S13, S15, S19, and Ciprofloxacin against *S. aureus* (**4URO**)

In the interaction diagrams shown in Figure 7 for Schiff base hybrids and *E. coli* Gyrase (6F86), the active site has a deep pocket that is mostly made up of hydrophobic molecules, with some polar amino acids, such as ASP73 and GLU50, acting as binding points for synthetic inhibitors (Narramore, Stevenson, Lawson, Maxwell, & Fishwick, 2019). This is exactly what we observed with our top candidate, S19. S19 forms a salt bridge with ASP 73 and a regular hydrogen bond with GLY 77. It also has several hydrophobic interactions with ARG 76, GLU 50, VAL 43, and VAL 167, which help keep the molecule in place (Fischer et al., 2021).

S15 makes a hydrogen bond with ASP 49, has an electrostatic attraction with GLU 50, and forms a carbon-hydrogen bond with ASP 73. It also benefits from hydrophobic interactions with GLU 50, LEU 52, ILE 78, and ALA 53, giving it a complete set of interactions (Meng et al., 2011; Pinzi & Rastelli, 2019).

S13 also forms a hydrogen bond with ASP 49, has an electrostatic attraction with GLU 50, and is supported by hydrophobic interactions that improve its binding (Arnott & Planey, 2012).

S08 mainly relies on hydrophobic interactions for its binding. For the reference drug ciprofloxacin, the diagram shows its typical binding pattern, including a hydrogen bond with ASN 46 and a halogen (fluorine) bond with GLU 50 and GLY 77. It also has additional hydrophobic interactions with ILE 78 and GLU 50. This combination shows how well-documented its mechanism of Gyrase inhibition is (Trott & Olson, 2010; Wilcken et al., 2013). The detailed interaction diagrams for all other compounds (S08, S13, S15) are provided in Supplementary Figure S3.

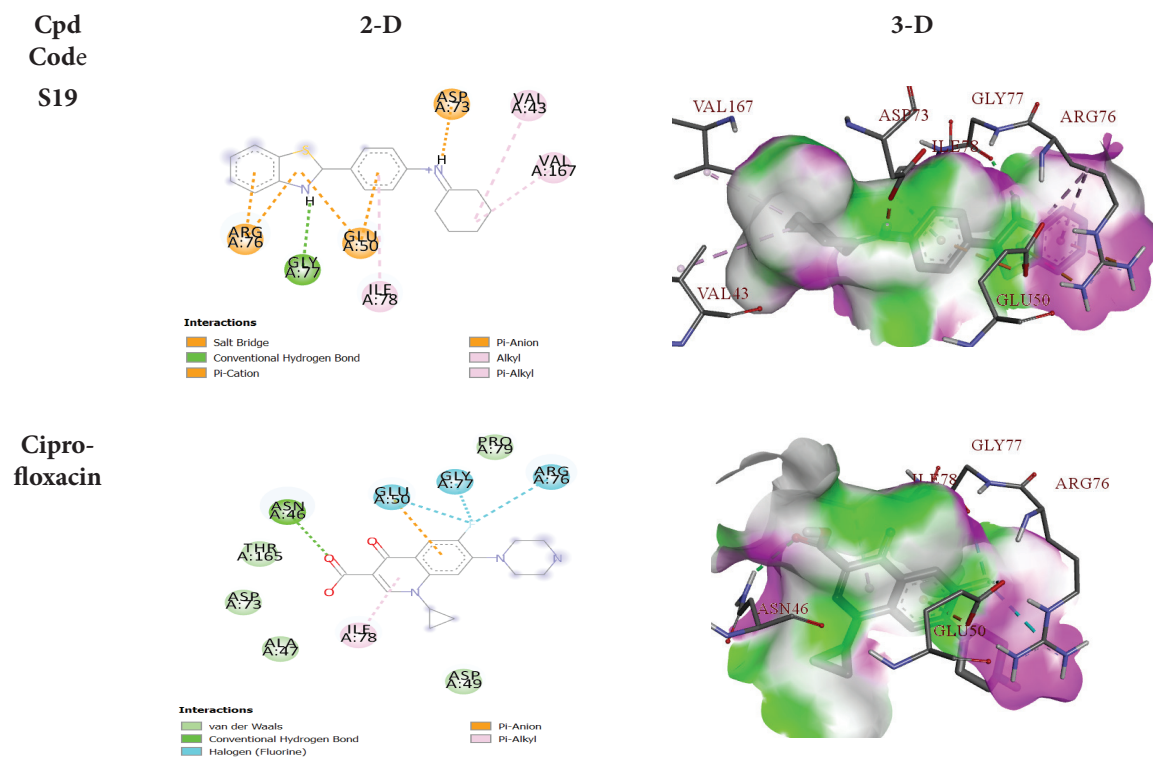


Figure 7. Molecular interactions of the lead compound S19 and the reference drug Ciprofloxacin with the active site *of E. coli* (**6F86**). The detailed interaction diagrams for all other compounds (S08, S13, S15) are provided in Supplementary Figure S3.

Drug-likeness and prediction of ADMET properties

Lipinski rule of five

Any molecular entity must exhibit distinct physical and chemical characteristics to qualify as an orally bioactive pharmaceutical agent (Ramos et al., 2020). To identify the most suitable compounds with drug-like properties, Lipinski's Rule of Five was applied. This principle posits that for a candidate molecule to be deemed appropriate for oral administration, it must demonstrate an Octanol-Water Partition Coefficient (Log P) ≤ 5, a hydrogen bond acceptor (HBA) count of ≤ 10, a molecular weight (MW) ≤ 500 g/mol, and a hydrogen bond donor (HBD) count of ≤ 5 (Lipinski et al., 1997). The criteria of Lipinski's Rule are satisfied if the compound incurs no more than one violation (Pauwels, 2004). Thus, S08, S13, S15, S19, and the standard drug (ciprofloxacin) have all adhered to Lipinski's Rule. The predicted molecular properties of the benzothiazole Schiff base hybrids satisfying Lipinski's Rule of Five are shown in Table 5.

Table 5. Predicted molecular properties of compounds satisfying Lipinski's Rule of Five

Compounds	MW(g/mol)	HBA	HBD	LogP	Lipinski Violation
S08	357.47	2	0	5.78	1
S13	360.43	4	1	5.43	1
S15	404.48	5	0	5.74	1
S19	306.42	2	0	6.00	1
Ciprofloxacin	331.34	5	2	1.18	1

ADMET properties prediction

The ADMET properties of the benzothiazole Schiff base hybrids and the standard drug that follows Lipinski's rule are listed in Table 6. S19 and ciprofloxacin are non-mutagenic, according to the Ames toxicity test, and all compounds have a high gastrointestinal absorption rate. P-glycoprotein (P-gp) is a membrane transport protein that exports toxins and pharmaceuticals outside the cell (Finch & Pillans, 2014). S19 and ciprofloxacin are found to be P-gp substrates. Moreover, the brain is protected from pathogens and toxins by the Blood-Brain Barrier (BBB), which allows selective permeability from the bloodstream to the brain (Amin, 2013; Weiss, Miller, Cazaubon, & Couraud, 2009). The BBB permeability prediction was conducted to assess the compounds' permeability; all the compounds, including the standard drug (ciprofloxacin), do not have effective Blood-Brain permeability.

Around 70-80% of pharmaceuticals in clinical settings undergo metabolic conversion via cytochrome P450 enzymes CYP3A4 and CYP2D6, which are the most relevant drug-metabolizing enzymes (Taylor et al., 2020). None of the compounds was a CYP2D6 inhibitor. S08, S13, S15, and S19 inhibited CYP3A4, indicating caution due to potential drug-drug interactions with substrates such as immunosuppressants, calcium channel blockers, and statins (Taylor et al., 2020). However, potent inhibitors of CYP3A4, like verapamil and ketoconazole, do not necessarily hinder further development of these compounds as drug candidates (Lin & Lu, 1998). Moreover, the hERG-related cardiotoxicity of compounds was predicted; none of the compounds showed action against hERG I. However, other than S19, all of the compounds inhibited hERG II. Notably, S19 and ciprofloxacin inhibited neither hERG I nor II, making them safer references (Gintant, Sager, & Stockbridge, 2016).

S19 is the best candidate based on ADMET properties, with high GI absorption and a perfect safety profile (Ames-negative, no hERG I/II inhibition). S19's structural simplicity allows for tractable optimization potential, despite its CYP3A4 inhibition and P-gp substrate activity, which are tolerable liabilities.

These options align with current FDA regulations, which prioritize safety over potency when developing early-stage antibiotics (U.S. Food and Drug Administration, 2021). S08, S13, and S15 are mutagenic, as determined by the Ames toxicity test, so they cannot be considered as potential drug candidates. Thus, S19 is identified as the top candidate through ADMET profiling.

Table 6. Predicted ADMET properties of compounds

Compound	Ames toxicity	GI Absorption	hERG I inhibitor	hERG II inhibitor	P-gp substrate	BBB Permeability	CYP3A4 inhibitor	CYP2D6 inhibitor
S08	Yes	High	No	Yes	No	No	Yes	No
S13	Yes	High	No	Yes	No	No	Yes	No
S15	Yes	High	No	Yes	Yes	No	Yes	No
S19	No	High	No	No	Yes	No	Yes	No
Ciprofloxacin	No	High	No	No	Yes	No	No	No

S19, despite its promising ADMET profile, is under scrutiny for its inhibition of cytochrome P450 3A4 (CYP3A4), the most abundant drug-metabolizing enzyme in the human liver, responsible for the oxidation of various drugs (Lin & Lu, 1998; Zanger & Schwab, 2013). This inhibition is a well-documented mechanism for drug-drug interactions (DDIs), as it can decrease the metabolic clearance of co-administered drugs, potentially increasing plasma concentrations and risk of adverse effects. Common medications that are substrates of CYP3A4 include statins, calcium channel blockers, and immunosuppressants (Guengerich, 2022).

However, CYP3A4 inhibition is often encountered in early-stage candidates and does not automatically preclude further development (Lin & Lu, 1998). Many successful drugs, such as antibiotic erythromycin and antifungal ketoconazole, are known CYP3A4 inhibitors but are used clinically with appropriate prescribing guidelines and monitoring for DDIs (Zanger & Schwab, 2013). The identification of this property in S19 is valuable for directing future medicinal chemistry efforts. The lead optimization phase could focus on structural modifications to the benzothiazole-Schiff base scaffold to mitigate CYP3A4 inhibition while preserving S19's core antimicrobial activity and safety features, such as its non-mutagenicity and lack of hERG cardiotoxicity (Hughes, Rees, Kalindjian, & Philpott, 2011).

CONCLUSION

This extensive *in silico* examination investigated the potential of benzothiazole-Schiff base hybrids (S08, S13, S15, and S19) as antimicrobial agents through the integration of DFT, molecular docking studies, and ADMET profiling. The DFT analysis indicated that the hybrids exhibit reduced HOMO-LUMO energy gaps (4.05 to 4.11 eV) and elevated electrophilicity indices (2.669 to 3.156 eV) in comparison to ciprofloxacin, suggesting enhanced chemical reactivity and improved charge transfer efficiency, which correlates with their significant experimental MIC values (3.91 to 15.6 μg/mL). Molecular docking studies corroborated robust and selective binding to bacterial gyrase targets (specifically, *S. aureus* Gyrase B and *E. coli* Gyrase B), with binding energies that are either comparable to or exceed those of the reference drug. The analysis of binding configurations revealed stabilizing interactions, encompassing hydrogen bonding and hydrophobic interactions with critical active site residues.

The assessment of drug-likeness and ADMET profiling designated S19 as the leading candidate. Although all compounds demonstrated favorable binding affinities and compliance with drug-like properties, S19 exhibited an enhanced safety profile, characterized by its non-mutagenic properties and absence of hERG cardiotoxicity concerns. Its predicted inhibition of CYP3A4 represents a manageable liability that

does not hinder the prospect of further development. In conclusion, the amalgamation of potent target affinity, advantageous electronic characteristics, and a promising ADMET profile positions S19 as a compelling candidate for further exploration. These computational findings offer a solid basis for its subsequent synthesis and empirical validation in the quest for innovative antimicrobial therapies.

AUTHOR CONTRIBUTION STATEMENT

AOS: Conceptualization, Methodology, Software, Formal analysis, Investigation, Data Curation, Writing - Original Draft. OAM: Validation, Investigation, Resources, Writing - Review & Editing. BS: Supervision, Project administration, Validation, Resources, Writing - Review & Editing, Funding acquisition.

CONFLICT OF INTEREST

The authors declare that there is no conflict of interest.

REFERENCES

Abd El-Hamid, S. M., Sadeek, S. A., Mohammed, S. F., Ahmed, F. M., & El-Gedamy, M. S. (2023). N_2O_2-chelate metal complexes with Schiff base ligand: Synthesis, characterization, and contribution as a promising antiviral agent against human cytomegalovirus. *Applied Organometallic Chemistry*, *37*(2). https://doi.org/10.1002/aoc.6958

Abdel Aziz, A. A., Ramadan, R. M., Sidqi, M. E., & Sayed, M. A. (2023). Structural characterization of novel mononuclear Schiff base metal complexes, DFT calculations, molecular docking studies, free radical scavenging, DNA binding evaluation, and cytotoxic activity. *Applied Organometallic Chemistry*, *37*(2). https://doi.org/10.1002/aoc.6954

Abedin, M. M., Pal, T. K., Chanmiya Sheik, M., & Alam, M. A. (2024). Investigation on synthesized sulfonamide Schiff base with DFT approaches and in silico pharmacokinetic studies: Topological, NBO, and NLO analyses. *Heliyon*, *10*(14). https://doi.org/10.1016/j.heliyon.2024.e34499

Akbari, Z., Stagno, C., Iraci, N., Efferth, T., Omer, E. A., Piperno, A.,… Micale, N. (2024). Biological evaluation, DFT, MEP, HOMO-LUMO analysis, and ensemble docking studies of Zn(II) complexes of bidentate and tetradentate Schiff base ligands as antileukemia agents. *Journal of Molecular Structure*, *1301*, 137400. https://doi.org/10.1016/j.molstruc.2023.137400

Alasadi, Y. K., Jumaa, F. H., & Mukhlif, M. G. (2023). Preparation, Characterization, Anti-cancer and Antibacterial Evaluation of New Schiff Base and Tetrazole Derivatives. *Tikrit Journal of Pure Science*, *28*(2), 12–19. https://doi.org/10.25130/tjps.v28i2.1333

Alfonso-Herrera, L. A., Rosete-Luna, S., Hernández-Romero, D., Rivera-Villanueva, J. M., Olivares-Romero, J. L., Cruz-Navarro, J. A.,… Colorado-Peralta, R. (2022). Transition Metal Complexes with Tridentate Schiff Bases (ONO and ONN) Derived from Salicylaldehyde: An Analysis of Their Potential Anticancer Activity. *ChemMedChem*, *17*(20). https://doi.org/10.1002/cmdc.202200367

Aljameel, A. I. (2022). DFT Study of 4-Acetamido-N-(3-amino-1,2,4-triazol-1-yl) Benzene Sulfonamide and its Potential Application as a Copper Corrosion Inhibitor. *International Journal of Electrochemical Science*, *17*(5), 220524. https://doi.org/10.20964/2022.05.39

Amin, Md. L. (2013). P-glycoprotein Inhibition for Optimal Drug Delivery. *Drug Target Insights*, *7*(1). https://doi.org/10.33393/dti.2013.1349

Arnott, J. A., & Planey, S. L. (2012). The influence of lipophilicity in drug discovery and design. *Expert Opinion on Drug Discovery*, *7*(10), 863–875. https://doi.org/10.1517/17460441.2012.714363

Aroua, L. M., Alhag, S. K., Al-Shuraym, L. A., Messaoudi, S., Mahyoub, J. A., Alfaifi, M. Y., & Al-Otaibi, W. M. (2023). Synthesis and characterization of different complexes derived from Schiff base and evaluation as a potential anticancer, antimicrobial, and insecticide agent. *Saudi Journal of Biological Sciences*, *30*(3), 103598. https://doi.org/10.1016/j.sjbs.2023.103598

Arulaabaranam, K., Muthu, S., Mani, G., & Ben Geoffrey, A. S. (2021). Speculative assessment, molecular composition, PDOS, topology exploration (ELF, LOL, RDG), ligand-protein interactions, on 5-bromo-3-nitropyridine-2-carbonitrile. *Heliyon*, *7*(5), e07061. https://doi.org/10.1016/j.heliyon.2021.e07061

Awolope, R. O., Ejidike, I. P., & Clayton, H. S. (2022). Schiff base metal complexes as dual antioxidant and antimicrobial agents. *Journal of Applied Pharmaceutical Science*. https://doi.org/10.7324/JAPS.2023.91056

Aytac, S., Gundogdu, O., Bingol, Z., & Gulcin, İ. (2023). Synthesis of Schiff Bases Containing Phenol Rings and Investigation of Their Antioxidant Capacity, Anticholinesterase, Butyrylcholinesterase, and Carbonic Anhydrase Inhibition Properties. *Pharmaceutics*, *15*(3), 779. https://doi.org/10.3390/pharmaceutics15030779

Babaei, P., Rezvan, V. H., Gilani, N. S., & Mansour, S. R. (2024). Molecular docking and in vitro biological studies of a Schiff base ligand as anticancer and antibacterial agents. *Results in Chemistry*, *7*. https://doi.org/10.1016/j.rechem.2024.101517

Benet, L. Z., Hosey, C. M., Ursu, O., & Oprea, T. I. (2016). BDDCS, the Rule of 5, and drugability. *Advanced Drug Delivery Reviews*, *101*, 89–98. https://doi.org/10.1016/j.addr.2016.05.007

Boulechfar, C., Ferkous, H., Delimi, A., Berredjem, M., Kahlouche, A., Madaci, A.,…Benguerba, Y. (2023). Corrosion inhibition of Schiff base and their metal complexes with [Mn (II), Co (II) and Zn (II)]: Experimental and quantum chemical studies. *Journal of Molecular Liquids*, *378*, 121637. https://doi.org/10.1016/j.molliq.2023.121637

Castro-Alvarez, A., Costa, A., & Vilarrasa, J. (2017). The Performance of Several Docking Programs at Reproducing Protein–Macrolide-Like Crystal Structures. *Molecules*, *22*(1), 136. https://doi.org/10.3390/molecules22010136

Daina, A., Michielin, O., & Zoete, V. (2017). SwissADME: a free web tool to evaluate pharmacokinetics, drug-likeness, and medicinal chemistry friendliness of small molecules. *Scientific Reports*, *7*(1), 42717. https://doi.org/10.1038/srep42717

Domingo, L., Ríos-Gutiérrez, M., & Pérez, P. (2016). Applications of the Conceptual Density Functional Theory Indices to Organic Chemistry Reactivity. *Molecules*, *21*(6), 748. https://doi.org/10.3390/molecules21060748

Edim, M. M., Enudi, O. C., Asuquo, B. B., Louis, H., Bisong, E. A., Agwupuye, J. A.,…Bassey, F. I. (2021). Aromaticity indices, electronic structural properties, and fuzzy atomic space investigations of naphthalene and its aza-derivatives. *Heliyon*, *7*(2), e06138. https://doi.org/10.1016/j.heliyon.2021.e06138

Ejalonibu, M. A., Elrashedy, A. A., Lawal, M. M., Soliman, M. E., Sosibo, S. C., Kumalo, H. M., & Mhlongo, N. N. (2020). Dual targeting approach for Mycobacterium tuberculosis drug discovery: insights from DFT calculations and molecular dynamics simulations. *Structural Chemistry*, *31*(2), 557–571. https://doi.org/10.1007/s11224-019-01422-w

Ejiah, F. N., Rofiu, M. O., Oloba-Whenu, O. A., & Fasina, T. M. (2023). Schiff bases as analytical tools: synthesis, chemo-sensor, and computational studies of 2-aminophenol Schiff bases. *Materials Advances*, *4*(10), 2308–2321. https://doi.org/10.1039/D3MA00097D

Elangovan, N., Sowrirajan, S., Arumugam, N., Rajeswari, B., Mathew, S., Priya, C. G.,…Mahalingam, S. M. (2024). Theoretical Investigation on Solvents Effect in Molecular Structure (TD-DFT, MEP, HOMO-LUMO), Topological Analysis and Molecular Docking Studies of N-(5-((4-Ethylpiperazin-1-yl)Methyl)Pyridin-2-yl)-5-Fluoro-4-(4-Fluoro-1-Isopropyl-2-Methyl-1H-Benzo[d] Imidazol-6-yl) Pyrimidin-2-Amine. *Polycyclic Aromatic Compounds*, *44*(7), 4467–4490. https://doi.org/10.1080/10406638.2023.2254896

El-Shamy, N. T., Alkaoud, A. M., Hussein, R. K., Ibrahim, M. A., Alhamzani, A. G., & Abou-Krisha, M. M. (2022). DFT, ADMET and Molecular Docking Investigations for the Antimicrobial Activity of 6,6′-Diamino-1,1′,3,3′-Tetramethyl-5,5′-(4-chlorobenzylidene)bis[pyrimidine-2,4(1H,3H)-dione]. *Molecules*, *27*(3). https://doi.org/10.3390/molecules27030620

Erol, M., Celik, I., & Kuyucuklu, G. (2021). Synthesis, Molecular Docking, Molecular Dynamics, DFT, and Antimicrobial Activity Studies of 5-substituted-2-(p-methylphenyl)benzoxazole Derivatives. *Journal of Molecular Structure*, *1234*, 130151. https://doi.org/10.1016/j.molstruc.2021.130151

Finch, A., & Pillans, P. (2014). P-glycoprotein and its role in drug-drug interactions. *Australian Prescriber*, *37*(4), 137–139. https://doi.org/10.18773/austprescr.2014.050

Fischer, A., Smieško, M., Sellner, M., & Lill, M. A. (2021). Decision Making in Structure-Based Drug Discovery: Visual Inspection of Docking Results. *Journal of Medicinal Chemistry*, *64*(5), 2489–2500. https://doi.org/10.1021/acs.jmedchem.0c02227

Gintant, G., Sager, P. T., & Stockbridge, N. (2016). Evolution of strategies to improve preclinical cardiac safety testing. *Nature Reviews Drug Discovery*, *15*(7), 457–471. https://doi.org/10.1038/nrd.2015.34

Guengerich, F. P. (2022). Inhibition of Cytochrome P450 Enzymes by Drugs: Molecular Basis and Practical Applications. *Biomolecules & Therapeutics*, *30*(1), 1–18. https://doi.org/10.4062/biomolther.2021.102

Hadigheh Rezvan, V., & Aminivand, Y. (2024). DFT computational study of optical properties for bis-Schiff bases of 8-aminoquinoline derivatives and furan-2, 3-dicarbaldehyde. *Structural Chemistry*, *35*(5), 1577–1587. https://doi.org/10.1007/s11224-024-02296-3

Hahn, P. (2024). Role of Heterocyclic Compounds in Drug Development: An Overview. *Research & Reviews: Journal of Medicinal and Organic Chemistry JOMC*, *11*(8). https://doi.org/10.4172/J

Hooper, D. C. (2001). Mechanisms of Action of Antimicrobials: Focus on Fluoroquinolones. *Clinical Infectious Diseases*, *32*(Supplement_1), S9–S15. https://doi.org/10.1086/319370

Hosny, N. M., Samir, G., & Abdel-Rhman, M. H. (2024). N′-(Furan-2-ylmethylene)-2-hydroxybenzohydrazide, and its metal complexes: synthesis, spectroscopic investigations, DFT calculations, and cytotoxicity profiling. *BMC Chemistry*, *18*(1), 1–17. https://doi.org/10.1186/s13065-023-01098-8

Hughes, J., Rees, S., Kalindjian, S., & Philpott, K. (2011). Principles of early drug discovery. *British Journal of Pharmacology*, *162*(6), 1239–1249. https://doi.org/10.1111/j.1476-5381.2010.01127.x

In Silico Study of Pyrazolylaminoquinazoline Toxicity by Lazar, Protox, and Admet Predictor. (2018). *Journal of Applied Pharmaceutical Science*, *8*(9), 119–129. https://doi.org/10.7324/JAPS.2018.8918

Karton, A., & Spackman, P. R. (2021). Evaluation of density functional theory for a large and diverse set of organic and inorganic equilibrium structures. *Journal of Computational Chemistry*, *42*(22), 1590–1601. https://doi.org/10.1002/jcc.26698

Krishna, G. A., Dhanya, T. M., Shanty, A. A., Raghu, K. G., & Mohanan, P. V. (2023). Transition metal complexes of imidazole-derived Schiff bases: Antioxidant/anti-inflammatory/antimicrobial/enzyme inhibition and cytotoxicity properties. *Journal of Molecular Structure*, *1274*, 134384. https://doi.org/10.1016/j.molstruc.2022.134384

Lin, J. H., & Lu, A. Y. H. (1998). Inhibition and Induction of Cytochrome P450 and the Clinical Implications. *Clinical Pharmacokinetics*, *35*(5), 361–390. https://doi.org/10.2165/00003088-199835050-00003

Lipinski, C. A., Lombardo, F., Dominy, B. W., & Feeney, P. J. (1997). Experimental and computational approaches to estimate solubility and permeability in drug discovery and development settings. *Advanced Drug Delivery Reviews*, *23*(1–3), 3–25. https://doi.org/10.1016/S0169-409X(96)00423-1

Listyarini, R. V. (2021). Implementation of the Molecular Visualization Program for Chemistry Learning. *Prisma Sains : Jurnal Pengkajian Ilmu Dan Pembelajaran Matematika Dan IPA IKIP Mataram*, *9*(1), 64. https://doi.org/10.33394/j-ps.v9i1.3941

Lu, J., Patel, S., Sharma, N., Soisson, S., Kishii, R., Takei, M., … Singh, S. B. (2014). Crystal Structure of Staph Gyrase B 24kDa in complex with Novobiocin. In the *Worldwide Protein Data Bank*. https://doi.org/10.2210/pdb4uro/pdb

Macabeo, A. P. G., Pilapil, L. A. E., Garcia, K. Y. M., Quimque, M. T. J., Phukhamsakda, C., Cruz, A. J. C.,…Stadler, M. (2020). Alpha-Glucosidase- and Lipase-Inhibitory Phenalenones from a New Species of Pseudolophiostoma Originating from Thailand. *Molecules*, *25*(4), 965. https://doi.org/10.3390/molecules25040965

Manolopoulos, D. E., May, J. C., & Down, S. E. (1991). Theoretical studies of the fullerenes: C34 to C70. *Chemical Physics Letters*, *181*(2–3), 105–111. https://doi.org/10.1016/0009-2614(91)90340-F

Maria Julie, M., Prabhu, T., Elamuruguporchelvi, E., Asif, F. B., Muthu, S., & Irfan, A. (2021). RETRACTED: Structural (monomer and dimer), wavefunctional, NCI analysis in aqueous phase, electronic and excited state properties in different solvent atmospheres of 3-{(E)-[(3,4-dichlorophenyl)imino]methyl} benzene-1,2-diol. *Journal of Molecular Liquids*, *336*, 116335. https://doi.org/10.1016/j.molliq.2021.116335

Meng, X.-Y., Zhang, H.-X., Mezei, M., & Cui, M. (2011). Molecular Docking: A Powerful Approach for Structure-Based Drug Discovery. *Current Computer-Aided Drug Design*, *7*(2), 146–157. https://doi.org/10.2174/157340911795677602

Miar, M., Shiroudi, A., Pourshamsian, K., Oliaey, A. R., & Hatamjafari, F. (2021). Theoretical investigations on the HOMO–LUMO gap and global reactivity descriptor studies, natural bond orbital, and nucleus-independent chemical shifts analyses of 3-phenylbenzo[*d*]thiazole-2(3H)-imine and its *para-substituted* derivatives: Solvent and substituent effects. *Journal of Chemical Research*, *45*(1–2), 147–158. https://doi.org/10.1177/1747519820932091

Narramore, S. K., Stevenson, C. E. M., Lawson, D. M., Maxwell, A., & Fishwick, C. W. G. (2019). Crystal Structure of E. coli GyraseB 24kDa in complex with 4-(4-bromo-1H-pyrazol-1-yl)-6-[(ethylcarbamoyl)amino]-N-(pyridin-3-yl)pyridine-3-carboxamide. In the *Worldwide Protein Data Bank*. https://doi.org/10.2210/pdb6f86/pdb

Nnyigide, O. S., Nnyigide, T. O., Lee, S.-G., & Hyun, K. (2022). Protein Repair and Analysis Server: A Web Server to Repair PDB Structures, Add Missing Heavy Atoms and Hydrogen Atoms, and Assign Secondary Structures by Amide Interactions. *Journal of Chemical Information and Modeling*, *62*(17), 4232–4246. https://doi.org/10.1021/acs.jcim.2c00571

Ouhazza, H., Abdelaziz, M., Alaoui, E., Soussi, S., Idrissi, A., Habsaoui, A., & Bouzakraoui, S. (2025). Molecular Docking, ADMET, DFT Studies, and Retrosynthesis Strategy of New Benzimidazolone Derivatives as HIV-1 Reverse Transcriptase (RT) Inhibitors. *Journal of Medicinal and Chemical Sciences*, *8*, 119–135. https://doi.org/10.26655/JMCHEMSCI.2025.2.1

Pal, T. K., Mumit, M. A., Hossen, J., Paul, S., Alam, Md. A., Islam, Md. A.-A.-A.-A., & Sheik, Md. C. (2021). Computational and experimental insight into antituberculosis agent, (E)-benzyl-2-(4-hydroxy-2-methoxybenzylidene) hydrazinecarbodithioate: ADME analysis. *Heliyon*, *7*(10), e08209. https://doi.org/10.1016/j.heliyon.2021.e08209

Paul, M. Kr., Dilipkumar Singh, Y., Bedamani Singh, N., & Sarkar, U. (2015). Emissive bis-salicylaldiminato Schiff base ligands, and their zinc(II) complexes: Synthesis, photophysical properties, mesomorphism, and DFT studies. *Journal of Molecular Structure*, *1081*, 316–328. https://doi.org/10.1016/j.molstruc.2014.10.031

Pauwels, R. (2004). New non-nucleoside reverse transcriptase inhibitors (NNRTIs) are being developed for the treatment of HIV infections. *Current Opinion in Pharmacology*, *4*(5), 437–446. https://doi.org/10.1016/j.coph.2004.07.005

Pibiri, I. (2024). Recent Advances: Heterocycles in Drugs and Drug Discovery. *International Journal of Molecular Sciences*, *25*(17), 9503. https://doi.org/10.3390/ijms25179503

Pinzi, L., & Rastelli, G. (2019). Molecular Docking: Shifting Paradigms in Drug Discovery. *International Journal of Molecular Sciences*, *20*(18), 4331. https://doi.org/10.3390/ijms20184331

Pore, A., Gaikwad, G., Hegade, S., Jadhav, Y., Mane, R., & Kumbhar, R. (2023). Analyzing the Impact of the Substituent on the Quinazolinone Schiff Base and the Interaction of the Fe (III) and Cr (III) with Different Quinazolinone Schiff Bases for Antioxidant and Anti-inflammatory Activity. *Analytical Chemistry Letters*, *13*(1), 39–59. https://doi.org/10.1080/22297928.2023.2173647

Preethi, V., Vijukumar, V. G., AnilaRaj, S., & Vidya, V. G. (2024). Synthesis, characterization, DFT studies, and evaluation of the potential anti-tumor activity of nicotinic hydrazide-based Schiff base using in vitro and molecular docking techniques. *Heliyon*, *10*(9). https://doi.org/10.1016/j.heliyon.2024.e29689

Rajimon, K. J., Elangovan, N., Amir Khairbek, A., & Thomas, R. (2023). Schiff bases from chlorine-substituted anilines and salicylaldehyde: Synthesis, characterization, fluorescence, thermal features, biological studies, and electronic structure investigations. *Journal of Molecular Liquids*, *370*, 121055. https://doi.org/10.1016/j.molliq.2022.121055

Ramos, R. S., Macêdo, W. J. C., Costa, J. S., da Silva, C. H. T. de P., Rosa, J. M. C., da Cruz, J. N.,…Santos, C. B. R. (2020). Potential inhibitors of the enzyme acetylcholinesterase and juvenile hormone with insecticidal activity: study of the binding mode via docking and molecular dynamics simulations. *Journal of Biomolecular Structure and Dynamics*, *38*(16), 4687–4709. https://doi.org/10.1080/07391102.2019.1688192

Rezaei, M. T., Keypour, H., Hajari, S., Yaghoobi, F., Moazzami Farida, S. H., Saadati, M., & Gable, R. W. (2023). Theoretical and solid-state structures of three new macroacyclic Schiff base complexes and the investigation of their anticancer, antioxidant, and antibacterial properties. *RSC Advances*, *13*(14), 9418–9427. https://doi.org/10.1039/D3RA00153A

Ruiz-Morales, Y. (2002). HOMO–LUMO Gap as an Index of Molecular Size and Structure for Polycyclic Aromatic Hydrocarbons (PAHs) and Asphaltenes: A Theoretical Study. I. *The Journal of Physical Chemistry A*, *106*(46), 11283–11308. https://doi.org/10.1021/jp021152e

Semire, B., Mutiu, O., & Oyebamiji, A. K. (2017). *DFT and AB INITIO Methods on NMR, IR, and Reactivity Indices of Indol-3-Carboxylate and Indazole-3-Carboxylate Derivatives of Cannabinoids: Comparative Study*. www.SID.ir

Singh, M., Kumar Singh, S., Thakur, B., Ray, P., & Singh, S. K. (2015). Design and Synthesis of Novel Schiff Base-Benzothiazole Hybrids as Potential Epidermal Growth Factor Receptor (EGFR) Inhibitors. *Anti-Cancer Agents in Medicinal Chemistry*, *16*(6), 722–739. https://doi.org/10.2174/1871520615666151007160115

Singh, M., Sellamuthu, S., Singh, S. K., Gangwar, M., Nath, G., & Singh, S. K. (2017). Antimicrobial Potency and Molecular Mechanism of Benzothiazole Schiff Base Hybrids. *Saudi Journal of Medical and Pharmaceutical Sciences*. https://doi.org/10.36348/sjmps.2017.v03i12.017

Sule, A. O., Obiyenwa, K. G., Salawu, O. W., & Semire, B. (2025). In silico evaluation of Co(II), Mn(II), Cu(II), and Zn(II) complexes with hydrazide ligands: DFT, spectroscopic, and molecular docking studies. *International Journal of Chemical Studies*, *13*(3), 96–113. https://doi.org/10.22271/chemi.2025.v13.i3b.12545

Taylor, C., Crosby, I., Yip, V., Maguire, P., Pirmohamed, M., & Turner, R. M. (2020). A Review of the Important Role of CYP2D6 in Pharmacogenomics. *Genes*, *11*(11), 1295. https://doi.org/10.3390/genes11111295

Trott, O., & Olson, A. J. (2010). AutoDock Vina: Improving the speed and accuracy of docking with a new scoring function, efficient optimization, and multithreading. *Journal of Computational Chemistry*, *31*(2), 455–461. https://doi.org/10.1002/jcc.21334

Tsuneda, T., Song, J.-W., Suzuki, S., & Hirao, K. (2010). On Koopmans' theorem in density functional theory. *The Journal of Chemical Physics*, *133*(17). https://doi.org/10.1063/1.3491272

U.S. Food and Drug Administration. (2021). *Novel Drug Approvals for 2021. https://www.fda.gov/drugs/novel-drug-approvals-fda/novel-drug-approvals-2021*.

Weiss, N., Miller, F., Cazaubon, S., & Couraud, P.-O. (2009). The blood-brain barrier in brain homeostasis and neurological diseases. *Biochimica et Biophysica Acta (BBA) - Biomembranes*, *1788*(4), 842–857. https://doi.org/10.1016/j.bbamem.2008.10.022

Wilcken, R., Zimmermann, M. O., Lange, A., Joerger, A. C., & Boeckler, F. M. (2013). Principles and Applications of Halogen Bonding in Medicinal Chemistry and Chemical Biology. *Journal of Medicinal Chemistry*, *56*(4), 1363–1388. https://doi.org/10.1021/jm3012068

Wu, P., Bhamidipati, M., Coles, M., & Rao, D. V. G. L. N. (2004). Biological nano-ceramic materials for holographic data storage. *Chemical Physics Letters*, *400*(4–6), 506–510. https://doi.org/10.1016/j.cplett.2004.10.129

Yassen, T. M., & AL-Azzawi, A. M. (2023). Synthesis and Characterization of New Bis-Schiff Bases Linked to Various Imide Cycles. *Iraqi Journal of Science*, 1062–1070. https://doi.org/10.24996/ijs.2023.64.3.3

Zanger, U. M., & Schwab, M. (2013). Cytochrome P450 enzymes in drug metabolism: Regulation of gene expression, enzyme activities, and impact of genetic variation. *Pharmacology & Therapeutics*, *138*(1), 103–141. https://doi.org/10.1016/j.pharmthera.2012.12.007

FABAD J. Pharm. Sci., 51, 1, 23-40, 2026
Doi: 10.55262/fabadeczacilik.1753199
RESEARCH ARTICLE

Development and Validation of RP-HPLC for Determination Bedaquiline Fumarate in Nanostructured Lipid Carriers, Tablets, and Human Plasma Using Design of Experiment Method

Asti RAHAYU[*], SATRIALDI[**], Neng Fisheri KURNIATI[***], Rachmat MAULUDIN[****°]

Development and Validation of RP-HPLC for Determination Bedaquiline Fumarate in Nanostructured Lipid Carriers, Tablets, and Human Plasma Using Design of Experiment Method

SUMMARY

A reversed-phase HPLC (RP-HPLC) technique was established to quantify Bedaquiline fumarate (BDQ), a hydrophobic drug for multidrug-resistant tuberculosis. Effective separation was achieved with a mobile phase of methanol and ammonium acetate buffer (pH 4.7) in a 85:15 (v/v) ratio, at a flow rate of 1.2 mL/min. The validated method exhibited excellent linearity in multiple matrices: tablet formulations (20-200 µg/mL; R^2=0.9993), nanostructured lipid carriers (NLCs) (40-300 µg/mL; R^2=0.9991), and human plasma (0.1-10 µg/mL; R^2=0.9975). Method sensitivity was confirmed with limits of detection (0.7483 µg/mL) and limit of quantification (2.2677 µg/mL). Comprehensive validation demonstrated satisfactory recovery rates (98-102%), precision, and robustness (relative standard deviation <2%), meeting all International Council for Harmonisation requirements. This study presents a systematically optimized RP-HPLC method for the quantification of BDQ. The main advantages over existing methods include a significantly shorter retention time (<3 minutes) achieved through DoE optimization and successful validation across diverse sample types (tablets, NLCs, and human plasma), and offering a reliable time-efficient solution for routine analysis.

Keywords: *Chromatography, design of experiments, validation method, lipid, tablet, plasma.*

Tasarım Deney Yöntemi Kullanılarak Nanoyapılı Lipid Taşıyıcılar, Tabletler ve İnsan Plazmasında Bedaquilin Fumarat Tayini İçin RP-HPLC Yönteminin Geliştirilmesi ve Validasyonu

ÖZ

Çoklu ilaca dirençli tüberküloz tedavisinde kullanılan hidrofobik bir ilaç olan bedaquiline fumaratın (BDQ) kantitatif analizi için ters fazlı HPLC (RP-HPLC) yöntemi geliştirilmiştir. Metanol ve amonyum asetat tamponunun (pH 4,7) 85:15 (v/v) oranında karıştırılmasıyla hazırlanan mobil faz ve 1,2 mL/dak akış hızı ile etkin bir ayırma sağlanmıştır. Validasyon çalışmaları, yöntemin farklı matrislerde mükemmel doğrusallık gösterdiğini ortaya koymuştur: tablet formülasyonları (20-200 µg/mL; R^2=0,9993), nanoyapılı lipid taşıyıcılar (40-300 µg/mL; R^2=0,9991) ve insan plazması (0,1-10 µg/mL; R^2=0,9975). Yöntemin hassasiyeti, tespit limiti (0,7483 µg/mL) ve kantifikasyon limiti (2,2677 µg/mL) ile doğrulanmıştır. Kapsamlı validasyon çalışmaları, tatmin edici geri kazanım oranları (%98-102), kesinlik ve sağlamlık (bağıl standart sapma <%2) ile Uluslararası Harmonizasyon Konseyi (ICH) gerekliliklerini karşıladığını göstermiştir. Bu çalışma, BDQ kantitatif analizi için sistematik olarak optimize edilmiş bir RP-HPLC yöntemi sunmaktadır. Mevcut yöntemlere kıyasla başlıca avantajları arasında Deneysel Tasarım (DoE) optimizasyonu ile elde edilen önemli ölçüde daha kısa tutulma süresi (<3 dakika) ve tabletler, NLY'ler ve insan plazması gibi çeşitli örnek tiplerinde başarıyla validasyonu yer almaktadır; bu da rutin analizler için güvenilir ve zaman açısından verimli bir çözüm sunmaktadır.

Anahtar Kelimeler: *Kromatografi, deneysel tasarım, validasyon yöntemi, lipid, tablet, plazma.*

Recieved: 29.07.2025
Revised: 17.10.2025
Accepted: 5.11.2025

[*] ORCID: 0009-0004-4731-942X, Doctoral Program in Pharmacy, School of Pharmacy, Institut Teknologi Bandung, Bandung, Indonesia; Department of Pharmaceutics, Faculty of Health Sciences, Universitas PGRI Adi Buana Surabaya, Indonesia
[**] ORCID: 0000-0001-9973-4044, Department of Pharmaceutics, School of Pharmacy, Institut Teknologi Bandung, Bandung, Indonesia
[***] ORCID: 0000-0001-9973-4044, Department of Pharmacology and Clinical Pharmacy, School of Pharmacy, Institut Teknologi Bandung, Bandung, Indonesia
[****] ORCID: 0000-0002-3729-0254, Department of Pharmaceutics, School of Pharmacy, Institut Teknologi Bandung, Bandung, Indonesia

[°] Corresponding Author; Rachmat MAULUDIN
E-mail: rachmat@itb.ac.id

INTRODUCTION

In December 2022, the World Health Organization published therapeutic protocols for multidrug-resistant tuberculosis (MDR-TB), incorporating bedaquiline fumarate (BDQ) as a key therapeutic agent (World Health Organization, 2022). These updated recommendations introduce a more streamlined, patient-centred treatment paradigm with improved equity of access (Vanino et al., 2023). BDQ, commercially available as Sirturo® (Janssen-Cilag), is administered as 100 mg immediate-release uncoated tablets (Petersen et al., 2023). The drug faces significant bioavailability challenges (10-30%) due to its poor aqueous solubility, despite high permeability (Jaw-Tsai et al., 2023). These physicochemical properties classify BDQ as a Biopharmaceutics Classification System (BCS) Class II compound, underscoring the need for formulation strategies to improve its dissolution (Guglielmetti et al., 2020).

This study developed a reversed-phase HPLC (RP-HPLC) method for the analysis of BDQ in pharmaceutical formulations (tablets and lipid nanocarriers) and biological samples. The development of this methodology aimed to achieve a balance between analytical performance (efficiency, accuracy) and practical considerations, including cost and solvent consumption (Abd-AlGhafar et al., 2022). While several HPLC and LC-MS/MS methods for BDQ analysis have been reported, many exhibit prolonged retention times or lack a systematic approach for optimization. Previous analytical approaches for BDQ determination have predominantly employed gradient HPLC systems, typically exhibiting retention times greater than 5 minutes (Chandrudu & Gandhimathi, 2024). Isocratic methods reported in the literature demonstrate even more protracted elution profiles, with retention times extending to 7.5 minutes (Ayodele et al., 2024). Notably, mobile phases incorporating methanol as the organic modifier have been associated with particularly extended chromatographic run times, ranging from 10 to 30 minutes in specific analytical protocols (Pardhi et al., 2024). Consequently, the development of an optimized HPLC method employing an appropriate methanol-ammonium acetate buffer ratio represents a critical advancement, combining the economic benefits of methanol with the chromatographic efficiency afforded by ammonium acetate buffers.

The implementation of a multivariate strategy through Design of Experiments (DoE) methodology permits the simultaneous optimization of multiple critical parameters to enhance chromatographic performance (Ajayi et al., 2024). The selection of an appropriate experimental design for HPLC method development requires careful consideration of multiple factors, including study objectives, practical constraints, resource availability, and temporal considerations (Abdallah et al., 2023). Method validation followed a tiered approach, commencing with analysis of simple tablet formulations before progressing to more complex matrices such as nanostructured lipid carriers and human plasma specimens (Bezawada et al., 2024). This systematic validation strategy ensures methodological robustness across diverse sample types while permitting thorough evaluation of the technique's pharmaceutical applications. The developed analytical procedure incorporates several innovative aspects that collectively reduce hazardous solvent consumption, minimise chemical waste generation, and improve energy efficiency. The method underwent strict validation in accordance with ICH International Council for Harmonisation (ICH) guidelines (Ermer, 2025), including comprehensive statistical evaluation. This optimized HPLC methodology represents a significant advancement in BDQ analysis, addressing several limitations associated with existing techniques.

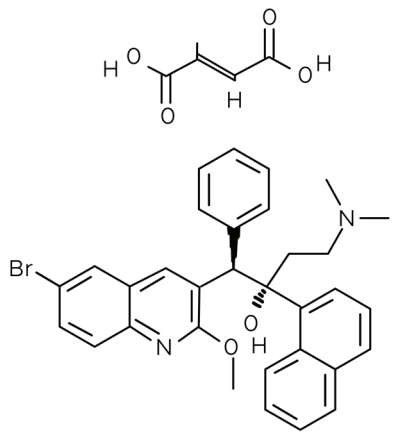


Figure 1. Chemical structure of Bedaquiline fumarate

MATERIALS AND METHODS

Materials

Bedaquiline fumarate was obtained commercially. All chemical reagents, including ammonium acetate, cetyl alcohol, oleic acid, Plantacare® 2000, and HPLC-grade methanol, were of analytical or pharmaceutical grade. Ultrapure water was produced using a laboratory water purification system. Marketed tablet formulation (Sirturo®) and fresh human blood samples were acquired for method validation.

Chromatographic apparatus and conditions

Chromatographic analysis was performed using an HPLC system equipped with a UV detector. Separation was achieved on a C18 column (250 × 4.6 mm, 5 µm) maintained at ambient temperature. The mobile phase, consisting of methanol and ammonium acetate buffer (pH 4.7) in a ratio of 85:15 (v/v), was delivered isocratically at a flow rate of 1.2 mL/min. Detection was carried out at 225 nm with an injection volume of 10 µL. Before use, the mobile phase was filtered through a 0.22 µm membrane filter.

Standard solution preparation

BDQ stock solutions (1000 µg/mL) were prepared by dissolving 10 mg of the compound in methanol within 10 mL volumetric flasks. Working standards were generated through serial methanolic dilutions of the stock solution, with thorough mixing ensured by vortex agitation. All solutions were filtered through 0.22 µm membrane filters before HPLC analysis to remove particulate matter. This dilution protocol produced the required concentration range for method validation while maintaining solution integrity.

Optimization and development of the RP-HPLC method

This study employed a full factorial design to optimize three critical parameters: flow rate (A), pH of buffer (B), and mobile phase ratio (C). As bedaquiline fumarate exhibits weak acidic properties, ammonium acetate buffer pH values (4.3, 4.5, 4.7) were selected to be slightly below the compound's pKa for enhanced reversed-phase retention (Pardhi et al., 2020). Methanol was chosen as the organic modifier due to its favourable low viscosity characteristics, which minimizes column backpressure (Abdu Hussen, 2022). Mobile phase compositions of buffer to methanol (15:85, 20:80, 25:75 v/v) were tested at flow rates (0.8, 1.0, 1.2 mL/min), with each parameter assessed at three coded levels (-1, 0, +1) for low, medium, and high values (Table 1.). A total of 27 experimental runs were executed to systematically assess the influence of these variables on two key chromatographic performance indicators: peak tailing factor (Y1), retention time (Y2), and theoretical plate count (Y3). The complete experimental matrix is detailed (Table 2.).

Table 1. Independent variables of the full factorial design method

Independent variables	Levels		
	-1	0	+1
Flow rate (mL/min)	0.8	1.0	1.2
Mobile phase ratio (buffer to methanol)	15:85	20:80	25:75
pH of buffer	4.3	4.5	4.7

Validation of analytical methods

Method validation followed ICH criteria, evaluating system performance, linear range, sensitivity (LOD/LOQ), precision, accuracy, and robustness (Chavan & Desai, 2022; Ermer, 2025).

Preparation of the mobile phase

The mobile phase comprised methanol-buffer mixtures ranging from 85:15 to 75:25 (v/v). A 10 mM ammonium acetate solution was prepared in 1000 mL HPLC-grade water, with pH precisely regulated to 4.3-4.7 using glacial acetic acid to achieve ideal separation conditions.

Table 2. 3^3 full factorial design optimization for Bedaquiline fumarate quantification

Run.	Independent variables			Dependent variables		
	Flow rate (mL/min) (A)	pH of Buffer (B)	Ratio of mobile phase buffer to methanol (%) (C)	Tailing Factor (Y_1)	Retention time (Y_2)	Theoretical plate (Y_3)
Run. 1	0.8	4.7	20:80	1.37	6.28	11916
Run. 2	0.8	4.7	25:75	1.30	12.83	12569
Run. 3	1.2	4.7	25:75	1.46	11.40	9851
Run. 4	1.2	4.3	25:75	1.97	9.32	8374
Run. 5	0.8	4.3	25:75	1.83	10.02	8670
Run. 6	1.2	4.5	20:80	1.51	4.63	9463
Run. 7	1.0	4.7	20:80	1.38	5.47	11120
Run. 8	0.8	4.3	20:80	1.37	3.66	11185
Run. 9	1.2	4.3	15:85	1.38	2.51	8838
Run. 10	1.0	4.5	25:75	1.53	10.68	9981
Run. 11	1.0	4.7	25:75	1.34	11.66	10752
Run. 12	1.2	4.5	25:75	1.62	11.41	9745
Run. 13	1.0	4.3	25:75	1.88	9.35	8608
Run. 14	0.8	4.3	15:85	1.32	3.21	9650
Run. 15	1.2	4.5	15:85	1.10	1.67	9084
Run. 16	0.8	4.5	25:75	1.52	9.50	9910
Run. 17	1.0	4.3	20:80	1.58	3.34	9207
Run. 18	0.8	4.5	20:80	1.48	5.57	10859
Run. 19	1.0	4.5	20:80	1.52	4.83	9521
Run. 20	1.2	4.3	20:80	1.58	3.41	8944
Run. 21	1.0	4.3	15:85	1.33	2.64	8964
Run. 22	0.8	4.7	15:85	1.09	3.46	10564
Run. 23	1.0	4.5	15:85	1.13	1.90	9715
Run. 24	1.0	4.7	15:85	1.08	2.77	10181
Run. 25	0.8	4.5	15:85	1.15	2.94	10777
Run. 26	1.2	4.7	20:80	1.38	5.39	11120
Run. 27	1.2	4.7	15:85	1.08	2.89	10417

System suitability

A 2.2 µg/mL BDQ solution was used to assess system suitability. Multiple injections verified compliance with acceptance criteria for peak area, tailing factor (TF), and theoretical plates (N). Mean values and percentage relative standard deviation (RSD) were calculated to assess method precision, ensure consistent chromatographic performance.

Linearity

The method showed strong linear responses within specified ranges: 20-200 µg/mL for BDQ tablets, 40-300 µg/mL for nanostructured lipid carriers (NLCs), and 0.1-10 µg/mL for human plasma. All standard curves achieved correlation coefficients exceeding 0.999, with satisfactory precision for all regression parameters.

Precision and accuracy

Method precision was investigated through both intra-day and inter-day studies (ICH Harmonised Guideline, 2022). Intra-day precision was evaluated by analyzing replicate calibration standard during a single session, whereas inter-day precision was assessed by conducting repeated tests over several days. Method accuracy was verified through recovery studies, in which a 100 µg/mL sample solution was spiked with standard solutions at 80%, 100%, and 120% of the original concentrations. Recovery percentages were then calculated to validate the method's trueness.

Selectivity

Method selectivity was rigorously evaluated by challenging the chromatographic system with potential interferents commonly present in the sample matrices. The standard addition method was employed for this purpose. A standard solution of BDQ was spiked into a placebo mixture mimicking the tablet excipients, blank nanostructured lipid carriers (without BDQ), and drug-free human plasma.

Limit of detection (LOD) and limit of quantitation (LOQ)

The limit of detection (LOD) and limit of quantification (LOQ) were derived from the calibration curve slope (SP) and the response standard deviation (r), following ICH criteria. LOD was defined as 3.3r/SP, whereas LOQ was calculated as 10r/SP. These values reflect the method's sensitivity and precision at low analyte concentrations.

Robustness

Method robustness was evaluated by intentionally modifying to chromatographic parameters, including mobile phase composition (83:17 to 87:13), flow rate (1.1-1.3 mL/min), and wavelength (224-226 nm). The impact on retention times and peak areas was analyzed using % RSD to verify consistency across altered conditions (Kohler et al., 2023).

Method application

Sample processing for BDQ in tablet dosage forms

The exact mass of Sirturo® 100 mg tablets was determined by precisely measuring the powdered tablet weight. BDQ tablet powder (100 mg) was dissolved in methanol within a volumetric flask for subsequent analysis.

Sample processing for BDQ in nanostructured lipid carriers

BDQ-loaded NLCs were prepared via ultrasonic emulsification (Hariyanti et al., 2023). The lipid phase (3.5% cetyl alcohol, 1.5% oleic acid). BDQ mixed into the lipid phase. The aqueous phase (4% PlantaCare® 2000, deionized water) was heated to 65°C. A heated microemulsion was prepared by homogenizing at 8000 rpm for 2 minutes, then probe-sonicated for 6 minutes (45:15 pulse cycle, 60% amplitude) to form NLCs. Following vortex mixing (2 min) and centrifugation (6000 rpm, 25 min) of 10 mL BDQ-NLC, 250 µL supernatant was diluted in methanol (2000 µL) and acetonitrile (3000 µL) before HPLC analysis.

Sample processing for BDQ in human plasma

Human plasma samples were obtained from Palang Merah Indonesia (PMI), Surabaya. 250 µL of human plasma was combined with BDQ standard solutions in separate centrifuge tubes. Following thorough mixing, protein precipitation was achieved

using 500 µL acetonitrile and 250 µL methanol, followed by 3 minutes of vortexing and 10 minutes of centrifugation at 15,000 rpm. The clear supernatant obtained was isolated and analyzed using the specified HPLC method.

Statistical analysis

A full factorial design was implemented in Minitab 21 (Minitab LLC, USA) to assess factor effects and interactions systematically.

RESULTS AND DISCUSSION

System suitability

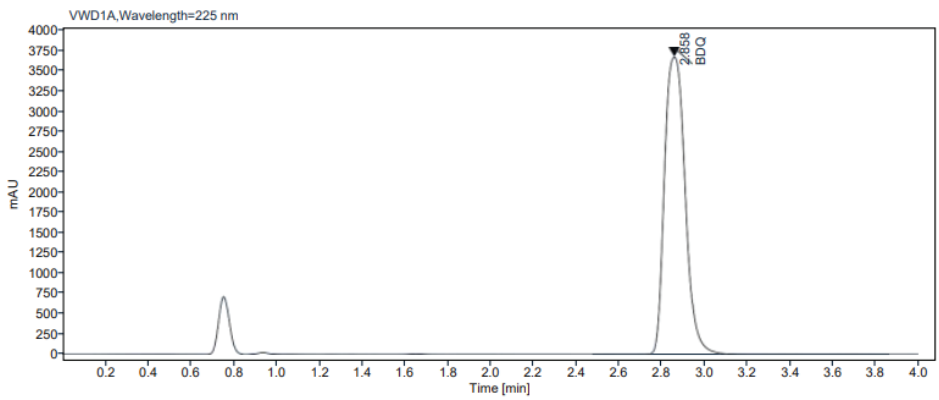
System suitability testing was conducted by determining %RSD for three critical chromatographic parameters: peak area reproducibility, tailing factor, and theoretical plate count (Isane et al., 2022). Analytical validation involved six replicate injections of a 2.2 µg/mL BDQ standard solution. The calculated %RSD values for both peak area and theoretical plate number demonstrated excellent precision, with all measurements yielding variations below the 2% threshold (Table 3.).

Table 3. System suitability test using 2.2 µg/mL

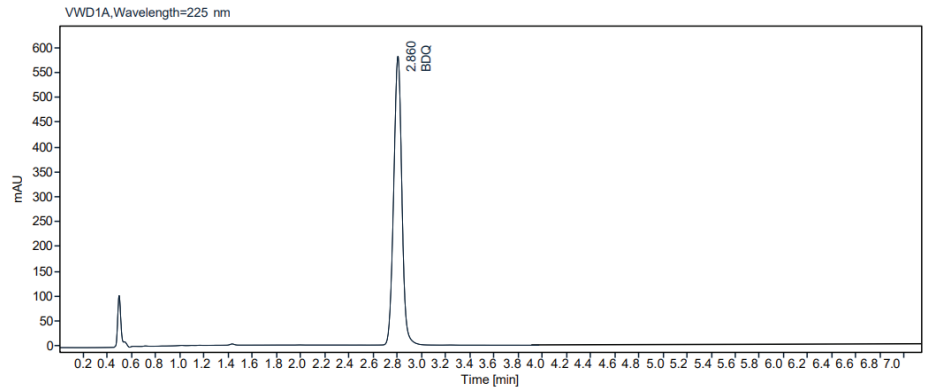
No.	Parameters	Results		
		Mean	SD	% RSD
1	Peak area	188.26	0.48	0.26
2	Number of theoretical plates	4536	29.04	0.64

Selectivity

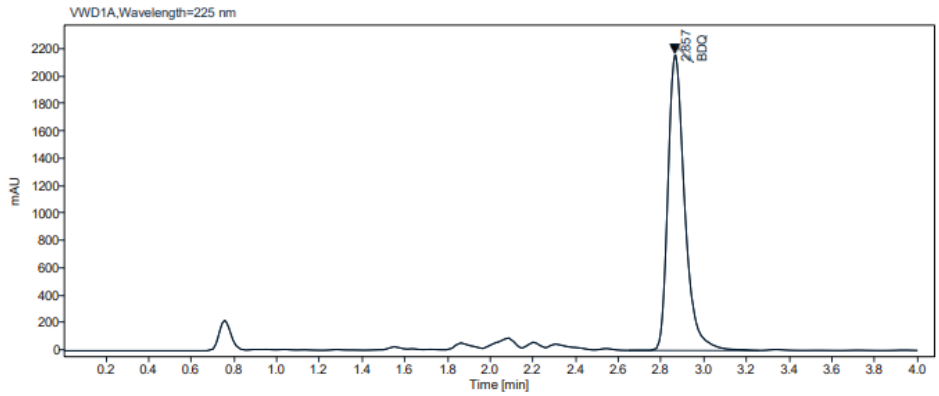
The experimental protocol adhered strictly to the validation requirements outlined in ICH Q2(R1) guidelines (Rajmane & Shinde, 2023). Representative chromatograms (Figure 2.) illustrate the separation profiles for: (a) blank matrix, (b) BDQ standard solution (500 µg/mL), (c) tablet formulation extract, (d) nanostructured lipid carrier preparation, and (e) human plasma sample. The chromatographic system demonstrated consistent retention characteristics, with BDQ eluting at 2.858 ± 0.003 minutes across all sample matrices, confirming method robustness and also offering an environmental benefit through reduced solvent consumption per run due to the shorter analysis time compared to many existing methods.



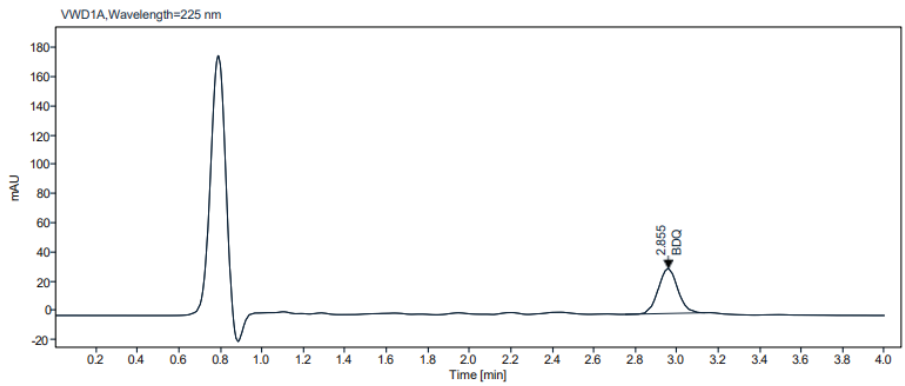
(a)



(b)



(c)



(d)

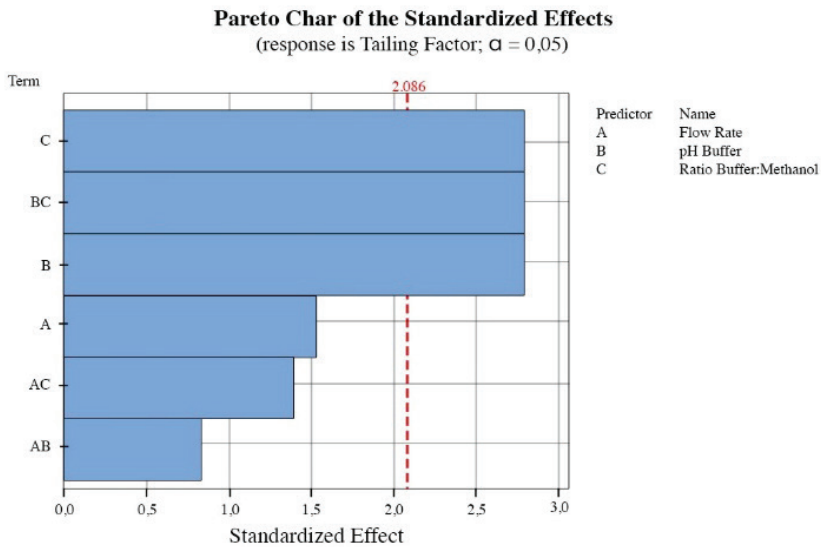
Figure 2. Chromatogram of BDQ in (a) standard at 500 µg/mL, (b) tablet dosage form, (c) nanostructured lipid carrier, (d) human plasma sample

Development and optimization of the RP-HPLC method

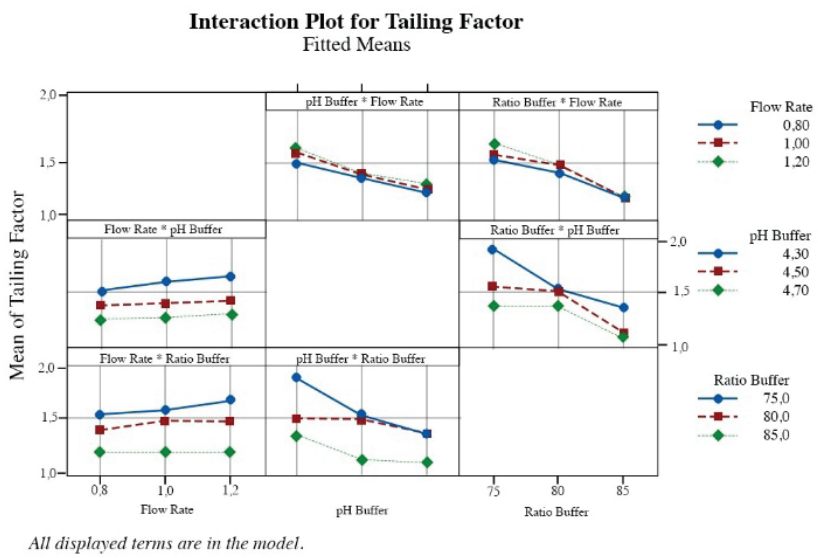
Twenty-seven chromatographic runs were performed, to evaluate peak area, tailing characteristics, and plate counts. Regarding the experimental design selection, a full factorial design (3^3) was deliberately chosen over more efficient response surface methodologies (RSM) such as Central Composite Design (CCD) or Box-Behnken Design (BBD). While CCD or BBD require fewer runs for a quadratic model, a full facto-

rial design provides the most reliable and unbiased estimates of all interaction effects without confounding (Montgomery, 2017). Minitab 21-generated Pareto analysis demonstrated statistically significant effects (p=0.011) of mobile phase composition (Factor C), buffer pH (Factor B), and their interaction (BC) on peak symmetry (Patil & Chalikwar, 2024). Flow rate variations proved inconsequential. Both linear and quadratic effects of pH and solvent ratio predominated in influencing tailing behaviour, either independently or synergistically. These results establish that mobile-phase pH and composition are pivotal parameters for chromatographic optimization. Visual representations of factor-response relationships are provided for standardized effects (Figure 4a.) and interaction plots (Figure 4b.), illustrating the dependence of chromatographic performance on these critical variables. The buffer pH (B), mobile phase ratio (C), and their interaction (BC) had statistically significant effects on chromatographic performance as their standardized effects exceeded the critical threshold, indicating that these parameters meaningfully influence separation outcomes.

a



b



All displayed terms are in the model.

Figure 3. Pareto chart illustrating standardised effects (a) and tailing factor interaction plot (b)

Minitab's response optimization tool established threshold values (minimum, target, maximum) for three critical responses (Table 4.), determining ideal operational parameters and corresponding desirability metrics (Sahu et al., 2018). The composite desirability index (D), scaled 0-1, quantified method robustness, with D=1 representing optimal performance as shown in (Table 4.) (Stojanović et al., 2021). The optimized chromatographic conditions comprised: 15:85 (v/v) buffer to methanol mobile phase, 1.2 mL/min flow rate, pH 4.7 buffer, and 30°C column temperature, demonstrating excellent robustness (D=1).

Table 4. Response optimization of a 3^3 full factorial design for RP-HPLC of BDQ

Parameters							Optimum condition pH = 4.7, methanol = 85%, flow rate 1.2 mL/min	
							Composite desirability (D) = 1	
Responses	Goal	Lower	Target	Upper	Weight	Importance	Predicted responses	Individual desirability (d)
TF	Minimize	1.08	1.0	1.97	1	1	1.08	1

The response optimization analysis established the ideal chromatographic conditions for BDQ analysis: ammonium acetate buffer (pH 4.7) and methanol in a 15:85 (v/v) ratio, delivered at a flow rate of 1.2 mL/min. This specific combination is grounded in fundamental reversed-phase chromatography principles to achieve an optimal balance of speed, efficiency, and peak integrity. The methanol-rich mobile phase (85%) is critical for the rapid elution of the highly hydrophobic BDQ (Nag et al., 2020). The high organic modifier content competitively reduces analyte interaction with the C18 stationary phase, thereby enabling the significantly shorter retention times (<3 minutes). This choice also enhances the method's greenness and cost-effectiveness compared to acetonitrile-based methods. The buffer pH of 4.7 was strategically selected based on BDQ's acid-base properties. Maintaining a pH slightly below its pKa ensures the molecule remains predominantly non-ionized, maximizing consistent hydrophobic interactions with the stationary phase (Dharuman et al., 2023). This controlled pH, synergized with the strong eluting power of 85% methanol, yields sharp, symmetrical peaks with minimal tailing. The flow rate of 1.2 mL/min represents an optimal compromise between analysis speed and chromatographic efficiency. While higher flow rates reduce retention time, they can compromise theoretical plate count, as evidenced by the negative coefficient for flow rate in the theoretical plate model (Y3). This selected rate provides fast analysis while maintaining high efficiency and acceptable backpressure.

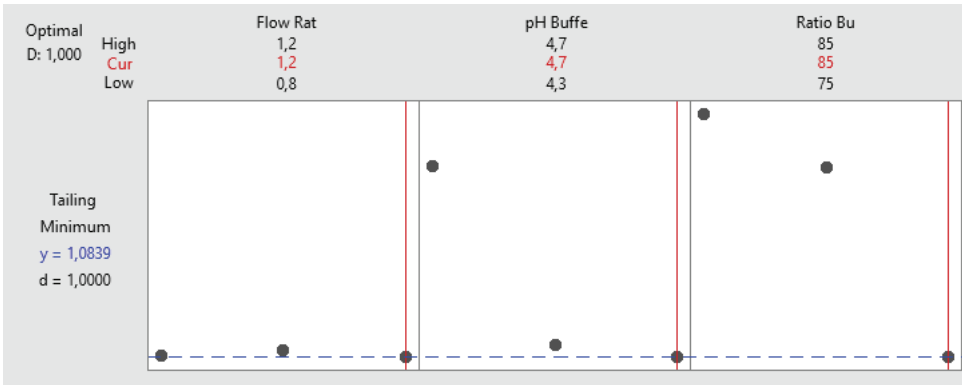


Figure 4. 3^3 Factorial design optimization plot for chromatographic parameter evaluation.

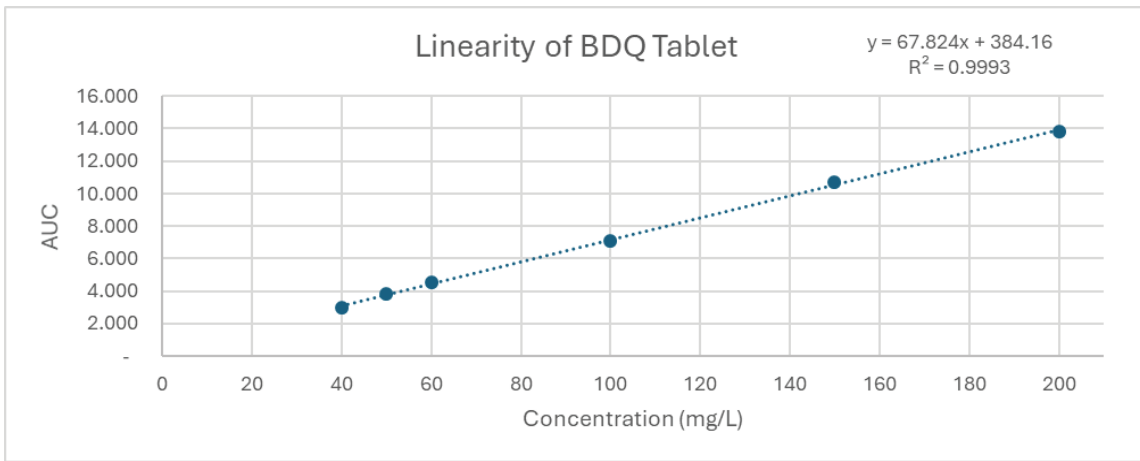
The model's adequacy was evaluated by analyzing pure error from central composite design points. Statistical assessment revealed significant model fit ($p<0.05$) for all response variables, confirming satisfactory predictive capability without evidence of lack of fit. Polynomial regression equations demonstrated quantitative relationships between independent and dependent variables, with positive regression coefficients indicating synergistic effects and negative values representing antagonistic interactions (Kumar et al., 2015). Coefficient magnitude directly correlated with parameter influence strength, with larger values denoting greater impact. The derived equations (Y1, Y2, and Y3) showed statistically significant correlations with all measured responses. The equations (1), (2), and (3) demonstrate how flow rate (A), buffer pH (B), and mobile phase ratio (C) affect chromatographic performance. A higher flow rate increases the tailing factor (Y1) but reduces the retention time (Y2). Alkaline pH decreases tailing while increasing theoretical plates (Y3). Mobile phase ratio shows minimal individual impact but interacts significantly with other parameters.

Tailing factor (Y1) = 27.13 + 5.17A – 5.60B – 0.309C – 0.508AB – 0.0337AC +0.0667BC	(1)
Retention Time (Y2) = -167 +25.6A + 49.5B +1.80C - 2.55 AB - 0.193AC – 0.536BC	(2)
Theoretical Plate (Y3) = -120.721 – 3.423A + 3.0516B + 1.382C – 653AB + 44AC – 318BC	(3)

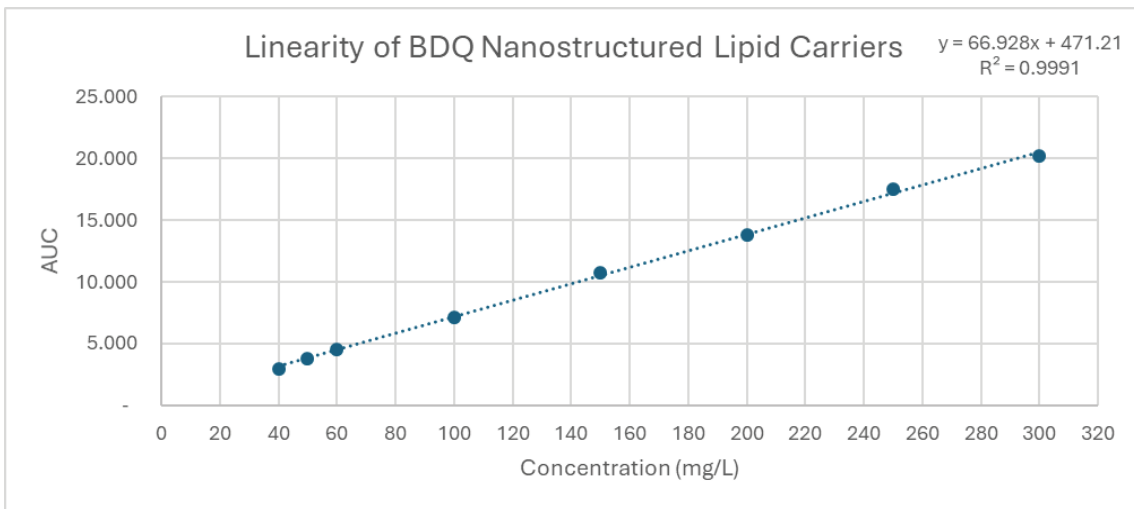
The model for the tailing factor (Y1) indicates that a higher flow rate (positive coefficient for A) adversely affects peak symmetry by increasing tailing. In contrast, an alkaline buffer pH (negative coefficient for B) is the most significant factor for improving peak shape by reducing tailing. While the mobile phase ratio (C) has a minimal standalone effect, its synergistic interaction with pH (positive BC coefficient) suggests that the beneficial effect of high pH is slightly enhanced at higher organic solvent concentrations. For retention time (Y2), buffer pH (B) has the profound positive effect, significantly increasing the analyte's residence time on the column. The flow rate (A) also shows a strong positive effect, which is counterintuitive but explained by its dominant interaction terms. This underscores that the system is best controlled by balancing these two parameters rather than adjusting them in isolation. The theoretical plate count (Y3), a measure of chromatographic efficiency, is primarily and favorably influenced by the buffer pH (B), as indicated by its significant positive coefficient. A higher flow rate (A) negatively impacts column efficiency. The most significant interaction is the strong antagonistic effect between flow rate and pH (negative AB coefficient), demonstrating that the combined increase of these two parameters drastically reduces the number of theoretical plates, thereby compromising separation efficiency. This highlights that achieving high efficiency requires a lower flow rate coupled with a higher pH.

Linearity

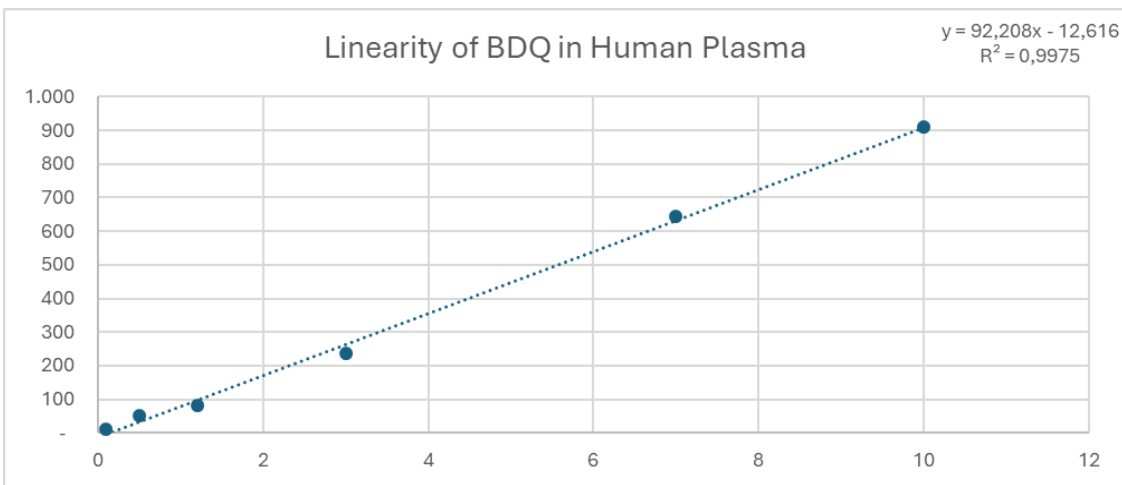
For tablet formulations Sirturo® (40-200 µg/mL), the linear regression equation $y = 67.8240x + 384.1611$ demonstrated excellent linearity (R^2=0.9993). Nanostructured lipid carrier analysis (40-300 µg/mL) showed comparable linearity (R^2=0.9991) with the equation $y = 66.9280x + 471.2101$. Plasma samples (0.1-10 µg/mL) showed satisfactory linearity (R^2 = 0.9975), described by $y = 92.2083x - 12.6161$. All calibration curves exhibited strong correlation coefficients exceeding 0.9975, confirming method validity across the studied concentration ranges.



(a)



(b)



(c)

Figure 5. Calibration Curve of BDQ in (a) tablet, (b) nanostructured lipid carrier, (c) human plasma sample

Precision

The analytical method's precision was rigorously assessed through intra-day (n=6) and inter-day variability studies, determined via peak area %RSD calculations (Çağlar et al., 2022). Accuracy validation examined BDQ in tablet formulations (70 µg/mL), nanostructured lipid carriers (240 µg/mL), and human plasma (2.5 µg/mL) through replicate analyzes. Both precision evaluations demonstrated exceptional reproducibility, with all %RSD values remaining below the 2% acceptance threshold (Table 5.), confirming method reliability for quantitative analysis across different matrices and time intervals.

Table 5. Intra-day and inter-day precision of BDQ in tablets, nanostructured lipid carriers, and plasma

Sample	Conc. (µg/mL)	Intra-day precision				Inter-day precision			
		Peak area	Mean area	SD	% RSD	Peak area	Mean area	SD	% RSD
BDQ in tablet	70	4,822.63	4,867.48	34.62	0.71	4,795.44	4,842.07	36.54	0.75
		4,891.44				4,837.76			
		4,843.36				4,861.11			
		4,922.59				4,895.24			
		4,884.07				4,866.09			
		4,840.80				4,796.77			
BDQ in nanostructured lipid carrier	240	16,264.32	16,295.29	36.83	0.23	16,508.97	16,427.55	193.78	1.18
		16,301.14				16,109.46			
		16,237.02				16,462.29			
		16,353.05				16,483.28			
		16,301.49				16,727.03			
		16,314.70				16,274.27			
BDQ in human plasma	2.5	188.50	188.26	0.48	0.26	188.11	188.28	0.24	0.13
		187.48				188.38			
		188.38				188.40			
		187.75				187.84			
		188.65				188,36			
		188.82				188.58			

Accuracy

Method accuracy was evaluated through standard addition at three concentrations (80%, 100%, 120%) across matrices: pure samples, nanostructured lipid carriers, and human plasma. Recovery rates demonstrated excellent accuracy, ranging from 98.46% to 101.11%, confirming the method's reliability for quantitative analysis.

Table 6. The percentage recovery of BDQ in tablet dosage form, nanostructured lipid carrier, and in human plasma

Sample	% Level	Conc. (µg/mL)	Found Conc. (µg/mL)	Mean	SD	% RSD	% Recovery
BDQ in tablet dosage form	80	80.01	80.02	80.42	0.43	0.54	100.52
			81.02				
			80.22				
	100	100.14	99.42	99.96	0.54	0.54	100.16
			100.52				
			100.56				
	120	120.03	119.99	119.33	0.49	0.41	99.44
			119.18				
			118.82				
BDQ in lipid-based nanocarriers	80	217.86	216.03	216.95	0.90	0.42	99.58
			218.18				
			216.65				
	100	236.67	235.97	236.02	0.39	0.17	99.90
			236.52				
			235.56				
	120	245.63	246.50	248.35	1.65	0.67	101.11
			248.04				
			250.51				
BDQ in human plasma	80	1.76	1.76	1.76	0.01	0.65	99.79
			1.76				
			1.74				
	100	2.20	2.17	2.17	0.01	0.15	98.46
			2.17				
			2.18				
	120	2.60	2.58	2.59	0.01	0.29	99.49
			2.59				
			2.60				

Limit of detection and limit of quantitation

Method sensitivity was established through signal-to-noise ratio calculations, with experimentally derived limits of 0.75 µg/mL for detection and 2.27 µg/mL for quantification, indicating robust bedaquiline measurement capability.

Robustness

The developed RP-HPLC method demonstrated consistent repeatability and specificity under optimized conditions. Robustness was evaluated through controlled variations in flow rate, temperature, and organic phase composition (Surapuraju & Juturu,

2022). Increasing temperature negligibly impacted retention time (%RSD < 2%) or BDQ peak area (recovery: 97.0–98.9%). Conversely, lower temperatures reduced retention time by 2.9% and slightly decreased peak stability (recovery: 93.2–96.7%). A 0.1 mL/min flow rate reduction delayed elution (9.66% difference) but maintained acceptable recovery (96.2–101.6%). These results confirm the method's reliability under minor operational modifications.

Table 7. Summary of BDQ validation parameter

Validation parameters	Tablet dosage forms	Nanostructured lipid carriers	Human plasma	Acceptance Criteria
Optimum wavelength (nm)	225	225	225	225
System suitability				
Peak area (%RSD)	0.71	0.23	0.26	
Retention time (%RSD)	0.13	0.13	0.25	<2%
Tailing factor (%RSD)	1.53	0.50	1.50	
Linearity				
Linearity range (µg/mL)	20-200	40-300	0.1-10	
Slope	67.8240	66.9280	92.2083	
Intercept	+384.1611	+471.2101	–12.6161	
Regression-coefficient (R^2)	0.9993	0.9991	0.9975	
Sensitivity				
LoD (µg/mL)	0.75			Sensitive
LoQ (µg/mL)	2.27			
Precision				
Intra-day (%RSD)	0.79	0.23	0.24	<2%
Inter-day (%RSD)	0.71	1.21	0.13	
Accuracy				
80% recovery (%)	100.52 ± 0.43	99.58 ± 0.90	99.79 ± 0.01	
100% recovery (%)	100.16 ± 0.54	99.90 ± 0.17	98.46 ± 0.15	98-102%
120% recovery (%)	99.44 ± 0.49	101.11 ± 1.65	99.49 ± 0.01	
Robustness				
Ratio of mobile phase (%RSD)	1.75			
Rate of flow (%RSD)	0.50			<2%
Detection wavelength (%RSD)	0.83			

Method application

Recovery assay in tablet dosage form

Content analysis of Sirturo® tablets demonstrated high BDQ purity (99.44–100.52%), with excellent reproducibility (%RSD 0.41–0.54). The developed method reliably quantified active pharmaceutical ingredient content, meeting pharmacopeial standards for drug formulation assessment (Sahu et al., 2018). This result is consistent with the findings of Chandrudu & Gandhimathi (2024), who reported a high BDQ purity of 100.78% in their analysis of Sirturo® tablets using an RP-HPLC method. The excellent reproducibility (%RSD 0.41–0.54) achieved in our study further corroborates the reliability of HPLC methods for the quality control of BDQ in pharmaceutical dosage forms.

Entrapment efficiency of BDQ nanostructured lipid carrier

The characterization of the NLCs has been streamlined to focus specifically on encapsulation efficiency and recovery data, as these parameters are most directly relevant to demonstrating the applicability and accuracy of the developed HPLC method for quantifying Bedaquiline in this complex formulation. The

developed NLCs demonstrated favourable physicochemical properties, with a monodisperse size distribution (157.88 ± 0.12 nm; PDI 0.254 ± 0.06) and excellent colloidal stability (zeta potential -45.9 ± 0.12 mV). High encapsulation efficiency (96.2 ± 0.24%) confirmed effective BDQ incorporation. Method validation through sextuplicate analyzes yielded consistent recovery rates (99.5 to 99.9%), verifying the reliability of the quantification approach (Table 6.).

Recovery assay in human plasma samples

LC-MS provides superior specificity and unambiguous compound identification through mass detection, unlike the non-specific UV detection in RP-HPLC. While advanced techniques such as LC-MS/MS are predominantly reported for BDQ analysis in biological samples (Gray et al., 2019), our validated RP-HPLC method offers a highly reliable, more accessible alternative. The excellent recovery rates (98.9-99.8%) confirm that this method provides the fundamental accuracy required for bioanalytical applications, such as therapeutic drug monitoring, without the need for sophisticated mass spectrometry instrumentation. This represents a critical first step in the bioanalytical method validation workflow, establishing the fundamental reliability for quantifying BDQ in plasma. However, it is acknowledged that analysing of plasma from patients undergoing BDQ treatment or from a formal pharmacokinetic study would have greater translational impact. Such applications would demonstrate the method's robustness in the presence of real-world metabolic interferences and its utility in therapeutic drug monitoring (TDM) or clinical pharmacokinetic research. Therefore, the application of this validated method to real patient samples is a clear and recommended direction for future work to fully leverage its potential in optimizing multi-drug-resistant tuberculosis therapy.

CONCLUSION

In conclusion, a rapid RP-HPLC method for BDQ was successfully optimized using a full-factorial DoE, achieving a key improvement analysis time under 3 minutes. The method was comprehensively validated across tablets, NLCs, and human plasma. The validation parameters confirmed the method's reliability, demonstrating excellent linearity (R^2 > 0.9975 across all matrices), high accuracy (mean recovery: 98.46-101.11%), exceptional precision (intra-day and inter-day %RSD < 2%), and satisfactory sensitivity (LOD: 0.75 µg/mL; LOQ: 2.27 µg/mL). Although the use of HPLC for BDQ analysis is established, a systematic DoE approach was developed to achieve rapid separation and validate it across a broad application scope. While the current study successfully demonstrates the method's suitability for quantifying BDQ in spiked human plasma, its application to pharmacokinetic studies or patient samples is a necessary next step to confirm its translational value in therapeutic drug monitoring and clinical research.

ACKNOWLEDGEMENTS

The authors express sincere appreciation to the Center for Higher Education Funding and Assessment, Ministry of Higher Education, Science, and Technology of the Republic of Indonesia for their invaluable financial support and funding of this research endeavour.

AUTHOR CONTRIBUTION STATEMENT

Concept (AR, RM), Design (AR, RM), Supervision (RM, ST, NFK), Resources (AR, RM), Materials (AR, RM), Data Collection and/or Processing (AR), Analysis and/ or Interpretation (RM, ST, NFK), Literature Search (AR), Writing (AR), Critical Reviews (RM, ST, NFK).

CONFLICT OF INTEREST

The authors declare that there is no conflict of interest.

REFERENCES

Abd-AlGhafar, W. N., Aly, F. A., Sheribah, Z. A., & Saad, S. (2022). Factorial design-assisted reverse phase HPLC-UV approach for the concurrent estimation of cetirizine and azelastine in aqueous humor. *Scientific Reports*, *12*(1), 22435. https://doi.org/10.1038/s41598-022-26774-y

Abdallah, N. A., Tolba, M. M., El-Brashy, A. M., Ibrahim, F. A., & Fathy, M. E. (2023). Hydro-organic mobile phase and factorial design application to attain a green HPLC method for simultaneous assay of paracetamol and dantrolene sodium in combined capsules. *BMC Chemistry*, *17*(1), 92. https://doi.org/10.1186/s13065-023-00990-7

Abdu Hussen, A. (2022). High-Performance Liquid Chromatography (HPLC): A review. *Annals of Advances in Chemistry*, *6*(1), 010–020. https://doi.org/10.29328/journal.aac.1001026

Ajayi, T. O., Poka, M. S., & Witika, B. A. (2024). Development of bedaquiline nanoemulsions intended for paediatric multidrug-resistant tuberculosis: excipient selection and preformulation studies. *Frontiers in Medical Technology*, *6*, 1388113. https://doi.org/10.3389/fmedt.2024.1388113

Ayodele, S., van Eyk, A. D., Kumar, P., & Choonara, Y. E. (2024). A sensitive, rapid, and cost-effective RP-HPLC-UV method for the detection and quantification of bedaquiline in physiological fluid (pH 7.4). *Analytical Methods*, *16*(42), 7169–7177. https://doi.org/10.1039/D4AY01143K

Bezawada, V., Mogili, P., Rao Polagani, S., & Dodda, S. (2024). Bioanalysis of bedaquiline in human plasma by liquid chromatography-tandem mass spectrometry: Application to pharmacokinetic study. *Journal of Mass Spectrometry and Advances in the Clinical Lab*, *31*, 27–32. https://doi.org/10.1016/j.jmsacl.2024.01.001

Çağlar, E. Ş., Okur, N. Ü., & Karasulu, H. Y. (2022). Development and validation of an HPLC method for the determination of hyaluronic acid active substance in pharmaceutical formulations. *Journal of Research in Pharmacy*, *26*(1), 112–122. https://dx.doi.org/10.29228/jrp.108

Chandrudu, J., & Gandhimathi, R. (2024). Method Development and Validation for Estimation of Bedaquiline and in Tablet Dosage form by HPTLC and RP-HPLC Study. *Biomedical and Pharmacology Journal*, *17*(1), 299–307. https://doi.org/10.13005/bpj/2858

Chavan, S. D., & Desai, D. M. (2022). Analytical method validation: A brief review. *World Journal of Advanced Research and Reviews*, *16*, 389–402. https://doi.org/10.30574/wjarr.2022.16.2.1165

Dharuman, N., Lakshmi, K. S., & Krishnan, M. (2023). An Environmental benign RP-HPLC method for the simultaneous estimation of anti-hypertensive drugs using analytical quality by design. *Green Chemistry Letters and Reviews*, *16*(1). https://doi.org/10.1080/17518253.2023.2214176

Ermer, J. (2025). ICH Q2 (R2): validation of analytical procedures. In J. Ermer, & P. W. Nethercote (Eds.), *Method validation in pharmaceutical analysis: a guide to best practice* (pp. 351–372). John Wiley & Sons. https://doi.org/10.1002/9783527831708.ch13

Gray, W. A., Waldorf, B., Rao, M. G., Stiles, B. L., Griffiss, J. M., Salata, R. A., & Blumer, J. L. (2019). Development and validation of an LC-MS/MS method for the simultaneous determination of bedaquiline and rifabutin in human plasma. *Journal of Pharmaceutical and Biomedical Analysis*, *176*, 112775. https://doi.org/10.1016/j.jpba.2019.07.023

Guglielmetti, L., Chiesi, S., Eimer, J., Dominguez, J., Masini, T., Varaine, F.,…Robert, J. (2020). Bedaquiline and delamanid for drug-resistant tuberculosis: a clinician's perspective. *Future microbiology*, *15*(9), 779–799. https://doi.org/10.2217/fmb-2019-0309

ICH Harmonised Guideline. (2022). Validation of analytical procedures Q2 (R2). *ICH: Geneva, Switzerland*.

Hariyanti, H., Kurniati, N. F., Sumirtapura, Y. C., & Mauludin, R. (2023). Development and validation of an analytical method for the determination of nanostructured lipid carrier's cinchonine using a direct method modified by liquid-liquid extraction using high-performance liquid chromatography. *Journal of Research in Pharmacy*, *27(2)*, 913–923. https://doi.org/10.29228/jrp.371

Isane, S. P., Waghmare, S. A., & Kamble, H. V. (2022). A Review on Method Development, Validation, Optimization, and Applications of HPLC. *International Journal of Research in Applied Science and Engineering Technology*, *10*, 1860–1867. https://doi.org/10.22214/ijraset.2022.42685

Jaw-Tsai, S., Barry, R., Pande, P. G., Taneja, R., & Yang, T. (2023). Comparison of pharmacokinetics and bioavailability of bedaquiline fumarate, benzoate, and maleate in dogs. *The International Journal of Tuberculosis and Lung Disease*, *27*(1), 28–33. https://doi.org/10.5588/ijtld.22.0326

Kohler, N., Karakose, H., Grobbel, H. P., Hillemann, D., Andres, S., Konig, C.,…Sanchez Carballo, P. M. (2023). A Single-Run HPLC-MS Multiplex Assay for Therapeutic Drug Monitoring of Relevant First- and Second-Line Antibiotics in the Treatment of Drug-Resistant Tuberculosis. *Pharmaceutics*, *15*(11). https://doi.org/10.3390/pharmaceutics15112543

Kumar, L., Sreenivasa Reddy, M., Managuli, R. S., & Pai, K. G. (2015). Full factorial design for optimization, development, and validation of an HPLC method to determine valsartan in nanoparticles. *Saudi Pharmaceutical Journal, 23*(5), 549–555. https://doi.org/10.1016/j.jsps.2015.02.001

Montgomery, D. C. (2017). *Design and analysis of experiments*. John Wiley & Sons, Inc.

Nag, M., Kar, A., Chanda, J., & Mukherjee, P. K. (2020). RP-HPLC analysis of the methanol extract of Viscum articulatum. *Journal of Ayurveda and Integrative Medicine*, *11*(3), 277–280. https://doi.org/10.1016/j.jaim.2018.02.135

Pardhi, V., Pant, G., & Flora, S. J. S. (2020). RP-HPLC method development and validation for bedaquiline fumarate to evaluate its forced degradation behaviour and stability in official dissolution media. *Future Journal of Pharmaceutical Sciences*, *6*(1). https://doi.org/10.1186/s43094-020-00061-x

Pardhi, V. P., Patel, M., & Jain, K. (2024). Formulation development, characterization, and evaluation of bedaquiline fumarate–Soluplus®–solid dispersion. *Pharmaceutical Development and Technology*, *29*(5), 492–503. https://doi.org/10.1080/10837450.2024.2348585

Patil, S. D., & Chalikwar, S. S. (2024). A brief review of the application of the design of experiments for the analysis of pharmaceuticals using HPLC. *Annales Pharmaceutiques Françaises*, *2,* 203-228. https://doi.org/10.1016/j.pharma.2023.12.011

Petersen, E., Hui, D. S., Nachega, J. B., Ntoumi, F., Goletti, D., Aklillu, E.,…Satta, G. (2023). End of the Bedaquiline patent–a crucial development for moving forward with affordable drugs, diagnostics, and vaccines for infectious diseases in low- and middle-income countries. *International Journal of Infectious Diseases*, *131*, 180–182. https://doi.org/10.1016/j.ijid.2023.04.386

Rajmane, A. D., & Shinde, K. P. (2023). A Review of HPLC Method Development and Validation as per ICH Guidelines. *Asian Journal of Pharmaceutical Analysis*, *13*(2), 143–151. https://doi.org/10.52711/2231-5675.2023.00024

Sahu, P. K., Ramisetti, N. R., Cecchi, T., Swain, S., Patro, C. S., & Panda, J. (2018). An overview of experimental designs in HPLC method development and validation. *Journal of Pharmaceutical and Biomedical Analysis*, *147*, 590–611. https://doi.org/10.1016/j.jpba.2017.05.006

Stojanović, J., Krmar, J., Protić, A., Svrkota, B., Djajić, N., & Otašević, B. (2021). DoE Experimental design in HPLC separation of pharmaceuticals : A review. *Archives of Pharmacy*, *71*, 279–301. https://doi.org/10.5937/arhfarm71-32480

Surapuraju, P. K. R., & Juturu, R. R. (2022). Development and validation of a stability-indicating-HPLC method for the determination of related substances in the novel nitroimidazole antituberculosis drug pretomanid: Robustness study by Design-Expert and application to stability studies. *Biomedical Chromatography*, *36*(12). https://doi.org/10.1002/bmc.5498

Vanino, E., Granozzi, B., Akkerman, O. W., Munoz-Torrico, M., Palmieri, F., Seaworth, B.,… Tadolini, M. (2023). Update of drug-resistant tuberculosis treatment guidelines: A turning point. *International Journal of Infectious Diseases*, *130* (Suppl 1), S12–S15. https://doi.org/10.1016/j.ijid.2023.03.013

World Health Organization. (2022). *WHO consolidated guidelines on tuberculosis. Module 4: treatment-drug-resistant tuberculosis treatment, 2022 update*.

FABAD J. Pharm. Sci., 51, 1, 41-52, 2026
Doi: 10.55262/fabadeczacilik.1786034
RESEARCH ARTICLE

Unveiling The Therapeutic Potential of *Nyctanthes arbor-tristis* Linn. In Breast Cancer: A Network Pharmacology and Molecular Docking Approach

Omkar TIPUGADE[*], Jyotiram SAWALE[**°], Namdeo JADHAV[***]

Unveiling The Therapeutic Potential of Nyctanthes arbor-tristis Linn. In Breast Cancer: A Network Pharmacology and Molecular Docking Approach

SUMMARY

Nyctanthes arbor-tristis Linn., a traditionally valued medicinal plant, exhibits anticancer activity, yet its mechanisms against breast cancer remain inadequately defined. This study explored its bioactive compounds, molecular targets, and pathways using network pharmacology, molecular docking, Absorption, Distribution, Metabolism, Excretion, and Toxicity (ADMET) profiling. Fifty-seven bioactive compounds were identified from databases, with potential targets predicted through SwissTargetPrediction and breast cancer proteins retrieved from the Therapeutic Target Database. Protein–protein interaction and Kyoto Encyclopedia of Genes and Genomes (KEGG) pathway analyses revealed the PI3K–Akt signalling pathway as a key mechanism. Molecular docking highlighted caffeic acid with strong binding affinity to the Epidermal Growth Factor Receptor (EGFR) kinase receptor (-27.44 kcal/mol), while lupeol was predicted to regulate the maximum number of targets. ADMET and drug-likeness profiling further identified nicotiflorin the highest drug-likeness score. Overall, lupeol and caffeic acid emerged as major active constituents, modulating breast cancer via phosphatidylinositol 3-kinase- Protein Kinase B (PI3K-Akt) and EGFR pathways. These findings provide mechanistic insights supporting the therapeutic potential of Nyctanthes arbor-tristis in breast cancer management.

Keywords: *Nyctanthes arbortristis Linn., breast cancer, network pharmacology, molecular docking, targets.*

Nyctanthes arbor-tristis Linn.'in Meme Kanserindeki Terapötik Potansiyelinin Ortaya Çıkarılması: Bir Ağ Farmakolojisi ve Moleküler Yerleştirme Yaklaşımı

ÖZ

Geleneksel olarak değerli bir tıbbi bitki olan Nyctanthes arbor-tristis Linn., antikanser aktivite göstermesine rağmen, meme kanserine karşı etkime mekanizmaları yeterince tanımlanmamıştır. Bu çalışmada, bitkinin biyoaktif bileşikleri, moleküler hedefleri ve etki yolları ağ farmakolojisi, moleküler yerleştirme (docking) ve Emilim, Dağılım, Metabolizma, Atılım ve Toksisite (ADMET) analizleri kullanılarak araştırılmıştır. Veritabanlarından elli yedi biyoaktif bileşik tanımlanmış; potansiyel hedefler SwissTargetPrediction aracılığıyla, meme kanseri ile ilişkili proteinler ise Therapeutic Target Database'den elde edilmiştir. Protein–protein etkileşimleri ve Kyoto Genleri ve Genomları Ansiklopedisi (KEGG) yolak analizleri, PI3K–Akt sinyal yolunun temel mekanizma olduğunu ortaya koymuştur. Moleküler yerleştirme analizleri, kafeik asidin Epidermal Büyüme Faktörü Reseptörü (EGFR) kinaz reseptörüne yüksek bağlanma afinitesi (-27,44 kcal/mol) gösterdiğini, lupeolün ise en fazla hedefi düzenlediğini ortaya koymuştur. ADMET ve ilaç-benzerliği analizleri sonucunda, en yüksek ilaç-benzerliği skoruna sahip bileşik olarak nikotiflorin belirlenmiştir. Genel olarak, lupeol ve kafeik asit, fosfatidilinozitol 3-kinaz–Protein Kinaz B (PI3K–Akt) ve EGFR yolakları aracılığıyla meme kanserini modüle eden başlıca aktif bileşenler olarak öne çıkmaktadır. Bu bulgular, Nyctanthes arbor-tristis'in meme kanseri tedavisinde terapötik potansiyelini destekleyen mekanistik kanıtlar sunmaktadır.

Anahtar Kelimeler: *Nyctanthes arbor-tristis Linn., meme kanseri, ağ farmakolojisi, moleküler yerleştirme, hedefler.*

Recieved: 17.09.2025
Revised: 29.10.2025
Accepted: 15.11.2025

[*] ORCID: 0000-0002-3723-9133, Research Scholar, Krishna Institute of Pharmacy, Krishna Vishwa Vidyapeeth (Deemed to be University), Karad, Maharashtra, India, 415539
**ORCID: 0000-0002-8383-7249, Department of Pharmacognosy, Krishna Institute of Pharmacy, Krishna Vishwa Vidyapeeth (Deemed to be University), Karad, Maharashtra, India, 415539
***ORCID: 0000-0001-5230-6659, Department of Pharmaceutics, Krishna Institute of Pharmacy, Krishna Vishwa Vidyapeeth (Deemed to be University), Karad, Maharashtra, India, 415539

° Corresponding Author; Dr. Jyotiram Sawale
E-mail: jyotisawale@gmail.com

INTRODUCTION

Cancer is a major global public health concern, with an estimated 2,001,140 new cases and 611,720 related deaths projected in the United States in 2024 (Siegel, Giaquinto, & Jemal, 2024) and approximately 4.8 million new cases and 3.2 million cancer-related deaths reported in China (Xia et al., 2022). One of the most common malignancies in the world is still breast cancer. Despite extensive research on its prevention and tumorigenesis over the past decades (Britt, Cuzick, & Phillips, 2020), its incidence continued to rise by 0.5% annually from 2014 to 2018 (Siegel, Miller, Fuchs, & Jemal, 2022). Breast cancer is an incurable metastatic disease that can spread to the brain, liver, lungs, and bones. However, early detection significantly improves prognosis and increases the chances of survival (DeSantis et al., 2016). According to the World Health Organization (WHO), early detection is the cornerstone of breast cancer management, as it significantly improves outcomes and survival rates. Various modern medicines are prescribed for breast cancer treatment, including antiestrogens like raloxifene and tamoxifen, which may help prevent the disease in individuals at high risk. In some cases, preventive mastectomy is considered for those with a significantly increased likelihood of developing breast cancer. Treatment options for people with breast tumours include radiation therapy, surgery, chemotherapy, hormone therapy, and targeted therapy. The main goals of management in situations of distant metastases are to increase survival and improve quality of life (Akram, Iqbal, Daniyal, & Khan, 2017). The adverse effects of conventional breast cancer treatments have driven interest in alternative therapies. Herbal medicine is regarded as a natural option, as certain plants may possess bioactive compounds with potential anticancer properties (Abdull Razis & Noor, 2013).

The quantity of bioactive chemicals in plants has led to extensive research into herbal medicine as a possible source of drugs against cancer (Dehelean et al., 2021). Through a variety of mechanisms, such as causing cancer cells to undergo apoptosis (programmed cell death), preventing angiogenesis (the growth of new blood vessels supplying tumours), and altering important signalling pathways involved in cancer progression and metastasis, some compounds derived from plants have shown promising anticancer properties (Abdulridha et al., 2020). Herbal medicine has been used for centuries to treat a variety of illnesses, including cancer. Herbal treatments have long been utilised to treat cancer in traditional medical systems like Ayurveda and Traditional Chinese Medicine (TCM), which laid the groundwork for current studies into their potential as therapeutics. However, with the rise of industrial medicine, the use of herbal treatments declined for some time. Recent advancements in technology have helped overcome challenges associated with natural compounds, reigniting interest in their integration into pharmaceutical development. Traditional treatments continue to be important, since the World Health Organisation estimates that 80% of the world's population uses them (Jenča et al., 2024). Advancements in biomolecular science have enhanced our understanding of the pharmacological effects of herbal compounds, including their anticancer, anti-inflammatory, and antiviral properties (Jenča et al., 2024). Research on the anticancer effects of herbal remedies is still ongoing. To get around issues including poor solubility, low bioavailability, and non-specific distribution, sophisticated drug delivery systems such as nanoparticles have been created (Coy-Barrera, Ogungbe, & Schmidt, 2023; Gaikwad et al., 2023; Garcia-Oliveira et al., 2021; Singh, Singh, Kanwar, & Chauan, 2020). The therapeutic efficacy, targeted delivery, and bioavailability of herbal anticancer medicines are all enhanced by these methods. However, issues including the requirement for standardisation, possible drug interactions, and variations in the quality of bioactive compounds must be addressed. Furthermore, many herbal substances' exact processes are still unknown, necessitating more investigation to clarify their biological pathways and interactions (Atanasov et al., 2021; Mali, 2023).

Nyctanthes arbor-tristis Linn., a member of the Oleaceae family, is commonly known in India as harsingar or night-flowering jasmine. It has long been used in Ayurvedic, Siddha, and Unani medicine and remains integral to traditional healing practices among indigenous tribal communities (Chabattula et al., 2024). Native to South and Southeast Asia, particularly India, Nepal, Pakistan, and Thailand, *Nyctanthes arbor-tristis* Linn. thrives in dry deciduous forests and rocky soils up to 1500 m altitude. The plant typically flowers between July and October and is now widely cultivated across Asia, Africa, and other tropical regions for its medicinal and ornamental value**.** Ethnomedicinally, its leaves act as laxative, diuretic, and diaphoretic agents; flowers are employed to treat skin and eye disorders; the bark is used against malaria and bronchitis; and the seeds serve as anthelmintic and are applied in alopecia. Tribal communities in India traditionally consume leaf extracts mixed with honey to manage malaria, fever, and blood disorders. Beyond its therapeutic applications, *Nyctanthes arbor-tristis* Linn. holds deep spiritual and cultural significance, being planted in temple gardens for its fragrant blossoms and symbolic purity (Tipugade, Sawale, & Jadhav, 2025a). Phytochemically, the plant is rich in benzoic acid, carotene, oleanolic acid, friedelin, essential oils, tannic acid, and lupeol, among other compounds. These bioactive constituents confer a broad spectrum of pharmacological properties, including antioxidant (Gahtori et al., 2024), anti-inflammatory (Sana et al., 2024), anti-cancer (Karan, Maity, Pal, Singha, & Jana, 2019), immunomodulatory (Bharshiv, Garg, & Bhatia, 2016), anti-leishmania, anti-allergic, and antimicrobial properties (ALNadhari, Alsakkaf, & Albarakat, 2024). Using network pharmacology and molecular docking, the current study explores the multiple bio-actives–many targets interaction paradigm in an effort to clarify the likely mode of action of *Nyctanthes arbor-tristis* Linn. By establishing connections between compounds, genes, and diseases, the network pharmacology technique sheds light on the target proteins' regulatory mechanisms (Sekaran et al., 2024). By examining the compounds' binding affinities to druggable receptor proteins, molecular docking was used to evaluate the compounds' therapeutic potential (Nxumalo et al., 2024).

It was hypothesized that the bioactive constituents of *Nyctanthes arbor-tristis* Linn. exert anticancer effects against breast cancer through multi-target and multi-pathway modulation, primarily involving key signaling cascades such as the PI3K-Akt and EGFR pathways. By integrating network pharmacology and molecular docking, the study aimed to delineate the compound–target–pathway interactions underlying the plant's therapeutic efficacy. This approach was expected to provide mechanistic insights into how phytochemicals from *Nyctanthes arbor-tristis* synergistically regulate oncogenic proteins, thereby offering a scientific rationale for its traditional use and identifying potential lead compounds for future drug development.

MATERIALS AND METHODS

Mining of phytoconstituents and targets

A list of reported phytoconstituents was obtained from Dr. Duke's Phytochemical and Ethnobotanical Databases (https://phytochem.nal.usda.gov/) and the IMPPAT: Indian Medicinal Plants, Phytochemistry, and Therapeutics Database (https://cb.imsc.res.in/imppat/#browse). The PubChem database (https://pubchem.ncbi.nlm.nih.gov/) provided the molecular formula, molecular weight, PubChem CID, InChI key, and canonical SMILES. Targets associated with breast cancer were retrieved from the Therapeutic Target Database (http://db.idrblab.net/ttd/) and GeneCards: The Human Gene Database (https://www.genecards.org/) using the keyword "Breast cancer" and cross-referenced with proteins regulated by the bio-actives of *Nyctanthes arbortristis* Linn., as identified from bio-actives-regulated proteins in SwissTargetPrediction (http://www.swisstargetprediction.ch/) (Daina, Michielin, & Zoete, 2019).

Drug-likeness and ADMET profile of bio-actives

By entering their SMILES, each bioactive compound's drug-likeness score was acquired from MolSoft (https://molsoft.com/mprop/) (Gad et al., 2020). Additionally, the absorption, distribution, metabolism, excretion, and toxicity (ADMET) profile of each bioactive was predicted utilizing SwissADME (http://www.swissadme.ch/index.php#) (Daina, Michielin, & Zoete, 2017) and PreADMET (https://preadmet.webservice.bmdrc.org/toxicity/) (Maliehe, Tsilo, & Shandu, 2020). P-glycoprotein (P-gp) inhibition, P-gp substrate potential, Colon Adenocarcinoma-2 (Caco-2) permeability, blood–brain barrier permeability, human intestinal absorption, and CYP1A2, CYP2C19, CYP2C9, CYP2D6, and CYP3A4 enzyme inhibition were all evaluated utilizing these tools (Gandla et al., 2023).

Gene expression and enrichment analysis

The gene codes of the regulated proteins were found using the UniProt database (https://www.uniprot.org/), and they were subsequently queried in STRING (https://string-db.org/) for Gene Ontology (GO) analysis (Szklarczyk et al., 2017). Similarly, the pathways associated with breast cancer were identified using the KEGG database (https://www.genome.jp/kegg/). Additionally, Cytoscape version 3.7.2 (https://cytoscape.org/) was utilised to build a network of bioactive compounds, proteins, and pathways (Shannon et al., 2003), excluding any duplication.

Molecular docking

Ligand preparation

The ligands' 2D structures were downloaded to the workspace in .sdf format after being obtained from the PubChem database (https://pubchem.ncbi.nlm.nih.gov) (Setlur, Chandrashekar, Bhattacharjee, Kumar, & Niranjan, 2023; Tipugade, Sawale, & Jadhav, 2025b).

Preparation of macromolecule

The docking simulation study of bioactive compounds was conducted on EGFR kinase (PDB ID: 1XKK), obtained from the Protein Data Bank (https://www.rcsb.org). The protein structure was prepared using the Molsoft ICM Pro, which involved adding hydrogen atoms, removing water molecules, assigning partial charges, determining protonation states, and applying restraints. After the ligand was removed, the binding sites were identified, and a grid box was used to create a grid (Bello, 2018; Ongko et al., 2022).

Ligand–protein docking

Each bioactive compound was docked into the appropriate binding site inside the grid utilising Molsoft ICM Pro's Glide module. It is a rapid and efficient docking program designed for docking small molecules into receptor-binding sites. The program incorporates a scoring function that considers shape complementarity, electrostatic interactions, and van der Waals forces between the ligand and receptor. Key active site interactions and corresponding scoring functions were thoroughly evaluated (Agu et al., 2023).

RESULTS

Mining of phytoconstituents and targets involved in breast cancer

In the pursuit of identifying potential phytoconstituents and their molecular targets in breast cancer, an extensive database mining approach was employed. The Dr. Duke and IMPPAT databases revealed fifty-seven bio-actives in the plant *Nyctanthes arbor-tristis* Linn., all of which altered proteins implicated in breast cancer. According to the GeneCards: The Human Gene Database, 3,722 proteins have been linked to breast cancer; of these, 144 have been altered by the bio-actives from *Nyctanthes arbortristis* Linn. The list of bio-actives, together with their molecular formula, molecular weight, and PubChem CID, is summarised in Table S1.

Drug-likeness score and ADMET profile of bio-actives

Computational analysis was carried out to evaluate the drug-likeness, pharmacokinetic behavior, and

toxicity profiles (ADMET properties) of the identified bioactive compounds. Among them, Nicotiflorin showed the highest drug-likeness score of 0.90 out of 18 compounds with positive scores (Table S2.). The pharmacokinetic characteristics of each bioactive were visualized in a heat map, showing their water solubility, intestinal permeability (Caco-2), skin permeability, and human intestinal absorption. Additional parameters such as P-glycoprotein substrate or inhibitor activity, blood–brain barrier (BBB) permeability, and cytochrome P450 (CYP) enzyme interactions were also analyzed (Figure S1.).

Phenylacetaldehyde and 4-Methoxybenzaldehyde demonstrated the highest intestinal absorption and permeability values, while Tetratriacontane and Tritriacontane showed the greatest BBB permeability. Cassiarins A and B were predicted to have strong P-glycoprotein inhibitory activity. Several other compounds, including Melanin, Syringic acid, Naringetol, Loganin, Chlorogenic acid, Astragalin, Nicotiflorin, and Crocin, were identified as potential P-glycoprotein substrates, suggesting possible roles in drug transport and metabolism.

In terms of toxicity prediction, α-Carotene and Melanin showed potential mutagenic (AMES) and hepatotoxic effects. Likewise, compounds such as 4-hydroxy hexahydrobenzofuran-7-one, Linolenic acid, Ursolic acid, Oleanolic acid, Betulinic acid, and Lignoceric acid were predicted to be hepatotoxic. Overall, the ADMET analysis provided valuable insights into the absorption, distribution, metabolism, excretion, and toxicity properties of NAT bioactives, helping to identify those with promising pharmacokinetic potential and safety profiles.

Enrichment and network analysis

Enrichment and network analyses were performed to explore the molecular mechanisms modulated by bio-actives. Lupeol was predicted to modulate the highest number of genes (33), as shown in Table S3. Likewise, all regulated proteins' protein–protein interactions are depicted in Figure S2. NFKB1 was the main target of the greatest amount of bioactives in the network of bioactives, targets, and pathways that was created. Similarly, Table S4 shows that the PI3K-Akt pathway was primarily controlled by affecting the greatest number of genes (22).

Similarly, the gene ontology analysis of protein interactions (Figure S3.) identified 917 biological processes, with response to oxygen-containing compounds (GO:1901700) exhibiting the lowest false discovery rate. This process was modulated through 74 genes *CFTR, MAPK1, APEX1, SERPINE1, NFKB1, MAPK14, SIRT2, CHRM3, PDGFRA, CDK4, PDGFRB, PIK3CA, STAT3, CDK2, CYSLTR2, HPGD, NOS3, MC4R, MMP3, ACHE, CHRM1, P2RY12, PTPN2, HSD11B2, NOS2, PRKCD, HSP90AA1, ESR2, C5AR1, BLM, RET, MAP3K5, PDE3A, DNMT1, CES1, NTRK3, STAT1, EGLN1, PTGS2, CNR1, CHUK, CACNA1B, GRIN1, HSP90AB1, PTPN1, TLR4, CNR2, RXRB, AR, F7, RORB, RPS6KA3, AKR1C3, CDK1, NFE2L2, PTK2B, GSTP1, ABCC1, KDM1A, OPRM1, CHRM2, ESR1, CHRM4, GLRA1, SLC2A1, RXRA, CDK5, PIK3R1, HDAC2, IDO1, HIF1A, NR4A1*, *FPR2* and *ACACA* against a background of 1,547 genes, with a strength of 0.82. Similarly, 134 molecular functions were identified in which Catalytic activity (GO:0003824) scored the lowest false discovery rate via modulation of 94 genes (*CFTR, HSD17B10, MIF, MAPK1, APEX1, DHODH, DUSP3, MAPK14, CTSD, FLT3, PIN1, SIRT2, ALOX12, CHRM3, PDGFRA, CDK4, ADAM10, PDGFRB, MAP2K2, BRD4, PIK3CA, HDAC4, F13A1, CDK2, GGPS1, HPGD, NOS3, MMP3, ANPEP, GUSB, ACHE, CHRM1, F2, PTPN7, TERT, PTPN2, AURKB, HSD11B2, METAP2, NOS2, PRKCD, HSP90AA1, TDP1, TRIM24, MAOA, CTSB, BLM, RET, MAP3K5, PDE3A, DNMT1, CES1, NTRK3, TOP1, PTGS1, EGLN1, PTGS2, CHUK, HSP90AB1, PTPN1, NOX1, HDAC8, TLR4, F7, CSNK2B, PIK3CD, XDH, RPS6KA3, NQO2, AKR1C3, DUT, GRK5, PRCP, CDK1, PTK2B, GSTP1, ABCC1, FKBP1A, KDM1A, CHEK1, ITK, PRKCA, TOP2A, CDK5, HDAC2, IDO1, CAPN1, RPS6KA1, ADK, PAK4, ACACA, PTPN11, CYP3A4, PIK3CB*)

against 5522 background genes at a strength of 0.37. Likewise, 84 cellular components were identified in which intrinsic plasma membrane (GO:0005886) scored the minimum false discovery rate by modulation of 84 genes (*CFTR, HSD17B10, MIF, MAPK1, SERPINE1, DUSP3, TFPI, FLT3, SIRT2, ALOX12, CHRM3, PDGFRA, ADAM10, PDGFRB, KCNH2, MAP2K2, PIK3CA, STAT3, NPC1, CYSLTR2, HPGD, NOS3, MC4R, ANPEP, ACHE, ADORA2B, CHRM1, P2RY12, F2, PTPN7, TERT, PTPN2, TLR8, METAP2, NOS2, PRKCD, HSP90AA1, TDP1, CTSB, C5AR1, RET, MAP3K5, NTRK3, ADORA1, PTGS2, ADRB1, CNR1, CHUK, CACNA1B, GRIN1, HSP90AB1, NOX1, TACR2, TLR4, CNR2, AR, F7, S1PR3, PIK-3CD, GRK5, PRCP, NFE2L2, PTK2B, ABCC1, FKBP1A, OPRM1, SCN4A, ITK, CHRM2, ESR1, PRKCA, CHRM4, FCGRT, GLRA1, SLC2A1, CDK5, PIK3R1, CAPN1, SLC6A5, ADK, FPR2, FPR1, S1PR2, PIK3CB*) against 5544 background genes at a strength of 0.32. Figure S3 illustrates the top 15 biological processes, molecular functions, and cellular components. Additionally, network analysis identified Lupeol as the bioactive regulating the highest number of proteins, with NFKB1 being the primary target protein and the PI3K-Akt signalling pathway as the most modulated pathway. Similarly, Figure S4 presents the interactions between individual bio-actives, their respective modulated proteins, and the regulated pathways.

***In silico* Molecular Docking**

A molecular docking study was conducted using *Nyctanthes arbor-tristis* Linn. structures as ligand groups and EGFR kinase as the target macromolecule. The docking analysis was performed using Molsoft ICM Pro. The downloaded structures of *Nyctanthes arbor-tristis* Linn. and reference standards were docked against EGFR kinase to determine binding conformations and binding affinity. A total of 57 structures of *Nyctanthes arbor-tristis* Linn., along with three standard inhibitors (Aderbasib, Erlotinib, and Gefitinib), were docked, and their binding affinities were compared. The molecular docking study revealed that among all docked *Nyctanthes arbor-tristis* Linn. compounds, Caffeic acid exhibited the highest binding affinity of −27.44 kcal/mol with the EGFR kinase domain complexed with a quinazoline inhibitor (GW572016, PDB: 1XKK). The binding affinities of the standard inhibitors were as follows: Gefitinib (STD1) at -30.7 kcal/mol, Erlotinib (STD2) at -19.94 kcal/mol, and Aderbasib (STD3) at -10.17 kcal/mol. Additionally, Caffeic acid, Naringetol, Crocetin, Astragalin, Linoleic acid, Pelargonic acid, Melanin, Curlone, Gallic acid, and Calceolarioside A demonstrated lower binding affinities compared to the reference standards. The visualized interactions of ligands within the binding pocket of PDB: 1XKK confirmed that all docked ligands were successfully bound to the identified binding site (Figure S5.). Figure S6 presents a 3D visualization of the *Nyctanthes arbor-tristis* Linn. compound interacting within the binding pocket of PDB: 1XKK. Molecular docking results revealed that 53 out of 57 docked *Nyctanthes arbor-tristis* Linn. compounds exhibited binding affinity with the EGFR kinase domain complexed with a quinazoline inhibitor (GW572016, PDB: 1XKK). Table S5 provides a summary of these docked compounds' specific interactions and binding affinities.

The integration of network pharmacology and molecular docking in this study provides translational insights into how the bioactive compounds of *Nyctanthes arbor-tristis* may contribute to breast cancer therapy. The identification of Lupeol and Caffeic acid as major regulators of the PI3K-Akt and EGFR signaling pathways underscores their potential as lead molecules for targeted anticancer drug development. These findings align with the current shift toward multi-target therapeutic strategies, emphasizing the relevance of phytochemicals in overcoming resistance mechanisms associated with single-target drugs. Moreover, the favourable ADMET and drug-likeness profiles of several bio-actives support their potential for oral formulations or adjuvant roles alongside standard chemotherapeutics. Collectively, *the in-silico* results form a mechanistic foundation for subsequent

in vitro and *in vivo* validations, bridging traditional medicinal knowledge of *Nyctanthes arbor-tristis* with modern translational oncology.

DISCUSSION

Traditional medicinal plants have long served as a cornerstone for modern drug discovery, offering a vast repository of bioactive compounds that often resemble pharmacologically relevant scaffolds or secondary metabolites (Tolstikova, Khvostov, & Bryzgalov, 2009). *Nyctanthes arbor-tristis* Linn. has been traditionally recognized for its diverse therapeutic potential, including demonstrated anticancer activity against HeLa, HepG2, and normal human peripheral lymphocyte cells (Bibechana Timsina, 2016). In contemporary research, the integration of *in silico* tools such as molecular modelling, structure–activity relationship analysis, pharmacophore identification, and network pharmacology has accelerated the exploration of complex herbal systems. These computational approaches, supported by machine learning and data mining, have become essential in identifying multi-target interactions and predicting pharmacokinetic behavior (Ekins, Mestres, & Testa, 2007).

The present study applied a network pharmacology and molecular docking framework to elucidate the mechanistic landscape of *Nyctanthes arbor-tristis* Linn. in breast cancer. Instead of focusing on isolated outcomes, the findings reveal a holistic, multi-target pharmacological profile consistent with the complex etiology of breast cancer. The identification of 57 bioactive compounds that collectively regulate 144 breast cancer-associated proteins underscores the plant's polypharmacology potential. Such multitarget interactions are particularly relevant in breast cancer, where overlapping pathways often contribute to drug resistance and tumor progression.

Among the identified compounds, Lupeol emerged as a central modulator, with NFKB1 and the PI3K–Akt signaling pathway serving as pivotal molecular nodes. Modulation of the PI3K–Akt cascade, a pathway frequently dysregulated in breast carcinogenesis, suggests that *Nyctanthes arbor-tristis* Linn. may restore cellular equilibrium by inhibiting aberrant proliferation and promoting apoptosis. This aligns with prior evidence indicating that Lupeol and related triterpenoids suppress Akt phosphorylation and NF-kB activation, thus impeding tumor growth and metastasis. Consequently, the synergistic interplay among NAT's constituents may offer therapeutic advantages over conventional single-target strategies.

ADMET and drug-likeness assessments further revealed that compounds such as Nicotiflorin and Lupeol possess favourable pharmacokinetic and safety profiles, indicating potential for oral bioavailability and systemic tolerability. Nonetheless, it is important to acknowledge that these computational findings serve as predictive indicators rather than conclusive evidence. The reliability of such analyses is constrained by database accuracy and algorithmic limitations; therefore, empirical validation through *in vitro* and *in vivo* studies remains essential to confirm bioavailability, metabolism, and toxicity outcomes.

Notably, Caffeic acid displayed a strong binding affinity (−27.44 kcal/mol) toward the EGFR kinase domain, suggesting a potential mechanism comparable to that of established EGFR inhibitors such as gefitinib. Since EGFR overexpression is implicated in aggressive breast cancer subtypes, particularly triple-negative breast cancer, this observation supports the therapeutic promise of *Nyctanthes arbor-tristis* Linn. bioactives as adjunctive or combinatorial agents rather than standalone drugs.

Despite these promising findings, the study has certain limitations that must be acknowledged. While this study provides valuable mechanistic insights into the anticancer potential of *Nyctanthes arbor-tristis* Linn., several limitations should be noted. The results are based solely on *in silico* analyses, which, despite their predictive value, cannot fully represent biological complexity. The accuracy of these findings depends on database quality and computational assumptions. Notably, the biological significance of mo-

lecular docking scores (e.g., −27 kcal/mol) remains uncertain, as such values do not directly translate to *in vivo* efficacy. The absence of *in vitro* and *in vivo* validation restricts confirmation of the predicted targets, pathways, and interactions. Importantly, while docking results indicated strong binding affinities (e.g., −27 kcal/mol for Caffeic acid), the biological significance of such scores remains uncertain. Docking energy values are computational estimates and do not necessarily reflect the true binding strength or pharmacological activity in biological systems. Thus, the predicted interactions should be interpreted cautiously and validated experimentally to determine their real therapeutic relevance. Therefore, future studies should include molecular assays, cell-based models, and animal experiments to validate these predictions and assess pharmacokinetics, bioavailability, and toxicity, ensuring the translational reliability of *Nyctanthes arbor-tristis* in cancer therapy.

CONCLUSION

The present study systematically explored the therapeutic potential of *Nyctanthes arbor-tristis* Linn. in breast cancer using a comprehensive network pharmacology and molecular docking approach. A total of 57 bioactive compounds were identified, among which Lupeol and Caffeic acid emerged as key regulators of multiple breast cancer-associated targets, particularly through the PI3K-Akt and EGFR signaling pathways. Gene Ontology and pathway enrichment analyses further revealed the plant's multi-target, multi-pathway mode of action, suggesting synergistic regulation of cellular proliferation, apoptosis, and immune modulation. The strong binding affinities of several bioactives with EGFR kinase underscore their potential as natural inhibitors capable of modulating tumor progression mechanisms. From a clinical perspective, these findings highlight *Nyctanthes arbor-tristis* as a promising candidate for adjunctive or complementary breast cancer therapy. The plant's bioactives, particularly Lupeol, Nicotiflorin, and Caffeic acid, display favorable drug-likeness and ADMET profiles, supporting their potential for oral bioavailability and minimal toxicity, an important advantage over conventional chemotherapeutics that often cause severe adverse effects. Furthermore, the modulation of multiple signaling pathways indicates that *Nyctanthes arbor-tristis* could contribute to overcoming drug resistance and enhancing therapeutic efficacy when integrated with existing treatment regimens. Overall, this study establishes a scientific foundation for the traditional use of *Nyctanthes arbor-tristis* and supports its potential translation into clinically relevant phytopharmaceutical formulations. However, rigorous *in vitro, in vivo*, and clinical investigations are essential to validate these computational findings, optimize dosage strategies, and confirm their safety and therapeutic effectiveness in breast cancer management.

ACKNOWLEDGEMENT

This research was conducted without any financial support from public, commercial, or non-profit funding agencies.

AUTHOR CONTRIBUTION STATEMENT

O.T. and J.S. conceptualized and designed the study, with O.T. handling data collection. J.S. conducted data analysis and prepared the initial draft of the article. N.J. supervised the study, contributed to data analysis and interpretation, and provided essential revisions. All authors have reviewed and approved the final version of the manuscript.

CONFLICT OF INTEREST

The authors declare that there is no conflict of interest.

REFERENCES

Abdull Razis, A. F., & Noor, N. M. (2013). Cruciferous Vegetables: Dietary Phytochemicals for Cancer Prevention. *Asian Pacific Journal of Cancer Prevention*, *14*(3), 1565–1570. https://doi.org/10.7314/APJCP.2013.14.3.1565

Abdulridha, M. K., Al-Marzoqi, A. H., Al-awsi, G. R. L., Mubarak, S. M. H., Heidarifard, M., & Ghasemian, A. (2020). Anticancer Effects of Herbal Medicine Compounds and Novel Formulations: a Literature Review. *Journal of Gastrointestinal Cancer*, *51*(3), 765–773. https://doi.org/10.1007/s12029-020-00385-0

Agu, P. C., Afiukwa, C. A., Orji, O. U., Ezeh, E. M., Ofoke, I. H., Ogbu, C. O., … Aja, P. M. (2023). Molecular docking as a tool for the discovery of molecular targets of nutraceuticals in disease management. *Scientific Reports*, *13*(1), 13398. https://doi.org/10.1038/s41598-023-40160-2

Akram, M., Iqbal, M., Daniyal, M., & Khan, A. U. (2017). Awareness and current knowledge of breast cancer. *Biological Research*, *50*(1), 33. https://doi.org/10.1186/s40659-017-0140-9

ALNadhari, S., Alsakkaf, W. A. A., & Albarakat, F. A. (2024). Biochemical and *In silico* Aspects of Active Compounds From Nyctanthes arbor-tristis Flower As Antidiabetic Agent. *Biotechnology and Applied Biochemistry*. https://doi.org/10.1002/bab.2709

Atanasov, A. G., Zotchev, S. B., Dirsch, V. M., Orhan, I. E., Banach, M., Rollinger, J. M., … Supuran, C. T. (2021). Natural products in drug discovery: advances and opportunities. *Nature Reviews Drug Discovery*, *20*(3), 200–216. https://doi.org/10.1038/s41573-020-00114-z

Bello, M. (2018). Binding mechanism of kinase inhibitors to EGFR and T790M, L858R, and L858R/T790M mutants through structural and energetic analysis. *International Journal of Biological Macromolecules*, *118*, 1948–1962. https://doi.org/10.1016/j.ijbiomac.2018.07.042

Bharshiv, C., Garg, S., & Bhatia, A. (2016). Immunomodulatory activity of aqueous extract of *Nyctanthes arbor-tristis* flowers with particular reference to splenocytes proliferation and cytokines induction. *Indian Journal of Pharmacology*, *48*(4), 412. https://doi.org/10.4103/0253-7613.186210

Bibechana Timsina, V. K. N. (2016). Purification and Evaluation of Bioactive Fractions for Anti-cancer Potentials from the Flowers and Leaves of Nyctanthes arbortristis L. *Chiang Mai J. Sci.*, *43*(1), 100–111.

Britt, K. L., Cuzick, J., & Phillips, K. A. (2020). Key steps for effective breast cancer prevention. *Nature Reviews Cancer*, *20*(8), 417–436. https://doi.org/10.1038/s41568-020-0266-x

Chabattula, S. C., Gupta, P. K., Govarthanan, K., Varadaraj, S., Rayala, S. K., Chakraborty, D., & Verma, R. S. (2024). Anti-cancer Activity of Biogenic Nat-ZnO Nanoparticles Synthesized Using *Nyctanthes arbor-tristis* (Nat) Flower Extract. *Applied Biochemistry and Biotechnology*, *196*(1), 382–399. https://doi.org/10.1007/s12010-023-04555-1

Coy-Barrera, E., Ogungbe, I. V., & Schmidt, T. J. (2023). Natural Products for Drug Discovery in the 21st Century: Innovations for Novel Therapeutics. *Molecules*, *28*(9), 3690. https://doi.org/10.3390/molecules28093690

Daina, A., Michielin, O., & Zoete, V. (2017). SwissADME: a free web tool to evaluate pharmacokinetics, drug-likeness, and medicinal chemistry friendliness of small molecules. *Scientific Reports*, *7*(1), 42717. https://doi.org/10.1038/srep42717

Daina, A., Michielin, O., & Zoete, V. (2019). SwissTargetPrediction: updated data, and new features for efficient prediction of protein targets of small molecules. *Nucleic Acids Research*, *47*(W1), W357–W364. https://doi.org/10.1093/nar/gkz382

Dehelean, C. A., Marcovici, I., Soica, C., Mioc, M., Coricovac, D., Iurciuc, S., … Pinzaru, I. (2021). Plant-Derived Anticancer Compounds as New Perspectives in Drug Discovery and Alternative Therapy. *Molecules*, *26*(4), 1109. https://doi.org/10.3390/molecules26041109

DeSantis, C. E., Fedewa, S. A., Goding Sauer, A., Kramer, J. L., Smith, R. A., & Jemal, A. (2016). Breast cancer statistics, 2015: Convergence of incidence rates between black and white women. *CA: A Cancer Journal for Clinicians*, *66*(1), 31–42. https://doi.org/10.3322/caac.21320

Ekins, S., Mestres, J., & Testa, B. (2007). *In silico* pharmacology for drug discovery: applications to targets and beyond. *British Journal of Pharmacology*, *152*(1), 21–37. https://doi.org/10.1038/sj.bjp.0707306

Gad, E. M., Nafie, M. S., Eltamany, E. H., Hammad, M. S. A. G., Barakat, A., & Boraei, A. T. A. (2020). Discovery of New Apoptosis-Inducing Agents for Breast Cancer Based on Ethyl 2-Amino-4,5,6,7-Tetra Hydrobenzo[b]Thiophene-3-Carboxylate: Synthesis, In Vitro, and *In vivo* Activity Evaluation. *Molecules*, *25*(11), 2523. https://doi.org/10.3390/molecules25112523

Gahtori, R., Tripathi, A. H., Chand, G., Pande, A., Joshi, P., Rai, R. C., & Upadhyay, S. K. (2024). Phytochemical Screening of *Nyctanthes arbor-tristis* Plant Extracts and Their Antioxidant and Antibacterial Activity Analysis. *Applied Biochemistry and Biotechnology*, *196*(1), 436–456. https://doi.org/10.1007/s12010-023-04552-4

Gaikwad, S. S., Morade, Y. Y., Kothule, A. M., Kshirsagar, S. J., Laddha, U. D., & Salunkhe, K. S. (2023). Overview of phytosomes in treating cancer: Advancement, challenges, and future outlook. *Heliyon*, *9*(6), e16561. https://doi.org/10.1016/j.heliyon.2023.e16561

Gandla, K., Islam, F., Zehravi, M., Karunakaran, A., Sharma, I., Haque, M. A., … Khandaker, M. U. (2023). Natural polymers as potential P-glycoprotein inhibitors: Pre-ADMET profile and computational analysis as a proof of concept to fight multidrug resistance in cancer. *Heliyon*, *9*(9), e19454. https://doi.org/10.1016/j.heliyon.2023.e19454

Garcia-Oliveira, P., Otero, P., Pereira, A. G., Chamorro, F., Carpena, M., Echave, J., … Prieto, M. A. (2021). Status and Challenges of Plant-Anticancer Compounds in Cancer Treatment. *Pharmaceuticals*, *14*(2), 157. https://doi.org/10.3390/ph14020157

Jenča, A., Mills, D., Ghasemi, H., Saberian, E., Jenča, A., Karimi Forood, A. M., … Ebrahimifar, M. (2024). Herbal Therapies for Cancer Treatment: A Review of Phytotherapeutic Efficacy. *Biologics: Targets and Therapy*, *18*, 229–255. https://doi.org/10.2147/BTT.S484068

Karan, B. N., Maity, T. K., Pal, B. C., Singha, T., & Jana, S. (2019). Betulinic Acid, the first lupane-type triterpenoid isolated via bioactivity-guided fractionation, and identified by spectroscopic analysis from leaves of Nyctanthes arbor-tristis : its potential biological activities *in vitro* assays. *Natural Product Research*, *33*(22), 3287–3292. https://doi.org/10.1080/14786419.2018.1470171

Mali, S. B. (2023). Cancer treatment: Role of natural products. Time to have a serious rethink. *Oral Oncology Reports*, *6*, 100040. https://doi.org/10.1016/j.oor.2023.100040

Maliehe, T. S., Tsilo, P. H., & Shandu, J. S. (2020). Computational Evaluation of ADMET Properties and Bioactive Score of Compounds from Encephalartos ferox. *Pharmacognosy Journal*, *12*(6), 1357–1362. https://doi.org/10.5530/pj.2020.12.187

Nxumalo, K. A., Adeyemi, J. O., Leta, T. B., Pfukwa, T. M., Okafor, S. N., & Fawole, O. A. (2024). Antifungal properties and molecular docking of ZnO NPs mediated using medicinal plant extracts. *Scientific Reports*, *14*(1), 18071. https://doi.org/10.1038/s41598-024-68979-3

Ongko, J., Setiawan, J. V., Feronytha, A. G., Juliana, A., Effraim, A., Wahjudi, M., & Antonius, Y. (2022). In-silico screening of inhibitors on the protein epidermal growth factor receptor (EGFR). *IOP Conference Series: Earth and Environmental Science*, *1041*(1), 012075. https://doi.org/10.1088/1755-1315/1041/1/012075

Sana, T., Khan, M., Siddiqui, B. S., Baig, T. A., Jabeen, A., Begum, S., … Shah, L. (2024). Anti-inflammatory and urease inhibitory iridoid glycosides from *Nyctanthes arbor-tristis* Linn. *Journal of Ethnopharmacology*, *319*, 117368. https://doi.org/10.1016/j.jep.2023.117368

Sekaran, K., Karthik, A., Varghese, R. P., Sathiyarajeswaran, P., Shree Devi, M. S., Siva, R., & George Priya Doss, C. (2024). *In silico* network pharmacology study on Glycyrrhiza glabra: Analyzing the immune-boosting phytochemical properties of Siddha medicinal plant against COVID-19. *Adv Protein Chem Struct Biol, 138*, 233-255. https://doi.org/10.1016/bs.apcsb.2023.04.003

Setlur, A. S., Chandrashekar, K., Bhattacharjee, R., Kumar, J., & Niranjan, V. (2023). Deciphering the interaction mechanism of natural actives against larval proteins of Aedes aegypti to identify potential larvicides: a computational biology analysis. *Journal of Biomolecular Structure and Dynamics*, *41*(22), 12480–12502. https://doi.org/10.1080/07391102.2023.2166993

Shannon, P., Markiel, A., Ozier, O., Baliga, N. S., Wang, J. T., Ramage, D., … Ideker, T. (2003). Cytoscape: A Software Environment for Integrated Models of Biomolecular Interaction Networks. *Genome Research, 13*(11), 2498–2504. https://doi.org/10.1101/gr.1239303

Siegel, R. L., Giaquinto, A. N., & Jemal, A. (2024). Cancer statistics, 2024. *CA: A Cancer Journal for Clinicians*, *74*(1), 12–49. https://doi.org/10.3322/caac.21820

Siegel, R. L., Miller, K. D., Fuchs, H. E., & Jemal, A. (2022). Cancer statistics, 2022. *CA: A Cancer Journal for Clinicians*, *72*(1), 7–33. https://doi.org/10.3322/caac.21708

Singh M. R., Singh, D., Kanwar, J., Chauan, N. S. (2020). Advances and Avenues in the Development of Novel Carriers for Bioactives and Biological Agents. Academic Press.

Szklarczyk, D., Morris, J. H., Cook, H., Kuhn, M., Wyder, S., Simonovic, M., … von Mering, C. (2017). The STRING database in 2017: quality-controlled protein–protein association networks, made broadly accessible. *Nucleic Acids Research*, *45*(D1), D362–D368. https://doi.org/10.1093/nar/gkw937

Tipugade, O., Sawale, J. A., & Jadhav, N. (2025a). *Nyctanthes arbor-tristis* Linn.: comprehensive insights into its medicinal, phytochemical, and safety profiles. *Natural Product Research*, 1–14. https://doi.org/10.1080/14786419.2025.2456086

Tipugade, O., Sawale, J., & Jadhav, N. (2025b). Network Pharmacology and Molecular Docking-Based Exploration of Rubiaceous Plants for Breast Cancer: Phytochemicals, Preclinical Studies, And Regulatory Perspectives. *Asian Journal of Pharmaceutical and Clinical Research*, 52–71. https://doi.org/10.22159/ajpcr.2025v18i7.54934

Tolstikova, T., Khvostov, M., & Bryzgalov, A. (2009). The Complexes of Drugs with Carbohydrate-Containing Plant Metabolites as Pharmacologically Promising Agents. *Mini-Reviews in Medicinal Chemistry*, *9*(11), 1317–1328. https://doi.org/10.2174/138955709789878123

Xia, C., Dong, X., Li, H., Cao, M., Sun, D., He, S., … Chen, W. (2022). Cancer statistics in China and the United States, 2022: profiles, trends, and determinants. *Chinese Medical Journal*, *135*(5), 584–590. https://doi.org/10.1097/CM9.0000000000002108

FABAD J. Pharm. Sci., 51, 1, 53-66, 2026
Doi: 10.55262/fabadeczacilik.1804119
RESEARCH ARTICLE

Intranasal Delivery of Nicotine Via Thermoresponsive Hydrogel Systems: Design, Characterization, and *In Vitro* Evaluation

Sema ARISOY[*°], Özlem YAPAR[**], Betül KARAKURT[***], Ramazan BAKAL[****], Dilara ÖRGÜL[*****]

Intranasal Delivery of Nicotine Via Thermoresponsive Hydrogel Systems: Design, Characterization, and In Vitro Evaluation

SUMMARY

Nicotine replacement therapy (NRT) remains a cornerstone strategy in smoking cessation programs, yet conventional nasal sprays are often limited by mucosal irritation and low patient adherence. This study aimed to develop and characterize a novel thermoresponsive hydrogel nasal formulation that combines Kolliphor P 407 and chitosan to enhance mucosal retention, control nicotine release, and improve patient compliance. Nicotine-containing and nicotine-free hydrogels were prepared with varying concentrations of Kolliphor P 407 and a constant chitosan level. Analytical method validation was performed in accordance with ICH Q2 (R1) guidelines. The physicochemical properties of the formulations, including sol-gel transition temperature, pH, FTIR spectrum, viscosity, and homogeneity, as well as in vitro drug release, were assessed. FTIR analysis confirmed the molecular interactions among the formulation components. In vitro drug release studies demonstrated a controlled, biphasic nicotine release from optimized hydrogel formulations (F2 and F8), characterized by favorable pH and viscosity profiles suitable for nasal administration. The findings suggest that the developed thermoresponsive hydrogel system is a promising and patient-friendly alternative for intranasal nicotine delivery in NRT.

Keywords: *Nicotine Replacement Therapy (NRT), Thermoresponsive hydrogel, Kolliphor® P 407, Chitosan, Intranasal drug delivery.*

Termoresponsif Hidrojel Sistemler ile Nikotinin İntranazal Uygulaması: Tasarım, Karakterizasyon ve İn Vitro Değerlendirme

ÖZ

Nikotin replasman tedavisi (NRT), sigara bırakma programlarında temel stratejilerden biri olmaya devam etmektedir. Ancak, konvansiyonel nazal spreylerde sıklıkla mukozal irritasyon ve düşük hasta uyumu gibi sınırlamalarla karşılaşmaktadır. Bu çalışmanın amacı, mukozal tutunmayı artırmak, nikotin salımını kontrol altına almak ve hasta uyumunu iyileştirmek amacıyla Kolliphor® P 407 ve kitosan kombinasyonu ile yeni bir termoresponsif hidrojel nazal formülasyonu geliştirmek ve karakterize etmektir. Farklı konsantrasyonlarda Kolliphor® P 407 ve sabit miktarda kitosan içeren nikotinli ve nikotinsiz hidrojel formülasyonları hazırlanmıştır. Analitik yöntem doğrulaması, ICH Q2 (R1) kılavuzlarına uygun şekilde gerçekleştirilmiştir. Formülasyonların sol-jel geçiş sıcaklığı, pH, FTIR, viskozite ve homojenlik gibi fizikokimyasal özellikleri ve in vitro ilaç salımı değerlendirilmiştir. FTIR analizleri ile formülasyon bileşenleri arasındaki moleküler etkileşimleri doğrulamıştır. İn vitro ilaç salım çalışmaları, nazal uygulama için uygun pH ve viskozite profiline sahip olan optimize edilen hidrojel formülasyonları (F2 ve F8) için kontrollü ve bifazik bir nikotin salımını ortaya koymuştur. Elde edilen bulgular, geliştirilen termoresponsif hidrojel sisteminin, NRT kapsamında intranazal nikotin uygulaması için umut vadeden ve hasta dostu bir alternatif olabileceğini göstermektedir.

Anahtar Kelimeler: *Nikotin Replasman Tedavisi (NRT), Termoresponsif hidrojel, Kolliphor® P 407, Kitosan, İntranazal ilaç uygulaması.*

Recieved: 15.10.2025
Revised: 31.10.2025
Accepted: 2.12.2025

[*] ORCID: 0000-0003-2798-1884, Department of Pharmaceutical Technology, Faculty of Pharmacy, Selcuk University, Konya, Turkey
[**] ORCID: 0009-0003-4602-3339, Faculty of Pharmacy, Selcuk University, Konya, Turkey
[***] ORCID: 0009-0007-4137-2387, Faculty of Pharmacy, Selcuk University, Konya, Turkey
[****] ORCID: 0009-0000-0112-7087, ILKO Pharmaceuticals, 42280, Konya, Turkey
[*****] ORCID: 0000-0002-8947-4995, Department of Pharmaceutical Technology, Faculty of Pharmacy, Selcuk University, Konya, Turkey

[°] Corresponding Author; Sema Arısoy
Address: Department of Pharmaceutical Technology, Faculty of Pharmacy, Selcuk University, Konya, Turkey
E-mail: sema.arisoy@selcuk.edu.tr

INTRODUCTION

Tobacco smoke is a highly complex mixture, comprising approximately 5,000 chemically active and reactive constituents. Reports from the World Health Organization (WHO) indicate that tobacco consumption is responsible for about 5.4 million premature deaths globally each year. Furthermore, scientific investigations suggest that the total number of distinct compounds present in cigarette smoke may surpass 100,000 (Al-Dahhan et al., 2022). Among these, nicotine is the most prominent psychoactive alkaloid, found almost exclusively in tobacco plants such as *Nicotiana tabacum* and *Nicotiana rustica*. Structurally, nicotine is a tertiary amine composed of pyrrolidine and pyridine rings (Brandon et al., 2009). Nicotine can enter the body through smoking, chewing, or intranasal inhalation of fine tobacco powders. It readily crosses the blood–brain barrier and distributes rapidly to the central nervous system. When inhaled via smoking, nicotine is absorbed through the pulmonary epithelium into the systemic circulation and quickly reaches the brain (Brandon et al., 2009; Wadgave & Nagesh, 2016). Acting as a full agonist, nicotine stimulates neuronal nicotinic acetylcholine receptors in the ventral tegmental area, thereby triggering dopamine release in the nucleus accumbens and reinforcing addiction (Devi et al., 2020; Prochaska & Benowitz, 2019).

The most widely investigated pharmacological approach for nicotine dependence is nicotine replacement therapy (NRT) (Wadgave & Nagesh, 2016). Purified nicotine formulations have long served as the first-line treatment to alleviate withdrawal symptoms and reduce physical dependence (Prochaska & Benowitz, 2019). NRT has been demonstrated to significantly decrease craving and improve cessation outcomes (Stead et al., 2012). A variety of NRT dosage forms are available, including gums, lozenges, transdermal patches, nasal sprays, and oral inhalers. While patches deliver nicotine continuously at a controlled rate, nasal sprays, gums, and tablets provide acute dosing (Wadgave & Nagesh, 2016). These therapies deliver lower and slower nicotine levels than cigarettes, reducing withdrawal with a diminished risk of dependence and relapse (Stead et al., 2012).

Commercial nasal sprays, such as Nicorette®, deliver 0.5 mg of nicotine per 50 µL spray and are typically administered once per nostril, corresponding to a total of 1 mg per dose. They are recommended for use 1–2 times per hour, with a maximum of five administrations per day (Brandon et al., 2009; Devi et al., 2020). Owing to their rapid absorption, nicotine nasal sprays produce a pharmacokinetic profile similar to that of cigarette smoking (Uzaslan, 2003). However, their clinical utility has been limited due to poor patient compliance, largely attributed to local side effects such as dryness and irritation, which can lead to reduced efficacy (Devi et al., 2020).

Several alternative nicotine delivery systems have been investigated. For instance, cellulose-based hydrogels with ultrasound-triggered release have been developed. However, they were primarily designed for neurological disorders such as Alzheimer's and Parkinson's disease. Cellulose hydrogel drug carrier was created with cellulose concentrations ranging from 0.45 wt% to 1.8 wt%, and 1 wt% nicotine solution was added to the system at a weight ratio of 9:1 (cellulose: nicotine). So the formulation contains a different dose of nicotine from those used in NRT (Iresha & Kobayashi, 2021). In another study, nicotine was incorporated into chitosan hydrogels, with or without glutaraldehyde crosslinking, for evaluation in transdermal delivery systems. While these systems offered prolonged release till 48 h, they did not provide the dosage per hour required for smoking cessation (Lino et al., 2017). Intranasal administration of nicotine at a dose of 1 mg/kg, along with proliposomes containing either nicotine base or nicotine hydrogen tartrate salt, or a mixture of powdered nicotine hydrogen tartrate salt and sorbitol, was applied for the prolonged delivery of nicotine to the systemic circulation. Nasal nicotine absorption from these formulations was ex-

tremely quick (less than 10 minutes to achieve plasma peaks) and resulted in significantly sustained plasma nicotine levels when compared to NB and NS saline solutions, as well as previous nasal nicotine sprays (Jung et al., 2000). The combination of pulsatile and sustained plasma nicotine profiles for smoking cessation was achieved by developing a nasal formulation of a powder containing a nicotine-Amberlite resin complex, which is a cationic exchange material (Cheng et al., 2002). All these formulations were developed for NRT; however, they do not provide mucoadhesion, which is essential to overcome mucociliary clearance for prolonged delivery of nicotine via the nasal route.

Hydrogels, which are three-dimensional hydrophilic polymeric networks, can retain large amounts of water and biological fluids. Their insolubility is ensured by chemical crosslinks (junctions, tie-points) and physical associations (entanglements, crystallites) (Peppas et al., 2000). Some hydrogels exhibit responsiveness to external stimuli such as pH or temperature. For example, Kolliphor® P 407-based formulations are well known for their thermoresponsive properties, undergoing sol–gel transitions in response to small temperature changes (Darge et al., 2019; Dumortier et al., 2006; Kojarunchitt et al., 2011). Hydrogels are also used as carriers that can interact with the mucosa lining in various parts of the body, including the gastrointestinal (GI) tract, colon, vagina, nose, and others, due to their ability to prolong residence time at the delivery location (Peppas et al., 2000). Additionally, thermoresponsive gels undergo a sol–gel transition at nasal temperature, allowing for in situ gelation and prolonged retention at the application site. The polymeric matrix further modulates drug diffusion by forming a three-dimensional network that slows the release of the incorporated drug (Arisoy & Dortunc, 2020).

Chitosan represents a multifunctional polymer, featuring both mucoadhesive and permeation-enhancing properties, and therefore is a widely studied excipient for mucosal drug delivery. Regarding nasal administration, chitosans have been used for the preparation of gels, solid inserts, powders, and nanoparticles, in which a three-dimensional network can be recognized (Luppi et al., 2010). Its mucoadhesive properties enable it to interact with the negatively charged mucin layer, thereby prolonging residence time and resisting clearance mechanisms (Arısoy et al., 2024; Arisoy & Dortunc, 2020). Consequently, combining chitosan with thermoresponsive polymers offers a rational strategy for sustained nasal delivery.

In the present study, thermoresponsive hydrogel formulations composed of Kolliphor® P 407 and chitosan were developed for nicotine replacement therapy. This system was designed to address the limitations of existing nasal sprays by providing controlled release, reduced dosing frequency, and enhanced patient compliance. Furthermore, the water-retention capacity of the hydrogels supports regional moisturization, potentially improving tolerability. By combining thermoresponsive gelation with mucoadhesive properties, these formulations are expected to maintain longer residence in the nasal cavity, overcome mucociliary clearance, and achieve a sustained release profile, consistent with findings from previous studies on nasal mucoadhesive systems (Arisoy, Sayiner, & Comoglu, 2020).

MATERIALS AND METHODS

Materials

Kolliphor® P 407 (102.13 g/mol) was a gift from BASF. Nicotine (d: 1.010 g/mL, liquid form), Sodium dihydrogen phosphate, Sodium Hydroxide, and Medium molecular weight chitosan (Acetylation degree: 75-85%) were from Sigma. Mucin from porcine stomach, Type II was from Sigma.

Methods

Analytical method validation

A high-concentration nicotine stock solution (100 µg/ml) was prepared using a buffer solution (pH 6.5). Standard solutions were obtained at concentrations of

1, 2.5, 5, 7.5, 10, and 12.5 µg/ml with several dilutions (Østergaard et al., 2010). The absorbance of the dilutions, measured at 254 nm using a UV-visible spectrophotometer (Cary 60 UV-vis), was plotted versus the concentration (Al-Dahhan et al., 2022; Østergaard et al., 2010). The study was repeated in three parallel groups, and the average values were graphed with their standard errors. The method was validated according to the ICH guideline Q2 (R1) with the parameters of accuracy, precision (intermediate precision), Limit of Detection (LOD), Limit of Quantification (LOQ), and linearity (Arisoy et al., 2021).

Preparation of Kolliphor® P 407-chitosan thermoresponsive hydrogel

0.5 mL of acetic acid was added to 9.5 mL of distilled water, and 0.05 g of chitosan was weighed and added. The mixture was then stirred with a magnetic stirrer until homogeneous. It was then stored in the refrigerator overnight. Different amounts of Kolliphor® P 407 were weighed and mixed with 1 mL of cold buffer 6.5. Then, 0.8 mL of buffer was added 1 hour later (Hulambukie et al., 2022). Half an hour later, 0.2 mL of the 0.5% chitosan solution was added. To achieve a homogenous system, it was agitated in an ice bath at 250 rpm using a magnetic stirrer (Multi-Channel Stirrer, MS-53M) for 24 hours (Sayiner et al., 2020). To obtain 50 mg of nicotine in each formulation, 50 µL of nicotine (d = 1.01 g/mL) and 50 µL of water were added during the preparation step. Thus, nicotine and nicotine-free formulations were created using Kolliphor® P 407 ratios ranging from 16% to 18% and chitosan at a constant ratio (Table 1.).

Table 1. Formulation Parameters

Formulation	Kolliphor® P 407	Nicotine	Chitosan (5 %)
F1	18 %	-	+
F2	18 %	+	+
F3	17 %	-	+
F4	17 %	+	+
F5	16 %	-	+
F6	16 %	+	+
F7	18 %	-	-
F8	18 %	+	-

Homogeneity

Nicotine and nicotine-free Kolliphor® P 407 hydrogels were visually examined for homogeneity. The resulting gels were heated to 40°C, which is above the transformation temperature, and gel images were recorded (Sayiner et al., 2020).

Determination of sol-gel transition temperature

The hydrogel's sol-gel transition was determined using the inverse test tube method. A test tube containing 1 mL of the hydrogel formulation was put in a water bath (Water Bath, Wisconsin). The temperature of the water bath was raised from 10°C to 40°C at a rate of 1°C per minute. The tubes were inverted every 30 seconds to check for flow, and the temperature showed that no flow was recorded as the transition temperature (Gu et al., 2020; Sayiner et al., 2020; Watts & Smith, 2009). The experiment was conducted in three parallel groups.

pH

A drop of the sample was dissolved in 10 mL of water, and the pH was measured using a pH meter (Inolab). The experiment was carried out in 3 parallel (Watts & Smith, 2009).

Viscosity

Viscosity was calculated at a speed of 5 rpm at a temperature of 33°C, which is above the sol-gel transition temperature of the gels (Sayiner et al., 2020). The experiment was conducted in three parallel runs using a rotational viscometer (Brookfield DV2-T) with a CPA-51Z spindle.

Swelling index

The swelling ratio was evaluated by recording the sample weights before and after swelling at various time intervals. Pre-weighed specimens were immersed in phosphate-buffered saline (pH 6.5). After carefully removing excess surface buffer with filter paper, the swollen samples were weighed at predetermined intervals of 0, 10, and 15 minutes. The swelling ratio at a given time (Wt) was calculated using equation 1:

$$Wt = \frac{Ws - Wd}{Wd} \quad \text{(Eq 1.)}$$

where Ws represents the swollen weight of the sample at a specific time and Wd is the corresponding dry weight. The point at which no further change in weight was observed was defined as the equilibrium swelling ratio (Wt) (Arısoy et al., 2023).

Fourier transform infrared spectroscopy (FT-IR) analysis

To investigate the molecular integration of hydrogel and nicotine, it was analyzed using FTIR spectrometry. Briefly, the spectra were recorded with 40 scans in the wave number range from 4000 cm^{-1} to 400 cm^{-1} at a resolution of 1 cm^{-1}. All measurements were performed at room temperature (Akkuş-Dağdeviren et al., 2023).

Mucoadhesion test

The mucoadhesive property was evaluated using a modified balance method (Thangarajoo et al., 2023). A 5% mucin solution was prepared in a pH 6.5 buffer (Thirawong et al., 2008). A filter paper impregnated with 0.4 mL of mucin solution was affixed to a clean glass slide, while on the opposite side, the lyophilized formulation was secured to the lower arm of the balance using double-sided adhesive tape in the same manner. Following 10 seconds of contact between the mucin and the formulation, the weight on the balance was gradually increased by adding water dropwise to the empty pan of the balance until detachment occurred. The mucoadhesive strength of each formulation was defined as the minimum weight necessary to separate the mucin-impregnated filter paper from the formulation. This method demonstrates the formulation's ability to remain attached at the site of application, which is crucial for localized therapeutic efficacy. The mucoadhesive property was quantified by calculating the mucoadhesive strength and the corresponding force of adhesion. The force of adhesion for the formulations and chitosan was calculated using the following equation 2:

$$Force\ of\ adhesion\,(N) = \frac{Mucoadhesive\ strength\,(g) \times 9.81}{1000} \quad \text{(Eq 2.)}$$

where mucoadhesive strength (g) represents the minimum weight required for detachment, and 9.81 is the gravitational acceleration constant.

***In vitro* drug release**

A phosphate buffer solution with a pH of 6.5 was used as a buffer to simulate the nasal area for in vitro release experiments (Arisoy et al., 2020). Hydrogel, nicotine solution in pH 6.5 buffer, and Nicorette® nasal spray, each containing 2.5 mg nicotine were filled into separate dialysis bags (MWCO of 10 kDa) (Arisoy & Comoglu, 2020). Then, the bags were placed in beakers containing 500 mL of pH 6.5 buffer, the temperature was set at 37°C, and mixed at 50 rpm using the USP 2 apparatus (dissolution device, PHARMA TEST). At predetermined time intervals, 1 mL samples were taken from the beakers, and the release medium was balanced with an equal amount of preheated refreshing medium. Nicotine content of the samples was calculated with UV at 254 nm.

RESULTS AND DISCUSSION

Nicotine has a tertiary amine structure and can exist in either ionized or non-ionized forms, depending on the pH of its surroundings. After smoking, nicotine travels rapidly to the arterial circulation and brain in 15 to 20 seconds, where it displays its addictive effects. The speed of delivery to the brain is regarded as playing a key role in the addictive potential of inhaled nicotine when compared to other routes. Nicotine dependence from drugs that give nicotine slowly, such as nicotine patches, gum, and lozenges, seems to be minimal (Prochaska & Benowitz, 2019).

Drugs can be transported directly to the brain via the olfactory and trigeminal nerve pathways, making the intranasal route an exciting alternative to traditional parenteral and oral routes. Additionally, it bypasses hepatic first-pass effects, ensuring a rapid onset of action and providing a patient-friendly method of administration (Koo et al., 2024). Smokers typically absorb about 1 to 1.5 milligrams of nicotine with

each inhalation. While nicotine's half-life is about two hours, environmental and genetic variables may influence its concentration in blood vs time. Blood nicotine levels climb over four to six hours due to regular smoking, plateau throughout the day, and then fall overnight (Prochaska & Benowitz, 2019).

In this formulation study, a nicotine-loaded nasal spray was prepared to obtain a direct and rapid action compared to the oral route. It contains 0.5 mg of nicotine per 50 µL to sustain steady nicotine levels in the brain, equivalent to smoking one cigarette. Consequently, in a daily smoker, the brain is exposed to nicotine for 24 hours every day, resulting in symptoms and tolerance development (Prochaska & Benowitz, 2019). Formulation characterization studies were conducted to ensure the quality of the developed thermoresponsive nicotine-containing hydrogel, and the results are discussed in this paper.

Analytical method

All examinations were conducted in 3 parallel groups. The average values were graphed with the standard errors. The deviation of the data obtained as a result of accuracy and precision studies was found to be less than 2%. The accuracy and precision of the method were evaluated at three concentration levels, representing low, medium, and high concentrations (5 µg/mL, 7.5 µg/mL, and 10 µg/mL, respectively). The accuracy of the analytical method was evaluated based on recovery studies. The mean percentage recoveries were found to be 100.38%, 99.51%, and 103.42% at the tested concentration levels. The corresponding standard deviations were 0.143, 0.094, and 0.047, respectively, with relative standard deviations (RSD%) of 0.143, 0.094, and 0.045. These values are within the acceptable limits, indicating the accuracy and reliability of the method. The precision of the method was assessed at three concentration levels (5 µg/mL, 7.5 µg/mL, and 10 µg/mL). The mean concentrations obtained were 5.0188, 7.4630, and 10.3423 µg/mL, respectively. The standard deviations were 0.01, 0.01, and 0.00, with relative standard deviations (RSD%) of 0.14, 0.09, and 0.04, respectively. These results demonstrate the high precision and reproducibility of the developed analytical method (Arisoy, Sayiner, & Comoglu, 2020). The LOD value was found to be 0.04 µg/mL, and the LOQ value was found to be 0.126 µg/mL. The calibration equation was prepared at 5 points as specified in the ICH guide, and R2 was evaluated as the linearity parameter. The R2 value was found to be as suitable as 0.998 (Figure 1.). All results indicate that the method was validated (Arisoy et al., 2021).

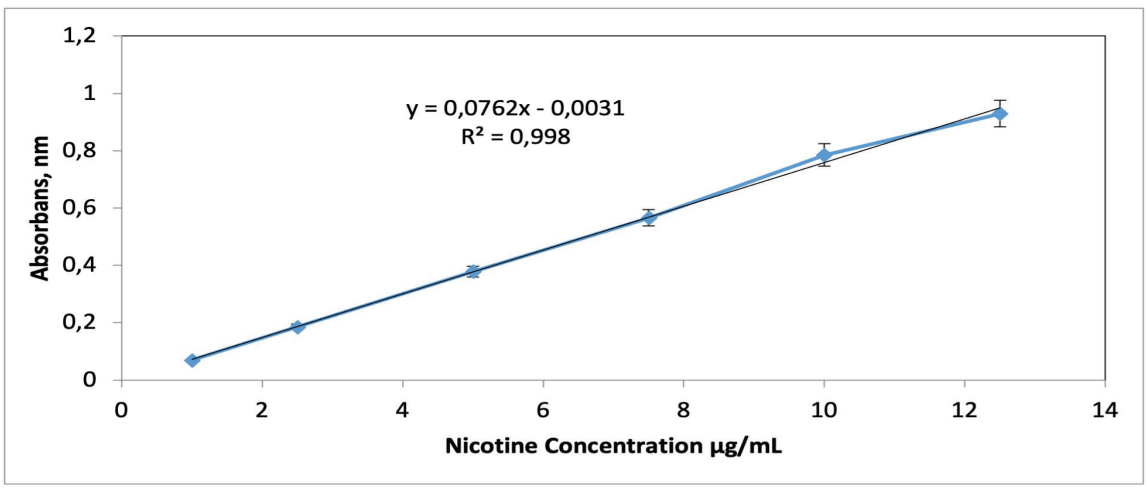


Figure 1. Calibration graph of nicotine concentration (µg/mL) vs. absorbance (nm)

Characterization studies

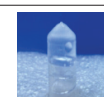
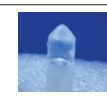
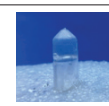
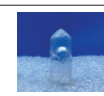
The primary limitation of intranasal application is the removal of drugs before they are sufficiently absorbed through nasal drainage (Arisoy et al., 2020). The use of mucoadhesive polymers, such as chitosan, has been proposed in drug delivery to increase the residence time at the mucosal surface and facilitate the permeation of various drugs into the brain (Ojeda-Hernández et al., 2024). Kolliphor® P 407 was used for its thermo-reversible behavior to formulate an intranasal sol–gel that accumulates in the nasal area after easy application in a solution state, while chitosan was used for its mucoadhesive properties (Riaz et al., 2023).

All hydrogels have a homogeneous appearance (Table 2.). All experiments were carried out in three parallel tests to determine the sol-gel transition of the hydrogel using the inverse test-tube method. The turn was observed in one minute for all formulations, as the experiment showed a 1°C increase in heat over this period.

F5 and F6, with the lowest Kolliphor® P 407 ratio (16%), did not form a gel state during the experiment, which was heated to 40°C. This result is supported by the literature, which shows that higher sol-gel transition temperatures occur with the decreased Kolliphor® P 407 concentration. In this study, nicotine addition, which was + for F6 and – for F5, did not alter this phenomenon, while the increase in pH might be attributed to nicotine's tertiary amine structure (Table 1-2.) (Prochaska & Benowitz, 2019; Riaz et al., 2023).

F1, F2, F3, and F4 showed a sol to gel transition at about 25°C, while F7 and F8 showed it at about 30°C, indicating that nicotine addition did not affect the transition temperature, while chitosan (5%) addition lowered the transition temperature due to it is gel state at 25°C.

Table 2. Characterization of formulations

Formulation	Transition temperature (°C)	pH	Appearance
F1	24.3 ± 0.1	6.04 ± 0.006	
F2	23.53 ± 0.16	7.84 ± 0.05	
F3	25.46 ± 0.46	6.02 ± 0.01	
F4	24.93 ± 0.16	8.14 ± 0.02	
F5	-	5.15 ± 0.06	
F6	-	8.02 ± 0.07	
F7	31.43 ± 0.29	7.77 ± 0.03	
F8	29.13 ± 0.15	6.77 ± 0.01	
Nicotine solution in the buffer pH 6.5	-	7.5 ± 0.03	-
Nicorette® nasal spray	-	7.00 ± 0.05	-
Nicotine solution in the water	-	9.72 ± 0.03	-

The pH of the healthy nasal mucosa is between 5.5 and 6.5. Formulations with a pH close to that of the nasal mucosa are associated with reduced discomfort following nasal administration (Watts & Smith, 2009). All formulations have a suitable pH to apply to biological membranes (Table 2.). It was shown that the addition of chitosan lowered the pH of the formulation, whereas the addition of nicotine led to a higher pH in the formulation (Table 2.). Chitosan is a cationic biopolymer that relies on pH for its solubility; it does not dissolve in neutral or alkaline water but can become soluble in acidic aqueous solutions through the protonation of its amine groups (Darge et al., 2019). In the formulation studies, chitosan was initially dissolved in an acidic solution and added, resulting in a rise in the pH of the formulation produced with the addition of the chitosan solution. Since nicotine possesses a basic chemical structure, its addition led to an increase in the pH of the chitosan solution.

Nicotine is a weak base with a pKa of 8.0, which means that at a physiological pH of 7.4, 69% of it is ionized while 31% remains unionized. The unionized form, referred to as freebase nicotine, easily crosses membranes such as the nasal mucosa (Prochaska & Benowitz, 2019). F1, F2, F7, and F8 have a pH range between 6.04 and 7.84, which favors the non-ionized form of nicotine, facilitating the mucosal transition.

Table 3. Viscosity of formulations

Formulation	Viscosity (cP)	Relative standard deviation (RSD) (%)
F1	34126 ± 975	2.86
F2	49373 ± 817.39	1.66
F7	4459.67 ± 207.32	4.65
F8	6255.00 ± 31	0.50
Chitosan (5%)	5.52 ± 2.60	47.11

It was found that as the Kolliphor® 407 concentration increased, the viscosity of the formulation also increased; however, due to the fluidic nature of chitosan solution, chitosan-added formulations showed lower viscosity (Riaz et al., 2023). F1, F2, F7, and F8 have suitable viscosity for a stable state in the nasal area (Gu et al., 2020). F2 and F8, with and without chitosan, were chosen as optimum formulations for further studies due to their acceptable viscosity, pH, transition temperature, and appearance.

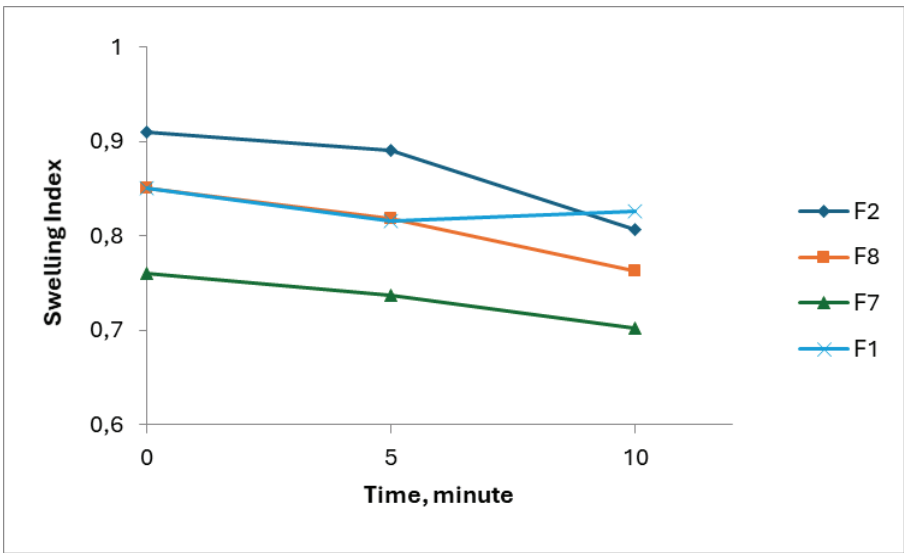


Figure 2. Swelling index vs. time of formulations

All formulations exhibited a high swelling index close to 1 (Figure 2.). By 15 minutes, however, all formulations degraded and lost their structural integrity. Among them, F7, which lacked both chitosan and nicotine, showed the lowest swelling, whereas F2, containing both chitosan and nicotine, demonstrated the highest swelling. F8 and F1 displayed similar swelling indices.

FTIR analysis

In the spectrum of Kolliphor® P 407 (Figure 3.), characteristic signals are observed mainly at wavelengths of ~2878 cm^{-1} (C-H aliphatic stretching), ~1372 cm^{-1} (O-H bending), and ~1279 cm^{-1} (C-O stretching). In the F8 (containing nicotine and Kolliphor® P 407), peaks belonging to nicotine were also observed in addition to the peaks belonging to Kolliphor® P 407. The peak observed at 716.76 cm^{-1} characterizes the different chemical functions of nicotine and corresponds to the out-of-plane bending of the C-H bond of the mono-substituted pyridinic cycle (Al-Dahhan et al., 2022). The vibration band for chitosan at 3266 cm^{-1} is related to N–H stretching, as well as –OH linked to both intermolecular and intramolecular hydrogen bonding. An absorption band near 2872 cm^{-1}, associated with asymmetric C–, was detected. The H stretching of the $–CH_2$ group appeared as a vibration band at 1634 cm^{-1}, attributed to C=O stretching of amide I. The N–H deformation of amide II was seen at 1542 cm^{-1}, with bands corresponding to the $C–CH_3$ deformation observed at 1256 cm^{-1}, and the C–O–C stretching of the saccharide structure at 1152, 1067, and 1023 cm^{-1} were recorded (Becerra et al., 2022).

In the FTIR analysis of the formula containing chitosan and Kolliphor® P407 without nicotine, peaks belonging to Kolliphor® P407 were observed next to the peaks belonging to chitosan. The presence of characteristic signals belonging to Kolliphor® P407 was observed at wavelengths of ~2879 cm^{-1} (C-H aliphatic stretching vibration), ~1372 cm^{-1} (O-H bending vibration), and ~1279 cm^{-1} (C-O stretching vibration) (Becerra et al., 2022). Characteristic peaks of nicotine (e.g., C–H stretching at ~3020–3100 cm^{-1}, N–H stretching at ~3300 cm^{-1}, and C–N stretching at ~1200–1350 cm^{-1}) were observed in the nicotine-loaded hydrogel (F2) (Al-Dahhan et al., 2022).

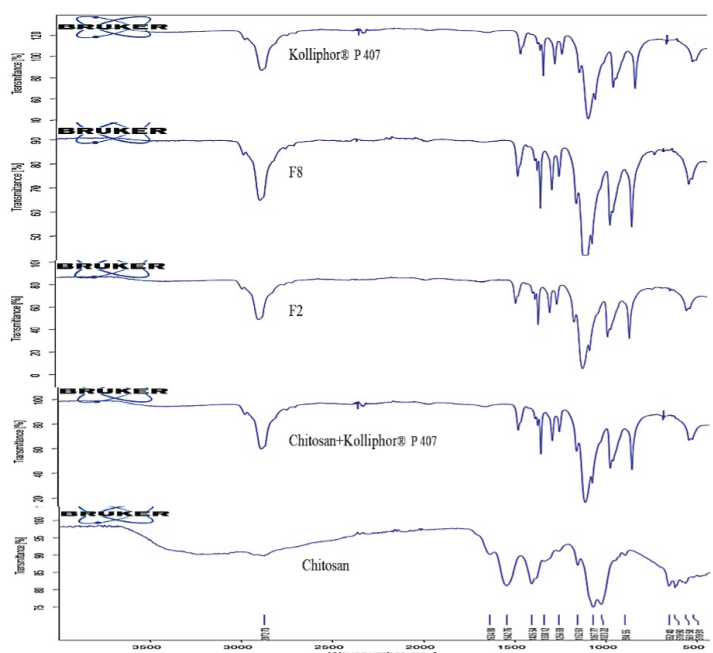


Figure 3. FTIR spectrum

***In vitro* mucoadhesive strength**

The mucoadhesive property of the formulation helps establish the ability of a topical formulation to retain at the site of action when applied to a specific area, such as the nasal area (Thangarajoo et al., 2023). In the development of an in situ gel system, the mucoadhesive strength is a crucial factor to be modulated in order to promote the retention of the formulation at the application site.

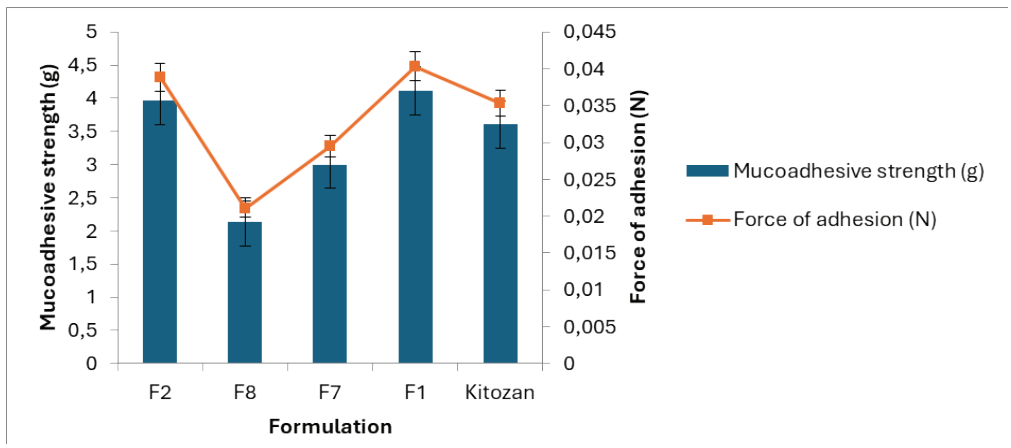


Figure 4. Mucoadhesive strength and force of adhesion of the formulations

Since formulations F1, F2, F7, and F8 exhibited suitable viscosity for maintaining stability in the nasal cavity and contained the same amount of Kolliphor® P 407, their mucoadhesive properties were investigated. Furthermore, these formulations provide a suitable model for investigating the effects of chitosan and poloxamer content, as well as nicotine incorporation, on mucoadhesion. Although Kolliphor® P 407 thermo-responsive hydrogels are not inherently mucoadhesive, they have been widely investigated as mucosal drug delivery systems owing to their thermosensitive gelation at the application site, which prolongs residence time and supports effective drug delivery. Incorporation of chitosan into Kolliphor®-based gels enhanced both gel strength and mucoadhesive properties, as the protonated amino groups of chitosan can readily interact with the negatively charged mucin components of the mucosal layer (Giuliano et al., 2018). As shown in Figure 4, the addition of chitosan enhanced mucoadhesiveness, whereas nicotine incorporation led to a reduction.

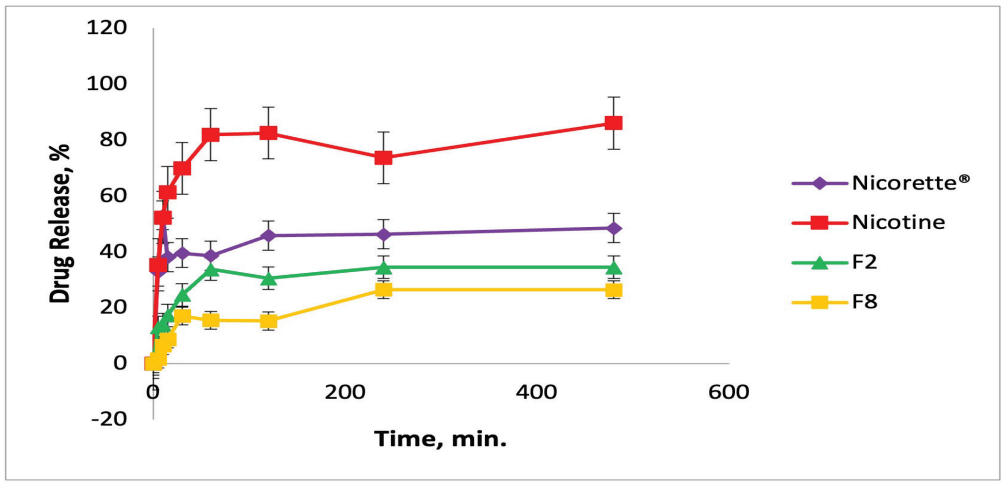


Figure 5. *In vitro* release profile of nicotine from the drug-loaded formulations in PBS (pH 6.5) at 37°C

***In vitro* drug release**

Numerous substances with a range of uses are found in Nicorette® nasal spray; NNS aroma DZ-03226 (B-ionone) as a flavoring agent, sodium chloride as a tonicity adjuster, sodium phosphate dodecahydrate, anhydrous citric acid as buffered, polysorbate 80 as a surfactant, methyl parahydroxybenzoate, propyl parahydroxybenzoate as antimicrobials, disodium edetate as a chelating agent, and purified water as a solvent. It was observed that Nicorette® nasal spray released 53.14% of the loaded nicotine within the first ten minutes. The percentage release rate increased over the first two hours and remained constant until the eighth hour, when the total release rate reached 48.57%.

The nicotine solution was prepared using only a phosphate buffer (pH 6.5) as a solvent. The nicotine solution showed a higher release %, 86.11%, than the formulations and Nicorette® nasal spray, which might be due to the absence of other substances that could potentially affect the release rate of nicotine through molecular interaction (Arısoy et al., 2024).

When the releases of nicotine from formulations, Nicorette® nasal spray and nicotine solution, were evaluated together, it was observed that the release was affected by pH as well as molecular interaction. Since the nicotine solution had a basic pH, nicotine was present in a non-ionized form in this solution and could therefore move more easily from the membrane to the release medium (Table 2, Figure 5.) (Al-Dahhan et al., 2022; Arısoy & Şalva, 2023).

F8 formula released 15.57% of the loaded nicotine into the buffer medium during the first hour. The percentage release increased during the first hour but stabilized during the second hour. It climbed again after the second hour, eventually releasing 26.53% of the loaded nicotine in the fourth hour. It was observed that F8 released the nicotine in its content in a controlled manner, exhibiting biphasic release (Arisoy & Comoglu, 2020).

The F2 formulation released 13% of the loaded nicotine in the first ten minutes and released 33.84% in the following hour. The release after the first hour continued stably until the eighth hour, and 34.55% of the loaded drug was released in total. It was observed that the F2 formulation released the nicotine content in a controlled manner after the burst release that occurred in the first five minutes (Arisoy & Comoglu, 2022).

These findings are consistent with the literature, as formulations F8 and F2 demonstrated the advantages of in situ gelling systems for intranasal drug delivery: their gel structure prolongs residence time in the nasal cavity, enables sustained drug release, and ultimately enhances bioavailability (Giuliano et al., 2018). The difference in burst release between F2 and F8 can be attributed to the absence of chitosan in F8, which causes a portion of nicotine to remain unincorporated within the gel matrix and localize on the surface, leading to its rapid release (Arısoy & Şalva, 2023).

The difference in the release profile between the F2 and F8 formulas might be due to a pH difference (Table 2.). F2 might have shown a higher release than F8 at the 8th hour due to its higher pH. Additionally, the differences between F2, F8, and Nicorette® may be attributed to the molecular interactions of Kolliphor® and chitosan with nicotine. The discrepancy between the two formulations› release patterns and percentage release rates at the conclusion of the eighth hour may be associated with the hydrophilic nature of chitosan, which is present in F2 but not in F8 (Arısoy et al., 2024).

CONCLUSION

This study successfully formulated and evaluated thermoresponsive hydrogel systems incorporating Kolliphor® P 407 and chitosan for intranasal nicotine replacement therapy. The developed formulations exhibited desirable gelation behavior at physiological temperatures, appropriate viscosity for nasal retention, and a pH compatible with the nasal mucosa. Controlled *in vitro* nicotine release profiles were observed, particularly in F2 and F8 formulations, indicating effective modulation of drug delivery. FTIR spectroscopy confirmed the presence of key function-

al interactions between nicotine, chitosan, and Kolliphor® P 407. Overall, these results demonstrate that the hydrogel system holds substantial potential as a patient-compliant and effective alternative to conventional nicotine nasal sprays, overcoming limitations such as rapid drug clearance.

ACKNOWLEDGEMENT

TUBITAK supported this study with application number 1139B412200347.

AUTHOR CONTRIBUTION STATEMENT

The conceptualization, methodology, investigation, data curation, formal analysis, visualization, writing – original draft, writing – review & editing, project administration (SA), the investigation, literature review, writing – original draft, data curation, formal analysis, project administration (ÖY), the investigation, literature review, writing – original draft, data curation, formal analysis, project administration (BK), the conceptualization, methodology, formal analysis, data curation, project administration (RB), the formal analysis, data curation, writing – review & editing (DÖ).

CONFLICT OF INTEREST

The authors declare that there is no conflict of interest.

REFERENCES

Akkuş-Dağdeviren, Z. B., Arısoy, S., Friedl, J. D., Fürst, A., Saleh, A., & Bernkop-Schnürch, A. (2023). Polyphosphate coated nanoparticles: Enzyme-activated charge-reversal gene delivery systems. *International Journal of Pharmaceutics, 646*, 123474.

Al-Dahhan, W. H., Kadhom, M., Yousif, E., Mohammed, S. A., & Alkaim, A. (2022). Extraction and determination of nicotine in tobacco from selected local cigarettes brands in iraq. *Letters in Applied NanoBioScience, 11*(1), 3278-3290.

Arısoy, S., Bux, K., Herwig, R., & Şalva, E. (2024). Development, evaluation, and molecular dynamics study of ampicillin-loaded chitosan–hyaluronic acid films as a drug delivery system. *ACS Omega, 9*(18), 19805-19815. doi: 10.1021/acsomega.3c08076

Arisoy, S., & Comoglu, T. (2020). Kinetic evaluation of l-dopa loaded wga-grafted nanoparticles. *Medicine, 9*(2), 385-388.

Arisoy, S., & Comoglu, T. (2022). Effect of formulation variables for the production of wga-grafted, levodopa-loaded plga nanoparticles. *Journal of Biomimetics, Biomaterials and Biomedical Engineering, 54*, 1-15.

Arisoy, S., & Dortunc, B. (2020). Thermosensitive hydrogels for controlled drug delivery. *Journal of Literature Pharmacy Sciences, 9*(1), 90-100. doi: 10.5336/pharmsci.2019-70783

Arisoy, S., Sayiner, Ö., & Comoglu, T. (2020). Evaluation of release of l-dopa from plga nanopartıcles with different in vitro release methods by an optimized hplc method. *Bezmialem Science*. doi: 10.14235/bas.galenos.galenos.2020.3860

Arisoy, S., Sayiner, O., Comoglu, T., Onal, D., Atalay, O., & Pehlivanoglu, B. (2020). In vitro and in vivo evaluation of levodopa-loaded nanoparticles for nose to brain delivery. *Pharmaceutical Development and Technology, 25*(6), 735-747.

Arisoy, S., Sayiner, Ö., & Çomoğlu, T. (2021). Development and validation of an in vitro dissolution method based on hplc analysis for l-dopa release from plga nanoparticles. *Bezmialem Science, 9*(1), 9.

Arısoy, S., & Şalva, E. (2023). Preparation and in vitro characterization of curcumin loaded chitosan-hyaluronic acid polyelectrolyte complex based hydrogels. *Drug Development and Industrial Pharmacy, 49*(10), 637-647.

Becerra, J., Rodriguez, M., Leal, D., Noris-Suarez, K., & Gonzalez, G. (2022). Chitosan-collagen-hydroxyapatite membranes for tissue engineering. *Journal of Materials Science: Materials in Medicine, 33*(2), 18.

Brandon, T.H., Drobes, D.J., Ditre, J.W., & Elibero, A. (2009). Nicotine. In L. M. Cohen, F. L. Collins, A. M. Young, D. E. McChargue, T. R. Leffingwell & K. L. Cook (Eds.), *Pharmacology and treatment of substance abuse: Evidence- and outcome-based perspectives* (pp. 267–293). Routledge: Taylor & Francis Group.

Cheng, Y. H., Watts, P., Hinchcliffe, M., Hotchkiss, R., Nankervis, R., Faraj, N.F., Smith, A., Davis, S.S., & Illum, L. (2002). Development of a novel nasal nicotine formulation comprising an optimal pulsatile and sustained plasma nicotine profile for smoking cessation. *Journal of Controlled Release, 79*(1), 243-254. doi: https://doi.org/10.1016/S0168-3659(01)00553-3

Darge, H. F., Andrgie, A. T., Tsai, H. C., & Lai, J. Y. (2019). Polysaccharide and polypeptide based injectable thermo-sensitive hydrogels for local biomedical applications. *International journal of biological macromolecules, 133*, 545-563.

Devi, R.E., Barman, D., Sinha, S., Hazarika, S.J., & Das, S. (2020). Nicotine replacement therapy: A friend or foe. *Journal of Family Medicine and Primary Care, 9*(6), 2615-2620.

Dumortier, G., Grossiord, J. L., Agnely, F., & Chaumeil, J.C. (2006). A review of poloxamer 407 pharmaceutical and pharmacological characteristics. *Pharmaceutical research, 23*, 2709-2728.

Giuliano, E., Paolino, D., Fresta, M., & Cosco, D. (2018). Mucosal applications of poloxamer 407-based hydrogels: An overview. *Pharmaceutics, 10*(3), 159.

Gu, F., Fan, H., Cong, Z., Li, S., Wang, Y., & Wu, C. (2020). Preparation, characterization, and in vivo pharmacokinetics of thermosensitive s nasal gel of donepezil hydrochloride. *Acta Pharmaceutica, 70*(3), 411-422.

Hulambukie, E., Abdeltawab, H., Duarah, S., Svirskis, D., & Sharma, M. (2022). Injectable in situ gelling system for sustained nicotine delivery as a replacement therapy for smoking cessation. *Gels, 8*(2), 114.

Iresha, H., & Kobayashi, T. (2021). Ultrasound-triggered nicotine release from nicotine-loaded cellulose hydrogel. *Ultrasonics Sonochemistry, 78*, 105710. doi: https://doi.org/10.1016/j.ultsonch.2021.105710

Jung, B. H., Chung, B. C., Chung, S. J., Lee, M. H., & Shim, C. K. (2000). Prolonged delivery of nicotine in rats via nasal administration of proliposomes. *Journal of Controlled Release, 66*(1), 73-79. doi: https://doi.org/10.1016/S0168-3659(99)00258-8

Kojarunchitt, T., Hook, S., Rizwan, S., Rades, T., & Baldursdottir, S. (2011). Development and characterisation of modified poloxamer 407 thermoresponsive depot systems containing cubosomes. *International journal of pharmaceutics, 408*(1-2), 20-26.

Koo, J., Lim, C., & Oh, K. T. (2024). Recent advances in intranasal administration for brain-targeting delivery: A comprehensive review of lipid-based nanoparticles and stimuli-responsive gel formulations. *International Journal of Nanomedicine*, 1767-1807.

Lino, M. E. S., Ruela, A. L. M., Trevisan, M. G., & Pereira, G. R. (2017). Influence of hydration and crosslinking in transdermal delivery of nicotine from chitosan-based gels by thermal analysis. *Journal of Thermal Analysis and Calorimetry, 130*(3), 1455-1461. doi: 10.1007/s10973-017-6129-3

Luppi, B., Bigucci, F., Cerchiara, T., & Zecchi, V. (2010). Chitosan-based hydrogels for nasal drug delivery: From inserts to nanoparticles. *Expert opinion on drug delivery, 7*(7), 811-828.

Ojeda-Hernández, D. D., Velasco-Lozano, S., Fraile, J. M., Mateos-Díaz, J. C., Rojo, F. J., Benito-Martín, M. S.,…Gomez-Pinedo, U. (2024). Thermosensitive chitosan-based hydrogel: A vehicle for overcoming the limitations of nose-to-brain cell therapy. *Acta Biomaterialia, 188*, 157-168. doi: https://doi.org/10.1016/j.actbio.2024.09.002

Østergaard, J., Meng-Lund, E., Larsen, S. W., Larsen, C., Petersson, K., Lenke, J., & Jensen, H. (2010). Real-time uv imaging of nicotine release from transdermal patch. *Pharmaceutical research, 27*, 2614-2623.

Peppas, N. A., Bures, P., Leobandung, W., & Ichikawa, H. (2000). Hydrogels in pharmaceutical formulations. *European journal of pharmaceutics and biopharmaceutics, 50*(1), 27-46.

Prochaska, J. J., & Benowitz, N. L. (2019). Current advances in research in treatment and recovery: Nicotine addiction. *Science advances, 5*(10), eaay9763.

Riaz, M., Zaman, M., Hameed, H., Sarwar, H. S., Khan, M. A., Irfan, A., Shazly, G. A.,…Jardan, Y. A. B. (2023). Lamotrigine-loaded poloxamer-based thermo-responsive sol–gel: Formulation, in vitro assessment, ex vivo permeation, and toxicology study. *Gels, 9*(10), 817.

Sayiner, O., Arisoy, S., Comoglu, T., Ozbay, F.G., & Esendagli, G. (2020). Development and in vitro evaluation of temozolomide-loaded plga nanoparticles in a thermoreversible hydrogel system for local administration in glioblastoma multiforme. *Journal of Drug Delivery Science and Technology*, 101627.

Stead, L. F., Perera, R., Bullen, C., Mant, D., Hartmann-Boyce, J., Cahill, K., & Lancaster, T. (2012). Nicotine replacement therapy for smoking cessation. *Cochrane database of systematic reviews*(11).

Thangarajoo, T., Hsin, Y. K., Pandey, M., Choudhury, H., Meng, L. W., Md, S.,…Gorain, B. (2023). A stimuli-responsive in situ spray hydrogel co-loaded with naringenin and gentamicin for chronic wounds. *Open Chemistry, 21*(1). doi: doi:10.1515/chem-2022-0357

Thirawong, N., Kennedy, R. A., & Sriamornsak, P. (2008). Viscometric study of pectin–mucin interaction and its mucoadhesive bond strength. *Carbohydrate Polymers, 71*(2), 170-179. doi: https://doi.org/10.1016/j.carbpol.2007.05.026

Uzaslan, E. (2003). Sigarayı bırakma yöntemleri. *Sted Journal of Continuing Medical Education, 12*(5), 166-171.

Wadgave, U., & Nagesh, L. (2016). Nicotine replacement therapy: An overview. *International journal of health sciences, 10*(3), 425.

Watts, P., & Smith, A. (2009). Pecsys: In situ gelling system for optimised nasal drug delivery. *Expert opinion on drug delivery, 6*(5), 543-552.

FABAD J. Pharm. Sci., 51, 1, 67-88, 2026
Doi: 10.55262/fabadeczacilik.1688795
RESEARCH ARTICLE

Analgesic and Anti-Inflammatory Activity of Ethanolic Extract of *Ipomoea Hederifolia* Linn

Kailas Krishnat MALI[*°], Nitin Hindurao SALUNKHE[**], Suraj Ashok SUTAR[***], Remeth Jacky DIAS[****], Balaji Dattatray JADHAV[*****]

Analgesic and Anti-Inflammatory Activity of Ethanolic Extract of Ipomoea Hederifolia Linn

SUMMARY

Pain and inflammation represent significant global health burdens, with plant-derived medicines contributing substantially to modern therapeutics. Ipomoea hederifolia L. has been traditionally employed for inflammation management, but scientific validation of its anti-inflammatory properties remains limited. This study systematically evaluates the analgesic and anti-inflammatory potential of I. hederifolia through comprehensive phytochemical characterization and preclinical pharmacological assessments. The ethanolic extract was prepared via continuous hot extraction and subjected to detailed phytochemical quantification (tannins, phenolics, alkaloids, flavonoids) and GC-MS analysis. Pharmacological evaluation included antioxidant capacity and protein denaturation inhibition in vitro, acute toxicity testing per OECD guidelines 423, acetic acid-induced writhing (peripheral analgesia), hot plate test (central analgesia), and carrageenan-induced paw edema (anti-inflammatory activity). Test groups received 200/400 mg/kg extract, compared against diclofenac (10/50 mg/kg) and tramadol (40 mg/kg) controls. Phytochemical analysis revealed substantial bioactive content (tannins 8.3%, flavonoids 8.02%). GC-MS identified 23 therapeutically relevant compounds correlating with observed bioactivities. The extract demonstrated potent DPPH radical scavenging activity (IC50 54.2 µg/mL) and 78.52% protein denaturation inhibition at 31.25 µg/mL. Significant analgesia occurred through both peripheral (57.3% writhing inhibition) and central (latency increase >150%) mechanisms, with dose-dependent anti-inflammatory effects (68.4% edema reduction). Remarkably, no toxicity was observed at 2000 mg/kg, indicating an exceptional safety profile for therapeutic development. This study provides conclusive pharmacological validation of I. hederifolia's traditional use, demonstrating its multifunctional therapeutic potential through robust antioxidant, analgesic, and anti-inflammatory activities. Further research should focus on compound isolation to fully realize its therapeutic value in pain and inflammation management.

Keywords: *Antioxidant, analgesic activity, anti-inflammatory activity, Ipomoea hederifolia.*

Ipomoea Hederifolia Linn'in Etanolik Ekstraktının Analjezik ve Anti-inflamatuar Aktivitesi

ÖZ

Ağrı ve inflamasyon, küresel sağlık açısından önemli bir yük oluşturmaktadır ve bitki kaynaklı ilaçlar modern tedavilere önemli katkı sağlamaktadır. Ipomoea hederifolia L. geleneksel olarak inflamasyonun tedavisinde kullanılmaktadır, ancak anti-inflamatuar özelliklerinin bilimsel olarak doğrulanması sınırlı kalmaktadır. Bu çalışma, kapsamlı fitokimyasal karakterizasyon ve preklinik farmakolojik değerlendirmeler yoluyla I. hederifolia'nın analjezik ve anti-inflamatuar potansiyelini sistematik olarak değerlendirmektedir. Etanolik ekstrakt, sürekli sıcak ekstraksiyon yoluyla hazırlanmış ve ayrıntılı fitokimyasal kantifikasyona (tanenler, fenolikler, alkaloidler, flavonoidler) ve GC-MS analizine tabi tutulmuştur. Farmakolojik değerlendirme, in vitro antioksidan kapasite ve protein denatürasyonu inhibisyonu, OECD kılavuzları 423'e göre akut toksisite testi, asetik asit kaynaklı kıvrılma (periferik analjezi), sıcak plaka testi (santral analjezi) ve karragenan kaynaklı pençe ödemi (antiinflamatuar aktivite) içermektedir. Test gruplarına 200/400 mg/kg ekstrakt verilirken, kontrol gruplarına diklofenak (10/50 mg/kg) ve tramadol (40 mg/kg) verildi. Fitokimyasal analiz, önemli miktarda biyoaktif içerik (tanenler %8,3, flavonoidler %8,02) olduğunu ortaya çıkarmıştır. GC-MS, gözlemlenen biyoaktivitelerle ilişkili 23 terapötik olarak önemli bileşik tespit etti. Ekstrakt, güçlü DPPH radikal temizleme aktivitesi (IC50 54,2 µg/mL) ve 31,25 µg/mL'de %78,52 protein denatürasyonu inhibisyonu gösterdi. Doz bağımlı antiinflamatuar etkilerle (ödemde %68,4 azalma) hem periferik (%57,3 kıvranma inhibisyonu) hem de merkezi (latens artışı >%150) mekanizmalar yoluyla önemli analjezi meydana geldi. Dikkat çekici bir şekilde, 2000 mg/kg'da herhangi bir toksisite gözlemlenmemiştir, bu da terapötik geliştirme için olağanüstü bir güvenlik profili olduğunu göstermektedir. Bu çalışma, I. hederifolia'nın geleneksel kullanımının kesin farmakolojik doğrulamasını sağlar ve güçlü antioksidan, analjezik ve antiinflamatuar aktiviteler yoluyla çok işlevli terapötik potansiyelini gösterir. İleri araştırmalar, ağrı ve inflamasyon yönetiminde terapötik değerini tam olarak gerçekleştirmek için bileşik izolasyonuna odaklanmalıdır.

Anahtar Kelimeler: *Antioksidan, analjezik aktivite, anti-inflamatuar aktivite, Ipomoea hederifolia.*

Recieved: 1.05.2025
Revised: 13.12.2025
Accepted: 16.12.2025

[*] ORCID: 0000-0002-1789-3592, Adarsh College of Pharmacy, Vita, A/p - 421/2, Near MIDC, Khambale (Bha.), Vita, Tal- Khanapur 415311 Dist- Sangli, Maharashtra, India
[**]ORCID: 0009-0002-1526-4423, Adarsh College of Pharmacy, Vita, A/p - 421/2, Near MIDC, Khambale (Bha.), Vita, Tal- Khanapur 415311 Dist- Sangli, Maharashtra, India
[***]ORCID: 0009-0009-8795-2672, Adarsh College of Pharmacy, Vita, A/p - 421/2, Near MIDC, Khambale (Bha.), Vita, Tal- Khanapur 415311 Dist- Sangli, Maharashtra, India
[****]ORCID: 0000-0002-8234-9630, Department of Pharmacy, Government College of Pharmacy, Karad 415124 Dist- Satara, Maharashtra, India
[*****]ORCID: 0009-0003-8727-0854, Adarsh College of Pharmacy, Vita, A/p - 421/2, Near MIDC, Khambale (Bha.), Vita, Tal- Khanapur 415311 Dist- Sangli, Maharashtra, India

[°] Corresponding Author; Dr. Kailas Krishnat Mali
E-mail: malikailas@gmail.com

INTRODUCTION

Pain and inflammation are widespread health concerns that, if unmanaged, may progress into chronic conditions like arthritis (Punchard, Whelan, & Adcock, 2004). Pain results from inflammatory mediators released after tissue injury or due to nerve compression from edema (Kidd & Urban, 2001). Similarly, inflammation involves biochemical changes such as cell membrane disruption, triggering arachidonic acid release. This activates cyclooxygenase (COX), producing thromboxanes and prostaglandins, key drivers of inflammation (Ijeoma, Aderonke, Ogbonna, Augustina, & Ifeyinwa, 2011).

Pain is a major global health issue, affecting an estimated 1 in 5 people worldwide, with an additional 1 in 10 adults diagnosed with chronic pain. Approximately 10% of the global population, around 60 million people, suffer from pain. In individual countries, the prevalence of pain ranges from 20% to 25% (Goldberg & McGee, 2011). Despite the availability of numerous medications for pain and inflammation, they remain among the most challenging and debilitating health issues, affecting 80% of adults globally. They are considered major clinical, social, and economic concerns in most communities worldwide (Yimer, Birru, Adugna, Geta, & Emiru, 2020). Prolonged, untreated pain is a pervasive disorder that can cause both physical damage and psychological issues (Krummenacher et al., 2014; Treede et al., 2019; Woolf, 2011). Uncontrolled inflammation not only hinders daily activities such as work, school, or social events but also accelerates the development of severe inflammatory diseases like rheumatoid arthritis, inflammatory bowel disease, atherosclerosis, and chronic periodontitis (Serhan & Levy, 2018). If left untreated, these debilitating illnesses are the primary causes of disability and can be fatal (Yimer et al., 2020).

Synthetic drugs are widely used for the treatment of pain and inflammation (Kidd & Urban, 2001; Punchard et al., 2004). Nonsteroidal anti-inflammatory drugs (NSAIDs) and opioid analgesics are commonly used for the treatment. However, these medications can cause numerous adverse effects (Grace, 1961; Punchard et al., 2004). These drugs cause various adverse effects such as nausea, vomiting, headache, dizziness, abdominal pain, indigestion, diarrhoea, and sickness (Sostres, Gargallo, Arroyo, & Lanas, 2010). They also lead to serious adverse effects, including hepatotoxicity (Sriuttha, Sirichanchuen, & Permsuwan, 2018), nephrotoxicity (Whelton, 1999), and gastrointestinal issues such as ulcers (Harirforoosh, Asghar, & Jamali, 2014). Therefore, herbal drugs can be a potential source to replace them. According to literature, alkaloids, flavonoids, steroids, and tannins exhibit analgesic and anti-inflammatory activity (Fan, Ali, & Basri, 2014; Ijeoma et al., 2011). Ipomoea species of plants have traditionally been employed to treat a wide range of ailments, including diabetes, constipation, hypertension, dysentery, arthritis, exhaustion, meningitis, rheumatism, kidney disease, and inflammation. Phytochemical analyses of the Ipomoea genus reveal that these plants possess antimicrobial, spasmogenic, hypotensive, anticancer, psychotomimetic, analgesic, and anti-inflammatory properties (Joel & Uwabunkeonye, 2020). Analgesic activity to some of the Ipomea species, such as Ipomoea imperati (Vahl.) Griseb. (Paula-Zurron et al., 2010), Ipomoea involucrate (Ijeoma et al., 2011), Ipomoea pes-caprae (Vieira et al., 2013), and Ipomoea pes-tigridis (Ramesh, 2010) are reported in the literature.

Ipomoea hederifolia L. (*I. hederifolia*), commonly known as "Jitirana," is a medicinal herb belonging to the family Convolvulaceae. It is also referred to as scarlet morning glory or scarlet creeper (Kurian, Banurekha, Venkateswarlu, & Kumar, 2023). While native to tropical and subtropical America, it is widely found in countries such as Brazil, Bangladesh, and India (Santos, Nurit-Silva, Arruda, & Leite, 2023). This plant features climbing, striated stems ranging from green to vinaceous, bright red corolla flowers, and simple, alternate, membranaceous, cordiform, or three-lobed leaves with semi-circular petioles around

7 cm long, resembling Ivy (Runner plant) (Santos et al., 2023). Phytochemical analysis reveals that *I. hederifolia* contains various constituents, including quinine, terpenoids, glycosides, alkaloids, steroids, flavonoids, saponins, and carbohydrates (Hossain, Uddin, Baral, Ferdus, & Bhowmik, 2022). The main chemical constituents include ergoline alkaloids, indolizidine alkaloids, nortropanic alkaloids, phenolic compounds, coumarins, norisoprenoids, diterpenes, isocoumarins, benzenoids, flavonoids, anthocyanosides, glycolipids, lignans, and triterpenes.

In traditional medicine systems, *I. hederifolia* is utilized for its hypotensive, anti-inflammatory, psychotomimetic, anticancer, laxative, diuretic, cathartic, and expectorant properties (Kurian et al., 2023; Meira, Silva, David, & David, 2012). Infusions and decoctions made from various parts of the plant, including the leaves, stems, roots, and fruits, are commonly used. They are employed as purgatives and treatments for tumors, dermatitis, rheumatism, nervous system issues, stomachaches, and intestinal parasites. The roots serve as a sternutatory, while the seeds can act as expectorants, diuretics, cathartics, and anti-inflammatory agents for conditions like constipation, edema, and parasitosis (Santos et al., 2023).

I. hederifolia has been traditionally used for its purported antinociceptive and anti-inflammatory effects, and preliminary phytochemical studies suggest the presence of bioactive compounds that may support these properties. However, no systematic scientific studies have yet validated its analgesic and anti-inflammatory potential. Therefore, this study aimed to evaluate the ethanolic extract of *I. hederifolia* for these activities using rodent models.

MATERIALS AND METHODS

Drugs and chemicals

Carrageenan, acetic acid, diclofenac, distilled water, tramadol, 1,1-diphenyl-2-picrylhydrazyl (DPPH), and egg albumin were obtained from the local vendors.

Collection, identification, and preparation of plant material

The *I. hederifolia* plant was collected in October 2023 from the roadside near the village of Khambale, Dist. Sangli 415311, Maharashtra, India. The plant was identified as *Ipomoea hederifolia* L. and confirmed by Dr. Shankar M. Shendage, Associate Professor, Department of Botany, Balwant College, Vita (Sangli), India. The voucher specimen (Specimen No. SS 002) has been deposited in the laboratory of Balwant College, Vita, for future reference.

Preparation of plant extract

After collecting the *I. hederifolia* plant, the material was washed under tap water, and the flowers were removed. The remaining plant parts were shade-dried for two weeks. The shade-dried material was then ground to obtain a coarse powder. For the extraction process, 40 grams of the powdered material was placed in a bag of cotton cloth, and the bag was kept in a glass thimble. Sufficient ethanol was added to the reservoir, and the hot continuous extraction process was initiated using a Soxhlet extractor at 70°C (K. Mali, Sutar, Devade, & Dias, 2019). This extraction continued until the ethanol in the thimble became colorless, which took about 6 hours. The ethanolic extract was then dried using a rotary evaporator, resulting in a brownish gummy residue. From 13 batches of 40 grams of crude *I. hederifolia* powder, a total of 38.1 grams of residue was obtained, yielding a percentage of 7.33%. The *I. hederifolia* extract (IHE) was stored in a desiccator for further use (Kaushik, Kumar, Kaushik, & Rana, 2012). The dry extract was dissolved in (0.5%) carboxymethyl cellulose (CMC) and administered orally to the animals as per body weight (AlRashdi et al., 2012).

Preliminary phytochemical screening of the extract

Standard phytochemical screening tests were carried out to detect the presence of secondary metabolites to relate the analgesic and anti-inflammatory activity of IHE with the presence or absence of active

constituents. Thus, the test for carbohydrate, tannin, saponin, flavonoid, alkaloid, quinine, terpenoid, glycoside, anthraquinone glycoside, triterpenoid, phenol, steroid, cardiac glycoside, and cyanogenic glycoside (Vanlalhruaia & Lalbiaknunga, 2020) was performed using reference procedures (Hossain et al., 2022).

Determination of alkaloids

A sample extract of I. *hederifolia* was prepared by dissolving 100 mg of plant extract in 10 mL of 2N hydrochloric acid and filtering. 1 mL of filtrate was transferred to a separating funnel and washed three times with 10 mL of chloroform. After washing, the extract was separated, and the pH was maintained at 7 by using 0.1 N sodium hydroxide. Solution of atropine sulphate (100 µg/mL) was prepared in distilled water. After preparation of the sample extract, 1 mL of the extract was mixed with 5 mL of pH 4.7 phosphate buffer. Subsequently, 5 mL of bromocresol green (BCG) was added, and the mixture was shaken with 1 mL, then 2 mL, 3 mL, and 4 mL of chloroform in a separating funnel. The chloroform layer extracts were collected in a 10 mL volumetric flask. If the volume is less than 10 mL, it was adjusted by adding chloroform. The same procedure was repeated for the standard solution of atropine sulphate at concentrations of 20 to 100 µg/mL to establish a calibration curve. The assay was compared with atropine equivalents. Finally, the absorbance of the chloroform layer containing the complex was measured at 470 nm against a blank prepared similarly but without the extract (Madhu, Sailaja, Satyadev, & Satyanarayana, 2016). This absorbance measurement allows for the determination of the concentration of the alkaloids in the sample extract.

Determination of flavonoids

A sample extract of *I. hederifolia* was prepared by dissolving 100 mg of plant extract in 100 mL of distilled water (1 mg/mL), and a solution of quercetin (100 µg/mL) was prepared in methanol. After preparation of the sample extract, 1 mL of the extract was mixed with 4 mL of distilled water in a 10 mL volumetric flask. Then, 0.3 mL of 5% sodium nitrite was added, followed by the addition of 0.3 mL of 10% aluminum chloride after 5 minutes. After another 5 minutes, 2 mL of 1M sodium hydroxide was added. The volume was then made up to 10 mL using distilled water. For the reference standard quercetin, solutions ranging from 10 to 100 µg/mL were prepared in the same manner as described above, without the sample extract. The absorbance of the resulting solutions was measured at 510 nm against a blank prepared similarly but without the sample extract. The assay is then expressed in terms of quercetin equivalent concentration (Chandran & Kavitha Chandran, 2016).

Determination of phenolics

A sample extract of *I. hederifolia* was prepared by dissolving 100 mg of plant extract in 100 ml of distilled water (i.e., 1 mg/mL), and a solution of gallic acid (100 µg/mL) was prepared in distilled water. Then 1 mL of the sample extract was mixed with 1 mL of Folin-Ciocalteu reagent (FC reagent). After 5 minutes, 10 mL of 7% sodium carbonate solution was added to the mixture. Distilled water was then added and mixed thoroughly to make up the volume to 25 mL in a volumetric flask. The mixture was kept in the dark for 90 minutes at 23 °C. After incubation, the absorbance of the sample extract and standard was measured at 760 nm against a blank. For the reference standard, gallic acid solutions ranging from 30 to 210 µg/mL were prepared in the same manner as described above. The total phenolic compound content is expressed as gallic acid equivalent concentration. (Chandran & Kavitha Chandran, 2016).

Determinations of tannins

A sample extract of *I. hederifolia* was prepared by dissolving 100 mg of plant extract in 100 mL of distilled water (i.e., 1 mg/mL), and a solution of tannic acid (100 µg/ml) was prepared in distilled water. In a 10 mL volumetric flask, 1 mL of sample extract was mixed with 7.5 mL of distilled water. Subsequently, 0.5 mL of Folin-Ciocalteu reagent was introduced, followed by the addition of 1 mL of 35% sodium car-

bonate solution. The flask was then filled to the 10 mL mark with distilled water and thoroughly shaken before being left at room temperature for 30 minutes. Meanwhile, a series of reference standard solutions containing tannic acid at concentrations of 20 to 100 µg/mL was prepared. Using a UV/Visible spectrophotometer, the absorbance of both the test and standard solutions was measured against a blank at 700 nm. The tannin content was quantified in terms of tannic acid equivalent concentration (Lahare, Yadav, Bisen, & Dashahre, 2021).

Gas chromatography-mass spectroscopy (GCMS) analysis

The ethanolic IHE was subjected to analysis using GC–MS (Shimadzu TQ 8050 Plus with HS 20, Japan), equipped with an automation tool AOC-20i+s, which was used for rinsing with pre-solvent 2 times, rinsing with post-solvent 2 times. Its injection port dwell time was 0.3 seconds with 5 times pumping. The washing volume was 8 µL. In the presence of purge flow of 3 mL/min, the pressure, column oven temperature, and injection temperature were maintained at 54.4 kPa, 50°C, and 260°C, holding time 2 minutes respectively. The column flow rate was maintained at 1.01 mL/min. Throughout the experiment run time of 4 min to 50 min, the injection mode was direct at a linear velocity of 36.5 cm/sec, and the injection temperature was 250 °C. The column oven temperature was 50°C. To have control of the system and acquire the data, we engaged the Shimadzu GC–MS solution software provided by the supplier. By comparing their mass spectra to data from the library NIST14.lib (National Institute of Standards and Technology), the compounds present in ethanolic IHE were identified (Willie, Uyoh, & Aikpokpodion, 2020).

DPPH radical scavenging activity

The antioxidant activity of the ethanolic extract of *I. hederifolia* was assessed using the scavenging activity of DPPH free radicals. Initially, a 0.1 mM DPPH solution was prepared by dissolving 10 mg of DPPH in 250 mL of methanol. Subsequently, 2 mL of the extract and standard ascorbic acid, each at various concentrations, were transferred to separate 10 mL volumetric flasks. To each volumetric flask, 3 mL of the DPPH solution was added. All samples of extract and ascorbic acid at different concentrations were covered with aluminium foil and incubated in a dark area for half an hour. After the 30-minute incubation period, the absorbance of each sample was measured using a UV-visible spectrophotometer at 517 nm. The DPPH solution without any extract or standard served as the control. The antioxidant activity of the extract was determined by calculating the reduction in DPPH absorbance compared to the control, using a suitable formula (Hossain et al., 2022).

$$Percentage\ of\ free\ radical\ DPPH\ scavenging = \frac{Ac - As}{Ac} \times 100 \qquad (01)$$

Where Ac is the absorbance of the control and As is the absorbance of the sample.

***In vitro* anti-inflammatory assay**

The assay was carried out with minor modifications in accordance with the procedures described by Mali et al. (Mali, Kokate, Ghorpade, Dias, & Mahajan, 2025). For the protein denaturation assay, egg albumin was prepared by diluting 1 mL of albumin in 10 mL of distilled water. Plant extracts and solutions of diclofenac were prepared at concentrations of 31.25 µg/mL to 1000 µg/mL in distilled water. Each reaction vessel was assembled with 0.2 mL of egg albumin, 1.4 mL of phosphate-buffered saline, and 1 mL of the test extract. For the negative control, distilled water was utilized. After 15 minutes of incubation at 37 °C, the mixtures were heated for 5 minutes at 70 °C. The absorbance was measured at 660 nm after cooling. The percentage inhibition of protein denaturation was calculated using the following formula:

$$\%Denaturation\ inbition = \frac{1 - D}{C} \times 100 \qquad (02)$$

Where D is the absorbance reading of the test sample, and C is the absorbance reading without the test sample (negative control).

Acute oral toxicity study

The extract of *I. hederifolia* was evaluated for its *in vivo* toxicological properties following the OECD guideline 423, which involves a single-dose 14-day acute oral toxicity study by using six healthy female Albino Wistar rats. Then the animals were kept fasting overnight, providing water only. After that, a 2000 mg/kg body weight aqueous solution with suspending agent (0.5%) CMC of IHE was administered orally by oral gavage. The dose volume of 10 mL/kg body weight was selected. Animals were observed individually after dosing at least once during the first 30 minutes, periodically during the first 24 hrs, with special attention given during the first 4 hrs. and daily thereafter, for a total of 14 days. The acute toxicity range of the test substance is determined based on the mortality status of the animals. This information assists in categorizing the toxicity level of the tested drug (OECD, 2002).

Experimental animals

Adult Wistar albino rats, weighing between 180 - 280 g, and Swiss albino mice, weighing between 20 - 35 g, of either gender were procured from National Institute of Biosciences 69, At Post Dhangawadi, Off Pune-Bangalore Highway, Tal Bhor, Dist Pune 412205 (1091/GO/BT/S/07/CPCSEA) and utilized for the study. The animals were housed in cages in rooms with regulated temperature, air-cooling, and a 12-hour light-dark cycle. They were provided with free access to water and a standard laboratory diet. A one-week acclimatization period to the laboratory conditions was allowed for the animals, and they were fasted overnight before the commencement of the experiments. The study protocol was approved by the Institutional Animal Ethics Committee of Biocyte Institute of Research and Development, Sangli, Maharashtra, India 416416 (IAEC/BiRD/Sangli/2024-25-03), and all experiments were conducted in accordance with the guidelines laid down by the Committee for the Purpose of Control and Supervision of Experiments on Animals (CPCSEA).

Animal grouping and dosing

Wistar albino rats and Swiss albino mice of either sex were randomly divided into four groups, each consisting of 6 rats and 6 mice, respectively. Group I served as the normal control and received distilled water only. Group II served as the positive control and was treated with standard drug tramadol (40 mg/kg, *p.o.*) for the hot plate test, diclofenac (50 mg/kg, *p.o.*) for the writhing test in mice, and diclofenac (10 mg/kg, *p.o.*) for the carrageenan-induced paw edema in rats. Groups III and IV were designated as test groups and received the IHE at doses of 200 and 400 mg/kg (*p.o.*), respectively. The doses were selected based on an acute toxicity study. All treatments were administered orally, and the maximum volume administered was 10 mL/kg.

Hot plate method

The Wistar albino rats were divided into four groups, each carrying six animals. Animals were fasted overnight prior to study, and each of them acclimatized to Eddy's hot plate for 5 min. After this, the hot plate temperature was maintained at 55°C, and then the rat was placed on it. The reaction time was recorded as the time taken for the rat to exhibit a response to the thermal pain, such as paw licking or jumping. Reaction times were recorded before (0 min) and at 30, 60, 90, and 120 min after the administration of the test extracts and standard drug (Tramadol). A maximum reaction time of 45 seconds was set to prevent any injury to the rats (Greene, 1972; Kumar, Singh, Pranav, & Ray, 2011). If the recorded reaction time exceeded 45 seconds, the animal was immediately removed from the hot plate, and it was considered to have reached maximum analgesia (Raveendran et al., 2019).

The maximum possible analgesia (MPA) was calculated as follows:

$$MPA = \frac{Reaction\ time\ for\ treatment - Reaction\ time\ for\ control}{(45\,\mathrm{sec} - Reaction\ time\ for\ control)} \times 100 \quad (03)$$

Acetic acid-induced writhing test

The writhing model is a chemical nociceptive test involving the intraperitoneal injection of irritating compounds into animals to induce peritonitis. Swiss albino mice were divided into four groups, each carrying six mice, and fasted overnight prior to the study. In this study, intraperitoneal injection of 10 mg/kg of a 0.6% acetic acid solution was administered 30 minutes after drug administration. Each mouse was placed into a glass beaker, and a five-minute observation period was allowed. The number of writhes, characterized by stretching of the abdomen and at least one hind limb simultaneously, was recorded for 10 minutes of observation. The writhing percentage was calculated and compared to the standard (Kaushik et al., 2012).

$$\%\ inhibition\ of\ writhing = \frac{Mean\ number(control) - Mean\ number(test)}{Mean\ number(control)} \times 100 \quad (04)$$

Carrageenan-induced paw edema method

Rats were divided into four groups, each containing six rats. Inflammation was induced in the left hind paw using carrageenan (1% carrageenan suspended in 0.9% NaCl) injected in subplantar region. The test drug, normal saline, and standard drug were administered to the rats before one hour of giving carrageenan injection. Group I served as the normal control and received the vehicle, group II served as the positive control and received the standard drug, and group III-IV received the test extract. Paw volume was measured using the volume displacement technique with a plethysmometer apparatus. Paw volume was measured immediately after carrageenan injection and after 30, 60, 90, 120, and 150 minutes. The percentage inhibition of inflammation was calculated using the following ratio (Ijeoma et al., 2011)**:**

$$Percentages\ inhibition\ of\ inflammation = \frac{[(Vt - Vo)control - (Vt - Vo)]test}{(Vt - Vo)control} \times 100 \quad (05)$$

Where Vt is the average volume for each group after treatment, and Vo is the average volume for each group before any treatment.

Statistical analysis

Results are expressed as mean ± Standard Error of Mean (SEM). Data was analysed using GraphPad Prism software version 10.1.0. Comparison between different groups was done by One-Way Analysis of Variance (ANOVA) followed by Tukey's test. A *p*-value less than 0.05 was considered statistically significant.

RESULTS

Preliminary phytochemical screening

Preliminary phytochemical screening of the extract (Table 1.) revealed the absence of anthraquinone glycosides and cyanogenic glycosides. However, the analysis confirmed the presence of multiple bioactive compounds, including carbohydrates, tannins, saponins, flavonoids, alkaloids, quinine, terpenoids, glycosides, triterpenoids, phenols, steroids, and cardiac glycosides. These findings suggest that IHE contains phytoconstituents potentially responsible for analgesic and anti-inflammatory effects.

Table 1. Results of preliminary phytochemical screening

Sr. No.	Phytoconstituent	Test name	Observation	Result
1	Carbohydrate	Benedict test	Reddish brown colour	+ ve
		Molisch test	Reddish or purple colour	+ ve
2	Tannin	Ferric chloride test	Green or black colour	+ ve
3	Saponin	Foam test	White foam	+ ve
4	Flavonoid	Shinoda test	Magneta or red colour	+ ve
5	Alkaloid	Mayer's test	Yellow colour	+ ve
		Wagner's test	Brown or reddish colour	+ ve
		Dragendroff test	Orange-red colour	+ ve
6	Quinine	Test for quinine	Red hue obtained	+ ve
7	Terpenoids	Salkowski test	Reddish brown colour	+ ve
8	Glycoside	Bromine water test	Yellow colour	+ ve
9	Anthraquinone Glycoside	Bontrager's test	Pink, Violet, or red colour	- ve
10	Triterpenoid	Liebermann Burchard test	Deep red colour	+ ve
11	Phenol	Ferric chloride test	Green colour	+ ve
12	Steroid	Salkowski test	Brown colour	+ ve
13	Cardiac glycoside	Test for cardiac glycoside	Blood red colour	+ ve
14	Cyanogenic glycoside	Picrate-impregnated paper test	Picrate-impregnated paper colour changes	- ve

+ ve: positive; -ve: negative

Quantitative estimation of phytoconstituents

Quantitative analysis of phytoconstituents in IHE is presented in Table 2. Tannins, phenolic compounds, alkaloids, and flavonoids were quantified and expressed as gram percentage (gm%) relative to standard reference compounds. The analysis revealed a higher concentration of tannins compared to phenolic compounds in the extract.

Table 2. Total secondary metabolite content in gm% equivalent to standards

Phytoconstituent	According to the calibration curve of the standard	Result expressed for the extract in	Secondary metabolites (gm%)
Tannins	Tannic acid	gm% equivalent to tannic acid	8.332
Phenolic compounds	Gallic acid	gm% equivalent to gallic acid	4.928
Alkaloids	Atropine sulphate	gm% equivalent to atropine sulphate	7.186
Flavonoids	Quercetin	gm% equivalent to quercetin	8.021

Gas chromatography mass spectrometry analysis

GC-MS analysis of *I. hederifolia* extract (Figure 1.) identified 73 compounds through NIST14 library matching. Among these, 23 bioactive compounds with established pharmacological properties are presented in Table 3. The majority of these identified compounds demonstrate significant antioxidant, analgesic, and anti-inflammatory activities.

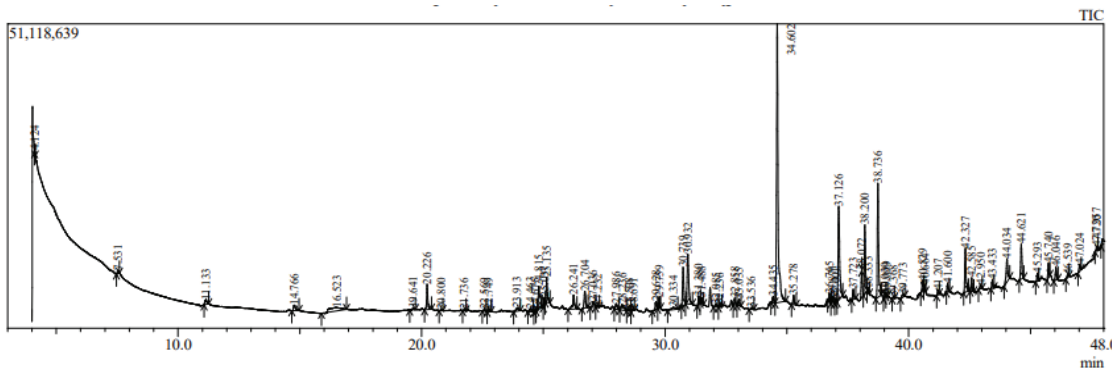


Figure 1. GCMS Chromatogram of the ethanolic extract of *I. hederifolia*

Table 3. Bioactive compounds present in the ethanolic extract of *I. hederifolia*

RT	Compound	Class	Area %	Activity	Reference
11.133	Propane, 1,1,3-triethoxy-	Retinaldehyde	0.53	Antioxidant activity, Anti-inflammatory, Upper respiratory infections.	(Willie et al., 2020)
14.766	Dodecane	Alkane	0.65	Antibacterial activity	(Padma et al., 2019)
20.226	Tetradecane	Alkane	1.81	Antimicrobial Activity, Wound healing activity, Anti-viral and Antitumor activities	(Velmurugan & Anand, 2017)
22.749	Pentadecane	Alkane	0.19	Anti-inflammatory, Analgesic, and Antipyretic	(Okechukwu, 2020)
23.913	2(4H)-Benzofuranone, 5,6,7,7a-tetrahydro-4,4	Benzofurans	0.42	Antimicrobial	(Mujeeb, Bajpai, & Pathak, 2014)
24.463	9,19-Cyclolanostan-3-ol, acetate, (3. beta.)-	Triterpenoid	0.29	Anti-mosquito larvicidal activity	(Ali, Mohammed, & Imad, 2016)
25.135	Hexadecane	Alkane	1.82	Antibacterial, Antioxidant activities	(Velmurugan & Anand, 2017)
28.236	1,1,4,7-Tetramethyldeca-hydro-1H-cyclopropa [e] azulene-4,7-diol	Azulene	0.82	Antioxidant, Antimicrobial	(Willie et al., 2020)
28.661	Thunbergol	Diterpene alcohol	0.08	Antidiabetic, Anticancer, Analgesic, anti-inflammatory, and Antimicrobial.	(Shah et al., 2023)
29.628	Tetradecanoic acid, ethyl ester	Fatty acid ester	0.62	Antioxidant, Anticancer, Nematicide, Hypocholesterolemic, Lubricant.	(Krishnamoorthy & Subramaniam, 2014)
30.739	Neophytadiene	Sesquiterpene	3.05	Analgesic, Anti-inflammatory, Antimicrobial, Antioxidant, Antifungal	(Pratama, Tunjung, Sutikno, & Daryono, 2019; Willie et al., 2020)
31.380	3,7,11,15-Tetramethyl-2-hexadecen-1-ol	Terpene alcohol	0.49	Anti-inflammatory, Antioxidant, and Analgesic	(Musa et al., 2022; Rajeswari, Murugan, & Mohan, 2012)

RT	Compound	Class	Area %	Activity	Reference
33.035	Hexadecanoic acid, methyl ester	Fatty acid ester	0.45	Anti-inflammatory, Hypocholesterolemic, Cancer preventive, Hepatoprotective, Nematicide, Insectifuge, Antihistaminic, Antieczemic, Antiacne, Alpha reductase inhibitor, Antiandrogenic, Antiarthritic, Anti coronary, Antifibrotic.	(Krishnamoorthy & Subramaniam, 2014; Usha et al., 2021)
33.536	Isophytol	Terpenoid alcohol	0.15	Anti-inflammatory and Antioxidant	(Musa et al., 2022)
34.602	Hexadecanoic acid, ethyl ester	Fatty acid ester	25.18	Antioxidant activities and Anti-inflammatory	(Musa et al., 2022; Sheela & Uthayakumari, 2013)
35.278	E, E, Z-1,3,12-Nonadeca-triene-5,14-diol	Fatty alcohol	0.76	Antimicrobial activity	(Mohammed, Ghaidaa, & Imad, 2016)
36.871	9-Octadecenoic acid, methyl ester, (E)-	Fatty acid ester	0.47	Anti-inflammatory, Antiandrogenic cancer preventive, Dermatitigenic hypocholesterolemic, 5-alpha reductase inhibitor, Anemiagenic, Insectifuge	(Krishnamoorthy & Subramaniam, 2014)
37.126	Phytol	Diterpene	8.76	Anticancer, Antioxidant, Anti-inflammatory, Diuretic, Antitumor, Chemopreventive, Antimicrobial, Use in vaccine formulations.	(Krishnamoorthy & Subramaniam, 2014; Musa et al., 2022; Sheela & Uthayakumari, 2013; Velmurugan & Anand, 2017; Willie et al., 2020)
38.333	(E)-9-Octadecenoic acid ethyl ester	Fatty acid ester	0.21	Steroids, fertility.	(Idu, Aihiokhai, Imoni, Akokigho, & Olali, 2021)
38.736	Octadecanoic acid, ethyl ester	Saturated fatty acid ethyl ester	8.73	Antioxidant, Anti-inflammatory, Antifungal, Antitumor, Antibacterial	(Ganesh & Mohankumar, 2017; Idu et al., 2021)
41.600	4,8,12,16-Tetramethylhepta-decan-4-olide	Diterpenoid	0.57	Anticancer	(Pratama et al., 2019)
42.327	Methyl 19-methyl-eicosa-noate	Fatty acid ester	3.48	Antifungal and antigenotoxic	(Ganesh & Mohankumar, 2017)
49.900	Squalene	Triterpene	1.37	Antioxidant, Antistatic, Antibacterial, Anticancer, Antitumor.	(Sheela & Uthayakumari, 2013; Willie et al., 2020)

DPPH radical scavenging activity

The antioxidant potential of *I. hederifolia* was evaluated using the DPPH free radical scavenging assay. As shown in Figure 2, the extract demonstrated concentration-dependent antioxidant activity, with percentage inhibition increasing proportionally with extract concentration. The maximum inhibition of 83.87% was observed at 250 µg/mL, while the minimum inhibition (36.95%) occurred at 1.9 µg/mL. The IC_{50} value of the extract (54.2 µg/mL) was significantly higher than that of ascorbic acid (2.28 µg/mL), indicating comparatively lower antioxidant potency relative to the reference standard.

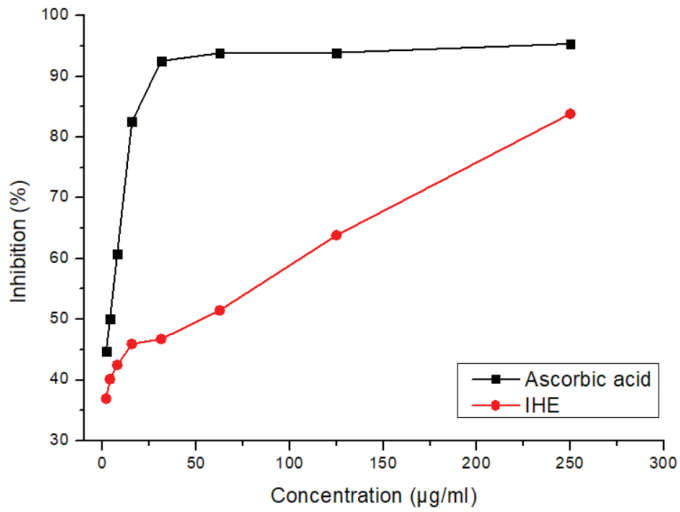


Figure 2. DPPH radical scavenging activity of ethanolic extract of *I. hederifolia* and ascorbic acid

***In vitro* anti-inflammatory assay**

The *in vitro* anti-inflammatory activity of IHE was assessed using the protein denaturation assay. As illustrated in Figure 3, both IHE and the reference standard (diclofenac sodium) exhibited concentration-dependent inhibition of protein denaturation. At the highest tested concentration (1000 µg/mL), IHE demonstrated 89.21% inhibition compared to 95.19% for diclofenac. Similarly, at the lowest concentration (31.25 µg/mL), the inhibition percentages were 78.52% for IHE and 81.30% for the standard drug, indicating comparable dose-response profiles between the test extract and positive control.

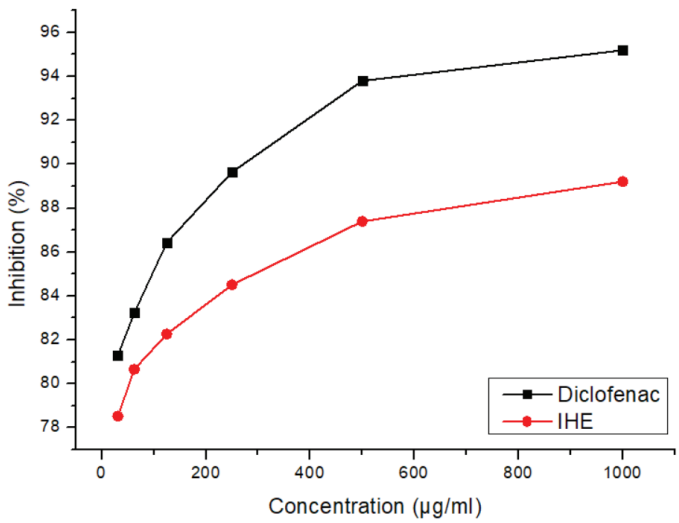


Figure 3. Comparison of protein denaturation inhibition by diclofenac and ethanolic extract of *I. hederifolia*

Acute oral toxicity study

The acute oral toxicity study revealed no adverse effects at the maximum tested dose (2000 mg/kg). All animals survived the observation period with normal food intake and body weight gain. Comprehensive clinical evaluations, including assessments of skin, fur, eyes, mucous membranes, respiratory function, and neurological status (with particular attention to tremors, convulsions, and coma), showed no abnormalities. Behavioral patterns and autonomic functions remained unaffected, with no signs of toxicity or mortality observed. Based on these results, doses of 200 mg/kg (10% of the maximum dose) and 400 mg/kg were selected for subsequent analgesic and anti-inflammatory evaluations.

Hot plate test

The results of the analgesic effect by using the hot plate method are shown in Table 4 and Figure 4. This method was performed to determine the central analgesic activity of IHE in rats. Low dose of IHE showed significant (p<0.05) central analgesic activity by delaying the reaction time at 30-minutes time interval of observation as compared with the normal control (Figure 4.). Similarly, all other groups showed significant (p<0.001) analgesic activity at 30, 60, 90, and 120-minutes time intervals when compared with the normal control group. At a 90-minutes time interval the low-dose extract showed significant (p<0.05) analgesic activity when compared with the standard drug, and the high-dose extract showed significant (p<0.001) analgesic activity. The intergroup comparison between low-dose and high-dose extract showed significant (p<0.05) analgesic activity at a 30-minutes time interval. The maximum possible analgesic activities were observed at 60 minutes for extracts 200 mg/kg and 400 mg/kg which were 39.45% and 52.35% respectively, as compared with the standard drug (tramadol 40 mg/kg), which produced 56.95% analgesic activity. The maximum analgesic activities observed at 90 minutes for extracts 200 mg/kg and 400 mg/kg were 31.87% and 75.54% respectively, as compared with the standard drug (tramadol 40 mg/kg) that produced 79.05% analgesic activity.

Table 4. Effect of ethanolic extract of *I. hederifolia* on hot plate latency time in rats

Group	**Normal Control**	**Standard**		**Low-dose extract**		**High dose extract**	
Drug	Distilled water	Tramadol		IHE		IHE	
Dose	10 mL/kg	40 mg/kg		200 mg/kg		400 mg/kg	
Time (Min)	**Paw licking and jumping response (Sec) ± SEM and % MPA**						
0	16.90±0.47	17.84±1.03	3.36%	24.69±3.88	27.74%	22.17±3.11	18.75%
30	17.02±0.36	26.05±1.65$^{\#c}$	32.25%	28.82±3.68$^{\#a*a}$	42.17%	26.04±2.74$^{\#c*a}$	32.24%
60	17.32±0.57	33.08±2.05$^{\#c}$	56.95%	28.24±3.25$^{\#c}$	39.45%	31.81±2.80$^{\#c}$	52.35%
90	17.76±0.61	39.29±1.21$^{\#c}$	79.05%	26.45±3.61$^{\#c\dagger a}$	31.87%	38.34±1.91$^{\#c\dagger c}$	75.54%
120	17.19±0.62	40.11±3.41$^{\#c}$	82.42%	18.64±1.33$^{\#c}$	05.19%	23.55±1.95$^{\#c\dagger c}$	22.84%

Values represent mean ± standard error of the mean; n=6, analysis was performed using One-Way ANOVA followed by Tukey's multiple comparison test, p value less than 0.05 was considered statistically significant. a: p<0.05, b: p<0.01, c: p<0.001, #: Data compared with control, †: Data compared with standard treatment, *: Data compared with low dose and high dose.

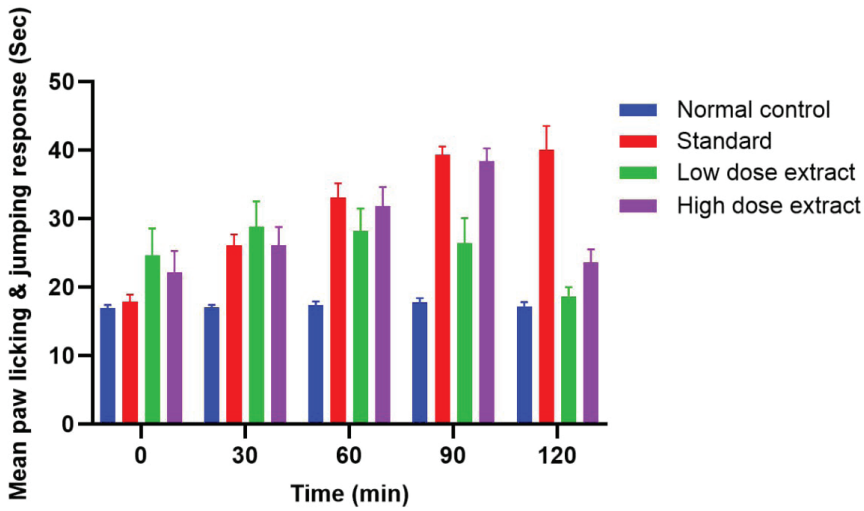


Figure 4. Comparison between groups vs mean response (sec) of the hot plate method

Acetic acid-induced writhing test

The results of the acetic acid-induced writhing test model in mice by using ethanolic IHE are shown in Table 5 and Figure 5. In this test, IHE at both test doses (i.e., 200 and 400 mg/kg) showed statistically significant (p<0.05) peripheral analgesic activity in a dose-dependent manner as compared to the normal control. High-dose (400 mg/kg) of the extract produced significant (p<0.001) protection against the number of writhings induced by acetic acid. The extent of reduction of writhing in the different doses of the extract was different, i.e., significantly lower in 200 mg/kg (p<0.01) and comparable with 400 mg/kg (p<0.001) as compared to the standard drug of 50 mg/kg (p<0.001) diclofenac sodium.

Inter-group comparison between the two extract doses does not show a statistically significant (p > 0.05) difference. The high dose of IHE (400 mg/kg) along with the standard drug (diclofenac sodium 50 mg/kg) showed comparable % protection of the numbers of writhing with percentage protection values of 50.23 % and 57.20 % respectively.

Table 5. Effect of the ethanolic extract of *I. hederifolia* on acetic acid-induced writhing in mice

Group	Drug	Dose	Mean number of writhing ± SEM	% Protection
Normal Control	Normal Saline	10 mL/kg	35.83±2.76	0
Standard	Diclofenac Sodium	50 mg/kg	15.33±1.11$^{\#c}$	57.20
Low dose IHE	IHE	200 mg/kg	24.66±1.52$^{\#b\dagger b}$	31.16
High dose IHE	IHE	400 mg/kg	17.83±1.25$^{\#c}$	50.23

Values represent mean ± standard error of the mean; n=6, analysis was performed using One-Way ANOVA followed by Tukey's multiple comparison test, p value less than 0.05 was considered statistically significant. a: $p<0.05$, b: $p<0.01$, c: $p<0.001$, #: Data compared with control, †: Data compared with standard treatment.

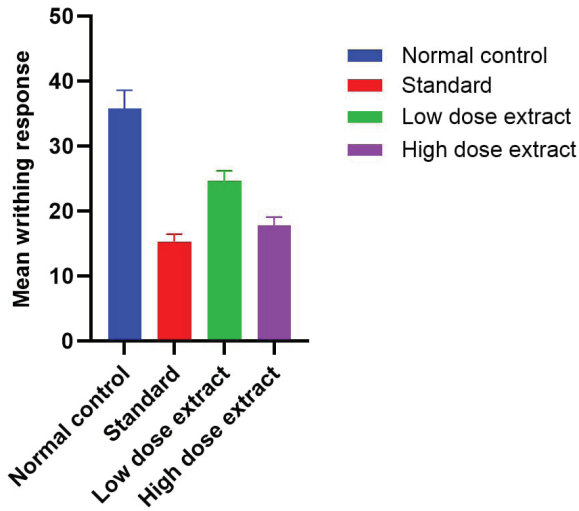


Figure 5. Comparison between groups and the mean number of writhing in the writhing test

The carrageenan-induced paw edema method

The results of the anti-inflammatory effect by using the carrageenan-induced paw edema method are shown in Table 6 and Figure 6. This method was performed to determine the acute inflammatory activity of IHE in rats. The mean paw volume was taken 60 minutes before each carrageenan induction. The results showed that low dose (200 mg/kg), high dose (400 mg/kg) of IHE and standard drug (Diclofenac 10 mg/kg) at 60, 90, 120,150 minutes showed significant (p<0.001) anti-inflammatory activity as compared with the control group. Low dose of extract at 120 minutes showed significant (p<0.05) anti-inflammatory activity as compared to the standard. Both low and high doses of extract at 150 minutes showed significant (p<0.001) anti-inflammatory activity. The inter-group comparison between low-dose and high-dose extract showed significant (p<0.05) anti-inflammatory activity. The maximum anti-inflammatory activity at 150 minutes of low-dose and high-dose extracts showed 52.77 % and 61.69 % respectively, as compared with the standard drug that produced 74.69 %.

Table 6. Effect of ethanolic IHE on carrageenan-induced paw edema method

Group	**Normal Control**	**Standard**		**Low-dose extract**		**High dose extract**	
Drug	Distilled water	Diclofenac		IHE		IHE	
Dose	10 mL/kg	10 mg/kg		200 mg/kg		400 mg/kg	
Time (min)	**Mean paw volume (CC) ± SEM and % Inhibition**						
-60	0.383±0.014	0.372±0.02		0.418±0.008		0.412±0.003	
30	0.740±0.009	0.728±0.009	0.28%	0.779±0.016	-1.12%	0.751±0.025	5.04%
60	0.815±0.012	0.701±0.021$^{\#c}$	23.84%	0.745±0.020$^{\#a*a}$	24.30%	0.690±0.007$^{\#c*a}$	35.64%
90	0.810±0.011	0.686±0.008$^{\#c}$	26.46%	0.682±0.02$^{\#c}$	38.17%	0.642±0.014$^{\#c}$	46.13%
120	0.801±0.005	0.608±0.010$^{\#c}$	43.54%	0.664±0.02$^{\#c\dagger a}$	41.15%	0.620±0.014$^{\#c}$	50.24%
150	0.798±0.015	0.477±0.015$^{\#c}$	74.69%	0.614±0.017$^{\#c\dagger c}$	52.77%	0.571±0.007$^{\#c\dagger c}$	61.69%

Values represent mean ± standard error of the mean; n=6, analysis was performed using One-Way ANOVA followed by Tukey's multiple comparison test, p value less than 0.05 was considered statistically significant. a: p<0.05, b: p<0.01, c: p<0.001, #: Data compared with control, †: Data compared with standard treatment, *: Data compared of low dose and high dose.

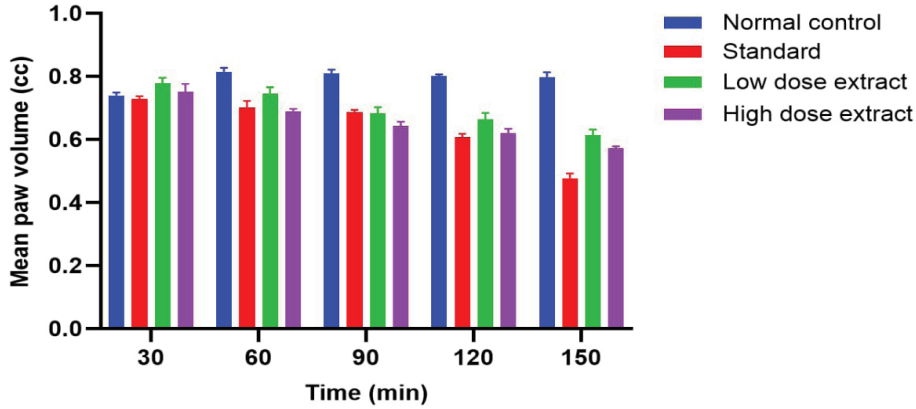


Figure 6. Comparison between groups vs. the mean paw volume of inflammation

DISCUSSION

The literature survey revealed that the herb *I. hederifolia* has been used as a traditional medicine for the treatment of inflammation (Kurian et al., 2023). The herb contains alkaloids, flavonoids, tannins, steroids, *etc* phytoconstituents which are responsible for analgesic and anti-inflammatory activity (Fan et al., 2014; Ijeoma et al., 2011). Thus, the present study was designed to evaluate traditional claims for the above-mentioned use of *I. hederifolia*.

The results showed significant analgesic and anti-inflammatory effects, which can be attributed to the presence of bioactive compounds within the extract. These effects were evaluated through *in vitro* assays, including protein denaturation and antioxidant assay, complemented by phytochemical screening, GC-MS analysis, *in vivo* study of analgesic effect evaluated by hot plate method and acetic acid induced writhing method, and anti-inflammatory effect evaluated by carrageenan-induced paw edema method.

The phytochemical analysis of ethanolic IHE revealed the presence of various bioactive compounds such as carbohydrates, alkaloids, tannins, saponins, flavonoids, cardiac glycosides, anthraquinone, steroids, phenol, triterpenoids, and glycosides. The quantitative study of IHE shows tannins 8.33%, flavonoids 8.02%, phenolics 4.93%, and alkaloids 7.18%, respectively. These results indicated that the ethanolic extract contains a high % of tannins and flavonoids.

The percentages of phenolics and flavonoids were found to be higher than those reported previously for the leaves of the plant (Suchiang, Devi, Zuala, & Shantabi, 2024). According to the literature, alkaloids, flavonoids, steroids, and tannins show analgesic and anti-inflammatory activity (Fan et al., 2014; Ijeoma et al., 2011). The presence of these compounds supports the pharmacological activities of the extract. Flavonoids and steroids act by inhibiting prostaglandin production, which inhibits pain and inflammation (Rafieian-kopaei, Shakiba, Sedighi, & Bahmani, 2017). GCMS analysis showed that most of the compounds present in IHE possess antioxidant, analgesic, and anti-inflammatory activity. Previous phytochemical studies have reported that *I.* hederifolia contains several bioactive constituents, including the pyrrolizidine alkaloids ipanguline and isoipanguline; the nortropane alkaloids calystegines B1 and B2, known for their glycosidase inhibitory activity; as well as cyanogenic glycosides, ergoline derivatives, isoenzymes, and hederifolic acids A–D, which are peracetylated glycosidic acid derivatives classified as resin glycosides (Ravikumara, Kaveri, & Umesha, 2025). The synergistic action of these phytochemicals may contribute to the overall analgesic and anti-inflammatory activity of the IHE (Fan et al., 2014; Ijeoma et al., 2011).

Oxidative stress is a major contributor to inflammation and pain, as excessive free radical generation

amplifies inflammatory signalling and tissue injury. Antioxidants play a crucial role in mitigating oxidative stress by neutralizing these reactive species. The ethanolic extract of IHE exhibited dose-dependent DPPH free radical scavenging activity comparable to that of ascorbic acid. However, since this study employed only the DPPH assay, the observed results represent the extract's potential for DPPH radical neutralization and do not reflect its overall antioxidant capacity, which would require evaluation through additional assays based on different mechanisms. The IC_{50} value obtained for the extract was higher than that reported by Suchiang et al. (2024), which may be attributed to variations in plant collection, extraction methods, and processing conditions. The antioxidant property of *I. hederifolia* may contribute to its analgesic and anti-inflammatory effects by reducing oxidative stress and preventing cellular damage. These protective effects, together with possible direct protein stabilization mechanisms (Hossain et al., 2022), may underlie the extract's efficacy in managing pain and inflammation. Future studies employing assays such as ABTS, FRAP, or ORAC, which operate through different antioxidant mechanisms, are warranted to provide a more comprehensive evaluation of the antioxidant potential of *I. hederifolia*.

Protein denaturation is a process in which proteins lose their tertiary and secondary structures, leading to loss of function. Inflammation involves the denaturation of proteins, but bioactive compounds present in IHE may inhibit protein denaturation and therefore, can be considered as potential anti-inflammatory agents (Osman, Sidik, Awal, Adam, & Rezali, 2016). The ethanolic IHE shows dose-dependant protein denaturation as compared with the standard drug diclofenac. The protein denaturation inhibition percentage of IHE was found to be 78.52% to 89.20% and standard diclofenac was 81.30% to 95.19%, respectively. This indicates that the IHE contains bioactive compounds that may stabilize proteins and prevent their denaturation, thereby exhibiting anti-inflammatory properties. It suggests that IHE may show therapeutic potential in treating inflammatory conditions.

The hot plate test measures the paw licking and jumping response to thermal pain, which indicates central analgesic activity. The IHE significantly (P<0.05) increased the pain threshold in low-dose (200mg/kg) animals at 30-minutes times compared to the normal control group. Similarly, all other low and high dose of IHE at 30, 60, 90, 120 minutes shows very significant (p<0.001) analgesic activity that suggesting the involvement of central mechanisms like activation of μ-receptor at supraspinal sites, $_{K}$-receptor within the spinal cord and δ-receptor involved at both spinal and supraspinal level (Fan et al., 2014; Faujdar, Sharma, Sati, Pathak, & Paliwal, 2016). At a 90-minute time interval, the low-dose extract shows significant (p<0.05) analgesic activity when compared with the standard drug, and the high-dose extract shows very significant (p<0.001) analgesic activity. The maximum possible analgesia at a 90-minute time interval was less than 50% analgesic activity in low-dose extract, while the high-dose extract showed 75.54% activity. Similarly, standard drug tramadol showed 82.42% analgesic activity at a 120-minute time interval. It suggests that IHE showed time-dependent analgesic activity at a specific time level, but after a certain time, there is a decrease in activity.

The acetic acid-induced writhing test measures the number of writhes in response to an irritant, which is indicative of peripheral analgesic activity. This activity may be mediated through the inhibition of COX or lipoxygenase enzyme (Faujdar et al., 2016). Both low (200 mg/kg) and high (400 mg/kg) dose of IHE shows dose-dependent reduction in the number of writhes, implying that it possesses peripheral analgesic properties compared to the normal control group. Both doses of IHE show significant results as compared to the normal control group at P<0.05. Standard drug shows a significant result as compared to the low-dose extract at P<0.05.

The analgesic effects observed in IHE may be due to the modulation of endogenous opioid pathways, inhibition of pain mediators, or anti-inflammatory properties that reduce the underlying cause of pain (Tracey & Mantyh, 2007). It suggests that both the hot plate method and the acetic acid-induced writhing test method show the analgesic effect of ethanolic IHE. According to the study observation in both studied models, IHE shows a significant analgesic effect. From this, we conclude that the extract has central as well as peripherally acting analgesic effects.

The carrageenan-induced paw edema model is used to evaluate acute inflammation. The IHE significantly reduced paw edema in treated rats, which indicates its effectiveness in reducing acute inflammatory responses. Inflammation is inhibited by COX-2 inhibitors, which leads to inhibition of prostaglandins (Wani et al., 2012). This reduction suggests the inhibition of mediators like histamine, serotonin, and prostaglandins, which are involved in the early phase of inflammation (Kaushik et al., 2012; Rafieian-kopaei et al., 2017). According to these mechanisms, our extract may show an anti-inflammatory effect.

Previous studies on other *Ipomoea* species, such as *Ipomoea pes-caprae* (Vieira et al., 2013) and *Ipomoea involucrate* (Ijeoma et al., 2011), have reported significant antinociceptive activity and anti-inflammatory activities. These findings support the possibility that similar bioactive constituents present in *I. hederifolia* may contribute to its observed analgesic and anti-inflammatory effects in the present study.

The overall study of ethanolic IHE shows no toxicity and promising analgesic and anti-inflammatory activity.

CONCLUSION

The present study provides compelling scientific evidence supporting the traditional use of *I. hederifolia* for pain and inflammation management. The ethanolic extract demonstrated significant antioxidant, analgesic, and anti-inflammatory activities, which were attributed to its rich phytochemical composition, including tannins, phenolics, alkaloids, and flavonoids. GC-MS analysis identified 23 bioactive compounds that likely contribute to these pharmacological effects.

The extract exhibited dual analgesic mechanisms (both central and peripheral) in rodent models and showed dose-dependent anti-inflammatory activity in the carrageenan-induced paw edema test. Importantly, acute toxicity studies revealed an excellent safety profile at doses up to 2000 mg/kg, suggesting its potential therapeutic window.

These findings validate the ethnomedicinal claims of *I. hederifolia* and highlight its potential as a source of novel bioactive compounds for developing natural analgesic and anti-inflammatory agents. Future studies should focus on isolating and characterizing the active constituents, elucidating their molecular mechanisms, and evaluating clinical efficacy.

ACKNOWLEDGEMENTS

The authors express their sincere gratitude to Adv. Vaibhav (Dada) Patil, President of the Loknete Hon. Hanmantrao Patil Charitable Trust, Vita, for providing the necessary facilities to conduct this research. The authors also acknowledge Dr. Sandip Patil from Biocyte, Sangli, for his valuable assistance with the in vivo studies. Shivaji University, Kolhapur, is acknowledged for assistance with analytical work.

FUNDING

The authors acknowledge that they received no funding in support of this research.

AUTHOR CONTRIBUTION STATMENT

Developing hypothesis (K.K.M., S.A.S), experimenting and statistics (K.K.M., B.D.J.), study text (B.D.J), literature research (S.A.S), interpretation of the data and reviewing (N.H.S., R.J.D.).

CONFLICT OF INTEREST

The authors declare that there is no conflict of interest.

REFERENCES

Ali, H. A. M., Mohammed, Y. H., & Imad, H. H. (2016). Determination of metabolites products by Cassia angustifolia and evaluate antimicobial activity. *Journal of Pharmacognosy and Phytotherapy*, *8*(2), 25–48. https://doi.org/10.5897/JPP2015.0367

AlRashdi, A. S., Salama, S. M., Alkiyumi, S. S., Abdulla, M. A., Hadi, A. H. A., Abdelwahab, S. I., … Asykin, N. (2012). Mechanisms of Gastroprotective Effects of Ethanolic Leaf Extract of Jasminum sambac against HCl/Ethanol-Induced Gastric Mucosal Injury in Rats. *Evidence Based Complementary and Alternative Medicine*, *2012*, 1–15. https://doi.org/10.1155/2012/786426

Chandran, K. C., & Kavitha Chandran, C. C. (2016). Quantitative estimation of total phenolic, flavonoids, tannin and chlorophyll content of leaves of Strobilanthes Kunthiana (Neelakurinji). *Journal of Medicinal Plants Studies*, *4*(4), 282–286. Retrived from https://www.plantsjournal .com/archives/?year=2016&vol=4&issue=4&part=D&ArticleId=408

Fan, S., Ali, N. A., & Basri, D. F. (2014). Evaluation of Analgesic Activity of the Methanol Extract from the Galls of Quercus infectoria (Olivier) in Rats. *Evidence-Based Complementary and Alternative Medicine*, *2014*(1), 1–6. https://doi.org/10.1155/2014/976764

Faujdar, S., Sharma, S., Sati, B., Pathak, A. K., & Paliwal, S. K. (2016). Comparative analysis of analgesic and anti-inflammatory activity of bark and leaves of Acacia ferruginea DC. *Beni-Suef University Journal of Basic and Applied Sciences*, *5*(1), 70–78. https://doi.org/10.1016/j.bjbas.2016.02.002

Ganesh, M., & Mohankumar, M. (2017). Extraction and identification of bioactive components in Sida cordata (Burm.f.) using gas chromatography–mass spectrometry. *Journal of Food Science and Technology*, *54*(10), 3082–3091. https://doi.org/10.1007/s13197-017-2744-z

Goldberg, D. S., & McGee, S. J. (2011). Pain as a global public health priority. *BMC Public Health*, *11*(1), 770. https://doi.org/10.1186/1471-2458-11-770

Grace, E. J. (1961). *Modern Medicine*, *JAMA*, *175*(12), 1111. https://doi.org/10.1001/jama.1961.03040120073027

Greene, M. J. (1972). Some aspects of the pharmacology of droperidol. *British Journal of Anaesthesia*, *44*(12), 1272–1276. https://doi.org/10.1093/bja/44.12.1272

Harirforoosh, S., Asghar, W., & Jamali, F. (2014). Adverse Effects of Nonsteroidal Antiinflammatory Drugs: An Update of Gastrointestinal, Cardiovascular and Renal Complications. *Journal of Pharmacy & Pharmaceutical Sciences*, *16*(5), 821. https://doi.org/10.18433/J3VW2F

Hossain, M. M., Uddin, M. S., Baral, P. K., Ferdus, M., & Bhowmik, S. (2022). Phytochemical screening and antioxidant activity of Ipomoea hederifolia stems: A potential medicinal plant. *Asian Journal of Natural Product Biochemistry*, *20*(2), 41–47. https://doi.org/10.13057/biofar/f200201

Idu, M., Aihiokhai, M. O., Imoni, C. A., Akokigho, C. E., & Olali, N. C. (2021). Gas Chromatography-Mass Spectrometry (GC-MS) Analysis and Phytochemical Screening of Polyherbal Aqueous Leaves Extract (PALE). *Journal of Complementary and Alternative Medical Research*, *14*(2), 10–18. https://doi.org/10.9734/jocamr/2021/v14i230240

Ijeoma, U. F., Aderonke, S. O., Ogbonna, O., Augustina, M. A., & Ifeyinwa, C.-N. (2011). Antinociceptive and anti-inflammatory activities of crude extracts of Ipomoea involucrata leaves in mice and rats. *Asian Pacific Journal of Tropical Medicine*, *4*(2), 121–124. https://doi.org/10.1016/S1995-7645(11)60050-3

Joel, U. C., & Uwabunkeonye, O. C. (2020). Comparative Phytochemical Study of The Parts of Ipomoea Species. *Journal of Medicinal Plants Studies*, *8*(4), 257–261. Retrieved from https://www.plantsjournal.com/archives/?year=2020&vol=8&issue=4&part=D&ArticleId=1174

Kaushik, D., Kumar, A., Kaushik, P., & Rana, A. C. (2012). Analgesic and Anti-Inflammatory Activity of Pinus roxburghii Sarg. *Advances in Pharmacological Sciences*, *2012*, 1–6. https://doi.org/10.1155/2012/245431

Kidd, B. L., & Urban, L. A. (2001). Mechanisms of inflammatory pain. *British Journal of Anaesthesia*, *87*(1), 3–11. https://doi.org/10.1093/bja/87.1.3

Krishnamoorthy, K., & Subramaniam, P. (2014). Phytochemical Profiling of Leaf, Stem, and Tuber Parts of Solena amplexicaulis (Lam.) Gandhi Using GC-MS. *International Scholarly Research Notices*, *2014*, 1–13. https://doi.org/10.1155/2014/567409

Krummenacher, P., Kossowsky, J., Schwarz, C., Brugger, P., Kelley, J. M., Meyer, A., & Gaab, J. (2014). Expectancy-induced placebo analgesia in children and the role of magical thinking. *Journal of Pain*, *15*(12), 1282–1293. https://doi.org/10.1016/j.jpain.2014.09.005

Kumar, R., Singh, S. S., Pranav, & Ray, S. B. (2011). Nimodipine potentiates the analgesic effect of morphine in the rat hot-plate test: Implications in the treatment of pain. *Indian Journal of Anaesthesia*, *55*(4), 413–416. https://doi.org/10.4103/0019-5049.84843

Kurian, P., Banurekha, J., Venkateswarlu, B., & Kumar, M. (2023). Pharmacognostic Evaluation of Ipomoea hederifolia L. *Research Journal of Pharmacy and Technology*, *16*(5), 2399–2402. https://doi.org/10.52711/0974-360X.2023.00395

Lahare, R. P., Yadav, H. S., Bisen, Y. K., & Dashahre, A. K. (2021). Estimation of Total Phenol, Flavonoid, Tannin and Alkaloid Content in Different Extracts of Catharanthus roseus from Durg District, *Chhattisgarh, India. Scholars Bulletin*, *7*(1), 1–6. https://doi.org/10.36348/sb.2021.v07i01.001

Madhu, M., Sailaja, V., Satyadev, T., & Satyanarayana, M. V. (2016). Quantitative phytochemical analysis of selected medicinal plant species by using various organic solvents. *Journal of Pharmacognosy and Phytochemistry*, *5*(2), 25–29. Retrived from https://www.phytojournal.com/archives/2016.v5.i2.752/quantitative-phytochemical-analysis-of-selected-medicinal-plant-species-by-using-various-organic-solvents

Mali, K., Sutar, G., Devade, O., & Dias, R. (2019). Evaluation of nootropic activity of Limonia acidissima against scopolamineinduced amnesia on rats. *Turkish Journal of Pharmaceutical Sciences*, *8*(1), 3-9. https://doi.org/10.4274/tjps.galenos.2018.30316

Mali, K. K., Kokate, M. D., Ghorpade, V. S., Dias, R. J., & Mahajan, N. S. (2025). Exploring the anti-arthritic potential of Caralluma fimbriata: Phytochemical screening and preliminary observations in a rat model. *Journal of Ethnopharmacology*, *353*(Pt B), 120417. https://doi.org/10.1016/j.jep.2025.120417

Meira, M., Silva, E. P. da, David, J. M., & David, J. P. (2012). Review of the genus Ipomoea: traditional uses, chemistry and biological activities. *Revista Brasileira de Farmacognosia*, *22*(3), 682–713. https://doi.org/10.1590/S0102-695X2012005000025

Mohammed, Y. H., Ghaidaa, J. M., & Imad, H. H. (2016). Analysis of bioactive chemical compounds of Nigella sativa using gas chromatography-mass spectrometry. *Journal of Pharmacognosy and Phytotherapy*, *8*(2), 8–24. https://doi.org/10.5897/JPP2015.0364

Mujeeb, F., Bajpai, P., & Pathak, N. (2014). Phytochemical Evaluation, Antimicrobial Activity, and Determination of Bioactive Components from Leaves of Aegle marmelos. *BioMed Research International*, *2014*, 1–11. https://doi.org/10.1155/2014/497606

Musa, M., Jan, G., Jan, F. G., Hamayun, M., Irfan, M., Rauf, A., … Ali, N. (2022). Pharmacological activities and gas chromatography–mass spectrometry analysis for the identification of bioactive compounds from Justicia adhatoda L. *Frontiers in Pharmacology*, *13*(September), 1–14. https://doi.org/10.3389/fphar.2022.922388

Organisation for Economic Co-operation and Development (OECD). (2002). *Test No. 423: Acute oral toxicity—Acute toxic class method. In OECD guidelines for the testing of chemicals* (Section 4). Paris, France: OECD Publishing. https://doi.org/10.1787/9789264071001-en

Okechukwu, P. N. (2020). Evaluation of anti-inflammatory, analgesic, antipyretic effect of Eicosane, Pentadecane, Octacosane, and Heneicosane. *Asian Journal of Pharmaceutical and Clinical Research*, *13*(4), 29–35. https://doi.org/10.22159/ajpcr.2020.v13i4.36196

Osman, N., Sidik, N., Awal, A., Adam, N., & Rezali, N. (2016). In vitro Xanthine Oxidase (XO) and Albumin Denaturation Inhibition Assay of Barringtonia racemosa L. and Total Phenolic Content Analysis for Potential Anti-Inflammatory Use in Gouty Arthritis. *Journal of Intercultural Ethnopharmacology*, *5*(4), 343. https://doi.org/10.5455/jice.20160731025522

Padma, M., Ganesan, S., Jayaseelan, T., Azhagumadhavan, S., Sasikala, P., Senthilkumar, S., & Mani, P. (2019). Phytochemical screening and GC–MS analysis of bioactive compounds present in ethanolic leaves extract of Silybum marianum (L). *Journal of Drug Delivery and Therapeutics*, *9*(1), 85–89. https://doi.org/10.22270/jddt.v9i1.2174

Paula-Zurron, A. C. B. De, Petraglia, N. M. M. A., Aur, C. R., Moura, S. H. P., Imamura, P. M., Freitas, J. C. De, & Catanzaro-Guimarães, S. A. (2010). Antinociceptive activity of Ipomoea imperati (Vahl) Griseb., Convolvulaceae. *Revista Brasileira de Farmacognosia*, *20*(2), 180–185. https://doi.org/10.1590/S0102-695X2010000200008

Pratama, O. A., Tunjung, W. A. S., Sutikno, S., & Daryono, B. S. (2019). Bioactive compound profile of melon leaf extract (Cucumis melo L. 'Hikapel') infected by downy mildew. *Biodiversitas Journal of Biological Diversity*, *20*(11), 3448–3453. https://doi.org/10.13057/biodiv/d201143

Punchard, N. A., Whelan, C. J., & Adcock, I. (2004). The Journal of Inflammation. *Journal of Inflammation*, *1*, 1–4. https://doi.org/10.1186/1476-9255-1-1

Rafieian-kopaei, M., Shakiba, A., Sedighi, M., & Bahmani, M. (2017). The Analgesic and Anti-Inflammatory Activity of Linum usitatissimum in Balb/c Mice. *Journal of Evidence-Based Complementary & Alternative Medicine*, *22*(4), 892–896. https://doi.org/10.1177/2156587217717416

Rajeswari, G., Murugan, M., & Mohan, V. R. (2012). GC-MS analysis of bioactive components of Hugonia mystax L. (Linaceae). *Research Journal of Pharmaceutical, Biological and Chemical Sciences*, *3*(4), 301–308. Retrived form https://www.rjpbcs.com/pdf/2012_3(4)/%5B32%5D.pdf

Ramesh, R. (2010). Analgesic effects of the aqueous extracts of plant Ipomoea pes-tigridis studied in albino mice. *Global Journal of Pharmacology*, *4*(1), 31–35. Retrived from https://www.idosi.org/gjp/4(1)10/5.pdf

Raveendran, S., Tilak, A. V, Yadav, S., Das, S., Madrewar, V., & Kulkarni, V. (2019). A study to evaluate the analgesic activity of Origanum vulgare in mice using hot plate method. *International Journal of Basic & Clinical Pharmacology*, *8*(7), 1563. https://doi.org/10.18203/2319-2003.ijbcp20192650

Ravikumara, K., Kaveri, T. M., & Umesha, S. (2025). A comprehensive exploration of phytochemistry and pharmacological activities of Ipomoea hederifolia. *Journal of Pharmacognosy and Phytochemistry*, *14*(5), 43–49. https://doi.org/10.22271/phyto.2025.v14.i5a.15552

Santos, E. A. V., Nurit-Silva, K., Arruda, E. C. P., & Leite, A. V. (2023). Morphoanatomical and histochemical study of Ipomoea hederifolia L. (Convolvulaceae). *Anales de Biología*, *45*, 9–21. https://doi.org/10.6018/analesbio.45.02

Serhan, C. N., & Levy, B. D. (2018). Resolvins in inflammation: emergence of the pro-resolving superfamily of mediators. *The Journal of Clinical Investigation*, *128*(7), 2657–2669. https://doi.org/10.1172/JCI97943

Shah, M., Khan, F., Ullah, S., Mohanta, T. K., Khan, A., Zainab, R., … Al-Harrasi, A. (2023). GC-MS Profiling and Biomedical Applications of Essential Oil of Euphorbia larica Boiss.: A New Report. *Antioxidants*, *12*(3), 662. https://doi.org/10.3390/antiox12030662

Sheela, D., & Uthayakumari, F. (2013). GC-MS analysis of bioactive constituents from coastal and dune taxon- Sesuvium Portulacastrum (L.). *Bioscience Discovery*, *4*(55), 47–53. Retrived from https://www.jbsd. in/Volume%204%20No1%20Jan%2013/D%20Sheela%2047-53.pdf

Sostres, C., Gargallo, C. J., Arroyo, M. T., & Lanas, A. (2010). Adverse effects of non-steroidal anti-inflammatory drugs (NSAIDs, aspirin and coxibs) on upper gastrointestinal tract. *Best Practice & Research Clinical Gastroenterology*, *24*(2), 121–132. https://doi.org/10.1016/j.bpg.2009.11.005

Sriuttha, P., Sirichanchuen, B., & Permsuwan, U. (2018). Hepatotoxicity of Nonsteroidal Anti-Inflammatory Drugs: A Systematic Review of Randomized Controlled Trials. *International Journal of Hepatology*, *2018*, 1–13. https://doi.org/10.1155/2018/5253623

Suchiang, I. S., Devi, S. V., Zuala, L., & Shantabi, L. (2024). Quantification of Total Phenolics, Flavonoids and Evaluation of In Vitro Antioxidant Potential of Ipomoea hederifolia Linn. *Indian Journal of Pharmaceutical Sciences*, *86*(3), 832–838. https://doi.org/10.36468/pharmaceutical-sciences.1339

Tracey, I., & Mantyh, P. W. (2007). The cerebral signature for pain perception and its modulation. *Neuron*, *55*(3), 377–391. https://doi.org/10.1016/j.neuron.2007.07.012

Treede, R.-D., Rief, W., Barke, A., Aziz, Q., Bennett, M. I., Benoliel, R., … Wang, S.-J. (2019). Chronic pain as a symptom or a disease: the IASP Classification of Chronic Pain for the International Classification of Diseases (ICD-11). *Pain*, *160*(1), 19–27. https://doi.org/10.1097/j.pain.0000000000001384

Usha, T., Middha, S. K., Shanmugarajan, D., Babu, D., Goyal, A. K., Yusufoglu, H. S., & Sidhalinghamurthy, K. R. (2021). Gas chromatography-mass spectrometry metabolic profiling, molecular simulation and dynamics of diverse phytochemicals of Punica granatum L. leaves against estrogen receptor. *Frontiers in Bioscience-Landmark*, *26*(9), 423–441. https://doi.org/10.52586/4957

Vanlalhruaia, & Lalbiaknunga, J. (2020). Detection of cyanogenic glycosides in ethnomedicinal plants of Euphorbiaceae used by Tribes in Mizoram, India. *Journal of Pharmacognosy and Phytochemistry*, *9*(3), 735–737. https://doi.org/10.22271/phyto.2020.v9.i3l.11361

Velmurugan, G., & Anand, P. S. (2017). GC-MS Analysis of Bioactive Compounds on Ethanolic Leaf Extract of Phyllodium pulchellum L. Desv. *International Journal of Pharmacognosy and Phytochemical Research*, *9*(1), 114–118. https://doi.org/10.25258/ijpapr.v9i1.8050

Vieira, D., Padoani, C., Soares, J. dos S., Adriano, J., Cechinel Filho, V., de Souza, M. M., … Couto, A. G. (2013). Development of hydroethanolic extract of Ipomoea pes-caprae using factorial design followed by antinociceptive and antiinflammatory evaluation. *Revista Brasileira de Farmacognosia*, *23*(1), 72–78. https://doi.org/10.1590/S0102-695X2012005000126

Wani, T. A., Kumar, D., Prasad, R., Verma, P. K., Sardar, K. K., Tandan, S. K., & Kumar, D. (2012). Analgesic activity of the ethanolic extract of Shorea robusta resin in experimental animals. *Indian Journal of Pharmacology*, *44*(4), 493–499. https://doi.org/10.4103/0253-7613.99322

Whelton, A. (1999). Nephrotoxicity of nonsteroidal anti-inflammatory drugs: physiologic foundations and clinical implications. *The American Journal of Medicine*, *106*(5B), 13S-24S. https://doi.org/10.1016/s0002-9343(99)00113-8

Willie, P., Uyoh, E. A., & Aikpokpodion, P. O. (2020). Gas Chromatography-Mass Spectrometry (GC-MS) Assay of Bioactive Compounds and Phytochemical Analyses in Three Species of Apocynaceae. *Pharmacognosy Journal*, *13*(2), 383–392. https://doi.org/10.5530/pj.2021.13.49

Woolf, C. J. (2011). Central sensitization: Implications for the diagnosis and treatment of pain. *Pain*, *152*(3), S2–S15. https://doi.org/10.1016/j.pain.2010.09.030

Yimer, T., Birru, E. M., Adugna, M., Geta, M., & Emiru, Y. K. (2020). Evaluation of analgesic and anti-inflammatory activities of 80% methanol root extract of Echinops kebericho m. (Asteraceae). *Journal of Inflammation Research*, *13*, 647–658. https://doi.org/10.2147/JIR.S267154

FABAD J. Pharm. Sci., 51, 1, 89-104, 2026
Doi: 10.55262/fabadeczacilik.1811982
RESEARCH ARTICLE

Evaluation for Dissolution Profile Similarity of Multisource Generic Products Containing Favipiravir in the Treatment of COVID-19: Model-independent Bootstrap f_2 and Model-dependent Approaches

Duygu YILMAZ USTA[*°]

Evaluation for Dissolution Profile Similarity of Multisource Generic Products Containing Favipiravir in the Treatment of COVID-19: Model-independent Bootstrap f_2 and Model-dependent Approaches

SUMMARY

Favipiravir (FAV) has emerged as a potential antiviral drug for treating COVID-19 and has received emergency use approval in many countries, including Türkiye. This study aimed to assess the similarity of the dissolution profiles of FAV products using model-independent bootstrap f_2 and model-dependent approaches, particularly in cases of high variability in dissolution profiles at early time points and cumulative drug release less than 85%. Five generic FAV tablets were tested in pH 4.5 acetate and 6.8 phosphate buffers. The DDSolver®, Bootf2BCA_v1.3, and PhEq_bootstrap v1.2 software were used for similarity evaluation. At pH 4.5, none of the products reached 85% dissolution within 60 minutes. However, F2 and F4 achieved this within 30 minutes at pH 6.8. High variability was observed at early time points. Model-dependent analyses revealed differences in dissolution kinetics that were specific to the product and pH. For bootstrap f_2, DDSolver® identified similarity between F1-F2 at pH 4.5 and F1-F5 at pH 6.8. However, Bootf2BCA and PhEq_bootstrap could only confirm this for F1-F2 at pH 4.5 due to the lower limits of the confidence interval falling below 50. These findings demonstrate the importance of conducting dissolution tests to demonstrate therapeutic equivalence among multisource generic drugs, particularly during public health emergencies such as the COVID-19 pandemic. Bootstrap f_2 has been observed to provide more robust results, particularly when the classical f_2 assessment criteria commonly used are not met. This reliable approach also meets the expectations of regulatory authorities such as the EMA and FDA.

Keywords: *Favipiravir, COVID-19, high variable dissolution profile comparison, bootstrap f_2, model-dependent approach.*

COVID-19 Tedavisinde Favipiravir İçeren Çok Kaynaklı Jenerik Ürünlerin Çözünme Profili Benzerliğinin Değerlendirilmesi: Modelden Bağımsız Bootstrap f_2 ve Modele Bağımlı Yaklaşımlar

ÖZ

Favipiravir (FAV), COVID-19 tedavisi için potansiyel bir antiviral ilaç olarak ortaya çıkmış ve Türkiye dahil birçok ülkede acil kullanım onayı almıştır. Bu çalışma, özellikle erken zaman noktalarında çözünme profillerinde yüksek değişkenlik ve kümülatif ilaç salımının %85'ten az olduğu durumlarda, model bağımsız bootstrap f_2 ve modele bağlı yaklaşımlar kullanarak FAV ürünlerinin çözünme profillerinin benzerliğini değerlendirmeyi amaçlamıştır. Beş jenerik FAV tableti, pH 4,5 asetat ve 6,8 fosfat tamponlarında test edilmiştir. Benzerlik değerlendirmesi için DDSolver®, Bootf2BCA_v1.3 ve PhEq_bootstrap v1.2 yazılımları kullanılmıştır. pH 4,5'te hiçbir ürün 60 dakika içinde %85 çözünme oranına ulaşamadı; ancak pH 6,8'de F2 ve F4 30 dakika içinde bu orana ulaşmıştır. Erken zaman noktalarında yüksek değişkenlik gözlemlenmiştir. Modele bağlı analizler, ürüne ve pH'ya özgü çözünme kinetiğinde farklılıklar olduğunu ortaya koymuştur. Bootsrap f_2 için, DDSolver® pH 4,5'te F1-F2 ile pH 6,8'de F1-F5 arasında benzerlik tespit etti. Ancak Bootf2BCA ve PhEq_bootstrap, güven aralığının alt sınırlarının 50'nin altına düşmesi nedeniyle bunu sadece pH 4,5'te F1-F2 için doğrulayabilmiştir. Bu bulgular, özellikle COVID-19 pandemisi gibi halk sağlığı acil durumlarında, çok kaynaklı jenerik ilaçlar arasında terapötik eşdeğerliği göstermek için çözünme testleri yapmanın önemini ortaya koymaktadır. Bootstrap f_2'nin, özellikle yaygın olarak kullanılan klasik f_2 değerlendirme kriterleri karşılanmadığında daha sağlam sonuçlar sağladığı gözlemlenmiştir. Bu güvenilir yaklaşım, EMA ve FDA gibi düzenleyici kurumların beklentilerini de karşılamaktadır.

Anahtar Kelimeler: *Favipiravir, COVİD-19, yüksek değişkenli çözünme profili karşılaştırması, bootstrap f_2, model bağımlı yaklaşım.*

Recieved: 29.10.2025
Revised: 16.12.2025
Accepted: 20.12.2025

[*] ORCID: 0000-0003-4035-7656, Gazi University Faculty of Pharmacy, Department of Pharmaceutical Technology, Ankara, Türkiye

[°] Corresponding Author; Duygu YILMAZ USTA
E-mail: yilmazduyguusta@gazi.edu.tr

INTRODUCTION

The coronavirus outbreak was first observed in Wuhan, China, in 2019, when it was identified as an unknown acute respiratory infection. After spreading to many countries, the World Health Organization (WHO) declared it a pandemic on 11 March 2020 (Dousari et al., 2020; Usta & Teksin, 2020). Since the start of the pandemic, countries have implemented different treatment approaches (FDA 2020; Jamshaid et al., 2020; Tsang et al., 2021). In view of the urgency of the situation, it has been deemed preferable to use approved drugs prescribed for other diseases that have an acceptable safety profile. This is because it could take months or even years to develop a drug molecule from scratch and prove its effectiveness in treating the disease (Liu et al., 2020; Pilkington et al., 2020).

One such drug is the antiviral Favipiravir (FAV), which is assumed to be therapeutically effective against the disease. FAV ($C_5H_4FN_3O_2$), also known as 6-fluoro-3-hydroxy-2-pyrazine carboxamide, is a pyrazine carboxamide derivative (Furuta et al., 2013). FAV has a molecular weight of 157.1 g/mol and is a prodrug (T-705). Its elimination half-life is 2–5.5 hours, and its bioavailability is 97.6%. The mean C_{max} is 51.5 μg/mL, the main volume of distribution is 15–20 L, and it is metabolized via the kidney (Joshi et al., 2021). There is no effect of food on FAV bioavailability. FAV was developed by the Japanese company Fujifilm Toyama Chemical in 2002 and approved for the treatment of influenza in 2014 (Dindar et al., 2022). FAV is an oral, broad-spectrum RNA-dependent RNA polymerase inhibitor with a well-defined safety profile (Joshi et al., 2021). It is thought that antiviral drugs administered shortly after the onset of symptoms may shorten the clinical course of the disease and reduce viral shedding when used to treat coronaviruses, thus reducing transmission, and these drugs have been included in treatment protocols. Avigan®, the reference drug for FAV included in the treatment protocol, was not available on the Turkish pharmaceutical market; however, the Ministry of Health has approved and used five generic products as of film-coated tablets (each includes 200 mg of FAV).

When a pharmaceutical product is taken orally, the active ingredient must be dissolved in gastrointestinal fluids before it can be absorbed. Dissolution is crucial for predicting *in vivo* drug behavior, ensuring consistent quality across all production batches and" post-approval adjustments, optimizing the drug manufacturing process, and determining bioequivalence and therapeutic equivalence between generic and reference drugs (McAllister et al., 2020). The most popular method of examining the effect of dissolution on these processes is to conduct *in vitro* dissolution studies in accordance with the relevant guidelines and pharmacopoeias (Muselík et al., 2021).

Dissolution studies enable drug behavior and performance in the gastrointestinal tract to be observed under *in vitro* conditions (Yılmaz Usta & Teksin, 2017). A key aspect of dissolution studies in drug development and regulatory approval is comparing dissolution profiles (Zuo et al., 2014). To this end, regulatory guidelines and legal authorities recommend using different methodologies to compare *in vitro* dissolution profiles based on dissolution data obtained from the dosage forms under study. The similarity factor (f_2) is the most widely used method for this purpose due to its simplicity and ease of calculation (Diaz et al., 2016). Recognized by numerous regulatory agencies worldwide, f_2 has become the standard approach for assessing dissolution profile similarity. However, specific conditions must be met for its application: the dissolution profile must include at least three time points beyond the initial measurement; testing must be conducted on 12 dosage units per formulation; the total dissolved drug percentage must exceed 85%; and the coefficient of variation (CV) must remain within acceptable limits - less than 20% at the first time point and below 10% for subsequent points

(Wang et al., 2016). In addition, the f_2 method has several limitations. These include assumptions about sample distribution and sensitivity to the number of time points. Furthermore, it is unable to pinpoint where variations occur within the dissolution profile. Furthermore, it does not account for high variability in dissolution data effectively.

Given the high variability observed at the start of the study and the fact that the cumulative percentage of the active ingredient dissolved remained below 85% for some products, it is important to determine the most appropriate method for evaluating the similarity of dissolution profiles and assessing generic formulations. Alternative approaches have been explored to address the shortcomings of the similarity factor (f_2). One such method uses a 90% confidence interval (CI) for f_2, applying bootstrap resampling techniques to evaluate similarity without relying on f_2 as a single-point estimator. This approach has attracted considerable interest from regulatory authorities, including the US Food and Drug Administration (FDA) and the European Medicines Agency (EMA), in recent years for evaluating dissolution profile similarity, especially when the prerequisites for using classical f_2 are not met (Paixão et al., 2017).

This study aimed to demonstrate the equivalence of generic products containing FAV in the Turkish pharmaceutical market, which have been approved for emergency use in the Ministry of Health's treatment protocol for patients with COVID-19, through dissolution studies. Dissolution profiles exhibiting high variability at early time points and a dissolved FAV amount of less than 85% were evaluated using both model-independent bootstrap f_2 methods and model-dependent approaches. The results obtained from these different approaches were then compared. As there are no dissolution or dissolution profile comparison studies in the literature for generic products containing FAV in the Turkish pharmaceutical market, this study is scientifically innovative.

MATERIALS AND METHODS

Materials

FAV was provided by Atabay Drug Company (İstanbul, Türkiye). Acetic acid ($C_2H_4O_2$), sodium acetate trihydrate ($NaC_2H_3O_2 \cdot 3H_2O$), potassium dihydrogen phosphate (KH_2PO_4), and sodium hydroxide (NaOH) were purchased from Merck, Germany. The batch numbers for generic products are as follows: F1, 204332; F2, 3388006; F3, 20N702; F4, 33927; F5,10100006. The F2 product was requested from the manufacturer, while the other generics are products provided to patients by contact tracing teams for emergency treatment.

Analytical quantification of FAV

pH 4.5 acetate and pH 6.8 phosphate buffers were used as media. A stock solution of FAV was prepared by dissolving 25 mg in 250 mL of buffer to obtain a concentration of 100 µg/mL. Working standard solutions in the concentration range (for pH 4.5, 10-20 µg/mL and pH 6.8, 4–12 µg/mL) were prepared by suitable dilution of the stock solution. All the samples were filtered with a 0.45µm membrane filter. The standard solutions (10 µg/mL) were scanned in the range of 200 -800 nm by a UV-spectrophotometer (Cary 60 UV-Vis, Agilent, Germany). The maximum absorbances were observed at 360 nm for both, and this wavelength was used for all measurements. The methods were validated using FDA guidelines and ICH Q2(R2) (FDA 2018; ICH 2023).

Preparation of buffer media

Preparation of pH 4.5 acetate buffer. The pH 4.5 acetate buffer was prepared by mixing 2.99 g $NaC_2H_3O_2 \cdot 3H_2O$ and 14 mL 2N acetic acid solution, and the required amount of distilled water was added up to 1 L. The pH was checked and adjusted to 4.5, if necessary, by adding small volumes of either acid or base. The solution was filtered through a 0.45 µm membrane filter before use.

Preparation of pH 6.8 phosphate buffer. The pH 6.8 phosphate buffer was prepared by mixing 250 mL of

0.2 M potassium dihydrogen phosphate (KH_2PO_4) with 112 mL of 0.2 M sodium hydroxide (NaOH) solution. Adjust the volume to 1000 mL with distilled water. The pH was checked, and the pH was adjusted to 6.8, if necessary, by adding small volumes of either acid or base. The solution was filtered through a 0.45 µm membrane filter before use.

0.2 M potassium dihydrogen phosphate solution: Dissolve 22.7 g of KH_2PO_4 in distilled water and dilute to 1000 mL.

0.2 M sodium hydroxide solution: Dissolve 2 g of NaOH in distilled water and dilute to 1000 mL.

Dissolution studies

There is no official monograph available for tablet dosage forms containing FAV. In such cases, it is recommended to perform dissolution testing for immediate release (IR) tablets using the basket or paddle method with different rotation speeds in different dissolution media (pH 1.0 to 6.8) (FDA, 1997). The dissolution testing of FAV generic tablets was conducted at 37 ± 0.5°C at 50 rpm using the USP apparatus II. pH 4.5 acetate buffer and pH 6.8 phosphate buffer, with 900 mL, were used as dissolution media. Aliquots of 5 mL were withdrawn at the 5, 10, 15, 20, 30, 45, and 60 min from each dissolution vessel, an equivalent volume of the corresponding fresh media was added. All samples were filtered 0.45µm membrane filter and analyzed by UV analysis at 360 nm. The studies were conducted in 12 parallel studies.

Software used for data analysis

For comparing estimations of the similarity factor (f_2, unbiased f_2 (bc- f_2), or the expected value ($_{2,exp}$)) and their corresponding 90% confidence intervals (CIs), three widely used and freely accessible software tools were selected: DDSolver®, Bootf2BCA (Version 1.3), and PhEq_bootstrap (Version 1.2). The method is implemented in Bootf2BCA, an open-source tool developed in the R statistical environment (Noce et al., 2020). Analyses were conducted in R (Version 4.1.3) and RStudio (Version 2022.02.1) using the bootf2 and bootf2BCa functions. All three compute the conventional f_2 metric, and each of these platforms employs a bootstrap approach to approximate the sampling distribution of the similarity factor. In addition, PhEq_bootstrap is the only platform that provides bc- f_2, while both Bootf2BCA and PhEq_bootstrap can calculate $_{2,exp}$ (Table 1.) (Noce et al., 2020). The primary functionalities and tools offered by these platforms are summarized in Table 2.

Table 1. Equations for different f_2 types calculated by software tools

f_2 types	Equations	Parameters
f_2	$f_2 = 50\log\left\{\left[1+\left(\frac{1}{n}\right)\sum_{k=1}^{n}(R_k-T_k)^2\right]^{-0.5}.100\right\}$	n: Number of time points R_t and T_t: Mean dissolution amount of reference and test products at time t
Estimated f_2 ($\hat{f}_2$)	$\hat{f}_2 = 100-25\log\left(1+\left(\frac{1}{n}\right)\sum_{k=1}^{n}(\overline{X}_{T,k}-\overline{X}_{R,k})^2\right)$	n: number of time points $\bar{X}_{R,k}$ *and* $\bar{X}_{T,k}$: Mean dissolution data at the k^{th} time point of random samples chosen from the reference and test populations, respectively.
Bias-corrected f_2 ($\hat{f}_{2,bc}$)	$\hat{f}_{2,bc} = 100-25\log\left(1+\left(\frac{1}{n}\right)\left(\sum_{k=1}^{n}(\overline{X}_{T,k}-\overline{X}_{R,k})^2-\left(\frac{1}{n}\right)\sum_{k=1}^{n}(S^2_{T,k}+S^2_{R,k})\right)\right)$	n: sample size $S^2_{R,k}$ and $S^2_{T,k}$: Unbiased estimates of variance at the k^{th} time points of random samples chosen from reference and test population, respectively.
Unbiased f_2	$bc-f_2 = 50\log\left\{\left[1+\left(\frac{1}{n}\right)\sum_{k=1}^{n}(R_k-T_k)^2-\sum_{k=1}^{n}(S^2_{R,k}+S^2_{T,k})/n\right]^{-0.5}.100\right\}$	$S^2_{R,k}$ and $S^2_{T,k}$: The sample variances at the k^{th} time point of reference and test products
Expected f_2 ($\hat{f}_{2,bc}$)	$E(\hat{f}_2) = 100-25\log(1+(\frac{1}{n})(\sum_{k=1}^{n}(\mu_{T,k}-\mu_{R,k})^2+(\frac{1}{n})\sum_{k=1}^{n}(\sigma^2_{T,k})^2+\sigma^2_{R,k})^2)))$	$\sigma^2_{R,k}$ and $\sigma^2_{T,k}$: Population variance at k^{th} time points of the reference and the test product, respectively.
Types of CI		
Normal interval	$\hat{f}_{2,L} = \hat{f}_{2,S}-E_B-\sqrt{V_B}.Z_{1-\alpha}$ $\quad$ $\hat{f}_{2,U} = \hat{f}_{2,S}-E_B-\sqrt{V_B}.Z_{1-\alpha}$ $E_B = \frac{1}{B}\sum_b^B \hat{f}_{2,b}-\hat{f}_{2,S} = \bar{f}_2-f_{2,S}$ $\quad$ $V_B = \frac{1}{B-1}\sum_b^B(\hat{f}^*_{2,b}-\bar{f}^*_2)^2$	$\hat{f}_{2,L}$ and $\hat{f}_{2,u}$: Lower and upper limit of the confidence interval estimated from bootstrap samples $Z_{1-\alpha}$: The inverse of the standard normal cumulative distribution function with type I error α: E_B and V_B are the resampling estimates of bias and variance B: Number of bootstrap samples $\hat{f}_{2,S}$: f_2 estimate with b^{th} bootstrap sample and $\bar{f}^*_2$: mean value
Basic interval	$\hat{f}_{2,L} = 2\hat{f}_{2,S}-\hat{f}^*_{2,(B+1)(1-\alpha)}$ $\quad$ $\hat{f}_{2,U} = 2\hat{f}_{2,S}-\hat{f}^*_{2,(B+1)\alpha}$ $\hat{f}^*_{2,(B+1)\alpha} = \hat{f}^*_{2,k}+\frac{\Phi^{-1}(\alpha)-\Phi^{-1}(\frac{k}{B+1})}{\Phi^{-1}(\frac{k+1}{B+1})-\Phi^{-1}(\frac{k}{B+1})}(\hat{f}^*_{2,k+1}-\hat{f}^*_{2,k})$	$\hat{f}^*_{2,(B+1)\alpha}$ and $\hat{f}^*_{2,(B+1)(1-\alpha)}$: (B+1)αth and (B+1)(1- α)th ordered resampling estimates of f_2 k: The integer part of (B+1)α, $\hat{f}^*_{2,k+1}$ and $\hat{f}^*_{2,k}$ the (k+1)th and the k^{th} ordered resampling estimates of f_2, respectively.
Bias-corrected and accelerated (BCa) intervals	$\hat{f}_{2,L} = \hat{f}^*_{2,\alpha_1}$ $\quad$ $\hat{f}_{2,U} = \hat{f}^*_{2,\alpha_2}$ $\alpha_1 = \Phi\left(\hat{Z}_0+\frac{\hat{z}_0+\hat{z}_\alpha}{1-\hat{a}(\hat{z}_0+\hat{z}_\alpha)}\right)$ $\quad$ $\alpha_2 = \Phi\left(\hat{Z}_0+\frac{\hat{z}_0+\hat{z}_{1-\alpha}}{1-\hat{a}(\hat{z}_0+\hat{z}_{1-\alpha})}\right)$	$\hat{f}^*_{2,\alpha_1}$ and $\hat{f}^*_{2,\alpha_2}$: The 100α$_1^{th}$ and the 100α$_2^{th}$ percentile of the resampling estimates of f_2 $\hat{z}_0$ and $\hat{a}$: Bias-correction and acceleration

CI: Confidence interval

Table 2. The summary of features, functionality, and parameters of the software tools

	Coding language	Using similarity parameters	Confidence interval	Sampling mode	Key advantages	Limitations
DDSolver[*,**]	Visual basic	*CI* for f_2	Percentile bootstrap	Whole vectors	Free Excel add-in Easy to use	Limited to n<36 No BCa CI
Bootf2BCA[**]	R language	*CI* for $E(f_2)$	Normal Basic Percent BCa (adjusted)	Individual values Whole vectors	Highly flexible Customizable Supports all CI methods	Requires coding skills
PhEq_bootstrap[***]	Lazarus RAD language in Pascal	*CI* for f_2 *CI* for $E(f_2)$	Percentile bootstrap	Individual values Whole vectors	Free Open-source Handles large datasets	No BCa CI Limited f_2 variants for CI

CI: Confidence interval; **BCa:** Bias-corrected and accelerated; **$E(f_2)$:** Expected f_2; **RAD:** Rapid application development
[*] Zhang et al., 2010
[**] Sourceforge.net, 2016
[***] Sourceforge.net, 2014

RESULTS and DISCUSSION

Dissolution studies

The apparatus, dissolution medium, sampling time, and rotation speed must be carefully selected in accordance with the relevant dissolution test conditions before conducting an *in vitro* dissolution test. There is no official monograph for tablet dosage forms containing FAV. In such cases, it is recommended that dissolution testing be performed under various conditions (pH 1 - 6.8) using a basket or paddle at different rotation speeds for IR tablets (FDA, 1997). When reviewing dissolution studies of FAV in the literature, it was found that studies had been conducted at different pH levels (pH 2.0 - 7.2), speeds (25 - 100 rpm), and media volumes (500 - 1000 mL) (Chakraborty & Mondal, 2023; Marzouk et al., 2022). The most important parameter when selecting the dissolution medium and volume is the solubility of the active ingredient. Solubility studies conducted for FAV in the literature show that solubility increases with pH (with the highest solubility occurring at pH 6.8) (Timur et al., 2021).

Considering suitable media volumes for dissolution studies, the theoretical solubility under sink conditions is 1.2 mg/mL for a volume of 500 mL and 0.7 mg/mL for a volume of 900 mL (Göktuğ et al., 2021). However, the solubility of FAV in different pH media (0.526 mg/mL at pH 1.2, 0.818 mg/mL at pH 4.5, and 0.815 mg/mL at pH 6.8) did not meet the sink conditions for a medium volume of 500 mL (as the solubility of FAV at these pH levels was less than 1.2 mg/mL), so the medium volume was increased to 900 mL. The sink condition saturation solubility (C_S)/drug concentration (C_D) ratio was calculated by dividing the dose by the 900 mL dissolution medium (Incecayir et al., 2021). According to the USP, the sink condition is met when the C_S/C_D value is greater than 3 (Hamed et al., 2016). For 200 mg of FAV in 900 mL, the sink condition was found to be 2.37, 3.68, and 3.67 at pH 1.2, 4.5, and 6.8, respectively. As the sink condition was not met at pH 1.2, and larger volumes are generally not favored in dissolution studies, comparisons were made using media at pH 4.5 and 6.8. A rotation speed of 50 rpm was selected, as recommended by the FDA and EMA for new studies (EMA, 2017; FDA, 1997).

Avigan®, the reference product, is unavailable on the Turkish pharmaceutical market; therefore, evaluations were carried out using F1, the first generic product to be launched, as the reference. The dissolution profiles are given in Figure 1 for the studies conducted at pH 4.5 and pH 6.8. The percentage of FAV dissolved at pH 6.8 was higher for F1, F2, and F4 than at pH 4.5, while the results for F3 and F5 were similar at both pH values. At pH 4.5, the percentage of dissolved FAV remained below 85% for all products after 60 minutes. At pH 6.8, however, F2 and F4 reached 85% within 30 minutes. F1, F3, and F5 remained below 85% at the end of the study. Examining the profiles revealed high variation at the early points.

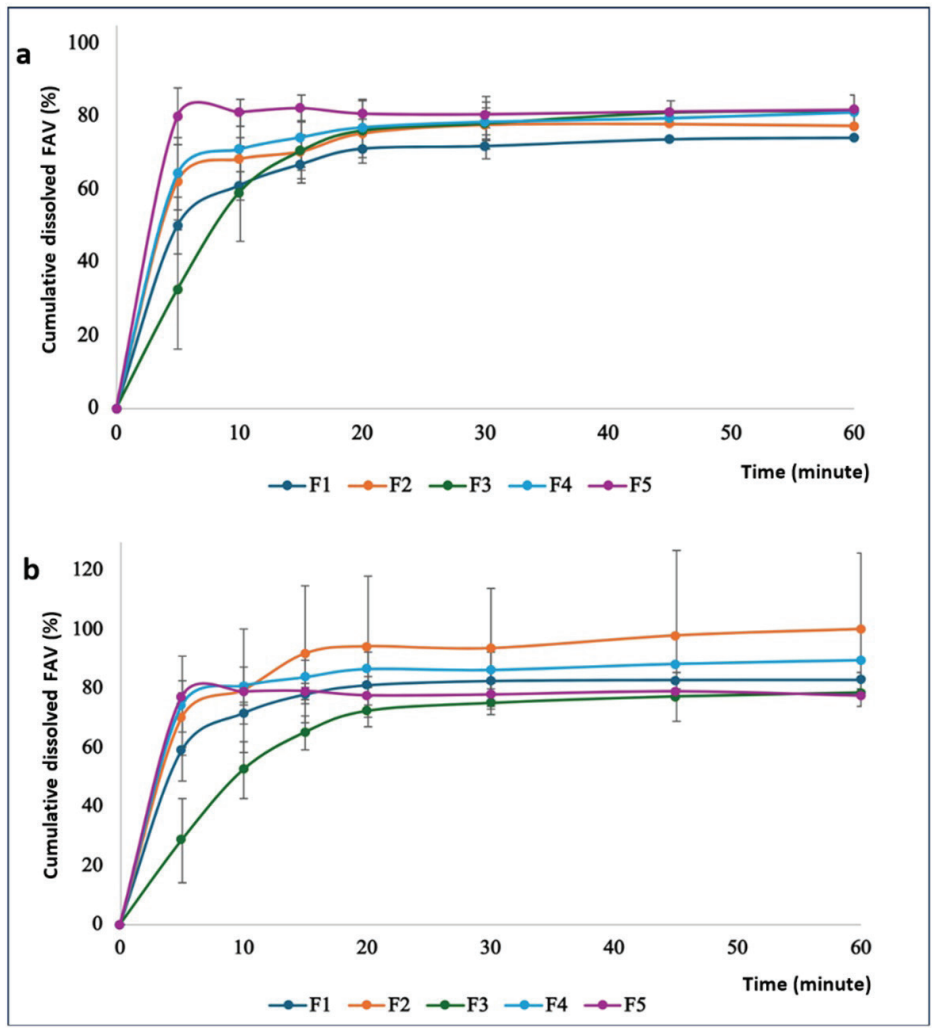


Figure 1. Dissolution profiles of FAV a) at pH 4.5 and b) at pH 6.8 (n=12, mean ± standard deviation)

Results of data analysis

Accurately assessing the similarity between dissolution profiles is important when analyzing dissolution data. Various approaches have therefore been developed to facilitate this comparison. These approaches can be broadly classified as either model-dependent or model-independent methods (Usta & Incecayir, 2022). Model-dependent methods involve fitting dissolution data to a specific mathematical or kinetic model for evaluation. These methods aim to determine the parameters that define the dissolution process and to make comparisons based on these

parameters. In these models, experimental dissolution data are fitted to mathematical equations, and the model parameters are determined. Statistical analyses of these parameters are then performed. Statistical measures such as the coefficient of determination, the root mean square error, corrected determination coefficient (R^2_{adj}), Akaike information criterion (AIC), and/or model selection criterion (MSC) are used to evaluate the model's fit.

DDSolver® is a free, menu-driven, computer-based program developed in Visual Basic for Microsoft Excel. It is designed to simplify the comparison, modelling, and calculation of dissolution profiles (Zhang et al., 2010). It is the first program of its kind to offer a user-friendly interface for analyzing pharmaceutical dissolution data. The software's primary objectives are to facilitate the evaluation of similarity between dissolution profiles, build a library of models that fit dissolution data using non-linear optimization methods, and enable reliable comparison of dissolution profiles. From the model library, the program can quickly determine which model best fits the release data. It can then generate fitted curves for each dataset, complete with error bars and mean dissolution curves (Yılmaz Usta & Teksin, 2017). In addition to profile fitting, DDSolver® provides over 40 built-in mathematical models, including zero-order, first-order, Higuchi, Korsmeyer–Peppas, and Weibull models. This enables both empirical and mechanistic analyses. The software also includes statistical tools for profile comparison, such as the f_2, the difference factor (f_1), and multivariate CIs. It also provides model selection criteria, such as the AIC and the MSC. By integrating directly into Excel, DDSolver® automates calculations, minimizes the risk of human error, and does not require advanced programming skills. Due to these advantages, it has become a widely used tool in pharmaceutical research, particularly in formulation development, quality control, and regulatory submissions. In addition to the classic f_2 statistic, the similarity of percentile CIs can be assessed using different resampling levels (5000, 10000, and 20000) and sample sizes (n = 12 and n = 24) for dissolution profiles with various levels of variability (10–20%, 40–50%, and 70–80% RSD). One limitation of the interface is that it cannot perform similarity assessments when the sample size is large (≥ 36).

The most suitable model for each product was determined by the lowest AIC value and the highest MSC and R^2_{adj}. The AIC evaluates both the complexity of the model and the quality of the fit, depending on the size of the dataset and the number of parameters. When comparing models with different numbers of parameters, the model with the lower AIC value is considered to provide a better fit. MSC is derived from AIC and normalized so that it is independent of the scaling of the data points. MSC is relatively easier to interpret, with a value above 3 indicating a good fit (Usta et al., 2018). R^2_{adj} is recommended for model selection and for comparing models with different numbers of parameters. As it considers the explanatory power of the included parameters when being calculated, R^2_{adj} more accurately reflects the true performance of the model. It may decrease if unnecessary parameters are added (Çoban et al., 2024). The reliability of model-dependent methods largely depends on the correct selection and statistical validation of the model. Incorrect model selection can lead to dissolution behavior being misinterpreted.

In this study, the AIC, MSC, and R^2_{adj} criteria were used for evaluation. Table 3 shows the models to which tablets containing FAV were fitted. Although different models were observed for different pH levels and generic products, it was determined that the tablet's dissolution behavior of is affected by β (shape factor) and α (scale factor), which characterize the dissolution profile parameters.

Table 3. Results of the evaluation of model-dependent methods using DDSolver® for FAV generic tablets

		F1	F2	F3	F4	F5
pH 4.5	**Model parameters**	**Gompertz 2**	**Probit 2**	**Gompertz 2**	**Logistic 2**	**Gompertz 1**
		α: 1.83	α: 0.05	α: 67.9	α: 41.5	α: 0.22
		β: 2.12	β: 0.963	β: 2.82	β: 1.69	β: 0.048
		F_{max}: 77.8	F_{max}: 81.7	F_{max}: 85.5	F_{max}: 85.1	
	R^2_{adj}	0.998	0.997	0.992	1	0.999
	AIC	21.4	24.5	33.9	5.57	11.5
	MSC	4.17	3.61	3.53	6.01	5.15
pH 6.8	**Model parameters**	**Gompertz 2**	**Weibull 2**	**Gompertz 2**	**Gompertz 2**	**Weibull 2**
		α: 1.36	α: 1.92	α: 7.45	α: 0.606	α: 0.662
		β: 2.04	β: 0.53	β: 2.90	β: 1.40	β: 0.003
		F_{max}: 87.1		F_{max}: 82.5	F_{max}: 94.1	
	R^2_{adj}	0.994	0.995	0.995	0.999	0.999
	AIC	31.3	31.8	30.0	14.7	14.7
	MSC	3.11	3.40	4.04	5.01	4.67

$\boldsymbol{F_{max}}$: Maximum fraction of drug released at infinite time; $\boldsymbol{\beta}$: Shape factor; $\boldsymbol{\alpha}$: Scale factor

Unlike model-dependent methods, model-independent methods are unaffected by errors resulting from incorrect model selection. This characteristic makes them widely preferred for regulatory submissions, bioequivalence assessments, and formulation optimization studies. However, when applying these methods, factors such as sampling design, the number of time points, and variability in dissolution data must be carefully evaluated. The f_2 method proposed by Moore and Flanner is the preferred criterion for this purpose, as it is simple (Muselík et al., 2021). Nevertheless, neither the EMA nor the FDA provides specific instructions for comparing dissolution curves beyond calculating the f_2 similarity factor. Furthermore, since f_2 is insensitive to the shape of the profiles, it is difficult to assess consumer risk (type I) and manufacturer risk (type II) errors (Hoffelder et al., 2022). In recent years, resampling techniques such as bootstrapping have been employed to mitigate the impact of factors such as variability in dissolution data and sample size on statistical reliability. These techniques generate a distribution of f_2 values and multiple simulated datasets from observed dissolution data (Efron 1992; Xu et al., 2021). Among multivariate, model-independent approaches, bootstrap statistics have become a widely used statistical approach for regulatory submissions and determining dissolution similarity (EMA, 2018). Bootstrap is a software-based statistical inference method that enables CIs and standard errors to be calculated for hypothesis testing without making classical statistical assumptions about probability distributions (Jamil & Polli, 2024; Kaity et al., 2023). Including CIs in the bootstrap method proposed by Shah et al. provides an interval estimate for assessing similarity, as opposed to the single point estimate provided by the classical f_2 method (Shah et al., 1998). These approaches strengthen the reliability of statistical inferences and evaluations by considering data variability and uncertainty (Rabelo & Lourenço, 2025).

In this study, due to some CV values exceeding the acceptable maximum (CV > 20 at initial time points and CV > 10 at subsequent time points) and the percentage of the active substance remaining

dissolved being below 85% (see *Dissolution studies,* Figure 1.), comparisons were performed using bootstrap f_2 (with CI), as recommended by EMA guidelines (Mendyk et al., 2013; Muselík et al., 2021). For bootstrap f_2 evaluations of dissolution profiles, the sample size was at least 12 units per batch or product. However, if a higher level of confidence is required, larger sample sizes should be used. The bootstrap f_2 approach is particularly important when f_2 is less than 60. In the bootstrap evaluation, the lower limit of the bootstrap CI is accepted if it is above 50. This meets the EMA guideline requirement that 'the f_2 value should be between 50 and 100' (EMA 2010; 2018). As the guidelines do not explain the details of the estimators or different CI types, this study presents the results obtained from estimators provided by different programs. The CI can be determined based on bootstrap analysis using various methods, including the normal approximation, the percentile method, and the BCa method (Boddu et al., 2023).

Bootf2BCA is a statistical approach designed to evaluate similarity between dissolution profiles by combining the bootstrap method with bias-corrected and accelerated (BCa) CIs. The analysis can be performed with varying numbers of bootstrap replications (5000, 10000, and 20000), different sample sizes (n = 12, 24, and 36), and across a wide range of dissolution profile variabilities (10–20%, 40–50%, and 70–80% RSD). The Bootf2BCA method uses a resampling strategy to generate thousands of bootstrap datasets, randomly sampling the original dissolution data with replacement. The BCa adjustment corrects for bias and skewness in the bootstrap distribution, enabling more accurate estimation of the f_2 of CIs. This allows multiple forms of similarity factors to be calculated, including estimated, expected, bias-corrected, variance-corrected and combined variance, and bias-corrected f_2, along with percentile and BCa CIs for each.

PhEq_bootstrap is freely available open-source statistical software, which was developed to compare the dissolution profiles of test and reference pharmaceutical products, using both conventional and advanced similarity assessment methods. It can calculate the conventional f_2, the bc- f_2, the $_{2,exp}$, and the percentile CI similarity limits through a bootstrap resampling approach (Noce et al., 2020). Unlike traditional methods, which produce only a single point estimate, the bootstrap technique repeatedly resamples dissolution data to generate a distribution of the similarity metric. This distribution can then be used to derive CIs. Previous studies have demonstrated that the conventional f_2 statistics are a biased, yet asymptotically unbiased, estimator of the true population similarity (Shah et al., 1998). This bias arises from the combined within-batch variance of the test and reference products. PhEq_Bootstrap overcomes these limitations by providing $_{2,exp}$, and percentile CI estimates, offering a more probabilistic understanding of similarity. In practical applications, the software enables evaluations under varying conditions, including different numbers of bootstrap resamples and sample sizes, and across profiles with different levels of variability (Table 6.). However, it should be noted that percentile CI limits can only be generated for $_{2,exp}$, and not for conventional f_2 or bc- f_2. This makes this method particularly valuable for cases involving high variability or limited data points, where conventional similarity factors may not fully capture the uncertainty in dissolution profile comparisons.

The results of profiles evaluated using DDSolver®, Bootf2BCA, and PhEq_Bootstrap are presented in Tables 4–6. Bootstrap f_2 values calculated using the software differed for the pH 4.5 and 6.8 media, but similar similarity assessment results were obtained. Comparisons were made using the first generic product (F1 was accepted as the reference), and only the similarity factor was found > 50 for F2 in the pH 4.5 media using all software. For a pH of 6.8, F5 was similar to F1 in the DDSolver® bootstrap assessment (Table 4.). However, similarity could not be achieved using the Bootf2BCA and PhEq_bootstrap methods because the lower limits of the CIs remained below 50 (Tables 5 and 6.).

Table 4. Results and evaluation of the bootstrap f_2 method with DDSolver®

	Observed similarity factor (f_2)	Bootstrap (Mean)	5000 Bootstrap (5^{th} percentile)	5000 Bootstrap (95^{th} percentile)	Similarity
pH 4.5					
F1-F2	60.8	60.7	53.8	68.6	*Yes*
F1-F3	55.1	54.6	49.0	60.4	*No*
F1-F4	54.7	55.2	47.7	67.1	*No*
F1-F5	41.0	40.9	38.8	43.4	*No*
pH 6.8					
F1-F2	45.4	46.4	34.2	68.3	*No*
F1-F3	42.2	42.3	38.0	47.0	*No*
F1-F4	55.5	55.5	48.9	63.5	*No*
F1-F5	55.8	55.7	51.5	61.8	*Yes*

Table 5. Results and evaluation of the bootstrap f_2 method with Bootf2BCA

	f_2 type	CI type	F2		F3		F4		F5	
pH 4.5	$\hat{f}_2$		$f_{2\,avr}$: 60.6		$f_{2\,avr}$: 54.5		$f_{2\,avr}$: 55.1		$f_{2\,avr}$: 41.0	
			L	U	L	U	L	U	L	U
		Normal	53.5	68.4	49.9	61.5	44.1	64.5	38.7	43.3
		Basic	53.0	67.6	49.7	61.3	42.3	61.9	38.6	43.2
		PI	53.9	68.6	48.9	60.5	47.4	67.0	38.8	43.5
		BCa	54.7	70.1	50.3	62.5	49.0	75.9	39.1	43.8
		Similarity	*Yes*		*No*		*No*		*No*	
	$\hat{f}_{2,exp}$		$f_{2\,avr}$: 59.5		$f_{2\,avr}$: 53.3		$f_{2\,avr}$: 53.7		$f_{2\,avr}$: 40.9	
			L	U	L	U	L	U	L	U
		Normal	53.0	66.5	49.3	59.5	45.9	61.3	38.6	43.2
		Basic	52.5	66.0	49.1	59.4	44.6	60.1	38.5	43.0
		PI	53.3	66.7	48.3	58.6	47.2	62.8	38.8	43.3
		BCa	54.0	67.6	49.4	59.9	48.5	66.3	39.0	43.6
		Similarity	*Yes*		*No*		*No*		*No*	
pH 6.8	$\hat{f}_2$		$f_{2\,avr}$: 52.0		$f_{2\,avr}$: 42.2		$f_{2\,avr}$: 53.0		$f_{2\,avr}$: 55.7	
			L	U	L	U	L	U	L	U
		Normal	32.2	65.4	37.7	46.8	43.0	61.9	50.5	61.2
		Basic	28.3	61.1	37.4	46.6	41.9	60.5	49.7	60.1
		PI	39.8	72.6	37.9	47.1	44.9	63.5	51.4	61.8
		BCa	41.3	78.1	38.2	47.4	45.6	65.2	52.4	66.5
		Similarity	*No*		*No*		*No*		*No*	
	$\hat{f}_{2,exp}$		$f_{2\,avr}$: 46.9		$f_{2\,avr}$: 41.9		$f_{2\,avr}$: 52.0		$f_{2\,avr}$: 55.1	
			L	U	L	U	L	U	L	U
		Normal	39.5	55.4	37.4	46.3	43.2	60.1	50.5	60.0
		Basic	39.7	55.2	37.1	46.1	42.4	59.1	49.8	59.2
		PI	39.1	54.7	37.7	46.6	44.5	61.3	51.2	60.5
		BCa	39.8	55.3	37.8	46.8	45.0	62.2	52.1	63.9
		Similarity	*No*		*No*		*No*		*No*	

5000 bootstrap replicates; $f_{2\,avr}$: Avarage f_2; $_2$: Observed similarity factor; $_{2,exp}$: Expected similarity factor; **CI**: Confidence interval; **L**: Lower limit of 90% CI; **U**: Upper limit of the 90% CI; **PI**: Percentile; **BCa**: Bias-corrected and accelerated

Table 6. Results and evaluation of the bootstrap f_2 method with PhEq_bootstrap

	f_2		$_{2,average}$	bc-f_2	$_{2,exp}$	*Similarity*
	L	U				
			pH 4.5			
F2	51.6	65.3	59.2	60.4	58.1	*Yes*
F3	46.8	57.2	53.1	54.4	52.0	*No*
F4	46.0	61.1	53.7	*	52.3	*No*
F5	37.3	42.0	39.5	39.7	39.4	*No*
			pH 6.8			
F2	32.4	50.0	45.2	*	40.8	*No*
F3	36.4	45.1	40.8	41.1	40.4	*No*
F4	46.9	60.4	54.0	55.1	53.1	*No*
F5	49.8	58.9	54.2	54.9	53.6	*No*

* An unbiased estimator for f_2 is not valid because of the large variance of dissolution points. Seek for values "-1" for unbiased f_2; **bc-f_2**: unbiased f_2; $_{2,exp}$: expected f_2; **L**: Lower limit of 90% confidence interval (CI); **U**: Upper limit of the 90% confidence interval (CI)

CONCLUSION

During the pandemic, FAV tablets were included in emergency treatment protocols for off-indication use, and various generic products became available for treatment. The dissolution profiles of the FAV tablets examined in this study were evaluated at pH 4.5 and pH 6.8 according to solubility and sink conditions. Significant differences in dissolution behavior were observed between products, particularly regarding the amount of dissolved substance remaining below 85%, and high intra-batch variation for the same product. These findings suggest that differences in bioavailability between generics may directly impact treatment efficacy. Although model-dependent methods identified parameters affecting the dissolution process (such as F_{max}, β, α), the high variation and the fact that the cumulative percentage of the dissolved substance was below the desired level (i.e., < 85%) for an IR product led to the use of the model-independent, bootstrap-based f_2 method to enable a more reliable comparison. DDSolver®, Bootf2BCA, and PhEq_bootstrap software generally provided consistent results. However, it was observed that similarity findings varied for some products due to program-dependent factors (e.g., changes in CI limits, skewness, and adjusted f_2). In conclusion, including different generic products in treatment, especially during periods of urgent use, suggests that differences in dissolution profiles may impact the clinical response. These findings emphasize the critical importance of dissolution testing when comparing generics, as well as the importance of accurately evaluating these tests, particularly when variation is high, or 85% dissolution cannot be achieved. Bootstrap f_2 approaches provide more robust results than classical f_2 assessments and are considered a reliable method compatible with the expectations of regulatory authorities such as EMA and FDA in bioequivalence assessments and formulation development studies.

ACKNOWLEDGEMENTS

The author thanks Atabay Drug Company (Türkiye) for kindly providing the active pharmaceutical ingredient, favipiravir.

AUTHOR CONTRIBUTION STATEMENT

The author was responsible for developing the hypothesis, conducting literature research, performing experiments, and preparing and reviewing the manuscript (DYU).

CONFLICT OF INTEREST

The author declares that there is no conflict of interest.

REFERENCES

Boddu, R., Kollipara, S., Bhattiprolu, A. K., Parsa, K., Chakilam, S. K., Daka, K. R., ... Ahmed, T. (2023). Dissolution profiles comparison using conventional and bias corrected and accelerated f2 bootstrap approaches with different software's: Impact of variability, sample size and number of bootstraps. *AAPS PharmSciTech*, *25*(1), 5. https://doi.org/10.1208/s12249-023-02710-9

Chakraborty, S., & Mondal, S. (2023). A Green Eco-friendly Analytical Method Development, Validation, and Stress Degradation Studies of Favipiravir in Bulk and Different Tablet Dosages Form by UV-spectro-photometric and RP-HPLC Methods with their Comparison by Using ANOVA and in-vitro Dissolution Studies. *International Journal of Pharmaceutical Investigation, 13*(2). https://dx.doi.org/10.5530/ijpi.13.2.039

Çoban, Ö., Usta, D., & Pinar, S. (2024). Evaluation of Different Methods for Dissolution Profile Similarity Comparison of Montelukast Tablets in Türkiye. *Dissolution Technologies, 31*(1). dx.doi.org/ 10.14227/dt310124p40

Diaz, D. A., Colgan, S. T., Langer, C. S., Bandi, N. T., Likar, M. D., & Van Alstine, L. (2016). Dissolution similarity requirements: how similar or dissimilar are the global regulatory expectations?. *The AAPS Journal*, *18*(1), 15-22. https://doi.org/10.1208/s12248-015-9830-9

Dindar, C. K., Bozal-Palabiyik, B., Uslu, B. (2022). Development of a Diamond Nanoparticles-based Nanosensor for Detection and Determination of Antiviral Drug Favipiravir. *Electroanalysis, 34*(7), 1174-1186. https://doi.org/10.1002/elan.202100571

Dousari, A. S., Moghadam, M. T., Satarzadeh, N. (2020). COVID-19 (Coronavirus disease 2019): a new coronavirus disease. *Infection and Drug Resistance,* 2819-2828. https://doi.org/10.2147/IDR.S259279

Efron, B. (1992). Bootstrap methods: another look at the jackknife. In S. Kotz, & N. L. Johnson (Eds.), *Breakthroughs in statistics: Methodology and distribution* (pp. 569-593). New York, NY: Springer New York.

EMA. (2010). *Guideline on the Investigation of Bioequivalence.* Retrieved from https://www.ema.europa.eu/en/documents/scientific-guideline/guideline-investigation-bioequivalence-rev1_en.pdf

EMA. (2017). *Committee for Medicinal Products for Human Use. Reflection Paper on the Dissolution Specification for Generic Solid Oral Immediate Release Products with Systemic Action. EMA/CHMP/CVMP/QWP/336031/2017.*

EMA. (2018). *The Adequacy of the Mahalanobis Distance to Assess the Comparability of Drug Dissolution Profiles.* Retrieved from https://www.ema.europa.eu/en/documents/scientific-guideline/question-answer-adequacy-mahalanobis-distance-assess-comparability-drug-dissolution-profiles_en.pdf

Furuta, Y., Gowen, B. B., Takahashi, K., Shiraki, K., Smee, D. F., & Barnard, D. L. (2013). Favipiravir (T-705), a novel viral RNA polymerase inhibitor. *Antiviral Research, 100*(2), 446-454. https://doi.org/10.1016/j.antiviral.2013.09.015

Göktuğ, Ö., Altaş, E., Kayar, G., & Gökalp, M. (2021). The development and the validation of a novel dissolution method of favipiravir film-coated tablets. *Scientia Pharmaceutica, 90*(1), 3. https://doi.org/10.3390/scipharm90010003

Hamed, R., Awadallah, A., Sunoqrot, S., Tarawneh, O., Nazzal, S., AlBaraghthi, T., ... Abbas, A. (2016). pH-dependent solubility and dissolution behavior of carvedilol—case example of a weakly basic BCS class II drug. *AAPS PharmSciTech, 17*(2), 418-426. https://doi.org/10.1208/s12249-015-0365-2

Hoffelder, T., Leblond, D., Van Alstine, L., Diaz, D. A., Suarez-Sharp, S., Witkowski, K., ... Abend, A. (2022). Dissolution profile similarity analyses—statistical principles, methods and considerations. *The AAPS Journal, 24*(3), 54. https://doi.org/10.1208/s12248-022-00697-y

Incecayir, T., Olgac, S., Usta, D. Y., & Teksin, Z. S. (2021). Role of surfactants on dissolution behavior of tamoxifen. *Dissolution Technologies, 28*(2), 6-15. dx.doi.org/10.14227/DT280221P6

International Council for Harmonisation of Technical Requirements for Pharmaceuticals for Human Use, ICH Harmonised Guideline. (2023). *Validation of Analytical Procedures Q2(R2).* Retrieved from https://database.ich.org/sites/default/files/ICH_Q2%28R2%29_Guideline_2023_1130.pdf

Jamil, R., & Polli, J. E. (2024). Application of bootstrap f2 to dissolution data from biorelevant media and evidence of the conservative nature of bootstrap f2. *European Journal of Pharmaceutical Sciences, 196*, 106745. https://doi.org/10.1016/j.ejps.2024.106745

Jamshaid, H., Zahid, F., Din, I. U., Zeb, A., Choi, H. G., Khan, G. M., & Din, F. U. (2020). Diagnostic and treatment strategies for COVID-19. *AAPS PharmSciTech, 21*(6), 222. https://doi.org/10.1208/s12249-020-01756-3

Joshi, S., Parkar, J., Ansari, A., Vora, A., Talwar, D., Tiwaskar, M., ... Barkate, H. (2021). Role of favipiravir in the treatment of COVID-19. *International Journal of Infectious Diseases, 102*, 501-508. https://doi.org/10.1016/j.ijid.2020.10.069

Kaity, S., Sah, S. K., Karanwad, T., & Banerjee, S. (2023). Bootstrap statistics and its application in disintegration and dissolution data analysis. *Molecular Pharmaceutics, 20*(8), 3791-3803. https://doi.org/10.1021/acs.molpharmaceut.3c00222

Liu, X., Liu, C., Liu, G., Luo, W., & Xia, N. (2020). COVID-19: Progress in diagnostics, therapy and vaccination. *Theranostics, 10*(17), 7821-7835. https://doi.org/10.7150/thno.47987

Marzouk, H. M., Rezk, M. R., Gouda, A. S., & Abdel-Megied, A. M. (2022). A novel stability-indicating HPLC-DAD method for determination of favipiravir, a potential antiviral drug for COVID-19 treatment; application to degradation kinetic studies and in-vitro dissolution profiling. *Microchemical Journal, 172*, 106917. https://doi.org/10.1016/j.microc.2021.106917

McAllister, M., Flanagan, T., Boon, K., Pepin, X., Tistaert, C., Jamei, M., ... Mackie, C. (2020). Developing clinically relevant dissolution specifications for oral drug products—industrial and regulatory perspectives. *Pharmaceutics, 12*(1):19. https://doi.org/10.3390/pharmaceutics12010019

Mendyk, A., Pacławski, A., Szlek, J., & Jachowicz, R. (2013). PhEq_bootstrap: Open-source software for the simulation of f2 distribution in cases of large variability in dissolution profiles. *Dissolution Technologies, 20*(1), 13-7. dx.doi.org/10.14227/DT200113P13

Muselík, J., Komersová, A., Kubová, K., Matzick, K., & Skalická, B. (2021). A critical overview of FDA and EMA statistical methods to compare in vitro drug dissolution profiles of pharmaceutical products. *Pharmaceutics, 13*(10), 1703. https://doi.org/10.3390/pharmaceutics13101703

Noce, L., Gwaza, L., Mangas-Sanjuan, V., & Garcia-Arieta, A. (2020). Comparison of free software platforms for the calculation of the 90% confidence interval of f2 similarity factor by bootstrap analysis. *European Journal of Pharmaceutical Sciences, 146*, 105259. https://doi.org/10.1016/j.ejps.2020.105259

Paixão, P., Gouveia, L. F., Silva, N., & Morais, J. A. (2017). Evaluation of dissolution profile similarity–Comparison between the f2, the multivariate statistical distance and the f2 bootstrapping methods. *European Journal of Pharmaceutics and Biopharmaceutics, 112*, 67-74. https://doi.org/10.1016/j.ejpb.2016.10.026

Pilkington, V., Pepperrell, T., & Hill, A. (2020). A review of the safety of favipiravir–a potential treatment in the COVID-19 pandemic? *Journal of Virus Eradication, 6*(2), 45-51. https://doi.org/10.1016/S2055-6640(20)30016-9

Rabelo, J., & Lourenço, F. R. (2025). Measurement uncertainty and risk of false decisions for similarity factor (f2): Boostrapping method or Kragten spreadsheet? *Chemometrics and Intelligent Laboratory Systems, 264*, 105475. https://doi.org/10.1016/j.chemolab.2025.105475

Shah, V. P., Tsong, Y., Sathe, P., & Liu, J. P. (1998). In vitro dissolution profile comparison—statistics and analysis of the similarity factor, f2. *Pharmaceutical Research, 15*(6), 889-896. https://doi.org/10.1023/A:1011976615750

Sourceforge.net. (2014). Retrieved from https://sourceforge.net/projects/pheqbootstrap/

Sourceforge.net. (2016). Retrieved from https://sourceforge.net/projects/bootf2bca/

Timur, S. S., Ataşoğlu, M., Öner, Y., Karabulut, T. C., & Eroğlu, H. (2021). In vitro studies for BCS classification of an antiviral agent, favipiravir. *Journal of Research in Pharmacy, 25*(6), 944-952. https://dx.doi.org/10.29228/jrp.91

Tsang, H. F., Chan, L. W. C., Cho, W. C. S., Yu, A. C. S., Yim, A. K. Y., Chan, A. K. C., ... Wong, S. C. C. (2021). An update on COVID-19 pandemic: the epidemiology, pathogenesis, prevention and treatment strategies. *Expert Review of Anti-İnfective Therapy, 19*(7), 877-888. https://doi.org/10.1080/14787210.2021.1863146

Usta, D. Y., Demirtaş, Ö., Ökçelik, C., Uslu, A., & Teksin, Z. Ş. (2018). Evaluation of in vitro dissolution characteristics of flurbiprofen, a BCS class IIa drug. *FABAD Journal of Pharmaceutical Sciences, 43*(2), 27-34.

Usta, D. Y., & Teksin, Z. Ş. (2020). COVID-19 Tedavisinde Kullanılan İlaçların Biyofarmasötik, Farmakokinetik ve Patent Değerlendirmeleri: Ülkemizde Eşdeğer İlaçların Geliştirilmesindeki Güncel Durum. *Gazi Medical Journal, 31*(3):498-509. http://dx.doi.org/10.12996/gmj.2020.119

Usta, D. Y., & Incecayir, T. (2022). Modeling of in vitro dissolution profiles of carvedilol immediate-release tablets in different dissolution media. *AAPS PharmSciTech, 23*(6), 201. https://doi.org/10.1208/s12249-022-02355-0

U.S. Food and Drug Administration. (1997). *Center for Drug Evaluation and Research. Guidance for Industry, Dissolution Testing of Immediate Release Solid Oral Dosage Forms*; US Food and Drug Administration, Center for Drug Evaluation and Research: Rockville, MD, USA.

U.S. Food and Drug Administration. (2018). *Guidance for Industry Bioanalytical Method Validation*. Retrieved from https://www.fda.gov/files/drugs/published/Bioanalytical-Method-Validation-Guidance-for-Industry.pdf

U.S. Food and Drug Administration Department of Health and Human Services (2020). *Center for Drug Evaluation and Research (CDER), Center for Biologics Evaluation and Research (CBER), COVID-19: Developing Drugs and Biological Products for Treatment or Prevention Guidance for Industry.*

Wang, Y., Snee, R. D., Keyvan, G., & Muzzio, F. J. (2016). Statistical comparison of dissolution profiles. *Drug Development and Industrial Pharmacy, 42*(5), 796-807. https://doi.org/10.3109/03639045.2015.1078349

Xu, Z., Merino-Sanjuan, M., Mangas-Sanjuan, V., & García-Arieta, A. (2021). Estimators and confidence intervals of f2 using bootstrap methodology for the comparison of dissolution profiles. *Computer Methods and Programs in Biomedicine, 212*, 106449. https://doi.org/10.1016/j.cmpb.2021.106449

Yılmaz Usta, D., & Teksin, Z. S. (2017). In Vitro Çözünme Hizi Çalismalarinda Yeni Yaklasimlar/ New approaches to in vitro dissolution rate studies. *FABAD Journal of Pharmaceutical Sciences, 40*(1), 33.

Zhang, Y., Huo, M., Zhou, J., Zou, A., Li, W., Yao, C., & Xie, S. (2010). DDSolver: an add-in program for modeling and comparison of drug dissolution profiles. *The AAPS Journal, 12*(3), 263-271. https://doi.org/10.1208/s12248-010-9185-1

Zuo, J., Gao, Y., Bou-Chacra, N., & Löbenberg, R. (2014). Evaluation of the DDSolver software applications. *BioMed Research International, 2014*(1), 204925. https://doi.org/10.1155/2014/204925

FABAD J. Pharm. Sci., 51, 1, 105-114, 2026
Doi: 10.55262/fabadeczacilik.1804862
RESEARCH ARTICLE

Rethinking Oral Infection Control: Antimicrobial Peptides and Essential Oils as Alternative Antibacterial Agents

Murat Sefa KARAASLAN[*], Nurten ALTANLAR[**°], Sinem ASLAN ERDEM[***]

Rethinking Oral Infection Control: Antimicrobial Peptides and Essential Oils as Alternative Antibacterial Agents

SUMMARY

Oral health has a direct impact on an individual's overall health status. Infections observed here not only affect individuals' quality of life but also decrease their productivity. Additionally, these infections can lead to systemic infections by affecting other parts of the body. Among the major causes that disrupt oral health are untreated dental caries and advanced periodontal diseases. Factors such as the loss of drug efficacy due to antimicrobial resistance, challenges in discovering new drug classes, and the limitation of existing treatment options due to observed side effects increase the need for new treatment strategies for the prevention and treatment of oral infections. The chemical composition of commercial essential oils (EO) was determined using gas chromatography-mass spectrometry (GC-MS). The antibacterial activities of antimicrobial peptides and essential oils were evaluated using the minimum inhibitory concentration method. Combinations of essential oils with antimicrobial peptides at a 1:1 ratio were prepared to investigate their efficacy. The main components of the essential oils were identified as carvacrol (82.675%) for Thymus vulgaris EO, eugenol (79.367%) for Syzygium aromaticum EO, menthol (47.199%) for Mentha piperita EO, and eucalyptol (63.642%) for Eucalyptus globulus EO. Among the essential oils, T. vulgaris exhibited the best antibacterial effect. The efficacy of combinations varied among the test bacteria. The most effective combination was determined with peppermint essential oil. Peppermint essential oil reduced the minimum inhibitory concentration value of both antimicrobial peptides by fourfold. The combination of lactoferrin and thyme essential oil led to a decrease in efficacy against all test bacteria. Although antimicrobial peptides alone showed limited activity, their combination with certain essential oils enhanced their antibacterial effectiveness against oral pathogens. These findings suggest that natural agent combinations exhibit species-specific efficacy and hold promise for the development of alternative therapeutic strategies.

Keywords: *Essential oils, Antimicrobial peptides, pathogens, oral, thymus.*

Oral Enfeksiyonların Kontrolünü Yeniden Değerlendirmek: Alternatif Antibakteriyel Ajanlar Olarak Antimikrobiyal Peptitler ve Uçucu Yağlar

ÖZ

Ağız sağlığı, bireylerin genel sağlık durumunu doğrudan etkiler. Bu bölgede görülen enfeksiyonlar yalnızca bireylerin yaşam kalitesini azaltmakla kalmaz, aynı zamanda üretkenliklerini de düşürür. Ayrıca bu enfeksiyonlar, vücudun diğer bölgelerini etkileyerek sistemik enfeksiyonlara yol açabilir. Ağız sağlığını bozan başlıca nedenler arasında tedavi edilmemiş diş çürükleri ve ileri periodontal hastalıklar yer alır. Antimikrobiyal direnç nedeniyle ilaç etkinliğinin azalması, yeni ilaç sınıflarının keşfindeki zorluklar ve mevcut tedavi seçeneklerinin yan etkiler nedeniyle sınırlı kalması, oral enfeksiyonların önlenmesi ve tedavisi için yeni stratejilere duyulan gereksinimi artırmaktadır. Ticari uçucu yağların (EO) kimyasal bileşimi gaz kromatografisi-kütle spektrometresi (GC-MS) yöntemiyle belirlenmiştir. Antimikrobiyal peptitlerin ve uçucu yağların antibakteriyel aktiviteleri minimum inhibitör konsantrasyon (MIC) yöntemiyle değerlendirilmiştir. Etkinliklerini incelemek için uçucu yağlar ve antimikrobiyal peptitler 1:1 oranında kombine edilmiştir. Uçucu yağların başlıca bileşenleri; Thymus vulgaris için karvakrol (%82,675), Syzygium aromaticum için öjenol (%79,367), Mentha piperita için mentol (%47,199) ve Eucalyptus globulus için ökaliptol (%63,642) olarak tanımlanmıştır. Uçucu yağlar arasında en güçlü antibakteriyel etki T. vulgaris'te gözlenmiştir. Kombinasyonların etkinliği test edilen bakterilere göre değişiklik göstermiştir. En etkili kombinasyon nane uçucu yağı ile elde edilmiştir. Nane uçucu yağı, her iki antimikrobiyal peptitin minimum inhibitör konsantrasyon değerini dört kat azaltmıştır. Laktoferrin ve kekik uçucu yağı kombinasyonu ise tüm test bakterilerinde etkinlik azalmasına neden olmuştur. Antimikrobiyal peptitler tek başına sınırlı aktivite göstermesine rağmen, belirli uçucu yağlarla kombinasyonları oral patojenlere karşı antibakteriyel etkinliği artırmıştır. Bu bulgular, doğal ajan kombinasyonlarının tür-spesifik etkinlik sergilediğini ve alternatif tedavi stratejilerinin geliştirilmesi için umut vadettiğini göstermektedir.

Anahtar Kelimeler: *Uçucu yağlar, antimikrobiyal peptitler, patojenler, oral, kekik.*

Recieved: 17.10.2025
Revised: 4.12.2025
Accepted: 26.12.2025

[*] ORCID: 0009-0001-8215-2491, Department of Pharmaceutical Microbiology, Faculty of Pharmacy, Ankara University, Ankara, Türkiye; Graduate School of Health Sciences, Ankara University, Ankara, Türkiye
[**] ORCID: 0000-0003-2977-2269, Department of Pharmaceutical Microbiology, Faculty of Pharmacy, Ankara University, Ankara, Türkiye
[***] ORCID: 0000-0003-1504-1916, Department of Pharmacocnosy, Faculty of Pharmacy, Ankara University, Ankara, Türkiye

[°] Corresponding Author; Nurten ALTANLAR
E-mail: naltanlar@ankara.edu.tr

INTRODUCTION

The general health status of individuals is directly linked to oral health. A deterioration in oral health can negatively impact individuals' quality of life by affecting their daily functioning physically, emotionally, socially, and psychologically (Peres et al., 2019). Moreover, oral diseases have been associated with systemic conditions such as cardiovascular diseases, rheumatoid arthritis, and osteoporosis (Palombo, 2011).

The World Health Organization (WHO) reports that approximately 50% of the global population is affected by one or more forms of oral diseases, among which dental caries is identified as the most common oral health issue (Jain et al., 2024; Kassebaum et al., 2017). *Streptococcus mutans* is considered the primary etiological agent responsible for dental caries, while species of *Lactobacillus*, such as *L. acidophilus* and *L. casei*, are implicated in the development and progression of carious lesions. Another bacterium present in the oral cavity, *Enterococcus faecalis*, is frequently associated with endodontic infections (Alghamdi & Shakir, 2020; Wen et al., 2022).

Reducing the oral microbial load decreases the risk of infection. Although daily tooth brushing is a recommended mechanical cleaning method, it cannot reach all colonization sites of oral bacteria. Chemical mouthwashes, another group of hygiene products, have limitations such as poor long-term usability due to mucosal absorption, potential discoloration of teeth and tongue, and risk of allergic reactions (Balappanavar et al., 2013; Batista et al., 2014).

Antimicrobial peptides (AMPs) are naturally occurring molecules found across all life forms, from prokaryotes to humans. Also referred to as host defense peptides, AMPs are key components of the innate immune system that protect the host from infections in higher organisms (Mahlapuu et al., 2016). Due to their short amino acid sequences, AMPs are notable for being easy to synthesize, for exerting broad-spectrum antimicrobial activity, and for degrading into non-toxic products such as amino acids (Rima et al., 2021).

Plants have been used for medicinal purposes for thousands of years. Natural products derived from medicinal plants form the basis for the development of numerous drugs. Essential oils obtained from plants are widely used in oral care products due to both their antimicrobial properties and their aromatic characteristics. Their low toxicity, pharmacological effects, and economic feasibility are among the main reasons for their frequent use in oral formulations (Nagy-Bota et al., 2021). Essential oils of thyme, mint, eucalyptus, and clove are widely used herbal products with various applications in the general population.

Given the limitations of current oral hygiene products in preventing oral infections and the public health significance of these infections, there is a clear need for safer and more effective products derived from natural sources (Palombo, 2011).

MATERIALS AND METHODS

Bacterial strains and growth conditions

In this study, *Streptococcus mutans* ATCC 25175, *Lactobacillus casei* RSKK 06029, and *Lactobacillus acidophilus* ATCC 11975 test bacteria were incubated on Brain Heart Infusion (BHI) and de Man Rogosa Sharp (MRS) agar media, respectively, at 37°C in a 5% CO_2 environment for 24-48 hours. The *Enterococcus faecalis* ATCC 29212 standard bacterium was incubated aerobically on BHI agar medium at 37°C for 24 hours.

Antimicrobial peptides and essential oil

In this study, commercially obtained human cathelicidin LL-37 (MedChemExpress) and human lactoferricin (Anaspec) antimicrobial peptides were used. The essential oils of *Thymus vulgaris* L. (TEO), *Mentha piperita* L. (MEO), *Eucalyptus globulus* Labill. (EEO), and *Syzygium aromaticum* L. (SEO) were used, obtained commercially.

GC and GC/MS analysis of essential oils

GC/MS analysis of the essential oil samples was performed using the Shimadzu GCMS-QP2020NX system. The analysis was performed using an Inert-Cap WAX column (30.0 m × 0.25 mm × 0.25 µm) (GL Sciences Inc., Japan) and helium as the carrier gas (1.78 ml min-1). The operating conditions were: The oven temperature was set at 40°C for 5 min after injection, then increased to 240°C with a heating ramp of 4°C/min for 10 min, and then increased to 240°C with a heating ramp of 4°C/min without holding; the injector and detector (FID) temperatures were 250°C; the split ratio was set at 10:1; the injection volume was 1.0 µl. MS conditions were as follows: ion source temperature 200°C; interface temperature 250°C; mass range 35-550 atomic mass units. The compounds were identified by comparing their relative retention indices and mass spectra with the corresponding literature (Bathily et al., 2023; Bota et al., 2022; Dolghi et al., 2022; Hamdoon et al., 2024) and by comparing their mass spectra with the Wiley and NIST libraries. The percentages of the components were calculated from the GC peak areas using the normalization method.

Antibacterial activity

The Minimum Inhibitory Concentration (MIC) values of the essential oils and antimicrobial peptides against the test bacteria were determined by the broth microdilution method. Essential oils were prepared as stock solutions at 100 mg/ml in 10% DMSO and 0.1% Tween 80, while antimicrobial peptides were prepared at 1 mg/ml in sterile distilled water. In this study, Mueller-Hinton Broth was used for *E. faecalis*, BHI Broth for *S. mutans* (Galvão et al., 2012), and MRS Broth for *L. acidophilus* and *L. casei* (Anisimova & Yarullina, 2019). Serial two-fold dilutions of the samples were prepared in suitable media. Test bacteria were prepared from overnight subcultures, and the final test concentration of bacteria was adjusted to $5x10^5$ CFU/mL. Plates were incubated according to the requirements of the test bacteria. At the end of the incubation period, the concentration of the last well showing no growth was recorded as the MIC value (mg/ml). In the study, a solvent containing 10% DMSO and 0.1% Tween 80 was used as a negative control, and ciprofloxacin (Merck) was used as a positive control. All experiments were performed in triplicate.

Antibacterial activity of antimicrobial peptide-essential oil combinations

Effective essential oils with antibacterial activity were mixed at a 1:1 ratio with antimicrobial peptides at stock concentration, and the antibacterial efficacy of this prepared mixture was investigated using the method described above.

RESULTS AND DISCUSSION

The general health status of individuals is associated with oral health. Oral diseases reduce the quality of life and working capacity of individuals. Oral infections affect daily life with symptoms such as pain and discomfort and have also been linked to systemic infections that impact other parts of the body. Worldwide, oral infections have a high prevalence, and there is a need for preventive measures against these infections (Palombo, 2011; Peres et al., 2019).

The results of combination experiments involving antimicrobial peptides, which did not exhibit antibacterial activity at the studied concentrations (250-1.95 µg/ml), were interpreted based on essential oils for which MIC values were determined. Due to the inability to detect MIC values for antimicrobial peptides, synergy tests involving combinations at different concentrations could not be conducted (Black et al., 2023). In this study, combinations of essential oils and antimicrobial peptides at a 1:1 ratio from stock concentrations were prepared for activity tests. In the antibacterial activity tests, the combinations were studied with TEO, MEO, and SEO, which demonstrated individual effectiveness.

Characterization of essential oils

The characterization results of the commercially obtained essential oils are shown below (Table 1.). The main components of the essential oils were identified as carvacrol for *Thymus vulgaris* EO, eugenol for *Syzygium aromaticum* EO, menthol for *Mentha piperita* EO, and eucalyptol for *Eucalyptus globulus* EO.

Table 1. Composition of the essential oil samples

NO	RRI	Compound	% Amount			
			T. vulgaris **EO**	***S. aromaticum*** **EO**	***M. piperita*** **EO**	***E. globulus*** **EO**
1.	1106	*α*-Pinene	-	-	-	21.533
2.	1171	D-Limonene	-	-	2.390	-
3.	1179	Eucalyptol	-	-	5.095	-
4.	1233	dl-Limonene	-	-	-	4.749
5.	1240	Eucalyptol	-	-	-	63.642
6.	1270	γ-Terpinene	2.587	-	-	-
7.	1291	*p*-Cymene	5.207	-	-	1.284
8.	1452	*I*-Menthone	-	-	27.120	-
9.	1474	Menthofuran	-	-	2.234	-
10.	1480	*p*-Menthone	-	-	4.348	-
11.	1551	Linalool	6.818	-	-	-
12.	1558	Menthyl acetate	-	-	5.338	-
13.	1592	Caryophyllene	-	-	2.783	-
14.	1593	(+)-Neomenthol	-	-	3.493	-
15.	1599	*trans*-Caryophellene	-	5.932	-	-
16.	1608	Aromadendrene	-	-	-	4.435
17.	1641	Menthol	-	-	47.199	-
18.	1647	Alloaromadendrene	-	-	-	0.972
19.	1658	*trans*-Pinocarveol	-	-	-	0.908
20.	1671	*α*-Humulene	-	0.667	-	-
21.	1698	*α*-Terpinyl acetate	-	-	-	2.477
22.	1728	*β*-Bisabolone	2.713	-	-	-
23.	2180	Eugenol	-	79.367	-	-
24.	2223	Carvacrol	82.675	-	-	-
25.	2267	Eugenyl acetate	-	14.034	-	-
		TOTAL	100	100	100	100

Antibacterial activity

The effects of essential oils and antimicrobial peptides on test bacteria were determined using the broth microdilution method. Essential oils were tested at concentrations ranging from 250 to 0.195 µg/ml, and antimicrobial peptides at concentrations from 250 to 0.001 µg/ml. At the end of the incubation period, the lowest concentration with no observed bacterial growth was recorded as the MIC value (Table 2.). Among the essential oils, TEO demonstrated the highest activity against *L. casei* RSKK 06029 at a concentration of 0.78 mg/ml. Antimicrobial peptides showed no antibacterial activity against the test bacteria at the tested concentrations. Additionally, the mixture of 10% DMSO and 0.1% Tween 80 used for dispersing the essential oils exhibited no antibacterial effect on the test bacteria.

In the study by de Oliveira Carvalho et al. (2020), which evaluated the efficacy of essential oils against oral pathogens, MIC values of SEO were reported as 0.315 mg/ml against *S. mutans* and 1.25 mg/ml against *E. faecalis*, and MIC values of TEO were reported as 0.625 mg/ml for these bacteria. Elgamily et al. (2019) reported MIC values of SEO as 15.56 mg/ml and 13.92 mg/ml against *S. mutans* and *L. acidophilus*, respectively. In another study, MIC values of SEO were reported as 2 mg/ml against *S. mutans*, 1 mg/ml against *L. casei*, and 4 mg/ml against *E. faecalis* (Agu-

iar et al., 2013). In our study, MIC values of SEO were determined as 3.12 mg/ml against *S. mutans*, 12.5 mg/ml against *E. faecalis*, and 12.5 mg/ml against *L. acidophilus*.

Fani & Kohanteb (2017) reported the MIC value of TEO as 1.9 µg/ml against clinical *S. mutans* isolates. In another study, an MIC value of 50 mg/ml was reported against the standard strain of *S. mutans* (Figueira et al., 2020). In the study by de Oliveira Carvalho et al. (2020), the MIC values of TEO were reported as 0.625 mg/ml against *S. mutans* and *E. faecalis*. In our study, MIC values of TEO were determined as 1.56 mg/ml against *S. mutans* and *E. faecalis*. It is thought that this discrepancy in MIC values may be due to the bacterial strains or the components of the essential oil used.

Goldbeck et al. (2014) reported an MIC value of 0.013 mg/ml for EEO against *S. mutans*, attributing its effect to the 1,8-cineole component. In another study, Harkat-Madouri et al. (2015) reported an MIC value of 11.4 mg/ml for EEO. In our study, EEO showed no antibacterial effect on the test bacteria at the tested concentrations.

Golestannejad et al. (2017) reported an MIC value of 10.5 µg/ml for MEO against *S. mutans* test bacteria. In another study, the MIC values of MEO were reported as 0.63 mg/ml against *S. mutans*, 0.27 mg/ml against *L. acidophilus*, and 0.23 mg/ml against *E. faecalis* (Nikolić et al., 2014). In our study, the MIC values of MEO were determined as 1.56 mg/ml against *S. mutans* and *L. acidophilus*, and 25 mg/ml against *E. faecalis*.

The antibacterial efficacy of essential oils shows significant variability in the literature. The efficacy of these oils depends on the composition and concentrations of the chemical molecules they contain.

In their study investigating the antibacterial activities of LL-37 and human lactoferricin against oral pathogens, Wuersching et al. (2021) reported that exposure to LL-37 inhibited the growth of co-cultured bacteria by 11%-65%, and lactoferricin exposure inhibited growth by 52%-64%. In our study, no MIC value was detected against *S. mutans* for antimicrobial peptides used at the same concentrations.

Schmidtchen et al. (2002) examined the interactions of LL-37 with various pathogenic bacteria, including *E. faecalis*, reported that *E. faecalis* proteases degrade the structure of LL-37, preventing the peptide from binding to the cell and causing it to lose its effectiveness. Contrary to this study, Lima et al. (2017), in a study on endodontic infection agents, reported that LL-37 had an MIC concentration of 256 µg/ml against *E. faecalis*, and at a concentration of 128 µg/ml, it inhibited bacterial growth by 54%. The degradation of LL-37 by *E. faecalis* is likely dose-dependent. In our study, LL-37 showed no antibacterial activity against *E. faecalis* at the tested concentrations.

Enigk et al. (2020) evaluated the efficacy of five antimicrobial peptides against various pathogenic bacteria using the agar dilution method, and reported that LL-37 and lactoferrin, a precursor molecule of lactoferricin, did not affect the growth of *E. faecalis* and *S. mutans* at concentrations of 0.125-8 µg/ml. In our study, the broth microdilution method was used for the MIC test of antimicrobial peptides, and no efficacy was observed against *E. faecalis* and *S. mutans* at concentrations ranging from 250-1.95 µg/ml.

In the study by Ouhara et al. (2005), which evaluated the efficacy of antimicrobial peptides on cariogenic bacteria, two different MIC methods were used. The first method involved spreading bacteria on an agar plate after a 2-hour exposure to various concentrations of antimicrobial peptides, as reported by Midorikawa et al. (2003). In the other method, bacterial cultures were incubated with antimicrobial peptide dilutions prepared in bovine serum albumin and acetic acid phosphate buffer, as reported by Wu & Hancock (1999). Using the first method, they reported that LL-37 inhibited the growth of *S. mutans* by 80.1% and *L. casei* by 45.9% at a concentration of 1 mg/ml. Using the other method, the MIC values of LL-37 were determined as 25 µg/ml against *S. mutans* and 50 µg/ml against *L. casei*.

In our study, further research is required to investigate the growth inhibition effects of antimicrobial peptides on test bacteria, for which no MIC values were determined.

Table 2. MIC test results of essential oils and antimicrobial peptides.

		Standard Strain			
		E. faecalis ATCC 29212	*L. acidophilus* ATCC 11975	*L. casei* RSKK 06029	*S. mutans* ATCC 25175
Essential Oils (mg/ml)	TEO	1.56	3.15	0.78	1.56
	MEO	25	1.56	1.56	1.56
	SEO	12.5	12.5	6.25	3.12
	EEO	-	-	-	-
Antimicrobial Peptides (µg/ml)	LL-37	-	-	-	-
	Laktoferricin	-	-	-	-
Control	Ciprofloxacin (µg/ml)	2	128	8	2
	Solvent	-	-	-	-

Results of antibacterial activity tests for combinations

To evaluate the combined effects, stock concentrations of essential oils and antimicrobial peptides were mixed in equal ratios (1:1), and dilutions were prepared from this mixture. Since MIC values for antimicrobial peptides alone were not observed at the tested concentrations, synergy testing was not conducted, and the results were interpreted based on the essential oils.

The presence of LL-37 (Table 3.):

- Increased the MIC value of thyme essential oil against *L. casei* RSKK 06029 by 4-fold.
- Increased the MIC value of peppermint essential oil by 8-fold against the same bacterium.
- Reduced the MIC value of peppermint essential oil by 4-fold against *E. faecalis* ATCC 29212.
- Reduced the MIC value of clove essential oil by 4-fold against *L. acidophilus* ATCC 11975

The presence of lactoferricin (Table 4.):

- Increased the MIC values of thyme essential oil for all test bacteria.
- Increased the MIC value of clove essential oil by 4-fold against *L. casei* RSKK 06029.
- Reduced the MIC value of peppermint essential oil by 4-fold against *E. faecalis* ATCC 29212.

Table 3. MIC values (mg/ml) of LL-37 and essential oil combinations

	TEO		MEO		SEO	
	A	**C**	**A**	**C**	**A**	**C**
E. faecalis ATCC 29212	1.56	3.12	25	6.25	12.5	6.25
L. acidophilus ATCC 11975	3.12	3.12	1.56	3.12	12.5	3.12
L. casei RSKK 06029	0.78	3.12	1.56	12.5	6.25	6.25
S. mutans ATCC 25175	1.56	1.56	1.56	3.12	3.12	1.56

*A: Alone, C: Combination

Table 4. MIC values (mg/ml) of lactoferricin and essential oil combinations

	TEO		MEO		SEO	
	A	**C**	**A**	**C**	**A**	**C**
E. faecalis ATCC 29212	1.56	>12.5	25	6.25	12.5	12.5
L. acidophilus ATCC 11975	3.12	>12.5	1.56	1.56	12.5	12.5
L. casei RSKK 06029	0.78	>12.5	1.56	1.56	6.25	12.5
S. mutans ATCC 25175	1.56	12.5	1.56	3.12	3.12	12.5

*A: Alone, C: Combination

Moon et al. (2011) evaluated the efficacy of SEO alone and in combination with antibiotics against oral pathogenic bacteria. In the study, the MIC value of SEO was reported as 0.2 mg/ml against *S. mutans*, and the MIC values of its combinations with ampicillin and gentamicin were each reported as 0.05 mg/ml. In our study, the MIC value of SEO against *S. mutans* was reduced 2-fold with the LL-37 combination, while it increased 4-fold with the lactoferricin combination.

In our study, the combinations of MEO with LL-37 and lactoferricin reduced the MIC value of MEO by 4-fold against *E. faecalis*. Furthermore, the LL-37 combination reduced the MIC value of clove essential oil by 4-fold against *L. acidophilus*.

The LL-37 combination increased the MIC value of TEO by 4-fold against *L. casei* and the MIC value of MEO by 8-fold. The lactoferricin combination reduced the antibacterial activity of TEO against all test bacteria. Additionally, the lactoferricin combination increased the MIC value of SEO by 4-fold against *S. mutans*.

In the peptide and essential oil combinations prepared in the study, both increases and decreases in the MIC values of essential oils were observed in the presence of antimicrobial peptides, depending on the bacterial species. Particularly, in the combinations of MEO with LL-37 or lactoferricin peptides, a 4-fold reduction in MIC values against *E. faecalis* was detected, indicating a notable increase in activity. In contrast, a strong antagonistic effect was found in the combination of lactoferricin with TEO, where activity decreased in all tested bacteria. The data obtained from this study show that essential oils and antimicrobial peptides have a high interaction potential. At the same time, the species-specific nature of these interactions indicates the necessity of prior evaluation for therapeutic applications.

The mechanisms underlying the enhancing or reducing effects of antimicrobial peptides on the activities of essential oils may depend on various factors. For example, activity enhancement may occur due to essential oils disrupting the bacterial cell membrane, increasing permeability, and allowing peptides to reach intracellular targets. Conversely, activity reduction may develop when essential oil components affect peptide stability and structural conformation. In conclusion, further studies are needed to fully elucidate the underlying mechanisms. A literature review revealed no studies evaluating the activities of antimicrobial peptides and essential oil combinations. In this respect, the results obtained from our study will contribute to the literature.

CONCLUSION

In this study, the effects of antimicrobial peptides and essential oils on oral pathogens were evaluated both individually and in combination at stock concentrations. While the antimicrobial peptides did not exhibit antibacterial activity at the tested concentrations when used alone, their efficacy appeared to increase in the presence of certain essential oils. Moreover, it was determined that the effectiveness of the combina-

tions varied depending on the bacterial species. These variations in activity highlight the need for a detailed investigation into the interactions between essential oils and peptides. In this context, evaluating combinations of natural agents may represent an important step toward the development of alternative therapeutic approaches.

ACKNOWLEDGMENT

This study was supported by the Scientific Research Projects Coordination Unit of Ankara University under project number TYL-2023-2776.

AUTHOR CONTRIBUTION STATEMENT

MSK: Conceptualization, Data curation, Formal analysis, Writing – original draft. NA: Methodology, Project administration, Writing – review and editing. SAE: Formal analysis, Methodology, Validation.

CONFLICT OF INTEREST

The authors declare that there is no conflict of interest.

REFERENCES

Aguiar, G. P., Carvalho, C. E., Dias, H. J., Reis, E. B., Martins, M. H. G., Wakabayashi, K. A. L., … Crotti, A. E. M. (2013). Antimicrobial activity of selected essential oils against cariogenic bacteria. *Natural Product Research, 27*(18), 1668–1672. https://doi.org/10.1080/14786419.2012.751595

Alghamdi, F., & Shakir, M. (2020). The influence of *Enterococcus faecalis* as a dental root canal pathogen on endodontic treatment: A systematic review. *Cureus, 12*(3). https://doi.org/10.7759/CUREUS.7257

Anisimova, E. A., & Yarullina, D. R. (2019). Antibiotic resistance of *Lactobacıllus* Strains. *Current Microbiology, 76*(12), 1407–1416. https://doi.org/10.1007/s00284-019-01769-7

Balappanavar, A., Sardana, V., & Singh, M. (2013). Comparison of the effectiveness of 0.5% tea, 2% neem and, 0.2% chlorhexidine mouthwashes on oral health: A randomized control trial. *Indian Journal of Dental Research, 24*(1), 26. https://doi.org/10.4103/0970-9290.114933

Bathily, M., Cissé, K., Youssefi, Y., Ou-Ani, O., Oucheikh, L., Ngom, B., … Costa, J. (2023). Evaluation of the inhibiting power of essential oil extracted from cloves (*Syzygium aromaticum*) on corrosion of steel C24 in medium HCl 1M. *Analytical and Bioanalytical Electrochemistry, 15*(10), 891–913. https://doi.org/10.22034/abec.2023.708677

Batista, A. L. A., Diógenes Alves UchÔa Lins, R., de Souza Coelho, R., do Nascimento Barbosa, D., Moura Belém, N., & Alves Celestino, F. J. (2014). Clinical efficacy analysis of the mouth rinsing with pomegranate and chamomile plant extracts in the gingival bleeding reduction. *Complementary Therapies in Clinical Practice, 20*(1), 93–98. https://doi.org/10.1016/J.CTCP.2013.08.002

Black, C., Al Mahmud, H., Howle, V., Wilson, S., Smith, A. C., & Wakeman, C. A. (2023). Development of a polymicrobial checkerboard assay as a tool for determining combinatorial antibiotic effectiveness in polymicrobial communities. *Antibiotics, 12*(7). https://doi.org/10.3390/antibiotics12071207

Bota, V., Sumalan, R. M., Obistioiu, D., Negrea, M., Cocan, I., Popescu, I., & Alexa, E. (2022). Study on the sustainability potential of thyme, oregano, and coriander essential oils used as vapours for antifungal protection of wheat and wheat products. *Sustainability (Switzerland), 14*(7). https://doi.org/10.3390/su14074298

de Oliveira Carvalho, I., Purgato, G. A., Píccolo, M. S., Pizziolo, V. R., Coelho, R. R., Diaz-Muñoz, G., & Alves Nogueira Diaz, M. (2020). *In vitro* anticariogenic and antibiofilm activities of toothpastes formulated with essential oils. *Archives of Oral Biology, 117*, 104834. https://doi.org/10.1016/J.ARCHORALBIO.2020.104834

Dolghi, A., Coricovac, D., Dinu, S., Pinzaru, I., Dehelean, C. A., Grosu, C., … Sarau, C. A. (2022). Chemical and antimicrobial characterization of *Mentha piperita* L. and *Rosmarinus officinalis* L. essential oils and *in vitro* potential cytotoxic effect in human colorectal carcinoma cells. *Molecules, 27*(18). https://doi.org/10.3390/molecules27186106

Elgamily, H., Safy, R., & Makharita, R. (2019). Influence of medicinal plant extracts on the growth of oral pathogens *Streptococcus mutans* and *Lactobacillus acidophilus*: An *in-vitro* study. *Macedonian Journal of Medical Sciences, 7*(14), 2328. https://doi.org/10.3889/oamjms.2019.653

Enigk, K., Jentsch, H., Rodloff, A. C., Eschrich, K., & Stingu, C. S. (2020). Activity of five antimicrobial peptides against periodontal as well as non-periodontal pathogenic strains. *Journal of Oral Microbiology, 12*(1). https://doi.org/10.1080/20002297.2020.1829405

Fani, M., & Kohanteb, J. (2017). *In vitro* antimicrobial activity of *Thymus vulgaris* essential oil against major oral pathogens. *Journal of Evidence-Based Complementary & Alternative Medicine, 22*(4), 660. https://doi.org/10.1177/2156587217700772

Figueira, L. W., de Oliveira, J. R., Camargo, S. E. A., & de Oliveira, L. D. (2020). *Curcuma longa* L. (turmeric), *Rosmarinus officinalis* L. (rosemary), and *Thymus vulgaris* L. (thyme) extracts aid murine macrophages (RAW 264.7) to fight *Streptococcus mutans* during *in vitro* infection. *Archives of Microbiology, 202*(8), 2269–2277. https://doi.org/10.1007/s00203-020-01945-5

Galvão, L. C. D. C., Furletti, V. F., Bersan, S. M. F., Da Cunha, M. G., Ruiz, A. L. T. G., Carvalho, J. E. De, … Rosalen, P. L. (2012). Antimicrobial activity of essential oils against *Streptococcus mutans* and their antiproliferative effects. *Evidence-Based Complementary and Alternative Medicine*, 2012. https://doi.org/10.1155/2012/751435

Goldbeck, J. C., do Nascimento, J. E., Jacob, R. G., Fiorentini, Â. M., & da Silva, W. P. (2014). Bioactivity of essential oils from *Eucalyptus globulus* and *Eucalyptus urograndis* against planktonic cells and biofilms of *Streptococcus mutans*. *Industrial Crops and Products, 60*, 304–309. https://doi.org/10.1016/J.INDCROP.2014.05.030

Golestannejad, Z., Gavanji, S., Mohammadi, E., Motamedi, A., Bahrani, M., Rezaei, F., … Bakhtari, A. (2017). Comparison of antibacterial activity of essential oils of *Foeniculum vulgare* Mill, *Mentha arvensis,* and *Mentha piperita* against *Streptococcus mutans*. *Advanced Herbal Medicine*, *3*(1), 3–13. Retrieved from https://fnp.skums.ac.ir/Article/fnp-67

Hamdoon, A. M., Aspatwar, A., Aljarbooa, A. F., & Qureshi, K. A. (2024). Comparative study of volatile oil constituents, anti-microbial properties, and antibiofilm activities in *Eucalyptus camaldulensis* and *Eucalyptus globulus*: Insights from central Saudi Arabia. *Journal of Essential Oil Bearing Plants, 27*(2), 341-355. https://doi.org/10.1080/0972060X.2024.2324343

Harkat-Madouri, L., Asma, B., Madani, K., Bey-Ould Si Said, Z., Rigou, P., Grenier, D., … Boulekbache-Makhlouf, L. (2015). Chemical composition, antibacterial, and antioxidant activities of essential oil of *Eucalyptus globulus* from Algeria. *Industrial Crops and Products, 78*, 148–153. https://doi.org/10.1016/J.INDCROP.2015.10.015

Jain, N., Dutt, U., Radenkov, I., & Jain, S. (2024). WHO's global oral health status report 2022: Actions, discussion, and implementation. *Oral Diseases, 30*(2), 73–79. https://doi.org/10.1111/ODI.14516

Kassebaum, N. J., Smith, A. G. C., Bernabé, E., Fleming, T. D., Reynolds, A. E., Vos, T., … Yonemoto, N. (2017). Global, regional, and national prevalence, incidence, and disability-adjusted life years for oral conditions for 195 countries, 1990-2015: A systematic analysis for the global burden of diseases, ınjuries, and risk factors. *Journal of Dental Research, 96*(4), 380–387. https://doi.org/10.1177/0022034517693566

Lima, S. M. F., Freire, M. S., Gomes, A. L. O., Cantuária, A. P. C., Dutra, F. R. P., Magalhães, B. S., … Rezende, T. M. B. (2017). Antimicrobial and immunomodulatory activity of host defense peptides, clavanins and LL-37, *in vitro*: An endodontic perspective. *Peptides, 95*, 16–24. https://doi.org/10.1016/J.PEPTIDES.2017.07.005

Mahlapuu, M., Håkansson, J., Ringstad, L., & Björn, C. (2016). Antimicrobial peptides: An emerging category of therapeutic agents. *Frontiers in Cellular and Infection Microbiology, 6*(DEC), 235805. https://doi.org/10.3389/FCIMB.2016.00194/BIBTEX

Midorikawa, K., Ouhara, K., Komatsuzawa, H., Kawai, T., Yamada, S., Fujiwara, T., & Sugai, M. (2003). *Staphylococcus aureus* susceptibility to innate antimicrobial peptides, beta-defensins, and CAP18, expressed by human keratinocytes. *Infection and Immunity, 71*(7), 3730–3739. https://doi.org/10.1128/IAI.71.7.3730-3739.2003

Moon, S. E., Kim, H. Y., & Cha, J. D. (2011). Synergistic effect between clove oil and its major compounds and antibiotics against oral bacteria. *Archives of Oral Biology, 56*(9), 907–916. https://doi.org/10.1016/J.ARCHORALBIO.2011.02.005

Nagy-Bota, M. C., Man, A., Santacroce, L., Brinzaniuc, K., Pap, Z., Pacurar, M., … Kovacs, M. (2021). Essential oils as alternatives for root-canal treatment and infection control against *Enterococcus faecalis*—A preliminary study. *Applied Sciences, 11*(4), 1422. https://doi.org/10.3390/APP11041422

Nikolić, M., Jovanović, K. K., Marković, T., Marković, D., Gligorijević, N., Radulović, S., & Soković, M. (2014). Chemical composition, antimicrobial, and cytotoxic properties of five Lamiaceae essential oils. *Industrial Crops and Products, 61,* 225–232. https://doi.org/10.1016/J.INDCROP.2014.07.011

Ouhara, K., Komatsuzawa, H., Yamada, S., Shiba, H., Fujiwara, T., Ohara, M., … Sugai, M. (2005). Susceptibilities of periodontopathogenic and cariogenic bacteria to antibacterial peptides, β-defensins, and LL37, produced by human epithelial cells. *Journal of Antimicrobial Chemotherapy, 55*(6), 888–896. https://doi.org/10.1093/JAC/DKI103

Palombo, E. A. (2011). Traditional medicinal plant extracts and natural products with activity against oral bacteria: Potential application in the prevention and treatment of oral diseases. *Evidence-Based Complementary and Alternative Medicine: ECAM*, 15. https://doi.org/10.1093/ECAM/NEP067

Peres, M. A., Macpherson, L. M. D., Weyant, R. J., Daly, B., Venturelli, R., Mathur, M. R., … Watt, R. G. (2019). Oral diseases: A global public health challenge. *The Lancet, 394(10194)*, 249–260. https://doi.org/10.1016/S0140-6736(19)31146-8

Rima, M., Rima, M., Fajloun, Z., Sabatier, J. M., Bechinger, B., & Naas, T. (2021). Antimicrobial peptides: A potent alternative to antibiotics. *Antibiotics, 10*(9), 1095. https://doi.org/10.3390/ANTIBIOTICS10091095

Schmidtchen, A., Frick, I. M., Andersson, E., Tapper, H., & Björck, L. (2002). Proteinases of common pathogenic bacteria degrade and inactivate the antibacterial peptide LL-37. *Molecular Microbiology, 46*(1), 157–168. https://doi.org/10.1046/J.1365-2958.2002.03146.X

Wen, Z. T., Huang, X., Ellepola, K., Liao, S., & Li, Y. (2022). Lactobacilli and human dental caries: More than mechanical retention. *Microbiology (United Kingdom), 168*(6), 001196. https://doi.org/10.1099/mic.0.001196

Wu, M., & Hancock, R. E. W. (1999). Interaction of the cyclic antimicrobial cationic peptide bactenecin with the outer and cytoplasmic membrane. *The Journal of Biological Chemistry, 274*(1), 29–35. https://doi.org/10.1074/JBC.274.1.29

Wuersching, S. N., Huth, K. C., Hickel, R., & Kollmuss, M. (2021). Inhibitory effect of LL-37 and human lactoferricin on growth and biofilm formation of anaerobes associated with oral diseases. *Anaerobe, 67,* 102301. https://doi.org/10.1016/J.ANAEROBE.2020.102301

FABAD J. Pharm. Sci., 51, 1, 115-128, 2026
Doi: 10.55262/fabadeczacilik.1830968
RESEARCH ARTICLE

Investigation of Synthesis, X-Ray Characterization and Biological Activities of Copper(II) Imidazole Complexes

Sevda ER[*°], Hakan ÜNVER[**], Banu BARUTCA[***]

Investigation of Synthesis, X-Ray Characterization, and Biological Activities of Copper(II) Imidazole Complexes

SUMMARY

Copper, a transition metal, possesses antimicrobial and anticancer properties. This trace element plays a critical role in various biological functions in the human body. Copper complexes have been found to enhance the effects of pharmaceuticals, with significant interest in studying their biological activities, especially when coordinated with therapeutic ligands like thiosemicarbazones, phosphines, imidazole, and benzimidazole. In this research, copper complexes containing imidazole and benzimidazole derivatives were synthesized and thoroughly characterized. Their antimicrobial and cytotoxic properties were evaluated. The antimicrobial effects of these complexes against bacterial strains were assessed using the Microbroth Dilution Technique. Additionally, the cytotoxicity of the synthesized complexes was tested on the Panc-1 and Clone-9 cell lines through LDH and MTT assays. The antimicrobial tests revealed that the copper(II) complex with the imidazole ligand (Complex 1) exhibited superior antimicrobial activity compared to the benzimidazole-based complex (Complex 2). On the other hand, MTT and LDH assays indicated that Complex 2 had a stronger cytotoxic effect on Clone-9 cells than Complex 1. However, Complex 1 showed greater activity against Panc-1 cells overall. The findings suggest that the copper(II)-imidazole complex could serve as a potential candidate for developing alternative chemotherapeutic agents.

Keywords: *Antimicrobial Activity, Benzimidazole, Copper(II) Complexes, Cytotoxicity, Imidazole, Panc-1 Cell Line.*

Bakır(II) İmidazol Komplekslerinin Sentezi, X-Ray Karakterizasyonu ve Biyolojik Aktivitelerinin Araştırılması

ÖZ

Bir geçiş metali olan bakır, antimikrobiyal ve antikanser özelliklere sahiptir. Bu eser element, insan vücudundaki çeşitli biyolojik işlevlerde kritik bir rol oynamaktadır. Bakır komplekslerinin, özellikle tiyosemikarbazonlar, fosfinler, imidazol ve benzimidazol gibi terapötik ligandlarla koordine edildiğinde, ilaçların etkilerini artırdığı bulunmuş ve biyolojik aktivitelerinin incelenmesine önemli ilgi gösterilmiştir. Bu araştırmada, imidazol ve benzimidazol türevleri içeren bakır kompleksleri sentezlenmiş ve kapsamlı bir şekilde karakterize edilmiştir. Antimikrobiyal ve sitotoksik özellikleri değerlendirilmiştir. Bu komplekslerin bakteri suşlarına karşı antimikrobiyal etkileri Mikrobroth Dilüsyon Tekniği kullanılarak değerlendirilmiştir. Ayrıca, sentezlenen komplekslerin sitotoksisitesi Panc-1 ve Klon-9 hücre hatları üzerinde LDH ve MTT analizleri ile test edilmiştir. Antimikrobiyal aktivite testleri, imidazol ligandlı bakır(II) kompleksinin (Kompleks 1), benzimidazol bazlı komplekse (Kompleks 2) kıyasla daha etkili olduğunu ortaya koymuştur. Öte yandan, MTT ve LDH analizleri, Kompleks 2'nin Klon-9 hücreleri üzerinde Kompleks 1'den daha güçlü bir sitotoksik etkiye sahip olduğunu göstermiştir. Ancak Kompleks 1'in, genel olarak Panc-1 hücrelerine karşı daha yüksek aktivite gösterdiği sonucuna varılmıştır. Bulgular, bakır(II)-imidazol kompleksinin alternatif kemoterapötik ajanların geliştirilmesi için potansiyel bir aday olabileceğini düşündürmektedir.

Anahtar Kelimeler: *Antimikrobiyal Aktivite, Benzimidazol, Bakır(II) Kompleksleri, Sitotoksisite, İmidazol, Panc-1 Hücre Hattı.*

Recieved: 27.11.2025
Revised: 10.01.2026
Accepted: 20.01.2026

[*] ORCID: 0000-0002-8210-0915, Department of Pharmacy, Yunus Emre Vocational School, Anadolu University, 26470, Eskişehir, Turkey
[**] ORCID: 0000-0002-4858-4039, Department of Chemistry, Faculty of Science, Eskisehir Technical University, 26470, Eskişehir, Turkey
[***] ORCID: 0000-0003-3533-170X, Yunus Emre Vocational School, Anadolu University, 26470, Eskişehir, Turkey

[°] Corresponding Author; Sevda ER
E-mail: sevdaer@anadolu.edu.tr

INTRODUCTION

Copper plays an important role in regulating intracellular redox states by acting as a cofactor for several enzymes within the human body. It has been recognized for its antimicrobial and anticancer properties (Nakahata et al., 2017; Ünver et al., 2022).

The global rise of antibiotic resistance, coupled with the limited number of available antibiotics, poses significant risks to public health. The challenge of treating infections caused by resistant pathogens contributes to the increased prevalence of chronic diseases (Mahmood et al., 2019).

This underscores the urgent demand for new antimicrobial solutions. Among the promising candidates, transition metal complexes, especially those involving copper, have become a focal point in research due to their ability to serve as effective antimicrobial agents (Saddam Hossain et al., 2018). Copper complexes, in particular, have garnered significant attention for their demonstrated antimicrobial properties (Ren et al., 2011).

These copper complexes also exhibit synergistic effects when combined with other drugs (Ren et al., 2011). The ability of copper-imidazole and copper-benzimidazole complexes to demonstrate a wide array of biological activities continues to fuel interest in their synthesis (Mendoza et al., 2013). Previous studies have reported various biological activities of copper (II) complexes containing imidazole and benzimidazole ligands, such as antibacterial, antifungal, antiamoebic, and antiparasitic effects (Bandopadhyay et al., 2022; Beheshti et al., 2021; Chen et al., 2012; Mañozca-Dosman et al., 2025). For instance, Atria et al. (2011) demonstrated that copper complexes with imidazole derivatives exhibited antimicrobial properties against several bacterial strains. In another study, a copper complex containing an imidazole ring was shown to possess antimicrobial activity against *Staphylococcus aureus* and *Escherichia coli* (Chai et al., 2018). Furthermore, 2-benzimidazole derivatives have been shown to have both antibacterial and mycobacterial effects (Chen et al., 2012). In a study by Ajibola et al. (2020), a copper-benzimidazole complex demonstrated superior antibacterial activity against *S. aureus*, *Klebsiella pneumoniae*, and *Acinetobacter baumannii* when compared to the benzimidazole ligand.

Cancer continues to be a major global health threat, with the World Health Organization forecasting that cancer-related deaths may rise to 13.1 million by 2030 (Paul et al., 2021). Since the 1970s, there has been a growing interest in developing more effective anticancer agents, particularly those with higher efficacy than platinum-based drugs (Alshehri et al., 2022). Copper, an essential endogenous metal, has gained attention for its low toxicity and high coordination ability, making it a promising candidate for anticancer therapy (Cai et al., 2021).

Increased concentrations of copper in the bloodstream have been associated with the advancement of several types of cancer, as malignant cells often accumulate more copper compared to normal cells. This heightened copper absorption could potentially inhibit angiogenesis, the process by which new blood vessels develop to nourish tumors with oxygen and nutrients (Qiao et al., 2014). Numerous studies have explored the anticancer potential of copper complexes in cancers such as liver, cervical, lung, and breast cancers (Manjuraj et al., 2018). Research indicates that copper-based therapeutics could offer a promising strategy for targeted cancer treatment (Qiao et al., 2014). In addition, copper complexes with therapeutic ligands such as thiosemicarbazones, imidazoles, and phosphines have attracted considerable attention in recent years (Alshehri et al., 2022).

In this research, we describe the synthesis of two copper (II) complexes, each incorporating imidazole and benzimidazole-derived ligands. Comprehensive structural analysis of these complexes was carried out using single-crystal X-ray diffraction techniques. Furthermore, the antimicrobial activities of the complexes were assessed against a variety of bacterial strains. Their cytotoxic effects were also evaluated on the Panc-1 human pancreatic cancer cell line and Clone-9 rat liver epithelial cells using LDH and MTT assays.

MATERIALS AND METHODS

General considerations

Copper(II) perchlorate hexahydrate ($Cu(ClO_4)_2 6H_2O$), 4-dimethylaminopyridine (DMAP), and solvents were purchased from commercial suppliers (TCI, Sigma, J&K Scientific). The imidazole-based ligand 1-(4-(trifluoromethyl)benzyl)-1*H*-imidazole (ImCF3) and the benzimidazole derivative 1-benzyl-1*H*-benzo[d]imidazole (Benzim) were synthesized following published procedures with slight modifications (RSC Adv., 2018, 8, 40000, doi: 10.1039/c8ra08897g). Elemental analysis was conducted with an Elementar Vario EL III microanalyzer. FT-IR spectra were obtained using a Perkin Elmer Spectrum 100 Spectrometer, covering the 4000–400 cm^{-1} range, with KBr pellets. The process for synthesizing the copper complexes is illustrated in Figure 1.

Synthesis of copper complexes 1 and 2

Complex 1 [$Cu(ImCF_3)_4(ClO_4)_2$]

A 10 mL methanol solution containing 4 equivalents of ImCF3 (0.4 mmol, 90.5 mg) was prepared, to which copper(II) perchlorate hexahydrate (0.1 mmol, 37 mg) was added. The mixture was stirred at 60°C for 24 hours. After filtration, the resulting deep blue solution was allowed to evaporate at room temperature, leading to the formation of deep blue crystals after five days. The copper complex was isolated with a yield of 49% (63 mg). The elemental analysis confirmed the chemical formula: $[Cu(C_{11}H_9N_2F_3)_4(ClO_4)_2]$. **Elemental Analysis:** Anal. Calcd (%) for $C_{44}H_{36}N_8O_8Cl_2F_{12}Cu$: C, 45.28; H, 3.11; N, 9.60. Found (%): C, 45.16; H, 3.18; N, 9.58. **FT-IR (KBr, cm^{-1}):** 3144, 1323, 1091.

Complex 2 [$Cu(Benzim)_2(DMAP)_2](ClO_4)_2$

In a 10 mL methanol solution, copper(II) perchlorate hexahydrate (0.1 mmol, 37 mg) was mixed with two equivalents of Benzim (0.2 mmol, 41.6 mg) and two equivalents of DMAP (0.2 mmol, 24.4 mg). The resulting mixture was stirred at 60°C for 12 hours. After 6 days, crystals were formed, and the final yield was 50% (52 mg). Elemental analysis confirmed the composition as $[Cu(C_{14}H_{12}N_2)_2(C_6H_{10}N_2)_2](ClO_4)_2$. **Elemental Analysis:** Anal. Calcd (%) for $C_{42}H_{44}N_8O_8Cl_2Cu$: C, 54.64; H, 4.80; N, 12.14. Found (%): C, 54.68; H, 4.75; N, 12.19. **FT-IR (KBr, cm^{-1}):** 3146, 1617, 1056.

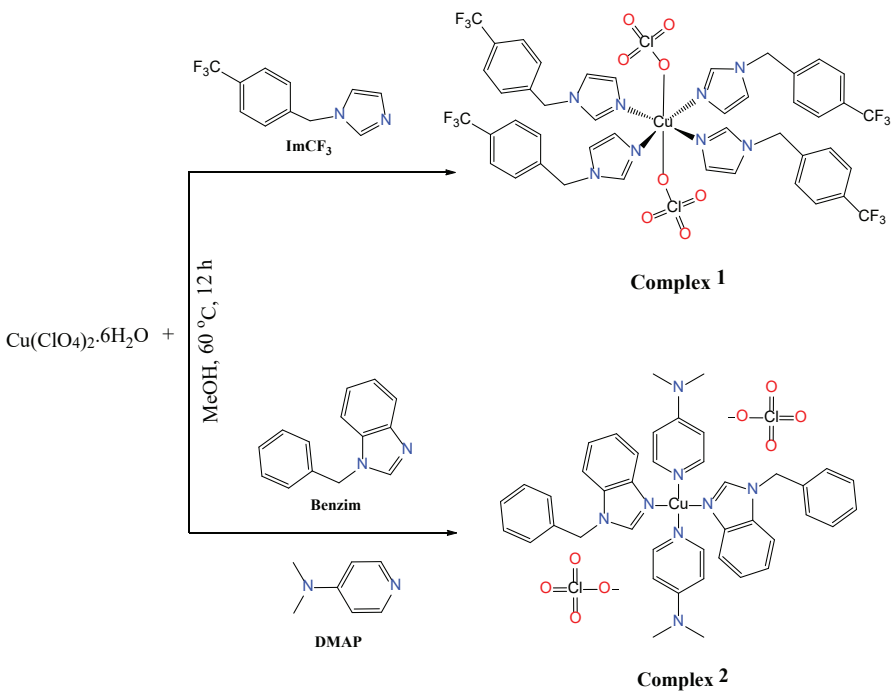


Figure 1. Synthesis procedure of two copper(II) complexes

X-ray crystallography

Single crystals of Complexes 1 and 2 were obtained by evaporating the solvents used in the reactions. X-ray diffraction analysis was conducted at 296.15 K using a Bruker APEX-II D8 Venture diffractometer with Mo Kα radiation (λ = 0.71073 Å). The data were processed with Bruker SMART software, and the structure was solved using the SHELXS program. Refinement was carried out using full-matrix least-squares (Shedrick, 2008), with hydrogen atoms placed at calculated positions. Molecular structures were visualized using the MERCURY software (Macrae et al., 2006).

Antimicrobial activity with MTT assay

Test bacteria

Acinetobacter baumannii ATCC 19606, *Enterococcus faecalis* ATCC 29210, *Escherichia coli* ATCC 25922, *Klebsiella pneumoniae* ATCC 70063, *Klebsiella pneumoniae* MCTC 13438, MRSA ATCC 43300, *Pseudomonas aeruginosa* ATCC 27853, *Pseudomonas aeruginosa* PA01, *Staphylococcus aureus* ATCC 25923, and *Staphylococcus epidermidis* CECT 4183 bacteria were used in the experiment. These strains were stored in a -86°C (EQUITEC) incubated in brain-heart infusion broth (Merck) at 37°C for 24 hours before use.

Minimum inhibitory concentration (MIC)

The MIC values were determined using the Microbroth Dilution Method (CLSI, 2006). Copper complexes containing imidazole and benzimidazole derivatives (Complex 1, Cu, Imi¸ Complex 2, DMAP, and Benzim) were dissolved in¸ dimethyl sulfoxide (DMSO) and then diluted in Mueller Hinton Broth. Following bacterial inoculation, the plates were incubated at 37°C for 24 hours. The MIC was defined as the lowest concentration at which no purple color appeared upon adding MTT reagent. Chloramphenicol was used as the positive control, while DMSO served as the negative control.

Minimum bactericidal concentration (MBC)

To ascertain the MBC, the wells that showed the MIC were streaked onto Mueller-Hinton agar plates and incubated at 37°C for 24 hours. The MBC was noted as having the lowest concentration where no bacterial growth was visible (Er et al., 2023).

Cytotoxicity assessment in Panc-1 and Clone-9 cell lines

Cell lines and culture conditions

Panc-1 (human pancreatic carcinoma, ATCC CRL-1469) and Clone-9 (rat liver epithelium, ATCC CRL-1439) cell lines were cultured under standard 37°C, 5% CO_2 conditions using DMEM or F-12K media (Capricorn Scientific GmbH) supplemented with 10% FBS (Sigma-Aldrich) and 1% penicillin–streptomycin. Complexes 1 and 2 were dissolved in DMSO (Sigma-Aldrich), with the final solvent concentration maintained below 0.01%. Cells were exposed to 0.0078–0.062 mg/mL of each compound, and viability was assessed after 24 and 48 hours.

MTT reduction assay

The cytotoxic effects of Complexes 1 and 2 were assessed via an MTT viability assay, following established protocols (Liu et al., 1997; Mosmann, 1983). Cells were seeded at 1×10^4 per well in 96-well plates and allowed to adhere for 24 hours before treatment. Serial concentrations of each compound (0.16–33.3 μM) were added for either 24 or 48 hours. After exposure, the medium was replaced with 100 μL of MTT solution (0.5 mg/mL) (Sigma-Aldrich Co.) and incubated for 3 hours at 37 °C to allow for formazan formation. The supernatant was then removed, and 200 μL of DMSO was added to dissolve the crystals. Absorbance at 570 nm was recorded using a BioTek 800 TS reader. All conditions were tested in triplicate, each with eight technical replicates.

Membrane integrity: LDH release assay

The integrity of the cell membrane was assessed by measuring LDH release using the CytoTox-ONE kit (Promega). Clone-9 and Panc-1 cells (10×10^3 per well) were treated with Complexes 1 and 2, or DMSO (solvent control), after 24 and 48 hours. Cytotoxicity was assessed by comparing the LDH release in treated cells with control cells (Garcia et al., 2012).

Statistical analysis

All experiments were performed in triplicate, and data were analyzed with one-way ANOVA using SPSS 22.0. Results are presented as mean ± SD, with statistical significance defined as $p \leq 0.05$. IC_{50} values were determined by nonlinear regression from at least three independent assays using GraphPad Prism 6.01 (GraphPad Software, La Jolla, CA, USA). Selectivity Index (SI) values were determined by calculating the ratio of IC_{50} values in normal cells to those in cancer cells (SI = IC50 normal / IC50 cancer). A SI value greater than 1 indicates preferential cytotoxicity toward cancer cells.

RESULTS AND DISCUSSION

Structural characterization of complexes 1 and 2

The formation of two copper(II) complexes, referred to as Complex 1 and Complex 2, was confirmed using X-ray diffraction analysis. Figure 2 presents the ORTEP representations of their molecular structures, and Tables 1 and 2 summarize the crystallographic data, including bond lengths and angles.

Table 1. Crystal data and structure refinement parameters for copper(II) complexes.

	Complex 1	Complex 2
Molecular Formula	$[Cu(ImCF_3)_4(ClO_4)_2]$	$[Cu(Benzim)_2(DMAP)_2](ClO_4)_2$
CCDC number	1989602	1956477
Empirical formula	$C_{22}H_{18.16}ClCu_{0.5}F_{5.84}N_4O_4$	$C_{21}H_{22}ClCu_{0.5}N_4O_4$
Formula weight	580.79	461.64
Temperature	273.15 K	296.15
Wavelength	0.71073 Å	0.71073 Å
Crystal system, space group	Triclinic, P-1	Monoclinic, $P2_1/c$
Unit cell dimensions	a = 9.0363(17) Å alpha = 65.120(4)° b = 16.804(3) Å beta = 90° c = 18.146(3) Å gamma = 90°	a = 11.366(2) **Å alpha = 90°** b = 9.716(2) **Å beta** = 101.193(13)° c = 19.329(4) **Å gamma = 90°**
Volume	2499.7(8) A^3	2093.9(8) A^3
Z, Calculated density	4, 1.543 mg/m^3	4, 1.464 mg/m^3
Absorption coefficient	0.647 mm^{-1}	0.713 mm^{-1}
F(000)	1177.0	958.0
Crystal size	0.3 × 0.2 × 0.2 mm	0.1 × 0.08 × 0.07 mm
Theta range	6.258 to 56.982 deg	3.652 to 56.862 deg
Limiting indices	-12 ≤ h ≤ 12, -22 ≤ k ≤ 22, -24 ≤ l ≤ 24	-15 ≤ h ≤ 15, -12 ≤ k ≤ 12, -23 ≤ l ≤ 25
Reflections coll. / unique	63706/ 12564 [R_{int} **= 0.1899**]	20884/ 5138 [R_{int} = 0.0461]
Completeness to theta	99.3% 28.491	97.9% 28.431
Absorption correction	Integration	Integration
Refinement method	Full-matrix least-squares on F^2	Full-matrix least-squares on F^2
Data/rest/parameters	12564/21/698	5138/0/279
Goodness-of-fit on F^2	0.946	1.051
Final R indices [I>2sigma(I)]	R_1 **= 0.0821, wR_2 = 0.1817**	R_1 = 0.0505, wR_2 = 0.1239
R indices (all data)	R_1 **= 0.2816, wR_2 = 0.2606**	R_1 = 0.1105, wR_2 = 0.1492
Largest diff. peak and hole	0.45 and -0.37 $e.A^{-3}$	0.58 and -0.47$e.A^{-3}$

Complex 1 crystallizes in the triclinic system with the P-1 space group, whereas Complex 2 adopts a monoclinic structure with the P21/c space group. Both complexes exhibit mononuclear coordination. In Complex 1, the copper center is coordinated by four nitrogen atoms from monodentate $ImCF_3$ ligands and two oxygen atoms from perchlorate anions. The nitrogen and oxygen bond lengths are 1.987–1.999

Å and 2.597 Å, respectively. The overall geometry of Complex 1 is a distorted octahedron, attributed to the elongated copper-oxygen bonds. The observed bond angles include N(1)-Cu(1)-O(1'), N(1)-Cu(1)-N(3), and N(3)-Cu(1)-O(1'), measuring 80.40°, 87.86°, and 90.51°, respectively.

In Complex 2, the copper ion coordinates with two benzimidazole (Benzim) and two 4-DMAP ligands. The bond distances range between 1.994 and 2.001 Å. The coordination geometry is classified as distorted square planar, with notable bond angles such as N(3)-Cu(1)-N(1), N(3)-Cu(1)-N(1'), and O(1)-Cl(1)-O(3), recorded at 89.67°, 90.33°, and 109.10°, respectively. Additionally, both complexes exhibit π–π stacking and hydrogen bonding interactions, which enhance their crystallographic stability.

Table 2. Selected bond distances (Å) and bond angles of two copper(II) complexes

Complex 1	
Bond Distances (Å)	**Bond Angles (°)**
Cu(1)-N(1) 1.987	N(1)-Cu(1)-N(3) 87.86
Cu(1)-N(3) 1.999	N(1)- Cu(1)-O(1') 83.40
Cu(1)-O(1') 2.597	N(3)- Cu(1)-O(1') 90.51
Complex 2	
Bond Distances (Å)	**Bond Angles (°)**
Cu(1)-N(1) 2.001	N(3)-Cu(1)-N(1) 89.67
Cu(1)-N(3) 1.994	N(3)-Cu(1)-N(1') 90.33
Cl(1)-O(1) 1.370	O(1)-Cl(1)-O(3) 109.10

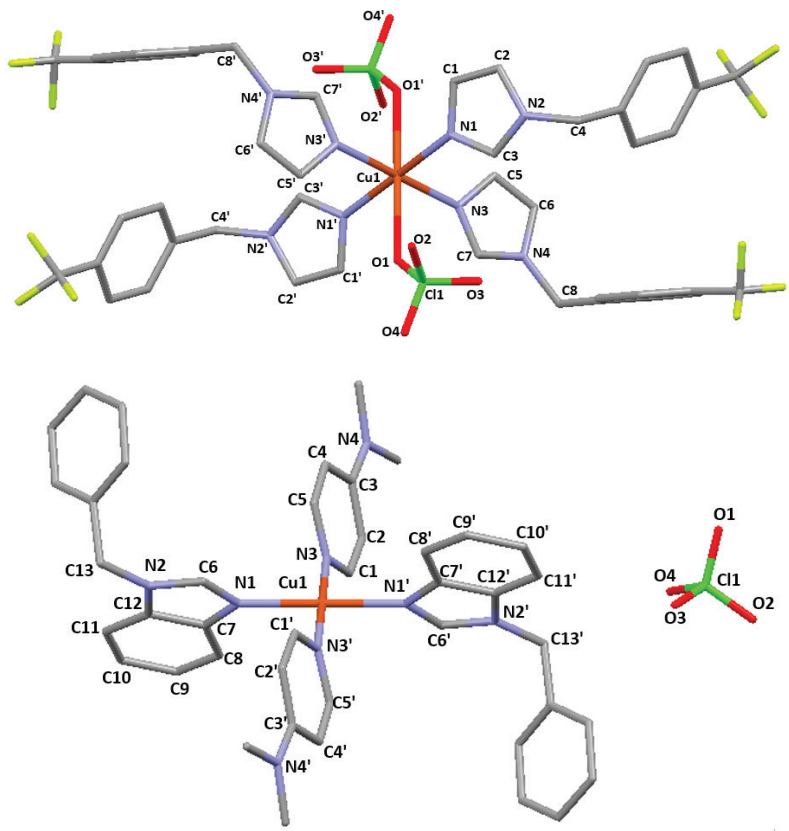


Figure 2. Molecular structures of copper complexes with thermal ellipsoid plots at the 20% probability level. Hydrogen atoms of both complexes were omitted for clarity.

Antimicrobial activity

Table 3 presents the MIC and MBC determined for the synthesized compounds. The results of the study showed that Complex 1 of the MIC values of *E. coli* ATCC 25922, *E. faecalis* ATCC 29210, *S. aureus* ATCC 25923 and *S. epidermidis* CECT 4183 bacteria were found to be 0.5, 0.5, 1, and 0.5 mg / mL, respectively. MIC values of other microorganisms (*A. baumannii* ATCC 19606, *K. pneumoniae* ATCC 70063, *K. pneumoniae* MCTC 13438, *P. aeruginosa* ATCC 27853, *P. aeruginosa* PA01, and MRSA ATCC 43300) were found above 2 mg / mL. The bactericidal activity of Complex 1 was observed above 2 mg/mL, except for *S. aureus* ATCC 25923 (1 mg / mL). When we look at the antimicrobial activity results of the Complex 2, the MIC and MBC values of all tested microorganisms were found to be above 2 mg / mL, except for the MIC value of *E. faecalis* ATCC 29210 (0.5 mg / mL) (Table 3.).

The Benzim ligand has MIC and MBC values similar to those of Complex 2. However, the MIC values of Imi ligand against Escherichia coli ATCC 25922, MRSA ATCC 43300, and Staphylococcus aureus ATCC 25923 bacteria were recorded as 0.25, 0.5, and 0.25 mg/mL, respectively (Table 3.). Imi ligand was observed to have a higher antibacterial effect against these bacteria compared to Complex 1. In Complex 1, imidazole is bound to copper, while in the Imi ligand it is free. Therefore, it is thought that the antimicrobial effect may be higher. No studies on this subject were found in the literature.

Table 3. Antibacterial activity results of Complex 1 and Complex 2 (mg / mL). MIC: Minimum inhibitory concentration; MBC: Minimum bactericidal concentration.

Microorganism name	Imidazole						Benzimidazole						Cloramphenicol	
	Complex 1		Cu		Imi		Complex 2		DMAP		Benzim			
	MIC	MBC	MIC	MBC	MIC	MBC	MIC	MBC	MIC	MBC	MIC	MBC	MIC	MBC
***Acinetobacter baumannii* ATCC 19606**	〉 2	〉 2	〉 2	〉 2	〉 2	〉 2	〉 2	〉 2	〉 2	〉 2	〉 2	〉 2	〉 1	〉 1
***Escherichia coli* ATCC 25922**	0.5	〉 2	〉 2	〉 2	0.25	〉 2	〉 2	〉 2	〉 2	〉 2	〉 2	〉 2	0.0078	0.0078
***Enterococcus faecalis* ATCC 29210**	0.5	〉 2	〉 2	〉 2	〉 2	〉 2	0.5	〉 2	〉 2	〉 2	〉 2	〉 2	0.0156	0.0156
***Klebsiella pneumoniae* ATCC 70063**	〉 2	〉 2	〉 2	〉 2	〉 2	〉 2	〉 2	〉 2	〉 2	〉 2	〉 2	〉 2	0.125	〉 1
***Klebsiella pneumoniae* MCTC 13438**	〉 2	〉 2	〉 2	〉 2	〉 2	〉 2	〉 2	〉 2	〉 2	〉 2	〉 2	〉 2	0.125	〉 1
***Pseudomonas aeruginosa* ATCC 27853**	〉 2	〉 2	〉 2	〉 2	〉 2	〉 2	〉 2	〉 2	〉 2	〉 2	〉 2	〉 2	〉 1	〉 1
***Pseudomonas aeruginosa* PA01**	〉 2	〉 2	〉 2	〉 2	〉 2	〉 2	〉 2	〉 2	〉 2	〉 2	〉 2	〉 2	〉 1	〉 1
MRSA ATCC 43300	〉 2	〉 2	〉 2	〉 2	0.5	0.5	〉 2	〉 2	〉 2	〉 2	〉 2	〉 2	0.0156	0.0156
***Staphylococcus aureus* ATCC 25923**	1	〉 2	〉 2	〉 2	0.25	0.5	〉 2	〉 2	〉 2	〉 2	〉 2	〉 2	0.0156	0.0312
***Staphylococcus epidermidis* CECT 4183**	0.5	1	〉 2	〉 2	0.5	0.5	〉 2	〉 2	〉 2	〉 2	1	1	0.0156	0.0156

In a study conducted by Rodríguez-Argüelles et al. (2005), MIC of imidazole-containing copper complexes on *E. coli* and *S. aureus* bacteria was reported above 0.1 mg / mL. In another study, MIC and MBC values of different copper complexes containing imidazole on *S. aureus* ATCC 25923 and *E. coli* ATCC 25922 were generally found to be 0.3 mg / mL and above 0.3 mg / mL (Gulya et al., 2013). In a study by Maru and Shah (2015), the MIC values of 2 different benzimidazole-containing copper complexes on *E. coli* MTCC 442, *P. aeruginosa* MTCC 44, and *S. aureus* MTCC 96 were found to be 0.5 mg / mL, 0.5 mg / mL, and 1 mg / mL, respectively.

Lobana et al. (2018) investigated the antimicrobial activity of copper complexes containing 11 different azole groups on different bacteria. As a result of the study, it was determined that each compound has different effects on the microorganism; it has been reported that the MIC values of 8 compounds on *S. aureus* bacteria vary between 10 and 1000 μg / mL, while the other 3 compounds have no effect. In addition, the MIC values of 10 compounds on *S. epidermidis* bacteria varied between 5-500 μg / mL, the other 1 compound had no effect on this bacteria; MIC values of 11 compounds on *E. faecalis* bacteria varied between 7-500 μg / mL; It has been reported that the MIC value of 1 compound on *E.coli* bacteria is 500 μg / mL, while the other 10 compounds have no effect on this bacteria.

Cytotoxic activity

The cytotoxic effects of Complexes 1 and 2 were assessed in Clone-9 normal hepatocytes and Panc-1 pancreatic cancer cells using MTT and LDH assays after 24 and 48 h of exposure to concentrations ranging from 0.0078 to 0.0625 mg/mL. These assays evaluate mitochondrial metabolic activity and membrane integrity, respectively. The results are shown in Figures 3A–D and 4A–B.

Both MTT and LDH assays indicated that Complex 1 did not induce appreciable cytotoxicity at lower concentrations (0.0078–0.015 mg/mL) in either cell line at either time point. In contrast, higher concentrations (0.031 and 0.0625 mg/mL) caused a statistically significant reduction in cell viability. After 24 h, this effect was more pronounced in Panc-1 cells, with viability decreases of approximately 25% and 45%, compared with reductions of approximately 14% and 54% in Clone-9 cells.

After 48 h of exposure, Clone-9 cell viability decreased by approximately 20% and 83% at 0.031 and 0.0625 mg/mL, respectively. In Panc-1 cells, viability remained comparable to controls at lower concentrations but declined markedly at higher concentrations, with reductions of approximately 68% and 97% at 0.031 and 0.0625 mg/mL, respectively.

The MTT assay showed that Complex 2 reduced Clone-9 cell viability in a time- and dose-dependent manner (Figure 3C.), with viability decreasing to approximately 50% and 25% at 0.062 mg/mL after 24 and 48 h, respectively. In Panc-1 cells, no cytotoxic effect was observed at lower concentrations (0.0078–0.031 mg/mL) after 24 h; however, viability declined by approximately 75% at the highest concentration. After 48 h, Panc-1 cell viability decreased in a concentration-dependent manner, reaching an approximate 80% reduction at 0.062 mg/mL (Figure 3D.).

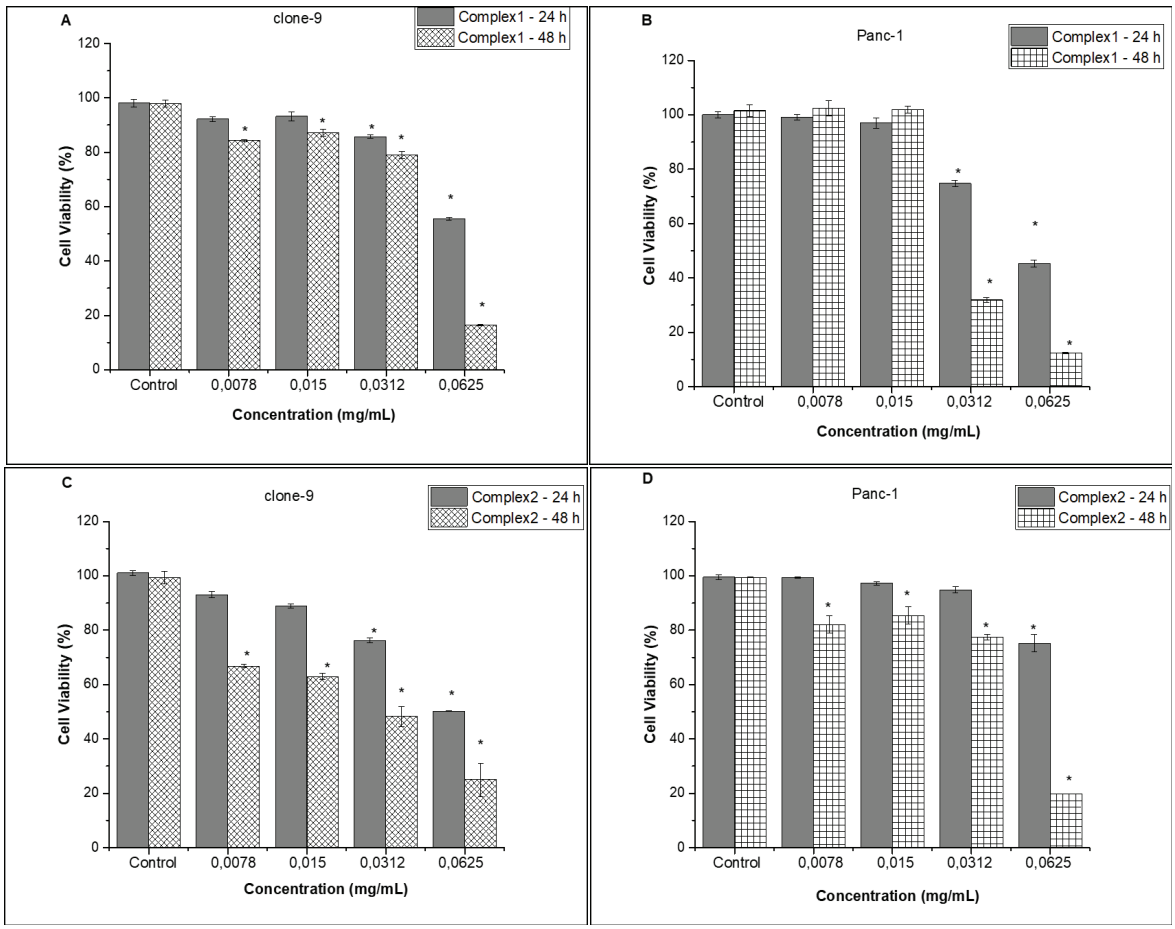


Figure 3. *In vitro* cytotoxic activities of complex 1 and complex 2. **A**) Cytotoxic activity of complex 1 on clone - 9 cell line. **B)** Cytotoxic activity of complex 1 on panc-1 cell line. **C)** Cytotoxic activity of complex 2 on clone - 9 cell line and **D)** Cytotoxic activity of complex 2 on panc - 1 cell line. Data are expressed as the mean ± SD. *Indicates significant difference from the control group (untreated cells) by the Tukey test ($p < 0.05$). The cytotoxic effect of cisplatin on the clone-9 and panc-1 cell lines should be described. Cisplatin $IC5_0$ value was used as a positive control. No data is provided.

Similar to the MTT results, Complex 1 showed no obvious cytotoxicity at lower concentrations (0.0078–0.015 mg/mL) in both cell lines in the LDH assay (Fig. 4A–B.). At the highest concentration, cytotoxicity cells were determined 40% and 80%, respectively, after 24 h and 48 h in clon-9 cells. However, in panc-1 cells, cytotoxicity reached 50% and 90% at 24 h and 48 h, respectively, at the highest concentration of Complex 1. Furthermore, in Clone-9 cells, cytotoxicity was increased in a concentration-dependent manner following 24 h and 48 h treatments. The significant increase in cell viability observed at the highest concentration (0.0625 mg/mL) of complex 2 was approximately % 80 (Figure 4A.). Complex 2 treatment of panc-1cells resulted in minimal changes in cytotoxicity after 24 h with lower concentrations (<0.0625 mg/mL), but the highest concentration (0.0625 mg/mL) cytotoxicity was increased to 30% and 83 % respectively after 24h and 48h (Figure 4B.).

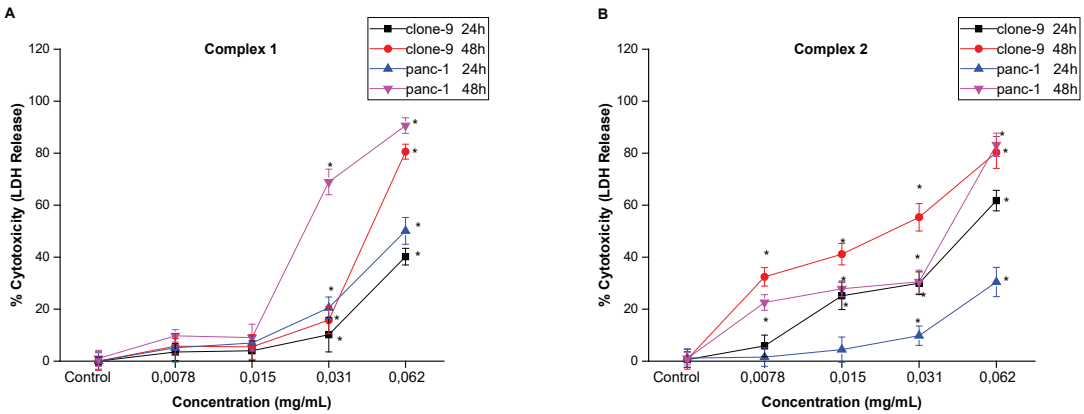


Figure 4. In vitro cytotoxic activities of complex 1 and complex 2. **A)** Complex 1 cytotoxic activity on clone-9 and panc-1 cell lines. **B)** Complex 2 cytotoxic activity on clone-9 and panc-1 cell lines. Data are expressed as the mean ± SD. *Indicates significant difference from the control group (untreated cells) by the Tukey test ($p < 0.05$).

Table 4. IC_{50} and selectivity index values of complex 1 and 2 on clone-9 and panc - 1 cell lines.

Complex	IC_{50} values mg/mL				Selectivity Index (SI)	
	Clone-9		**Panc-1**			
	Incubation Time					
	24 h	**48 h**	**24 h**	**48 h**	**24 h**	**48 h**
Complex 1	0.070 ± 1.56	0.04 ± 2.04	0.056 ± 0.78	0.034 ± 1.46	1.25	1.18
Complex 2	0.062 ± 1.63	0.029 ± 1.88	ND*	0.046 ± 2.25	<0.99	0.63

*ND: Not determined IC_{50} value >0.0625 mg/mL

In our study, for Complex 1, the IC_{50} values at 24 hours were 0.070 mg/mL and 0.056 mg/mL for Clone-9 and Panc-1 cells, respectively. After 48 hours, these values decreased to 0.04 mg/ and 0.034 mg/mL. For Complex 2, the IC_{50} for Clone-9 cells was 0.062 mg/mL at 24 hours, dropping to 0.029 mg/mL at 48 hours. In Panc-1 cells, the 24-h IC50 value could not be determined, as Complex 2 did not induce a sufficient reduction in cell viability. In contrast, the IC_{50} value at 48 h was calculated to be 0.041mg/mL (Table 4.). The selectivity of the tested complexes toward pancreatic cancer cells was evaluated by calculating the Selectivity Index (SI) based on IC50 values obtained in normal Clone-9 hepatocytes and panc-1 pancreatic cancer cells. For Complex 1, SI values were 1.25 at 24 h and 1.18 at 48 h, indicating a modest but consistent preferential cytotoxicity toward Panc-1 cells compared with normal cells. In contrast, Complex 2 did not demonstrate cancer cell selectivity. At 24 h, the IC_{50} value in Panc-1 cells exceeded the highest tested concentration, resulting in an estimated SI value below 1, while at 48 h, the SI decreased further to 0.63, suggesting greater sensitivity of normal cells relative to cancer cells. Overall, these findings indicate that Complex 1 exhibits limited yet favorable selectivity toward pancreatic cancer cells, whereas Complex 2 lacks selective anticancer activity.

The increased cytotoxicity observed for Complex 2 in normal Clone-9 cells compared with PANC-1 pancreatic cancer cells may be attributed to cell line–specific biological differences and intrinsic drug-resistance mechanisms. PANC-1 cells are well known for their chemoresistant phenotype, characterized by enhanced drug efflux, elevated anti-apoptotic protein expression,

and efficient DNA damage repair, which collectively limit intracellular drug accumulation and reduce cytotoxic efficacy (Amrutkar & Gladhaug, 2017).

In contrast, Clone-9 cells exhibited greater sensitivity to Complex 2, indicating that this compound has not yet achieved cancer cell selectivity despite its pronounced cytotoxic potential. This interpretation is supported by Selectivity Index values below 1. Overall, these findings suggest that although Complex 2 displays substantial cytotoxic activity, further optimization is required to improve its selective anticancer efficacy, potentially through targeted delivery strategies and mechanistic investigations of cellular uptake.

Although no studies have examined the cytotoxic effects of copper complexes with imidazole and benzimidazole on Panc-1 and Clone-9 cell lines, their effects on other cell lines, including M14, MCF-7, HeLa, A-549, HT-29, SGC7901, and EC109, have been reported (Alshehri et al., 2022; Paul et al., 2021; Zhao et al., 2013). Raducka et al. (2021) determined IC50 values for benzimidazole-based copper complexes on A-549 cells as 264.32–608.7 μM, while Alshehri et al. (2022) reported IC_{50} values of 6.65 and 8.83 mg/mL for imidazole-based copper complexes on M14 cells.

CONCLUSION

This research reports the preparation, structural analysis, and biological evaluation of copper(II) complexes containing imidazole and benzimidazole ligands. The complexes exhibited notable antibacterial activity, especially Complex 1, which showed better performance compared to Complex 2. In terms of cytotoxicity, Complex 1 demonstrated moderate effects, particularly against Panc-1 cells. In summary, the results suggest that Complex 1 may possess limited but favorable selectivity toward pancreatic cancer cells, while Complex 2 demonstrates reduced selectivity, warranting cautious interpretation and further investigation. The IC_{50} values suggest that both complexes could be promising candidates for further investigation in antimicrobial and anticancer drug development.

ACKNOWLEDGEMENT

The authors would like to thank Prof. Dr. Ayşe Tansu KOPARAL for her endless support.

AUTHOR CONTRIBITION STATEMENT

S.E. and H.Ü. designed and directed the project; S.E. wrote the manuscript with support from H.Ü. and B.B.; H.Ü. synthesized the test substances, S.E. performed the antimicrobial activity experiments, and B.B. performed the cell culture experiments.

CONFLICT OF INTEREST

The authors declare that there is no conflict of interest.

REFERENCES

Ajibola, A. A., Perveen, F., Jan, K., Anibijuwon, I. I., Shaibu, S. E., Sieroń, L., …Maniukiewicz, W. (2020). A Five-Coordinate Copper (II) Complex Constructed from Sterically Hindered 4-Chlorobenzoate and Benzimidazole: Synthesis, Crystal Structure, Hirshfeld Surface Analysis, DFT, Docking Studies and Antibacterial Activity. *Crystals, 10*(11), 991. https://doi.org/10.3390/cryst10110991

Alshehri, N. S., Sharfalddin, A. A., Domyati, D., Basaleh, A. S., & Hussien, M. A. (2022). Experiment versus theory of copper (II) complexes-based imidazole derivatives as anti-cancer agents. *Journal of the Indian Chemical Society, 99*(10), 100692. https://doi.org/10.1016/j.jics.2022.100692

Amrutkar, M., & Gladhaug, I. P. (2017). Pancreatic Cancer Chemoresistance to Gemcitabine. *Cancers, 9*(11), 157.

Atria, A., Cortes-Cortes, P., Garland, M. T., Baggio, R., Morales, K., Soto, M., …Corsini, G. (2011). X-ray studies and antibacterial activity in copper and cobalt complexes with imidazole derivative ligands. *Journal of the Chilean Chemical Society, 56*(3), 786-792. http://dx.doi.org/10.4067/S0717-97072011000300015

Bandopadhyay, N., Paramanik, K., Mudi, P. K., Sarkar, G., Kotakonda, M., Shit, M., …Das, H. S. (2022). A thiomethyl-substituted imidazolyl imine functionalized copper (II) complex: synthesis, structural characterization, phenoxazinone synthase mimics and biological activities. *Polyhedron, 218,* 115783. https://doi.org/10.1016/j.poly.2022.115783

Beheshti, A., Nozarian, K., Mousavifard, E. S., Abrahams, C. T., Mayer, P., Gajda, R., …Motamedi, H. (2021). Design and construction of the imidazole-2-thione-based copper (I) complexes by varying the co-anion and synthesis conditions and verifying their antimicrobial activity. *Journal of Solid State Chemistry, 294,* 121874. https://doi.org/10.1016/j.jssc.2020.121874

Cai, D. H., Zhang, C. L., Liu, Q. Y., He, L., Liu, Y. J., Xiong, Y. H., …Le, X. Y. (2021). Synthesis, DNA binding, antibacterial, and anticancer properties of two novel water-soluble copper (II) complexes containing gluconate. *European Journal of Medicinal Chemistry, 213,* 113182. https://doi.org/10.1016/j.ejmech.2021.113182

Chai, L. Q., Zhou, L., Zhang, K. Y., & Zhang, H. S. (2018). Structural characterizations, spectroscopic, electrochemical properties, and antibacterial activities of copper (II) and cobalt (II) complexes containing an imidazole ring. *Applied Organometallic Chemistry, 32*(12), e4576. https://doi.org/10.1002/aoc.4576

Chen, J. Y., Ren, X. X., Mao, Z. W., & Le, X. Y. (2012). Synthesis, characterization, and antibacterial activities of two new copper (II) glycinate complexes incorporating 2-(4′-thiazolyl) benzimidazole/2-(2-pyridyl) benzimidazole. *Journal of Coordination Chemistry, 65*(12), 2182-2191. https://doi.org/10.1080/00958972.2012.681380

CLSI. (2006). Clinical and Laboratory Standards Institute. Retrieved from: https://clsi.org/?gclid=Cj0KCQiAyracBhDoARIsACGFcS72LPCyllzdcrcERY81owvT6tuBsyAsCW dhSENgz9d0ltne5vn97LoaAkblE ALw_wcB_

Er, S, Ünver, H., & Dikmen, G. (2023). A New Dinuclear Copper (II)-Hydrazone Complex: Synthesis, Crystal Structure and Antibacterial Activity. *Letters in Organic Chemistry, 20*(4), 376-387. https://doi.org/10.2174/1570178620666221202090558

Garcia, R. C., Dati, L. M., Fukuda, S., Torres, L. H., Moura, S., de Carvalho, N. D., …Marcourakis, T. (2012). Neurotoxicity of anhydroecgonine methyl ester, a crack cocaine pyrolysis product. *Toxicological sciences: an official journal of the Society of Toxicology, 128*(1), 223–234. https://doi.org/10.1093/toxsci/kfs140

Gulya, A. P., Lozan-Tyrshu, K. S., Tsapkov, V. I., Chumakov, Y. M., Zhanno, E., & Rudik, V. F. (2013). Synthesis, structure, and antimicrobial activity of copper (II) chelates containing imidazole and condensation products of α-amino acids with salicylaldehyde and its derivatives. *Russian Journal of General Chemistry, 83,* 530-537. DOI: 10.1134/S1070363213030201

Liu, Y., Peterson, D. A., Kimura, H., & Schubert, D. (1997). Mechanism of cellular 3-(4,5-dimethylthiazol-2-yl)-2,5-diphenyltetrazolium bromide (MTT) reduction, *Journal of Neurochemistry, 69*(2), 581–593. https://doi.org/10.1046/j.1471-4159.1997.69020581.x

Lobana, T. S., Aulakh, J. K., Sood, H., Arora, D. S., Garcia-Santos, I., Kaur, M., …Jasinski, J. P. (2018). Synthesis, structures and antimicrobial activity of copper derivatives of N-substituted imidazolidine-2-thiones: unusual bio-activity against Staphylococcus epidermidis and Enterococcus faecalis. *New Journal of Chemistry, 42*(12), 9886-9900. https://doi.org/10.1039/C8NJ00206A

Macrae, C.F., Edgington, P.R., McCabe, P., Pidcock, E., Shields, G.P., Taylor, R., …Towler, M. (2006) Mercury: visualization and analysis of crystal structures. *Journal of Applied Crystallography, 39,* 453-457. https://doi.org/10.1107/S002188980600731X

Mahmood, K., Hashmi, W., Ismail, H., Mirza, B., Twamley, B., Akhter, Z., …Baker, R. J. (2019). Synthesis, DNA binding and antibacterial activity of metal (II) complexes of a benzimidazole Schiff base. *Polyhedron, 157,* 326-334. https://doi.org/10.1016/j.poly.2018.10.020

Manjuraj, T., Krishnamurthy, G., Bodke, Y. D., Naik, H. B., & Kumar, H. A. (2018). Synthesis, XRD, thermal, spectroscopic studies, and biological evaluation of Co (II), Ni (II), Cu (II) metal complexes derived from 2-benzimidazole. *Journal of Molecular Structure, 1171,* 481-487.

Mañozca-Dosman, I. V., Aragón-Muriel, A., & Polo-Cerón, D. (2025). Antibacterial Activity of Metal Complexes of Cu (II) and Ni (II) with the Ligand 2-(Phenylsubstituted) Benzimidazole. *Scientia Pharmaceutica*, *93*(2), 22. https://doi.org/10.1016/j.molstruc.2018.06.055

Maru, M.S., & Shah, M.K. (2015). Synthesis, Characterization and Antimicrobial Evaluation of Transition Metal Complexes of Monodentate 2-(Substituted Phenyl)-1*H*-benzo[d]imidazoles. *Chiang Mai Journal of Science, 42*(1), 216-227. http://epg.science.cmu.ac.th/ejournal/ Contributed Paper

Mendoza, Á., Mendoza-Díaz, G., Pedraza-Reyes, M., & Bernès, S. (2013). Copper (II) Complex with the Tridentate Ligand N, N-bis (2-ethyl-4-methyl-imidazol-5-ylmethyl) phenylethylamine (biaq). X-ray Crystal Structure and Biological Activity on Bacillus subtilis of [Cu (biaq) Cl2]. *Zeitschrift für anorganische und allgemeine Chemie, 639*(8-9), 1455-1460. https://doi.org/10.1002/zaac.201300082

Mosmann, T. (1983). Rapid Colorimetric Assay for Cellular Growth and Survival: Application to Proliferation and Cytotoxicity Assays. *Journal of Immunological Methods, 65,* 55-63. https://doi.org/10.1016/0022-1759(83)90303-4

Nakahata, D. H., Ribeiro, M. A., Corbi, P. P., Machado, D., Lancellotti, M., Lustri, W. R., …Formiga, A. L. (2017). Synthesis, characterization, and preliminary antimicrobial assays of copper (II) complexes with 2-(imidazole-2-yl) heteroaryl ligands. *Inorganica Chimica Acta, 458,* 224-232. https://doi.org/10.1016/j.ica.2017.01.015

Paul, A., Singh, P., Kuznetsov, M. L., Karmakar, A., da Silva, M. F. C. G., Koch, B., …Pombeiro, A. J. (2021). Influence of anchoring moieties on new benzimidazole-based Schiff base copper (ii) complexes towards estrogen-dependent breast cancer cells. *Dalton Transactions, 50*(10), 3701-3716. https://doi.org/10.1039/D0DT03873C

Qiao, X., Ma, Z. Y., Shao, J., Bao, W. G., Xu, J. Y., Qiang, Z. Y., …Lou, J. S. (2014). Biological evaluation of a cytotoxic 2-substituted benzimidazole copper (II) complex: DNA damage, antiproliferation and apoptotic induction activity in human cervical cancer cells. *Biometals, 27,* 155-172. DOI 10.1007/s10534-013-9696-1

Raducka, A., Czylkowska, A., Gobis, K., Czarnecka, K., Szymański, P., & Świątkowski, M. (2021). Characterization of metal-bound benzimidazole derivatives, effects on tumor cells of lung cancer. *Materials, 14*(11), 2958. https://doi.org/10.3390/ma14112958

Ren, X,, Chen, J., & Le, X. (2011). Antibacterial Activities and Nuclease Properties of Two New Ternary Copper(II) Complexes with 2-(4'-Thiazolyl)- benzimidazole and 2,2′-Bipyridine/1,10-phenanthroline. *Chinese Journal of Chemistry, 29,* 1380—1388. https://doi.org/10.1002/cjoc.201180257

Rodríguez-Argüelles, M. C., López-Silva, E. C., Sanmartín, J., Pelagatti, P., & Zani, F. (2005). Copper complexes of imidazole-2-, pyrrole-2-and indol-3-carbaldehyde thiosemicarbazones: inhibitory activity against fungi and bacteria. *Journal of inorganic biochemistry, 99*(11), 2231-2239. https://doi.org/10.1016/j.jinorgbio.2005.07.018

Saddam Hossain, Md., Zakaria, C. M., & Kudrat-E-Zahan, Md. (2018) Metal Complexes as Potential Antimicrobial Agents: A Review. *American Journal of Heterocyclic Chemistry, 4*(1), 1-21. doi: 10.11648/j.ajhc.20180401.11

Shedrick, G. M. (2008). A short of SHELX. *Acta Crystallographica, A64,* 11-122. https://doi.org/10.1107/S0108767307043930

Ünver, H., Berber, B., Kanat, B., Arafat, M., Koparal, A. T., & Doluca, O. (2022). DNA binding effects of 2, 2′-bipyridine and 1, 10-phenanthroline ligands synthesized with benzimidazole copper (II) complexes: Crystal structure, molecular docking, DNA binding and anti-cancer studies. *Polyhedron, 221,* 115834. https://doi.org/10.1016/j.poly.2022.115834

Zhao, J. A., Li, S., Zhao, D., Chen, S., & Hu, J. (2013). Metal and structure tuned in vitro antitumor activity of benzimidazole-based copper and zinc complexes. *Journal of Coordination Chemistry, 66*(9), 1650-1660. https://doi.org/10.1080/00958972.2013.789505

FABAD J. Pharm. Sci., 51, 1, 129-146, 2026
Doi: 10.55262/fabadeczacilik.1704650
RESEARCH ARTICLE

Mucoadhesive Delivery of Alfuzosin HCl Using Hupu Gum: Insights from *In Silico* Docking and *Ex Vivo - In Vivo* Adhesion Studies

Rajeswari ALETI[*°], Monika NIJHAWAN[**], Pavan KUMAR THOTA[***], Bhavana JIDIGE[****]

Mucoadhesive Delivery of Alfuzosin HCl Using Hupu Gum: Insights from In silico Docking and Ex vivo - In Vivo Adhesion Studies

SUMMARY

Benign prostatic hyperplasia (BPH) is an age-associated disorder of enlargement of the prostate that leads to urinary obstruction. Alfuzosin HCl, a selective α1-adrenoceptor antagonist, is well absorbed in the duodenum and is more effective in extended-release formulations. This study investigates the formulation of mucoadhesive compression-coated tablets (MCCT) of alfuzosin HCl using hupu gum to enhance gastric retention and achieve a 24-hour extended drug release, addressing bioavailability issues that affect therapeutic efficacy. The investigation is further validated by in silico and ex vivo studies. Alfuzosin HCl, hupu gum, and lactose were used in this study. Initially an in silico study was conducted using software CB Dock 2 to know the interaction between hupu gum and mucin. Optimized Inner Core tablets (ICT) prepared with varying concentrations of hupu gum were then compression-coated with hupu gum. The tablets obtained were characterized and optimized on the basis of in vitro and ex vivo studies determining mucoadhesive and drug release parameters. Results of in silico studies confirmed multiple interactions between the hupu gum and mucin through conventional hydrogen bond, C-H bond, and van der Waals interactions. The presence of these bonds suggests that the formulation exhibits an extended gastric retention time on mucosal surfaces, thereby enhancing the efficacy of the mucoadhesive system. Formulation MCCT1 was optimized as the maximum amount of drug release of 98.2 % was observed over a period of 24 hours in gastric medium, and mucoadhesive strength was found to be 0.26 N. A study of gastric retention time using X-ray imaging indicates effective in vivo adhesion and prolonged gastric retention. The extended release of alfuzosin HCl was achieved by gastroretentive mucoadhesive tablets using a compression coating technique.

Keywords: *Alfuzosin hydrochloride, hupu gum, compression coating technique, mucoadhesive, in silico studies, ex vivo studies.*

Hupu Sakızı Kullanarak Alfuzosin HCl'nin Mukoadezif Taşınması: In Silico Docking ve Ex Vivo - In Vivo Adezyon Çalışmalarından Elde Edilen Bulgular

ÖZ

Benign prostat hiperplazisi (BPH), yaşa bağlı olarak ortaya çıkan ve prostatın büyümesiyle idrar yolu tıkanıklığına yol açan bir hastalıktır. Seçici bir α1-adrenoseptör antagonisti olan Alfuzosin HCl, duodenumda iyi emilir ve uzatılmış salım formülasyonlarında daha etkilidir. Bu çalışma, biyoyararlanımı etkileyerek tedavi etkinliğini azaltan sorunları ele almak amacıyla, hupu zamkı kullanılarak mide tutulumunu artırmayı ve 24 saatlik uzatılmış ilaç salımını sağlamayı hedefleyen alfuzosin HCl'nin mukoadezif kompresyon kaplı tabletlerinin (MCCT) formülasyonunu araştırmaktadır. Araştırma, in silico ve ex vivo çalışmalarla desteklenmiştir. Çalışmada Alfuzosin HCl, hupu zamkı ve laktoz kullanılmıştır. İlk olarak, hupu zamkı ile müsin arasındaki etkileşimi belirlemek amacıyla CB dock 2 yazılımı kullanılarak in silico çalışma gerçekleştirilmiştir. Daha sonra, farklı konsantrasyonlarda hupu sakızı ile hazırlanan optimize edilmiş iç çekirdek tabletleri (ICT), hupu sakızı ile sıkıştırma yöntemiyle kaplandı. Elde edilen tabletler, in vitro ve ex vivo çalışmalara dayanarak mukoadeziflik ve ilaç salım parametreleri açısından karakterize edilmiş ve optimize edilmiştir. In silico çalışmaların sonuçları, hupu zamkı ile müsin arasında geleneksel hidrojen bağları, C-H bağları ve van der Waals etkileşimleri yoluyla çoklu etkileşim olduğunu doğrulamıştır. Bu bağların varlığı, formülasyonun mukozal yüzeylerde uzamış mide tutunma süresi gösterdiğini ve böylece mukoadezif sistemin etkinliğini artırdığını göstermektedir. MCCT1 formülasyonu, mide ortamında 24 saat boyunca %98,2 oranında maksimum ilaç salımı sağladığı ve 0,26 N mukoadezif kuvvete sahip olduğu için optimize edilmiştir. X-ışını görüntüleme kullanılarak yapılan mide tutunma süresi çalışması, etkili in vivo adezyon ve uzatılmış mide tutulumunu göstermiştir. Alfuzosin HCl'nin uzatılmış salımı, kompresyon kaplama tekniği kullanılarak hazırlanan gastroretentif mukoadezif tabletlerle başarıyla gerçekleştirilmiştir.

Anahtar Kelimeler: *Alfuzosin hidroklorür, hupu zamkı, kompresyon kaplama tekniği, mukoadezif, in silico çalışmalar, ex vivo çalışmalar.*

Recieved: 23.05.2025
Revised: 31.12.2025
Accepted: 3.02.2026

[*] ORCID: 0009-0001-8894-9063, Gland Institute of Pharmaceutical Sciences Medak District – 502313, Telangana, India
[**] ORCID: 0000-0002-3564-0257, Department of Pharmaceutics, Professor, GokarajuRangaraju College of Pharmacy, Osmania University, Hyderabad, Telangana, India.
[***] ORCID: 0009-0009-5890-3636, Department of Pharmaceutics, GokarajuRangaraju College of Pharmacy, Osmania University, Hyderabad, Telangana, India.
[****] ORCID: 0009-0007-0819-1357, Department of Pharmaceutics, GokarajuRangaraju College of Pharmacy, Osmania University, Hyderabad, Telangana, India.

[°] Corresponding Author; Dr. Rajeswari Aleti,
Email: razi.pharma.87@gmail.com

INTRODUCTION

Age-related health issues are common, and Benign Prostatic Hyperplasia (BPH) is a notable example, characterized by an enlarged prostate gland that obstructs urine flow, resulting in symptoms such as increased urinary frequency, urgency, and a weak stream (Kim et al., 2016). Alfuzosin HCl, a selective α1-adrenoceptor antagonist, is widely used in the management of BPH. Although it is classified as a BCS Class I drug with good water solubility, its oral bioavailability is only 49% when taken with food and drops to 25% under fasting conditions (Pattnaik et al., 2009). This low bioavailability is attributed to extensive first-pass hepatic metabolism and a narrow absorption window, with peak absorption occurring primarily in the duodenum and jejunum, followed by a decline along the remaining intestinal tract (Maggi et al., 2000).

These pharmacokinetic limitations highlight the necessity of adopting gastroretentive drug delivery systems (GRDDS) to enhance systemic availability. Although immediate-release Alfuzosin tablets (2.5 mg) are commercially available and typically administered thrice daily, this frequent dosing regimen fails to maintain consistent plasma concentrations. Extended-release formulations are also available; however, due to the drug's narrow absorption window, short gastric retention time, and minimal absorption in the lower gastrointestinal tract, their efficiency remains suboptimal (Streubel et al., 2006).

Recent developments have explored chitosan-based sponges embedded with magnetite, which demonstrated excellent floating capacity and mucoadhesive properties, ensuring gastric retention for up to 5 hours (Abd El-Aziz et al., 2020). Nevertheless, floating systems depend on buoyancy in gastric fluids and require a minimum level of stomach content to remain effective. In contrast, mucoadhesive systems offer a distinct advantage by directly adhering to the gastric mucosa, allowing prolonged gastric residence regardless of the fed or fasting state.

This study highlights the development of a mucoadhesive gastroretentive formulation using mucoadhesive polymers that enable electrostatic interactions and hydrogen bonding between the dosage form and gastric mucin. In this investigation, a natural polymer, Hupu gum derived from *Sterculia urens*, was employed to achieve gastric retention and ensure controlled drug release over 24 hours. It is a hydrophilic polysaccharide abundant in galactomannans and is known for its high swelling index, making it suitable for localized and controlled drug delivery. However, there is limited literature on its pharmaceutical application, particularly in gastroretentive systems, adding novelty to this study (Aleti et al., 2025).

The aim of the present study is to investigate the gastric mucoadhesive property of hupu gum by *in silico* studies and the development of mucoadhesive compression-coated tablets (MCCT) of Alfuzosin HCl using a natural mucoadhesive polymer, hupu gum, to enhance bioavailability by achieving controlled release over 24 hours.

According to USP, Alfuzosin HCl extended-release tablets are required to exhibit a controlled dissolution profile, delivering 10–20% drug release within 1 hour, 40–55% within 6 hours, 65–85% within 12 hours, and not less than 85% by 20 hours (USP 47–NF 42, 2024). Hence, in the present study, the core tablets were developed with increasing concentration of hupu gum to function as a rate- controlling polymer and subjected to compression coating with a fixed concentration of hupu gum to function as the mucoadhesive polymer.

MATERIALS AND METHODS

Alfuzosin hydrochloride was obtained from MSN Labs, Telangana. Hupu gum was procured from the Girijan Cooperative Corporation, Visakhapatnam, Andhra Pradesh. Microcrystalline cellulose, magnesium stearate, lactose, and isopropyl alcohol were procured from Pioneer Chemical Industries, Hyderabad.

***In silico* studies**

Molecular docking is one of the most important computational methods to predict binding affinity between protein and ligand. In the present study, CB-Dock2 was used for molecular docking, and Discovery Studio for binding pose visualization and analysis.

Preparation of protein and ligands

The target protein structure, Mucin-2 (6RBF), was obtained in PDBQT format from the Protein Data Bank (RCSB-PDB). Water molecules and unwanted bonds were removed from the crystalline structure of the target protein using Discovery Studio to prepare it for docking studies. Polysaccharides of hupu gum (α-L-Rhamnose, Arabinose, α-D-Mannose, α- and β-Glucose, α- and β-Galactose, Glucuronic acid, and α- and β-Galacturonic acid) are selected as ligands and downloaded in SDF format from PubChem for the molecular docking. Before docking, the ligands were optimized through energy minimization to ensure accurate interaction predictions.

Molecular docking studies

The protein and ligands were uploaded in PDBQT and SDF formats, respectively, for the docking process, which was carried out using the software CB-Dock2. Using default parameters, CB-Dock2 automatically detected the binding cavity. The Vina score was used to rank the best poses. Following the docking process, the top-ranked pose was downloaded and uploaded into Discovery Studio to find out the binding sites and type of binding between the protein & ligand.

Drug-excipients compatibility studies

Samples were analysed using a Fourier transform infrared spectrophotometer by the KBr pellet method, and spectra were recorded over the wavenumber range between 4000–250 cm ^{1}. Compatibility between alfuzosin HCl and hupu gum was evaluated by comparing the spectra of alfuzosin HCl and the final formulation.

Precompression parameters

The precompression parameters of the powder blend were determined as mentioned. Using the funnel method, the angle of repose was determined by the equation tan θ = h/r, considering the height and radius of the pile formed by pouring the powder blend through the funnel. Bulk density (BD) was recorded by carefully adding the powder into a graduated glassware and calculating the weight-to-volume ratio. Tapped density (TD) was measured by introducing a specified amount of powder into a graduated glassware and subjecting it to 100 taps using a tapped density apparatus, continually reducing volume until no more reduction is seen. The ratio of tapped to BD refers to the Hausner ratio, while Carr's index (CI) was determined using the formula: (TD−BD)/TD x 100 (Aulton, 2002).

Formulation development of mucoadhesive compression-coated tablets (MCCT)

This formulation strategy was designed to enhance the stability of hygroscopic drugs like alfuzosin HCl by applying a compression coating that protects the tablet core from moisture and helps prevent dose dumping. The development of MCCT followed a two-step process. First, inner core tablets (ICT) were formulated and evaluated to study the drug release profile. These core tablets were then coated with a mucoadhesive polymer, such as hupu gum, to extend the drug release and enhance gastric retention. The final MCCT formulation was optimized by focusing on key parameters of mucoadhesive gastroretentive drug delivery. The best-performing tablet, based on achieving maximum drug release over 24 hours, was selected for further *ex vivo* evaluation.

Preparation of ICT

The ICT was formulated using the direct compression method. The required quantities of alfuzosin HCl, hupu gum, and microcrystalline cellulose (MCC) were sieved and weighed accurately as per the composition mentioned in (Table 1.). The contents were transferred to a mortar and pestle and mixed thoroughly to ensure a uniform blend. Further lubricants were incorporated into the blend and triturated to achieve consistency. The resulting mixture was subjected to direct compression using a 6 mm punch.

Table 1. Formulation of core tablets of alfuzosin HCl

Ingredients (mg)	ICT1	ICT2	ICT3	ICT4	ICT5
Alfuzosin HCl	10	10	10	10	10
Hupu gum (%)	10	20	30	40	50
MCC	76	56	36	26	16
Mg. Stearate	2	2	2	2	2
Talc	2	2	2	2	2
Total weight (mg)	100	100	100	100	100

Evaluation of ICT characteristics

The ICT was characterized for different tableting parameters. The thickness of six ICT from each batch was determined using a Vernier calliper. Hardness was tested on six randomly selected tablets per batch using a hardness tester (Monsanto). Ten tablets from each batch were subjected to a friability test using a friabalator as per the Indian Pharmacopoeia, Section 2.5.5. For uniformity of weight, the individual weights of ICT were accurately measured, and the mean value along with % deviation was calculated as per the Indian Pharmacopoeia, Section 2.5.3. Drug content was analysed spectrophotometrically at 244 nm by randomly selecting twenty ICT from each batch (Sanki & Mandal, 2012).

Dissolution performance of ICT

A USP-type I dissolution apparatus was used at 100 rpm, 0.01 N HCl (pH 1.2), and 37 °C. Fresh medium was replaced after each sample (5 ml) was collected and analysed spectrophotometrically at 244 nm, to determine cumulative percentage drug release.

Preparation of coating granules

Coating granules with 10 % hupu gum were prepared by wet granulation using a 70:30 ratio of isopropyl alcohol and water as the granulating agent. The wet granules were screened through a BSS#30 sieve after passing through a BSS#22 sieve and drying for 1 hour at 40°C. Finally, they were lubricated, then mixed for 3 minutes to ensure uniform distribution.

Compression coating of ICT

The mucoadhesion of ICT is augmented by compression coating using a mucoadhesive polymer sufficient to coat evenly on all sides. In preliminary studies, it was determined that 150 mg of coating granules exhibited 1mm coat thickness on all sides. In the coating process, half of the required granules (75 mg) were first placed evenly in the die cavity, then ICT was positioned at the center of the powder bed, followed by the addition of the remaining granules to the die cavity. The entire contents were compacted using an 8-mm tablet punch to form the coated tablets (Aleti & Murthy, 2023).

Tableting properties of MCCT

MCCT tablets were tested for tableting properties following the same procedures outlined earlier for the evaluation of the ICT.

Dissolution performance of MCCT

The study was conducted in accordance with the specified dissolution conditions. At time points 1, 6, 12, 20, and 24 hours, samples withdrawn were subjected to quantitative analysis spectrophotometrically to determine the % release of the drug in all formulations. The optimized formulation % drug release is compared with the marketed product (ALFUNIL-10 ER).

***Ex vivo* studies**

Ex vivo experiments of mucoadhesive strength and mucoadhesive retention time determination were performed in triplicate (n = 3), and results were expressed as mean ± standard deviation.

Determination of mucoadhesive strength

Mucoadhesive strength is a critical parameter that reflects a formulation's ability to bond with the mucosal surface, directly influencing both the mucoadhesive retention time and drug release profile. The mucoadhesive strength was measured using a modified simple balance method. Goat stomach mucosal tissue was obtained from a local slaughterhouse, thoroughly rinsed with 0.01 N HCl, secured to a glass slide, and placed in a petri dish as shown in (Figure 1.). The petri dish was then filled with 0.01 N HCl buffer until the tissue was sufficiently moistened. Tablets from various formulations were affixed to the underside of the left pan using adhesive tape, allowing them to make contact with the mucus membrane. On the opposite pan, water was gradually added dropwise from a burette. As the weight of the water increased, it gradually caused the tablet to separate from the tissue. The total weight of water on the right pan at the point of separation represented the mucoadhesive strength, measured in grams (Park & Robinson, 1984). The method was validated through consistent repeatability across trials.

For each formulation, three trials were conducted, and the mean value was recorded and determined using the following equation.

$$N = W * g / 1000$$

Let N = Mucoadhesive force, W = Weight (g) sufficient to detach the tablet from tissue, and g = Acceleration due to gravity 9.81 m/s^2.

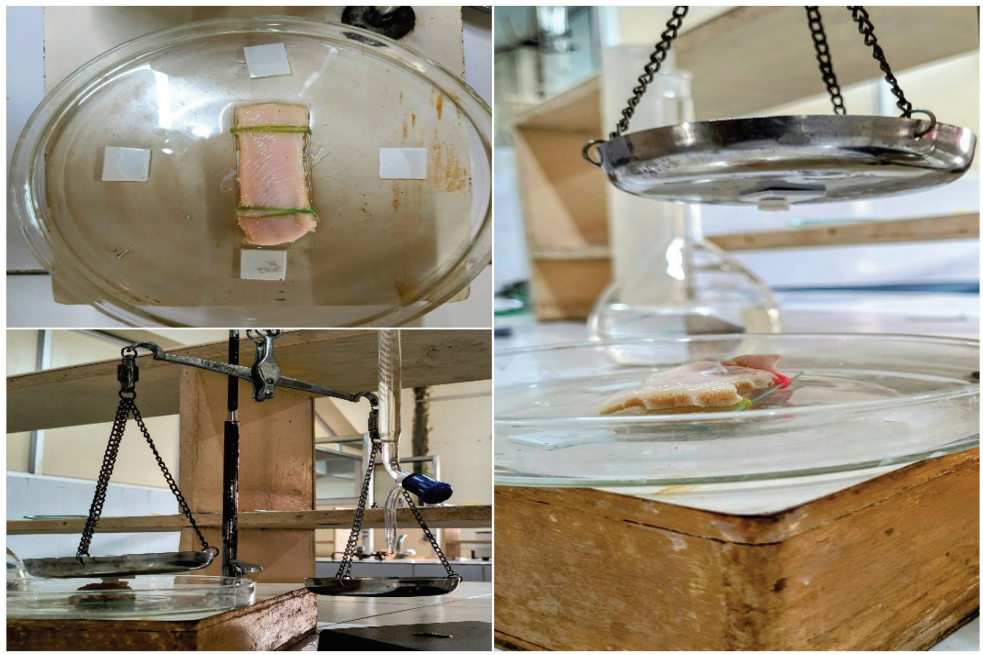


Figure 1. *Ex vivo* evaluation of mucoadhesive strength of MCCT using modified balance method

Determination of mucoadhesive retention time

The duration of mucoadhesive time is a crucial factor that reflects the formulation's ability to remain adhered to the mucosal surface, ensuring extended drug release and effective treatment. The *ex vivo* retention time, measured using a USP Type II apparatus, demonstrated consistent adherence across samples. Fresh goat stomach mucosal tissue was collected from a local slaughterhouse, cleaned with distilled water, and pH 1.2 buffer (0.01 N HCl). The mucosal tissue was then attached to a glass slide and adhered to the paddle of the dissolution apparatus, as shown in (Figure 2.). The tablet was placed in contact with the tissue for 30 seconds after hydrating one side of the tablet with 0.01 N HCl. The setup was then immersed in the dissolution medium at 37±0.5 °C, rotating at 100 rpm.

Tablet detachment time from the mucosal surface was recorded (Sankar & Jain, 2013; Kumar et al., 2020; Panda et al., 2022).

Each formulation was evaluated in triplicate (n = 3), and results were reported as mean ± s.d. Statistical comparisons were performed using appropriate post hoc tests.

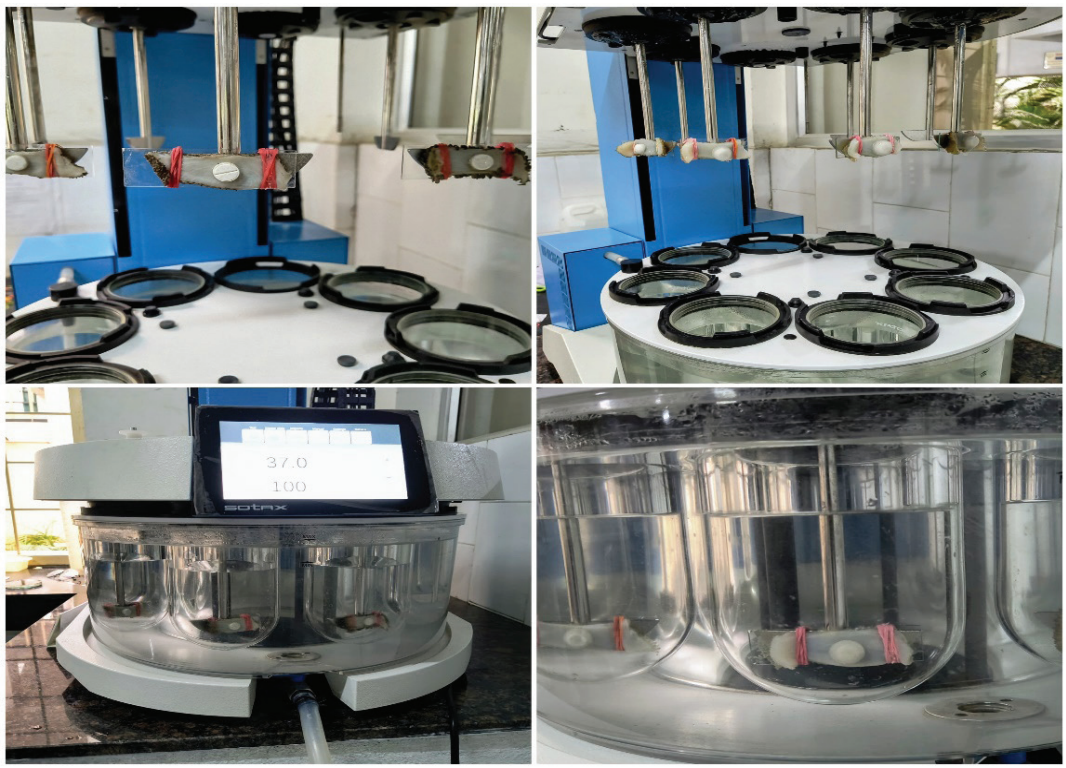


Figure 2. *Ex vivo* evaluation of mucoadhesive retention time using goat gastric mucosa

***In vivo* gastric retention time**

Visual evidence of retention time was validated through radiographic imaging (Ige & Gattani, 2013). The study was conducted with a single animal (n = 1) for preliminary confirmation of gastric retention behavior. Results were interpreted qualitatively based on radiographic visibility and positional consistency. All experimental procedures were performed in compliance with the ethical standards set by the Institutional Animal Ethics Committee (IAEC), Gokaraju Rangaraju College of Pharmacy. The study protocol was reviewed and approved under protocol no. GRCP/CEU/005/2024.

The optimized MCCT1 formulation was downsized to the appropriate animal dose. A healthy rabbit of approximately 2.5 Kg was selected as the subject and fasted overnight. The optimized formulation was administered the following morning along with 25 mL of water.

X-ray images were taken at intervals of 12 and 24 hours to monitor the tablet's position within the gastric region. After 5 hours of tablet administration, the rabbit was fed to assess the impact of food on gastric retention.

Stability profile of optimized formulation

Stability testing for the final optimized formulation (MCCT1) was conducted as per ICH Guidelines, 2018. Two sets of MCCT1 samples were sealed in hermetically sealed bottles and stored under controlled conditions: long-term (30°C/70% RH) and accelerated (40°C ± 2°C/75% ± 5% RH), as specified in the ICH

Guidelines for Zone IV and WHO standards (2021). Samples were evaluated at 3 and 6 months, for physicochemical properties, *in vitro* dissolution behaviour, and mucoadhesive performance.

RESULTS AND DISCUSSION

In silico studies

The docking analysis conducted using CB-Dock2 indicated that hupu gum exhibits strong binding affinity with the mucin protein. The interaction is evident from Vina scores ranging from -5.5 kcal/mol to -6.3 kcal/mol binding affinity in the order of Arabinose > α-D-Glucose > β-D-Glucose > α-L-Rhamnose > α-D-Mannose > D-Glucuronic acid > α-D-Galactose > β-D-galactose > β-D-Galacturonic acid > α-D-Galacturonic acid. Visualization by Discovery Studio indicates interactions between ligands and the amino acid residues located in the active site, as represented in (Figure 3.).

α-D-Galacturonic acid achieved the highest binding affinity among the ligands, with a Vina score of -6.3 kcal/mol. It formed four conventional hydrogen bonds with GLN B 956, ARG B 1112, ARG B 973, and SER B 1093, in addition to a carbon-hydrogen bond with GLU B 1089. β-D-Galacturonic acid showed a Vina score of -6.2 kcal/mol, forming hydrogen bonds with GLY B 955, GLU B 1176, and CYS B 1163, with additional van der Waals interactions involving TYR B 1124 and a carbon-hydrogen bond with VAL B 954. β-D-Galactose exhibited a Vina score of -6.2 kcal/mol, with conventional hydrogen bonds formed with ARG B 1140, ARG B 952, PHE B 1142, and ASN B 1154, as well as four van der Waals interactions with SER B 1153, VAL B 1157, TYR B 1164, and VAL B 954. α-D-Galactose showed a vina score of -6.1 kcal/mol, engaging in hydrogen bonds with ARG B 1112, GLN B 956, ARG B 973, and SER B 1093, along with carbon-hydrogen bonding with GLU B 1161, ALA B 1096, and ASP B 971, and one van der Waals interaction with GLU B 1089.

D-glucuronic acid displayed a Vina score of -6.0 kcal/mol, forming hydrogen bonds with ARG C 973, GLN C 956, PRO A 1114, and PRO C 118, along with a carbon-hydrogen bond with CYS C 1117. α-D-Mannose demonstrated a binding affinity of -5.8 kcal/mol, forming hydrogen bonds with ARG B 1112, GLN 956, and SER 1093, as well as two carbon-hydrogen bonds with GLU B 1089 and ARG B 973. Additionally, two van der Waals interactions were detected with ALA B 1096 and ASP B 971.

α-L-Rhamnose, with a Vina score of -5.7 kcal/mol, formed hydrogen bonds with ARG B 1112, GLN B 956, PRO B 1118, and ARG B 973, alongside a carbon-hydrogen bond with ASP B 1115. β-D-glucose had a binding affinity of -5.7 kcal/mol, forming hydrogen bonds with TYR A 1134, PRO C 1127, and GLU C 1129. α-D-Glucose exhibited a Vina score of -5.7 kcal/mol, with conventional hydrogen bonds observed between the ligand and the receptor amino acids GLN 956, ARG 973, PRO 1114, and ARG B 1112. Arabinose displayed a Vina score of -5.5 kcal/mol, interacting through conventional hydrogen bonds with ASP 971, SER B 1093, ARG B 973, and GLN B 956.

The presence of hydrogen bonding, C-H bond, and van der Waals interactions suggests a strong and stable binding affinity between the receptor and the ligand**.** These interactions suggest strong adhesion, as the hydrogen bonds enhance stability while the C-H bonds and van der Waals interactions facilitate additional molecular interactions (Peppas & Buri, 1985). The existence of these bonds suggests that the formulation exhibits an extended retention time on mucosal surfaces, thereby enhancing the efficacy of the mucoadhesive system (Andrews et al., 2009). This finding suggests that hupu gum could serve as an effective polymer in mucoadhesive delivery of alfuzosin HCl, thereby improving drug retention and release characteristics.

These docking studies provide a foundation for further investigation into mucoadhesive properties and drug release behaviour through *in vitro* and *ex vivo* experiments.

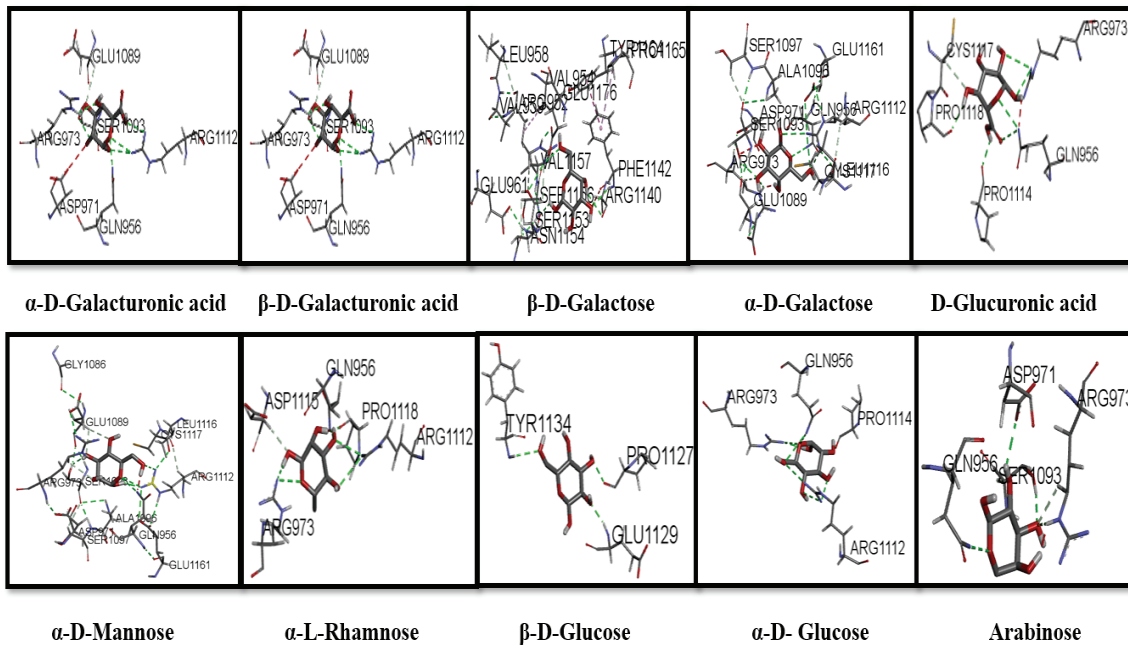


Figure 3. Protein-ligand interaction sites of hupu gum and mucin

Drug-excipients compatibility studies

The FTIR spectra for pure alfuzosin HCl and optimised formulation MCCT1 are compared (Vaishali et al., 2013) in Figure 4. The FTIR spectrum of pure alfuzosin HCl exhibited characteristic absorption bands at 1654.93 cm^{-1} (C=O stretching), 1240.23 cm^{-1} (C–O–C stretching), and 2843.08 cm^{-1} (C–H stretching), while the MCCT1 formulation showed corresponding peaks at 1656.86 cm^{-1}, 1240.23 cm^{-1}, and 2850.79 cm^{-1}. The absence of significant shifts in these characteristic peaks in the formulation blend suggests that no major interactions occurred between the drug and excipients. The functional groups remained unchanged, indicating that alfuzosin HCl did not undergo chemical degradation or form new compounds during the formulation process. This confirms the compatibility of alfuzosin HCl with Hupu gum.

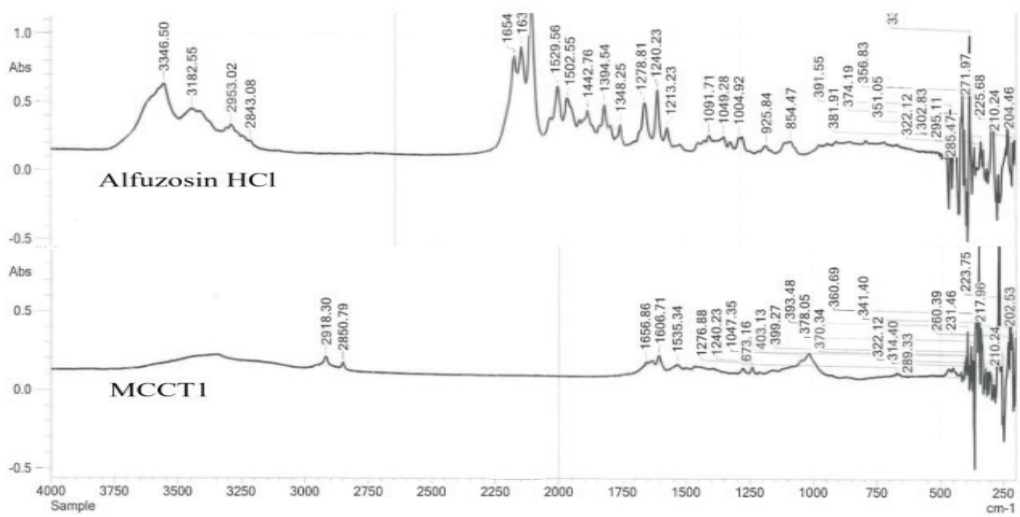


Figure 4. FTIR spectrum of alfuzosin HCl and optimized formulation MCCT1

Precompression parameters

The flow properties of the powder blend for various formulations, as shown in (Table 2.), demonstrated that all precompression parameters were within acceptable limits. Overall, the powder blend exhibited good flow and compaction characteristics suitable for tablet formulation.

Table 2. Results of precompression parameters of core tablets

Formulations	Angle of repose (°)	BD (gm/cm³)	TD (gm/cm³)	CI (%)	Hausner's ratio
ICT1	29.11.14	0.460.18	0.530.04	12	1.090.11
ICT2	30.18.53	0.420.07	0.490.26	16	1.060.03
ICT3	31.13.65	0.430.09	0.570.45	15	1.110.04
ICT4	32.04.31	0.450.11	0.510.19	13	1.150.08
ICT5	33.12.14	0.440.15	0.550.14	15	1.160.12

mean±s.d., n=3

Evaluation of ICT characteristics

The characteristics of the formulated ICT, summarized in (Table 3.), showed a hardness of 5.1-5.6 kg/cm², indicating sufficient mechanical strength, and a friability of less than 0.5%, confirming their suitability for compression coating. The tablet's thickness ranged from 4.2 to 4.5 mm, with consistent weight uniformity across the batch. The drug content was 99.91±0.02%, confirming uniform drug distribution within the tablets.

Table 3. Tableting characteristics of core tablets

Formulations	Thickness (mm)	Hardness (kg/cm2)	Friability (%)	Weight variation (mg)	Drug content (%)
ICT1	3.20.14	5.1.2	0.350.11	100±0.1	99.910.02
ICT2	3.40.21	5.40.16	0.420.06	100±0.3	99.970.18
ICT3	3.40.16	5.20.12	0.320.03	100±0.2	99.650.07
ICT4	3.30.18	5.60.16	0.290.05	100±0.5	99.950.25
ICT5	3.50.11	5.30.14	0.280.10	100±0.9	98.320.32

mean±s.d., n=3

Dissolution performance of ICT

The percentage drug release of all ICT formulations, represented graphically in Figure 5, indicates that among all formulations, ICT1 demonstrated maximum drug release within 12 hours, while ICT2, ICT3, and ICT4 extended the release to 15, 16, and 18 hours, respectively. ICT5, which had the highest polymer concentration, achieved drug release up to 20 hours due to the formation of a dense, highly viscous gel layer that restricted drug diffusion (Ford, 2014; Siepmann & Peppas, 2012).

As the formulation strategy focused on extending the drug release profile not by further increasing polymer concentration in the core, which could negatively affect tablet performance, but by applying an external mucoadhesive compression coating, as mucoadhesion is a surface-dependent phenomenon (Smart, 2005). Accordingly, all the core tablets were subjected to compression coating.

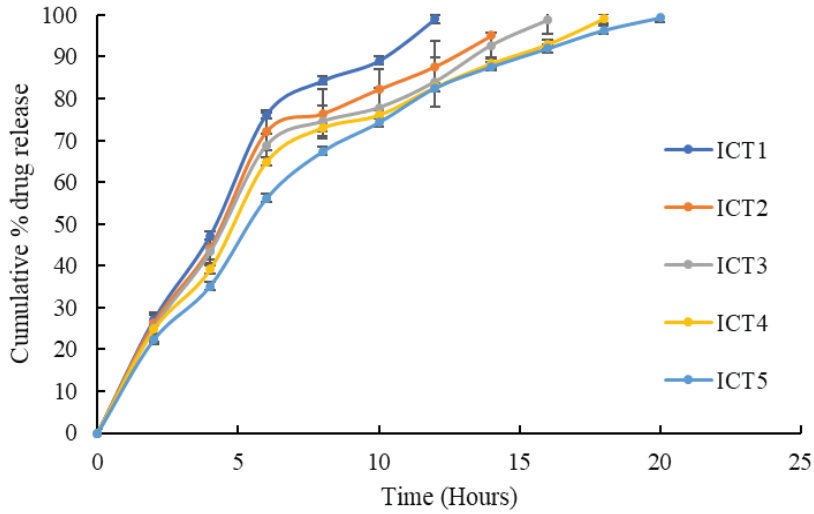


Figure 5. *In-vitro* drug release profiles of ICT1–ICT5 core tablets (n = 3, mean ± SD) in USP apparatus II, 900 mL phosphate buffer pH 6.8, 37 ± 0.5 °C, 50 rpm.

Tableting characterization of MCCT

The tableting characteristics of the formulated MCCT were assessed, and the results are represented in (Table 4.). The evaluated parameters indicate that all the formulations are as per the USP specified limits. The drug content ranged from 98.28 ± 0.30 % - 99.96±0.19 %, ensuring precise dosing. The tablet thickness was between 5.1 and 5.6 mm, while the hardness ranged from 5.1 to 5.7 kg/cm², confirming adequate mechanical strength. The friability values range between 0.24 - 0.38 %, indicating good resistance to abrasion. All tablets exhibited consistent uniformity of weight, demonstrating the reliability of the compression-coating process in producing uniform and high-quality tablets.

Table 4. Tableting characteristics of MCCT

Formulations	Thickness (mm)	Hardness (kg/cm²)	Friability (%)	Weight variation (mg)	Drug content (%)
MCCT1	5.10.17	5.1±0.32	0.37±0.02	250±0.5	99.94±0.16
MCCT2	5.30.12	5.1±0.21	0.38±0.03	250±0.6	99.96±0.19
MCCT3	5.10.16	5.3±0.18	0.35±0.01	250±0.8	98.60±0.04
MCCT4	5.70.18	5.5±0.42	0.27±0.05	250±0.4	99.90±0.24
MCCT5	5.60.15	5.6±0.12	0.24±0.03	250±0.1	98.28±0.30

mean±s.d., n=3

Dissolution performance of MCCT

The cumulative % release of formulations MCCT1-MCCT5 were represented in (Figure 6.). Dissolution profile of the MCCT1 formulation closely matched with that of the USP monograph for alfuzosin HCl, with maximum drug release observed in 24 hours. However, the remaining formulations MCCT2, MCCT3, and MCCT4 did not meet the USP standard release criteria. The difference in dissolution profile among the formulations is likely due to the higher concentration of polymer in the core tablet which resulted in excessive swelling of the tablet, which in turn reduced the porosity in the swollen polymer matrix, causing delayed drug release.

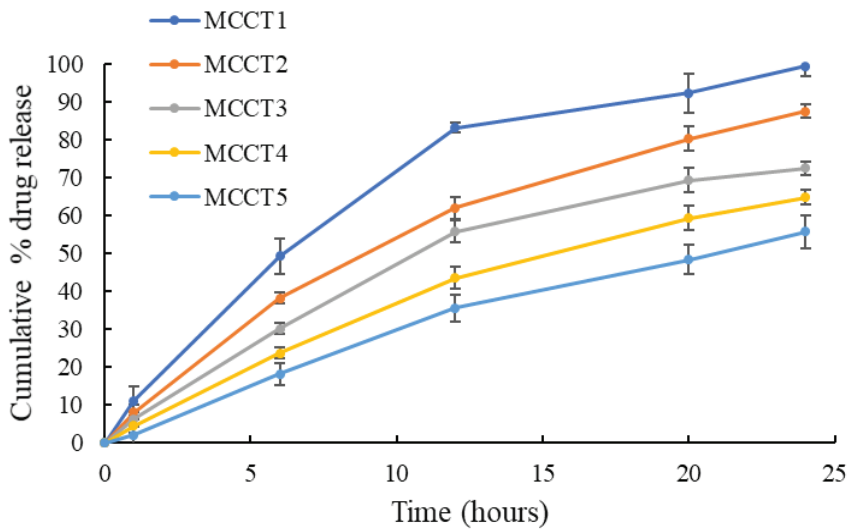


Figure 6. *In-vitro* drug release profiles of MCCT1–MCCT5 tablets (n = 3, mean ± SD) in USP apparatus II, 900 mL phosphate buffer pH 6.8, 37 ± 0.5 °C, 50 rpm.

The ratio of 1:1 hupu gum in the core and coat layer effectively extends drug release up to 24 hours while maintaining prompt initial drug availability and improved gastric retention. To support this selection, drug release kinetics of all formulations were fitted into various mathematical models and the results are represented in (Table 5.) (Korsmeyer et al., 1983).

Table 5: Mathematical modelling of mucoadhesive compression-coated tablets

Formulation	Zero-order (R^2)	Higuchi (R^2)	Peppas (R^2)	Peppas n	Mechanism
MCCT1	0.983	0.991	0.994	0.62	Non-Fickian diffusion
MCCT2	0.961	0.987	0.993	0.68	Anomalous transport
MCCT3	0.957	0.984	0.991	0.74	Anomalous transport
MCCT4	0.942	0.976	0.982	0.81	Case-II transport
MCCT5	0.936	0.972	0.980	0.84	Case-II transport

Among the developed mucoadhesive compression-coated tablet formulations, MCCT1 emerged as the optimized gastroretentive system capable of sustaining drug release over 24 hours**.** MCCT1 exhibited the highest correlation with the Korsmeyer–Peppas model (R^2 = 0.994), along with strong agreement with the Higuchi (R^2 = 0.991) and zero-order (R^2 = 0.983) models, indicating a well-controlled and predictable release pattern.

The Peppas release exponent (n = 0.62) confirms a non-Fickian diffusion mechanism**,** demonstrating a balanced contribution of drug diffusion and polymer relaxation. This dual mechanism enabled uniform hydration, stable gel formation, and sustained matrix integrity, which are critical for effective mucoadhesion and prolonged gastric residence (Peppas & Buri, 1983).

Compared with higher-polymer formulations (MCCT2–MCCT5), MCCT1 avoided excessive matrix rigidity and over-retardation, ensuring complete and continuous drug release throughout the 24-hour period. The optimized polymer content in MCCT1 thus provided an ideal balance between mucoadhesive strength, gastroretentive behavior, and controlled drug release, making it the most suitable formulation for once-daily mucoadhesive gastroretentive delivery.

Comparison of drug release profiles

The comparative dissolution profiles of the optimized formulation (MCCT1) and the marketed product are represented in (Figure 7.). The marketed product exhibited a complete drug release within 8 hours, whereas the optimized formulation (MCCT1) demonstrated an extended-release profile, achieving 100% drug release over 24 hours. This indicates that the optimized formulation provides a more controlled and prolonged release compared to the marketed product, potentially enhancing therapeutic efficacy and patient compliance.

A quantitative assessment was carried out using the similarity factor (f_2), which yielded a value of 42.6, indicating dissimilarity between the MCCT1 and the marketed product.

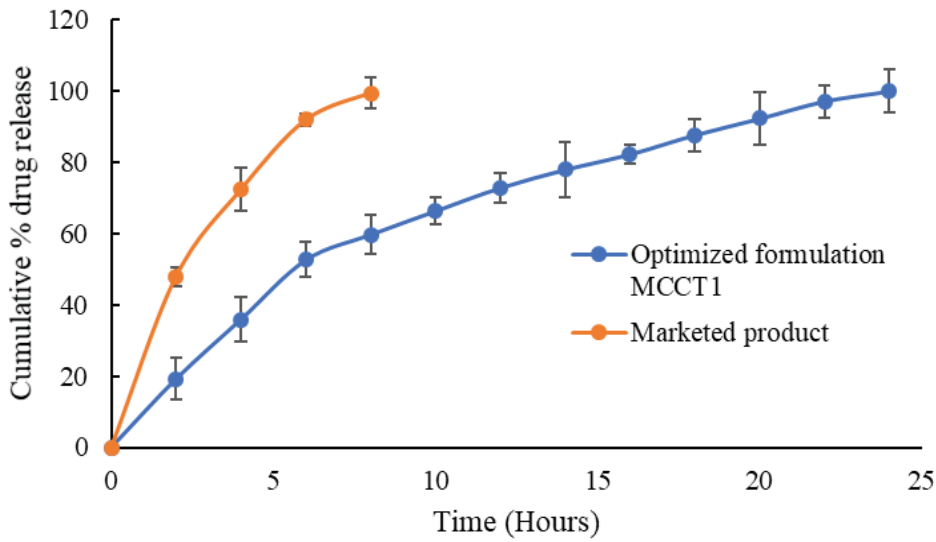


Figure 7. Comparative dissolution profiles of MCCT1 and marketed formulation (n = 3, mean ± s.d.,)

***Ex vivo* mucoadhesion strength**

Mucoadhesive strength testing was conducted on all ICT and MCCT formulations, as presented in Figure 8. The results revealed that the compression-coated formulations (MCCT1–MCCT5) consistently exhibited higher mucoadhesive strength compared to the core ICT tablets. Effective mucoadhesion of Hupu gum depends on adequate surface hydration and subsequent chain entanglement with mucin present on the gastrointestinal mucosa. Emphasizes that internal polymer does not significantly contribute to mucoadhesion. Earlier studies emphasizes that internal polymer does not significantly contribute to mucoadhesion (Khutoryanskiy, 2011). Compression coating offers a distinct advantage by localizing the mucoadhesive polymer on the tablet surface, thereby maximizing polymer exposure to the mucosal tissue This configuration promotes stronger and more sustained mucoadhesive interactions compared to matrix-based systems.

An incremental rise in mucoadhesive strength was observed with increasing polymer content in the ICT. To determine the statistical significance of the observed differences in mucoadhesive strength, one-way ANOVA was conducted among all formulations. The results showed a statistically significant difference (p

< 0.05), validating the role of polymer concentration and coating architecture in enhancing mucoadhesion.

To support these observations, *ex vivo* mucoadhesive retention time was evaluated for all MCCT formulations. This additional analysis provided further evidence of the strong and prolonged adhesion properties of the coated tablets, reinforcing the impact of the coating strategy on mucoadhesion.

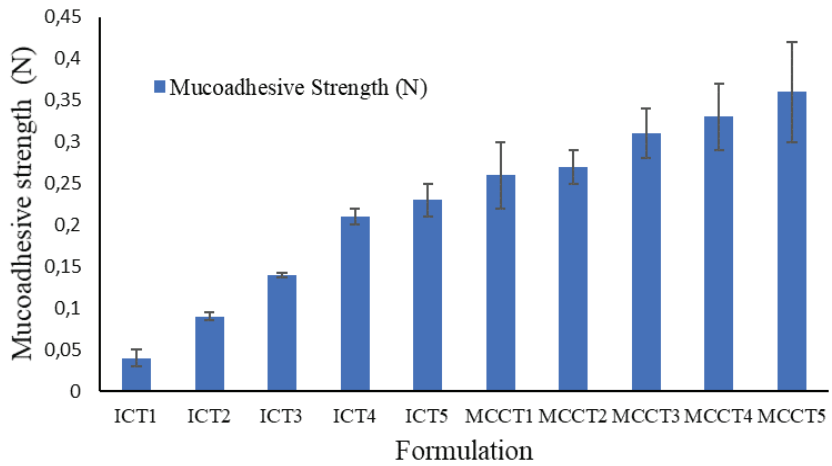


Figure 8. Mucoadhesive strength of all formulations (mean ± s.d., n = 3; $p < 0.05$, ANOVA with Tukey's test)

***Ex vivo* mucoadhesive retention time**

Mucoadhesive retention time of all MCCT formulations was tested and represented in (Figure 9.) All MCCT formulations exhibited retention times exceeding 24 hours, with MCCT1 exhibiting mucoadhesion over a 24-hour duration, while MCCT5 demonstrated the longest retention, nearly up to 29 hours. These findings confirm the strong and sustained mucoadhesive property of hupu gum. This prolonged adhesion supports the formulation's potential to deliver the drug over an extended period, enhancing its therapeutic efficacy. However, compression-coated mucoadhesive systems were optimized based on superior release control, enhanced mucoadhesive efficiency, and lower polymer load compared to the high-polymer matrix system.

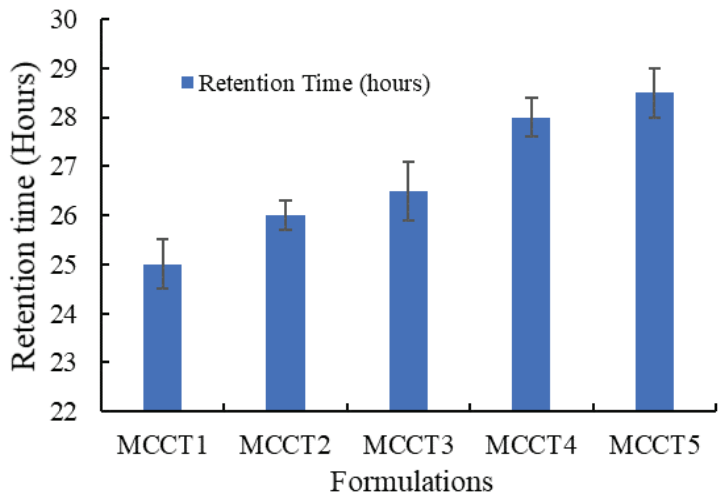


Figure 9. Mucoadhesive retention time of MCCT formulations (mean ± s.d., n = 3)

Among the evaluated formulations, MCCT1 demonstrated a gastric retention time of approximately 25 hours, which was adequate to maintain the dosage form intact within the gastric environment until complete drug release. This outcome successfully met the study objective of achieving prolonged gastric residence, thereby enabling sustained and complete drug delivery over 24 hours. Consequently, MCCT1 was identified as the most suitable formulation, offering an optimal balance between gastric retention efficiency, structural integrity, and controlled drug release within the intended therapeutic timeframe.

***In vivo* gastric retention time**

X-ray images of a rabbit after drug administration demonstrated that the alfuzosin HCl compression-coated tablet adhered to the gastric mucosa effectively over 24 hours. X-ray images taken at intervals of 12 and 24 hours were represented in (Figure 8.). This finding confirmed the tablet's retention in the stomach without significant displacement. At the 12-hour mark, the tablet remained positioned firmly in the gastric region, and by 24 hours, it showed consistent adherence, indicating strong mucoadhesive properties. These findings validate the formulation's potential for prolonged gastric retention, aligning with the stipulated extended drug delivery profile. This strong retention correlates well with *ex vivo* mucoadhesive data, supporting the *in vivo* relevance of the formulation's design. The persistent gastric localization is particularly advantageous for drugs like alfuzosin HCl that benefit from localized release and improved bioavailability in upper GI tract conditions.

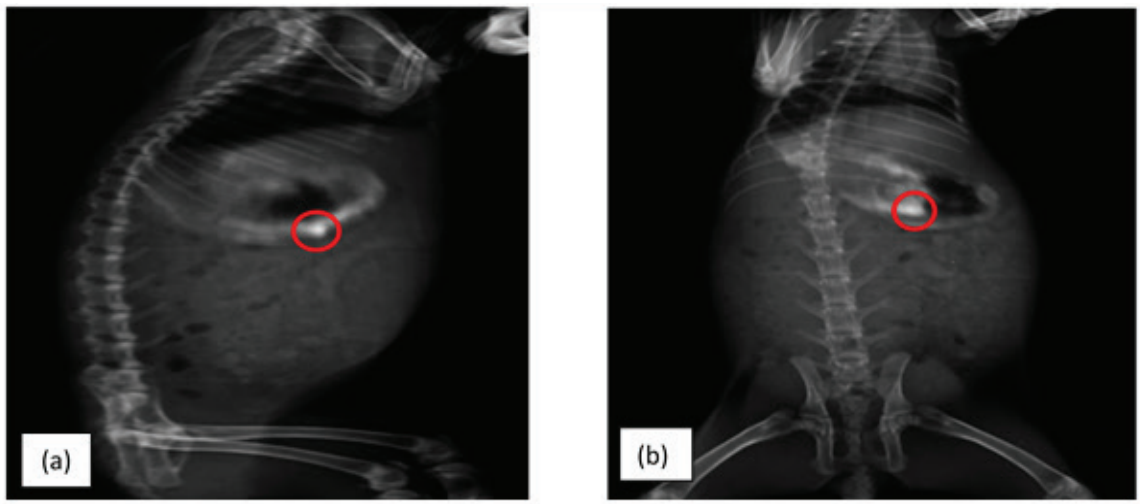


Figure 8. X-ray images of MCCT1 mucoadhesive gastric retention in a rabbit at (a)12 hours (b) 24 hours

Optimized formulation: stability profile

The stability study results in (Table 5.) showed no visible or physical changes in the product stored under both long-term and accelerated conditions. As shown in Table 9, drug release remained consistent before and after storage, with similarity factor (f2) values of 91.25 for long-term and 87.41 for accelerated conditions. These findings confirm that the coating thickness and polymers used in the formulation effectively protected the drug from environmental factors, with no changes in drug content or mucoadhesive properties, demonstrating the product's stability in line with ICH guidelines.

Table 5. Stability studies of optimized formulation MCCT1

Test	Fresh samples	Storage condition			
		Acelerated		Longterm	
		3 months	6 months	3 months	6 months
Thickness[a] (mm)	5.1±0.17	5.1±0.15	5.1±0.13	5.1±0.16	5.1±0.14
Hardness[a] (Kg/cm^2)	5.1±0.32	5.1±0.29	5.1±0.28	5.1±0.30	5.1±0.31
Weight variation[b] (mg)	250±0.5	250±0.4	250±0.3	250±0.7	250±0.6
Drug content[c] (%)	99.94±0.16	99.94±0.13	99.94±0.14	99.94±0.18	99.94±0.15
Mucoadhesive strength	0.26 ± 0.04	0.26 ± 0.07	0.25 ± 0.03	0.25 ± 0.06	0.25 ± 0.05
Mucoadhesive retention time	24±0.5	24±0.3	24±0.2	24±0.4	24±0.3

n=3

CONCLUSION

The study successfully established a mucoadhesive gastroretentive drug delivery system capable of sustaining the release of alfuzosin HCl for a full 24-hour period. Among all the developed formulations, MCCT1 demonstrated superior performance, exhibiting a gastric residence time of approximately 25 hours while retaining its structural integrity in the gastric environment until complete drug release. This confirmed the achievement of the primary objective of prolonged gastric retention.

The enhanced performance of MCCT1 was primarily attributed to efficient polymer utilization and improved mucoadhesive behaviour achieved through the compression-coated design. By localizing the mucoadhesive polymer on the tablet surface, the formulation maximized interaction with the gastric mucosa while limiting the overall polymer load. This approach resulted in more predictable drug release, better formulation reproducibility, and improved patient acceptability.

Molecular docking studies further reinforced the mucoadhesive potential of the system, revealing the involvement of hydrogen bonding, C–H interactions, and van der Waals forces. The presence of these interactions indicates strong and stable binding between the polymer and mucosal components, which is likely to enhance mucosal adhesion and prolong retention at the site of action, thereby supporting sustained drug release.

The findings clearly identify Hupu gum as an effective mucoadhesive polymer for the gastroretentive delivery of alfuzosin HCl. Overall, MCCT1, formulated with a 1:1 ratio of Hupu gum in the core and coating layers, emerged as the most suitable and optimized formulation for once-daily mucoadhesive gastroretentive therapy. In addition, the docking results provide a scientific foundation for further *in vitro* and *ex vivo* investigations into mucoadhesive performance and drug release behavior.

ACKNOWLEDGEMENTS

The authors are thankful to Gokaraju Rangaraju College of Pharmacy for providing the research facility.

AUTHOR CONTRIBUTION STATEMENT

RA, PKT, MN, BJ contributed to this article. RA contributed to conceptualisation, supervision. RA, PKT contributed to the literature search, data acquisition and calculations and writing of the preliminary draft of the manuscript. MN and BJ edited the manuscript and made critical revisions. All authors reviewed and approved the final manuscript.

CONFLICT OF INTEREST

The authors declare that there is no conflict of interest.

REFERENCES

Abd El-Aziz, M. F., Ismail, S., Tadros, M. I., & Elnabarawi, M. A. (2020). Alfuzosin hydrochloride-loaded low-density gastroretentive sponges: development, in vitro characterization and gastroretentive monitoring in healthy volunteers via MRI. *Pharmaceutical Development and Technology*, *25*(5), 566-578. doi.org/10.1080/10837450.2020.1720235

Aleti, R., & Murthy, K. V. R. (2023). Development and characterization of chronotherapeutic tablets of sacubitril-valsartan supramolecular complex using hupu gum and lannea gum by compression coating. *Journal of Applied Pharmaceutical Science*, *13*(7), 193-203. doi.org/10.7324/JAPS.2023.120714

Aleti, R., Nijhawan, M., Thota, P. K., & Jidige, B. (2025). Review on novel pharmaceutical applications of hupu gum: A versatile natural polymer. In *Annales Pharmaceutiques Françaises*, *83*(1), 22-32. Elsevier Masson. doi.org/10.1016/j.pharma.2024.09.008

Andrews, G. P., Laverty, T. P., & Jones, D. S. (2009). Mucoadhesive polymeric platforms for controlled drug delivery. *European journal of pharmaceutics and biopharmaceutics*, *71*(3), 505-518. doi.org/10.1016/j.ejpb.2008.09.028

Aulton, M. E. (2002). Pharmaceutics: The science of dosage form design. Oxford, Churchill Livingstone.

Ford, J. L. (2014). Design and evaluation of hydroxypropyl methylcellulose matrix tablets for oral controlled release: A historical perspective. In Hydrophilic matrix tablets for oral controlled release (pp. 17-51). New York, NY: Springer New York.

Ige, P. P., & Gattani, S. G. (2013). In vivo radio imaging studies on designed swelling gastro retentive drug delivery system. *Afr J Pharm Pharmacol*, *7*, 2846-2848. doi: 10.5897/AJPP11.587

Indian Pharmacopoeia, Govt of India. Ministry of Health and Family Welfare, IPC, Ghaziabad, India, 2018; 8th Edition, Vol 1; 2.5.3:308.

Indian Pharmacopoeia, Govt of India, Ministry of Health and Family Welfare, IPC, Ghaziabad, India, 2018; 8th Edition, Vol 1;2.5.5:309.

Khutoryanskiy, V. V. (2011). Advances in mucoadhesion and mucoadhesive polymers. *Macromolecular bioscience, 11*(6), 748-764. doi.org/10.1002/mabi.201000388

Kim, E. H., Larson, J. A., & Andriole, G. L. (2016), Management of benign prostatic hyperplasia, *Annual review of medicine, 67(*1), 137-151. doi.org/10.1146/annurev-med-063014-123902

Korsmeyer, R. W., Gurny, R., Doelker, E., Buri, P., & Peppas, N. A. (1983). Mechanisms of solute release from porous hydrophilic polymers. *International journal of pharmaceutics*, *15*(1), 25-35. doi.org/10.1016/0378-5173(83)90064-9

Kumar, K., Gurunath, S., Rao, M., & Ajitha, M. (2020). Formulation, Characterization and Evaluation to Establish the Bioavailability of Gastroretentive Mucoadhesive Dosage of Atenolol in Human Sub-

jects with Possible In-Vitro-In-Vivo Correlation: Gastroretentive Mucoadhesive Dosage Form of Atenolol. *Iranian Journal of Pharmaceutical Sciences*, *16*(4), 53-70.

Maggi, L., Conte, U., Grenier, P., Vergnault, G., Dufour, A., Jarreau, F. X., & Rauch-Desanti, C. (2000). U.S. Patent No. 6,149,940. Washington, DC: U.S. Patent and Trademark Office.

Panda, J., Rao, M. E. B., Swain, S., Patra, C. N., & Jena, B. R. (2022). Formulation development, optimization and characterization of mucoadhesive minitablets of cefuroxime axetil: in vitro, ex vivo and in vivo pharmacokinetic evaluation. *Beni-Suef University Journal of Basic and Applied Sciences*, *11*(1), 123. doi.org/10.1186/s43088-022-00303-2

Park, K., & Robinson, J. R. (1984). Bioadhesive polymers as platforms for oral-controlled drug delivery: method to study bioadhesion. *International journal of pharmaceutics*, *19*(2), 107-127. doi.org/10.1016/0378-5173(84)90154-6

Pattnaik, S., Kalpana, S., Choudhury, P., Acharya, P. K., & Mallick, S. (2009). Alfuzosin hydrochloride transdermal films: evaluation of physicochemical, *in vitro* human cadaver skin permeation and thermodynamic parameters. *International Brazilian Journal of Urology, 35*, 716-729. doi.org/10.1590/S1677-55382009000600010

Peppas, N. A., & Buri, P. A. (1985). Surface, interfacial and molecular aspects of polymer bioadhesion on soft tissues. *Journal of Controlled Release*, *2*, 257-275. doi.org/10.1016/0168-3659(85)90050-1

Roni, M. A., Kibria, G., & Jalil, R. (2009). Formulation and in vitro evaluation of alfuzosin extended release tablets using directly compressible eudragit. *Indian journal of pharmaceutical sciences*, *71*(3), 252. doi.org/10.4103/0250-474X.56019

Sankar, R., & Jain, S. K. (2013). Development and characterization of gastroretentive sustained-release formulation by combination of swelling and mucoadhesive approach: a mechanistic study. *Drug design, development and therapy*, 1455-1469. doi.org/10.2147/DDDT.S52890

Sanki, U. K., & Mandal, B. K. (2012). In vitro-in vivo correlation evaluation of generic alfuzosin modified release tablets. *International scholarly research notices*, *2012*(1), 813836. doi.org/10.5402/2012/813836

Siepmann, J., & Peppas, N. A. (2012). Modeling of drug release from delivery systems based on hydroxypropyl methylcellulose (HPMC). *Advanced drug delivery reviews*, *64*, 163-174. doi.org/10.1016/j.addr.2012.09.028

Smart, J. D. (2005). The basics and underlying mechanisms of mucoadhesion. *Advanced drug delivery reviews*, *57*(11), 1556-1568. doi.org/10.1016/j.addr.2005.07.001

Streubel, A., Siepmann, J., & Bodmeier, R. (2006). Gastroretentive drug delivery systems. *Expert opinion on drug delivery*, *3*(2), 217-233. doi.org/10.1517/17425247.3.2.217

USP 47–NF 42. (2024). United States Pharmacopeial Convention. Rockville (MD): USP. General Chapter <711> Dissolution; General Chapter <724> Drug Release

Vaishali, K., Imtiaz, K., & Nidhi, S. (2013). Novel sustained release drug delivery system of alfuzosin hydrochloride with improved bioavailability: Investigation of drug release kinetics. *Journal of Pharmaceutical Research*, *12*(4), 134-141. https://pdfs.semanticscholar.org/e92a/9a97e772d497fa4faf1784d00d9a5e90d991.pdf

FABAD J. Pharm. Sci., 51, 1, 147-162, 2026
Doi: 10.55262/fabadeczacilik.1746938
RESEARCH ARTICLE

Investigation of Maillard-Type Drug–Excipient Interaction Between Rivaroxaban and Lactose: Implications for Stability and *In Vitro* Anticoagulant Activity

Kunal BACHCHHAO[*°], Ajaygiri GOSWAMI[**], Chandragauda PATIL[***], Dipak PATIL[****]

Investigation of Maillard-Type Drug–Excipient Interaction Between Rivaroxaban and Lactose: Implications for Stability and In Vitro Anticoagulant Activity

SUMMARY

The study of drug–excipient interactions (DEI) is a critical aspect of the preformulation stage in pharmaceutical formulation development. The Maillard reaction is particularly reported in amine-containing excipients interacting with drug molecules possessing carbonyl groups, or vice versa, forming intermediate products that may be toxic in nature. The present study highlights the interaction between Rivaroxaban (RVI) and lactose monohydrate (LT) through the Maillard reaction. RVI is an oral anticoagulant with potent activity. The RVI–LT adduct was prepared by incubating RVI with LT at 60°C in borate buffer (pH 9.2) for 12 hours. The formation of the adduct was assessed using spectroscopic and thermal techniques such as UV–visible spectroscopy, Fourier-transform infrared spectroscopy, differential scanning calorimetry, high-performance liquid chromatography, and liquid chromatography–mass spectrometry. In silico molecular docking experiments were performed to evaluate the effect of adduct formation on the binding of RVI to its pharmacological target, Factor Xa. A significant loss of binding activity of the adduct, compared with native RVI, was revealed by docking experiments, indicating a potential reduction in anticoagulant potency. These were supported by in vitro chromogenic substrate assays for Factor Xa inhibition, with the adduct demonstrating reduced inhibitory activity. The present study identifies the susceptibility of RVI to Maillard-type interactions when formulated with LT, highlighting the imperative of prudent excipient selection in solid dosage forms to ensure therapeutic activity.

Keywords: *Rivaroxaban, Maillard reaction, drug–excipient interaction, in silico and in vitro study, Factor Xa inhibition.*

Rivaroksaban ve Laktoz Arasındaki Maillard Tipi İlaç-Yardımcı Madde Etkileşiminin Araştırılması: Stabilite ve İn Vitro Antikoagülan Aktivite Açısından Etkileri

ÖZ

İlaç–yardımcı madde etkileşimlerinin (DEI) incelenmesi, farmasötik formülasyon geliştirme sürecinin ön formülasyon aşamasında kritik bir unsurdur. Maillard reaksiyonu, özellikle karbonil grupları içeren ilaç molekülleri ile etkileşime giren amin içeren yardımcı maddelerde veya tersine durumda rapor edilmekte olup, toksik nitelikte olabilen ara ürünlerin oluşumuna yol açabilmektedir. Bu çalışma, Rivaroksaban (RVI) ile laktoz monohidrat (LT) arasındaki etkileşimi Maillard reaksiyonu aracılığıyla vurgulamaktadır. RVI, güçlü etkiye sahip oral bir antikoagülanttır. RVI–LT adüktü, RVI'nin LT ile borat tamponu (pH 9,2) içerisinde 60°C'de 12 saat inkübe edilmesiyle hazırlanmıştır. Adükt oluşumu; UV–görünür spektroskopisi, Fourier dönüşümlü kızılötesi spektroskopi, diferansiyel taramalı kalorimetri, yüksek performanslı sıvı kromatografisi ve sıvı kromatografi–kütle spektrometrisi gibi spektroskopik ve termal teknikler kullanılarak değerlendirilmiştir. In silico moleküler docking çalışmaları, adükt oluşumunun RVI'nin farmakolojik hedefi olan Faktör Xa'ya bağlanması üzerindeki etkisini değerlendirmek amacıyla gerçekleştirilmiştir. Docking deneyleri, adüktün bağlanma aktivitesinde doğal RVI'ye kıyasla belirgin bir azalma olduğunu ortaya koymuş ve bu durum antikoagülan etkinlikte potansiyel bir düşüşe işaret etmiştir. Bu bulgular, Faktör Xa inhibisyonuna yönelik in vitro kromojenik substrat testleriyle desteklenmiş olup, adüktün daha düşük inhibitör aktivite gösterdiği belirlenmiştir. Mevcut çalışma, LT ile formüle edildiğinde RVI'nin Maillard tipi etkileşimlere duyarlılığını ortaya koymakta ve terapötik etkinliğin korunması amacıyla katı dozaj formlarında dikkatli yardımcı madde seçiminin gerekliliğini vurgulamaktadır.

Anahtar Kelimeler: *Rivaroksaban, Maillard reaksiyonu, ilaç-yardımcı madde etkileşimi, in silico ve in vitro çalışma, Faktör Xa inhibisyonu.*

Recieved: 20.07.2025
Revised: 2.01.2026
Accepted: 5.02.2026

[*] ORCID: 0000-0003-1095-1961, University Institute of Chemical Technology, KBC North Maharashtra University, Jalgaon, Maharashtra, India.
[**] ORCID: 0000-0002-4472-863X, University Institute of Chemical Technology, KBC North Maharashtra University, Jalgaon, Maharashtra, India.
[***] ORCID: 0000-0001-8401-1978, Department of Pharmacology, R.C. Patel Institute of Pharmaceutical Education & Research Shirpur, Dist Dhule MS.425405
[****] ORCID: 0000-0002-4826-4537, Department of Quality Assurance K. K. Wagh College of Pharmacy, Nasik MS 422003

[°] Corresponding Author; Kunal Bachchhao
E-mail: kunalbachchhao@gmail.com

INTRODUCTION

The four cornerstones of safety, efficacy, quality, and formulation stability are the pillars of any new drug development process. If the physicochemical properties of the drug product are to be consistently preserved in a final dosage form, it is necessary to understand the physicochemical properties of the active pharmaceutical ingredient (API) and all other elements, such as excipients, manufacturing aids, and packaging materials (Patel, Ahir, Patel, Manani, & Patel, 2015). API and other formulation ingredients are typically completely investigated at the preformulation stage of the development of a new drug (Chaurasia, 2013; Mishra et al., 2023b). Drug solubility, dissolution rate, polymorph and salt screening, stability, particle size distribution, ionisation characteristics, and API–excipient compatibility are evaluated during the preformulation stage. Excipients are found in every drug product and contribute to the formation of the dosage form, stability, administration, distribution, and/or other aspects. Choice of excipients relies on their price, compatibility, and functionality. However, such interactions between API and excipient might lead to unstipulated stability problems and compromise the therapeutic performance of the formulation. Thus, conducting preformulation studies is essential to determine drug–excipient compatibility (Bachchhao, Patil, Patil, & Patil, 2017). The most common drug–excipient interactions involve physicochemical incompatibilities, such as acid–base interactions and the Maillard reaction (Monajjemzadeh et al., 2009).

Adequate assessment of possible incompatibilities between the drug and excipients, using appropriate analytical strategies, is required to prevent issues during drug development and post commercialization. These analytical techniques also help identify unexpected formulated related while providing valuable information on excipient compatibility with the medicinal compound (Mishra et al., 2023a). In recent years, interest in the interaction between carbonyl-containing excipients and APIs that contain nucleophilic amine groups, particularly due to the potential of Maillard-type reaction, has increased (Ghaderi & Monajjemzadeh, 2020). Since lactose monohydrate (LT) is inert, economical, non-toxic, and provides adequate stability, it is often used as a filler or filler-binder in oral tablets and capsule formulations. Different LT grades are selected based on their physicochemical characteristics, such as flow behavior and particle size distribution (Babazadeh miyandoab, Barghi, Yousefi, & Ghaderi, 2022). LT is, however, capable of participating in Maillard reactions with amine-containing drugs containing primary or secondary amines under specific conditions, i.e., elevated temperature and alkaline pH, to form drug-excipient adducts (Patil & Patil, 2013). Such adducts can alter the physicochemical properties, therapeutic activity, and stability of the original drug molecule. When mixed with reducing sugars such as LT, the functional groups of Rivaroxaban (RVI), a direct oral anticoagulant with specific action on Factor Xa, could be susceptible to such non-enzymatic browning reactions. Although RVI possesses excellent oral bioavailability and steady-state pharmacokinetics, information on its interaction with excipients under stress conditions is lacking (Samama, 2011).

Due to its high mortality and morbidity rate, venous thromboembolism (VTE) is a serious disease that poses a significant public health issue (Fox, Kahn, Langleben, Eisenberg, & Shimony, 2012). VTE refers to blood clots in the veins. Venous thromboembolism, a chronic disease that includes both pulmonary embolism (PE) and deep vein thrombosis (DVT), occurs in nearly 10 million people every year all over the globe. VTE is induced by venous stasis, or reduced venous blood flow, which triggers platelet and fibrin aggregation and thrombosis (Franchini & Mannucci, 2012; Upreti, Gongati, Pandey, Saad, & Vittorio, 2023). DVT is bound to cause PE and be fatal after it occurs. Direct oral anticoagulants are the first choice for treatment of nearly all VTE patients; however, low molecular weight heparins remain widely utilized

(Xu, 2024). Patients with VTE precipitated by a significant transient risk factor may discontinue anticoagulant therapy after the initial three to six months of treatment. Those patients with a greater long-term risk of recurrent VTE compared to major bleeding, including spontaneous VTE or serious malignant disease, should take anticoagulant medication indefinitely. In most cases, pharmacological prophylaxis for VTE is required in patients undergoing major orthopaedic or cancer surgery (Khan, Tritschler, Kahn, & Rodger, 2021).

Without altering existing thrombin activity, several trials with novel oral anticoagulants have shown that factor Xa inhibitors are beneficial in VTE by reducing thrombin generation, thereby decreasing thrombin-mediated platelet activation and coagulation (Ingason et al., 2023; Perzborn, Roehrig, Straub, Kubitza, & Misselwitz, 2011). RVI is the first direct, non-cofactor-dependent inhibitor of factor Xa approved for human use (Kearon et al., 2005). Specific inhibition of Factor Xa prevents fibrin clot formation by blocking both the intrinsic and extrinsic pathways of the coagulation cascade. Unlike traditional vitamin K antagonists, RVI has linear pharmacokinetics and does not require frequent monitoring. Especially at elevated pH or temperature, RVI with aromatic and carbonyl moieties can interact with excipients in covalent or non-covalent manners. An RVI–LT adduct can alter the drug's solubility, binding capacity to Factor Xa, or overall anticoagulant activity. Although LT-containing formulations of RVI are widely available, no extensive studies have investigated the impact of such interactions on drug efficacy.

In this research, the possibility of adduct formation between lactose monohydrate (LT) and RVI of a Maillard-type was explored with a battery of sophisticated analytical tools such as UV–visible spectroscopy, Fourier-transform infrared spectroscopy (FT-IR), differential scanning calorimetry (DSC), high-performance liquid chromatography (HPLC), and liquid chromatography–mass spectrometry (LC–MS). To probe the meaning of this interaction at the molecular level, *in silico* docking experiments were conducted to assess the binding interactions of RVI and its LT adduct to Factor Xa, the drug's major biological target (PDB code: 2W26). In addition, to confirm the functional relevance of adduct formation, an *in vitro* anti-coagulant activity assay was performed, comparing the thrombin generation inhibition effectiveness of RVI with that of the RVI–LT adduct.

MATERIALS AND METHODS

Materials

RVI was obtained as a gift sample from Alembic Pharmaceutical Ltd., Vadodara. The excipients, such as LT, were procured from Merck Specialties Pvt. Ltd., Mumbai, India, Organic solvents were used without purification.

Preparation of adduct

The LT (3 g) was dissolved in 50 mL of alkaline borate buffer, pH 9.2, which provided a buffered alkaline environment for the reaction. This borate buffer had to be used to prevent pH oscillations under heating since the alkaline systems in an unbuffered state can have a pH drift that may result in uncontrolled degradation instead of reproducible adduct formation. Furthermore, it is well known that the borate ion forms reversible complexes with the cis-diol group of LT, thereby offering controlled interaction of the sugar. The quantity of LT was selected in excess with respect to RVI as a model for excipient-rich conditions commonly found in solid oral dosage forms, and also to ensure adequate availability of the reducing sugar for condensation reactions. Then, 0.5 g RVI was added; this amount was selected to maintain adequate solubility of the reactant in the reaction medium and allow reliable physicochemical characterization. The mixture was ultrasonicated in a sonicating bath for 20 min until a clear solution was obtained and then transferred to a round-bottom flask. The solution was heated at 60°C on a water bath under reflux for 12 hours. During heating, the solution gradually discolored indicating adduct formation. After completing

the reaction, the solution was transferred to a Petri dish and dried in a hot-air oven at 50°C. The resulting powder was collected by scraping and stored for further characterization.

Stability under accelerated conditions

The dry physical mixture of RVI and LT (0.5:3 g, w/w) was exposed to 40°C/75% relative humidity for 15 days, simulating the process of Maillard reaction. Afterwards, the color, the content of water, and the thermal behaviour of the new pharmaceutical formulation were evaluated by DSC.

Analytical methods

UV–visible spectroscopy

The UV–visible spectra of RVI and the RVI–LT adduct were analysed using UV– visible spectrophotometer (UV-1700, Shimadzu, Japan) double-beam spectrophotometer. Solutions of RVI and the RVI–LT adduct at a concentration of 10 µg/mL were analysed in the UV–Vis range of 200–800 nm to determine shifts in absorbance intensity (Monajjemzadeh et al., 2009).

FT-IR

The FT-IR spectra of RVI and the RVI– LT adduct were acquired using an FT-IR spectrophotometer (iD3, Nicolet ST5, ATR, Thermofisher Scientific, Mumbai, India). The prepared samples were analysed in the 4000 – 400 cm^{-1} infrared range to determine the differences in the vibrational intensity.

DSC

DSC analysis was performed to examine thermal behavior and confirm adduct formation. sample of approximately 5–10 mg of the RVI and RVI–LT adduct sample was placed on the pan and heated between 30°C and 300°C at a rate of 10°C/min by employing a DSC apparatus (DSC1, STAR System, Mettler Toledo, USA).

Isocratic HPLC analysis

Chromatographic analysis of RVI and the RVI–LT adduct was performed using an HPLC system (Shimadzu, Japan) equipped with an LC-20AD pump, an SPD-20A UV detector, and a Rheodyne injector. The injection volume was kept constant at 20 µL, and data acquisition and analysis were performed using LC solution software. The Phenomenex Luna C18 (5 µ, 250 mm × 4.6 mm) column was used for the retention and elution of RVI and RVI-LT adduct. The mobile phase consisting of acetonitrile and water (55:45 v/v, pH 6.5) was used for the elution of RVI at a flow rate of 1.0 mL/min (Gouveia et al., 2020; Mestareehi, 2025). For adduct analysis, a water:methanol (95:5 v/v) mobile phase was employed. RVI was detected at 249 nm in both studies.

LC-MS

LC–MS was performed with an electrospray ionization source in positive mode (Varian Inc., USA 410 Prostar binary LC with 500 MS). The adduct was eluted on a Zorbax Eclipse XDB-C18 column (2.1 mm × 150 mm), 5 µm particle size as the stationary phase at a flow rate of 0.2 mL/min. Spectra were acquired between 50 and 2000 amu.

***In silico* evaluation**

Molecular docking studies were conducted using the GLIDE module of Schrödinger (Schrödinger Inc., USA, 2006). The crystal structure of Factor Xa complexed with an inhibitor (PDB ID: 2W26) was obtained from the Protein Data Bank (Kundu & Wu, 2021). The protein was prepared and optimized using the Protein Preparation Wizard in Maestro (version 9.0) through a two-step process involving structure refinement and energy minimization. Ligand structures were generated in the Maestro Build Panel and subsequently processed with LigPrep 2.2 to obtain low-energy conformers based on the OPLS-2005 force field. The most stable ligand conformations were then docked into the receptor's active site using the grid derived from the prepared protein, employing the standard precision (SP) docking protocol.

***In vitro* determination of anti-coagulant activity**

Blood samples of six normal human volunteers were drawn after informed consent. Prothrombin time was determined employing a regular prothrombin time test kit (company: BIOBASE) according to the manufacturer's guidelines. Three treatment

groups were assigned to the samples: untreated control, RVI-treated, and RVI–LT adduct-treated. The treatment was performed at 37°C for 30 min using RVI at a concentration of 10 µg/mL, and an equivalent concentration of the RVI–LT adduct was incubated under the same conditions. All samples were tested in triplicate. Statistical analysis was conducted using one-way ANOVA with Tukey's post hoc test to determine prothrombin times among groups, with $p < 0.001$ as statistically significant.

RESULTS AND DISCUSSION

The present study involved the characterization of a Maillard-type adduct formed between RVI and LT monohydrate. A combination of analytical techniques, including UV–visible spectroscopy, FT-IR, DSC, HPLC, and LC–MS, was employed to confirm adduct formation and evaluate its physicochemical properties. The anticoagulant activity of RVI was compared with that of the synthesized adduct using an *in vitro* Factor Xa inhibition assay. In addition, *in silico* molecular docking was performed to investigate key interactions between RVI and human Factor Xa and to elucidate the impact of adduct formation on target affinity and pharmacological activity.

Analytical methods

UV–visible spectroscopy

UV–visible absorption spectra of the pure RVI and the RVI–LT adduct were obtained with distilled water as a solvent from 200–800 nm, which covers the typical electronic transitions of the aromatic and amide groups in RVI. The adduct exhibited shifts in maximum absorbance and minor changes in intensity relative to the pure drug, suggesting potential alteration in the electronic environment due to Maillard-type interaction. The pure RVI was scanned from 800 – 400 nm in the visible range, showing no increase in the absorbance intensity, as shown in Figure 1. After formation of the adduct, RVI-LT shows an increase in the absorbance spectra post 600 nm, extending towards 400 nm. The increase in the absorbance intensity compared to pure RVI preliminary confirms the formation of an adduct (Han, Yi, Wang, & Huang, 2017). The increase in the absorbance spectra at 420 nm, as shown in Figure 1b, shows the browning effect of adduct formation. In the Maillard reaction, browning is considered an important and initial step after the aldehyde and amine polymerization reaction between amine and carboxylic surface groups. The browning effect was due to the formation of a heterocyclic nitrogen intermediate in the presence of moisture (Wu et al., 2014).

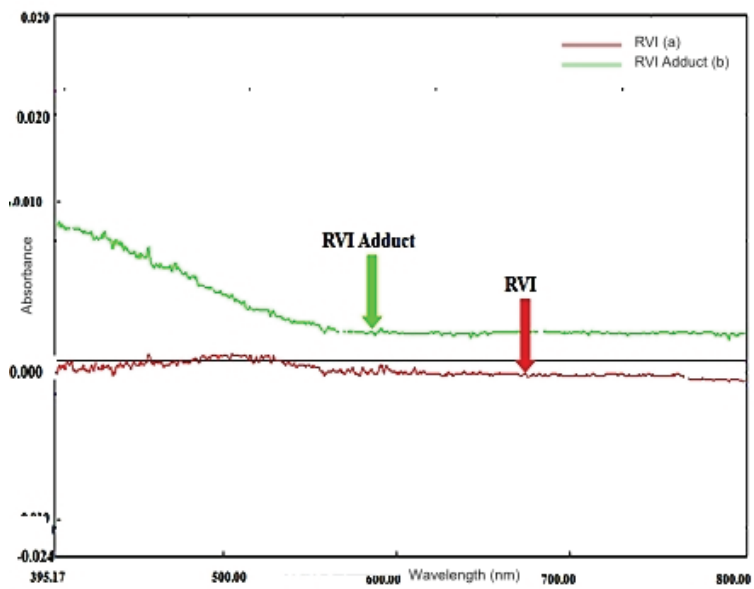


Figure 1. UV spectra of RVI and RVI-LT adduct.

FT-IR

The FT-IR absorption patterns of RVI and the RVI–LT adduct were recorded as shown in Figure 2. The vibration spectrum of pure RVI was recorded and depicted in Figure 2a, showing a distinct and sharp peak at about 3400 cm^{-1}, which represents the N-H stretching vibrations, typical of amide or amine functionalities in the molecule. Nevertheless, within the range of the RVI–LT adduct (Figure 2b.), this peak can be observed distinctly broadened and weaker, indicative of the engagement of hydrogen bonding interactions between RVI's N-H groups and LT's hydroxyl groups. Furthermore, a stretching vibration peak of C=O appears at 1750 cm^{-1} in the RVI spectrum, indicative of carbonyl groups (Shaligram et al., 2023). In the adduct, there is a shift and decrease in intensity of the carboxylic (C=O) peak, implying a modification of the electronic surrounding of the carbonyl functionality, possibly on account of contact with LT. Additionally, the spectral zone between 1600–1500 cm^{-1} similarly displays significant modification in peak position and intensity, further confirming intermolecular contact formation (Ozon et al., 2024). These spectral changes establish the formation of an RVI–LT adduct by non-covalent interactions, i.e., hydrogen bonding, as opposed to simple physical mixing (C-N stretching vibrations typically appear in the range of 1020–1350 cm^{-1}, while 1750 cm^{-1} is characteristically attributed to C=O stretching (particularly from esters or lactams). Thus, the peak at 1750 cm^{-1} in RVI is more accurately assigned to a carbonyl (C=O) group rather than C-N (Xu, Wu, Liu, Zhang, & Lu, 2017).

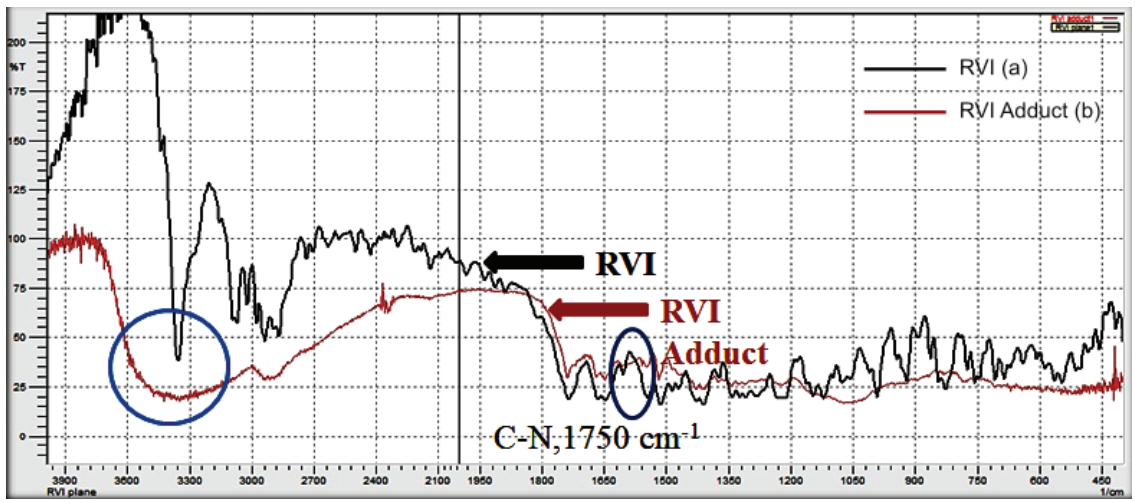


Figure 2. FT-IR spectrum of RVI (a) and RVI-LT adduct (b)

DSC

DSC is a crucial technique for figuring out whether an adduct was successfully produced. Figure 3a and 3b display the DSC curves of RVI and RVI-LT adduct. A sharp endothermic peak of RVI is displayed at 232°C, which corresponds to its melting point (Sherje & Jadhav, 2018). The clear, narrow peak illustrates the drug's crystalline structure and thermal purity. Unlike the pure form, the combination of RVI and LT shows a wide range of temperature changes instead of a clear melting point. The melting peak of RVI after the formation of the adduct decreased sharply, suggesting a loss of crystallinity, followed by the disappearance of the peak at 232°C (Ding, Chen, Zhai, Fu, & Sun, 2017). The adduct curve also has a small, broad endothermic hump in the region of 100 and 150°C. Desorption of adsorbed water or low-energy interactions, such as hydrogen bonding with LT, are likely the cause of this. The finding indicates that after coming in contact with LT, RVI has become an amorphous or largely amorphous state and also gives confirmatory evidence for the formation of the RVI–LT adduct.

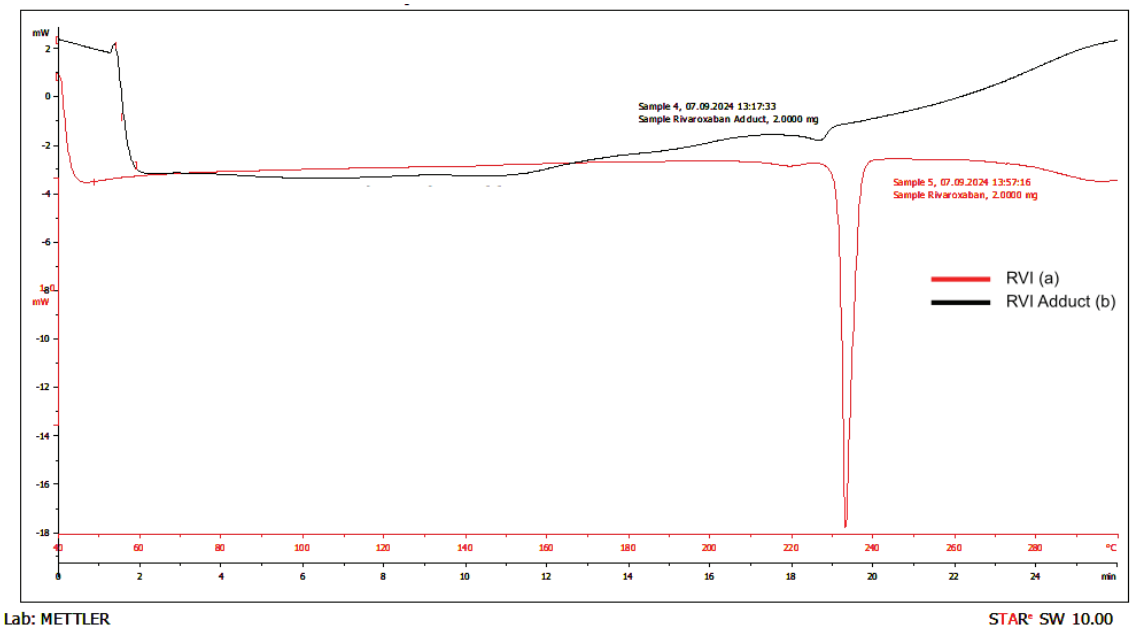


Figure 3. DSC Spectrum of RVI and RVI-LT adduct

HPLC analysis

HPLC was used to determine the chromatographic behavior of RVI and its Maillard adduct with LT, as shown in Figures 4a and 4b. The method was operated in isocratic mode using a Phenomenex Luna C18 column (250 × 4.6 mm, 5 µm, 100 Å) and a mobile phase containing ACN: Water (55:45 v/v) ratio. The same mixture was utilized as the diluent. The column temperature and sample temperatures were set to 25°C, at a 1.0 ml/min flow rate. The 20 µL injection volume was set, and detection occurred at a wavelength of 249 nm during a 10-minute runtime. Pure RVI produced a single, sharp peak on the chromatogram at a retention time of 4.203 minutes, ensuring the analyte was pure (Figure 4a.) (Rao et al., 2023). The RVI–LT adduct produced multiple peaks (Figure 4b.). The main peak of the RVI–LT Maillard adduct was found to occur at 6.988 minutes retention time, which is different from the pure compound. Other low-intensity minor peaks were at 0.142, 0.493, 1.628, 4.169, and 7.280 minutes, showing evidence of intermediate or side products that are generated under the Maillard reaction (Choi et al., 2023).

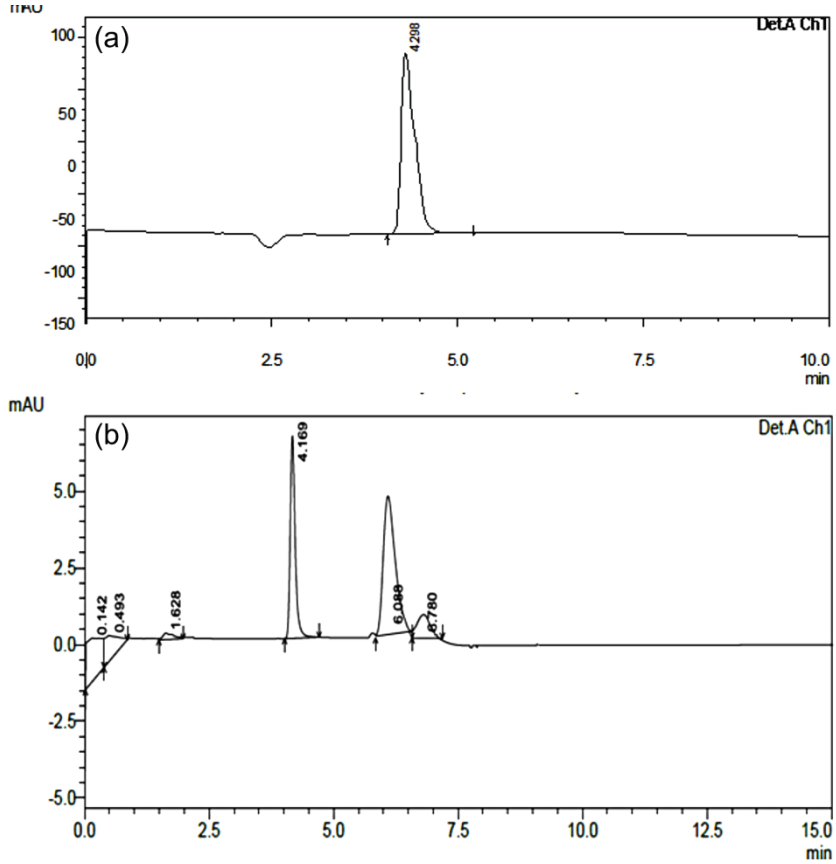


Figure 4. HPLC chromatogram of RVI (a), RVI-LT adduct (b).

LC-MS

LC-MS is commonly utilized to characterize amine–LT adducts (Babazadeh miyandoab et al., 2022; Gouveia et al., 2020). The adduct was investigated using the electrospray ionization method in positive ion mode. LC MS spectra revealed the precursor ion of the RVI– LT adduct to be a protonated molecule ([M + H] +) at m/ z 751.03 (Figure 5a.). The proposed structure of the RVI– LT adduct is illustrated in Figure 5b. The molecular weight of the RVI–LT adduct mass was in agreement with the Maillard condensation product adduct. The loss of a water molecule from a parent compound results in the production of the Maillard adduct (Wingert et al., 2015; Wirth et al., 1998). The interaction between RVI and LT was investigated to assess potential excipient–drug adduct formation. Mass spectrometric analysis (Figure 5a.) shows an ionization peak at m/z 751.03 [M+H]+, corresponding to a molecular weight of 750.018 Da. This mass aligns with the theoretical molecular weight of a covalent adduct formed between RVI ($C_{19}H_{18}O_5N_3S$-Cl; MW = 435.882 Da) and LT ($C_{12}H_{22}O_{11}$; MW = 342.2996 Da), with the elimination of a single water molecule (H_2O; 18.015 Da) via condensation. The proposed reaction mechanism (Figure 5b.) involves nucleophilic attack by the hydroxyl groups of LT on an electrophilic center of RVI, likely its ester or carbamate functional group, resulting in a covalent bond formation. Such adduct formation could have significant implications on the chemical stability, pharmacokinetics, and therapeutic efficacy of RVI when formulated with LT-containing excipients. This finding highlights the importance of thorough excipient compatibility studies during preformulation to mitigate unexpected drug–excipient interactions.

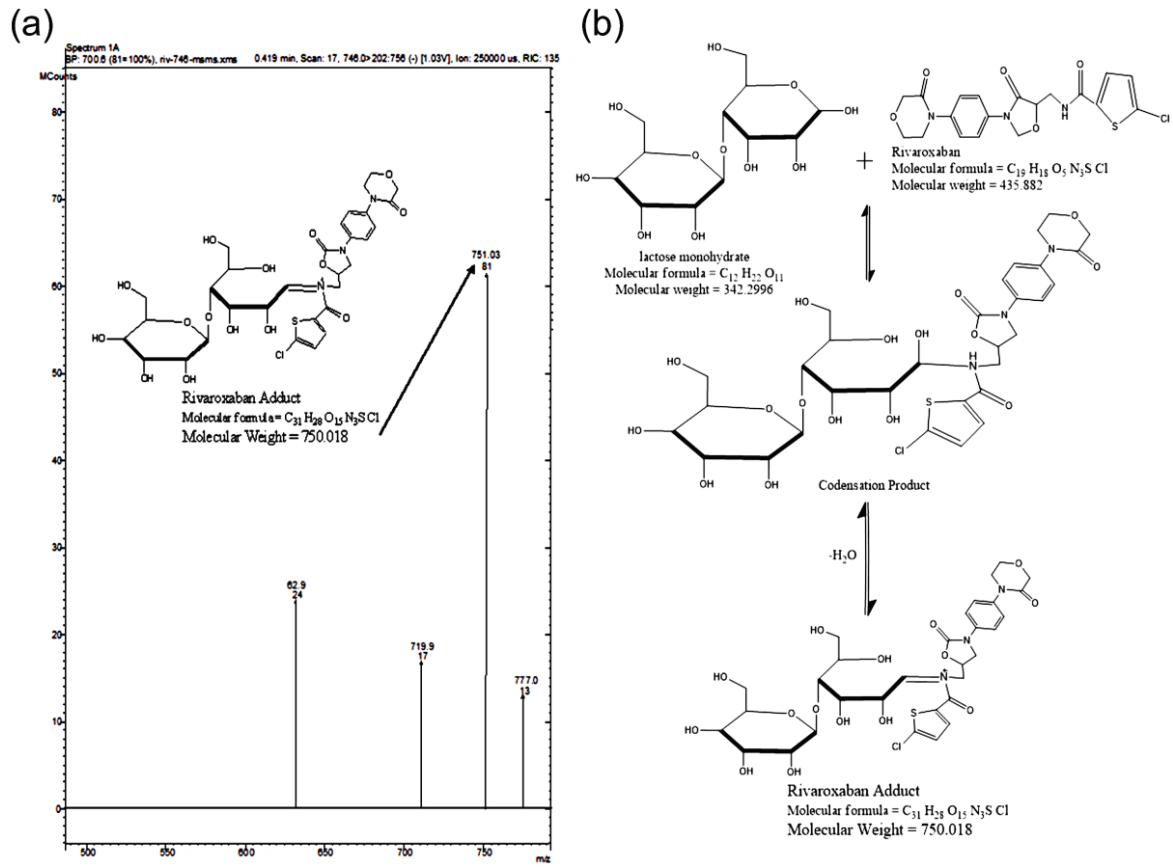


Figure 5. LC-MS spectra of RVI adduct (a), Reaction scheme for adduct formation using Maillard Reaction (b).

Docking study

RVI has an active binding site of Factor Xa in the molecular docking study with the Protein Data Bank (PDB code: 2W26) (Sabbagh, Al-Beik, & Hadid, 2023). It validated its established inhibitory activity against Factor Xa by establishing critical interactions with the ALA-121, GLY-219, and CYS-220 residues of the binding pocket (Schumacher, Luettgen, Quan, & Seiffert, 2010). These amino acid residues assist in keeping RVI stable and properly positioned within the catalytic domain of the enzyme, as depicted in Figure 6. Conversely, a binding orientation change was found when the same protein was docked with the RVI–LT adduct. LYS-148, GLU-147, GLY-216, and LYS-96 each (Figure 6.), which lie outside the traditional active site area, engaged the adduct (Esmon, 2017). These results suggest that RVI's conformation and binding energy are altered by the formation of Maillard-type adducts, possibly compromising its anticoagulant properties. The results *in vitro*, which showed that the adduct was less inhibitory of Factor Xa than the pure drug, were consistent with the *in silico* results. The introduction of the bulky LT moiety appears to interfere with the drug's ability to access and occupy its original binding site. As a result, the adduct failed to form interactions with the key catalytic residues identified for native RVI, indicating a potential reduction in binding affinity and target specificity (Du, Qian, Yao, & Xue, 2020).

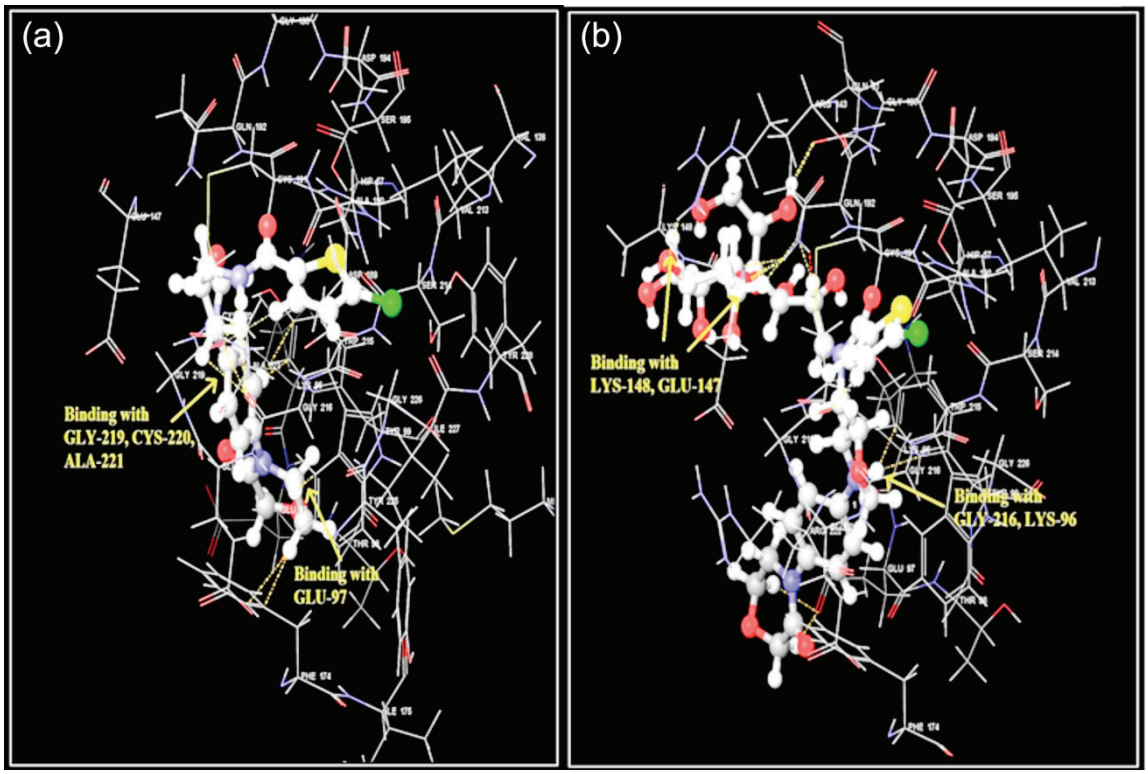


Figure 6. RVI docked with protein 2W26 (a), RVI-LT adduct docked with 2W26 (b)

***In vitro* anticoagulant activity**

By determination of prothrombin time (PT), the anticoagulant effect of RVI and its LT adduct was assessed. Six healthy human volunteers were selected for the research after the clinical practitioners ascertained their initial blood levels and secured their consent. Prothrombin time (PT) is often employed to measure the anticoagulant effect of pharmaceutical drugs and is an important clinical parameter for studying the extrinsic pathway of coagulation. The PT in the control, RVI-treated, and RVI–LT adduct groups was significantly altered in the present study, yielding data regarding the pharmacodynamic consequences of potential drug–excipient interactions (Marlu et al., 2017).

As seen from the graph, the control group had a mean PT of 43.23 ± 1.12 seconds, which was the physiological baseline. When RVI, a direct factor Xa inhibitor, was administered, a significant rise in PT to 60.29 ± 1.45 seconds was evident, an indication of its strong anticoagulant effect by inhibiting the conversion of prothrombin to thrombin (Figure 7.). This extension in PT is consistent with the established pharmacological profile of RVI and confirms its effectiveness in the modification of coagulation parameters. Perhaps most notably, the RVI–LT adduct group showed a decreased PT of 50.22 ± 1.28 seconds, significantly less than that of the pure RVI group. This decrease indicates a potential diminution of anticoagulant activity upon RVI complexation to LT, a frequently used drug excipient. Such modulation may be the result of non-covalent interaction or Maillard-type conjugation between LT and RVI (Marlu et al., 2017; Samuelson, Cuker, Siegal, Crowther, & Garcia, 2017), possibly modifying the bioavailability or molecular structure of the drug and hence its binding capacity to factor Xa. Statistical analysis with one-way ANOVA reveals a notable difference between the groups ($p < 0.001$). These findings indicate that interaction with LT resulted in reduced anticoagulant effect of RVI, as shown by the reduced PT compared to normal RVI (Pailleret et al., 2019).

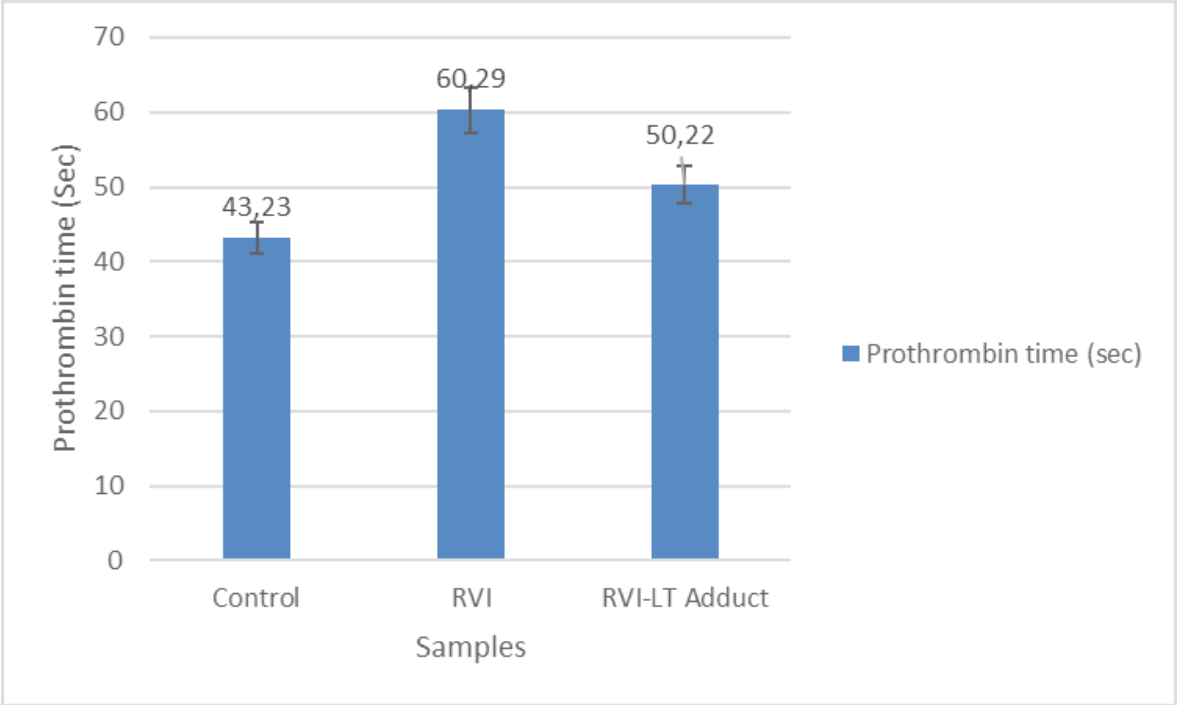


Figure 7. Prothrombin time (seconds) of control, RVI-treated, and RVI–LT adduct-treated blood samples (n = 6). Data are mean ± standard deviation. One-way ANOVA showed a statistically significant difference among the groups ($p < 0.001$)

Assessment of Maillard reaction under accelerated conditions

The physical mixture stored for 15 days underwent slight browning. This indicated that the Maillard reaction started between RVI and LT. The moisture content rose compared to that of the physical mixture. This increased moisture content helped to accelerate the Maillard reaction between the NH group of RVI and the reducing end of LT. The DSC curves of the fresh mixture revealed a sharp endothermic peak around 220°C due to RVI and another small peak due to LT at 148°C (Figure 8.). However, upon accelerated storage conditions, the DSC thermogram revealed widening and mild shift of the endothermic peak of RVI towards 220°C with reduced intensities indicative of its interaction with LT and reduced crystallinity of the remaining mixture due to Maillard reaction product formation. A small new peak emerged around 148°C, corresponding to possibly emerging Maillard reaction products. Thus, based on observations of browning reactions, increased moisture content, and changes in heat diffusivity of the mixture, it is established that the Maillard reaction proceeds in the RVI and LT mixture under accelerated conditions.

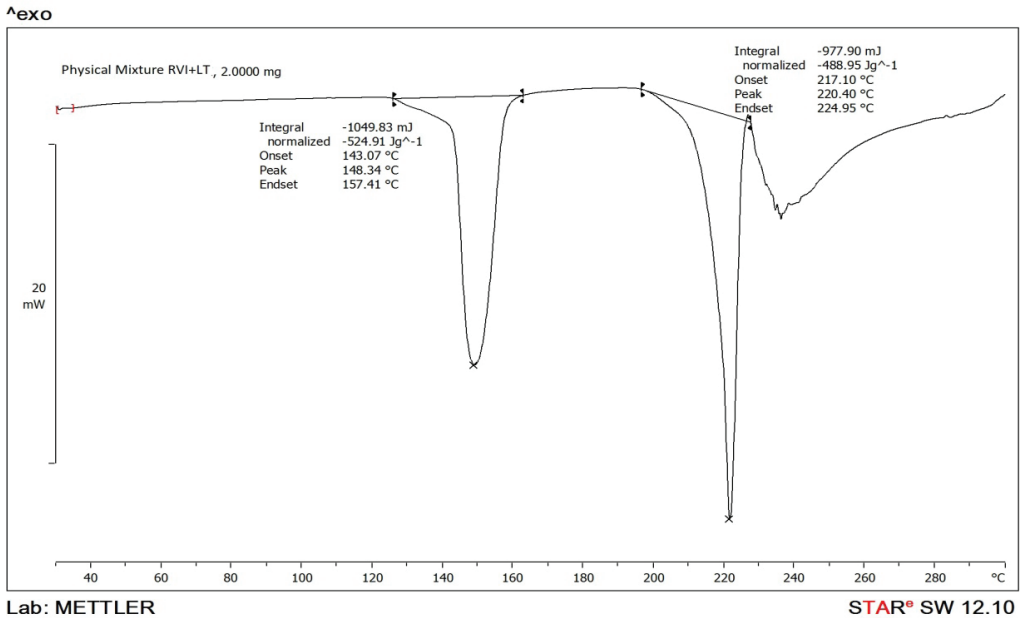


Figure 8. Physical Mixture of RVI-LT under accelerated condition

CONCLUSION

While it has long been recognized that amine-containing drug substances are capable of undergoing Maillard-type reactions with LT, LT continues to be widely used as an excipient because of its economical nature, good compressibility, and cost-effectiveness. The present study highlights the potential formation of a Maillard reaction adduct between LT and RVI in pharmaceutical formulations. Both *in vitro* anticoagulant assays and *in silico* docking studies confirmed that RVI–LT adduct formation reduced the anticoagulant activity of RVI, as evidenced by a reduced prothrombin time relative to the native drug. Given the critical therapeutic role of RVI as an anticoagulant, such excipient interactions are of significant concern. The findings suggest that the use of LT as an excipient in RVI formulations should be reconsidered. Further studies are warranted to investigate RVI–LT adduct formation under storage and environmental conditions and to assess its stability and clinical relevance over time.

CONFLICT OF INTEREST

The authors declare that there is no conflict of interest.

AUTHOR CONTRIBUTION STATEMENT

KB – Methodology, investigation, visualization, writing original draft, AG – Formal Analysis, Resources, Supervision, Writing – review and editing, CP – Investigation, statistical investigation, Analysis, DP – Supervision, Writing – review and editing.

REFERENCES

Babazadeh miyandoab, A. A., Barghi, L., Yousefi, N., & Ghaderi, F. (2022). Evaluation of Ampicillin-Lactose Incompatibility Reactions at Solid-State Using Physicochemical Methods. *Journal of Research in Applied and Basic Medical Sciences*, *8*(2), 69–74. https://doi.org/10.52547/rabms.8.2.69

Bachchhao, K. B., Patil, R. R., Patil, C. R., & Patil, D. D. (2017). Hydroxyurea-Lactose Interaction Study: In Silico and In Vitro Evaluation. *AAPS PharmSciTech*, *18*(8), 3034–3041. https://doi.org/10.1208/s12249-017-0791-4

Chaurasia, G. (2013). A Review On Pharmaceutical Preformulation Studies In Formulation And Development Of New Drug Molecules. *International Journal of Pharmaceutical Sciences and Research*, *7*.

Choi, M.-J., Woo, M. R., Baek, K., Park, J. H., Joung, S., Choi, Y. S., … Jin, S. G. (2023). Enhanced Oral Bioavailability of Rivaroxaban-Loaded Microspheres by Optimizing the Polymer and Surfactant Based on Molecular Interaction Mechanisms. *Molecular Pharmaceutics*, *20*(8), 4153-4164. https://doi.org/10.1021/acs.molpharmaceut.3c00281

Ding, T., Chen, L., Zhai, L.-H., Fu, Y., & Sun, B.-W. (2017). Compatibility study of rivaroxaban and its pharmaceutical excipients. *Journal of Thermal Analysis and Calorimetry*, *130*(3), 1569–1573. https://doi.org/10.1007/s10973-017-6412-3

Du, Q., Qian, Y., Yao, X., & Xue, W. (2020). Elucidating the tight-binding mechanism of two oral anticoagulants to factor Xa by using induced-fit docking and molecular dynamics simulation. *Journal of Biomolecular Structure and Dynamics*, *38*(2), 625–633. https://doi.org/10.1080/07391102.2019.1583605

Esmon, C. T. (2017). Targeting factor Xa and thrombin: Impact on coagulation and beyond. *Thrombosis and Haemostasis*, *111*, 625–633. https://doi.org/10.1160/TH13-09-0730

Fox, B. D., Kahn, S. R., Langleben, D., Eisenberg, M. J., & Shimony, A. (2012). Efficacy and safety of novel oral anticoagulants for treatment of acute venous thromboembolism: Direct and adjusted indirect meta-analysis of randomised controlled trials. *BMJ*, *345*, e7498. https://doi.org/10.1136/bmj.e7498

Franchini, M., & Mannucci, P. M. (2012). Association between venous and arterial thrombosis: Clinical implications. *European Journal of Internal Medicine*, *23*(4), 333–337. https://doi.org/10.1016/j.ejim.2012.02.008

Ghaderi, F., & Monajjemzadeh, F. (2020). Review of the physicochemical methods applied in the investigation of the maillard reaction in pharmaceutical preparations. *Journal of Drug Delivery Science and Technology*, *55*, 101362. https://doi.org/10.1016/j.jddst.2019.101362

Gouveia, F., Bicker, J., Santos, J., Rocha, M., Alves, G., Falcão, A., & Fortuna, A. (2020). Development, validation and application of a new HPLC-DAD method for simultaneous quantification of apixaban, dabigatran, edoxaban and rivaroxaban in human plasma. *Journal of Pharmaceutical and Biomedical Analysis*, *181*, 113109. https://doi.org/10.1016/j.jpba.2020.113109

Han, M.-M., Yi, Y., Wang, H.-X., & Huang, F. (2017). Investigation of the Maillard Reaction between Polysaccharides and Proteins from Longan Pulp and the Improvement in Activities. *Molecules*, *22*(6), 938. https://doi.org/10.3390/molecules22060938

Ingason, A. B., Hreinsson, J. P., Agustsson, A. S., Lund, S. H., Rumba, E., Palsson, D. A., … Bjornsson, E. S. (2023). Comparison of the effectiveness and safety of direct oral anticoagulants: A nationwide propensity score–weighted study. *Blood Advances*, *7*(11), 2564–2572. https://doi.org/10.1182/bloodadvances.2022009099

Kearon, C., Comp, P., Douketis, J., Royds, R., Yamada, K., & Gent, M. (2005). Dose–response study of recombinant human soluble thrombomodulin (ART-123) in the prevention of venous thromboembolism after total hip replacement. *Journal of Thrombosis and Haemostasis*, *3*(5), 962–968. https://doi.org/10.1111/j.1538-7836.2005.01251.x

Khan, F., Tritschler, T., Kahn, S. R., & Rodger, M. A. (2021). Venous thromboembolism. *The Lancet*, *398*(10294), 64–77. https://doi.org/10.1016/S0140-6736(20)32658-1

Kundu, S., & Wu, S. (2021). A Structure Based Study of Selective Inhibition of Factor IXa over Factor Xa. *Molecules*, *26*(17), 5372. https://doi.org/10.3390/molecules26175372

Marlu, R., Hodaj, E., Paris, A., Albaladejo, P., Crackowski, J. L., & Pernod, G. (2017). Effect of non-specific reversal agents on anticoagulant activity of dabigatran and rivaroxaban. *Thrombosis and Haemostasis*, *108*, 217–224. https://doi.org/10.1160/TH12-03-0179

Mestareehi, A. (2025). Development and validation of a stability-indicating reversed phase high-performance liquid chromatography method for quantifying rivaroxaban (XARELTO). *Journal of Chromatography B*, *1257*, 124573. https://doi.org/10.1016/j.jchromb.2025.124573

Mishra, A., Sinha, V. R., Sharma, S., Mathew, A. T., Kumar, R., & Yadav, A. K. (2023a). A comprehensive compatibility study of ganciclovir with some common excipients. *American Journal of Biopharmacy and Pharmaceutical Sciences*, *3*. https://doi.org/10.25259/AJBPS_4_2023

Mishra, A., Sinha, V. R., Sharma, S., Mathew, A. T., Kumar, R., & Yadav, A. K. (2023b). Molecular and qualitative characterization of compatibility between valacyclovir hydrochloride and excipients as raw materials for the development of solid oral dosage formulation. *American Journal of Biopharmacy and Pharmaceutical Sciences*, *3*. https://doi.org/10.25259/AJBPS_12_2023

Monajjemzadeh, F., Hassanzadeh, D., Valizadeh, H., Siahi-Shadbad, M. R., Mojarrad, J. S., Robertson, T. A., & Roberts, M. S. (2009). Compatibility studies of acyclovir and lactose in physical mixtures and commercial tablets. *European Journal of Pharmaceutics and Biopharmaceutics*, *73*(3), 404–413. https://doi.org/10.1016/j.ejpb.2009.06.012

Ozon, E. A., Mati, E., Karampelas, O., Anuta, V., Sarbu, I., Musuc, A. M., … Mitu, M. A. (2024). The development of an innovative method to improve the dissolution performance of rivaroxaban. *Heliyon*, *10*(12). https://doi.org/10.1016/j.heliyon.2024.e33162

Pailleret, C., Jourdi, G., Siguret, V., Gouin-Thibault, I., Gandrille, S., Stepanian, A., … Samama, C. M. (2019). Modified ROTEM for the detection of rivaroxaban and apixaban anticoagulant activity in whole blood: A diagnostic test study. *European Journal of Anaesthesiology | EJA*, *36*(6), 449. https://doi.org/10.1097/EJA.0000000000000903

Patel, P., Ahir, K., Patel, V., Manani, L., & Patel, C. (2015). Drug-Excipient compatibility studies: First step for dosage form development. *The Pharma Innovation Journal, 4*(5), 14-20.

Patil, D. D., & Patil, C. R. (2013). Modification of pharmacological activity of nebivolol due to Maillard reaction. *Pharmaceutical Development and Technology*, *18*(4), 844–851. https://doi.org/10.3109/10837450.2011.591802

Perzborn, E., Roehrig, S., Straub, A., Kubitza, D., & Misselwitz, F. (2011). The discovery and development of rivaroxaban, an oral, direct factor Xa inhibitor. *Nature Reviews Drug Discovery*, *10*(1), 61–75. https://doi.org/10.1038/nrd3185

Wingert, N. R., A.G. Nunes, M., T. Barden, A., Gomes, P., I. Muller, E., M.M. Flores, E., & Steppe, M. (2015). Ultra-performance LC-ESI/Q-TOF MS for the Rapid Analysis of Rivaroxaban: Method Validation Using Experimental Design for Robustness Evaluation. *Current Analytical Chemistry*, *11*(2), 124–129.

Rao, W., Li, L., Zhang, C., Zheng, J., Fan, X., Luan, B., … Wang, Z. (2023). Development and validation of a stability-indicating RP-HPLC method for the determination of fifteen impurities in rivaroxaban. *Journal of Pharmaceutical and Biomedical Analysis*, *228*, 115325. https://doi.org/10.1016/j.jpba.2023.115325

Sabbagh, G. M., Al-Beik, L. M., & Hadid, I. (2023). In Silico and In Vitro Anticoagulant Activity Detection of Quercetin, Rutin, and Troxerutin as New Potential Inhibitors of Factor Xa. *Egyptian Journal of Chemistry*, *66*(2), 151–166. https://doi.org/10.21608/ejchem.2022.140123.6144

Samama, M. M. (2011). The mechanism of action of rivaroxaban – an oral, direct Factor Xa inhibitor – compared with other anticoagulants. *Thrombosis Research*, *127*(6), 497–504. https://doi.org/10.1016/j.thromres.2010.09.008

Samuelson, B. T., Cuker, A., Siegal, D. M., Crowther, M., & Garcia, D. A. (2017). Laboratory Assessment of the Anticoagulant Activity of Direct Oral Anticoagulants: A Systematic Review. *Chest*, *151*(1), 127–138. https://doi.org/10.1016/j.chest.2016.08.1462

Schumacher, W. A., Luettgen, J. M., Quan, M. L., & Seiffert, D. A. (2010). Inhibition of Factor XIa as a New Approach to Anticoagulation. *Arteriosclerosis, Thrombosis, and Vascular Biology*, *30*(3), 388–392. https://doi.org/10.1161/ATVBAHA.109.197178

Sherje, A. P., & Jadhav, M. (2018). β-Cyclodextrin-based inclusion complexes and nanocomposites of rivaroxaban for solubility enhancement. *Journal of Materials Science: Materials in Medicine*, *29*(12), 186. https://doi.org/10.1007/s10856-018-6194-6

Shaligram, P. S., P. George, C., Sharma, H., R. Mahadik, K., Patil, S., Vanka, K., … G. Gonnade, R. (2023). Rivaroxaban eutectics with improved solubility, dissolution rates, bioavailability and stability. *CrystEngComm*, *25*(22), 3253–3263. https://doi.org/10.1039/D3CE00261F

Upreti, P., Gongati, S. R., Pandey, N., Saad, M., & Vittorio, T. (2023). Exploring the Causal Relationship Between Arterial and Venous Thromboembolism: A Case Series With Review of Literature. *Cureus*, *15*(4), e37660. https://doi.org/10.7759/cureus.37660

Wirth, D. D., Baertschi, S. W., Johnson, R. A., Maple, S. R., Miller, M. S., Hallenbeck, D. K., & Gregg, S. M. (1998). Maillard Reaction of Lactose and Fluoxetine Hydrochloride, a Secondary Amine. *Journal of Pharmaceutical Sciences*, *87*(1), 31–39. https://doi.org/10.1021/js9702067

Wu, S., Hu, J., Wei, L., Du, Y., Shi, X., & Zhang, L. (2014). Antioxidant and antimicrobial activity of Maillard reaction products from xylan with chitosan/chitooligomer/glucosamine hydrochloride/taurine model systems. *Food Chemistry*, *148*, 196–203. https://doi.org/10.1016/j.foodchem.2013.10.044

Xu, K. (2024). EFFECT OF LOW MOLECULAR WEIGHT HEPARIN IN THE PREVENTION OF SEVERE PNEUMONIA COMPLICATED WITH LOWER EXTREMITY DEEP VEIN THROMBOSIS. *FARMACIA*, *72*(2), 294–297. https://doi.org/10.31925/farmacia.2024.2.7

Xu, Y., Wu, S.-P., Liu, X.-J., Zhang, L.-J., & Lu, J. (2017). Crystal characterization and transformation of the forms I and II of anticoagulant drug rivaroxaban. *Crystal Research and Technology*, *52*(3), 1600379. https://doi.org/10.1002/crat.201600379

FABAD J. Pharm. Sci., 51, 1, 163-174, 2026
Doi: 10.55262/fabadeczacilik.1839938
RESEARCH ARTICLE

Anticancer Potential of Piperidine-Substituted Mannich Bases: Evidence of Cytotoxic Activity and Apoptotic Effects on Various Cancer Cells

Gülşah KARAKAYA[*], Canan SEVİMLİ GÜR[**], Mutlu AYTEMİR[***°]

Anticancer Potential of Piperidine-Substituted Mannich Bases: Evidence of Cytotoxic Activity and Apoptotic Effects on Various Cancer Cells

SUMMARY

Cancer remains the second leading cause of death worldwide, accounting for approximately 20% of annual mortalities. Lung, breast, colon, and melanoma are among the most common cancer types, especially in developing countries. Kojic acid and its synthetic derivatives are known for their wide range of biological activities and applications in medicine, cosmetics, food, and agriculture. Mannich base derivatives of kojic acid have been previously reported to exhibit promising cytotoxic potential on various tumor cell lines. In this study, a series of kojic acid–based Mannich bases containing a piperidine ring were synthesized and evaluated for their anticancer effects on several cancer cell lines (SK-MEL, MCF-7, MDA-MB-231, A549, HeLa, Hep3B, HT-29, Neuro2A) and one healthy cell line (Vero). Among the synthesized compounds, Compound 4, containing a piperidinopiperidine moiety, demonstrated the highest and broadest cytotoxic activity, with IC50 values of 5.02 ± 0.09, 5.80 ± 0.06, and 5.92 ± 0.12 μM against MCF-7, Neuro2A, and SK-MEL cells, respectively. Flow cytometric analysis using the Annexin V method suggested that Compound 4 may induce apoptosis in a time-dependent manner, accompanied by G1 phase arrest in MCF-7 cells, although further molecular verification is required.

Keywords: *Kojic acid, piperidine, cytotoxicity, apoptosis.*

Piperidin İçeren Kojik Asit Mannich Bazlarının Sentezi ve Antikanser Değerlendirmesi

ÖZ

Kanser, dünya çapında ikinci önde gelen ölüm nedeni olmaya devam etmekte ve yıllık ölümlerin yaklaşık %20'sini oluşturmaktadır. Akciğer, meme, kolon ve melanom, özellikle gelişmekte olan ülkelerde en yaygın kanser türleri arasındadır. Kojik asit ve sentetik türevleri, tıp, kozmetik, gıda ve tarım alanlarında geniş bir yelpazede biyolojik aktiviteleri ve uygulamalarıyla bilinmektedir. Kojik asidin Mannich bazı yapısındaki türevlerinin, çeşitli tümör hücre hatlarında umut verici sitotoksik potansiyel sergilediği daha önce bildirilmiştir. Bu çalışmada, piperidin halkası içeren bir dizi kojik asit türevi Mannich bazları sentezlenmiş ve çeşitli kanser hücre hatları (SK-MEL, MCF-7, MDA-MB-231, A549, HeLa, Hep3B, HT-29, Neuro2A) ve bir sağlıklı hücre hattı (Vero) üzerinde antikanser etkileri değerlendirilmiştir. Sentezlenen bileşikler arasında, piperidinopiperidin parçası içeren Bileşik 4, MCF-7, Neuro2A ve SK-MEL hücrelerine karşı sırasıyla 5,02 ± 0,09, 5,80 ± 0,06 ve 5,92 ± 0,12 μM IC50 değerleri ile en yüksek ve en geniş sitotoksik aktiviteyi göstermiştir. Annexin V yöntemi kullanılarak yapılan akış sitometrik analiz, daha fazla moleküler doğrulama gerekmekle birlikte, Bileşik 4'ün MCF-7 hücrelerinde G1 fazı durması ile birlikte zamana bağlı bir şekilde apoptozu indükleyebileceğini ortaya koymuştur.

Anahtar Kelimeler: *Kojik asit, piperidin, sitotoksisite, apoptoz.*

Recieved: 10.12.2025
Revised: 28.01.2026
Accepted: 7.02.2026

[*] ORCID: 0000-0002-3827-7537, Department of Pharmaceutical Chemistry, Faculty of Pharmacy, İzmir Katip Çelebi University, İzmir, Türkiye
[**] ORC ID: 0000-0002-2210-5925, Department of Basical Sciences, Faculty of Pharmacy, İzmir Katip Çelebi University, İzmir, Türkiye
[***] ORCID: 0000-0002-1433-0356, Department of Pharmaceutical Chemistry, Faculty of Pharmacy, Hacettepe University, Ankara, Türkiye

[°] Corresponding Author; Mutlu AYTEMİR
E-mail: mutlud@hacettepe.edu.tr

INTRODUCTION

Cancer is a major and growing global health issue, affecting millions of people each year regardless of region or socio-economic background. As a primary cause of death worldwide, it accounted for approximately 10 million deaths in 2020 (Filho et al., 2025). To effectively tackle this critical problem and overcome drug resistance, focused efforts are necessary to develop novel therapeutic agents that will improve both patient outcomes and quality of life (Koirala & DiPaola, 2024).

Kojic acid (5-hydroxy-2-hydroxymethyl-4*H*-pyran-4-one, KA), a natural chelating agent, is a versatile starting material for making new anticancer agents due to its known antioxidant, radioprotective, antiproliferative, and anti-inflammatory qualities (Brtko, 2022; Burnett et al., 2010; He et al., 2021; Mohamad et al., 2010; Phasha et al., 2022; Zilles et al., 2022). Its chelating properties, attributed to the hydroxyl group at position 3 and ketonic oxygen at position 4 of the hydroxypyranone ring, are particularly significant for its antimicrobial and antioxidant activities (Emami et al., 2022). Previously, some KA derivatives were tested for their antimelanogenic activity by our research group, and several compounds showed stronger inhibition than the reference drugs, while maintaining low toxicity toward normal cells (Karakaya et al., 2019a, b). Moreover, the structural resemblance of KA to allomaltol (ALM), another pyrone derivative, suggests a shared potential for modulating cellular pathways critical for cancer progression (Ercan et al., 2020) (Figure 1.). Given its structure and established biological activities, KA becomes an attractive scaffold for synthesizing novel Mannich bases with potential anticancer properties. Specifically, using Mannich reactions allows us to strategically attach diverse amine moieties, such as piperazine and piperidine rings. These additions can significantly boost the compound's affinity for biological targets and enhance its pharmacokinetic profiles.

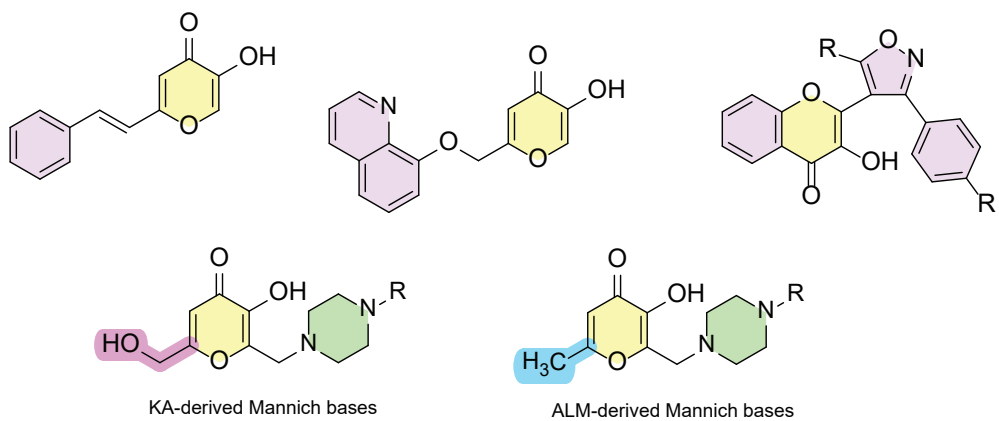


Figure 1. Chemical structures of KA derivatives with anticancer potential.

Piperidine rings are key structures in many important therapeutic compounds, showing various biological and pharmacological effects, including anticancer properties (El-Sayed Ebead et al., 2023) A series of arylidenes derivatives was synthesized under ultrasonic methodology via Knoevenagel condensation reaction of cyanoacetohydrazide derivative with the appropriate aldehydes and/or ketone. The anticancer properties of the newly synthesized compounds were tested against four different human cancer cell lines (HEPG-2, MCF-7, HCT-116, and PC-3. They are effective against many cancers, including drug-resistant prostate and ovarian cancers, by inducing mitotic arrest, terminal differentiation, and apoptosis (Mutahir et al., 2023).

These considerations led us to evaluate the cytotoxic effects of KA-based Mannich bases, specifically those incorporating a piperidine ring, across various cancer cell lines. Our chemical design was guided by previous structure–activity observations, which suggested that substitution at the Mannich position critically affects both potency and selectivity. The resulting compounds were assessed for their ability to induce apoptosis, with particular attention paid to their chemical structure–activity relationships. In this study, Compound 1 was synthesized and characterized for the first time using ^{1}H-NMR, ^{13}C-NMR, and LC-MS analysis techniques. The other derivatives (Compounds 2–9) were re-synthesized according to our previously reported procedures (Aytemir & Çalış, 2010; Karakaya et al., 2022) to evaluate their comparative anticancer activities. Their cytotoxic potential was tested on a panel of human cancer cell lines (SK-MEL, MCF-7, MDA-MB-231, A549, HeLa, Hep3B, HT-29, and Neuro2A) and the normal Vero cell line. For the most potent compound, it was investigated how it induces apoptosis, a type of programmed cell death, using the Annexin V method, and performed cell cycle analysis to understand its mechanism of action.

MATERIALS AND METHODS

Chemistry

All chemical reagents used in the synthesis were purchased from Merck and Aldrich Chemical Co. Melting points were determined using a Büchi M-560 Melting Point Apparatus and are reported without correction. NMR spectra were recorded on a Varian Mercury 500 MHz spectrometer in DMSO-d_6, with tetramethylsilane (TMS) serving as an internal standard. Mass spectra were obtained on a Micromass ZQ LC-MS instrument using the electrospray ionization (ESI) technique. HPLC analyses were performed on a Waters Alliance system equipped with a C18 column. Elemental analyses were conducted in the Central Laboratory of the Faculty of Pharmacy, Ankara University, using a Leco CHNS-932 analyzer. The purity of the compounds was verified by thin-layer chromatography (TLC) on Kieselgel 60 F_{254} plates (Merck®, Germany).

Synthesis of Compound 1

4-Phenyl-3,6-dihydropyridine (3 mmol) was mixed with formaldehyde under continuous stirring. KA (3 mmol) was then added to the reaction mixture, followed by 20 mL of methanol, and the solution was stirred at room temperature for 15–25 minutes. The resulting precipitate was collected by vacuum filtration, washed with cold methanol, and recrystallized from suitable solvents. The purity of the compound was confirmed by thin-layer chromatography (TLC) using a chloroform:methanol (9:1, v/v) solvent system.

3-Hydroxy-6-(hydroxymethyl)-2-((4-phenyl-3,6-dihydropyridin-1(2*H*)-yl)methyl)-4H-pyran-4-one (Compound 1)

$C_{18}H_{19}NO_4$ (M.W.: 313.35 g/mol); white solids, yield: 60%, M.p. 90-192°C; ^{1}H-NMR δ (DMSO$_{d6}$, 500 MHz) 2.50 (2H; t; *J*= 1.75; pyridine-*H*^{5}); 2.74 (2H; t; *J*= 5.65; pyridine-*H*^{6}); 3.17 (2H; d; *J*= 2.75; pyridine-*H*^{2}); 3.65 (2H; s; pyrane-C*H*$_2$-pyridine); 4.32 (2H; s; -C*H*$_2$-OH); 6.13 (1H; s; pyridine-*H*^{3}); 6.35 (1H; s; pyrane-*H*^{5}); 7.24 (1H; m; Ar-*H*^{4}); 7.32 (2H; m; Ar-*H*^{3,5}); 7.40 (2H; d; *J*= 8.4; Ar-*H*^{2,6}); ^{13}C-NMRδ (DMSO$_{d6}$, 125 MHz) 27.73, 50.06, 52.63, 53.54, 60.08, 109.41, 122.22, 125.01, 127.46, 128.80, 134.35, 140.54, 144.17, 147.12, 168.14, 174.11. ESI-MS (m/z): 160, 314 (%100, M^{+}+H).

Biological activity studies

The following instruments were used in bioactivity sudies: CO_2 incubator (Thermo Fisher Scientific, USA), Class II laminar flow cabinet (ESCO, Singapore), orbital shaker incubator (Biosan, Türkiye), flow cytometer (BD Accuri C5, BD Biosciences, USA), inverted phase-contrast microscope (Zeiss, Germany), light microscope (Olympus, Germany), spectrophotometer (Thermo Fisher Scientific, USA), bench centrifuge (Nüve, Türkiye), refrigerated microcentrifuge

(Hettich, Germany), water bath (LKTC-L Controller, Türkiye), vortex mixer (Thermo Fisher Scientific, USA), liquid nitrogen storage tank (50 L, Cryogenic), ultra-low freezer (−86 °C, Eppendorf, Germany), and refrigerator (+4°C, Uğur, Türkiye).

Cell culture and maintenance under two-dimensional conditions

Seven human cancer cell lines — SK-MEL (melanoma), MCF-7 and MDA-MB-231 (breast carcinoma), A549 (lung carcinoma), HeLa (cervical adenocarcinoma), Hep3B (hepatocellular carcinoma), HT-29 (colon adenocarcinoma), and one murine line, Neuro-2A (neuroblastoma) — together with one normal cell line, Vero (African green monkey kidney epithelial cells), were used in this study. Cells were cultured in RPMI-1640 or DMEM/Ham's F-12 media (Invitrogen, USA) supplemented with 10% fetal bovine serum (FBS, Sigma, USA), 100 IU/mL penicillin, and 1 µg/mL streptomycin at 37 °C in a humidified atmosphere containing 5% CO_2.

When cell confluency reached approximately 80%, the cells were sub-cultured using 0.25% trypsin-EDTA at 37°C for 3 minutes. Detached cells were collected by centrifugation at 1000 rpm for 5 minutes and re-suspended in fresh medium.

For long-term storage, cell stocks were frozen either in culture medium containing 5% dimethyl sulfoxide (DMSO) or in freezing medium composed of 10% DMSO in fetal bovine serum, and preserved at −86°C or in liquid nitrogen (−196°C) until further use (Sevimli-Gur et al., 2013; Üçkan et al., 2023).

Determination of cytotoxicity of synthesized compounds in 2D cell culture

Cell viability assay

The cytotoxic potential of the synthesized compounds was evaluated by the MTT [3-(4,5-dimethylthiazol-2-yl)-2,5-diphenyltetrazolium bromide] assay, a colorimetric method based on the reduction of tetrazolium salts by mitochondrial dehydrogenase enzymes of viable cells. The conversion of MTT (Sigma Chemicals, USA) into an insoluble blue formazan product was measured spectrophotometrically at 570 nm using a microplate reader (VersaMax™ Tunable Microplate Reader, Molecular Devices, USA). The percentage of cell viability was calculated relative to untreated controls as previously described (Sevimli-Gur et al., 2010, 2011, 2013).

Evaluation of apoptosis-inducing potential in 2D cell culture by Annexin V–FITC/PI assay

Apoptosis induction was assessed using the Annexin V–FITC/PI double-staining method, which detects the externalization of phosphatidylserine from the inner to the outer leaflet of the plasma membrane—a hallmark of early apoptosis. Annexin V, a calcium-dependent phospholipid-binding protein, binds to exposed phosphatidylserine with high affinity, allowing the detection of apoptotic cells when conjugated with a fluorochrome.

MCF-7 cells in the logarithmic growth phase were seeded in 6-well plates at a density of 2.5 × 10^5 cells/mL and incubated for 24 h at 37 °C in a humidified atmosphere containing 5% CO_2. Following incubation, cells were treated with compound 4 concentrations of 3.125, 1.562, and 0.781 µg/mL for 24 and 48 hours. After treatment, supernatants were discarded, and cells were washed with PBS and detached using trypsin-EDTA. The cell suspensions were collected and washed three times with PBS (2000 rpm, 5 min, 4°C). Cells were resuspended in 100 µL binding buffer (1×), stained with 1 µL FITC-conjugated Annexin V (BD Biosciences, USA), and incubated in the dark for 15 minutes. After washing twice with PBS, samples were resuspended in 200 µL PBS and analyzed by flow cytometry (BD Accuri C5, BD Biosciences, USA) using the FL1 (525 nm) channel (Bogurcu et al., 2011).

Cell cycle distribution was determined using the same Annexin V–FITC staining protocol to evaluate the effects of Compound 3 on MCF-7 cell proliferation. The proportion of cells in each phase (G_0/G_1, S, and G_2/M) was quantified by flow cytometry. Data were analyzed using BD Accuri C6 software to assess possible G_1-phase arrest in correlation with apoptotic induction.

Statistical analysis

All experiments were performed independently in triplicate. Results were expressed as mean ± standard deviation (SD). Statistical analysis was carried out using Microsoft Excel. Differences between groups were evaluated using one-way ANOVA followed by Dunnett's multiple comparison test. Significance between paired data was determined using the Student's t-test. Differences were considered statistically significant at *$p < 0.05$, **$p < 0.01$, and ***$p < 0.001$ (Sevimli-Gur et al., 2013).

RESULTS AND DISCUSSION

In medicinal chemistry, heterocyclic amines like piperidine and piperazine are key pharmacophores. They are vital for receptor binding and maintaining a favorable pharmacokinetic balance. Piperidine, a saturated six-membered heterocycle, offers a conformationally flexible, electron-rich scaffold. This feature is critical for influencing metabolic stability and molecular recognition. The Mannich reaction is powerful for structural diversification of KA because the resulting Mannich base introduces an b-amino methyl functionality at the C-6 or C-7 position of the pyrone ring. This modification significantly alters physicochemical properties such as lipophilicity, hydrogen-bonding capacity, and electronic distribution. Such modifications can improve cellular permeability and interaction with biological macromolecules, thereby enhancing biological activity (Roman, 2015).

Compounds 2-9 have been reported in our previous studies (Aytemir & Çalış, 2010; Karakaya et al., 2022). For this study, they were resynthesized, and their structures were confirmed (Figure 2.). Compound 1, however, is an original compound characterized for the first time in this study and included in the study to strengthen the understanding of the structure-activity relationships. Its chemical structure has been confirmed by appropriate spectral analysis methods.

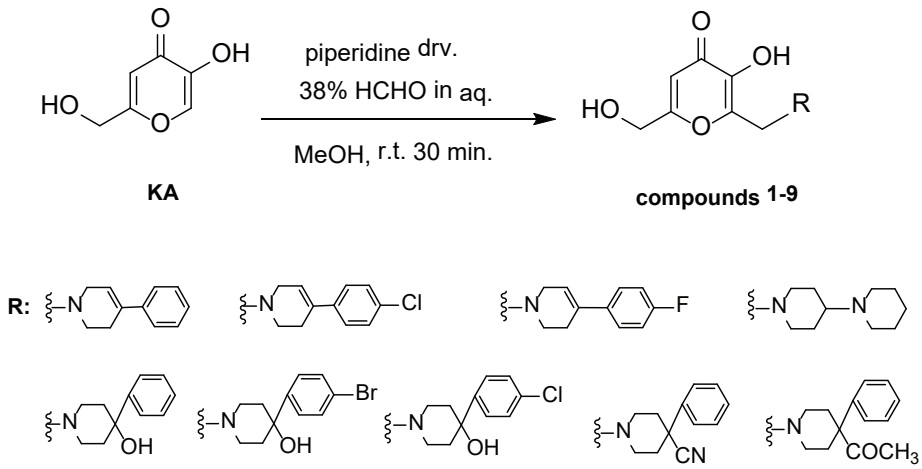


Figure 2. General synthetic route of KA–based Mannich base derivatives.

All target compounds were synthesized rapidly and in high yields under mild, room-temperature conditions. The spectral and physicochemical data supported the proposed molecular structures.

The cytotoxic effects of the Mannich bases synthesized within the scope of this study were evaluated on seven cancer cell lines — SK-MEL (human melanoma), MCF-7 and MDA-MB-231 (human breast carcinoma), A549 (human lung carcinoma), HeLa (human cervical adenocarcinoma), Hep3B (human hepatocellular carcinoma), HT-29 (human colon adenocarcinoma), and Neuro2A (mouse neuroblastoma) — and one normal cell line, Vero (African green monkey kidney epithelial cells). Cytotoxicity was determined using the MTT assay after 72 hours of incubation.

Doxorubicin (10 µg/mL), a clinically used chemotherapeutic agent, served as the positive control, while cells treated with 0.1% DMSO were used as the negative control. All compounds were tested at four concentrations — 12.5, 6.25, 3.125, and 1.56 µg/mL — to assess dose-dependent responses.

When the bioactivity results were evaluated on a cell line-specific basis, the Hep3B human hepatocellular carcinoma cell line proved to be the least responsive to the tested compounds, followed by the HeLa human cervical adenocarcinoma cell line. Intriguingly, the cytotoxic profiles of the compounds showed a similar trend against SK-MEL and Neuro2A cells, a parallelism that was not observed for the reference drug, doxorubicin.

In anticancer drug discovery, an ideal candidate should exert potent cytotoxic effects against tumor cells while exhibiting minimal toxicity toward healthy cells. Therefore, assessing the effects of the synthesized compounds on the Vero normal cell line is of particular importance. From this perspective, none of the synthesized compounds caused greater cytotoxicity to normal cells than doxorubicin at the lowest tested dose. These findings suggest that the newly synthesized compounds may represent promising and relatively safe anticancer candidates with selective activity toward cancer cells.

Considering all results together, Compounds 9 and 4 emerged as the most promising lead candidates among the synthesized KA-based Mannich derivatives. Although Compound 9 showed lower cell viability values against the MCF-7, SK-MEL, and Neuro2A cell lines at the lowest tested concentration, this effect was dose-independent. Rather than exhibiting the anticipated decrease in cell viability with increasing concentration, Compound 9 displayed an atypical, concentration-independent cytotoxic behavior.

In contrast, Compound 4 demonstrated consistent dose-dependent activity across a broader range of concentrations and achieved lower IC_{50} values (Figure 3 and Table 1.). Given its predictable and favorable dose-activity profile, Compound 4 was selected for further mechanistic evaluation to better elucidate its apoptosis-inducing potential. These investigations include the Annexin V–PI apoptosis assay and cell cycle analysis.

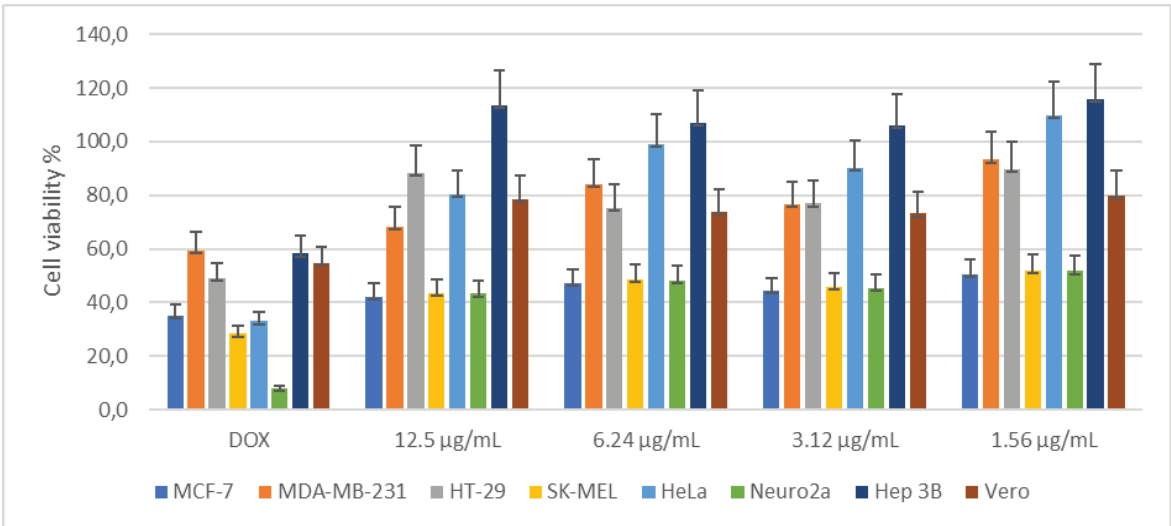
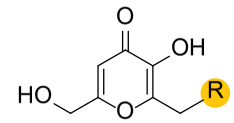
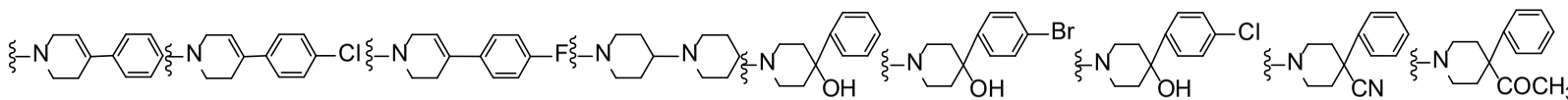


Figure 3. Cell viability results for Compound 4 at all tested doses

Table 1. The IC_{50} (μM) values of the compounds' cytotoxicity against the cell lines tested*



R



Cell line	Comp. 1	Comp. 2[a]	Comp. 3[b]	Comp. 4[b]	Comp. 5[a]	Comp. 6[a]	Comp. 7[a]	Comp. 8[a]	Comp. 9[a]	DOX
MCF7	140.93 ± 13.05	132.58 ± 12.31	90.12 ± 8.03	**5.02 ± 0.09**	124.06 ± 11.41	86.41 ± 7.85	100.60 ± 9.16	114.17 ± 10.46	35.06 ± 0.39	4.05 ± 0.18
MDA-MB-231	147.60 ± 11.27	129.50 ± 9.86	135.00 ± 10.26	132.66 ± 10.05	129.86 ± 9.84	112.76 ± 8.60	119.79 ± 9.08	98.69 ± 7.26	88.16 ± 6.44	3.68 ± 1.66
HT-29	147.50 ± 15.35	74.18 ± 7.30	121.63 ± 12.52	115.97 ± 11.88	133.48 ± 13.85	98.21 ± 10.12	125.99 ± 13.09	44.07 ± 3.94	126.61 ± 13.15	3.86 ± 0.74
SK-MEL	140.93 ± 8.36	132.58 ± 7.91	90.12 ± 5.01	**5.92 ± 0.12**	124.06 ± 7.27	86.41 ± 4.97	100.60 ± 5.82	114.17 ± 6.64	71.91 ± 3.89	4.78 ± 0.18
HeLa	147.60 ± 9.51	129.50 ± 8.31	135.00 ± 8.66	132.66 ± 8.47	129.86 ± 8.30	112.76 ± 7.26	119.79 ± 7.65	98.69 ± 6.08	88.16 ± 5.37	-
Neuro2a	140.93 ± 7.24	132.58 ± 6.87	90.12 ± 4.32	**5.80 ± 0.06**	124.06 ± 6.31	86.41 ± 4.29	100.60 ± 5.03	114.17 ± 5.76	71.91 ± 3.30	-
Hep 3B	137.20 ± 6.57	89.48 ± 4.02	138.68 ± 6.73	69.82 ± 2.85	126.48 ± 6.04	115.37 ± 5.61	86.85 ± 3.94	77.15 ± 3.32	91.13 ± 4.14	-
Vero	137.20 ± 14.20	89.48 ± 9.00	138.68 ± 14.43	69.85 ± 6.73	126.48 ± 13.07	115.37 ± 12.02	86.82 ± 8.75	77.15 ± 7.61	91.13 ± 9.21	3.81 ± 1.29

*Concentration range studied = 12.5–1.5 μg/mL (1/2 serial dilution, 4 concentrations for each compound) a: (Aytemir & Çalış, 2010). b: (Karakaya et al., 2022)

When all synthesized compounds were compared for their cytotoxic effects against tumor cell lines, compound 4 exhibited the highest potency and the broadest spectrum of activity. Its antitumor efficacy was approximately 7.7–28.8 times greater than that of the other compounds in the series. The calculated therapeutic index (TI) values of Compound 4 were 13.90 μg/mL for MCF-7 (human breast adenocarcinoma), 11.79 μg/mL for SK-MEL (human malignant melanoma), and 12.04 μg/mL for Neuro2A (mouse neuroblastoma) cells, indicating a favorable selectivity profile.

The IC_{50} values obtained for compound 5 ranged between 124.06 and 133.48 μM, while those for compound 3 were in the range of 90.12-138.68 μM. Compound 7 exhibited IC_{50} values between 86.82 and 125.99 μM across the same cell lines. Compound 9 displayed IC_{50} values ranging from 35.06 to 126.61 μM, with the lowest value recorded for the MCF-7 cell line, suggesting that this cell line was the most sensitive to its effects.

For compound 4, IC_{50} values varied between 5.02 and 132.66 μM, confirming it as the most potent cytotoxic agent among all synthesized derivatives. The most responsive cell lines to this compound were MCF-7, Neuro2A, and SK-MEL, with IC_{50} values of 5.02, 5.80, and 5.92 μM, respectively, whereas the corresponding IC_{50} value for the normal Vero cell line was 69.85 μM.

When all compounds and cell lines were collectively evaluated, the MCF-7 cell line emerged as the most sensitive, followed by Neuro2A and SK-MEL, while Hep3B was the least affected. In contrast, all compounds showed relatively low cytotoxicity toward the normal Vero cells, supporting their potential safety as anticancer agents.

Evaluation of the IC_{50} values reveals significant insights into the structure-activity relationships (SAR) of the synthesized Mannich bases. The most striking finding is the superior potency of Compound 4, which contains a bis-piperidine skeleton, compared to the phenyl-substituted derivatives (Compounds 1–3 and 5–9). While the phenyl-bearing compounds generally exhibited IC_{50} values above 35 μM against MCF-7 cells, the replacement of the aromatic phenyl ring with a saturated, pharmacologically flexible piperidine moiety in Compound 4 drastically improved the cytotoxicity (IC_{50}: 5.02 μM). This suggests that the absence of the rigid aromatic ring and the presence of a secondary piperidine group may enhance cellular uptake or binding affinity to the target protein.

A key observation lies in the electronic nature of the substituents at the 4-position of the piperidine ring. Compound 5, which bears a hydroxyl group (typically considered an electron-donating and polar group), exhibited relatively low cytotoxicity (IC_{50} > 120 μM). Interestingly, replacing this group with electron-withdrawing moieties altered the biological profile. The introduction of an acetyl group (-$COCH_3$) in Compound 9 significantly improved the cytotoxic potency (IC_{50}: 35.06 μM against MCF-7), suggesting that electron-withdrawing substituents at this position contribute positively to the anticancer activity compared to electron-donating ones. However, the strongest activity was achieved not by these substitutions, but by the unique bis-piperidine skeleton of Compound 4. This implies that while electronic properties are important, the conformational flexibility and specific steric features provided by the piperidinopiperidine moiety may be the primary drivers of the superior potency observed in this series.

Determination of the apoptotic effects of compound 4

Since Compound 4 exhibited the most potent cytotoxic activity among the synthesized derivatives, we aimed to investigate its mode of cell death to determine if the observed cytotoxicity was mediated through apoptosis, a preferred mechanism for anticancer agents, rather than non-specific necrosis. To investigate the potential cell death mechanism of Compound 4, MCF-7 cells were stained with Annexin V-FITC/PI following 24 and 48 hours of treatment. As shown in

Figures 4 and 5, treatment with Compound 4 resulted in a slight increase in the apoptotic cell population compared to the negative control. Specifically, at the 48th hour, a moderate elevation in early apoptotic cells was observed. However, unlike the positive control doxorubicin, Compound 4 did not exhibit a sharp, dose-dependent increase in the apoptotic population. The overlapping error bars and the modest increase in Annexin V-positive cells indicate that the apoptotic effect is limited under the tested conditions. These findings suggest that while Compound 4 possesses strong cytotoxic potential, its primary mechanism of cell death may involve pathways other than, or in addition to, classical apoptosis. Therefore, these flow cytometry results should be interpreted as preliminary evidence of a potential apoptotic process, which warrants further validation through extensive molecular studies, such as caspase activation assays or gene expression analysis.

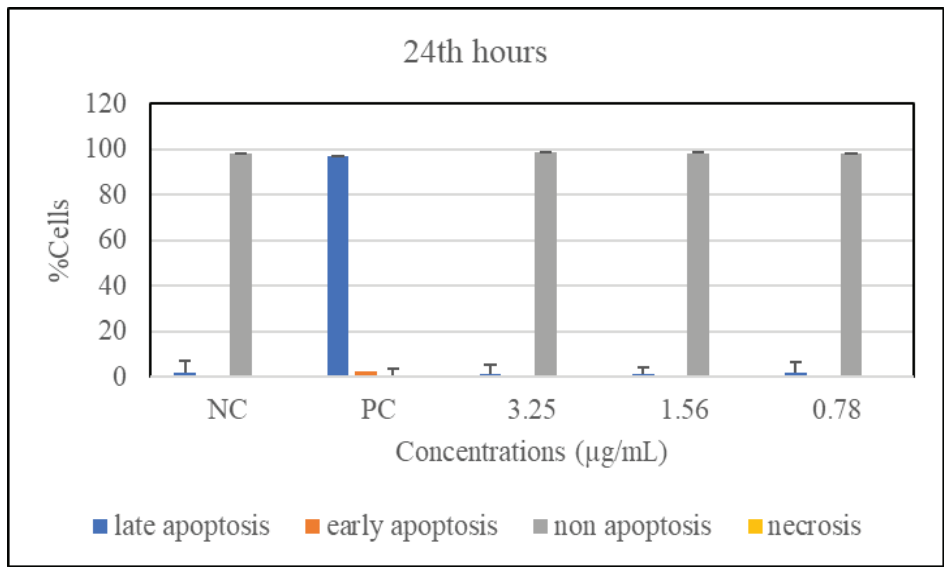


Figure 4. Determination of Apoptotic Effects of Compound 4. The results of 24 hours of treatment with 3.125, 1.56, and 0.78 µg/ml compound 4, the negative control (NC), and the positive control (PC) doxorubicin.

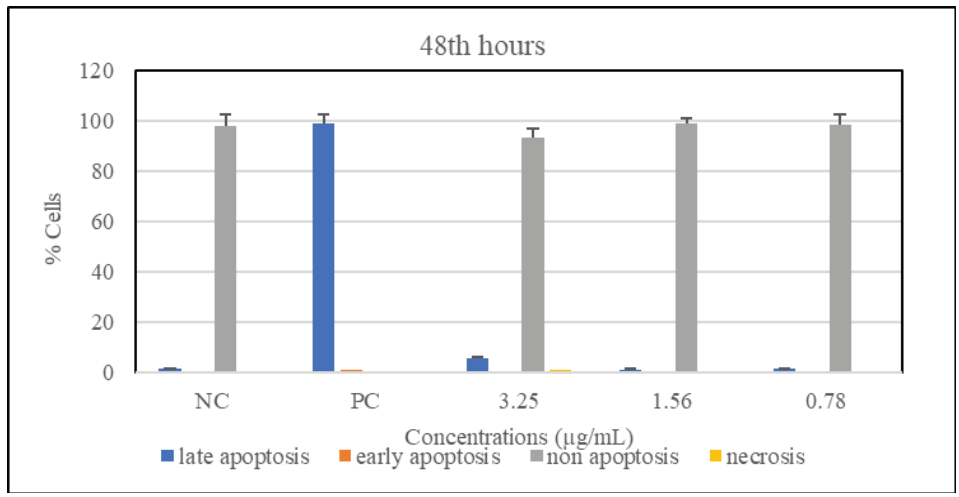


Figure 5. Determination of Apoptotic Effects of Compound 4. The results of 48 hours of treatment with 3.125, 1.56, and 0.78 µg/ml compound 4, the negative control (NC), and the positive control (PC) doxorubicin.

CONCLUSION

A series of KA-Mannich base derivatives was evaluated for their cytotoxic effects on various cancer cell lines using doxorubicin as a reference drug. Compound 4, which contains a piperidinopiperidine moiety, exhibited the strongest and broadest cytotoxic activity, particularly against MCF-7, Neuro2A, and SK-MEL cell lines, with IC_{50} values of 5.02, 5.80, and 5.92 μM, respectively. The compound showed low toxicity toward healthy Vero cells, indicating favorable selectivity. SAR analysis revealed that electron-withdrawing substituents, such as the cyano and acetyl groups, significantly enhance cytotoxic potency. Crucially, the absence of an aromatic ring, a feature unique to Compound 4, further optimized this activity. Subsequent flow cytometric analyses indicated that Compound 4 triggers a moderate and time-dependent apoptotic response in MCF-7 cells, rather than a strong dose-dependent effect.

Collectively, these results underscore Compound 4 as a promising lead molecule. Future studies will focus on clarifying its complete molecular mechanism and verifying the mode of cell death using more sensitive quantitative techniques such as RT-PCR and Western blot analyses.

ACKNOWLEDGEMENTS

This study was supported by İzmir Kâtip Çelebi University Scientific Research Projects Coordination Unit (Project number: 2021-GAP-ECZF-0058).

CONFLICT OF INTEREST

The authors declare that there is no conflict of interest.

AUTHOR CONTRIBUTION STATEMENT

Concept – G.K., C.S.G., M.D.A.; Design – G.K., C.S.G., M.D.A.; Supervision – M.D.A.; Resources – G.K., C.S.G., M.D.A.; Materials G.K., C.S.G., M.D.A.; Data Collection and/or Processing – G.K., C.S.G.; Analysis and/or Interpretation – G.K., C.S.G., M.D.A.; Literature Search – G.K.; Writing –G.K., C.S.G., M.D.A.; Critical Reviews – G.K., C.S.G., M.D.A.

REFERENCES

Aytemir, M. D., & Çalış, Ü. (2010). Anticonvulsant and Neurotoxicity Evaluation of Some Novel Kojic Acids and Allomaltol Derivatives. *Archiv Der Pharmazie*, *343*(3), 173–181. https://doi.org/10.1002/ardp.200900236

Bogurcu, N., Sevimli-Gur, C., Ozmen, B., Bedir, E., & Korkmaz, K. S. (2011). ALCAPs induce mitochondrial apoptosis and activate DNA damage response by generating ROS and inhibiting topoisomerase I enzyme activity in K562 leukemia cell line. *Biochemical and Biophysical Research Communications*, *409*(4), 738–744. https://doi.org/10.1016/j.bbrc.2011.05.078

Brtko, J. (2022). Biological functions of kojic acid and its derivatives in medicine, cosmetics, and food industry: Insights into health aspects. *Archiv Der Pharmazie*, *355*(10), 2200215. https://doi.org/10.1002/ardp.202200215

Burnett, C. L., Bergfeld, W. F., Belsito, D. V., Hill, R. A., Klaassen, C. D., Liebler, D. C., … Andersen, F. A. (2010). Final Report of the Safety Assessment of Kojic Acid as Used in Cosmetics. *International Journal of Toxicology*, *29*(6_suppl), 244S-273S. https://doi.org/10.1177/1091581810385956

El-Sayed Ebead, E., Aboelnaga, A., Nassar, E., Naguib, M. M., & Ismail, M. F. (2023). Ultrasonic-induced synthesis of novel diverse arylidenes *via* Knoevenagel condensation reaction. Antitumor, QSAR, docking and DFT assessment. *RSC Advances*, *13*(42), 29749–29767. https://doi.org/10.1039/D3RA05799B

Emami, S., Ahmadi, R., Ahadi, H., & Ashooriha, M. (2022). Diverse therapeutic potential of 3-hydroxy-4-pyranones and related compounds as kojic acid analogs. *Medicinal Chemistry Research*, *31*(11), 1842–1861. https://doi.org/10.1007/s00044-022-02954-3

Ercan, A., Oncul, S., Karakaya, G., & Aytemir, M. (2020). An allomaltol derivative triggers distinct death pathways in luminal a and triple-negative breast cancer subtypes. *Bioorganic Chemistry*, *105*, 104403. https://doi.org/10.1016/j.bioorg.2020.104403

Filho, A. M., Laversanne, M., Ferlay, J., Colombet, M., Piñeros, M., Znaor, A., … Bray, F. (2025). The GLOBOCAN 2022 cancer estimates: Data sources, methods, and a snapshot of the cancer burden worldwide. *International Journal of Cancer*, *156*(7), 1336–1346. https://doi.org/10.1002/ijc.35278

He, M., Fan, M., Peng, Z., & Wang, G. (2021). An overview of hydroxypyranone and hydroxypyridinone as privileged scaffolds for novel drug discovery. *European Journal of Medicinal Chemistry*, *221*, 113546. https://doi.org/10.1016/j.ejmech.2021.113546

Karakaya, G., Ercan, A., Öncül, S., & Aytemir, M. D. (2019a). Kojic acid derivatives as potential anticancer agents: Synthesis and cytotoxic evaluation on A375 human malignant melanoma cells. *Journal of Research in Pharmacy*, *23*(4), 596–607. https://doi.org/10.12991/jrp.2019.167

Karakaya, G., Ercan, A., Oncul, S., & Aytemir, M. D. (2019b). Synthesis and Cytotoxic Evaluation of Kojic Acid Derivatives with Inhibitory Activity on Melanogenesis in Human Melanoma Cells. *Anti-Cancer Agents in Medicinal Chemistry*, *18*(15), 2137–2148. https://doi.org/10.2174/1871520618666180402141714

Karakaya, G., Türe, A., Özdemir, A., Özçelik, B., & Aytemir, M. (2022). Synthesis and molecular modeling of some novel hydroxypyrone derivatives as antidermatophytic agents. *Journal of Heterocyclic Chemistry*, *59*(10), 1801–1812. https://doi.org/10.1002/jhet.4520

Koirala, M., & DiPaola, M. (2024). Overcoming Cancer Resistance: Strategies and Modalities for Effective Treatment. *Biomedicines*, *12*(8), 1801. https://doi.org/10.3390/biomedicines12081801

Mohamad, R., Mohamed, M. S., Suhaili, N., Salleh, M. M., & Ariff, A. B. (2010). Kojic acid: Applications and development of fermentation process for production. *Biotechnology and Molecular Biology Reviews*, *5*(2), 24–37.

Mutahir, S., Khan, M. A., Mushtaq, M., Deng, H., Naglah, A. M., Almehizia, A. A., … Refat, M. S. (2023). Investigations of Electronic, Structural, and In Silico Anticancer Potential of Persuasive Phytoestrogenic Isoflavene-Based Mannich Bases. *Molecules*, *28*(15), 5911. https://doi.org/10.3390/molecules28155911

Phasha, V., Senabe, J., Ndzotoyi, P., Okole, B., Fouche, G., & Chuturgoon, A. (2022). Review on the use of kojic acid—A skin-lightening ingredient. *Cosmetics*, *9*(3), 64.

Roman, G. (2015). Mannich bases in medicinal chemistry and drug design. *European Journal of Medicinal Chemistry*, *89*, 743–816. https://doi.org/10.1016/j.ejmech.2014.10.076

Sevimli-Gur, C., Akgun, I. H., Deliloglu-Gurhan, I., Korkmaz, K. S., & Bedir, E. (2010). Cytotoxic Naphthoquinones from *Alkanna cappadocica*. *Journal of Natural Products*, *73*(5), 860–864. https://doi.org/10.1021/np900778j

Sevimli-Gür, C., Onbaşılar, İ., Atilla, P., Genç, R., Çakar, N., Deliloğlu-Gürhan, İ., & Bedir, E. (2011). In vitro growth stimulatory and in vivo wound healing studies on cycloartane-type saponins of Astragalus genus. *Journal of Ethnopharmacology*, *134*(3), 844–850. https://doi.org/10.1016/j.jep.2011.01.030

Sevimli-Gur, C., Cetin, B., Akay, S., Gulce-Iz, S., & Yesil-Celiktas, O. (2013). Extracts from Black Carrot Tissue Culture as Potent Anticancer Agents. *Plant Foods for Human Nutrition*, *68*(3), 293–298. https://doi.org/10.1007/s11130-013-0371-z

Üçkan, P. N., Karakaya, G., Düzleyen, B., Sevimli Gür, C., & Aytemir, M. (2023). Synthesis and Investigation of Cytotoxicity in Different Cell Lines of Novel Hydroxypyranones. *Hacettepe University Journal of the Faculty of Pharmacy*. https://doi.org/10.52794/hujpharm.1374319

Zilles, J. C., Dos Santos, F. L., Kulkamp-Guerreiro, I. C., & Contri, R. V. (2022). Biological activities and safety data of kojic acid and its derivatives: A review. *Experimental Dermatology*, *31*(10), 1500–1521. https://doi.org/10.1111/exd.14662

FABAD J. Pharm. Sci., 51, 1, 175-188, 2026
Doi: 10.55262/fabadeczacilik.1777903
RESEARCH ARTICLE

Dornase Alfa as a Potential Treatment Option for SARS-CoV-2: *In Vitro* Insights

Derya DİLEK KANÇAĞI[*°], Cihan TAŞTAN[**], Kevser Buse KARADENİZ[***], Selen ABANUZ[****], Didem ÇAKIRSOY[*****], Yaren BÜYÜKÇOLAK[******], Sezer AKYÖNEY[*******], Gözde SIR KARAKUŞ[********], Bulut YURTSEVER[*********], Koray YALÇIN[**********], İsmail Tuncer DEĞİM[**********], Ercüment OVALI[***********]

Dornase Alfa as a Potential Treatment Option for SARS-CoV-2: In Vitro Insights

SUMMARY

The potential use of dornase alfa (DA) in severe acute respiratory syndrome coronavirus 2 (SARS-CoV-2) infection has been widely discussed, yet its mechanisms remain insufficiently characterized. Here, we investigated whether DA modulates SARS-CoV-2 through multiple in vitro readouts, including viral infectivity, viral RNA integrity, spike-mediated entry, T-helper cytokine polarization, and neutrophil extracellular trap (NET) formation. DA at 30 U reduced viral infectivity ($p < 0.05$). Quantum dot–based quantitative flow cytometry showed that DA (10 U and 30 U) decreased viral internalization, consistent with spike-binding–mediated entry inhibition ($p < 0.05$). qRT-PCR and sequencing suggested altered integrity/fragmentation of naked viral RNA after exposure to 30 U DA ($p < 0.05$). Cytokine bead array analyses of viral peptide–stimulated lymphocytes indicated a shift toward a Th2-skewed response in the presence of DA ($p < 0.05$). In addition, fluorescence microscopy demonstrated that 30 U DA suppressed phorbol myristate acetate–induced NETosis in polymorphonuclear leukocytes. Overall, these findings provide preliminary, hypothesis-generating evidence that DA may modulate SARS-CoV-2–related responses via multiple mechanisms. Larger, adequately powered studies are needed to validate these findings. However, clinical efficacy and any potential prophylactic role require confirmation in appropriately designed in vivo and patient-based studies.

Keywords: *Coronavirus disease 2019, severe acute respiratory syndrome coronavirus 2, dornase alfa, neutrophil extracellular traps.*

Dornaz Alfa'nın SARS-CoV-2 İçin Potansiyel Bir Tedavi Seçeneği Olarak Kullanımı: İn Vitro Bulgular

ÖZ

Dornaz alfa'nın (DA) şiddetli akut solunum sendromu koronavirüs 2 (SARS-CoV-2) enfeksiyonunda potansiyel kullanımı yaygın biçimde tartışılmakla birlikte, etki mekanizmaları yeterince aydınlatılmamıştır. Bu çalışmada DA'nın, viral enfektivite, viral RNA bütünlüğü, spike aracılı giriş, T-helper sitokin polarizasyonu ve nötrofil ekstrasellüler tuzak (NET) oluşumu gibi çoklu in vitro çıktılar üzerinden SARS-CoV-2'yi modüle edip etmediği araştırılmıştır. DA'nın 30 U dozunda viral enfektiviteyi azalttığı gösterilmiştir ($p < 0,05$). Kuantum nokta (quantum dot) tabanlı kantitatif akım sitometrisi, DA'nın (10 U ve 30 U) viral internalizasyonu azalttığını ve bunun spike proteinine bağlanma aracılı giriş inhibisyonu ile uyumlu olduğunu göstermiştir ($p < 0,05$). qRT-PCR ve sekanslama analizleri, 30 U DA maruziyeti sonrası "çıplak" viral RNA'nın bütünlüğünde/parçalanma düzeyinde olası bir değişime işaret etmiştir ($p < 0,05$). Viral peptitle uyarılan lenfositlerde yapılan sitokin boncuk dizisi (CBA) analizleri, DA varlığında Th2 ağırlıklı bir yanıt yönelimi olduğunu göstermiştir ($p < 0,05$). Ayrıca floresan mikroskopi, polimorfonükleer lökositlerde forbol miristat asetat ile indüklenen NETozis üzerinde 30 U DA'nın baskılayıcı etkisini ortaya koymuştur. Genel olarak bu bulgular, DA'nın SARS-CoV-2 ile ilişkili yanıtları çoklu mekanizmalar üzerinden modüle edebileceğine dair ön ve hipotez oluşturucu kanıtlar sunmaktadır. Bu bulguların doğrulanması için daha büyük örneklemli ve yeterli istatistiksel güce sahip çalışmalara ihtiyaç vardır. Bununla birlikte klinik etkinlik ve olası profilaktik rolün ortaya konması, uygun şekilde tasarlanmış in vivo ve hasta temelli çalışmalarla doğrulanmayı gerektirmektedir.

Anahtar Kelimeler: *Koronavirüs hastalığı 2019, şiddetli akut solunum yolu sendromu koronavirüs 2, dornaz alfa, nötrofil ekstraselüler tuzakları.*

Recieved: 4.09.2025
Revised: 22.12.2025
Accepted: 8.02.2026

[*] ORCID: 0000-0003-4725-3200, Department of Biochemistry, Faculty of Pharmacy, Fenerbahçe University, Istanbul, Turkey; Acibadem Labcell Cellular Therapy Laboratory, Istanbul, Turkey
[**] ORCID: 0000-0002-4173-6634, Acibadem Labcell Cellular Therapy Laboratory, Istanbul, Turkey; Transgenic Cell Technologies and Epigenetic Application and Research Center (TRGENMER), Üsküdar University, Istanbul, Turkey; Molecular Biology and Genetics Department, Faculty of Engineering and Natural Science, Üsküdar University, Istanbul, Turkey
[***] ORCID: 0000-0001-5370-6865, Institute of Health and Science, Department of Medical Biotechnology, Acibadem Mehmet Ali Aydinlar University, Istanbul, Turkey
[****] ORCID: 0000-0002-6136-5033, Institute of Health and Science, Department of Medical Biochemistry, Acibadem Mehmet Ali Aydinlar University, Istanbul, Turkey
[*****] ORCID: 0000-0002-1293-9520, Acibadem Labcell Cellular Therapy Laboratory, Istanbul, Turkey; Institute of Health and Science, Department of Medical Biotechnology, Acibadem Mehmet Ali Aydinlar University, Istanbul, Turkey
[******] ORCID: 0000-0002-5988-5312, Acibadem Labcell Cellular Therapy Laboratory, Istanbul, Turkey; Institute of Health and Science, Department of Medical Biotechnology, Acibadem Mehmet Ali Aydinlar University, Istanbul, Turkey
[*******] ORCID: 0000-0003-2514-4142, Institute of Health and Science, Department of Biostatistics and Bioinformatics, Acibadem Mehmet Ali Aydinlar University, Istanbul, Turkey
[********] ORCID: 0000-0002-0682-5869, Acibadem Labcell Cellular Therapy Laboratory, Istanbul, Turkey
[*********] ORCID: 0000-0002-9269-8383, Acibadem Labcell Cellular Therapy Laboratory, Istanbul, Turkey; Institute of Health and Science, Department of Medical Biochemistry, Acibadem Mehmet Ali Aydinlar University, Istanbul, Turkey
[**********] ORCID: 0000-0003-3454-9870, Acibadem Labcell Cellular Therapy Laboratory, Istanbul, Turkey; Institute of Health and Science, Department of Medical Biotechnology, Acibadem Mehmet Ali Aydinlar University, Istanbul, Turkey; Acıbadem Altunizade Hospital, Department of Pediatric Hematology and Oncology, Istanbul, Turkey
[***********] ORCID: 0000-0002-9329-4698, Pharmaceutical Technology Department, Faculty of Pharmacy, Biruni University, Istanbul, Turkey
[************] ORCID: 0000-0002-4782-5355, Acibadem Labcell Cellular Therapy Laboratory, Istanbul, Turkey

[°] Corresponding Author; Derya DİLEK KANÇAĞI
E-mail: derya.kancagi@gmail.com

INTRODUCTION

The SARS-CoV-2 virus, which was first identified in Wuhan, China, in December 2019, has since spread worldwide and tragically resulted in the loss of over 5 million lives (Msemburi et al., 2023). This virus causes Coronavirus disease 2019 (COVID-19) disease, primarily affecting the human respiratory system and leading to severe pneumonia, coagulopathy, hyperinflammation, and acute respiratory distress syndrome (ARDS). The onset of SARS-CoV-2 infection involves the spike protein-mediated infection of respiratory cells and subsequent cytokine release reactions that contribute to ARDS development (Matthay et al., 2019). In this context, neutrophil activation has been implicated in the disease pathology, particularly in the development of ARDS (Barnes et al., 2020).

Neutrophils, apart from their role in engulfing microbes and releasing antimicrobial substances, are involved in the formation of neutrophil extracellular traps (NETs), reticulated extensions containing granular proteins and DNA strands (Brinkmann et al., 2004; Schönrich Raftery, 2016). While NETs play a crucial role in the immune response, they can also contribute to the pathogenesis of various diseases, especially viral infections, causing secondary damage (Schönrich Raftery, 2016).

Dornase alfa, a recombinantly produced enzyme known as deoxyribonuclease I (rhDNAase I), specifically breaks down DNA and has been successfully used to reduce lung fluid viscosity in patients with cystic fibrosis (Fitzgerald et al., 2005). Its use in combination with standard therapies has been shown to promote pulmonary function recovery in cystic fibrosis treatment (Yang Montgomery, 2021). Remarkably, dornase alfa has also demonstrated potential in treating ARDS (Morris Mullan, 2004). COVID-19 caused by SARS-CoV-2 may trigger a cytokine-storm–like response, leading to sepsis and severe, potentially fatal ARDS. Cystic fibrosis patients also show cytokine imbalance and hyperinflammatory profiles that resemble aspects of the COVID-19 disease process. This mechanistic overlap provides a rationale for translating evidence from cystic fibrosis/ARDS into SARS-CoV-2–related settings (Peckham et al., 2020). Notably, some clinical studies have observed a lower risk of severe disease in cystic fibrosis patients with SARS-CoV-2 infection, possibly attributed to the use of dornase alfa (Colombo et al., 2022). This observation has sparked initiatives exploring the use of dornase alfa in COVID-19 treatment, such as COVI-Dornase and COVASE (Desilles et al., 2020). Additionally, DNase1L3 has been considered for its potential in reducing vascular occlusion due to COVID-19 (Jiménez-Alcázar et al., 2017). Previous clinical studies have reported the promising effects of nebulized dornase alfa in reducing inflammation and oxygen requirements in hospitalized patients with COVID-19 pneumonia (Porter et al., 2024).

Similarly, in our preliminary report (Okur et al., 2020), we presented early invitro and limited invivo evidence (Vero/MDBK experiments and n=3 cases) regarding the potential effects of dornase alfa (DA) in SARSCoV2 infection.

Because DA is a DNase that targets extracellular DNA, its activity does not directly explain an effect on an RNA virus such as SARS-CoV-2. Accordingly, whether DA acts indirectly by altering NET/extracellular DNA–rich airway microenvironments, inflammatory responses, or virus–host interactions remains insufficiently defined. Building on this research line, the present study aimed to test mechanistic hypotheses by evaluating whether DA modulates SARS-CoV-2 in vitro through spike-associated viral entry/internalization, viral RNA integrity and infectivity, NETosis, and Th1/Th2 polarization.

MATERIALS AND METHODS

SARS-CoV-2 isolation

The study included nasopharyngeal and oropharyngeal cavity samples from four volunteers who tested positive for SARS-CoV-2 via RT-PCR in Acıbadem Healthcare Group hospitals. The isolation of SARS-

CoV-2 RNA from the collected patient samples followed previously described procedures (Sir Karakus et al., 2021; Taştan et al., 2020). In brief, the Vero cell line (CCL-81, ATCC, USA) was utilized for virus isolation and propagation. The virus culture initiation occurred in a 96-well plate and was subsequently scaled up in volume in a viral medium composed of high-glucose DMEM (Thermo Fisher Scientific Inc., USA), 2% fetal bovine serum (Thermo Fisher Scientific Inc., USA), and 1% penicillin-streptomycin-amphotericin (PSA) solution (Pan-Biotech GmbH, Aidenbach, Germany). The progression of virus replication and isolation was monitored by observing cytopathic effects during the propagation process. The supernatants obtained at the end of the production were pooled and concentrated 10–15 times (Sir Karakus et al., 2021). Unless otherwise stated, experiments were repeated in at least three independent biological replicates (≥3 separate experiments performed on different days/independent preparations). Within each independent experiment, conditions were run in technical triplicate (three replicate wells/measurements). For analysis and plotting, technical triplicates were averaged within each experiment, and summary statistics [mean ± standard deviation (SD)] were calculated across independent experiments.

Viral inactivation assay

Vero cells were seeded at 10,000 cells/well in flat-bottom 96-well plates with complete DMEM (10% FBS; 1% penicillin/streptomycin/amphotericin B) and incubated overnight at 37°C. SARS-CoV-2 (100× $TCID_{50}$; Taştan et al., 2020) was pre-incubated 1 h at RT with dornase alfa, then added to cells. Final concentrations were 3, 10, and 30 U/mL (i.e., 3, 10, 30 µg/mL given 1 mg/mL = 1000 U/mL). These levels were chosen a priori from published rhDNase I applications—where short ex vivo incubations at approximately 10 U have been reported—to span a sub-maximal activity range suitable for Vero cells while enabling dose–response assessment (Fisher et al., 2021). After 96 h, MTT (3-(4,5-dimethylthiazol-2-yl)-2,5-diphenyltetrazolium bromide) was performed per manufacturer; absorbance was read at 450 nm (FLUOstar Omega). Plate included mock, virus-only, and DA-only controls. Data were background-subtracted, normalized to mock, and reported as mean ± SD; % viability and % inactivation were calculated relative to virus-only.

QDot's production and characterization

Quantum Dots (QDots) are minute crystalline structures in the nanoscale, functioning as semiconductors with just a few atomic sizes, typically ranging between 2 and 10 nm, derived from compounds found within the periodic table's II-VI or III-V elements (Ozkan, 2004). Due to their small dimensions, both metallic and non-metallic QDots exhibit quantum effects, emitting narrow-band light in the ultraviolet (UV) region and displaying strong fluorescence and remarkable photostability (Kuang et al., 2011; Xu Chen, 2012). This makes QDots suitable for several applications (Maysinger et al., 2007; Singh Lillard, 2009; Xu Chen, 2012).

Production

QDots were synthesized using a microwave-assisted method. In brief, 0.5 g of p-phenylenediamine (Sigma Aldrich Chemie GmbH, Eschenstraße 5, 82024 Taufkirchen, Germany) served as a carbon source, and 1g of formamide (Sigma Aldrich Chemie GmbH, Eschenstraße 5, 82024 Taufkirchen, Germany) acted as a hetero atom. This mixture, combined with 15 ml of distilled water, was thoroughly mixed and transferred to the microwave reactor (Microwave 300, Anton Paar, St. Albans, Hertfordshire, AL4 0LA, UK). After the reaction, N-doped QDots were obtained, confirmed by UV light (365 nm), which revealed a red emission. The mixture was gently stirred overnight at room temperature. A final confirmation under UV light (365 nm) was performed before dialyzing the QDots.

Characterization

Analysis of physical appearances, particle size, and zeta potential of QDots has been conducted (Supplementary Figure 1 and Supplementary Table 1.). The determination of particle size and distribution was accomplished using Anton Paar Lite Sizer 500, with a sample size of n = 6 for particle size measurements and n = 12 for zeta potential measurements.

Quantum yield

The optical properties of QDots were assessed using a Spectrofluorometer (Model 229129, Agilent Technologies, 5301 Stevens Creek Blvd., Santa Clara, CA 95051, USA). QDots were excited, and their emitted light was recorded. The experimental procedure was adapted from the literature (Mirtchev et al., 2012). The quantum yield was calculated according to the well-established method outlined in the literature (Camlik et al., 2022).

Spike labeling with qdots assay and analysis of labelled spike protein blockage with dornase alfa

10,000 cells/well were seeded into a flat-bottom 96-well plate with complete DMEM (Wisent, Multicell 319-066-CL; 10% Fetal-Bovine Serum, 1% penicillin/streptomycin). S (spike) PepTivator, a collection of freeze-dried peptides encompassing the dominant sequence regions of the surface glycoprotein (also known as the spike protein or "S") of SARS-CoV-2 (GenBank MN908947.3, Protein QHD43416.1) (Miltenyi Biotech, GmbH, Bergisch Gladbach, Germany; cat# 130-126-700), was incubated with QDots E3 for 1 hour at 37°C a CO_2 incubator. After incubation, 3U, 10U, and 30U dornase alfa were added to the Spike-QDots mixture. Treated Spike-QDots- dornase alfa mixture was added onto Vero cells. After 48-hour incubation at 37°C a CO_2 incubator, spike cultivators were tracked by QDots labeling in APC-A750-A via flow cytometry (Buranda et al., 2011). Flow analysis was performed with the CYTOFLEX (Beckman Coulter, USA). Qdot fluorescence was also visualized macroscopically under UV/405 nm illumination.

q-RT-PCR assay

q-RT-PCR analyses were conducted using two different experimental setups for active virus in BSL-3 conditions. (1) Infected supernatants: RNA was extracted with Direct-zol and analyzed using DiaCarta QuantiVirus on LightCycler 96 (targets ORF1ab/N/E; triplicates; standard curve $R^2 \geq 0.99$, efficiency 90–110%). (2) Naked RNA ± DA: Purified SARS-CoV-2 RNA was incubated with DA (3/10/30 U/mL; [37°C], 30–60 min) vs. RNA-only, RNA+$MgSO_4$. SARS-CoV-2–specific qRT-PCR was performed with the QuantiVirus SARS-CoV-2 Test Kit (DiaCarta) on a Roche LightCycler 96, following the manufacturer's instructions (Targets: ORF1ab, N, and E; kit-specific panels). Each sample was run in technical triplicate; no-template controls (NTC) and positive controls were included on every plate.

Sequencing

Whole-genome sequencing (WGS) was performed on live viral RNA after 100× $TCID_{50}$ SARS-CoV-2 had been pre-incubated for 1 h with dornase alfa (3, 10, or 30 U/mL) or buffer only (no DA). Then the samples were analyzed via whole-genome analysis. The quality controls of the raw data generated by the reading were carried out with the FastQC tool. The raw data obtained were first trimmed to certain lengths using cutadapt (v3.2) and fgbio tools, considering the quality parameters of the 5' and 3' ends and the primers used. It was then aligned against the reference genome (NCBI Reference Sequence: NC_045512.2) using the BWA (v.0.7.12) tool. The GATK v.4 tool was used for alignment corrections in Indel regions, normalization of DNA sequence quality values, and variant extraction. All obtained variants were visually checked with the GenomeBrowse (Golden Helix) tool. Then, the annotation of the variants was completed with the Variant Effect Predictor program.

Cytokine bead array

Peripheral blood mononuclear cells (PBMCs) were isolated from a healthy volunteer using Ficoll-paque plus overlay (GE Healthcare, Chalfont St Giles, UK).

Subsequently, 10,000 PBMCs per well were seeded in a 96-U bottom well plate with complete DMEM (containing 10% Fetal Bovine Serum, 1% penicillin/streptomycin). The cells were treated with a mix of spike (S), nucleocapsid (N), and membrane (M) PepTivator (Miltenyi Biotec, GmbH, Bergisch Gladbach, Germany), with 20 µL added to each well. Following this, they were incubated with 3U and 10U of dornase alfa, along with 420 µg/mL $MgSO_4$, for 72 hours in a humidified 37°C CO_2 incubator. After the incubation period, a Cytometric Bead Assay was conducted using a MACSPLEX Cytokine 10 kit (Miltenyi Biotec, GmbH, Bergisch Gladbach, Germany), following the manufacturer's protocol, on the supernatant from the cell suspension. Flow analysis of the samples was performed using the MACSQUANT Analyzer (Miltenyi Biotec, GmbH, Bergisch Gladbach, Germany) (Sir Karakus et al., 2021; Turan et al., 2021).

Clearance of NET formation by dornase alfa

PBMCs obtained as described previously were seeded on a 24-well plate with $1x10^6$ /well concentration in complete medium (RPMI enriched with 10% Fetal-Bovine Serum, 1% penicillin/streptomycin). As previously described in the literature, the culture was supplemented with 700 nM phorbol myristate acetate (PMA) for NET formation (Hoppenbrouwers et al., 2017). Then, the culture treated with 420 µg/mL $MgSO_4$ and 0, 3U, 10U, and 30U Dornase Alfa was incubated for 24 hours. After incubation, the wells were stained with DAPI (Sigma Aldrich, USA), and NET formation was examined under a fluorescent microscope (ZEISS Axio Vert.A1). PBMCs were assessed under unstimulated and PMA-stimulated conditions. DA + PMA was compared against PMA-only to evaluate changes consistent with NETosis suppression. No DA-only, heat-inactivated DNase, vehicle/buffer-only, or inhibitor controls were performed in this study.

Statistics

Student's t-tests were employed to assess normally distributed data presented on bar graphs, while the Mann-Whitney U test was utilized for comparing two groups of non-normally distributed data. Statistical analyses were conducted using both Graphpad Prism (trial version) and SPSS Statistics software. Each data point corresponds to an independent measurement and represents one of at least 3 separate experiments undertaken in triplicate, with the bar graph illustrating the mean and standard deviation of the mean. A significance threshold of $*p < 0.05$ was applied to all tests, with "ns" indicating non-significance.

RESULTS AND DISCUSSIONS

Role of dornase alfa in the blockade of SARS-CoV-2 infectivity

Cytotoxic effect of dornase alfa on the virus

In the MTT assay, dornase alfa treatment increased Vero cell viability after SARS-CoV-2 exposure. Although 10 U and 30 U showed higher viability than the virus-only control, the difference reached statistical significance only for 30 U ($p = 0.0172$) (Figure 1.).

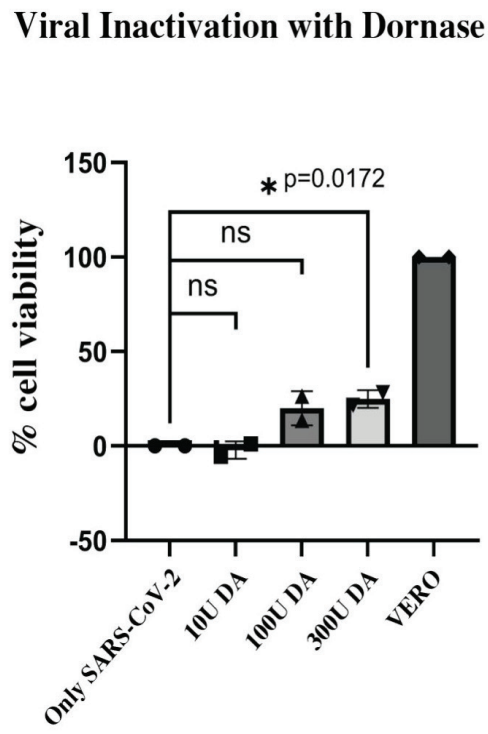


Figure 1. Vero cells were exposed to SARS-CoV-2 (100×$TCID_{50}$) pre-incubated with increasing concentrations of dornase alfa (DA). DA at 30 U significantly improved cell viability compared with the virus-only control. Cell viability (%) was quantified using a colorimetric ELISA-based assay. Each data point represents one independent biological replicate (one of ≥3 separate experiments from pooled virus), with each experiment performed in technical triplicate. Bars show the mean ± SD across independent experiments. Statistical significance was assessed using an unpaired two-tailed Student's t-test or Mann–Whitney U test, as appropriate ($p < 0.05$).

Effect of dornase alfa on SARS-CoV-2 neutralization: spike blocking analysis

Docking analyses suggested favorable binding between dornase alfa and the SARS-CoV-2 spike protein. Guided by this result, we evaluated whether dornase alfa affects spike availability using Qdot-labeled spike protein. Increasing dornase alfa concentrations produced a dose-dependent reduction in Qdot signal, with significant effects at 10 U ($p = 0.0122$) and 30 U ($p < 0.0001$) (Figure 2.).

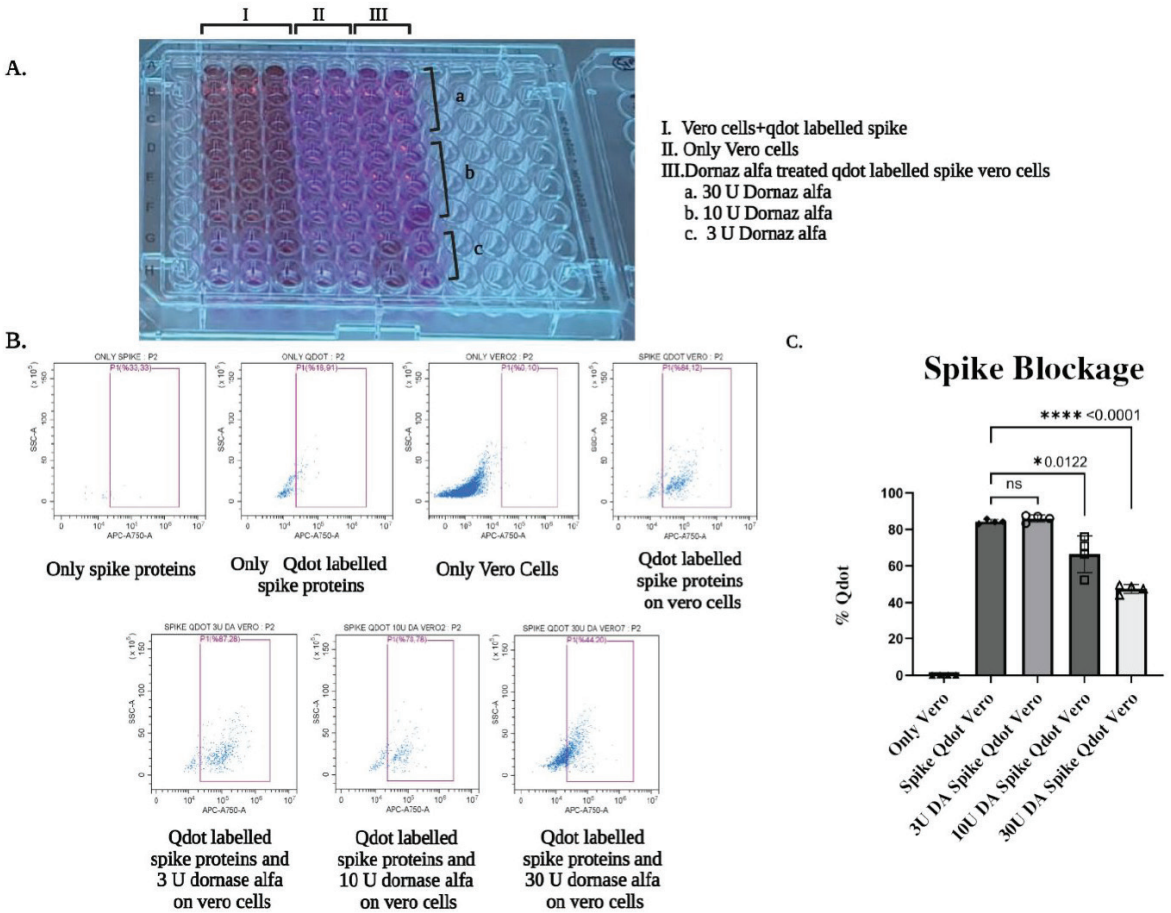


Figure 2. A. Macroscopic luminescence view of the plate under UV light. **B.** Plots show the amount of spike protein detected by flow cytometry after treatment with different concentrations of dornase alfa. A statistically significant neutralization of viral spike proteins has been detected, particularly in response to the use of 10U and 30U dornase alfa. **C.** The graph shows the mean fluorescence intensity (MFI) of Qdot signals across replicates. Each data point represents one independent biological replicate (one of ≥3 separate experiments from pooled virus), with each experiment performed in technical triplicate. Bars show the mean ± SD across independent experiments. Statistical significance was assessed using an unpaired two-tailed Student's t-test or Mann–Whitney U test, as appropriate ($p < 0.05$).

Effect of dornase alfa on naked SARS-CoV-2 RNA copy number: qRT-PCR analysis

Significant changes in viral copy numbers of isolated SARS-CoV-2 RNA were observed following treatment with different amounts of dornase alfa (p= 0.0163 for all concentrations). These changes in viral copy numbers due to dornase alfa usage were statistically significant (Figure 3.).

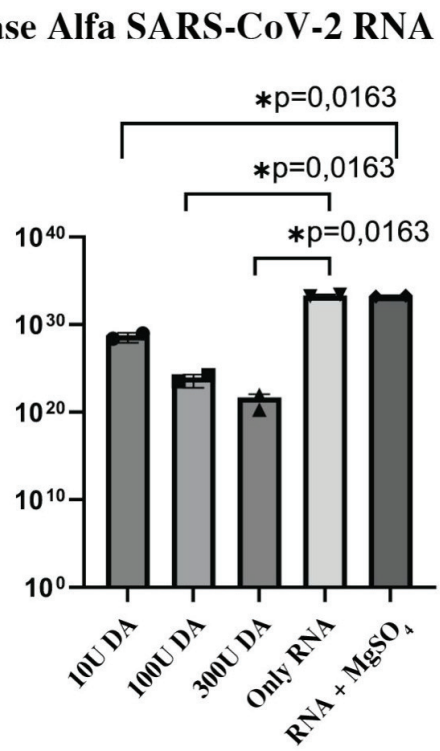


Figure 3. Purified ("naked") SARS-CoV-2 RNA was incubated with increasing concentrations of dornase alfa, and viral RNA levels were quantified by SARS-CoV-2–specific qRT-PCR. Viral copies/mL were calculated from a standard curve. Bars show viral copy number per mL for each condition (p values indicated). Each data point represents one independent biological replicate (one of ≥3 separate experiments from pooled virus), with each experiment performed in technical triplicate. Bars show the mean ± SD across independent experiments. Statistical significance was assessed using an unpaired two-tailed Student's t-test or Mann–Whitney U test, as appropriate ($p < 0.05$).

Effect of Dornase alfa on naked SARS-CoV-2 RNA sequence: Whole genome sequencing

Whole genome sequencing analysis was conducted to investigate potential changes in the genome sequence of the SARS-CoV-2 virus incubated with various concentrations of dornase alfa. Results revealed no significant difference between viral RNA left untreated and viral RNA treated with 3U and 10U dornase alfa (high coverage). However, viral RNA treated with 30U of dornase alfa exhibited poor quality, and whole genome sequencing was not feasible (low coverage level) (Supplementary Figure 2.). A minimum threshold of 100 depth was established for consensus fastas, with a mean depth >10000.

RNA copy number isolated from dornase alfa-treated SARS-CoV-2: qRT-PCR analysis

Evaluation of the effect of dornase alfa directly incubated with SARS-CoV-2 demonstrated no significant change in viral copy numbers (Figure 4.).

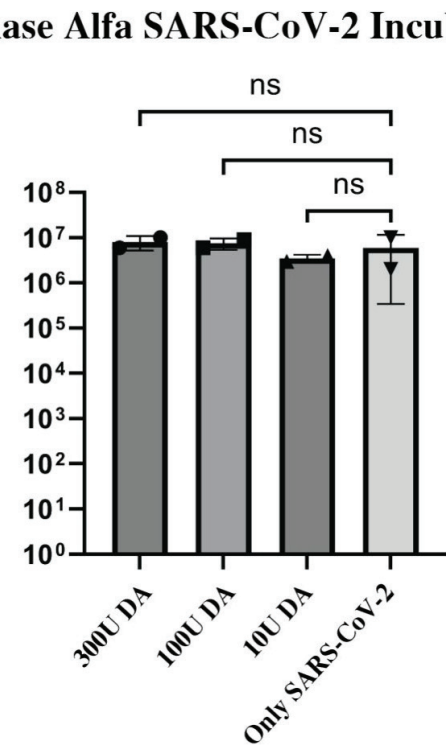


Figure 4. Following pre-incubation of SARS-CoV-2 (100×$TCID_{50}$) with increasing concentrations of dornase alfa, viral RNA was extracted and quantified by SARS-CoV-2–specific qRT-PCR. Viral copies/mL were calculated from a standard curve. Bars show viral copy number per mL for each condition. Each data point represents one independent biological replicate (one of ≥3 separate experiments from pooled virus), with each experiment performed in technical triplicate. Bars show the mean ± SD across independent experiments. Statistical significance was assessed using an unpaired two-tailed Student's t-test or Mann–Whitney U test, as appropriate ($p < 0.05$).

Effect of dornase alfa on the immune cytokine response due to the SARS-CoV-2 infection

Effect of dornase alfa on Th2 immunological response: Cytokine bead array analysis

PBMCs from two donors were stimulated with spike protein pre-incubated with dornase alfa, and cytokine responses were quantified by CBA. Dornase alfa shifted the response toward a Th2-skewed profile, with significant changes at 3 U in the IL-17/IL-10, TNF-α/IL-6, and IFN-γ/IL-6 ratios (p = 0.0095, p = 0.0198, and p = 0.0316, respectively). At 10 U, IFN-γ/IL-6 and TNF-α/IL-6 ratios also differed significantly compared with PBMC-only controls (p = 0.0358 and p = 0.0298, respectively) (Figure 5; Supplementary Table 2.).

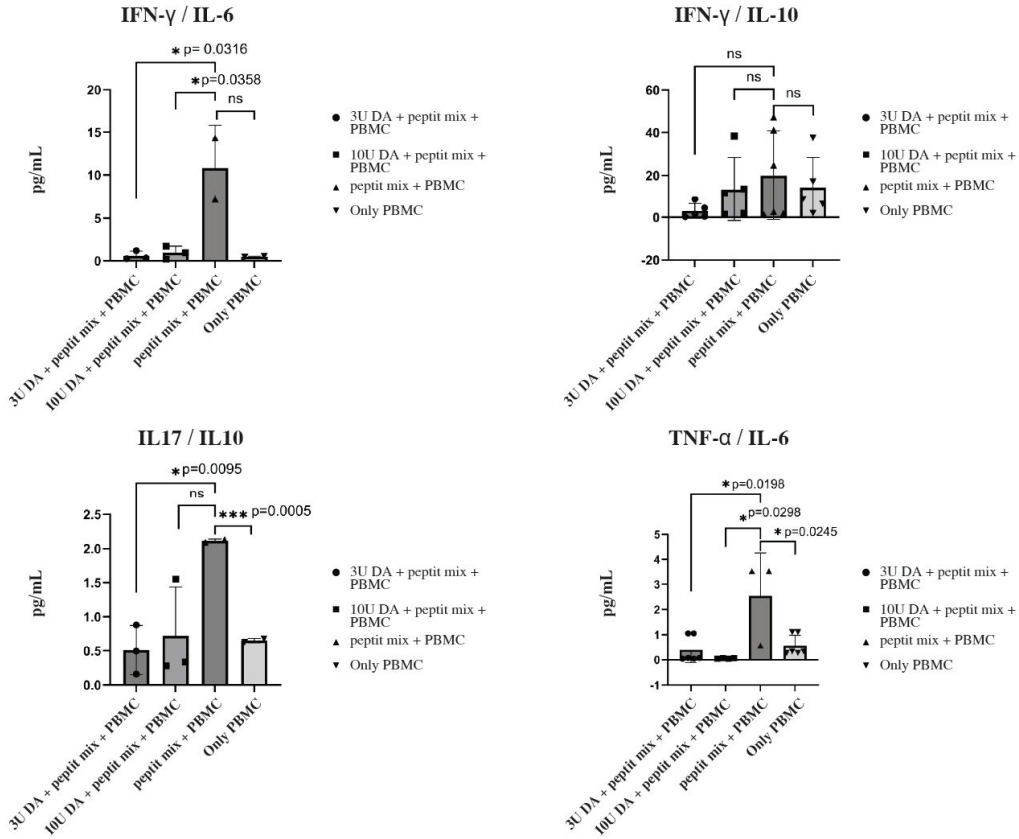


Figure 5. The immune response in PBMC cells treated with different concentrations of dornase alfa and viral peptide mix was examined by CBA assay after 72h. The bar charts indicate the ratio of Th1 response to Th2 response. Only PBMC: Negative Control; Peptide Mix + PBMC: Positive Control. Each data point represents one independent biological replicate (one of ≥3 separate experiments from pooled virus), with each experiment performed in technical triplicate. Bars show the mean ± SD across independent experiments. Statistical significance was assessed using an unpaired two-tailed Student's t-test (normal data) or Mann–Whitney U test (non-normal data), as indicated; $p < 0.05$ was considered significant.

NET formation with dornase alfa: Fluorescent microscopy analysis

To assess the impact of dornase alfa on NETs induced by PMA, NETs were treated with different concentrations of dornase alfa for 24 hours and stained with DAPI dye. Results indicated that virus pathophysiology was altered by 3U, 10U, and 30U dornase alfa (Figure 6.).

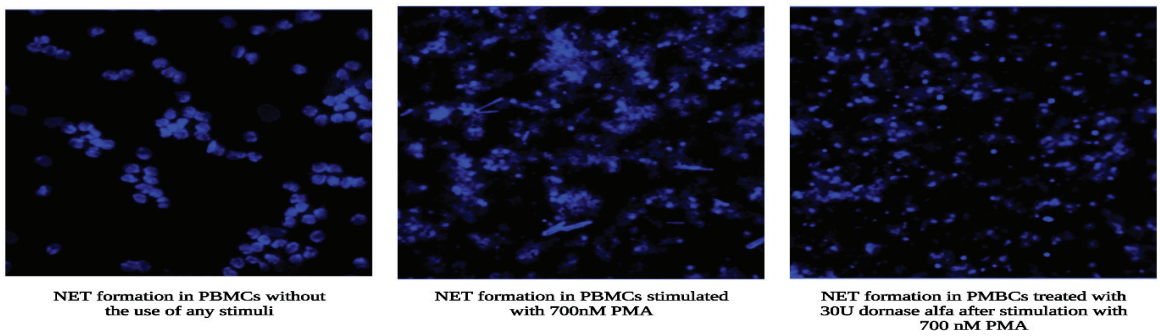


Figure 6. Image of NET formation in PBMC cells stained with DAPI dye under fluorescence microscopy**.**

CONCLUSION

Clinical studies have suggested that dornase alfa may benefit patients with SARS-CoV-2–related ARDS, reporting improvements in oxygenation, clinical status, and time to discharge (Desilles et al., 2020; Turan et al., 2021; Porter et al., 2024). In addition, Colombo et al. observed lower COVID-19 severity among cystic fibrosis patients receiving dornase alfa as part of standard care (Colombo et al., 2022). Building on these clinical observations, we sought to explore potential mechanisms by examining DA-driven immune modulation and its effects on viral components.

In our in vitro system, dornase alfa (DA; 10–30 U/mL) was associated with reduced SARS-CoV-2–induced cytopathic effects, potentially through two non-exclusive mechanisms: interference with spike-mediated entry and effects detected on purified ("naked") viral RNA. Qdot-based readouts supported a DA-dependent interaction with spike/entry processes, and pre-incubation of purified SARS-CoV-2 RNA with DA was associated with reduced qRT-PCR–derived copy number. In contrast, no copy-number reduction was observed when intact virions were incubated with DA before RNA extraction and qRT-PCR, which is biologically plausible given that the genome is shielded by the nucleocapsid and viral envelope. Importantly, DA is a DNase rather than an RNase; therefore, the "naked RNA" signal should be interpreted cautiously as hypothesis-generating only and may reflect indirect or matrix-related effects (e.g., carryover DNA, divalent cation–dependent assay effects, or other reaction-condition artifacts) rather than direct RNA cleavage. Accordingly, we do not interpret this observation as evidence of RNase-like activity, but as an indirect readout that requires orthogonal validation. Overall, these findings support biological plausibility for DA affecting entry-adjacent steps while cautioning against over-interpreting the "naked RNA" observation as RNase-like activity. A prior docking study is consistent with potential DA–spike interaction (Salman et al., 2020). Furthermore, Qdot-based quantitative flow cytometry showed a dose-dependent decrease in fluorescence with increasing dornase alfa, consistent with DA–spike interaction and reduced viral internalization as a surrogate measure of entry. These data do not directly quantify infectivity, which was assessed separately in the functional assays. Importantly, DA is a recombinant human DNase I and is not established as an RNase; therefore, the apparent "naked RNA" signal should be interpreted cautiously as hypothesis-generating and may reflect indirect or matrix-related effects rather than direct RNA cleavage. Under specific experimental conditions, DNA-mediated catalysis against RNA substrates has been described (e.g., DNAzymes) (Glick et al., 2014), and RNA digestion by other DNases has been reported in non-neutral environments (e.g., DNase II under mildly acidic conditions) (Zhuang et al., 2024). Accordingly, in complex mixtures where DNA and RNA co-exist, matrix effects—including potential contributions from cell-derived DNA fragments—could influence RNA integrity readouts. Orthogonal validation (e.g., RNase-inhibitor controls, heat-inactivated DA, and assays that discriminate true RNA cleavage from artifacts) will be required to resolve this mechanism. Early COVID-19 studies described a cytokine-storm phenotype with dysregulated T-cell immunity and broad shifts in inflammatory mediators; Guo et al. similarly reported widespread cytokine increases in patients, including IL-1β, IL-6, IL-8, IL-17, IFN-γ, and IL-10 (Guo et al., 2021). In this context,

our spike-stimulated PBMC data suggest that dornase alfa (DA) may modulate T-helper polarization toward a Th2-skewed profile, a concept that has been discussed as potentially relevant when effective antivirals are limited (Mamber et al., 2020). However, these observations are exploratory, derived from an in vitro system with a small donor number, and do not establish clinical benefit; validation in larger, longitudinal in vivo studies will be required (Gupta et al., 2022). Beyond cytokine dysregulation, NET formation has been implicated in ARDS and SARS-CoV-2 morbidity, and our microscopy-based readouts are consistent with a DNA/NET-directed effect of DA (Toma et al., 2021; Weber et al., 2020), aligning with ex vivo evidence of rapid NET dissolution in COVID-19 sputum after DNase I treatment (Fisher et al., 2021); nevertheless, these findings remain hypothesis-generating and require rigorous in vivo confirmation.

In this in vitro model, dornase alfa (DA) reduced assay-measured viral infectivity, decreased spike-associated viral internalization, and modulated inflammatory readouts, including a Th2-skewed response, while attenuating PMA-induced NETosis. Together with the hypothesis-generating observations reported by Okur et al. (2020), these results provide a preliminary mechanistic rationale to further investigate DA in the context of SARS-CoV-2 infection. However, given the limited sample size (n=3) and potential donor-to-donor variability despite harmonized procedures, statistical power is constrained, and the findings should be interpreted cautiously. Accordingly, this work should be considered preliminary and hypothesis-generating, and it requires validation in appropriately designed in vivo models and patient-based studies before any conclusions can be drawn regarding clinical efficacy or prophylactic use. In addition, further confirmatory experiments were beyond the scope of the present study due to laboratory and biosafety constraints and limited access to live virus materials. Future studies with larger sample sizes and independent replication will be essential to confirm and extend these findings.

ACKNOWLEDGEMENTS

The author(s) received no financial support for the research. The authors thank Acibadem Labcell Cellular Therapy Center for their support of the project.

ETHICS COMMITTEE APPROVAL

An informed consent form was obtained from the patients participating in the study (Ethics Committee Approval: Acıbadem Mehmet Ali Aydınlar University, number: 2020-06/03).

AUTHOR CONTRIBUTION STATEMENT

D.D.K., C.T., K.B.K., S.A., D.Ç., Y.B., G.S.K. and B.Y. designed, completed, and/or analyzed preclinical experiments. S.A. analyzed SARS-CoV-2 sequencing results. I.T.D. performed qdot production and its quality control analysis. D.D.K., C.T., K.B.K, Y.B. K.Y. and İ.T.D. wrote the manuscript. E.O. led the investigation and development project and contributed to the design and interpretation of the data. All authors contributed to the editing of the manuscript and approved the final version.

CONFLICTS OF INTEREST

The authors declare that there is no conflict of interest.

REFERENCES

Barnes, B. J., Adrover, J. M., Baxter-Stoltzfus, A., Borczuk, A., Cools-Lartigue, J., Crawford, J. M., ... Egeblad, M. (2020). Targeting potential drivers of COVID-19: Neutrophil extracellular traps. *Journal of Experimental Medicine*, *217*(6), e20200652. https://doi.org/10.1084/jem.20200652

Brinkmann, V., Reichard, U., Goosmann, C., Fauler, B., Uhlemann, Y., Weiss, D. S., ... Zychlinsky, A. (2004). Neutrophil extracellular traps kill bacteria. *Science*, *303*(5663), 1532-1535. https://doi.org/10.1126/science.1092385

Buranda, T., Wu, Y., Sklar, L. A. (2010). Quantum dots for quantitative flow cytometry. In *Flow Cytometry Protocols* (pp. 67-84). Totowa, NJ: Humana Press. https://doi.org/10.1007/978-1-61737-950-5_4

Camlik, G., Ozakca, I., Bilakaya, B., Ozcelikay, A. T., Velaro, A. J., Wasnik, S., Degim, I. T. (2022). Development of composite carbon quantum dots-insulin formulation for oral administration. *Journal of drug delivery science and technology*, *76*, 103833. https://doi.org/10.1016/j.jddst.2022.103833

Colombo, C., Cipolli, M., Daccò, V., Medino, P., Alghisi, F., Ambroni, M., ... Alicandro, G. (2022). Clinical course and risk factors for severe COVID-19 among Italian patients with cystic fibrosis: a study within the Italian Cystic Fibrosis Society. *Infection*, *50*(3), 671-679. https://doi.org/10.1007/s15010-022-01779-6

Desilles, J. P., Gregoire, C., Le Cossec, C., Lambert, J., Mophawe, O., Losser, M. R., ... Pottecher, J. (2020). Efficacy and safety of aerosolized intra-tracheal dornase alfa administration in patients with SARS-CoV-2-induced acute respiratory distress syndrome (ARDS): a structured summary of a study protocol for a randomised controlled trial. *Trials*, *21*(1), 548. https://doi.org/10.1186/s13063-020-04540-y

Fisher, J., Mohanty, T., Karlsson, C. A., Khademi, S. H., Malmström, E., Frigyesi, A., ... Linder, A. (2021). Proteome profiling of recombinant DNase therapy in reducing NETs and aiding recovery in COVID-19 patients. *Molecular Cellular Proteomics*, *20*, 100113. https://doi.org/10.1016/j.mcpro.2021.100113

Fitzgerald, D. A., Hilton, J., Jepson, B., Smith, L. (2005). A crossover, randomized, controlled trial of dornase alfa before versus after physiotherapy in cystic fibrosis. *Pediatrics*, *116*(4), e549-e554. https://doi.org/10.1542/peds.2005-0308

Glick, B. R., Patten, C. L., Delovitch, T. L. (Eds.). (2014). *Medical biotechnology*. John Wiley Sons.

Guo, J., Wang, S., Xia, H., Shi, D., Chen, Y., Zheng, S., ... Li, L. (2021). Cytokine signature associated with disease severity in COVID-19. *Frontiers in immunology*, *12*, 681516. https://doi.org/10.3389/fimmu.2021.681516

Gupta, G., Shareef, I., Tomar, S., Kumar, M. S. N., Pandey, S., Sarda, R., ... Sinha, S. (2022). Th1/Th2/Th17 cytokine profile among different stages of COVID-19 infection. *National Academy Science Letters*, *45*(4), 363-369. https://doi.org/10.1007/s40009-022-01123-9

Hoppenbrouwers, T., Autar, A. S., Sultan, A. R., Abraham, T. E., van Cappellen, W. A., Houtsmuller, A. B., ... de Maat, M. P. (2017). In vitro induction of NETosis: Comprehensive live imaging comparison and systematic review. *PloS one*, *12*(5), e0176472. https://doi.org/10.1371/journal.pone.0176472

Jiménez-Alcázar, M., Rangaswamy, C., Panda, R., Bitterling, J., Simsek, Y. J., Long, A. T., ... Fuchs, T. A. (2017). Host DNases prevent vascular occlusion by neutrophil extracellular traps. *Science*, *358*(6367), 1202-1206. https://doi.org/10.1126/science.aam8897

Kuang, H., Zhao, Y., Ma, W., Xu, L., Wang, L., Xu, C. (2011). Recent developments in analytical applications of quantum dots. *TrAC trends in analytical chemistry*, *30*(10), 1620-1636. https://doi.org/10.1016/j.trac.2011.04.022

Mamber, S. W., Krakowka, S., Osborn, J., Saberski, L., Rhodes, R. G., Dahlberg, A. E., ... McMichael, J. (2020). Can unconventional immunomodulatory agents help alleviate COVID-19 symptoms and severity? *MSphere*, *5*(3), 10-1128. https://doi.org/10.1128/mSphere.00288-20

Matthay, M. A., Zemans, R. L., Zimmerman, G. A., Arabi, Y. M., Beitler, J. R., Mercat, A., ... Calfee, C. S. (2019). Acute respiratory distress syndrome. *Nature reviews Disease primers*, *5*(1), 18. https://doi.org/10.1038/s41572-019-0069-0

Maysinger, D., Behrendt, M., Lalancette-Hébert, M., Kriz, J. (2007). Real-time imaging of astrocyte response to quantum dots: in vivo screening model system for biocompatibility of nanoparticles. *Nano Letters*, *7*(8), 2513-2520. https://doi.org/10.1021/nl071611t

Mirtchev, P., Henderson, E. J., Soheilnia, N., Yip, C. M., Ozin, G. A. (2012). Solution phase synthesis of carbon quantum dots as sensitizers for nanocrystalline TiO 2 solar cells. *Journal of Materials Chemistry*, *22*(4), 1265-1269. https://doi.org/10.1039/C1JM14219A

Morris, C., Mullan, B. (2004). Use of dornase alfa in the management of ARDS. *Anaesthesia*, *59*(12), 1249-1249. https://doi.org/10.1111/j.1365-2044.2004.04018.x

Msemburi, W., Karlinsky, A., Knutson, V., Aleshin-Guendel, S., Chatterji, S., Wakefield, J. (2023). The WHO estimates of excess mortality associated with the COVID-19 pandemic. *Nature*, *613*(7942), 130-137. https://doi.org/10.1038/s41586-022-05522-2

Okur, H. K., Yalcin, K., Tastan, C., Demir, S., Yurtsever, B., Karakus, G. S., ... Ovali, E. (2020). Preliminary report of in vitro and in vivo effectiveness of dornase alfa on SARS-CoV-2 infection. *New microbes and new infections*, *37*, 100756. https://doi.org/10.1016/j.nmni.2020.100756

Ozkan, M. (2004). Quantum dots and other nanoparticles: what can they offer to drug discovery? *Drug Discovery Today*, *9*(24), 1065-1071. https://doi.org/10.1016/s1359-6446(04)03291-x

Peckham, D., McDermott, M. F., Savic, S., Mehta, A. (2020). COVID-19 meets Cystic Fibrosis: for better or worse? *Genes Immunity*, *21*(4), 260-262. https://doi.org/10.1038/s41435-020-0103-y

Porter, J. C., Inshaw, J., Solis, V. J., Denneny, E., Evans, R., Temkin, M. I., ... Papayannopoulos, V. (2024). Anti-inflammatory therapy with nebulized dornase alfa for severe COVID-19 pneumonia: a randomized unblinded trial. *Elife*, *12*, RP87030. https://doi.org/10.7554/eLife.87030.4

Xu, L., Chen, C. (2012). Physiological behavior of quantum dots. *Wiley Interdisciplinary Reviews: Nanomedicine and Nanobiotechnology*, *4*(6), 620-637. https://doi.org/10.1002/wnan.1187

Salman, S., Shah, F. H., Chaudhry, M., Tariq, M., Akbar, M. Y., Adnan, M. (2020). In silico analysis of protein/peptide-based inhalers against SARS-CoV-2. *Future Virology*, *15*(9), 557-564. https://doi.org/10.2217/fvl-2020-0119

Schönrich, G., Raftery, M. J. (2016). Neutrophil extracellular traps go viral. *Frontiers in immunology*, *7*, 366. https://doi.org/10.3389/fimmu.2016.00366

Singh, R., Lillard Jr, J. W. (2009). Nanoparticle-based targeted drug delivery. *Experimental and molecular pathology*, *86*(3), 215-223. https://doi.org/10.1016/j.yexmp.2008.12.004

Sir Karakus, G., Tastan, C., Dilek Kancagi, D., Yurtsever, B., Tumentemur, G., Demir, S., ... Ovali, E. (2021). Preclinical efficacy and safety analysis of gamma-irradiated inactivated SARS-CoV-2 vaccine candidates. *Scientific reports*, *11*(1), 5804. https://doi.org/10.1038/s41598-021-83930-6

Taştan, C., Yurtsever, B., Karakuş, G., Kançağı, D. D., Demir, S., Abanuz, S., ... Kocagöz, A. S. (2020). SARS-CoV-2 isolation and propagation from Turkish COVID-19 patients. *Turkish Journal of Biology*, *44*(7), 192-202. https://doi.org/10.3906/biy-2004-115

Toma, A., Darwish, C., Taylor, M., Harlacher, J., Darwish, R. (2021). The use of dornase alfa in the management of COVID-19-associated adult respiratory distress syndrome. *Critical care research and practice*, *2021*(1), 8881115. https://doi.org/10.1155/2021/8881115

Turan, R. D., Tastan, C., Dilek Kancagi, D., Yurtsever, B., Sir Karakus, G., Ozer, S., ... Ovali, E. (2021). Gamma-irradiated SARS-CoV-2 vaccine candidate, OZG-38.61. 3, confers protection from SARS-CoV-2 challenge in human ACEII-transgenic mice. *Scientific reports*, *11*(1), 15799. https://doi.org/10.1038/s41598-021-95176-2

Weber, A. G., Chau, A. S., Egeblad, M., Barnes, B. J., Janowitz, T. (2020). Nebulized in-line endotracheal dornase alfa and albuterol administered to mechanically ventilated COVID-19 patients: a case series. *Molecular Medicine*, *26*(1), 91. https://doi.org/10.1186/s10020-020-00206-6

Yang, C., Montgomery, M. (2021). Dornase alfa for cystic fibrosis. *Cochrane Database of Systematic Reviews*, (3). https://doi.org/10.1002/14651858.CD001127.pub5

Zhuang, J., Du, X., Liu, K., Hao, J., Wang, H., An, R., Liang, X. (2024). DNase II Can Efficiently Digest RNA and Needs to Be Redefined as a Nuclease. *Cells*, *13*(18), 1525. https://doi.org/10.3390/cells13181525

FABAD J. Pharm. Sci., 51, 1, 189-206, 2026
Doi: 10.55262/fabadeczacilik.1814439
RESEARCH ARTICLE

Smoking Behavior, Nicotine Dependence, and Awareness of Cessation Methods Among Pharmacy Students: A Cross-Sectional Analysis

Nesligül ÖZDEMİR AYDURAN[*°], Nida AÇAR[**], Zeynep Ülkü GÜN[***]

Smoking Behavior, Nicotine Dependence, and Awareness of Cessation Methods Among Pharmacy Students: A Cross-Sectional Analysis

SUMMARY

Determining the smoking behaviors of pharmacy students and the factors that influence these behaviors is important for public health, as they are future healthcare professionals. This study assessed the prevalence of nicotine dependence among pharmacy students, evaluated perceptions of smoking-cessation methods, and identified correlates of dependence. This cross-sectional survey was conducted at a Faculty of Pharmacy in eastern Türkiye between June and July 2022. An online 25-item questionnaire, developed based on the literature and expert input, was administered to the students. Students' nicotine dependence was assessed using the Fagerström Test for Nicotine Dependence (FTND). The primary outcome was nicotine dependence severity. Secondary outcomes were the prevalence of current smoking, FTND distributions by demographics, and perceived effectiveness of cessation methods. Data from 232 students were analyzed (median age 23 years; ~70% female). Of these, 121 (52.2%) had never smoked; 54 (23.3%) had tried once; 11(4.7%) were former smokers; 13 (5.6%) smoked occasionally; and 33 (14.2%) smoked daily. The median (IQR) value of the FTND score of active smokers was 3(4). Among 46 current smokers, the distribution of nicotine-dependence levels was: very low: 22 (47.8%), low: 10 (21.7%), moderate: 3 (6.5%), high: 4(8.7%), and very high: 7 (15.2%). The presence of a family member who smoked led to an increase in the FTND Score (p=0.006). Face-to-face counseling and smoking cessation clinic interventions were rated significantly more effective than both mobile applications and posters and printed educational materials (p <0.05). In conclusion, students had low nicotine dependence and limited awareness of smoking-cessation methods.

Keywords: *Nicotine dependence, pharmacy students, smoking cessation methods, smoking prevalence.*

Eczacılık Fakültesi Öğrencilerinde Sigara Kullanım Davranışı, Nikotin Bağımlılığı ve Sigarayı Bırakma Yöntemlerine İlişkin Farkındalık: Kesitsel Bir Analiz

ÖZ

Geleceğin sağlık profesyonelleri olacak eczacılık öğrencilerinin sigara içme davranışlarını ve bu davranışları etkileyen faktörleri belirlemek halk sağlığı açısından önemlidir. Bu çalışmada eczacılık öğrencileri arasında nikotin bağımlılığının yaygınlığı ve sigara bırakma yöntemlerine ilişkin algıları değerlendirilmiş ve bağımlılığın ilişkili olduğu faktörler belirlenmiştir. Bu kesitsel anket, Haziran-Temmuz 2022 tarihleri arasında Türkiye'nin doğusundaki bir eczacılık fakültesinde gerçekleştirilmiştir. Literatür ve uzman görüşlerine dayanarak geliştirilen 25 soruluk çevrimiçi bir anket öğrencilere uygulanmıştır. Öğrencilerin nikotin bağımlılığı Fagerström Nikotin Bağımlılığı Testi (FTND) kullanılarak değerlendirilmiştir. Birincil çıktı nikotin bağımlılığı şiddetidir. İkincil çıktılar mevcut sigara içme yaygınlığı, demografik özelliklere göre FTND dağılımları ve sigara bırakma yöntemlerinin algılanan etkinliğidir. 232 öğrenciden alınan veriler analiz edilmiştir (ortanca yaş 23 yıl; ~%70 kadın). Bunlardan 121'i (%52,2) hiç sigara içmemişti; 54'ü (%23,3) bir kez denemişti; 11'i (%4,7) eskiden sigara içmiş ve bırakmıştı; 13'ü (%5,6) ara sıra sigara içiyordu ve 33'ü (%14,2) ise günlük sigara içiyordu. Aktif sigara içicilerinin FTND skorunun ortanca (IQR) değeri 3(4) idi. 46 mevcut sigara içicisinde nikotin bağımlılığı düzeylerinin dağılımı sırasıyla çok düşük: 22 (%47,8), düşük: 10 (%21,7), orta: 3 (%6,5), yüksek: 4 (%8,7) ve çok yüksek: 7 (%15,2) idi. Sigara içen aile üyesinin varlığı FTND Skorunda artışla ilişkilendirildi (p=0,006). Yüz yüze danışmanlık ve sigara bırakma kliniği müdahaleleri hem mobil uygulama hem de poster ve basılı eğitim materyallerinden önemli ölçüde daha etkili olarak derecelendirildi (p <0,05). Sonuç olarak, öğrencilerin nikotin bağımlılığı düşüktü ve sigara bırakma yöntemleri konusundaki farkındalıkları da sınırlıydı.

Anahtar Kelimeler: *Eczacılık öğrencileri, nikotin bağımlılığı, sigara bırakma yöntemleri, sigara içme yaygınlığı.*

Recieved: 4.11.2025
Revised: 6.02.2026
Accepted: 15.02.2026

[*] ORCID: 0000-0003-2551-9549, Department of Clinical Pharmacy, Faculty of Pharmacy, Gazi University, Ankara, Türkiye
[**] Faculty of Pharmacy, Inonu University, Malatya, Türkiye
[***] ORCID: 0000-0002-7131-6585, Department of Clinical Pharmacy, Faculty of Pharmacy, Trakya University, Edirne, Türkiye

[°] Corresponding Author; Nesligül ÖZDEMIR AYDURAN
E-mail: nesliozdmr@hotmail.com

INTRODUCTION

Tobacco use remains a leading cause of preventable morbidity and mortality worldwide and continues to pose a major public-health challenge in Türkiye (West, 2017). Based on global estimates for 2020–2022, the prevalence of smoking was 13.3% among individuals aged 15–24 years and 21.7% among those aged ≥15 years (WHO, 2024). According to nationally reported data for Türkiye, cigarette-smoking prevalence was 28.7 % among individuals aged ≥15 years, and %19.3 among individuals aged 15-24 years in 2022 (TÜİK, 2023). Compared with global estimates, Türkiye shows a higher prevalence of tobacco smoking across all age groups.

The onset and consolidation of tobacco use occur predominantly during adolescence and young adulthood; nearly nine in ten adult daily cigarette smokers report initiating use by age 18 (Tidey, 2020; CDC, 2024). Young people are more vulnerable to smoking because they develop addiction more quickly than adults (Goriounova & Mansvelder, 2012). Consequently, the rapidly developing addiction often persists into later life, placing individuals at increased risk for smoking-related diseases, including lung cancer, chronic obstructive pulmonary disease, and ischemic heart disease (Dai et al., 2022). Therefore, identifying smoking behavior and its causes among the young population and developing preventive strategies against them remains an important issue.

University students are a key population among whom smoking initiation and consolidation frequently occur. Multiple cross-sectional studies conducted in Türkiye among students from different disciplines have reported smoking rates ranging from 10.8% to 45.4% (Çapık et al., 2007; Tunçdemir, 2009; Ulukoca et al., 2013; Tarı-Selçuk et al., 2018; Çelik & Demirel, 2022). Although most Turkish studies sample students across multiple disciplines, only two have specifically examined smoking among pharmacy students (Yegenoglu et al., 2006; Kop et al., 2015). One used a mixed-methods design with first- and fifth-year cohorts at a state university (Yegenoğlu et al., 2006), and the other surveyed a private pharmacy school (Kop et al., 2015). Both were limited to describing smoking prevalence and patterns, without assessing nicotine dependence or its correlates. Beyond these pharmacy-specific investigations, the broader Turkish literature has largely focused on mixed groups of healthcare students, reporting overall nicotine use or dependence estimates without providing subgroup-specific analyses for pharmacy students (Çapık et al., 2007; Tunçdemir, 2009; Ulukoca et al., 2013; Tarı-Selçuk et al., 2018; Çelik & Demirel, 2022). However, as demonstrated in international research, smoking behaviors, levels of nicotine dependence, and attitudes toward tobacco use can vary considerably across different health-professional student groups (Rahman et al., 2022). These differences highlight the importance of examining pharmacy students as a distinct population in order to obtain discipline-specific data and to inform targeted educational and preventive strategies.

This distinction is particularly relevant in the context of pharmacists' professional responsibilities in smoking cessation. Smoking cessation is a key component of preventive health counseling provided by pharmacists, and pharmacist-led interventions have been shown to support behavioral change (Carson-Chahhoud et al., 2019). Pharmacists who perceive themselves as sufficiently trained in smoking cessation interventions demonstrate greater willingness to provide smoking cessation counseling to patients (Odukoya et al., 2016). Although limited evidence exists regarding the impact of pharmacists' own smoking status, a study reported no significant difference in willingness to counsel, while non-smoking pharmacists demonstrated higher counseling scores, suggesting that personal smoking behaviors may still influence engagement in smoking cessation counseling (Alzahrani et al., 2023).

Given this professional context, and recognizing that smoking behaviors and attitudes may differ across health-professional student groups, it is important to identify cigarette addiction among pharmacy students and to evaluate their perceptions of smoking

cessation approaches. Accordingly, this study aimed to determine the prevalence of smoking addiction among pharmacy students, to examine the perception of smoking cessation methods, and to identify factors associated with nicotine dependence. The findings are intended to raise awareness and inform the development of targeted strategies to encourage smoking cessation in this cohort.

MATERIALS AND METHODS

This cross-sectional survey was conducted at a Faculty of Pharmacy in Türkiye between June and July 2022. The study population comprised all pharmacy students enrolled at the faculty. Because a census approach was adopted (the intention was to reach the entire population, 484 students), no a priori sample-size calculation was performed. Eligibility was restricted to pharmacy students who consented to participate.

The questionnaire was developed based on a literature review and expert opinions, and administered online via Google Forms (Ergin et al. 2016; Karadag et al., 2021). Distribution occurred through students' class WhatsApp groups and institutional email lists. The questionnaire consisted of two sections with a total of 25 items: a demographics section (19 items) and the Fagerström Nicotine Dependence Test (6 items). Perceived effectiveness of smoking-cessation methods among smokers was evaluated using a four-point Likert-type ordinal scale comprising slightly effective (1), moderately effective (2), highly effective (3), and no opinion (0).

To assess the understandability of the questionnaire questions, a pilot study was conducted with 20 individuals with similar characteristics to the study population, and the language and clarity of the questionnaire were adjusted based on the obtained data. The questionnaire was revised and sent to the study population. Before participation, students were presented with an online information and consent page explaining the purpose of the study, the voluntary nature of participation, and their right to withdraw at any time. Electronic informed consent was obtained before access to the questionnaire was granted. The survey was conducted anonymously, and no personally identifiable information was collected.

Following the initial invitation, two reminder messages/emails were sent at two-week intervals. The questionnaire closed two weeks after the final reminder. All data were stored on a secure, password-protected system accessible only to the research team and were used solely for research purposes.

Fagerström test for nicotine dependence (FTND)

Nicotine dependence was assessed using the FTND, which was studied for validity and reliability in Turkish by Uysal et al. and showed moderate internal consistency (Cronbach's $\alpha = 0.56$) (Uysal et al., 2025). This test is a six-item instrument for cigarette smokers. The items cover: time to first cigarette after waking, difficulty refraining in restricted areas, the cigarette most difficult to give up, number of cigarettes per day, smoking more in the morning, and smoking during illness. Item scores are summed to yield a total score from 0 to 10, with higher scores indicating greater dependence. Scores of 0–2 indicate very low dependence, 3–4 low, 5 moderate, 6–7 high, and 8–10 very high dependence. Internal consistency in our sample was evaluated using Cronbach's alpha.

The primary outcome was nicotine-dependence severity, measured by the FTND total score. Secondary outcomes included the prevalence of current cigarette smoking among pharmacy students, the distribution of FTND scores across demographic subgroups (e.g., sex, year of study), and the perceived effectiveness of smoking-cessation methods.

This study was conducted in accordance with the ethical standards set out in the Declaration of Helsinki. The study was approved by the Inonu University Health Sciences Scientific Research Ethics Committee-Nonclinical Trials Ethics Committee (approval number: 2022/3642, date: 07.06.2022).

Statistical analysis

Data were summarized using descriptive statistics (numbers and percentages). For variables that were not normally distributed, medians and interquartile ranges (IQRs) were reported. Comparisons of demographic characteristics across the groups were performed using the Kruskal–Wallis test for continuous variables and the chi-square test for categorical variables. Smoking status was categorized as never smokers, experimenters (tried smoking once), current smokers (occasional or daily), and former smokers. Inclusion of variables in the analyses was guided by their conceptual relevance to the research questions and the availability of corresponding outcome measures. The items assessing perceived effectiveness were designed to obtain independent ordinal ratings of different smoking cessation methods rather than to constitute a unified psychometric scale or generate a composite score. Each item was therefore analyzed independently as an ordinal variable, and no total or summary score was calculated. Because the response options represented ordered categories rather than continuous measurements and did not meet normality assumptions, medians were used as measures of central tendency, and non-parametric tests were applied for comparisons.

The Friedman test was employed to examine differences in perceived effectiveness scores across the nine smoking cessation methods, as the data were ordinal and measured repeatedly for the same participants. Following a significant Friedman test result, post-hoc pairwise comparisons were conducted to identify specific differences between smoking cessation methods. These comparisons were performed using the Wilcoxon signed-rank test, and p-values were adjusted for multiple testing using the Bonferroni correction. Associations between FTND scores and categorical variables were examined with the Mann–Whitney U test for two-group comparisons and the Kruskal–Wallis H test for variables with three or more categories. Results are reported as median (IQR). Two-sided $p < 0.05$ was considered statistically significant.

Because the study targeted all accessible students, an a priori sample size calculation was not performed. However, a post hoc power analysis was performed using G*Power (version 3.1) for the primary outcome, which compared perceived effectiveness scores across multiple smoking cessation methods rated by the same participants (n=18). An equivalent repeated-measures model was applied. Assuming a moderate effect size ($f = 0.25$), $\alpha = 0.05$, nine repeated measurements, and a correlation of 0.5 among measures, the achieved power was 0.90, indicating that the sample size was sufficient to detect group differences. Effect size measures for FTND scores were calculated to evaluate the magnitude of subgroup differences and to support the interpretation of findings in the context of limited subgroup sample sizes. Effect sizes were interpreted according to established guidelines reported in the statistical literature (small ≈ 0.10, medium ≈ 0.30, large ≥ 0.50 for r; small ≈ 0.01, medium ≈ 0.06, large ≥ 0.14 for η^2) (Alpar, 2022).

RESULTS

The survey was completed by 234 of the 484 students enrolled in the Faculty of Pharmacy, corresponding to a response rate of 48.3%. Two students were excluded from the study due to incomplete answers to the survey questions, and data from 232 students were analyzed.

Approximately 70% of the participants were female, and the median age was 23 years. Of the 232 students, 111 (47.8%) were classified as ever smokers, including those who had tried smoking once, former smokers, and current smokers. Among the total sample, 46 students (19.8%) were current smokers (13 occasional and 33 daily smokers), and 11 students (4.7%) were former smokers. The remaining 121 students (52.2%) were never smokers. Demographic characteristics of the students are given in Table 1.

Significant differences were observed across smoking-status groups in terms of age, gender, place

of residence, income status, and presence of smokers in the family ($p < 0.05$). Current/former smokers were older and predominantly male. Experimenters were more likely to live with their families, while current/former smokers were less likely to do so. Lower income was more frequent among experimenters and current/former smokers than among never smokers. Moreover, having a family member who smokes increased progressively from never smokers to experimenters and current/former smokers. No significant differences were found for class level or presence of chronic disease.

Table 1. Demographic characteristics of the students (n=232)

	All students (n=232) n (%)	**Never smoker (n=121) n (%)**	**Experimenters (tried smoking once) (n=54) n (%)**	**Current and Former smokers (n=57) n (%)**	**p value**
Age [median(IQR)]	23 (2)	22 (2)	22 (2)	23 (3)	**<0.001***
Gender					**<0.001****
Female	161 (69.4)	101 (83.5)	37 (68.5)	23 (40.4)	
Male	71 (30.6)	20 (16.5)	17 (31.5)	34 (59.6)	
Class					0.867**
1st year student	24 (10.3)	12.5 (9.9)	5 (9.3)	7 (12.3)	
2nd year student	28 (12.1)	18 (14.9)	6 (11.1	4 (7.0)	
3rd year student	77 (33.2)	39 (32.2)	16 (29.6)	22 (38.6)	
4th year student	33 (14.2)	18 (14.9)	8 (14.8)	7(12.3)	
5th year student	70 (30.2)	34 (28.1)	19 (35.2)	17(29.8)	
Place of residence during university education					**0.001****
Shared student apartment	29 (12.5)	5 (4.1)	11 (20.4)	13(22.8)	
Living with family	62 (26.7)	42 (34.7)	34 (63.0	11(19.3)	
Dormitory	141 (60.8)	74 (61.2)	9(16.6)	33(57.9)	
Income status					0.005**
Good	32 (13.8)	18 (14.9)	10 (18.5)	4(7.0)	
Moderate	175 (75.4)	98 (81.0)	34 (63.0)	43(75.4)	
Poor	25 (10.8)	5 (4.1)	10 (18.5)	10(17.6)	
Presence of chronic disease					0.787**
Yes	16 (6.9)	8 (6.6)	3 (5.6)	5(8.8)	
No	216 (93.1)	113 (93.4)	51 (94.4)	52(91.2)	
Presence of smokers in the family					**0.016****
Yes	127 (54.7)	56 (46.3)	32 (59.3)	39(68.4)	
No	105 (45.3)	65 (53.7)	22 (40.7)	18(31.6)	

* Kruskal Wallis, **Chi-square Test,

Among ever smokers (n=111), the median (IQR) age at first smoking experience was 15 (6) years. Among current smokers (n=46), 43.5% smoked fewer than 10 cigarettes per day, 34.8% smoked 10–20 cigarettes per day, 13.0% smoked 21–30 cigarettes per day, and 8.7% smoked more than 31 cigarettes per day.

Among current and former smokers, 66.7% reported experiencing at least one health problem after starting to smoke. Among the reported problems, oral and dental health issues ranked highest (55.3%) in frequency, whereas skin problems ranked lowest (13.2%). Reported health problems in current and former smokers after starting to smoke are given in Figure 1.

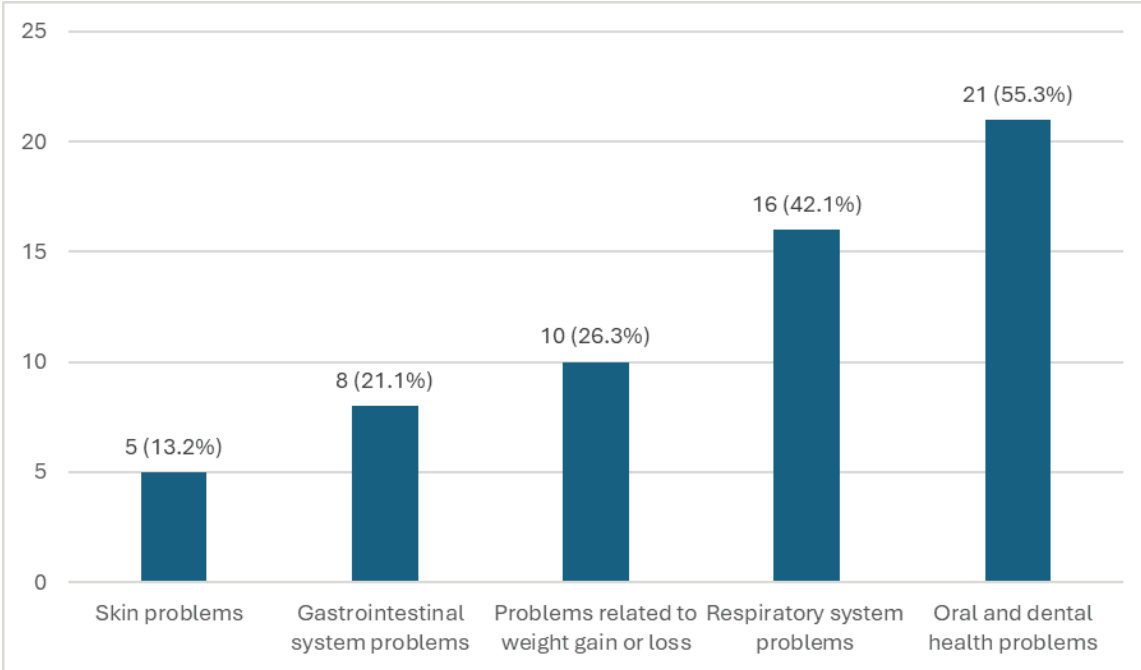


Figure 1. Reported problems in current and former smokers after starting to smoke (n=57).

The distribution of reasons for smoking among ever smokers is given in Figure 2. According to students' statements, the top three factors that lead to smoking are curiosity, influence from friends, and stress, respectively.

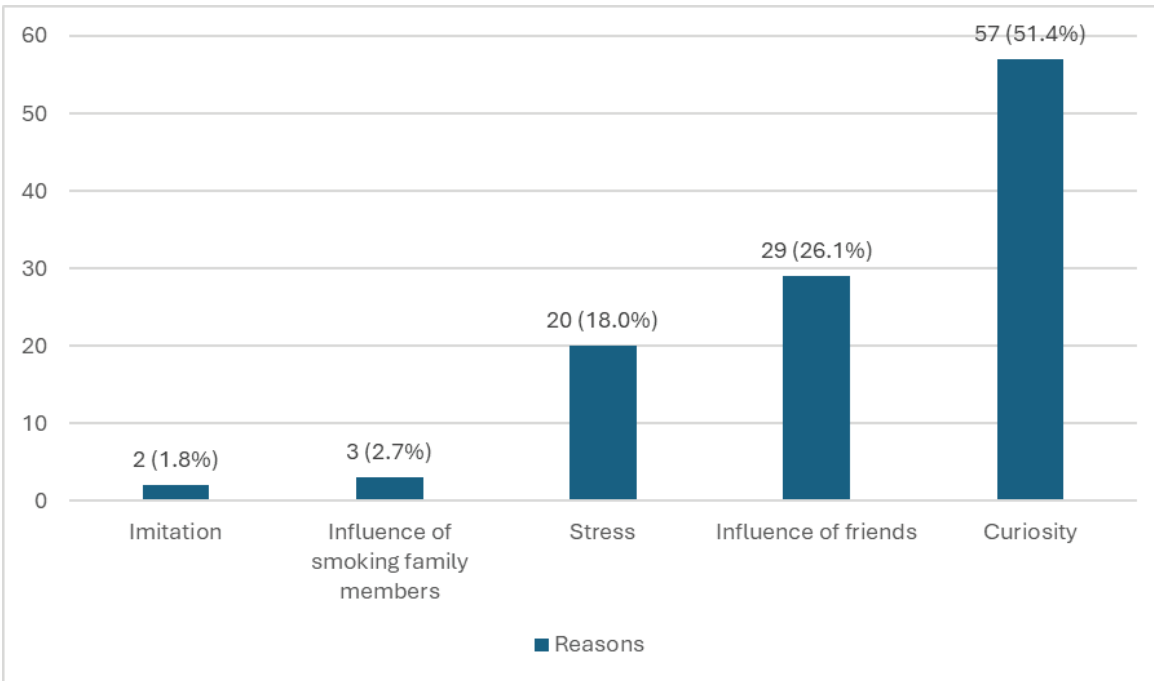


Figure 2. Distribution of reasons for smoking among ever smokers (n=111)

Behaviors and intentions related to smoking cessation among current-smoking students are given in Table 2. Three-quarters of current smokers reported at least one smoking cessation attempt. The most common pattern was four attempts. Only 17.1% of current smokers had tried at least one smoking cessation method. When students were questioned about their intentions for smoking cessation, only 28.2% expressed a desire to quit, and 26.1% wanted to seek counseling for smoking cessation.

Table 2. Smoking cessation behaviors and intentions of current-smoking students (n=46)

	n (%)
Attempted smoking cessation (n=46)	
Yes	35 (76.1)
No	11 (23.9)
Total	46 (100)
The number of smoking cessation attempts (n=35)	
1 time	8 (22.9)
2 times	7 (20.0)
3 times	7 (20.0)
>4 times	13 (37.1)
Total	46 (100)
Use of Smoking Cessation Methods (n=35)	
Yes	6 (17.1)
No	29 (82.9)
Total	35 (100)
Types of Smoking Cessation Methods Used (n=6)	
Smoking cessation clinic	1 (16.7)
Nicotine replacement therapy	1 (16.7)
Prescription medication therapy	1 (16.7)
Mobile smoking cessation application	3 (50.0)
Intention for Smoking Cessation (n=46)	
Yes	13 (28.2)
Undecided	16 (34.8)
No	17 (37.0)
Total	46 (100)
Willingness to Receive Counseling for Smoking Cessation (n=46)	
Yes	12 (26.1)
No	34 (73.9)
Total	46 (100)

Perceived effectiveness of smoking cessation methods among current and former smokers is given in Table 3. According to the results, the methods most frequently rated as "highly effective" were face-to-face counseling, smoking cessation clinics, and prescription medication therapy (each 21.2%). The method most frequently rated as "slightly effective" was posters and printed educational materials (70.2%).

Table 3. Perceived effectiveness of smoking cessation methods among current and former smokers (n=57)

	Slightly effective (1) n (%)	Moderately effective (2) n (%)	Highly effective (3) n (%)	No opinion (0) n (%)
Public service announcements	32 (56.1)	7 (12.3)	2 (3.5)	16 (28.1)
Posters and printed educational materials	40 (70.2)	4 (7.0)	2 (3.5)	11 (19.3)
Face-to-face counseling	8 (14.0)	24 (42.0)	12 (21.2)	13 (22.8)
Smoking cessation clinics	12 (21.2)	19 (33.3)	12 (21.2)	14 (24.3)
Nicotine replacement therapy (NRT)	5 (8.8)	21 (36.8)	10 (17.6)	21 (36.8)
Prescription medication therapy (e.g., varenicline, bupropion)	6 (10.5)	19 (33.3)	12 (21.2)	20 (35.0)
Acupuncture	11 (19.3)	16 (28.1)	2 (3.5)	28 (49.1)
Hypnosis	15 (26.3)	10 (17.6)	2 (3.5)	30 (52.6)
Mobile applications for smoking cessation	26 (45.6)	6 (10.5)	0 (0)	25 (43.9)

The Friedman test revealed a statistically significant difference in perceived effectiveness across the nine methods, $\chi^2(8) = 55.553$, $p<0.001$, Kendall's W=0.386 (Table 4.).

Table 4. Comparison of perceived effectiveness of smoking cessation methods among complete cases (n = 18)

	Mean Rank*	p- value*
Public service announcements	4.11	**<0.001**
Posters and printed educational materials	3.33	
Face-to-face counseling	7.03	
Smoking cessation clinics	6.44	
Nicotine replacement therapy (NRT)	5.75	
Prescription medication therapy (e.g., varenicline, bupropion)	5.89	
Acupuncture	4.69	
Hypnosis	4.44	
Mobile applications for smoking cessation	3.31	

* Mean ranks and p-values were calculated using the Friedman test among participants who provided valid ratings for all nine methods.

Post-hoc pairwise comparisons with Bonferroni adjustment indicated that face-to-face counseling and smoking cessation clinic interventions were rated significantly more effective than both mobile application and posters and printed educational materials ($p<0.05$). No other pairwise differences reached statistical significance after adjustment. Pairwise comparisons of perceived effectiveness between smoking cessation methods are given in Table 5.

Table 5. Pairwise comparisons of perceived effectiveness between smoking cessation methods (n=18)

Comparison pairs	Test statistics	p-value*
Public service announcements- Posters and printed educational materials	0.778	>0.05
Public service announcements- Face-to-face counseling	-2.917	0.05
Public service announcements- Smoking cessation clinics	-2.333	>0.05
Public service announcements- Nicotine replacement therapy	-1.639	>0.05
Public service announcements- Prescription medication therapy	-1.778	>0.05
Public service announcements- Acupuncture	-0.583	>0.05
Public service announcements- Hypnosis	-0.333	>0.05
Public service announcements- Mobile applications for smoking cessation	0.806	>0.05
Posters and printed educational materials- Face-to-face counseling	-3.694	**0.02**
Posters and printed educational materials- Smoking cessation clinics	-3.111	**0.02**
Posters and printed educational materials- Nicotine replacement therapy	-2.417	>0.05
Posters and printed educational materials- Prescription medication therapy	-2.556	>0.05
Posters and printed educational materials- Acupuncture	-1.361	>0.05
Posters and printed educational materials- Hypnosis	-1.111	>0.05
Posters and printed educational materials- Mobile applications for smoking cessation	0.028	>0.05
Face-to-face counseling- Smoking cessation clinics	0.583	>0.05
Face-to-face counseling- Nicotine replacement therapy	1.278	>0.05
Face-to-face counseling- Prescription medication therapy	1.139	>0.05
Face-to-face counseling- Acupuncture	2.333	>0.05
Face-to-face counseling- Hypnosis	2.583	>0.05
Face-to-face counseling- Mobile applications for smoking cessation	3.722	**0.02**
Smoking cessation clinics- Nicotine replacement therapy	0.694	>0.05
Smoking cessation clinics- Prescription medication therapy	0.556	>0.05
Smoking cessation clinics- Acupuncture	1.750	>0.05
Smoking cessation clinics- Hypnosis	2.000	>0.05
Smoking cessation clinics- Mobile applications for smoking cessation	3.139	**0.021**
Nicotine replacement therapy- Prescription medication therapy	-0.139	>0.05
Nicotine replacement therapy- Acupuncture	1.056	>0.05
Nicotine replacement therapy- Hypnosis	1.306	>0.05
Nicotine replacement therapy- Mobile applications for smoking cessation	2.444	0.267
Prescription medication therapy- Acupuncture	1.194	>0.05
Prescription medication therapy- Hypnosis	1.444	>0.05
Prescription medication therapy- Mobile applications for smoking cessation	2.583	>0.05
Acupuncture- Hypnosis	0.250	>0.05
Acupuncture- Mobile applications for smoking cessation	1.389	>0.05
Hypnosis- Mobile applications for smoking cessation	1.139	>0.05
* Wilcoxon signed-rank test		

Fagerström test for nicotine dependence (FTND)

The Cronbach alpha value of the FTND was found to be 0.759. The median (IQR) value of the FTND score of active smokers was 3 (4). Among 46 current smokers, the distribution of nicotine-dependence (FTND) levels was: very low, 22 (47.8%), low, 10 (21.7%), moderate, 3 (6.5%), high, 4 (8.7%), and very high, 7 (15.2%).

When the FTND score was evaluated to determine whether students' demographic characteristics differed, only the presence of a family member who smoked showed a statistically significant difference (p=0.006). The presence of a family member who smoked led to an increase in the FTND Score (Table 6.). Effect size analyses showed that the presence of smokers in the family had a moderate association with FTND scores (r = 0.40), whereas chronic disease status showed a small-to-moderate effect (r = 0.24). Gender demonstrated a negligible effect (r = 0.009). For Kruskal–Wallis comparisons, class level (η^2<0.001) and place of residence (η^2 = 0.007) showed negligible effects, while income status demonstrated a small effect (η^2 = 0.069).

Table 6. Comparison of FTND scores according to demographic characteristics.

	FTND Score [median(IQR)]	**p value**
Age [median(IQR)]	Correlation coefficient= 1.000	0.960*
Gender		
Female	3.5 (6)	0.952**
Male	2.5 (4)	
Class		
1st year student	5 (6)	0.407***
2nd year student	3 (0)	
3rd year student	4 (5)	
4th year student	1 (8)	
5th year student	2 (4)	
Place of residence during university education		
Shared student apartment	2.5 (3)	0.315***
Living with family	1 (4)	
Dormitory	4 (5)	
Income status		
Good	-	0.084***
Moderate	3.5 (4)	
Poor	3 (5)	
Presence of chronic disease		
Yes	7 (7)	0.099**
No	2.5 (4)	
Presence of smokers in the family		
Yes	4 (6)	**0.006****
No	1.5 (2)	
*Spearman correlation, **Mann-Whitney U Test, ***Kruskal Wallis		

DISCUSSION

In this cross-sectional study of pharmacy students, nicotine dependence among current smokers was generally low, and the presence of a smoker in the family was significantly associated with higher FTND scores. Although quit attempts were common, uptake of evidence-based cessation support was minimal. Participants rated face-to-face counseling and smoking-cessation clinics as more effective than mobile applications or printed educational materials.

In this study, nearly half of the students had tried, previously used, or were currently smoking cigarettes. About one-quarter of the students were active smokers. In a study conducted among university students, 38.4% were identified as current smokers, and the mean age at smoking initiation was 16.5 ± 2.78 years (Karadag et al., 2021). In a study, which included medical, pharmacy, and dentistry students, the smoking rate was found to be 20.3% (Alwhaibi et al., 2022). In a study conducted among medical and pharmacy students, the overall prevalence of smoking was 1.6% (n = 4) and was significantly higher among medical students (4.3%, n = 4) than among pharmacy students (0%, n = 0; p = 0.009) (Rahman et al., 2022). To date, the prevalence of cigarette smoking among pharmacy students in Türkiye has been documented in only two studies, with Kop et al. reporting 28.1% and Yegenoğlu et al. reporting 22.2% (Yeğenoğlu et al., 2006; Kop et al., 2015). In the present study, the percentage of students who smoke is higher than the smoking prevalence among individuals aged 15-24, both in Türkiye and worldwide (TÜİK, 2023; WHO, 2024). Relative to the 2015 study by Kop et al., the current prevalence among pharmacy students in Türkiye shows a slight decline, whereas relative to the 2006 study by Yegenoğlu et al., it reflects an increase; moreover, when benchmarked against international studies in student populations, smoking rates remain comparatively high. These findings indicate that awareness regarding smoking as a harmful behavior is low among pharmacy students in Türkiye.

Our findings indicate that smoking behavior among students is closely linked to several sociodemographic and familial characteristics. In particular, students who currently smoke or have smoked in the past tended to be slightly older and were more often male compared with the other groups. Living arrangements also differed across groups: those who had only experimented with smoking were more likely to reside with their families, whereas current/former smokers were less likely to do so. In addition, indicators of lower socioeconomic status were more common among students with any smoking experience than among those who had never smoked. A clear gradient was also observed for family smoking exposure, with higher proportions among experimenters and current/former smokers than among never smokers. In contrast, academic year and chronic disease status did not appear to influence smoking status. In a study of university students, the proportion of smokers was slightly higher among women than men (31.2% vs. 29.5%); however, this gender difference was not statistically significant (Milošević-Georgiev et al., 2019). In a study conducted among medical students, the probability of a student currently smoking increased significantly if there was a family member who smoked (Taher et al., 2014). The same study further reported a higher smoking prevalence among male than female students, while no statistically significant differences were observed across academic years. On the other hand, Ilic et al. reported that final-year pharmacy students were significantly more likely to smoke than younger cohorts (Ilic et al., 2020). In a study of university students, it was reported that smoking prevalence was significantly higher among individuals with lower income levels (Yurt-Öncel et al., 2011). Comparisons with the extant literature reveal heterogeneity in the associations between demographic characteristics and smoking behavior. This variation likely reflects differences in study populations (e.g., composition of student cohorts) and methodological features such as sampling frames and sample size.

The health harms of smoking rise with each additional cigarette per day and with more years of smoking (Inoue-Choi et al., 2018; 2019). And, it is well known that there is no safe level of smoking. In our study, students typically initiated cigarette use at approximately 15 years of age. Among current smokers, nearly half reported consuming more than 10 cigarettes per day, with some smoking as many as 30 per day. Considering the cumulative harms of smoking, this pattern points to moderate-to-heavy use among many pharmacy student smokers and underscores the need for targeted cessation support.

In our study, nearly 70% of current and former smokers reported at least one smoking-related health problem. The most frequently cited were oral/dental issues, respiratory symptoms, and weight-related problems. Prior studies indicate that smoking approximately doubles the risk of infectious respiratory illnesses, is associated with an 85% higher risk of periodontitis, contributes to oral mucosal lesions and tooth loss, has bidirectional effects on body weight (both gain and loss), is linked to inflammatory bowel disease, and increases the risk of peptic-ulcer recurrence (Chiolero et al., 2008; Berkowitz et al., 2018; McGeoch et al., 2023). Moreover, continued smoking is associated with the progression of these conditions over time and with an elevated long-term risk of cancer (Berkowitz et al., 2018; Leite et al., 2018; Chen, 2023; McGeoch et al., 2023). In a university-aged population, cumulative exposure is still limited; however, if smoking persists, the relatively mild problems observed are likely to progress to more serious disease over time.

Evaluations of smoking determinants among university students indicate that stress and unhappiness, peer influence, and curiosity are the most frequently cited reasons for initiation (Oğuz et al., 2018). Consistent with prior reports, students in our study most commonly cited curiosity, peer influence, and stress as reasons for smoking initiation. Addressing these modifiable determinants can change smoking trajectories. A life-course approach—improving family and environmental conditions from childhood—may prevent initiation; at the university stage, however, efforts should prioritize identifying and targeting the factors that sustain smoking (e.g., stress coping, social pressure, habit/dependence), which is crucial for effective tobacco control on campus.

Approximately three-quarters of current smokers reported at least one prior cessation attempt, and the greatest proportion had made four or more attempts in our study. Among students with prior cessation attempts, use of evidence-based cessation methods was rare. Cessation intent was likewise limited, with only one in four expressing willingness to seek cessation counseling. Across studies of university students in Türkiye, reported rates of at least one prior cessation attempt range from 45% to 77%, whereas cessation intent ranges from 27% to 60.4% (Kop et al., 2015; Ergin et al., 2016; Tarı-Selçuk et al., 2018). The smoking cessation attempts and intentions observed in our cohort are broadly similar to those reported in previous studies. Smoking cessation behavior and intention are multifactorial. In adults, key predictors include age, sex, education, health-insurance status, place of residence, and nicotine dependence (Suen et al., 2022; Al-Dahshan et al., 2023). Among adolescents and young adults, smoking behavior is significantly associated with male sex, increasing age, exposure to second-hand smoke, and favorable beliefs about smoking, such as perceiving it as socially prestigious, attractive, or difficult to quit (El Dalatony et al., 2025). Considering these age-specific determinants, cessation attempts and intentions differ between adults and young people. In our university sample, a substantial proportion had made at least one cessation attempt, yet intention to undertake further attempts was low. The limited uptake of evidence-based cessation approaches further suggests insufficient awareness of effective support options among students.

While motivation for smoking cessation is foundational, employing evidence-based cessation methods

is a key determinant of successful smoking cessation. Accordingly, smokers should possess high levels of knowledge and awareness regarding evidence-based strategies for smoking cessation.

Evidence-based approaches comprise behavioral, pharmacological, and combined modalities. Pharmacotherapies include nicotine replacement therapy (NRT), bupropion, and varenicline; behavioral interventions include cognitive-behavioral therapy, motivational interviewing, and contingency/incentive-based strategies to motivate and reinforce behavior change (Onwuzo et al., 2024). When students' perceptions of evidence-based methods were assessed, face-to-face counselling, smoking-cessation clinics, and pharmacological therapy were rated as the most effective. In a pairwise comparison of smoking cessation methods, face-to-face counseling and smoking cessation clinic interventions were rated significantly more effective than both mobile applications, posters, and printed educational materials. These results are partially consistent with previous studies. In the study conducted by Alwhaibi et al., it was determined that one-third of pharmacy faculty students found smoking cessation clinics effective (Alwhaibi et al., 2022). In a study involving university students studying health in Türkiye, an on-campus smoking cessation clinic and the idea of peer-assisted smoking cessation were evaluated as useful by more than half of the students (Ergin et al., 2016). In a meta-analysis of university students assessing the effectiveness of smoking-cessation interventions, technology-based approaches and motivational interviewing showed statistically significant effects, whereas reinforcement/reward interventions were comparatively less effective (Setchoduk et al., 2023). Students' approaches to smoking cessation methods and the real-life effectiveness of these methods appear to differ. In our study, similar to other studies, motivational interviews, such as face-to-face counseling and smoking cessation clinics, were found to be more effective than technological applications alone. These findings suggest insufficient knowledge and awareness of evidence-based smoking-cessation methods among students. If such gaps exist in health-sciences cohorts, they are likely even greater in non–health-sciences populations. These findings underscore the need to integrate structured instruction on smoking-cessation strategies into pharmacy curricula, particularly as a component of preventive health coursework.

The internal consistency of the FTND in our sample (Cronbach's $\alpha = 0.759$) was higher than that reported in the Turkish validation study ($\alpha = 0.56$). This difference may be related to the more homogeneous structure of our sample, which consisted of health sciences university students. Greater sample homogeneity is known to increase reliability coefficients.

In our study, among 46 current smokers, the median FTND score was 3, indicating low nicotine dependence. Approximately 30% of students exhibited moderate to very high nicotine dependence. In a study conducted among university students, 10.2% of the participants showed medium nicotine dependence, 15.1% exhibited high dependence, and 7.5% demonstrated very high dependence according to FTND scores (Karadag et al., 2021). In another study assessing university students' nicotine dependence, 31.4% were classified as moderately dependent and 13.4% as highly dependent (Terzi et al., 2019). In another study, the mean FTND score (± SD) among male university smokers was 4.37 ± 2.3, whereas among female smokers it was 3.90 ± 2.4 (Yurt-Öncel et al., 2011). Compared with prior studies, active smokers in our pharmacy-student sample appear to exhibit lower nicotine dependence. This disparity may reflect shorter smoking duration and fewer cigarettes per day, and could also be influenced by students' health-related training and greater awareness of tobacco harms relative to non–health sciences cohorts.

When FTND scores were compared across demographic subgroups, only having a family member who smokes was associated with a statistically significant increase in dependence scores. In contrast, gender, age, year of study, income level, and presence of a

chronic condition showed no significant associations with FTND score. In the study by Terzi et al., both the father's and the close friend's smoking levels were found to be higher in students with high nicotine addiction (Terzi et al., 2019). Öncel and colleagues reported that among university students, FTND scores increased with higher daily cigarette consumption and decreased with older age at smoking initiation (Yurt-Öncel et al., 2011). Previous studies show that FTND scores vary across populations and contexts. Even so, a clear dose-response relationship is evident: greater daily cigarette consumption is associated with higher nicotine dependence. In addition, smoking within the household remains an important risk factor, promoting initiation and increasing progression to dependence.

A key strength of this study is the combined assessment of pharmacy students' smoking behaviors with the FTND, alongside an evaluation of their perceptions of cessation methods. However, several limitations should be noted. First, the single-institution design limits the generalizability of the findings. Second, the data are based on self-reported survey responses rather than objective measurements, which may introduce reporting and recall bias. Although a census-based sampling strategy was planned, the response rate was 48.3%, which may introduce non-response bias and limit the representativeness of the findings. Moreover, subgroup analyses, particularly those involving FTND categories, should be interpreted with caution due to reduced sample sizes. The lack of multivariable regression analysis should be considered a limitation, as potential confounding and interaction effects could not be examined. Finally, the data were collected in 2022, and although the main patterns of smoking behavior remain informative, rapid developments in nicotine products and digital cessation tools may limit the direct applicability of our findings to current student populations.

CONCLUSION

In this cross-sectional sample of pharmacy students, nicotine dependence among current smokers was generally low, yet exposure to family members who smoke was associated with higher FTND scores. Although most smokers had attempted to quit at least once, engagement with evidence-based supports was limited; students perceived face-to-face counselling and smoking-cessation clinics as more effective than stand-alone technology or printed materials. Curriculum and campus initiatives that expand access to counseling and approved pharmacotherapies and strengthen students' awareness of smoking cessation methods appear to be needed.

AUTHOR CONTRIBUTION STATEMENT

Concept: N.Ö.A, N.A., Z.Ü.G.; Design: N.Ö.A, N.A., Z.Ü.G.; Supervision: Z.Ü.G.; Resources: N.A., N.Ö.A; Data Collection and/ or Processing: N.A.; Analysis and/or Interpretation: N.Ö.A., N.A., Z.Ü.G.; Literature Review: N.Ö.A.; Writing the Article: N.Ö.A; Critical Review: Z.Ü.G.

CONFLICT OF INTEREST

The authors declare that there is no conflict of interest.

REFERENCES

Al-Dahshan, A., Al-Muraikhi, H., Musa, S., Joudeh, A., Al-Baker, W., Selim, N., & Bougmiza, I. (2023). Prevalence and predictors of smoking cessation among smokers receiving smoking cessation intervention in primary care in Qatar: a 6-month follow-up study. *Front Public Health, 11*, 1166016. https://doi.org/10.3389/fpubh.2023.1166016

Alotibi, H. F., El-Moselhy, M. A., Ahmedani, E. I., & Yousef, B. A. (2025). Smoking behaviours, awareness and attitude among university students in Jeddah, Saudi Arabia: A Cross-Sectional Study. *Journal of Advances in Medical and Pharmaceutical Sciences, 27*(8), 67–77. https://doi.org/10.9734/jamps/2025/v27i8809

Alpar, R. (2022). *Uygulamalı istatistik ve geçerlik-güvenirlik.* 7. Baskı. Ankara: Detay Yayıncılık.

Alwhaibi, A., Wajid, S., Alenezi, A., Salami, Y., Alhaydan, I., Samreen, S., …Al-Arifi, M. N. (2022). Prevalence of smoking and beliefs and attitudes toward smoking habits and smoking cessation methods among pharmacy students: A Cross-Sectional Study in Saudi Arabia. *Frontiers in Public Health, 10,* 816101. https://doi.org/10.3389/fpubh.2022.816101

Alzahrani, F., Sandaqji, Y., Alharrah, A., Alblowi, R., Alrehaili, S., & Mohammed-Saeid, W. (2023). Community pharmacies' promotion of smoking cessation support services in Saudi Arabia: Examining current practice and barriers. *Healthcare, 11*(13), 1841. https://doi.org/10.3390/healthcare11131841

Berkowitz, L., Schultz, B. M., Salazar, G. A., Pardo-Roa, C., Sebastián, V. P., Álvarez-Lobos, M. M., & Bueno, S. M. (2018). Impact of cigarette smoking on the gastrointestinal tract inflammation: Opposing effects in Crohn's Disease and Ulcerative Colitis. *Frontiers in Immunology, 9,* 74. https://doi.org/10.3389/fimmu.2018.00074

Carson-Chahhoud, K. V., Livingstone-Banks, J., Sharrad, K. J., Kopsaftis, Z., Brinn, M. P., To-A-Nan, R., & Bond, C. M. (2019). Community pharmacy personnel interventions for smoking cessation. *The Cochrane Database of Systematic Reviews, 2019*(10), CD003698. https://doi.org/10.1002/14651858.

CDC. (2024). Youth and tobacco use. Retrieved from https://www.cdc.gov/tobacco/php/data-statistics/youth-data-tobacco/index.html Accessed 11 October 2025.

Chen, J. (2023). A comparative analysis of lung cancer incidence and tobacco consumption in Canada, Norway, and Sweden: A Population-Based Study. *International Journal of Environmental Research and Public Health, 20*(20), 6930. https://doi.org/10.3390/ijerph20206930

Chiolero, A., Faeh, D., Paccaud, F., & Cornuz, J. (2008). Consequences of smoking for body weight, body fat distribution, and insulin resistance. *The American Journal of Clinical Nutrition, 87*(4), 801–809. https://doi.org/10.1093/ajcn/87.4.801

Çapık, C., & Özbıçakcı, Ş. (2007). Hemşirelik yüksekokulu öğrencilerinin sigara bağımlılık düzeyleri ve etkileyen etmenler. *Uluslararası İnsan Bilimleri Dergisi, 4*(2).

Çelik, F. G. N., & Demirel, G. (2022). Impact of a coronavirus pandemic on smoking behavior in university students: An online survey in Türkiye. *Turkish Journal of Pharmaceutical Sciences, 19*(4), 416-421. https://doi.org/10.4274/tjps.galenos.2021.26985

Dai, X., Gil, G. F., Reitsma, M. B., Ahmad, N. S., Anderson, J. A., Bisignano, C.,… Gakidou, E. (2022). Health effects associated with smoking: A burden of proof study. *Nat Med, 10,* 2045-2055. https://doi.org/10.1038/s41591-022-01978-x

El Dalatony, M. M., Elkhobby, A. A., Shubayr, M. A., Monshi, S. S., Al-Zalabani, A. H., El Desouky, E. D.,… Aldossary, M. S. (2025). Prevalence and predictors of tobacco use among Saudi adolescents: the Global Youth Tobacco Survey (GYTS) 2022. *BMC Public Health, 25*(1), 2733. https://doi.org/10.1186/s12889-025-23974-9

Ergin, A., Uzun, S. U., & Bozkurt, A. İ. (2016). Knowledge and attitudes on smoking cessation techniques among healthcare professional students in Turkey. *Tob Prev Cessation, 63.*

Goriounova, N. A., & Mansvelder, H. D. (2012). Short- and long-term consequences of nicotine exposure during adolescence for prefrontal cortex neuronal network function. *Cold Spring Harbor Perspectives in Medicine, 2*(12), a012120. https://doi.org/10.1101/cshperspect.a012120

Ilic, I., Grujicic-Sipetic, S., Radovanovic, D., & Ilic, M. (2020). Cigarette smoking and e-cigarette use by pharmacy students in Serbia. *Behavioral Medicine (Washington, D.C.), 46*(1), 43–51. https://doi.org/10.1080/08964289.2018.1541863

Inoue-Choi, M., Hartge, P., Liao, L. M., Caporaso, N., & Freedman, N. D. (2018). Association between long-term low-intensity cigarette smoking and incidence of smoking-related cancer in the National Institutes of Health-AARP cohort. *International Journal of Cancer, 142*(2), 271–280. https://doi.org/10.1002/ijc.31059

Inoue-Choi, M., Hartge, P., Park, Y., Abnet, C. C., & Freedman, N. D. (2019). Association between reductions of number of cigarettes smoked per day and mortality among older adults in the United States. *American Journal of Epidemiology, 188*(2), 363–371. https://doi.org/10.1093/aje/kwy227

Karadag, M., Aydın-Guclu, O., Gorek-Dilektaslı, A., Coskun, F., & Uzaslan, E. (2021). Understanding university students' smoking behaviors towards tobacco-free campus policy. *Tuberk Toraks, 69*(1), 49-58.

Kesen-Yurtcanli, C. H., Bakar, M. T., Peker, Ş., & Ay, P. (2024). Factors related to tobacco cessation attempts among Turkish adolescents: A structural equation model analysis. *Thoracic Research and Practice, 25*(3), 197–202. https://doi.org/10.5152/ThoracResPract.2024.23129

Kop, B., Culduz, A., Kaspar, Ç., & Şencan, N. (2015). Yeditepe Üniversitesi Eczacılık Fakültesi öğrencileri sigara kullanım alışkanlıkları: Kalitatif ve kantitatif yaklaşım. *Marmara Pharmaceutical Journal, 19*(1), 36-42. https://doi.org/10.12991/mpj.2015198608

Leite, F. R. M., Nascimento, G. G., Scheutz, F., López, R. (2018). Effect of smoking on periodontitis: A systematic review and meta-regression. *American Journal of Preventive Medicine, 54*(6), 831–841. https://doi.org/10.1016/j.amepre.2018.02.014

McGeoch, L. J., Ross, S., Massa, M. S., Lewington, S., & Clarke, R. (2023). Cigarette smoking and risk of severe infectious respiratory diseases in UK adults: 12-year follow-up of UK biobank. *Journal of Public Health (Oxford, England), 45*(4), e621–e629. https://doi.org/10.1093/pubmed/fdad090

Milošević-Georgiev, A., Kotur-Stevuljević, J., & Krajnović, D. (2019). Socio-demographic factors associated with smoking habits among university students in Belgrade, Serbia. *Zdravstveno Varstvo, 58*(1), 11–20. https://doi.org/10.2478/sjph-2019-0002

Odukoya, O. O., Poluyi, E. O., Aina, B., Ejekam, C., & Faseru, B. (2016). Pharmacist-led smoking cessation: The attitudes and practices of community pharmacists in Lagos state, Nigeria. A mixed methods survey. *Tobacco Prevention & Cessation, 2,* 2. https://doi.org/10.18332/tpc/61546

Oğuz, S., Çamcı, G., & Kazan, M. (2018). The prevalence of cigarette smoking and knowing status for diseases caused by smoking among students of university. *Van Med J, 25*(3), 332-337. https://doi.org/10.5505/vtd.2018.02411

Onwuzo, C. N., Olukorode, J., Sange, W., Orimoloye, D. A., Udojike, C., Omoragbon, L., …Joseph-Erameh, U. (2024). A review of smoking cessation interventions: Efficacy, strategies for implementation, and future directions. *Cureus, 16*(1), e52102. https://doi.org/10.7759/cureus.52102

Rahman, A., Mambali, M., Keshavarzi, F., Baig, M. A. I., Hariadha, E., & Farrukh, M. J. (2022). Evaluation of smoking prevalence, secondhand smoke exposure, attitudes of tobacco control, and smoking cessation knowledge among pharmacy and medical students in a private university, Malaysia. *Journal of Pharmacy And Bioallied Sciences 14*(1), 38-45. https://doi.org/10.4103/jpbs.jpbs_334_21

Setchoduk, K., Pichayapinyo, P., Lapvongwatana, P., & Chansatitporn, N. (2023). The effectiveness of tobacco cessation programs for university students: A systematic review and meta-analysis. *Tobacco-induced Diseases, 21,* 73. https://doi.org/10.18332/tid/162001

Suen, L. W., Rafferty, H., Le, T., Chung, K., Straus, E., Chen, E., & Vijayaraghavan, M. (2022). Factors associated with smoking cessation attempts in a public, safety-net primary care system. *Preventive Medicine Reports, 26,* 101699. https://doi.org/10.1016/j.pmedr.2022.101699

Taheri, E., Ghorbani, A., Salehi, M., & Sadeghnia, H. R. (2014). Cigarette smoking behavior and the related factors among the students of Mashhad University of Medical Sciences in Iran. *Iranian Red Crescent Medical Journal, 17*(1), e16769. https://doi.org/10.5812/ircmj.16769

Tarı-Selçuk, K., Avcı, D., & Mercan, Y. (2018). Smoking addiction among university students and the willingness and self-efficacy to quit smoking. *Clinical and Experimental Health Sciences, 8*(1), 36-43.

Terzi, Ö., Kumcağız, H., & Dündar, C. (2019). Cigarette smoking and determination of nicotine dependence levels in university students. *Addicta, 6,* 168-181.

Tidey, J. W. (2020). Advancing our understanding of tobacco use in vulnerable populations. *Nicotine Tob Res, 22*(6), 865-866. https://doi.org/10.1093/ntr/ntaa045

Tunçdemir, A. (2009). *Adıyaman Üniversitesi öğrencilerinde sigara içme prevalansı araştırması*. (Master's thesis). İnönü University, Institute of Health Sciences, Department of Nursing, Public Health Nursing Division

TÜİK. (2023). Türkiye sağlık araştırması 2022. Retrieved from https://data.tuik.gov.tr/Bulten/Index?p=Turkiye-Saglik-Arastirmasi-2022-49747 Accessed 11 October 2025.

Ulukoca, N., Gökgöz, Ş., & Karakoç, A. (2013). Kırklareli Üniversitesi öğrencileri arasında sigara, alkol ve madde kullanım sıklığı. *Fırat Tıp Dergisi, 18*(4), 230-234.

Uysal, M. A., Kadakal, F., Karsidag, C., Bayram, G., Uysal, O., & Yilmaz, V. (2025). Fagerstrom test for nicotine dependence: Reliability in a Turkish sample and factor analysis. *Tüberküloz ve Toraks Dergisi, 52*(2), 115-121.

West, R. (2017). Tobacco smoking: Health impact, prevalence, correlates, and interventions. *Psychol Health, 32(8),* 1018-1036. doi: 10.1080/08870446.2017.1325890

WHO. (2024). WHO global report on trends in prevalence of tobacco use 2000–2030. Retrieved from https://www.who.int/publications/i/item/9789240088283 Accessed 11 October 2025.

Yegenoglu, S., Aslan, D., Erdener, S. E., Acar, A., & Bilir, N. (2006). What is behind smoking among pharmacy students: a quantitative and qualitative study from Turkey. *Substance Use & Misuse, 41*(3), 405–414. https://doi.org/10.1080/10826080500409142

Yurt-Öncel, S., Gebizlioğlu, Ö. L., & Aliev-Alioğlu, F. (2011). Risk factors for smoking behavior among university students. *Turk J Med Sci, 41*(6), 1071-1080.

FABAD J. Pharm. Sci., 51, 1, 207-222, 2026
Doi: 10.55262/fabadeczacilik.1843398
RESEARCH ARTICLE

A Cross-Sectional Survey on the Attitudes of Future Pharmacists Towards Phytotherapeutic Product Use and Safety

Suheda Rumeysa OSMANLIOGLU DAG[*°], Ceyhan CERAN SERDAR[**], Seyma YIGITBASI[***], Iffet Irem TATLI CANKAYA[****]

A Cross-Sectional Survey on the Attitudes of Future Pharmacists Towards Phytotherapeutic Product Use and Safety

SUMMARY

Phytotherapeutic products are widely used in both traditional and modern healthcare systems and are often perceived as risk-free due to their natural origin. However, a lack of adequate education, particularly among future healthcare professionals, can lead to significant safety concerns. This study aimed to evaluate the knowledge, attitudes, and perceptions of pharmacy students regarding the safe use of herbal products. A cross-sectional survey was conducted with 274 students enrolled in a Faculty of Pharmacy in Türkiye. A validated 57-item Likert-type scale was used to assess four key factors: common usage scenarios, safety and regulatory knowledge, practices related to obtaining and using herbal products, and risk perception with a professional approach. Findings revealed that only 26.3% of the students had previously received education on herbal products, while 85% expressed interest in such training. Male students scored significantly higher in common use (Factor 1, p = .023), and safety and regulatory knowledge (Factor 2, p = .002), whereas female students scored significantly higher in risk perception (Factor 4, p = .039). Age was not a significant factor. Notably, fourth-year students had lower scores in risk perception, indicating a possible curriculum gap during the clinical transition phase. Students who had prior education scored significantly higher in risk awareness. The scale showed high internal consistency (Cronbach's α = 0.908). These results highlight the need for structured and evidence-based phytotherapy education within pharmacy curricula, particularly during critical periods such as clinical training. Correcting the misconception that "natural" equals "safe" and ensuring students gain the competence to guide patients effectively is essential for promoting medication safety and supporting informed patient decisions.

Keywords: *Pharmacy, pharmacy students, phytotherapy, attitude, herbal products, education.*

Geleceğin eczacılarının bitkisel ürünlerin kullanımı ve güvenliğine yönelik tutumları üzerine kesitsel bir anket çalışması

ÖZ

Fitoterapötik ürünler hem geleneksel hem de modern sağlık sistemlerinde yaygın biçimde kullanılmakta ve doğal kökenli olmaları nedeniyle çoğu zaman risksiz olarak algılanmaktadır. Ancak yeterli bilgiye sahip olunmaması, özellikle sağlık profesyoneli adayları arasında, önemli güvenlik risklerine yol açabilir. Bu çalışma, Türkiye'de bir eczacılık fakültesinde öğrenim gören 274 öğrencinin bitkisel ürünlerin güvenli kullanımı konusundaki bilgi, tutum ve algılarını değerlendirmeyi amaçlamıştır. Kesitsel olarak yürütülen çalışmada, dört temel faktörü içeren (yaygın kullanım, güvenlik/mevzuat bilgisi, kullanım uygulamaları ve risk algısı/mesleki yaklaşım) ve 57 maddeden oluşan geçerli ve güvenilir bir Likert tipi ölçek kullanılmıştır. Bulgular, öğrencilerin yalnızca %26,3'ünün bitkisel ürünler konusunda daha önce eğitim aldığını, ancak %85'inin bu eğitimi almak istediğini göstermiştir. Erkek öğrenciler yaygın kullanım (Faktör 1, p = .023) ile güvenilirlik ve denetim (Faktör 2, p = .002) boyutlarında anlamlı derecede daha yüksek puan alırken, kadın öğrenciler risk algısı (Faktör 4, p = .039) boyutunda anlamlı derecede daha yüksek puan almıştır. Yaş değişkeni anlamlı fark yaratmamıştır. Dördüncü sınıf öğrencilerinin risk algısı puanlarında belirgin bir düşüş gözlenmiş, bu durum müfredattaki klinik geçiş sürecinde bir boşluk olabileceğini düşündürmüştür. Eğitim almış öğrenciler risk farkındalığında anlamlı olarak daha yüksek puanlar elde etmiştir. Ölçeğin iç tutarlılığı oldukça yüksektir (Cronbach's α = 0,908). Sonuçlar, eczacılık müfredatına yapılandırılmış, kanıta dayalı fitoterapi eğitiminin entegrasyonunun gerekliliğini ortaya koymaktadır.

Anahtar Kelimeler: *Eczacılık, eczacılık öğrencileri, fitoterapi, tutum, bitkisel ürünler, eğitim.*

Recieved: 17.12.2025
Revised: 7.02.2026
Accepted: 16.02.2026

[*] ORCID: 0000-0002-0243-3454, Department of Pharmaceutical Botany, Faculty of Pharmacy, Inonu University, Malatya, Turkiye
[**] ORCID: 0000-0002-2921-7030, Department of Medical Biology and Genetics, School of Medicine, Ankara Medipol University, Ankara, Turkiye
[***] ORCID: 0009-0006-0962-7362, Faculty of Pharmacy, Inonu University, Malatya, Turkiye
[****] ORCID: 0000-0001-8531-9130, Department of Pharmaceutical Botany, Faculty of Pharmacy, Hacettepe University, Ankara, Turkiye

[°] Corresponding Author; Suheda Rumeysa OSMANLIOGLU DAG
E-mail: rumeysa.osmanlioglu@inonu.edu.tr

INTRODUCTION

Phytotherapeutic products are medicinal preparations derived from plants or plant parts, and used for the prevention or treatment of diseases based on traditional knowledge and scientific evidence. These products include herbal medicines, standardized plant extracts, and medicinal teas, and they constitute a major component of traditional and complementary medicine systems worldwide (WHO, 2019). Traditional medicine remains an integral part of healthcare delivery, particularly in low- and middle-income countries, but its use has also increased substantially in developed societies due to cultural acceptance, accessibility, and patient preference for "natural" therapies (Ekor, 2014; Tilburt & Kaptchuk, 2008). The WHO estimates that a significant proportion of the global population relies on traditional medicine as a primary or complementary healthcare modality, underscoring the continued relevance of phytotherapeutic products in modern medical practice (WHO, 2019).

Despite their widespread use, phytotherapeutic and other natural products are commonly perceived by the public as inherently safe due to their natural origin. This assumption represents a critical misconception, as numerous studies have demonstrated that herbal products may cause adverse reactions, toxicity, contamination-related harm, and clinically significant herb–drug interactions (Izzo, Hoon-Kim, Radhakrishnan, & Williamson, 2016; Posadzki, Watson, & Ernst, 2013). The lack of stringent regulatory oversight in many countries further contributes to variability in product quality, composition, and labeling accuracy, increasing the risk of inappropriate use (Barnes, Anderson, & Phillipson, 2007; Heinrich, Barnes, Prieto-Garcia, Gibbons, & Williamson, 2017). Consequently, the irrational use of phytotherapeutic products may compromise patient safety, particularly among individuals with chronic diseases, polypharmacy, or vulnerable physiological conditions.

Healthcare professionals play a central role in ensuring the rational, safe, and evidence-based use of phytotherapeutic products. Among these professionals, pharmacists are uniquely positioned due to their accessibility, pharmacological expertise, and frequent involvement in patient counseling. Studies conducted among community pharmacists in various countries have evaluated their knowledge, attitudes, and practices related to complementary and alternative medicines, revealing significant gaps in safety awareness and patient counseling behaviors. Strengthening pharmacists' competence in this area is therefore essential for improving medication safety and promoting informed patient decision-making (Abudalo et al., 2022; Hijazi et al., 2019; Naja et al., 2024; Thin et al., 2022).

Survey-based studies have been widely used to assess knowledge, attitudes, and practices related to phytotherapeutic product use among healthcare professionals, including physicians, pharmacists, and nurses (Hilal & Hilal, 2017; Jafari, Zanganeh, Kazemi, Lael-Monfared, & Tehrani, 2021; Tahir et al., 2023). However, research focusing specifically on healthcare students, particularly pharmacy students, remains comparatively limited. This gap is noteworthy, as students represent future healthcare providers whose attitudes and preparedness will directly influence clinical practice and patient safety.

In light of these considerations, the present study conducts a cross-sectional survey to examine the knowledge, attitudes, and perceptions of future pharmacists regarding the use and safety of phytotherapeutic products. By investigating the factors that shape these attitudes within a population whose professional identity is rooted in medication expertise, this study aims to address a critical gap in pharmacy education. Through this approach, we seek to generate evidence-based insight into students' preparedness to provide safe and informed guidance on phytotherapeutic therapies and to identify areas in which curricular reinforcement may be required.

MATERIALS AND METHODS

Study design

This study was conducted as a quantitative, cross-sectional, survey-based empirical investigation to assess the knowledge and attitudes toward the safe use of herbal products among pharmacy students. The research was carried out at the Faculty of Pharmacy, İnönü University, Türkiye. A cross-sectional approach was selected to capture measurable data on attitudes and perceptions at a single point in time, allowing for the exploration of associations between key demographic and behavioral variables (Creswell & Creswell, 2017). A 5-point Likert-type scale was employed to quantify participants' attitudes toward the safe use of herbal products, as such instruments are widely validated for measuring behavioral tendencies and belief systems (DeVellis & Thorpe, 2021). Furthermore, the online survey format was chosen to ensure wide accessibility among students and to encourage more honest and unbiased responses through perceived anonymity (Wright, 2005).

Study setting and timeline

The study was conducted at the Faculty of Pharmacy, İnönü University, located in Malatya, Türkiye. Data collection occurred between 1 November and 1 December 2025. An online survey (Google Forms) was employed to facilitate anonymous participation, reduce response bias, and enable access to students across different academic years.

Study population and sampling

The target population for this study comprised all currently enrolled undergraduate students (Years 1–5) at the Faculty of Pharmacy, İnönü Universitytrkey, during the study period (N = 536). A census sampling approach was adopted, aiming to invite the entire student population rather than employing random sampling methods. The minimum required sample size was determined to be 200 participants, based on reliability considerations for scale validation and supported by G*Power analysis (alpha error probability = 0.05, statistical power = 0.80, and a medium effect size assumption). The primary inclusion criterion was active enrollment in the Faculty of Pharmacy at İnönü University. Questionnaires with incomplete or missing responses were excluded from the final analysis, which constituted an implicit exclusion criterion. No other exclusion criteria were applied.

Data collection instrument

The data was collected using an electronic questionnaire comprised of two main instruments.

Demographic information form

This form included five items gathering basic information on participants' age, gender, year of study, prior formal education on herbal products, and interest in receiving further education on this subject. Prior formal education was defined as having received structured training on herbal products either within the undergraduate pharmacy curriculum (e.g., compulsory or elective courses) or outside the university setting through certified or officially recognized educational programs. These items were included for descriptive purposes only and were not part of the validated scale.

Attitudes toward safe use of herbal products scale

Attitudes towards the safe use of herbal products were assessed using the 57-item, 5-point Likert scale developed and validated by Yıldız (2021). The instrument was originally developed for use among healthcare professionals (including physicians and nurses) to reveal their knowledge, attitudes, and behaviors regarding herbal products. The scale's construct validity was confirmed through Explanatory Factor Analysis (EFA), which demonstrated that the 57 items were gathered into four sub-dimensions explaining 40.263% of the total variance (Yıldız, 2021). These four subdimensions cover:

- Frequent use scenarios of herbal products
- Safety and regulatory perception
- Practices related to the collection, purchase, and usage of herbs

- Risk perceptions and healthcare professionals' attitudes

The original study reported high item-total score correlation and strong internal consistency, confirming the scale's reliability. In the present study, the original validated scale was used without modification. No additional items were added to the scale, and all psychometric analyses were conducted exclusively using the original 57 items. The questionnaire items were derived from the original validated scale; however, to preserve the integrity of the assessment tool and in accordance with ethical considerations regarding intellectual property, the full item set is not reproduced in this manuscript. The original instrument is publicly accessible through the cited source. In the present study, the scale's psychometric properties—specifically its internal consistency (Cronbach's alpha) and factorial structure—will be re-evaluated within a pharmacy student population to ensure its continued validity for this specific target group.

Data collection procedure

Data collection was performed via an online platform (Google Forms) to ensure broad reach and participant anonymity. Access to the questionnaire was granted only after the participants provided informed consent digitally. The estimated completion time for the survey was 15–20 minutes. To maintain data quality and prevent duplicate entries, each participant was intended to receive a single-use link, and only one response per IP address was accepted.

Variables

The study utilized the following variables for analysis.

Dependent Variable: The primary dependent variable was the Total attitude score towards the safe use of herbal products (continuous variable).

Independent Variables: Key independent variables examined for their potential influence on attitudes included Gender (categorical: binary), Year of study (categorical: 5 levels), and Status of prior education on herbal products (categorical: binary).

Statistical analysis

Data analysis will be performed using SPSS version 26.0. The significance threshold for all inferential tests was set at $p < 0.05$.

Descriptive statistics

Frequencies, percentages, means, and standard deviations will be reported for all relevant demographic and scale variables.

Inferential statistics

To compare differences in attitude scores across groups, appropriate inferential tests will be selected based on the assessment of data distribution characteristics: For comparisons based on binary variables (Gender and prior education), the Independent samples t-test (parametric) or the Mann–Whitney U test (non-parametric) was used. For comparisons across multiple groups (Year of study), the One-way ANOVA with Tukey HSD post-hoc test (parametric)was employed.

Reliability and validity analysis

Internal consistency of the attitude scale will be assessed using Cronbach's alpha (α) coefficient, with $\alpha \geq 0.70$ indicating acceptable reliability.

Study limitations

The primary limitation of the study is the reliance on self-reported data collected online, which may introduce response bias or variability in participation. However, the full population recruitment strategy (census) and the anonymity of the data collection process are expected to mitigate these risks.

Ethics approval

This study was approved by the Ethics Committee of İnönü University (2025/8100). Participants' informed consent was obtained before the survey questions.

RESULTS

A total of 274 pharmacy students participated in the study. Of these, 198 (72.3%) were female, and 76 (27.7%) were male, with a mean age of 20.90 ±1.87

years. When asked about prior exposure to education or training on the safe use of herbal phytotherapeutic products, 72 students (26.3%) reported having received such training, while 202 students (73.7%) indicated no prior experience. Despite the low prior exposure, interest in receiving education on this topic was notably high: 233 students (85.0%) expressed a willingness to take a course or training on the safe use of herbal products, whereas only 41 students (15.0%) declined (Figure 1.). These findings suggest a significant educational gap alongside a strong demand for structured learning opportunities in the area of herbal product safety among pharmacy students.

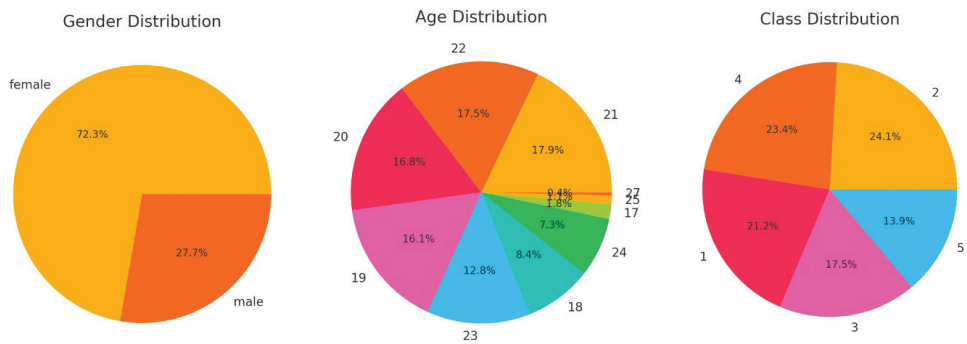


Figure 1. Demographic Distribution of the Pharmacy Student Sample.

Figure 2 presents the gender-based distribution of the study's pharmacy students (N=274) across four educational categories concerning herbal products. Female students constitute the vast majority across the entire sample and consistently represent the largest group in all categories examined. Specifically, 56 female and 16 male students reported having received prior formal education on herbal products. Conversely, the largest segment was the group that had not taken such a course (142 females, 60 males). Crucially, a significantly high level of interest in future education was observed, with 233 students (85% of the total sample) indicating their willingness to enroll in a course on the safe use of herbal products; this cohort comprised 168 females and 65 males. Only a small minority (30 females, 11 males) expressed no desire to pursue this specialized education. These findings underscore that female pharmacy students dominate both the current educational engagement and the prospective interest in herbal product studies within this population.

The reliability analysis demonstrated that all four factors exhibited acceptable to excellent internal consistency. Cronbach's alpha coefficients were .931 for Factor 1 (Common Situations Where Herbal Products Are Frequently Used), .756 for Factor 2 (Safety and Regulation of Herbal Products), .878 for Factor 3 (Harvesting, Purchasing, and Use of Medicinal Plants), and .861 for Factor 4 (Risks of Herbal Products and the Healthcare Professionals' Approach). The overall reliability for the total scale (57 items) was high ($\alpha = .908$), indicating strong internal consistency across all items (Table 1.).

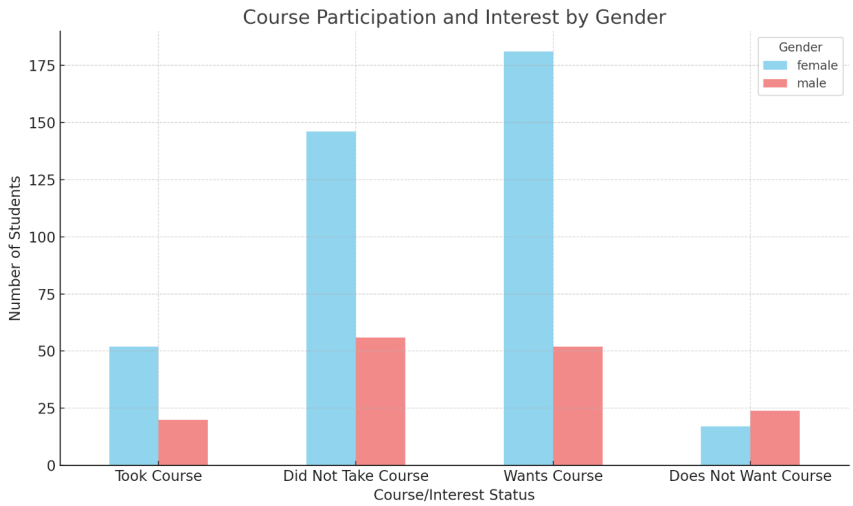


Figure 2. Distribution of Course Participation and Interest by Gender

Table 1. Internal consistency reliability of the attitude scale and its subscales as assessed by Cronbach's alpha coefficients.

Factor	Factor name	n	Cronbach's Alpha
Factor 1	Frequent use scenarios of herbal products	17	.931
Factor 2	Safety and Regulation of Herbal Products	18	.756
Factor 3	Practices related to the collection, purchase, and usage of herbs	14	.878
Factor 4	Risk perceptions and healthcare professionals' attitudes	8	.861
Total		57	.908

In terms of gender-based differences (Table 2.), statistically significant differences were found in Factors 1, 2, and 4. Male students scored significantly higher than females in Factor 1 (M = 65.14 vs. 61.35, p = .023) and Factor 2 (M = 64.63 vs. 60.13, p = .002) whereas female students scored significantly higher in Factor 4 (M = 34.84 vs. 33.61, p = .039). No significant difference was observed in Factor 3 (p = .387). These results suggest that male students tend to report slightly higher agreement with statements related to common usage situations, regulatory aspects, and risk perception of herbal products compared to their female counterparts.

Table 2. Comparison of attitude scale factor scores according to gender.

	Gender	N	Mean	Std. Deviation	Std. Error Mean	p value
Factor 1	Female	198	61.3485	12.43235	.88353	.023
	Male	76	65.1447	11.85547	1.35992	
Factor 2	Female	198	60.1313	7.48080	.53164	.002
	Male	76	64.6316	11.69369	1.34136	
Factor 3	Female	198	55.6263	5.55011	.39443	.387
	Male	76	54.7763	7.81554	.89650	
Factor 4	Female	198	34.8434	4.21392	.29947	.039
	Male	76	33.6053	4.95602	.56849	

When comparing students based on age (Table 3.), no statistically significant differences were found across any of the four factors ($p > .05$). Students younger than 20 and those aged 20 and above showed similar levels of response in all domains, indicating that age was not a discriminating variable in perceptions or knowledge levels regarding herbal products.

Table 3. Comparison of attitude scale factor scores according to age group (<20 years vs. ≥20 years)

	Age	N	Mean	Std. Deviation	Std. Error Mean	p value
Factor 1	<20	118	62.0169	12.20479	1.12354	.655
	≥20	156	62.6923	12.52693	1.00296	
Factor 2	<20	118	61.7881	8.17423	.75250	.517
	≥20	156	61.0705	9.68545	.77546	
Factor 3	<20	118	55.9322	5.45334	.50202	.200
	≥20	156	54.9808	6.79133	.54374	
Factor 4	<20	118	35.0085	4.03509	.37146	.101
	≥20	156	34.1154	4.72872	.37860	

When comparing factor scores across class levels (1st through 5th year students), no statistically significant differences were observed for Factor 1 ($p = .799$), Factor 2 ($p = .102$), or Factor 3 ($p = .160$) (Table 4.), indicating relatively consistent perceptions of commonly encountered herbal product usage scenarios, regulatory understanding, and knowledge related to harvesting and purchasing practices across academic years.

However, for Factor 4 (Risk perceptions and healthcare professionals' attitudes), a statistically significant difference was found ($p = .002$). Notably, 4th-year students scored lower (M = 32.53) than students in other years (e.g., 1st-year: M = 35.29; 5th-year: M = 35.37), suggesting a potential gap or decreased awareness regarding risk-related aspects of herbal products during this academic phase.

Table 4. Comparison of attitude scale factor scores across academic year (class level)

	Class	N	Mean	Std. Deviation	Std. Error Mean	p value
Factor 1	1	58	63.7069	12.02484	1.57894	.799
	2	66	62.1515	14.09009	1.73437	
	3	48	60.7292	11.85684	1.71139	
	4	64	62.8906	12.21516	1.52689	
	5	38	62.1316	10.87067	1.76346	
	Total	274	62.4015	12.37122	.74737	
Factor 2	1	58	62.7759	9.40333	1.23472	.102
	2	66	61.2727	8.05471	.99147	
	3	48	62.8542	11.36435	1.64030	
	4	64	61.0625	9.00771	1.12596	
	5	38	58.1053	5.97648	.96951	
	Total	274	61.3796	9.05670	.54714	

	Class	N	Mean	Std. Deviation	Std. Error Mean	p value
Factor 3	1	58	56.0862	6.14813	.80729	.160
	2	66	56.0303	5.02599	.61866	
	3	48	55.7708	8.11943	1.17194	
	4	64	53.6563	5.79605	.72451	
	5	38	55.6579	6.19623	1.00516	
	Total	274	55.3905	6.25737	.37802	
Factor 4	1	58	35.2931	4.24681	.55763	**.002**
	2	66	34.8485	3.66792	.45149	
	3	48	35.0000	4.27262	.61670	
	4	64	32.5313	5.03943	.62993	
	5	38	35.3684	4.44438	.72097	
	Total	274	34.5000	4.45757	.26929	

Comparisons based on prior education or training on herbal products revealed a statistically significant difference in Factor 3 (Harvesting, Purchasing, and Use of Medicinal Plants), with students who had prior education scoring higher than those without (M = 56.65 vs. 54.94, p = .046) (Table 5.). No statistically significant differences were observed in Factors 1, 2, or 4 (p > .05).

Table 5. Comparison of attitude scale factor scores according to prior education on herbal products.

	Prior Education on Herbal Products	N	Mean	Std. Deviation	Std. Error Mean	p value
Factor 1	Yes	72	61.7500	12.70993	1.49788	**.604**
	No	202	62.6337	12.27198	.86345	
Factor 2	Yes	72	61.1667	8.87789	1.04627	**.817**
	No	202	61.4554	9.14017	.64310	
Factor 3	Yes	72	56.6528	5.64728	.66554	**.046**
	No	202	54.9406	6.41410	.45129	
Factor 4	Yes	72	35.2083	4.40530	.51917	**.117**
	No	202	34.2475	4.45967	.31378	

Comparisons based on interest in receiving education on herbal products showed a statistically significant difference in Factor 4 (Risks of Herbal Products and the Healthcare Professionals' Approach), with students who expressed interest scoring higher than those who did not (M = 34.85 vs. 32.49, p = .021) (Table 6.). No statistically significant differences were observed in Factors 1–3 (p > .05).

Table 6. Comparison of attitude scale factor scores according to interest in receiving education on herbal products.

	Interest in receiving education	N	Mean	Std. Deviation	Std. Error Mean	p value
Factor 1	Yes	233	62.0386	12.29849	.80570	.248
	No	41	64.4634	12.73400	1.98872	
Factor 2	Yes	233	61.0558	8.49855	.55676	.263
	No	41	63.2195	11.69725	1.82680	
Factor 3	Yes	233	55.7082	5.60717	.36734	.151
	No	41	53.5854	8.99715	1.40512	
Factor 4	Yes	233	34.8541	4.00809	.26258	.021
	No	41	32.4878	6.12830	.95708	

DISCUSSION

The present cross-sectional survey examined the attitudes of pharmacy students at İnönü University toward the safe use of phytotherapeutic products, revealing important insights into educational preparedness, gender-based differences, and the influence of prior training. The findings underscore both the strengths and gaps in current pharmacy education regarding herbal medicine safety and highlight the need for curriculum enhancement in this domain.

A striking finding of this study was the substantial educational gap coupled with overwhelming student interest in phytotherapy training. Only 26.3% of participants reported having received prior education on the safe use of herbal products, yet 85.0% expressed willingness to undertake formal training in this area. This pattern aligns closely with international evidence demonstrating consistent student demand for complementary and alternative medicine (CAM) education despite inadequate curricular coverage (Abd Wahab, Sakthong, & Winit-Watjana, 2016; Ogaji, Lubayo, & Aliyu, 2021). In Nigeria, 99.1% of pharmacy students supported adding CAM topics to the undergraduate curriculum (Ibrahima & Lawal, 2022), while 89.1% of U.S. pharmacy students and pharmacists desired more instruction in herbal products (Mahmoud, Yousif, & Arbab, 2024). The convergence of these findings across diverse educational contexts suggests a global recognition among future pharmacists that phytotherapy competence is essential for contemporary practice, yet formal training opportunities remain insufficient. The high level of interest observed in the present study may reflect students' awareness of the prevalence of herbal product use in clinical practice and their anticipated role in patient counseling. Given that herbal medicines constitute a major component of healthcare delivery worldwide, particularly in Türkiye, where traditional medicine maintains cultural significance, pharmacy students appear to recognize the professional imperative to develop evidence-based competence in this area. This readiness to learn represents a valuable opportunity for curriculum developers to integrate structured phytotherapy education that addresses both efficacy and safety considerations.

The present study identified statistically significant gender differences across multiple dimensions of herbal product attitudes. Male students scored significantly higher than females in Factor 1 (common usage situations) and Factor 2 (safety and regulation), whereas females scored significantly higher in Factor 4 (risk perception and professional approach) ($p = .039$). These findings contrast with the heterogeneous pattern of gender effects reported in international literature, where results vary by country, cultural context, and specific CAM modality (Ahmad et al., 2015; James & Bah, 2014; Jamshed, Khan, Ahmad, & Elkalmi, 2016).

In some settings, male pharmacy students demonstrated more favorable attitudes toward traditional medicine systems. For instance, male final-year pharmacy students in Andhra Pradesh, India, were significantly more likely to hold positive beliefs about AYUSH (Ayurveda, Yoga, Unani, Siddha, and Homeopathy) medicines (OR = 4.62, 95% CI: 2.37–8.99) compared to females (Ahmad et al., 2015). Conversely, Malaysian pharmacy students revealed that females were more likely to express cautious safety perceptions regarding CAM use (p = 0.007) (Jamshed et al., 2016). On the other hand, in Sierra Leone, no significant difference in the overall positive attitude toward CAM was observed between male and female undergraduate pharmacy students (James & Bah, 2014).

The higher scores among male students in the present study, particularly in safety and regulatory domains (Factor 2), may reflect differential exposure to information sources, varying levels of engagement with pharmacological coursework, or distinct patterns of health-seeking behavior. However, the absence of a universal directional pattern in the literature suggests that gender differences in herbal medicine attitudes are shaped by complex interactions between cultural norms, educational exposure, and individual experiences rather than inherent biological or psychological factors. Further qualitative research is warranted to elucidate the mechanisms underlying these gender-based variations in the Turkish pharmacy education context.

No statistically significant differences were observed between students younger than 20 years and those aged 20 and above across any of the four attitude factors. This finding suggests that chronological age within the narrow range of undergraduate pharmacy students does not substantially influence perceptions of herbal product use and safety. The homogeneity of attitudes across age groups may reflect the relatively uniform life stage and educational exposure of undergraduate students, who typically progress through the curriculum at similar developmental phases. This result underscores that educational interventions targeting herbal medicine competence need not be age-differentiated within the pharmacy student population but should instead focus on year of study and prior training exposure as more relevant stratification variables.

Analysis across class levels revealed a concerning pattern: while Factors 1, 2, and 3 showed no significant differences across academic years, Factor 4 (risk perceptions and healthcare professionals' attitudes) demonstrated significant variation (p = 0.002), with fourth-year students scoring notably lower (M = 32.53) compared to first-year (M = 35.29) and fifth-year students (M = 35.37). This U-shaped pattern suggests a potential gap in risk awareness during the fourth year of pharmacy education, precisely when students are preparing for clinical rotations and patient-facing responsibilities.

Several explanations may account for this phenomenon. Fourth-year students may be experiencing curriculum overload focused on conventional pharmacotherapy, inadvertently deprioritizing attention to complementary medicine safety. Alternatively, the transition from theoretical learning to clinical preparation may create cognitive dissonance, wherein students prioritize evidence-based conventional treatments while temporarily undervaluing the clinical significance of herbal product risks. This finding is particularly concerning given that inadequate awareness of herb-drug interactions and adverse effects represents a major patient safety issue (Barnes et al., 2007; Heinrich et al., 2020). Studies have documented that over half of medical students are unaware that herbs can cause herb-drug interactions, and only 38.6% of Malaysian pharmacy students correctly answered questions about herbal product use with digoxin (Heinrich et al., 2020; Jamshed et al., 2016).

The recovery of risk awareness in fifth-year students may reflect the impact of clinical exposure, where real-world patient encounters reinforce the im-

portance of comprehensive medication history-taking, including herbal products. However, the temporary decline in fourth-year students warrants targeted curriculum intervention to ensure continuous reinforcement of herbal product safety throughout the educational continuum.

Students who had received prior education on herbal products scored significantly higher in Factor 3 (Harvesting, Purchasing, and Use of Medicinal Plants) compared to those without such training ($p = .046$) (Table 5.). In addition, students who expressed interest in receiving further education scored significantly higher in Factor 4 (risk perception and professional approach) ($p = .021$) (Table 6.). Together, these findings provide empirical support for the value of structured phytotherapy education and for students' motivation to engage with herbal product safety. The positive association between prior training and risk awareness aligns with international evidence demonstrating that curricular exposure improves students' knowledge, attitudes, and readiness for clinical integration of herbal medicine guidance (AbouZid, 2015; Hasen & Hashim, 2021). Furthermore, studies examining health professionals' awareness of herbal medicine safety reveal that having formal training is significantly associated with a higher awareness status, highlighting the role of education in promoting safer practices and better patient risk assessment, while Egyptian pharmacy students participating in active learning assignments reported improved knowledge and communication skills regarding herbal products (Thin et al., 2022). These findings collectively reinforce the principle that structured, evidence-based education—rather than incidental exposure or personal use—is essential for developing professional competence in phytotherapy counseling. However, the absence of significant differences in Factors 1, 2, and 3 suggests that prior education may have been narrowly focused on safety and risk aspects without comprehensively addressing common usage scenarios, regulatory frameworks, or practical harvesting and purchasing considerations. This highlights the need for holistic curriculum design that integrates multiple dimensions of herbal product knowledge, including efficacy evidence, quality assurance, legal regulation, and patient communication strategies.

The attitude scale demonstrated strong psychometric properties within the pharmacy student population, with Cronbach's alpha coefficients ranging from 0.756 to 0.931 for individual factors and 0.908 for the overall scale. These values indicate acceptable to excellent internal consistency, confirming the reliability of the instrument for assessing pharmacy students' attitudes toward herbal product safety. The successful adaptation of Yıldız's (2021) scale, originally developed for healthcare professionals, to a student population validates its applicability across different stages of professional development and supports its use in future educational research.

A critical issue highlighted by the literature and relevant to the present findings is the persistent misconception that herbal products are inherently safe due to their natural origin. Studies have documented that 46.85% of medical students considered herbal medicines risk-free (Heinrich et al., 2020), and community pharmacists reported alarmingly low rates of routine herbal product counseling: 50% never or rarely ask patients about herbal use, 80% rarely or never document it, and only 25% always discuss potential side effects (Braun & Cohen, 2014). This gap between perceived safety and actual risk represents a significant threat to patient safety, particularly given the well-documented potential for herb-drug interactions, contamination, adulteration, and adverse effects associated with phytotherapeutic products (Izzo et al., 2016; Moreira, Teixeira, Monteiro, De-Oliveira, & Paumgartten, 2014; Posadzki et al., 2013).

The present study's findings regarding risk perception (Factor 4) suggest that Turkish pharmacy students recognize the importance of professional caution regarding herbal products, particularly when they have received formal training. However, the lower scores among fourth-year students and those without

prior education indicate that this awareness is fragile and requires continuous reinforcement throughout the curriculum. Pharmacy educators must explicitly address the "natural equals safe" fallacy and emphasize that the absence of synthetic processing does not guarantee safety, efficacy, or quality.

The convergence of findings from the present study and the international literature points to several evidence-based recommendations for enhancing pharmacy education in phytotherapy:

Mandatory integration of phytotherapy modules

Given the high student demand (85.0% in the present study; >87% internationally) and documented knowledge gaps, phytotherapy should be incorporated as a mandatory component of the pharmacy curriculum rather than an elective offering (Abd Wahab et al., 2016; Ibrahima & Lawal, 2022; Ogaji et al., 2021). This integration should occur longitudinally across multiple years to ensure continuous exposure and reinforcement, with particular attention to the fourth year when risk awareness appears to decline.

Evidence-based content emphasizing safety and efficacy

Curriculum content must balance traditional knowledge with rigorous scientific appraisal of efficacy, safety, and quality (Abd Wahab et al., 2016; Hasen & Hashim, 2021). Key topics should include:

- **Herb-drug interactions**: Mechanisms, clinical significance, and patient counseling strategies
- **Adverse effects**: Recognition, reporting, and management
- **Product quality issues**: Standardization, contamination, adulteration, and regulatory frameworks
- **Evidence appraisal**: Critical evaluation of phytotherapy research and clinical guidelines
- **Legal and ethical considerations**: Scope of practice, professional liability, and informed consent

Active and experiential learning methods

Passive lecture-based instruction has proven insufficient for developing practical competence in herbal medicine counseling (AbouZid, 2015). Effective educational strategies include:

- **Problem-based learning**: Case studies involving patients using herbal products alongside conventional medications
- **Community-based assignments**: Interviews with traditional healers, herbalists, or patients to understand real-world usage patterns
- **Simulation exercises**: Role-playing patient counseling scenarios involving herbal product inquiries
- **Clinical integration**: Supervised documentation of herbal product use during pharmacy practice experiences

Egyptian pharmacy students who participated in active learning assignments involving community interviews reported significant improvements in knowledge and communication skills (AbouZid, 2015), demonstrating the value of experiential approaches.

Practical counseling skills development

Students must be trained in specific competencies essential for safe herbal product counseling (Braun & Cohen, 2014):

- Systematic documentation of herbal product use in patient medication histories
- Effective communication strategies for discussing herb-drug interactions without dismissing patients' cultural beliefs
- Point-of-care information retrieval skills using reliable databases (e.g., Natural Medicines Database, Cochrane Reviews)
- Collaborative practice with physicians and other healthcare providers regarding patients using herbal therapies

Addressing gender-specific educational needs

While the mechanisms underlying gender differences in herbal medicine attitudes remain unclear, educators should be aware that male and female students may approach phytotherapy topics with different perspectives and learning needs. Curriculum design should incorporate diverse teaching methods and case examples that resonate with students of all genders, while avoiding stereotypical assumptions about gendered health behaviors.

Continuous assessment and feedback

The fourth-year decline in risk awareness observed in the present study highlights the importance of continuous assessment throughout the curriculum. Regular formative assessments, reflective exercises, and feedback mechanisms can help identify and address knowledge gaps before students enter clinical practice.

Limitations and future research directions

Several limitations of the present study warrant acknowledgment. First, the reliance on self-reported data introduces potential response bias, although the anonymity of the online survey format likely mitigated this concern. Second, the cross-sectional design precludes causal inference regarding the relationship between prior education and attitudes; longitudinal studies tracking students' knowledge development throughout their pharmacy education would provide more robust evidence. Third, the study was conducted at a single institution in Türkiye, limiting generalizability to other cultural and educational contexts. Multi-institutional and international comparative studies would enhance understanding of how cultural factors shape pharmacy students' attitudes toward phytotherapy.

Future research should employ mixed-methods approaches combining quantitative surveys with qualitative interviews to elucidate the mechanisms underlying gender differences and the fourth-year knowledge gap. Additionally, intervention studies evaluating the effectiveness of specific educational strategies (e.g., active learning modules, clinical integration programs) on students' knowledge, attitudes, and counseling behaviors would provide actionable evidence for curriculum development. Finally, longitudinal follow-up of graduates into professional practice would clarify whether educational interventions translate into improved patient counseling and safety outcomes in real-world pharmacy settings.

CONCLUSION

This study reveals that Turkish pharmacy students demonstrate substantial interest in phytotherapy education despite limited prior training, with significant gender differences and a concerning decline in risk awareness during the fourth year of study. Prior education positively influences students' recognition of herbal product safety concerns, supporting the value of formal curricular integration. The findings align with international evidence documenting widespread educational gaps in pharmacy programs globally and underscore the urgent need for comprehensive, evidence-based phytotherapy modules that emphasize safety, herb-drug interactions, and practical counseling skills. By addressing these educational deficiencies, pharmacy schools can better prepare future pharmacists to serve as competent, trusted advisors on the safe and rational use of phytotherapeutic products, ultimately enhancing patient safety and healthcare quality.

ACKNOWLEDGEMENTS

The authors would like to sincerely thank the developers of the original attitude scale for granting permission to use the instrument in this study. We are grateful for their willingness to support academic research and for providing access to a validated measurement tool, which significantly contributed to the methodological rigor of our study.

AUTHOR CONTRIBUTION STATEMENT

S.R.O.D: Conceptualization, survey design, methodology, visualization, interpretation, writing. C.C.S: Data analysis. Ş.Y: Survey distribution. İ.İ.T.C: Supervision. All authors have read and approved the final version of the manuscript and agree to be accountable for all aspects of the work.

CONFLICT OF INTEREST

The authors declare that there is no conflict of interest.

REFERENCES

Abd Wahab, M. S., Sakthong, P., & Winit-Watjana, W. (2016). Pharmacy students' attitudes and perceptions about complementary and alternative medicine: a systematic review. *The Thai Journal of Pharmaceutical Sciences, 40*(2), 102-114. https://doi.org/10.56808/3027-7922.1932

AbouZid, S. (2015). An active learning assignment to improve pharmacy students' knowledge of herbal medicine. *Journal of Applied Pharmaceutical Science, 5*(3), 106-108. https://doi.org/10.7324/JAPS.2015.50318

Abudalo, R., Abudalo, R., Alqudah, A., Abuqamar, A., Abdelaziz, A., Alshawabkeh, M., & Taha, L. (2022). Pharmacy practitioners' practice, awareness, and knowledge about herbal products and their potential interactions with cardiovascular drugs. *F1000Research, 11*, 912. https://doi.org/10.12688/f1000research.121709.2

Ahmad, A., Khan, M. U., Kumar, B. D., Kumar, G. S., Rodriguez, S. P., & Patel, I. (2015). Beliefs, attitudes, and self-use of Ayurveda, yoga, and naturopathy, Unani, Siddha, and homeopathy medicines among senior pharmacy students: An exploratory insight from Andhra Pradesh, India. *Pharmacognosy Research, 7*(4), 302. https://doi.org/10.4103/0974-8490.158438

Barnes, J., Anderson, L. A., & Phillipson, J. D. (2007). *Herbal medicines*. Pharmaceutical Press.

Braun, L., & Cohen, M. (2014). *Herbs and natural supplements: An evidence-based guide* (Vol. 2): Elsevier Health Sciences.

Creswell, J. W., & Creswell, J. D. (2017). *Research design: Qualitative, quantitative, and mixed methods approaches*: Sage Publications.

DeVellis, R. F., & Thorpe, C. T. (2021). *Scale development: Theory and applications*: Sage Publications.

Ekor, M. (2014). The growing use of herbal medicines: issues relating to adverse reactions and challenges in monitoring safety. *Frontiers in Pharmacology, 4*, 177. https://doi.org/10.3389/fphar.2013.00177

Hasen, G., & Hashim, R. (2021). Current awareness of health professionals on the safety of herbal medicine and associated factors in the south west of Ethiopia. *Journal of Multidisciplinary Healthcare*, *14*, 2001-2008. https://doi.org/10.2147/JMDH.S321765

Heinrich, M., Appendino, G., Efferth, T., Fürst, R., Izzo, A. A., Kayser, O., . . . Viljoen, A. (2020). Best practice in research–overcoming common challenges in phytopharmacological research. *Journal of Ethnopharmacology, 246*, 112230. https://doi.org/10.1016/j.jep.2019.112230

Heinrich, M., Barnes, J., Prieto-Garcia, J., Gibbons, S., & Williamson, E. M. (2017). *Fundamentals of Pharmacognosy and Phytotherapy E-Book: Fundamentals of Pharmacognosy and Phytotherapy E-Book*: Elsevier Health Sciences.

Hijazi, M. A., Shatila, H., El-Lakany, A., Ela, M. A., Kharroubi, S., Alameddine, M., & Naja, F. (2019). Beliefs, practices, and knowledge of community pharmacists regarding complementary and alternative medicine: national cross-sectional study in Lebanon. *BMJ Open, 9*(3), e025074. https://doi.org/10.1136/bmjopen-2018-025074

Hilal, M., & Hilal, S. (2017). Knowledge, attitude, and utilization of herbal medicines by physicians in the Kingdom of Bahrain: a cross-sectional study. *Journal of the Association of Arab Universities for Basic and Applied Sciences, 24*, 325-333. https://doi.org/10.1016/j.jaubas.2016.11.001

Ibrahima, A., & Lawal, B. (2022). Assessment of awareness, use, attitude, and the perceived need for Complementary and Alternative Medicine (CAM) education, among undergraduate pharmacy students. *Nigerian Journal of Pharmaceutical Research, 18*(2), 143-155. https://dx.doi.org/10.4314/njpr.v18i2.6

Izzo, A. A., Hoon-Kim, S., Radhakrishnan, R., & Williamson, E. M. (2016). A critical approach to evaluating clinical efficacy, adverse events, and drug interactions of herbal remedies. *Phytotherapy Research, 30*(5), 691-700. https://doi.org/10.1002/ptr.5591

Jafari, A., Zanganeh, M., Kazemi, Z., Lael-Monfared, E., & Tehrani, H. (2021). Iranian healthcare professionals' knowledge, attitudes, and use of complementary and alternative medicine: a cross sectional study. *BMC Complementary Medicine and Therapies, 21*(1), 244. https://doi.org/10.1186/s12906-021-03421-z

James, P. B., & Bah, A. J. (2014). Awareness, use, attitude, and perceived need for Complementary and Alternative Medicine (CAM) education among undergraduate pharmacy students in Sierra Leone: a descriptive cross-sectional survey. *BMC Complementary and Alternative Medicine, 14*(1), 438. https://doi.org/10.1186/1472-6882-14-438

Jamshed, S. Q., Khan, M. U., Ahmad, A., & Elkalmi, R. M. (2016). Knowledge, perceptions, and attitudes toward complementary and alternative medicines among pharmacy students of a Malaysian Public University. *Journal of Pharmacy and Bioallied Sciences, 8*(1), 34-38. https://doi.org/10.4103/0975-7406.171686

Mahmoud, E. I., Yousif, M. A., & Arbab, A. H. (2024). Attitude and practice of pharmacy students toward traditional herbal medicines, Sudan. *Integrated Pharmacy Research and Practice*, *13*, 61-68. https://doi.org/10.2147/IPRP.S465056

Moreira, D. d. L., Teixeira, S. S., Monteiro, M. H. D., De-Oliveira, A. C. A., & Paumgartten, F. J. (2014). Traditional use and safety of herbal medicines. *Revista Brasileira de Farmacognosia, 24*(2), 248-257. https://doi.org/10.1016/j.bjp.2014.03.006

Naja, F., Abbas, N., Khaleel, S., Zeb, F., Osaili, T. A., Obaid, R. S., . . . Hassan, H. (2024). Beyond pillbox: a national cross-sectional study on the attitudes, practices, and knowledge of community pharmacists regarding complementary and alternative medicine. *BMC Complementary Medicine and Therapies, 24*(1), 107. https://doi.org/10.1186/s12906-024-04391-8

Ogaji, I., Lubayo, J., & Aliyu, F. O. (2021). Willingness of bachelor of pharmacy (B. Pharm.) students to be custodians of Complementary and Alternative Medicine (CAM): case study of Kenyatta University, Nairobi. *Journal of Pharmacy & Bioresources, 18*(1), 53-63. https://doi.org/10.4314/jpb.v18i1.8

Posadzki, P., Watson, L., & Ernst, E. (2013). Herb–drug interactions: an overview of systematic reviews. *British Journal of Clinical Pharmacology, 75*(3), 603-618. https://doi.org/10.1111/j.1365-2125.2012.04350.x

Tahir, A. H., Tanveer, M., Shahnaz, G., Saqlain, M., Ayub, S., & Ahmed, A. (2023). Knowledge, attitude, and perceptions of healthcare professionals towards complementary and alternative medicine: a cross-sectional survey from twin cities of Pakistan. *BMC Complementary Medicine and Therapies, 23*(1), 432. https://doi.org/10.1186/s12906-023-04187-2

Thin, S. M., Thet, D., Li, J. Y., Nakpun, T., Nitadpakorn, S., Phanudulkitti, C., . . . Kittisopee, T. (2022). A systematic review of community pharmacist practices in complementary medicine. *Pharmacy Practice, 20*(3), 2697. https://doi.org/10.18549/PharmPract.2022.3.2697

Tilburt, J. C., & Kaptchuk, T. J. (2008). Herbal medicine research and global health: an ethical analysis. *Bulletin of the World Health Organization, 86*, 594-599. https://doi.org/10.2471/BLT.07.042820

WHO. (2019). *WHO global report on traditional and complementary medicine 2019*. World Health Organization.

Wright, K. B. (2005). Researching Internet-based populations: Advantages and disadvantages of online survey research, online questionnaire authoring software packages, and web survey services. *Journal of Computer-Mediated Communication, 10*(3), JCMC1034. https://doi.org/10.1111/j.1083-6101.2005.tb00259.x

Yıldız, K. (2021). *Bitkisel ürünlerin güvenli kullanımına yönelik tutum ölçeği geliştirilmesi* (Doctoral dissertation, Selçuk University, Konya, Türkiye). Retrieved from https://tez.yok.gov.tr/UlusalTezMerkezi/

FABAD J. Pharm. Sci., 51, 1, 223-238, 2026
Doi: 10.55262/fabadeczacilik.1821521
RESEARCH ARTICLE

The Effects of Garlic (*Allium sativum* L.) and Allicin on Heart Rate: A Systematic Review and Meta-Analysis of Experimental and Clinical Studies

Rita RAKHMAWATI[*°], Rasmaya NIRURI[**]

The Effects of Garlic (Allium sativum L.) and Allicin on Heart Rate: A Systematic Review and Meta-Analysis of Experimental and Clinical Studies

SUMMARY

Garlic (Allium sativum L.) has long been recognized for its cardiovascular benefits, including antihypertensive, antihyperlipidemic, and antioxidant effects. However, evidence regarding its influence on heart rate (HR) remains inconsistent across studies. This systematic review and meta-analysis aimed to evaluate the effects of garlic, Allium sativum, or allicin administration on HR and to explore the underlying mechanisms contributing to HR modulation. A comprehensive literature search was conducted in the Scopus and PubMed databases following PRISMA guidelines. Studies published in English from 2010 onward were included if they investigated the effect of garlic or allicin on HR or elucidated mechanisms related to HR regulation. Data extraction was performed independently by two reviewers, and analysis was based on mean and standard deviation (SD). Out of 175 initially identified records, 19 studies met the inclusion criteria, and 13 were included in the meta-analysis. Most human studies reported a modest HR reduction following garlic supplementation, with a pooled mean difference of approximately –5.57 ± 10.36 beats per minute (bpm). Consistent trends were observed in animal models, showing an average HR decrease of –50.06 ± 21.25 bpm. Mechanistic studies revealed that garlic and allicin influence HR through modulation of ion channels (Nav1.5 and Cav1.2), regulation of HCN4 expression, and antioxidant and parasympathetic activation pathways. Garlic and its bioactive compound allicin demonstrate HR-lowering potential through electrophysiological and autonomic modulation. However, the extent of HR change depends on dosage, extract formulation, and baseline cardiovascular status. Further standardized clinical trials are warranted to define optimal formulations and dosing strategies for cardiovascular applications.

Keywords: *Allium sativum, allicin, heart rate, cardiovascular regulation, systematic review, meta-analysis.*

Sarımsağın (Allium sativum L.) ve Alisinin Kalp Atım Hızı Üzerindeki Etkileri: Deneysel ve Klinik Çalışmaların Sistematik Derlemesi ve Meta-Analizi

ÖZ

Sarımsak (Allium sativum L.), antihipertansif, antihiperlipidemik ve antioksidan etkiler dahil olmak üzere kardiyovasküler yararlarıyla uzun süredir bilinmektedir. Ancak, kalp atım hızı (HR) üzerindeki etkisine ilişkin kanıtlar çalışmalar arasında tutarsızlık göstermektedir. Bu sistematik derleme ve meta-analiz, sarımsak, Allium sativum veya allisin uygulamasının HR üzerindeki etkilerini değerlendirmeyi ve HR düzenlenmesine katkıda bulunan altta yatan mekanizmaları araştırmayı amaçlamıştır. PRISMA yönergelerine uygun olarak Scopus ve PubMed veri tabanlarında kapsamlı bir literatür taraması yapılmıştır. 2010 yılından itibaren İngilizce yayımlanan ve sarımsak veya allisinin HR üzerindeki etkisini ya da HR düzenlenmesine ilişkin mekanizmaları inceleyen çalışmalar dahil edilmiştir. Veriler iki araştırmacı tarafından bağımsız olarak çıkarılmış ve analizler ortalama ile standart sapma (SD) değerlerine dayanmıştır. Başlangıçta belirlenen 175 çalışmadan 19'u dahil edilme kriterlerini karşılamış ve 13'ü meta-analize alınmıştır. İnsan çalışmalarının çoğu, sarımsak takviyesi sonrasında ortalama –5,57 ± 10,36 atım/dk düzeyinde hafif bir HR azalması bildirmiştir. Hayvan modellerinde benzer şekilde, ortalama –50,06 ± 21,25 atım/dk düzeyinde HR düşüşü gözlenmiştir. Mekanistik çalışmalar, sarımsak ve allisinin HR'yi iyon kanalları (Nav1,5 ve Cav1,2), HCN4 gen ekspresyonu, antioksidan ve parasempatik aktivasyon yolları üzerinden modüle ettiğini ortaya koymuştur. Sarımsak ve biyoaktif bileşiği allisin, elektrofizyolojik ve otonom mekanizmalar aracılığıyla HR düşürücü potansiyele sahiptir. Ancak, bu etkinin derecesi doz, ekstre formülasyonu ve kardiyovasküler durum gibi faktörlere bağlıdır.

Anahtar Kelimeler: *Allium sativum, allisin, kalp atım hızı, kardiyovasküler düzenleme, sistematik derleme, meta-analiz.*

Recieved: 11.11.2025
Revised: 7.02.2026
Accepted: 17.02.2026

[*] ORCID: 0000-0001-8905-5531, Department of Pharmacy, Faculty of Mathematics and Natural Sciences, Universitas Sebelas Maret, Surakarta, Indonesia
[**] ORCID: 0000-0002-9684-2573, Department of Pharmacy, Faculty of Mathematics and Natural Sciences, Universitas Sebelas Maret, Surakarta, Indonesia

[°] Corresponding Author; Rita Rakhmawati
E-mail: ritarakhmawati@staff.uns.ac.id

INTRODUCTION

Garlic (*Allium sativum* L.) has long been recognized not only as a culinary ingredient that enhances the flavor of food but also as a medicinal plant with a broad spectrum of therapeutic activities (Ha et al., 2024). Throughout history, it has been utilized in various traditional medical systems for its beneficial effects on human health, particularly in the prevention and management of cardiovascular disorders. Modern pharmacological studies have confirmed that garlic exerts antihypertensive, antihyperlipidemic, antithrombotic, and antioxidant effects, as well as immunomodulatory properties. Garlic is characterized predominantly by organosulfur constituents, with intact cloves containing *S*-alk(en)yl-*L*-cysteine sulfoxides and related γ-glutamyl peptides. Upon tissue disruption, alliinase rapidly converts alliin to allicin (diallyl thiosulfinate), a reactive and transient compound that further yields secondary sulfur metabolites such as ajoene, vinyldithiins, and diallyl sulfides, alongside water-soluble derivatives (e.g., *S*-allyl cysteine) (Sasmaz et al., 2025). These sulfur-containing metabolites are pharmacologically significant and are widely linked to garlic's cardioprotective and vascular effects, inhibition of platelet aggregation, and antioxidant/anti-inflammatory as well as antimicrobial activities (Sleiman et al., 2024; Supa-aksorn et al., 2025).

Cardiovascular diseases (CVDs) remain the leading cause of morbidity and mortality worldwide, and heart rate (HR) is considered a vital physiological parameter closely associated with cardiovascular outcomes. Elevated HR has been independently linked to increased risks of hypertension, atherosclerosis, and cardiac mortality. Therefore, identifying natural agents capable of modulating HR may contribute to the development of complementary strategies for cardiovascular protection (Bernal-Sánchez et al., 2026; Mahfoud et al., 2024).

Interestingly, the relationship between garlic administration and HR regulation remains controversial. Some experimental and clinical studies have reported that garlic or allicin supplementation can lower HR through mechanisms involving vasodilation, enhanced parasympathetic activity, and reduced oxidative stress (Asdaq & Inamdar, 2011; Brankovic et al., 2011; Khastkhodaei et al., 2011). Conversely, other studies have shown either an increase or no significant change in HR, with variations attributed to differences in dosage, formulation, duration of administration, and experimental models used. These inconsistencies indicate that the effects of garlic on HR, as well as the underlying mechanisms, are not yet fully elucidated.

Given the growing interest in herbal-based cardiovascular therapies and the inconsistent findings across studies, a systematic review and meta-analysis are warranted to synthesize current evidence. This study therefore aims to identify changes in HR following administration of garlic, *A. sativum*, or allicin, in different formulations, including whole garlic preparations and standardized extracts, as well as isolated bioactive compounds such as allicin, and provide an integrated understanding of the mechanisms by which garlic influences HR regulation. By quantitatively synthesizing HR outcomes and integrating mechanistic evidence, this study addresses inconsistencies in the existing literature and provides a focused evaluation of formulation- and dose-dependent effects that have not been systematically examined in previous reviews. The findings are expected to clarify the cardiovascular role of garlic and strengthen the scientific foundation for its application as an evidence-based herbal intervention in modern medicine.

MATERIALS AND METHODS

Search strategy and study selection

This study was conducted in accordance with the Preferred Reporting Items for Systematic Reviews and Meta-Analyses (PRISMA) guidelines. Two independent researchers evaluated all retrieved manuscripts to ensure accuracy and minimize selection bias.

A comprehensive literature search was performed in two electronic databases, Scopus and PubMed, to identify relevant publications addressing both research objectives. The search strategy employed four sets of keywords, including both Medical Subject Headings (MeSH) and All Field terms.

For the first objective (to identify changes in heart rate following *garlic/Allium sativum/allicin* administration), the search strings applied were "((garlic [MeSH Terms]) OR (allium [MeSH Terms])) AND (heart rate [MeSH Terms])" for MeSH Terms, and "((("garlic") OR ("allium") OR ("allicin")) AND ("heart rate")" for All Field search. For the second objective, which aimed to explore the mechanisms underlying heart rate regulation influenced by garlic, the search strings were "((garlic[MeSH Terms]) OR (allium[MeSH Terms])) AND (heart rate[MeSH Terms]) AND (gene[MeSH Terms])" for MeSH Terms, and "((("garlic") OR ("allium") OR ("allicin")) AND ("heart rate") AND ("gene")" for All Field search.

Inclusion and exclusion criteria

The inclusion criteria comprised original research articles published in English from 2010 onward that investigated either changes in heart rate or the mechanisms influencing heart rate after administration of garlic, *A. sativum*, or allicin. Only studies that reported quantitative outcomes suitable for synthesis or meta-analysis were included. Studies were excluded if the full text was inaccessible, if duplicates were identified across databases, or if the publications consisted of reviews, commentaries, or conference abstracts without primary data.

Data extraction and analysis

Data extraction was performed independently by two reviewers, and discrepancies were resolved through discussion until consensus was reached. Extracted data included study characteristics, intervention details, and heart rate outcomes. For meta-analysis, the sample mean and standard deviation were used following the statistical approach described by (Chi et al., 2023).

RESULTS AND DISCUSSION

A total of 175 records were initially identified through the systematic search, of which 19 studies met the inclusion criteria for the qualitative synthesis and 13 were eligible for meta-analysis, as shown in Figure 1 (PRISMA Flowchart). The studies encompassed human clinical trials, experimental animal models, and *in vitro* mechanistic investigations, providing a broad and integrative perspective on the effect of garlic (*A. sativum*) and its principal bioactive compound, allicin, on heart rate (HR).

In human studies (summarized in Table 1.), garlic supplementation was generally associated with a modest reduction in HR. The pooled mean difference from the meta-analysis, approximately −5.57 ± 10.36 bpm (Table 4.), reflects a mild yet consistent bradycardic tendency across most trials. Notably, the study by Khastkhodaei et al. (2011) reported the greatest decrease (−14.95 bpm) after four weeks of daily organosulfur extract administration in patients with stable angina, whereas trials by Leitão et al. (2022) and Lopez et al. (2013) showed smaller or negligible effects in healthy or obese volunteers. Such differences are clinically meaningful and suggest that the chronotropic response to garlic is not uniform but instead depends heavily on the individual's cardiovascular condition and autonomic tone (Osailan et al., 2023). In subjects with heightened sympathetic activity, endothelial dysfunction, or ischemic heart disease, HR reduction may indicate a restoration of autonomic balance and vascular responsiveness. In contrast, individuals with normal cardiovascular regulation often exhibit minimal change, as homeostatic baroreflex mechanisms counteract further decreases in HR (Duong et al., 2020; Siepmann et al., 2022). This pattern aligns closely with previous studies on garlic's cardiovascular benefits, which consistently show that its blood pressure–lowering and endothelial effects are more pronounced in hypertensive than in normotensive populations (Ried et al., 2016; Wang et al., 2015). Collectively, these observations suggest that garlic's influence on HR likely represents part of a broader, adaptive cardiovascular modulation rather than a direct pharmacological suppression of cardiac rhythm.

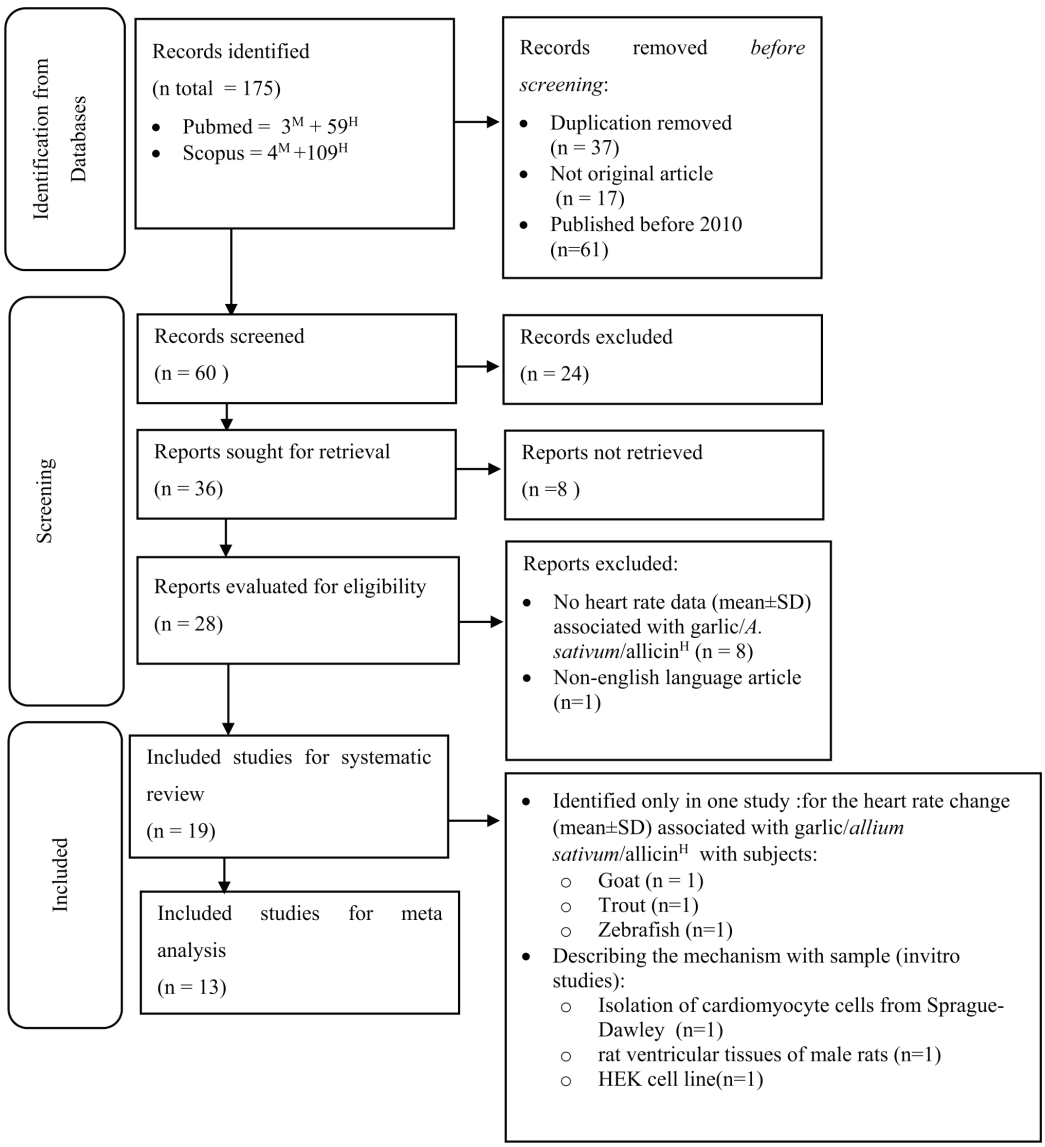


Figure 1. Prisma flowchart

M= Records based on mechanism keywords (MeSH term and All Field), H= Records based on heart rate value keywords (MeSH term and All Field), HR = Heart Rate

Table 1. Characteristics of included studies in the systematic review for changes in heart rate value in human

Subject	Study (Author, year, country, subject, method)	Garlic (dose), duration of treatment, N subject	Concomitant therapy	Outcome Heart rate	Other outcomes
Human					
	Khastkhodaei et al., 2011 • Iran • Patients with stable chest angina • RCT	• Garlic organosulfur extract • (407.4 mg/ml- 60 ml/day) • For four weeks • Ntotal=40	60 ml/day extract consisted of hawthtorn (44.44 mg/ml), ginger (14.8 mg/ml), bilberry (20.4 mg/ml), red pepper (9.3 mg/ml), chammomile (14.8 mg/ml), willow bark (26.6 mg/ml)	Pre: 87.55 ± 3.23 Post: 72.60 ± 3.00 Δ: -14.95 ± 4.41	Lower LDL triglyceride and total cholesterol level
	Leitão et al., 2022 • Brazil • Patients with stable chest angina • RCT Leitão et al., 2022 • Brazil • Patients with stable chest angina • RCT	• Age Garlic • (2,4 g/day), • N/A, • Ntotal=28	(-)	Pre: 66.30 ± 11.87 Post: 63.33 ± 10.03 Δ: -2.97 ± 15.54	Age garlic extract improved microvascular function in male (age: 67±6) with cardiovascular disease high risk factors
	Lopez et al., 2013 • USA • obese human with metabo diet (consisted of raspberry ketone, caffeine, capsaicin, gingerols, shogaols, *Citrus aurantium* and related alkaloids, B vitamins, and chromium) • RCT	• Garlic • (N/A) • • For eight weeks • • Ntotal=27	Thiamin, riboflavin, niacin, pyridoxine, methylcobalamin, biotin, patothenic acid, Chromium, raspberry ketone, caffeine, capsaicin, garlic, ginger, and *Citrus aurantium*	Pre: 70.1 + 8.2 Post: 70.1 + 8.4 Δ: +0.00 ± 11.74	• Increased weight loss program (from 94±23 to 92± 23kg) • Reduced systolic (from 119± 10 to 118±10 mmHg) and diastolic blood pressure (77±8 to 76 ±9mmHg)
	McCrea et al., 2015 • USA • Healthy subject with obese • RCT	• Garlic powder • (1.81 gram) • • N/A • • N total = 20	Black pepper (0.91g), cinnamon (1.11g), cloves (0.61g), ginger (1.51g), oregano (2.26g), paprika (2.85g), rosemary (0.61g), turmeric (2.79g)	Pre: 64.43 ± 1.56 Post: 64.98 ± 1.84 Δ: +0.00 ± 2.41	Significantly lower triglycerides level by 31% ($p<0,05$) at rest condition,.
	Morris et al., 2013 • USA • Healthy cyclist in hypoxia • Cohort	• Garlic bulb powder (4650 mg/day) • • For 7 days • • N total=9	(-)	Pre: 183±10 Post: 182±11 Δ: -1.00 ± 14.87	No significant effect on oxygen consumption/ saturation, peripheral blood pressures (both in exercise or resting condition), or exercise performance.

HR=heart rate; D HR=pre-post (result after garlic administration=minus (showed the HR reduction) or plus (demonstrated HR increase); D HR data was collected from the existing study or calculated based on formula proposed by Chi et al. (2023) and Arifin (2014); post and pre=after and before garlic administration; (-); No concomitant therapy with other treatment.

Animal studies presented in Table 2 showed a more robust HR reduction, with a pooled mean difference of approximately –50.06 ± 21.25 bpm (Table 5.). Studies in hypertensive, ischemic, or oxidative-stress-induced models demonstrated marked bradycardic responses after garlic or allicin administration, suggesting that the effect intensifies under pathological conditions characterized by sympathetic overactivation and oxidative stress (Grassi & Drager, 2024). In contrast, studies in normotensive or healthy animals showed smaller reductions or even transient HR increases at specific doses, underscoring that the effect is context- and concentration-dependent rather than universally bradycardic. Aqueous and aged garlic extracts, rich in stable organosulfur compounds, showed stronger HR-lowering effects than oil-based or ethanol extracts, which may contain different allicin derivatives. Excessively high doses sometimes produced paradoxical effects, possibly due to compensatory sympathetic activation or receptor desensitization. These inconsistencies instead reflect the pharmacodynamic complexity of garlic, a feature commonly observed in natural products, where multiple bioactive constituents may interact synergistically or antagonistically depending on dose and matrix composition (Sharma & Rani, 2021; Thomson et al., 2015).

Table 2. Characteristics of included studies in the systematic review for changes of heart rate value in rats

Subject	Study (Author, year, country, subject)	Garlic (dose), duration of treatment/evaluation period, N subject	Concomitant therapy	Outcome Heart rate	Other outcomes
Sprague-Dawley rats					
	Al-Qattan et al., 2017 • Kuwait • 2-kidney 1-clip rat model	• Raw garlic aqueous extract (30 mg / 100 g weight) • Five time i.v. administration of garlic • N=11	(-)	Pre: 188 ± 2 Post: 187 ± 1 Δ: -1.00 ± 2.24	Blocked angiotensin I converting enzyme dipeptidase activity and Angiotensin II generation
	Li et al., 2012 • China • cardiac hypertrophy rats	• Allicin 180 mg/kg/day • For 8 weeks • N=9	(-)	Pre: 321±15.6 Post: 306±17.6 D: -15.00 ± 23.53	Allicin inhibits the development of cardiac remodeling and cardiac hypertrophy, caused by increasing activity of Nrf2 antioxidant signaling pathways
	Manosroi et al., 2013 • Thailand • hypertensive Sprague-Dawley rats	• Extract garlic in water fraction (6.26 mg/kg) • After an administration the extract • N=6	(-)	D HR: -7.00±1.30	Reducing mean arterial blood pressure
	Manosroi et al., 2013 • Thailand • hypertensive Sprague-Dawley rats	• Extract garlic in butanol fraction (0.33 mg/kg) • After an administration the extract • N=6	(-)	D HR: -3.33±0.56	
	Manosroi et al., 2013 • Thailand • hypertensive Sprague-Dawley rats	• Extract garlic in ethyl acetate • (0.27 mg/kg) • After an administration the extract • N=6	(-)	D HR: +0.50±0.50	

Subject	Study (Author, year, country, subject)	Garlic (dose), duration of treatment/evaluation period, N subject	Concomitant therapy	Outcome Heart rate	Other outcomes
Sprague-Dawley rats					
Wistar rats					
	Asdaq et al., 2011 -India -rat with heart failure	• Extract garlic • (125 mg/kg BB) • • For 3 weeks • • N=8	(-)	Pre: 398.4 ± 3* Post: 353.2 ± 1 D: -44.20 ± 3.16	Lowering systolic blood pressure, cholesterol, triglycerides, glucose in HF rats.
		• Extract garlic (250 mg/kg BB) • For 3 weeks • • N=8	(-)	Pre: 398.4 ± 3 Post: 353.2 ± 1 D: -66.30 ± 3.16	
		• Extract garlic (500 mg/kg BB) • For 3 weeks • N=8	(-)	Pre: 398.4 ± 3 Post: 353.2 ± 1 D: -50.80 ± 3.61	
	Brankovic et al., 2011 • Serbia • Normotensive rat	• Garlic extract in ethanol • (6 mg/kg weight) • After an i.v. injection of the extract • N=6	(-)	Pre: 293 ± 10.76 Post: 196.31 ± 18.36 D: 96.69 ±21.28	Reducing arterial blood pressure
	Nwokocha et al., 2011 • Nigeria • Normotensive rat	• Aqueous garlic extract (20 mg/kg weight) • N=6	(-)	Pre: 378 ±5 Post: 207 ±5 D: 171 ±7.07	Decreasing blood pressure
	Nwokocha et al., 2011 • Nigeria • Hipertensive rat	• Aqueous garlic extract (20 mg/kg weight) • After garlic extract administration • N=6	(-)	Pre: 406 ±6 Post: 250 ±5 D: 156 ±7.81	Decreasing blood pressure
	Shackebaei et al., 2010 • Iran • Rat with Ischemia	• Garlic juice (0.01 mg/ml) was added to the perfusion solution 20 min before ischemia • After the hearts were perfused with the juice • (N=8)	(-)	Pre: 253 ± 10.27 Post: 217 ± 18 D: -36 ± 20.72	Improving on Rate pressure product and left ventricular developed pressure.
		• Garlic juice (0.01 mg/ml) was added to the perfusion solution min before and 10 min after ischemia • After the hearts were perfused with the juice • (N=7)	(-)	265 ± 13 227 ± 7.6 D: -38 ± 15.06	

Subject	Study (Author, year, country, subject)	Garlic (dose), duration of treatment/evaluation period, N subject	Concomitant therapy	Outcome Heart rate	Other outcomes
Sprague-Dawley rats					
	Supakul et al., 2014 • Thailand • Obese insulin-resistant rat	• Normal diet (250 mg/kg weight) • • For 28 days • (N=8)	(-)	Pre: 324 ± 24 Post: 311.05 ± 40 D: -12.95 ± 46.65	Decreasing plasma insulin, oxidative stress levels, and total cholesterol
		• Normal diet (500 mg/kg weight) • For 28 days • (N=8)	(-)	Pre 324 ± 24 Post: 333 ± 39 D: +9±45.79	
		• High fat diet (250 mg/kg weight) • For 28 days • (N=8)	(-)	Pre: 419 ± 3 Post: 307 ± 27 D: -112 ±27.17	
		• High fat diet (500 mg/kg weight) • For 28 days • (N=8)	(-)	Pre: 419 ± 3 Post: 315 ± 19 D: -104±19.24	

HR=heart rate; D HR=pre-post (result after garlic administration=minus (showed the HR reduction) or plus (demonstrated HR increase); D HR data was collected from the existing study or calculated based on formula proposed by Chi et al., (2023) and Arifin (2014); post and pre=after and before garlic administration; (-); No concomitant therapy with other treatment. i.v.= intravenous

Cross-species evidence summarized in Table 3 supports the consistency of this physiological trend. Experiments involving goats, trouts, and zebrafish all demonstrated significant HR reductions after garlic or allicin exposure. In zebrafish, for example, exposure to increasing concentrations of fresh garlic juice resulted in a dose-dependent decline in HR, ranging from 36 to 60 bpm reductions, which supports a conserved electrophysiological mechanism across vertebrates. Such findings reinforce the notion that garlic exerts a fundamental modulatory effect on cardiac pacemaker function rather than acting solely through secondary systemic changes.

Table 3. Characteristics of included studies in the systematic review for changes of heart rate value in goats, trouts, zebrafish

Subject	Study (Author, year, country, subject)	Garlic (*Allium sativum)*/Allicin (dose, N subject)	Concomitant therapy	Outcome Heart rate (HR)	Other outcomes
Goats,	Attia et al., 2021 • Egypt • One year old goat infected with with Escherichia coli	Allicin (2.7 mg /kg) twice a day at 12-h intervals for 42 days (N=4)	(-)	Pre: 104.0 ± 3.786 Post: 89.67 ± 2.728 Δ HR: 14.33 ± 4.67	Administration of allicin led to higher release of IL-6, IL-12, and TNF-α in both infected groups than in the untreated control
Trout	Papadopoulou et al., 2022 • Finland • Trout	• Allicin • (1000 mg/ml) for 6 weeks • (N=18)	(-)	Pre: 158.4 ± 4.70 Post: 143.6 ± 8.45 Δ HR: 14.80 ± 9.67	Alicin reduced the temperature coefficient of heart rate
Zebrafish	Majewski et al., 2017 • Poland • Zebrafish	Fresh garlic juice (0.01%) for 36 hours (N=7)	(-)	Pre: 131.60 ± 3.20 Post: 95.6 ± 9.7 Δ HR: 36.00 ± 10.21	Slow growth, swelling around the heart with heart defects, yolk deformities, absence of color, and body shape abnormalities have been observed at a level of 0.03% after 48 hours of exposure.
Zebrafish	Majewski et al., 2017 • Poland • Zebrafish	Fresh garlic juice (0.02%) for 36 hours (N=7)	(-)	Pre: 131.6 ± 3.2 Post: 84.9 ±7.3 Δ HR: 46.70± 7.97	Mortality was also higher with garlic exposure after being in contact for 12 hours at a level of 0.08%
Zebrafish	Majewski et al., 2017 • Poland • Zebrafish	Fresh garlic juice (0.03%) for 36 hours (N=7)	(-)	Pre: 131.6 ± 3.2 Post: 71.6 ± 4.7 Δ HR: 60 ± 5.69	

HR=heart rate; D HR=pre-post (result after garlic administration=minus (:showed the HR reduction) or plus (demonstrated HR increase); D HR data was collected from the existing study or calculated based on formula proposed by Chi et al., (2023) and Arifin (2014); post and pre=after and before garlic administration; (-); No concomitant therapy with other treatment; (-); No concomitant therapy with other treatment.

Mechanistic studies summarized in Table 6 offer crucial insight into why garlic and allicin lower HR. Chen et al. (2021) found that allicin significantly suppressed the late sodium current (INa,L) mediated by Nav1.5 channels in HEK293 cells expressing the KPQ-SCN5A mutation. This action stabilizes the cardiac action potential and reduces excitatory currents that drive arrhythmogenic and tachycardic responses. Similarly, Han et al. (2019) demonstrated that allicin inhibits Cav1.2 L-type calcium channel trafficking in rat ventricular tissues, reducing calcium influx and consequently decreasing sinoatrial node firing and contractility. Moreover, modulation of HCN4 expression further dampens sinoatrial node automaticity, providing a direct molecular rationale for HR reduction (Trieu et al., 2020). The same study reported that the ethyl acetate fraction of garlic produced the opposite effect, upregulating HCN4 expression and increasing beating rate, emphasizing that garlic's chronotropic effect is highly dependent on chemical composition and extraction solvent (Bar et al., 2022). This variability corresponds to the inconsistent results among studies in Tables 1–3, where certain extracts or doses caused minimal or paradoxical HR increases.

Table 4. Heart rate change after garlic administration in humans

Study	N Each study	Δ HR Each study	Ntotal	Δ HR total
Garlic treatment as single or in mixture ingredient				
Khastkhodaei et al., 2011	40	-14.95 ± 4.40	124	-5.57 ± 10.36
Leitão et al., 2022	28	-2.97 ±15.54		
Lopez et al., 2013	27	-0.00 ± 11.74		
McCrea et al., 2015	20	-0.00 ± 2.41		
Morris et al., 2013	9	-1.00 ± 14.86		
Garlic treatment as single ingredient				
Leitão et al., 2022	28	-2.97 ±15.54	37	-2.49 ± 15.39
Morris et al., 2013	9	-1.00 ± 14.86		

HR=heart rate; D HR=pre-post (result after garlic administration=minus (showed the HR reduction) or plus (demonstrated HR increase), classified into: D HR each study and D HR total [combining data (mean and standard deviation (using formula proposed by Axon et al., 2023 and Chi et al., 2023) from multi arm studies)]

Table 5. Heart rate change after garlic administration on rats

Study		N Each study	Δ HR Each study	Ntotal	Δ HR total
Sprague-Dawley rats					
Al-Qattan et al., 2017		11	-1.00 ± 2.24	29	-2.14 ± 1.56
Manosroi et al., 2013*	I	6	-7.00 ± 1.30		
	II	6	-3.30 ± 0.56		
	III	**6**	**-0.50 ± 0.50**		
Winstar rat				89	-61.25 ± 24.23
Asdaq et al., 2011*	I	8	-44.20 ± 3.16		
	II	8	-66.30 ± 3.16		
	II	8	-50.80 ± 3.61		
Brankovic et al., 2011		6	-96.69 ± 21.28		
Nwokocha et al., 2011*	I	6	-171 ± 7.07		
	II	6	-156 ± 7.81		
Shackebaei et al., 2010*	I	8	-36 ± 20.73		
	II	7	-38 ± 15.06		
Supakul et al., 2014*	I	8	-12 ± 46.65		
	II	8	+9 ± 45.79		
	III	8	-112 ± 27.17		
	IV	8	-104 ± 19.24		

HR=heart rate; D HR=pre-post (result after garlic administration=minus (showed the HR reduction) or plus (demonstrated HR increase), classified into: D HR each study and D HR total [combining data (mean and standard deviation) (using formula proposed by Axon et al., 2023 and Chi, 2023) from multi arm studies)]

Taken together, the evidence suggests that the HR-lowering activity of garlic and allicin is multifactorial. At the molecular level, the modulation of ion channels (Nav1.5, Cav1.2, HCN4) directly influences pacemaker automaticity and conduction velocity, producing negative chronotropy. On a systemic level, garlic enhances parasympathetic (vagal) tone, promotes vasodilation through improved nitric oxide bioavailability, and exerts antioxidant and anti-inflammatory actions that reduce sympathetic drive (Imaizumi et al., 2023). These pathways are interconnected: vasodilation reduces peripheral resistance and cardiac afterload, which in turn lowers reflex sympathetic activity and slows HR. Additionally, reduction of oxidative stress stabilizes the cardiac redox state, preserving ion channel function and reducing excitatory arrhythmogenic potential. The observed outcome is a physiologically mediated reduction in heart rate, which appears to be associated with restoration of autonomic balance rather than direct cardiac suppression (Hasan et al., 2022).

Table 6. Mechanistic pathways involved in the heart rate–lowering effects of garlic

(Study), Country, Garlic, Experimental Approach,	Mechanism associated with Heart rate
(Trieu et al., 2020) • Vietnam • Garlic *n*-hexane/dichloromethane/ethyl acetate extract, • Procedure: • ▸ Isolation of cardiomyocyte cells from Sprague-Dawley rat (1- to 2-day-old) • ▸ Inducing beating rate • ▸ HCN4 expression	Beating rate and HCN4 expression ▸ Garlic extract in n-hexane and dichloromethane (20 µg/mL) demonstrated lower beating rate and HCN4 expression than negative control groups ▸ Garlic ethyl acetate extract (20 µg/mL) showed higher beating rate and HCN4 expression than negative control groups
(Chen et al., 2021) • China, • Allicin, • Procedure: • ▸ Cell culture and transfection, Confocal Imaging, Western Blotting (HEK 293 cell line, ΔKPQ-SCN5A mutations) • ▸ Electrophysiological and current Recordings	Allicin (30 mM) significantly reduced the late sodium current (Ina,L) of the Nav1.5 channel current which encoded by 1KPQ-SCN5A,
(Han et al., 2019) • China, • Allicin, • Procedure: • ▸ Cell culture, Cell viability determination (ventricular tissues of male rats aged 5–8 weeks) • ▸ Cav1.2 protein expression	Allicin caused trafficking dysfunction, which resulted in the inhibition of cardiac Cav1.2 channels

When contextualized within broader literature, these findings align with a growing body of evidence on the cardioprotective and autonomic regulatory effects of garlic. Reviews by El-Saadony et al. (2024), Gao et al. (2024), and Li et al. (2023) have outlined garlic's ability to modulate oxidative stress, lipid peroxidation, and vascular inflammation, processes closely linked to autonomic function and HR control. Taken together, these studies reinforce that the HR-lowering property of garlic is mechanistically coherent with its other cardiovascular actions. HR reductions have been reported following administration of both complex garlic preparations/extracts and isolated allicin; however, the relative contribution of allicin is likely formulation-dependent due to its chemical instability and rapid conversion to downstream organosulfur metabolites. Consequently, preparations with different organosulfur profiles and allicin-generating capacity may produce HR effects through overlapping but not identical pathways. At the same time, they highlight critical research needs: improved extract standardization, standardized reporting of key chem-

ical markers (including allicin content/yield and other relevant organosulfur constituents), identification of key bioactive sulfur compounds responsible for autonomic modulation, and pharmacokinetic data defining effective human dosing.

Despite the consistency of these physiological trends, the strength of evidence remains limited by methodological weaknesses across included studies. Many human trials were small, single-center, and lacked details on randomization, blinding, or the chemical standardization of extracts. In several studies, intervention characterization was insufficient (e.g., absence of standardized marker reporting such as allicin content/yield or comparable organosulfur profiling), which limits inference regarding whether HR changes were driven by allicin specifically or by other constituents/metabolites present in the extract matrix. Similarly, most animal experiments did not report allocation methods or blinding of outcome assessment. These methodological shortcomings introduce potential bias that could either exaggerate or underestimate true effects. Therefore, the present findings should be interpreted with appropriate caution. Future systematic reviews should incorporate formal risk-of-bias assessment frameworks and ideally apply GRADE (Grading of Recommendations Assessment, Development, and Evaluation) criteria to evaluate certainty of evidence.

CONCLUSION

This systematic review and meta-analysis provide comprehensive evidence that garlic (*A. sativum* L.) and its active compound allicin exert a heart rate–lowering effect across human, animal, and cellular models. The HR reduction appears to be mediated through multiple pathways, including modulation of sodium and calcium channel currents, downregulation of HCN4 expression, enhancement of parasympathetic tone, and attenuation of oxidative stress. Nonetheless, the extent of HR modulation is dose-dependent and influenced by extract type and physiological condition, suggesting that garlic acts as a functional modulator rather than a fixed chronotropic agent. Notably, this study offers a novel contribution by quantitatively synthesize heart rate–specific outcomes while integrating mechanistic evidence to distinguish formulation- and pathway-dependent effects of garlic and allicin, thereby addressing inconsistencies in prior cardiovascular-focused reviews. These findings strengthen the scientific basis for garlic's cardioprotective properties and highlight its potential as an evidence-based herbal adjunct in cardiovascular therapeutics. Further well-controlled clinical studies are warranted to optimize formulation, dosage, and treatment duration for maximal efficacy and safety.

AUTHOR CONTRIBUTION STATEMENT

RR: Concept and design, drafting the manuscript, supervision, final approval; RN: Concept and design, data analysis, drafting the manuscript, critical revision of the manuscript, final approval

CONFLICT OF INTEREST

The authors declare that there is no conflict of interest.

REFERENCES

Al-Qattan, K. K., Thomson, M., & Ali, M. (2017). Garlic extract increases non-clipped kidney tubular natriuresis and diuresis in the 2-kidney, 1-clip rat model: significance in hypertension. *Pathophysiology*, *24*(4), 317–325. doi:10.1016/j.pathophys.2017.08.004

Arifin, W. N. (2014). Calculating standard deviation of difference for determination of sample size for planned paired t-test analysis. *Education in Medicine Journal*, *6*(2), 62–64. doi:10.5959/eimj.v6i2.252

Asdaq, S. M. B., & Inamdar, M. N. (2011). The potential benefits of a garlic and hydrochlorothiazide combination as antihypertensive and cardioprotective in rats. *Journal of Natural Medicines*, *65*(1), 81–88. doi: 10.1007/s11418-010-0467-9

Attia, N., Bayoumi, Y., & Bahnass, M. (2021). Prophylactic and therapeutic effects of allicin against goats experimentally infected with colibacillosis. *Slovenian Veterinary Research*, *58*(24-Suppl), 289–298. doi:10.26873/SVR-1448-2021

Axon, E., Dwan, K., & Richardson, R. (2023). Multiarm studies and how to handle them in a meta-analysis: A tutorial. *Cochrane Evidence Synthesis and Methods*, *1*(10), e12033. doi:10.1002/cesm.12033

Bar, M., Binduga, U. E., & Szychowski, K. A. (2022). Methods of isolation of active substances from garlic (*Allium sativum* L.) and its impact on the composition and biological properties of garlic extracts. *Antioxidants*, *11*(7), 1345. doi: 10.3390/antiox11071345

Bernal-Sánchez, J. J., Arboleda-Campo, V. H., Chavarro-Ortiz, P. A., Valencia-Ortiz, J. G., & Wilches-Luna, E. C. (2026). Changes in vital signs and functional performance during the 2-minute step test in healthy Colombian adults. *Journal of Bodywork and Movement Therapies*, *46*, 17–21. doi: 10.1016/j.jbmt.2025.10.056

Brankovic, S., Radenkovic, M., Kitic, D., Veljkovic, S., Ivetic, V., Pavlovic, D., & Miladinovic, B. (2011). Comparison of the hypotensive and bradycardic activity of ginkgo, garlic, and onion extracts. *Clinical and Experimental Hypertension*, *33*(2), 95–99. doi: 10.3109/10641963.2010.531833

Chen, Y., Huang, Y., Bai, J., Liu, C., Ma, S., Li, J., … Zhang, J. (2021). Effects of allicin on late sodium current caused by ΔKPQ-SCN5A mutation in HEK293 cells. *Frontiers in Physiology*, *12*, 1-8. doi: 10.3389/fphys.2021.636485

Chi, K.-Y., Li, M.-Y., Chen, C., & Kang, E. (2023). Ten circumstances and solutions for finding the sample mean and standard deviation for meta-analysis. *Systematic Reviews*, *12*(1), 62. doi: 10.1186/s13643-023-02217-1

Duong, H. T. H., Tadesse, G. A., Nhat, P. T. H., Hao, N. Van, Prince, J., Duong, T. D., … Thwaites, L. (2020). Heart rate variability as an indicator of autonomic nervous system disturbance in tetanus. *The American Journal of Tropical Medicine and Hygiene*, *102*(2), 403–407. doi: 10.4269/ajtmh.19-0720

El-Saadony, M. T., Saad, A. M., Korma, S. A., Salem, H. M., Abd El-Mageed, T. A., Alkafaas, S. S., … Ibrahim, S. A. (2024). Garlic bioactive substances and their therapeutic applications for improving human health: a comprehensive review. *Frontiers in Immunology*, *15*, 1-25. doi: 10.3389/fimmu.2024.1277074

Gao, Y., Wang, B., Qin, G., Liang, S., Yin, J., Jiang, H., … Li, X. (2024). Therapeutic potentials of allicin in cardiovascular disease: advances and future directions. *Chinese Medicine*, *19*(1), 93. doi: 10.1186/s13020-024-00936-8

Grassi, G., & Drager, L. F. (2024). Sympathetic overactivity, hypertension and cardiovascular disease: state of the art. *Current Medical Research and Opinion*, *40*(sup1), 5–13. doi: 10.1080/03007995.2024.2305248

Ha, J., Kim, J., Kim, S., Lee, K. J., & Shin, H. (2024). Garlic-induced enhancement of *Bifidobacterium*: Enterotype-specific modulation of gut microbiota and probiotic populations. *Microorganisms*, *12*(10), 1971. doi: 10.3390/microorganisms12101971

Han, D., Xu, L., Liu, P., Liu, Y., Sun, C., & Yin, Y. (2019). Allicin disrupts cardiac Cav1.2 channels via trafficking. *Pharmaceutical Biology*, *57*(1), 245–249. doi: 10.1080/13880209.2019.1577469

Hasan, A., Menon, S. N., Zerin, F., & Hasan, R. (2022). Dapagliflozin induces vasodilation in resistance-size mesenteric arteries by stimulating smooth muscle cell KV7 ion channels. *Heliyon*, *8*(5), e09503. doi: 10.1016/j.heliyon.2022.e09503

Imaizumi, V. M., Laurindo, L. F., Manzan, B., Guiguer, E. L., Oshiiwa, M., Otoboni, A. M. M. B., … Barbalho, S. M. (2023). Garlic: A systematic review of the effects on cardiovascular diseases. *Critical Reviews in Food Science and Nutrition*, *63*(24), 6797–6819. doi: 10.1080/10408398.2022.2043821

Khastkhodaei, S., Sharifi, G., Salahi, R., Rahnamaeian, M., & Moattar, F. (2011). Clinical efficacy of Stragol™ herbal heart drop in ischemic heart failure of stable chest angina. *European Journal of Integrative Medicine*, *3*(3). doi: 10.1016/j.eujim.2011.07.004

Leitão, R., de Oliveira, G. V., Rezende, C., Volino-Souza, M., Mesquita, J., de Carvalho, L. L., & Alvares, T. S. (2022). Improved microvascular reactivity after aged garlic extract intake is not mediated by hydrogen sulfide in older adults at risk for cardiovascular disease: a randomized clinical trial. *European Journal of Nutrition*, *61*(7), 3357–3366. doi: 10.1007/s00394-022-02895-y

Li, X.-H., Li, C.-Y., Xiang, Z.-G., Hu, J.-J., Lu, J.-M., Tian, R.-B., & Jia, W. (2012). Allicin ameliorates cardiac hypertrophy and fibrosis through enhancing of Nrf2 antioxidant signaling pathways. *Cardiovascular Drugs and Therapy*, *26*(6), 457–465. doi:10.1007/s10557-012-6415-z

Li, S., Guo, W., Lau, W., Zhang, H., Zhan, Z., Wang, X., & Wang, H. (2023). The association of garlic intake and cardiovascular risk factors: A systematic review and meta-analysis. *Critical Reviews in Food Science and Nutrition*, *63*(26), 8013–8031. doi: 10.1080/10408398.2022.2053657

Lopez, H. L., Ziegenfuss, T. N., Hofheins, J. E., Habowski, S. M., Arent, S. M., Weir, J. P., & Ferrando, A. A. (2013). Eight weeks of supplementation with a multi-ingredient weight loss product enhances body composition, reduces hip and waist girth, and increases energy levels in overweight men and women. *Journal of the International Society of Sports Nutrition*, *10*, 22. doi:10.1186/1550-2783-10-22

Mahfoud, F., Wang, J., & Ray, S. (2024). The current position of β-blockers in hypertension: guidelines and clinical practice. *Current Medical Research and Opinion*, *40*(sup1), 25–32. doi: 10.1080/03007995.2024.2318003

Manosroi, A., Lohcharoenkal, W., Khonsung, P., Manosroi, W., & Manosroi, J. (2013). Potent antihypertensive activity of Thai-Lanna medicinal plants and recipes from "MANOSROI III" database. *Pharmaceutical Biology*, *51*(11), 1426–1434. doi:10.3109/13880209.2013.796391

Majewski, M., Kasica, N., Jakubowski, P., & Podlasz, P. (2017). Influence of fresh garlic (Allium sativum L.) juice on zebrafish (Danio rerio) embryos: Developmental effects. *Journal of Elementology*, *22*(2), 475–486. doi:10.5601/jelem.2016.21.4.1261

McCrea, C. E., West, S. G., Kris-Etherton, P. M., Lambert, J. D., Gaugler, T. L., Teeter, D. L., ... Skulas-Ray, A. C. (2015). Effects of culinary spices and psychological stress on postprandial lipemia and lipase activity: Results of a randomized crossover study and in vitro experiments. *Journal of Translational Medicine*, *13*(1), 1–12. doi:10.1186/s12967-014-0360-5

Morris, D. M., Beloni, R. K., & Wheeler, H. E. (2013). Effects of garlic consumption on physiological variables and performance during exercise in hypoxia. *Applied Physiology, Nutrition, and Metabolism*, *38*(4), 363–367. doi:10.1139/apnm-2012-0210

Nwokocha, C. R., Ozolua, R. I., Owu, D. U., Nwokocha, M. I., & Ugwu, A. C. (2011). Antihypertensive properties of Allium sativum (garlic) on normotensive and two kidney one clip hypertensive rats. *Nigerian Journal of Physiological Sciences*, *26*(2), 213–218. doi:10.1007/s11418-010-0467-9

Osailan, A. M., Metsios, G. S., Duda, J. L., Kitas, G. D., Veldhuijzen van Zanten, J. J. C. S., & Elnaggar, R. K. (2023). Chronotropic Response and Risk Factors for Cardiovascular Disease in Patients with Rheumatoid Arthritis: A Cross-Sectional Study. *Journal of Clinical Medicine*, *12*(23), 7256. doi: 10.3390/jcm12237256

Papadopoulou, A., Pettinau, L., Seppänen, E., Sikanen, A., & Anttila, K. (2022). The interactive effects of exercise training and functional feeds on the cardiovascular performance of rainbow trout (Oncorhynchus mykiss) at high temperatures. *Current Research in Physiology*, *5*, 142–150. doi:10.1016/j.crphys.2022.02.005

Ried, K., Travica, N., & Sali, A. (2016). The effect of aged garlic extract on blood pressure and other cardiovascular risk factors in uncontrolled hypertensives: the AGE at Heart trial. *Integrated Blood Pressure Control*, *9*, 9-21. doi: 10.2147/IBPC.S93335

Sasmaz, H. K., Ilgaz, C., Kadiroglu, P., Erkin, O. C., Selli, S., & Kelebek, H. (2025). Comparative phytochemical analysis and bioactive potential of white and black garlic. *Scientific Reports*, *15*(1), 23427. doi: 10.1038/s41598-025-03843-6

Shackebaei, D., Ghazvineh, S., Godini, A., Pilehvarian, A., & Reshadat, S. (2010). Cardioprotective effect of garlic juice on the isolated rat heart in ischemia-reperfusion. *Journal of Medicinal Plants*, *9*(35), 71–79

Sharma, K., & Rani, V. (2021). Comparative phytochemical and antioxidative analysis of raw and aged garlic extract; indicating the therapeutic potential of stable organosulfur compounds. *Current Trends in Biotechnology and Pharmacy*, *15*, 96–103. doi: 10.5530/ctbp.2021.6.17

Siepmann, M., Weidner, K., Petrowski, K., & Siepmann, T. (2022). Heart rate variability: A measure of cardiovascular health and possible therapeutic target in dysautonomic mental and neurological disorders. *Applied Psychophysiology and Biofeedback*, *47*(4), 273–287. doi: 10.1007/s10484-022-09572-0

Sleiman, C., Daou, R. -M., Al Hazzouri, A., Hamdan, Z., Ghadieh, H. E., Harbieh, B., & Romani, M. (2024). Garlic and hypertension: Efficacy, mechanism of action, and clinical implications. *Nutrients*, *16*(17), 2895. doi:10.3390/nu16172895

Supa-aksorn, M., Tongsiri, S., Promya, J., Hongnueng, C., & Amornlerdpison, D. (2025). Synergistic effect of garlic and andrographis extracts on digestive enzyme activity, immune modulation, and anti- inflammation in nile tilapia (*Oreochromis niloticus*). *Comparative Immunology Reports*, *9*, 200257. doi: 10.1016/j.cirep.2025.200257

Supakul, L., Pintana, H., Apaijai, N., Chattipakorn, S., Shinlapawittayatorn, K., & Chattipakorn, N. (2014). Protective effects of garlic extract on cardiac function, heart rate variability, and cardiac mitochondria in obese insulin-resistant rats. *European Journal of Nutrition*, *53*(3), 919–928. doi:10.1007/s00394-013-0595-6

Thomson, M., Al-Qattan, K. K., JS, D., & Ali, M. (2015). Anti-diabetic and anti-oxidant potential of aged garlic extract (AGE) in streptozotocin-induced diabetic rats. *BMC Complementary and Alternative Medicine*, *16*(1), 17. doi: 10.1186/s12906-016-0992-5

Trieu, H. P., Nguyen, T. N., Do, T. P., Nguyen, T. C., Yen Pham, T. H., & Do, T. T. (2020). Primary study for possible transdifferentiation effects of several vietnamese plant extracts on isolated rat neonatal cardiomyocytes. *Vietnam Journal of Science and Technology*, *58*(4), 402–410. doi: 10.15625/2525-2518/58/4/14660

Wang, H., Yang, J., Qin, L., & Yang, X. (2015). Effect of garlic on blood pressure: A meta-analysis. *The Journal of Clinical Hypertension*, *17*(3), 223–231. doi: 10.1111/jch.12473

FABAD J. Pharm. Sci., 51, 1, 239-256, 2026
Doi: 10.55262/fabadeczacilik.1821524
RESEARCH ARTICLE

An Integrated Taguchi Design and Response Surface Methodological Approach for Development of Bedaquiline-Loaded Nanostructured Lipid Carriers

Rachmat MAULUDIN[*°], Asti RAHAYU[**], SATRIALDI[***], Neng Fisheri KURNIATI[****]

An Integrated Taguchi Design and Response Surface Methodological Approach for Development of Bedaquiline-Loaded Nanostructured Lipid Carriers

SUMMARY

Bedaquiline (BDQ), a poorly water-soluble drug, was successfully encapsulated in nanostructured lipid carriers (NLCs) to enhance its physicochemical properties. For the first time, BDQ-NLCs were optimized using a hybrid Taguchi and central composite design (CCD) methodology. This study selected cetyl palmitate, caprylic triglyceride, and Plantacare® 1200 in formulation development. The independent variables in this study, based on the Taguchi design approach, include the solid-liquid binary ratio, the surfactant concentration, and the sonication time. The dependent variables include particle size, encapsulation efficiency, and drug loading. The optimized BDQ-NLCs exhibited a particle size of 153.5 ± 2.3 nm, an encapsulation efficiency of 94.46 ± 0.09%, and a drug loading capacity of 3.04 ± 0.02%. The characterization of the optimum BDQ-NLCs revealed a zeta potential of -47.75 mV, a round particle morphology, and an endothermic event occurring between 45.94 and 54.60°C, indicating a transformation phase from solid to liquid. In vitro drug release profiles demonstrated that the optimized BDQ-NLCs formulation provides controlled and pH-dependent drug release, governed by a diffusion-driven mechanism. The stability evaluation of BDQ-NLCs demonstrated consistent stability under refrigerated conditions, while significant particle growth was observed at 25°C and 40°C, indicating temperature-dependent stability. Therefore, the developed BDQ-NLC formulation represents a physicochemically optimized system that may serve as a platform for further development of BDQ delivery, with therapeutic potential to be validated in future biological studies.

Keywords: *Design of Experiment, Bedaquiline, characterization, formulation, nanostructured lipid carriers.*

Tasarım Deney Yöntemi Kullanılarak Nanoyapılı Lipid Taşıyıcılar, Tabletler ve İnsan Plazmasında Bedaquilin Fumarat Tayini İçin RP-HPLC Yönteminin Geliştirilmesi ve Validasyonu

ÖZ

Su içinde düşük çözünürlüğe sahip bir ilaç olan Bedaquiline (BDQ), fizikokimyasal özelliklerini iyileştirmek amacıyla nanoyapılı lipid taşıyıcılar (NLC'ler) içinde başarıyla enkapsüle edilmiştir. BDQ-NLC'lerin optimizasyonu, bir hibrit Taguchi ve merkezi kompozit tasarım (CCD) metodolojisi kullanılarak ilk kez bu çalışmada gerçekleştirilmiştir. Formülasyon geliştirmede setil palmitat, kaprilik trigliserit ve Plantacare® 1200 seçilmiştir. Taguchi tasarımına dayalı bağımsız değişkenler, katı-sıvı ikili karışım oranı, surfaktan konsantrasyonu ve sonikasyon süresini içermekte olup; bağımlı değişkenler ise parçacık boyutu, enkapsülasyon verimi ve ilaç yükü olarak belirlenmiştir. Merkezi Kompozit Tasarım ile geliştirilen optimize BDQ-NLC'ler, 153,5 ± 2,3 nm'lik parçacık boyutu, %94,46 ± 0,09 enkapsülasyon verimi ve %3,04 ± 0,02 ilaç yük kapasitesi sergilemiştir. Optimum BDQ-NLC'lerin karakterizasyonu, -47,75 mV'luk zeta potansiyeli, yuvarlak veya oval parçacık morfolojisi ve katı-sıvı faz dönüşümünü işaret eden 45,94 ile 54,60°C arasında gerçekleşen endotermik bir olay ortaya koymuştur. İn vitro ilaç salım profilleri, optimize edilmiş BDQ-NLC'lerin difüzyon odaklı bir mekanizma ile kontrollü ve pH bağımlı bir ilaç salımı sağladığını göstermiştir. BDQ-NLC'lerin stabilite değerlendirmesi, soğutma koşullarında tutarlı bir kararlılık gösterirken, 25°C ve 40°C'de anlamlı partikül büyümesinin gözlemlenmesi, sıcaklığa bağlı bir kararlılığı işaret etmektedir. Bu nedenle, geliştirilen BDQ-NLC formülasyonu, BDQ taşınmasının daha ileri geliştirilmesi için bir platform olarak hizmet edebilecek fizikokimyasal açıdan optimize edilmiş bir sistem olup, terapötik potansiyelinin gelecekteki biyolojik çalışmalarla doğrulanması gerekmektedir.

Anahtar Kelimeler: *Deney Tasarımı, Bedaquilin, karakterizasyon, formülasyon, nanoyapılı lipid taşıyıcı.*

Recieved: 11.11.2025
Revised: 19.02.2026
Accepted: 25.02.2026

[*] ORCID: 0000-0002-3729-0254, Department of Pharmaceutics, School of Pharmacy, Institut Teknologi Bandung, Bandung, Indonesia
[**] ORCID: 0009-0004-4731-942X, Program Doctoral, School of Pharmacy, Institut Teknologi Bandung, Bandung, Indonesia; Department of Pharmaceutics, Faculty of Health Sciences, Universitas PGRI Adi Buana Surabaya, Indonesia
[***] ORCID: 0000-0001-9973-4044, Department of Pharmaceutics, School of Pharmacy, Institut Teknologi Bandung, Bandung, Indonesia
[****] ORCID: 0000-0001-9973-4044, Department of Pharmacology and Clinical Pharmacy, School of Pharmacy, Institut Teknologi Bandung, Bandung, Indonesia

[°] Corresponding Author; Rachmat MAULUDIN
E-mail: rachmat@itb.ac.id

INTRODUCTION

Mycobacterium tuberculosis (MTB), the primary causative pathogen of tuberculosis (TB), remains a critical public health challenge worldwide (Millington et al., 2024). Following an upward trend in TB cases during the COVID-19 pandemic, the global incidence rate has shown a decline in growth and is now stabilizing (Bussi & Gutierrez, 2019). Reported cases reached around 10.8 million in 2023, marking a marginal increase from 10.7 million in 2022 but still substantially higher than the 10.4 million and 10.1 million recorded in 2021 and 2020, respectively. Additionally, in 2023, an estimated 175,923 patients globally were identified and received treatment for multidrug-resistant or rifampicin-resistant TB (MDR/RR-TB), accounting for only 44% of the projected 400,000 cases (with a 95% uncertainty interval ranging from 360,000 to 440,000) that emerged that year. Among recent advancements in TB treatment, BDQ stands out as an innovative oral diarylquinoline-based antimycobacterial drug (Luo et al., 2020). Approved by the FDA in 2012, BDQ has become a crucial therapeutic option for managing MDR and extensively drug-resistant TB (MDR/XDR-TB). Functioning as a first-in-class ATP synthase inhibitor, BDQ exhibits exceptional specificity toward mycobacteria (Wei et al., 2024), with a binding affinity for mycobacterial ATP synthase over 20,000 times stronger than for its eukaryotic counterpart (Abraham et al., 2024).

BDQ has been widely studied for alternative delivery methods, such as oral and intranasal administration (Chae, Choi, Tanaka, & Choi, 2021). Commercially available as *Sirturo*® by Janssen-Cilag, it is formulated as an uncoated 100 mg immediate-release tablet for oral ingestion (Guglielmetti et al., 2017). However, oral BDQ administration is often associated with adverse effects such as nausea, vomiting, joint pain, and QTc prolongation (Gavras & Schluger, 2024). To reduce these side effects, researchers have explored intranasal delivery systems that enable direct lung targeting (Patil, Sawant, & Kunda, 2021). Despite this promise, achieving efficient pulmonary drug deposition, particularly in the alveolar region remains a significant challenge (Yadav, Rawal, & Baxi, 2016). Consequently, optimizing critical parameters like particle size, surface charge, and lipophilicity is essential to improve drug penetration across the respiratory barrier (Carnero Canales et al., 2024).

Currently, various methods are employed to address pulmonary barriers, including non-cellular and cellular barriers (Costabile et al., 2024). Among these, lipid-based nanoparticle carriers, or lipid nanocarriers, represent a promising approach (Gordillo-Galeano, Ospina-Giraldo, & Mora-Huertas, 2021). This methodology may enhance the pharmacodynamics of BDQ, addressing its poor aqueous solubility (0.002 μg/mL at 25°C) and high lipophilicity (log P ≈7.74) (PubChem). Nanostructured lipid carriers (NLCs) exhibit exceptional biocompatibility and drug-loading capacity, making them promising candidates for overcoming the solubility limitations of lipophilic drugs like BDQ (Jia et al., 2024). For example, research on the pulmonary administration of BDQ via nanolipid carriers for potential tuberculosis therapy highlights the critical role of targeted lung drug delivery in the effective management of respiratory diseases (De Matteis et al., 2018). NLCs constitute a superior generation of drug delivery vehicles, offering substantial improvemenregionts over conventional solid lipid nanoparticles. The strategic integration of liquid lipids into the NLC matrix fundamentally enhances system performance by overcoming multiple limitations of traditional formulations. These innovative carriers effectively resolve critical issues such as poor hydrophilic drug incorporation, reduced physical stability, and compound degradation, while simultaneously achieving superior drug payload capacity compared to earlier lipid-based systems (Mauludin, Garmana, & Fauzian, 2024; Müller, Radtke, & Wissing, 2002a). This unique structure not only enhances the payload capacity for lipophilic

drugs but also facilitates a sustained release profile, making NLCs a versatile platform for drug delivery (Kumar et al., 2023).

A significant gap exists in the current literature regarding the development of BDQ-NLCs using a hybrid Design of Experiments (DoE) methodology. This study bridges this gap by pioneering an integrated optimization strategy combining Taguchi design and CCD. The Taguchi method provides a robust screening phase, efficiently identifying critical formulation parameters with a minimal number of experimental runs through its orthogonal array design (Rajyalakshmi & Boggarapu, 2019). This synergistic Taguchi-CCD approach offers superior optimization capabilities compared to either method alone. The resulting optimized BDQ-NLCs formulation was thoroughly characterized for its particle size (PS), polydispersity index (PDI), zeta potential (ZP), entrapment efficiency (EE), drug loading (DL), and colloidal stability. Furthermore, we aimed to highlight the opportunity to integrate sustainable practices into the formulation development of our BDQ-NLCs by assessing our experimental designs and reducing energy and time consumption wherever possible.

MATERIALS AND METHODS

Materials

Bedaquiline fumarate with ≥ 98.5 % purity was procured from Hangzhou APIChem Technology Co., Ltd. Ammonium acetate was purchased from Merck KGaA, Darmstadt, Germany. Cetyl palmitate as Cutina® CP, Plantacare® 1200, Plantacare® 2000, Cremophor® RH 40, and Kolliphor® RH 40 were procured from BASF Co., Ltd. (Germany). Tego® Care 165 was procured from Evonik Co., Ltd (Germany). Capryl triglyceride, Span® 80, and Poloxamer 188 were obtained from Haihang Industry Co., Ltd. (China). The HPLC Grade Methanol and acetonitrile were acquired from Fisher Scientific Korea Ltd, Seoul, Korea. Analytical grade water (Onelab Waterone™) was obtained from PT. Jayamas Medica Industry (Sidoarjo, Indonesia).

Methods

Screening of lipids

The selection of solid and liquid lipids was based on their ability to solubilize BDQ. Solubility was assessed by incrementally adding solid lipids to 10 mg of BDQ at 80°C until no visible drug particles remained after 24 hours. Solubility behavior was evaluated visually via light microscopy. A lipid was deemed an effective solvent if it produced a clear solution (Satrialdi, Putri, & Lumintang, 2023); otherwise, it was classified as a non-solvent if a biphasic system formed (Kovačević, Müller, & Keck, 2020).

The preparation of BDQ-NLCs

Surfactants were screened for their ability to emulsify solid-liquid binary mixtures. Initial NLCs were formulated by combining 5% (w/v) solid-liquid binary (SLB) ratio with 5% (w/v) surfactants or blends at 70°C, followed by 5-minute ultrasonication (CY-500, Optic Ivymen System®, Spain) at 60% amplitude. Emulsification efficiency was evaluated via particle size and PDI using a Delsa™ Nano C Particle Analyzer (Beckman Coulter, USA).

Experiment design for the optimization and development of BDQ-NLCs

A Taguchi design was used to screen critical formulation parameters for NLCs. Seven independent variables were investigated: SLB ratio (X_1), total lipid amount (X_2), surfactant concentration (X_3), homogenization speed (X_4), and homogenization time (X_5), along with sonication amplitude (X_6) and sonication time (X_7), each evaluated at two concentration levels. This systematic approach assessed their influence on two critical quality attributes: particle size (Y_1) and PDI (Y_2). Statistical evaluation using Minitab software identified the most influential parameters through variance analysis, establishing their relative significance in the NLC fabrication process.

Central composite design for formulation optimization

Building on the Taguchi design outcomes, three critical parameters—SLB ratio (X_1), surfactant concentration (X_2), and sonication time (X_3)—were further investigated using a CCD. The CCD was selected for its superior flexibility and accurate detection of nonlinear relationships compared to other designs like Box-Behnken. This design evaluated the influence of these parameters on nanoparticle characteristics: particle size (Y_1), encapsulation efficiency (Y_2), and drug loading capacity (Y_3). A total of 20 BDQ-NLC formulations were composed (Table 3.). ANOVA facilitated the selection of the most appropriate model, and response surface methodology generated polynomial equations (Equation 1.) to locate optimal formulation conditions. Model significance was determined by ANOVA ($p < 0.05$), and validity was confirmed at a 95% confidence level by comparing predicted versus observed values. Subsequently, optimal conditions were established by applying specific criteria for each variable, ultimately identifying the solution with the highest desirability.

$$Y_i = \beta_0 + \beta_1 X_1 + \beta_2 X_2 + \beta_3 X_3 + \beta_{11} X_{12} + \beta_{22} X_{22} + \beta_{33} X_{33} + \beta_{12} X_1 X_2 + \beta_{13} X_1 X_3 + \beta_{23} X_2 X_3$$

(Equation 1)

Particle size, polydispersity index, and zeta potential determination

Particle size distribution and PDI were assessed by dynamic light scattering (DLS) following 20-fold dilution with Onelab Waterone™. Zeta potential measurements were conducted via electrophoretic light scattering (ELS) using a Malvern Instruments (UK) instrument, with 200-fold diluted samples analyzed in specialized flat-surface cells to ensure accurate surface charge determination.

Encapsulation efficiency and drug loading determination

The encapsulation efficiency (EE) and drug loading (DL) of BDQ-NLCs were determined through indirect quantification. Following centrifugation (13,000 rpm, 30 min) with a 10 kDa molecular weight cut-off filter (Amicon Ultra, USA), unentrapped BDQ was extracted using methanol. Chromatographic separation was achieved using a LiChrospher C18 column with UV detection at 225 nm. The mobile phase consisted of ammonium acetate buffer (pH 4.7) and methanol (15:85 v/v), which was membrane-filtered (0.22 µm) before use. Isocratic elution was maintained at 1.2 mL/min throughout the analysis. Results are reported as EE and DL, according to equations 1 and 2 below (Marques et al., 2025).

$$EE(\%) = \frac{Theoritical\ BDQ\ Concentration - Free\ BDQ\ Concentration}{Theoritical\ BDQ\ Concentration} \times 100\%$$

(Equation 2)

$$DL(\%) = \frac{Amount\ of\ entrapped\ BDQ}{Amount\ of\ lipid\ phase + Amount\ of\ entrapped\ BDQ} \times 100\%$$

(Equation 3)

Morphology analysis

The morphology of BDQ-NLCs was analyzed using TEM (JEOL JEM-1400, Japan) at 100 kV. A drop of the optimized BDQ-NLCs was placed on a 200 nm carbon-coated copper grid. Negative staining was performed using UranyLess EM Stain, with 15 µL applied for 1 min before imaging.

Thermal characteristic determination

Thermal characterization was performed using a Shimadzu DSC-60 Plus calorimeter. Sample preparation involved centrifugation (10,000 rpm, 30 min) to minimize water interference. Precisely weighed samples (2-8 mg) of cetyl palmitate, unloaded NLCs, and optimized BDQ-NLCs were hermetically sealed

in aluminum crucibles. The temperature program ramped from 20°C to 90°C at 10°C/min, with a constant nitrogen purge at 50 mL/min. An empty aluminum pan provided the reference baseline for all measurements.

***In vitro* drug release study**

The *in vitro* release of BDQ-NLCs was evaluated using a dialysis bag method with a USP Apparatus II dissolution system. The study was conducted under sink conditions in two distinct media: phosphate buffer (pH 7.4) to simulate intestinal fluid and acetate buffer (pH 5.5) to mimic a moderately acidic environment. The dissolution vessel contained 900 mL of medium maintained at 37 ± 0.5°C with a paddle rotation speed of 100 rpm. An aliquot of BDQ-NLCs equivalent to 10 mg of BDQ was placed in a pre-hydrated dialysis bag (MWCO 12-14 kDa) and immersed in the release medium. Samples (5 mL) were withdrawn at predetermined intervals up to 2880 minutes, with immediate replenishment of fresh medium. BDQ concentration in the samples was quantified using a validated RP-HPLC method. Release kinetics were analyzed by fitting the cumulative release data to various mathematical models, with the best-fit model selected based on the highest coefficient of determination (R^2). All experiments were performed in triplicate.

Stability testing

The optimized BDQ-NLC formulation underwent stability testing under three temperature conditions (4°C, 25°C, and 40°C) for 30 days. Samples were analyzed at predetermined intervals (days 0, 7, 14, and 30) to evaluate particle size (PS), encapsulation efficiency (EE), and drug loading (DL) throughout the storage duration.

Statistical analysis

Data analysis was performed using Minitab®21 software (Minitab, Inc., PA, USA). One-way analysis of variance (ANOVA) was used to determine intergroup differences, with $p<0.05$ set as the criterion for statistical significance. This threshold indicated significant differences between the experimental groups in the study.

RESULTS AND DISCUSSION

Classical lipid screening

The solubility profile of bedaquiline fumarate was systematically evaluated across eleven lipid excipients during a 60-minute observation period (Table 1.). Glyceryl monostearate (A1) demonstrated consistent solubility throughout all time points, whereas caprylic triglyceride (A7) required 30 minutes for complete dissolution. Partial solubility emerged after 45 minutes for cetyl palmitate (A2) and cetyl alcohol (A3), with remaining excipients showing no dissolution capacity. Comparative analysis identified glyceryl monostearate (A1) as the optimal excipient, followed by caprylic triglyceride (A7), with other lipids proving ineffective under experimental conditions (Pornputtapitak, Thiangjit, & Tantirungrotechai, 2024). Preliminary results suggest GMS may destabilize lipid nanoparticles, prompting the selection of cetyl palmitate for initial testing. Its composition—palmitic acid esterified with cetyl alcohol—provides a stable, adaptable matrix for drug encapsulation in NLCs (Kovačević et al., 2020).

Table 1. The solubility of Bedaquiline fumarate in various lipids

Time (min)	Lipid Excipients										
	A1	A2	A3	A4	A5	A6	A7	A8	A9	A10	A11
15	+	-	-	-	-	-	-	-	-	-	-
30	+	-	-	-	-	-	+	-	-	-	-
45	+	+	+	-	-	-	+	+	-	-	-
60	+	+	+	-	-	-	+	+	-	-	-

[(+) dissolved, (−) not dissolved]

Selection of surfactants

Surfactant screening evaluated emulsification capacities for the SLB ratio (Figure 1). Lower-molecular-weight surfactants, such as Alkyl Polyglucosides (APGs), showed promising results (Sułek, Ogorzałek, Wasilewski, & Klimaszewska, 2013) and yielded smaller, more stable particle sizes. Lower molecular weight surfactants, such as Plantacare® 1200 (320.4 g/mol) and Plantacare® 2000 (345.8 g/mol), produced NLCs with smaller particle sizes (159.4 ± 2.65 nm and 190.0 ± 2.23 nm) and lower PDI (0.190 ± 0.003 and 0.206 ± 0.005), indicating superior uniformity and stability. In contrast, higher molecular weight surfactants, such as Tego® Care 165 (~4,684.5 g/mol) and Pluracare® F 68 (~8,350 g/mol), resulted in larger particle sizes (839.5 ± 1.35 nm and 747.2 ± 2.54 nm) and higher PDI (0.377 ± 0.003 and 0.331 ± 0.006), suggesting reduced stability. Plantacare® 1200's shorter alkyl chain improved packing efficiency and reduced steric hindrance, yielding smaller particles. (Keck et al., 2014). High molecular weight surfactants, such as Tween® 80, Cremophor® RH 40, Kolliphor® RH 40, Tego® Care 165, and Poloxamer 188, often lead to destabilisation in NLC systems due to their increased steric hindrance and decreased diffusion rates at the oil-water interface.

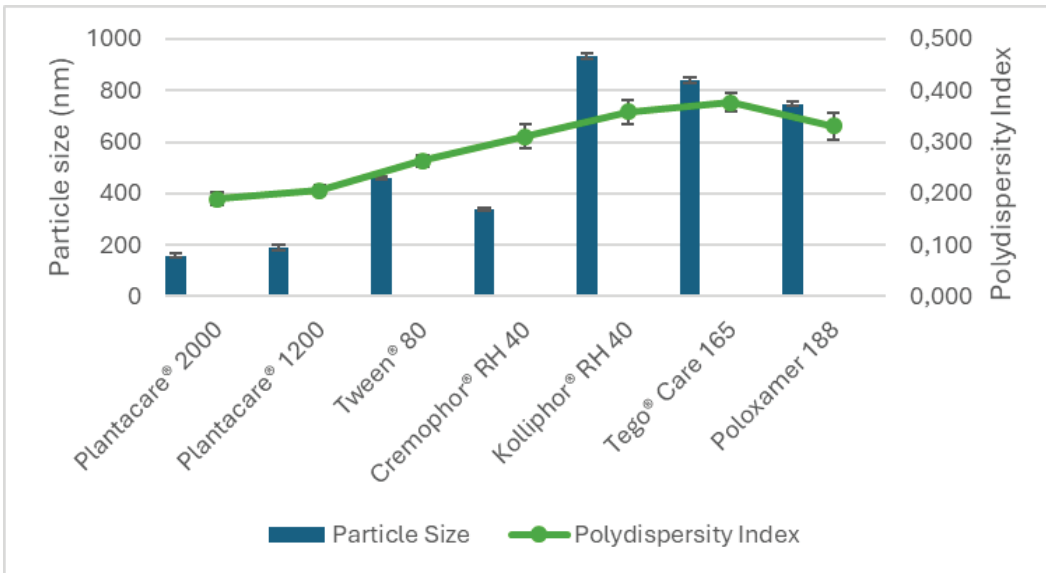


Figure 1. Particle size and PDI of the preliminary NLCs prepared from various surfactants, Plantacare® 2000; Plantacare® 1200; Tween® 80; Cremophor® RH 40; Kolliphor® RH 40; Tego® Care 165; and Poloxamer 188.

Formulation development and optimization using a hybrid design approach: Taguchi design for screening of relevant experimental factors

The Taguchi method enables systematic optimization of formulation parameters, enhancing product consistency and quality (Rajyalakshmi & Boggarapu, 2019). This experimental configuration employs a specialized array design that enables comprehensive analysis of multiple variables within limited trials, accounting for linear, quadratic, or higher-order effects while excluding factor interactions (Sathish, Giri, Rathinasamy, & Kanan, 2024). Particle size analysis demonstrated significant factorial modeling (p=0.0008), with derived equations maintaining 95% confidence intervals, confirming robust statistical validity. The Taguchi design optimized BDQ-NLCs by focusing on particle size (Y_1) and PDI (Y_2) as critical quality attributes (Table 2.). Seven factors (X_1–X_7) at two levels each were tested across 16 formulations. Sonication amplitude (X_6) had the greatest impact (rank 1), followed by

total lipid concentration (X_2, rank 2) and sonication time (X_7, rank 3). SLB ratio (X_1) and homogenization speed (X_4) were equally influential (rank 4), while homogenization time (X_5) had the least effect (rank 7). The results highlight the importance of sonication parameters and lipid concentration in achieving optimal particle size and uniformity. Although sonication amplitude (X_6) and total lipid amount (X_2) ranked highest for particle size control, the SLB ratio (X_1) and surfactant concentration (X_3) were prioritized for CCD optimization due to their critical influence on encapsulation efficiency and drug loading.

Table 2. Experimental design and results of BDQ-NLC formulations using the Taguchi method

Run	Experimental Factors							Dependent Variables	
Formulation	X_1	X_2	X_3	X_4	X_5	X_6	X_7	Y_1	Y_2
T1	60	4	3	6000	1	50	4	315	0.351
T2	60	4	3	8000	1	70	6	221	0.287
T3	60	4	5	6000	3	50	6	185	0.207
T4	60	4	5	8000	3	70	4	199	0.216
T5	60	6	3	6000	3	70	4	237	0.387
T6	60	6	3	8000	3	50	6	211	0.209
T7	60	6	5	6000	1	70	6	196	0.188
T8	60	6	5	8000	1	50	4	267	0.321
T9	80	4	3	6000	3	70	6	261	0.253
T10	80	4	3	8000	3	50	4	344	0.384
T11	80	4	5	6000	1	70	4	254	0.236
T12	80	4	5	8000	1	50	6	288	0.277
T13	80	6	3	6000	1	50	6	303	0.311
T14	80	6	3	8000	1	70	4	453	0.367
T15	80	6	5	6000	3	50	4	265	0.312
T16	80	6	5	8000	3	70	6	248	0.255

Formulation optimization using central composite design

The CCD offers superior methodological flexibility compared to the Box-Behnken Design in response surface methodology investigations. By incorporating axial points, CCD facilitates more accurate identification of nonlinear relationships between variables. This advanced design provides enhanced curvature detection and superior modeling capacity of response surfaces. Analysis of Taguchi results identified three key parameters: solid-liquid binary mixture (X_1), surfactant concentration (X_2), and sonication time (X_3) as the most influential experimental factors. The effects of these parameters on particle size (Y_1), entrapment efficiency (Y_2), and drug loading (Y_3) were further investigated, and the CCD was employed to optimize the results. Outcomes from 20 experimental trials in this study are presented (Table 3.). Utilizing Central Composite Design, three polynomial equations were developed to assess variable-response correlations and determine optimal conditions. All models demonstrated strong predictive validity with regression coefficients (R^2) > 0.800 (Table 4.), indicating excellent agreement between empirical data and theoretical predictions.

Table 3. Experimental design and results of BDQ-NLC formulations using the CCD

Run	Independent Variables			Dependent Variables			Polydispersity Index
	X_1	X_2	X_3	Y_1	Y_2	Y_3	
1	60	3.5	4	350	84.88	2.79	0.509
2	80	4.5	4	316	88.51	2.81	0.506
3	80	3.5	6	219	88.79	2.85	0.340
4	60	4.5	6	181	89.53	2.85	0.269
5	70	4	5	177	94.26	3.04	0.292
6	70	4	5	159	95.56	3.12	0.251
7	80	3.5	4	461	87.16	2.83	0.740
8	60	4.5	4	349	83.35	2.85	0.555
9	60	3.5	6	239	86.82	2.80	0.395
10	80	4.5	6	195	90.89	2.95	0.298
11	70	4	5	158	94.46	3.09	0.245
12	70	4	5	157	94.72	3.04	0.203
13	53.67	4	5	229	86.45	2.60	0.338
14	86.33	4	5	226	83.43	2.97	0.334
15	70	3.1835	5	215	86.34	2.89	0.337
16	70	4.8165	5	147	93.64	3.08	0.235
17	70	4	3.367	239	87.85	2.76	0.349
18	70	4	6.633	145	93.25	3.04	0.223
19	70	4	5	175	93.93	3.11	0.246
20	70	4	5	186	95.29	3.17	0.292

Effect of experimental factors on particle size, entrapment efficiency, drug loading of BDQ-NLCs

Effect of experimental factors on particle size of BDQ-NLCs

BDQ-NLCs particle size (147.5–461.7 nm) was significantly influenced ($p < 0.05$) by sonication time (X_3) and SLB ratio (X_2). The coefficients of each variable facilitated a direct comparison of their effects on particle size, as indicated by the sign and magnitude of the coefficients. Regression analysis (Equation 4) revealed negative coefficients for both surfactant concentration (-25.4) and sonication duration (-59.7), demonstrating their inverse correlation with BDQ-NLC particle size. The larger magnitude of the sonication time coefficient indicates its greater relative impact on particle size reduction compared to surfactant concentration. Response surface methodology (Figure 4A.) confirmed that elevated levels of both parameters consistently yielded smaller nanoparticles, with sonication time showing more pronounced effects on size diminution. Increased sonication time and surfactant concentration reduced particle size by forming a dense network, lowering interfacial tension, and preventing aggregation (Ma et al., 2014). The contour plots (Figure 4.) depict the response surfaces for PS, EE, and DL. In each plot, one independent variable was held at its hold values—surfactant concentration at 4% (w/v), sonication time at 5 min, and SLB ratio at 70, respectively. Prolonged ultrasonication enhances nanoparticle breakdown through cavitation-induced shear forces, effectively reducing particle size (Viegas et al., 2023). Conversely, elevated SLB ratio concentrations promote particle aggregation (Equation 4.), attributable to inadequate surfactant coverage, increased viscosity, and diminished sonication efficacy, ultimately yielding larger particle formations (Khosa, Reddi, & Saha, 2018).

Particle Size (nm):

$$166.9+5.0X_1 - 25.4X_2 - 59.7X + 41.6\,X_1^2 + 24.2\,X_2^2 + 28.3\,X_3^2 - 13.7\,X_1X_2 - 10.3\,X_1X_3 + 9.0X_2X_3$$

(Equation 4)

Effect of experimental factors on entrapment efficiency of BDQ-NLCs

Entrapment efficiency of BDQ-NLCs ranged from 83.35 to 95.56% (Table 3.). The ANOVA analysis revealed that the square effect of SLB ratio (X_1^2), square effect of surfactant concentration (X_2^2), square effect of sonication time (X_3^2), variable surfactant concentration (X_2), and sonication time (X_3) significantly affect the entrapment efficiency of BDQ-NLCs (P-value < 0.05). While the effects of the variables X_2 (surfactant concentration) and X_3 (sonication time) were insignificant toward the BDQ-NLCs encapsulation efficiency (P-value > 0.05). Contour plot analysis (Figure 4B.) and (Equation 5.) show that elevated levels of the SLB ratio, surfactant concentration, and sonication time collectively enhance the encapsulation efficiency of BDQ-NLCs. Increased surfactant concentration and prolonged sonication time reduce nanoparticle size, thereby increasing the surface area-to-volume ratio. This expanded interfacial area facilitates greater drug incorporation. During thermal processing, this promotes the preferential partitioning of BDQ into the lipid phase, thereby enhancing encapsulation efficiency during the subsequent homogenization and cooling stages (Beloqui, Solinís, Rodríguez-Gascón, Almeida, & Préat, 2016). Increased surfactant concentration stabilizes lipid nanoparticles, improving entrapment efficiency by minimizing aggregation (Khan, Sharma, & Jain, 2023). Prolonged sonication reduces particle size, strengthening drug-lipid interactions. Thermal processing dissolves BDQ, while subsequent cooling induces lipid solidification and drug entrapment. Size reduction through sonication enhances encapsulation efficiency via increased surface area.

Entrapment efficiency (%):

$$94.71+0.44X_1 + 1.24X_2 + 1.57X_3 - 3.71X_1^2 - 1.82X_2^2 - 1.61X_3^2 + 0.29X_1X_2 - 0.52X_1X_3 + 0.6X_2X_3$$

(Equation 5)

Effect of experimental factors on drug loading of BDQ-NLCs

Drug loading of BDQ-NLCs varied from 2.60 to 3.17% (Table 3). According to the ANOVA analysis, the variables X1, ratio of solid liquid mixture, square effect of SLB ratio (X_1^2), and square effect of sonication time (X_3^2) significantly affect the BDQ-NLCs drug loading (P-value < 0.05). In contrast, the variable surfactant concentration and sonication time were not significant for the BDQ-NLCs drug loading (P-value > 0.05). BDQ is the lipid-soluble active ingredient; therefore, the BDQ-NLCs drug loading was directly proportional to its encapsulation efficiency. On the contour plot (Figure 4C.) and according to (Equation 6.), it is shown that increasing the ratio of the solid-liquid lipid mixture (X_1), the surfactant concentration (X_2), and the sonication time (X_3) will increase the BDQ-NLCs drug loading. The 20 tested BDQ-NLC formulas exhibited high encapsulation efficiency (>90%) (Table 3.). Elevating the solid-to-liquid lipid ratio improves active ingredient incorporation by forming a more rigid, organized matrix that can accommodate greater lipophilic drug content while reducing leakage potential. Higher solid lipid content enhances loading stability, whereas increased surfactant levels promote superior emulsification and nanoparticle stabilization through improved interfacial activity. This dual optimization strategy effectively balances drug payload with system stability (Khosa et al., 2018). Sonication time critically influences BDQ incorporation into NLCs by facilitating drug migration from the aqueous to the lipid phase during

hot homogenization. This redistribution process, enhanced by subsequent cooling, promotes effective encapsulation within lipid matrices. As previously discussed, prolonged sonication time optimizes this phase-transfer mechanism, thereby improving overall drug-loading efficiency.

Drug loading (%)

$$3.09 + 0.06X_1 + 0.04X_2 + 0.05X_3 - 0.12X_1^2 - 0.05X_2^2 - 0.08X_3^2 - 0.004X_1X_2 + 0.02X_1X_3 + 0.01X_2X_3$$

(Equation 6)

The contour plots (Figure 4.) and optimization graphs (Figure 2.) provide critical insights into the relationships between independent variables and responses. Figure 4A reveals a nonlinear inverse correlation between sonication time (X_3) and particle size (Y_1), where extended sonication (>5 min) combined with higher surfactant concentrations (X_2 >4% w/v) yielded particles below 200 nm, attributable to enhanced cavitation and interfacial stabilization. Conversely, Figure 4B demonstrates that encapsulation efficiency (Y_2) plateaued at intermediate SLB ratio (X_1 ≈70:30) and surfactant levels (X_2 ≈4% w/v), reflecting a balance between lipid matrix capacity and surfactant-mediated drug partitioning. The global optimum (desirability = 0.9642) lies at the intersection of minimized particle size, maximized EE (>95%), and elevated drug loading (>3%), achieved at X_1 = 71.5:28.5, X_2 = 4.2% w/v, and X_3 = 5.4 min (Figure 2.). These findings confirm the predictive accuracy of the quadratic models and highlight the need for multi-factor optimization for BDQ-NLCs. The optimized BDQ-NLCs achieved high encapsulation (94.46%) but moderate drug loading (3.04%), equating to a lipid-to-drug ratio of ~33:1. Administering a 100 mg BDQ dose would require approximately 3.3 g of lipid, a payload that is substantial yet potentially feasible for pulmonary delivery with optimized formulation strategies, though dose volume and local tolerability must be carefully evaluated. While the present study focuses on the physicochemical optimization and in vitro characterization of BDQ-NLCs, it is important to note that demonstrating suitability for pulmonary delivery would require subsequent aerodynamic characterization in future studies.

Selection of optimum BDQ-NLC formulation

The ideal BDQ-NLC formulation was determined using Table 4 criteria, demonstrating minimal particle diameter, maximal encapsulation efficiency, and optimal drug payload. Minitab® 21's response optimizer tool enabled this selection by systematically evaluating critical quality attributes. The optimization graphs reveal that the optimal values for the independent variables X_1, X_2, and X_3 are 71.5:29.5 for the Solid-liquid binary mixture, 4.2% (w/v) for the surfactant concentration, and 5.4 minutes for the sonication duration. The final optimized formulation was selected based on its superior performance across all critical parameters: it demonstrated (1) the smallest particle size (Y_1) 141.1 nm, (2) the highest entrapment efficiency (Y_2) 95.38%, and (3) the maximum drug loading (Y_3) 3.12%, among all tested formulations, meeting our predetermined optimization criteria. A composite desirability value of 0.9642 was achieved for the optimized formulation, confirming its high reliability, where a value of 1.0 indicates all response goals are met simultaneously. This is visually supported by the optimization plots (Figure 2.), where the vertical lines pinpoint the optimal parameters (e.g., SLB ratio at 71.5) and the horizontal lines show the corresponding predicted responses (e.g., particle size of ~141 nm), collectively defining the global optimum.

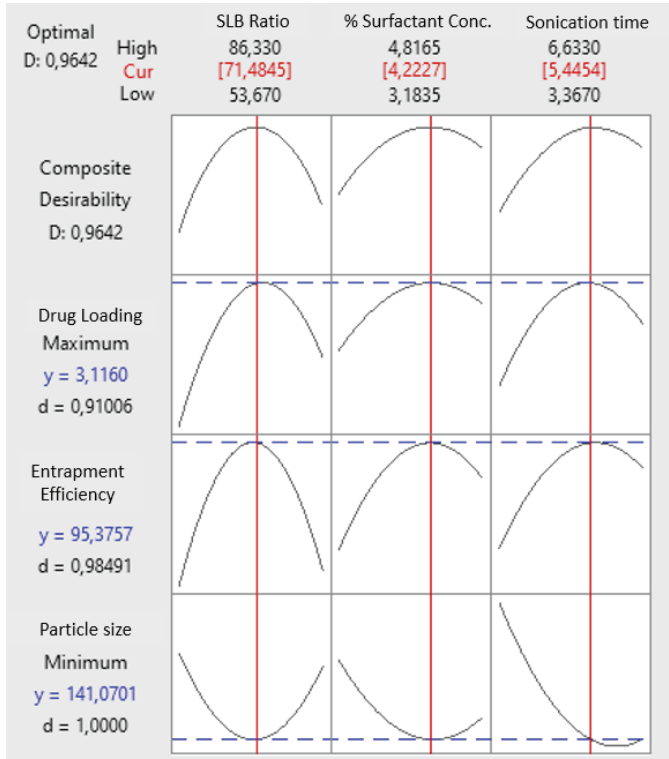


Figure 2. Optimization plots of Y_1: particle size (nm), Y_2: encapsulation efficiency (%), and Y_3: drug loading (%) based on independent variables X_1: SLB ratio (%, w/v), X_2: surfactant concentration (% w/v), and X_3: sonication time (min).

Confirmation of optimum BDQ-NLCs formulation

The BDQ-NLCs were fabricated utilizing the optimal formulation, and the outcomes were contrasted with the predicted values obtained from the CCD (Table 4.). The optimal formulation (Run 6) achieved a particle size of 159 nm, encapsulation efficiency of 95.56%, and drug loading of 3.12%, all of which closely matched the predictions with an error of less than 10%. This consistency underscores the robustness of the hybrid Taguchi-CCD approach in optimizing BDQ-NLCs. The experimental measurements for the responses Y_1 (PS), Y_2 (EE), and Y_3 (DL) were found to be 153.5 ± 2.3 nm, 94.46 ± 0.09%, and 3.04 ± 0.02%, respectively. The percentage of error calculated for the three responses was less than 10%, indicating that the predictive performance of models demonstrated significant predictive accuracy (Sabour & Amiri, 2017). Furthermore, the optimal BDQ-NLCs formulation exhibited PDI and zeta potential values of 0.29 ± 0.03 and -47.75 ± 4.22 mV, respectively. While the previous study achieved a smaller particle size of 65.57 nm, this can be attributed to their employment of high-shear homogenization (Rajendhiran & Bhattacharyya, 2024), a technique known to generate superior mechanical shear forces for nanoparticle size reduction compared to the ultrasonication method utilized in the present study. The optimized BDQ-NLCs showed higher entrapment efficiency attributed to the solid-liquid lipid ratio (71.5:29.5), Plantacare® 1200 surfactant (better stabilization), and extended sonication time (5.4 min) for improved drug encapsulation. This improvement likely results from our optimized solid-liquid lipid ratio (cetyl palmitate-caprylic triglyceride) and sonication parameters. The moderate drug loading (<5%) aligns with typical lipophilic drug limitations in NLCs due to lipid matrix crystallization. The value indicates a consistent particle

size distribution of the BDQ-NLCs, with no signs of particle aggregation. Meanwhile, the zeta potential value indicates excellent physical stability due to strong electrostatic repulsion between particles. This value is more negative than comparable Plantacare® 1200-based NLC systems, likely due to more uniform charge distribution from our optimized lipid-surfactant combination. The magnitude exceeding ± 30 mV (Müller, Radtke, & Wissing, 2002b) correlates with long-term colloidal stability.

Table 4. Comparison of the predicted and observed values from the optimized formulation

Response	Predicted value	Observed value	Error (%)
Y_1: Particle size (nm)	141.1	153.5 ± 2.3	8.78
Y_2: Entrapment efficiency (%)	95.38	94.46 ± 0.09	0.96
Y_3: Drug loading (%)	3.12	3.04 ± 0.02	2.56

Morphology analysis

Transmission electron microscopy (TEM) analysis of the optimized BDQ-NLC formulation revealed well-defined spherical to oval nanoparticles (Figure 3.). The observed particle diameters (150-200 nm) correlated well with dynamic light scattering measurements, confirming size uniformity. TEM micrographs showed discrete, non-aggregated particles with smooth surfaces, demonstrating excellent colloidal stability. This morphological characterization validates the successful preparation of monodisperse nanoparticles with the desired physicochemical characteristics.

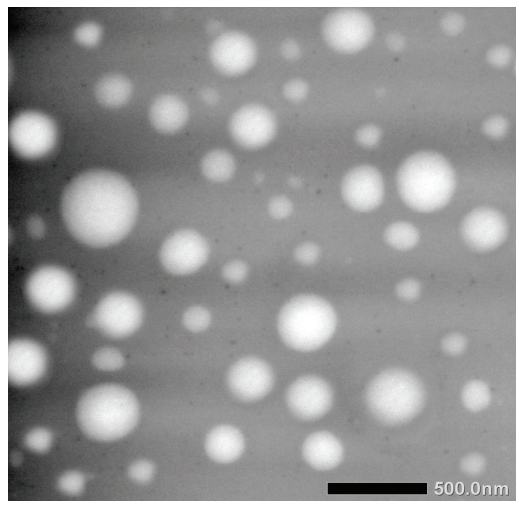


Figure 3. Transmission electron microscopy image showing the morphology of BDQ-NLCs at 25,000 × magnification.

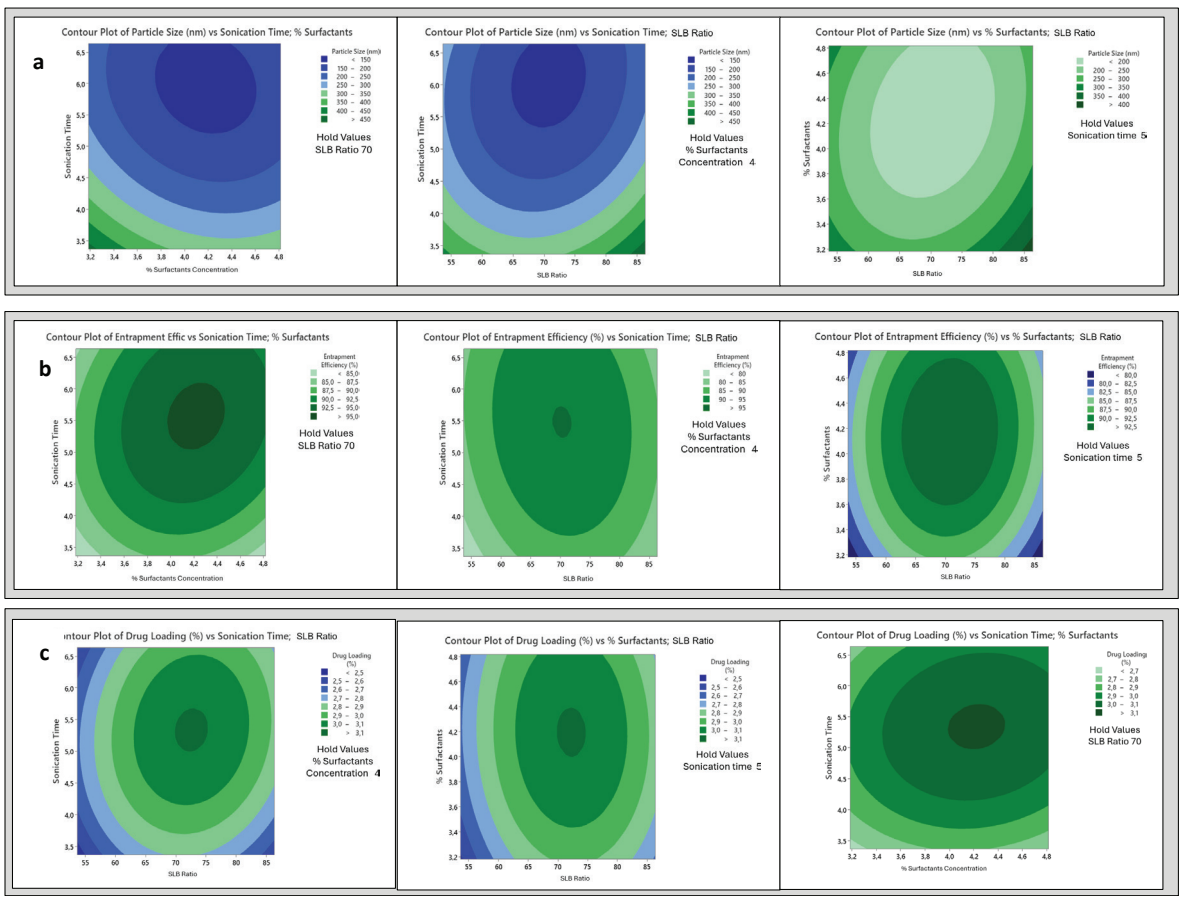


Figure 4. Contour plots for the effect of SLB ratio (%, w/v), surfactant concentration (%, w/v), and sonication time (min) on (a) particle size (nm); (b) encapsulation efficiency (%); (c) drug loading (%) of the BDQ-NLCs formula generated using CCD. In each plot, one independent variable was held at its hold values: surfactant concentration at 4% (w/v), sonication time at 5 min, and SLB ratio at 70, respectively.

Thermal characteristic analysis

Differential scanning calorimetry (DSC) was employed to assess the thermal characteristics of NLCs and their individual components. Pure cetyl palmitate displayed a melting transition beginning at 47.74°C, reaching maximum heat flow at 56.37°C, and completing at 59.10°C, suggesting its broad phase transition range could affect lipid matrix stability. Unloaded NLCs demonstrated an endothermic peak centered at 51.03°C (range: 45.01–53.72°C), corresponding to the glass transition (Tg) of the amorphous lipid phase, which represents a reversible thermodynamic process characteristic of disordered systems. The transition temperatures (onset, peak, and endset) were lower in NLCs compared to pure cetyl palmitate. This depression results from the incorporation of caprylic triglyceride, which introduces structural disorder into the lipid matrix. BDQ-loaded NLCs exhibited modified thermal transitions with an onset at 45.94°C, peak at 51.93°C, and completion at 54.6°C, reflecting subtle drug-lipid interactions. Notably, the negligible difference (ΔT = 0.9°C) in peak temperature between drug-loaded and blank NLCs indicates minimal perturbation of the lipid system by BDQ incorporation. The consistent appearance of endothermic transitions across all formulations verifies the preservation of a structurally intact solid lipid core in the NLC matrix (Müller et al., 2002b).

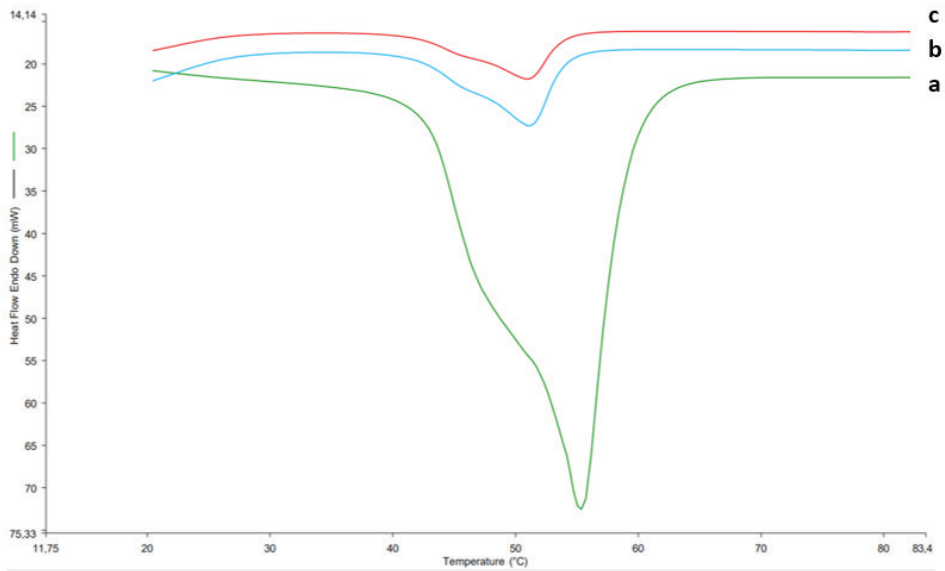


Figure 5. DSC thermograms of (a) cetyl palmitate; (b) blank NLCs; (c) BDQ-NLCs

***In vitro* drug release study**

The *in vitro* release study of BDQ-NLCs exhibited a pH-dependent release profile. At pH 7.4, the cumulative release was 65.78% over 2880 minutes, while a significantly higher release of 79.91% was achieved at pH 5.4 (Figure 6.). This enhanced release under acidic conditions suggests a favorable environment for BDQ diffusion from the lipid matrix. Kinetic modeling revealed that the release at both pH values best followed the Higuchi model (R^2 = 0.9747 at pH 7.4; R^2 = 0.9706 at pH 5.4), indicating a diffusion-controlled release mechanism (Table 5.). Furthermore, the Korsmeyer-Peppas model at pH 5.4 yielded a release exponent of 0.62, signifying a non-Fickian or anomalous transport where drug diffusion and lipid matrix erosion both contribute to the release kinetics. The sustained release profile across 2880 minutes demonstrates the potential of NLCs to provide prolonged BDQ delivery, which is advantageous for improving patient adherence in long-term tuberculosis therapy.

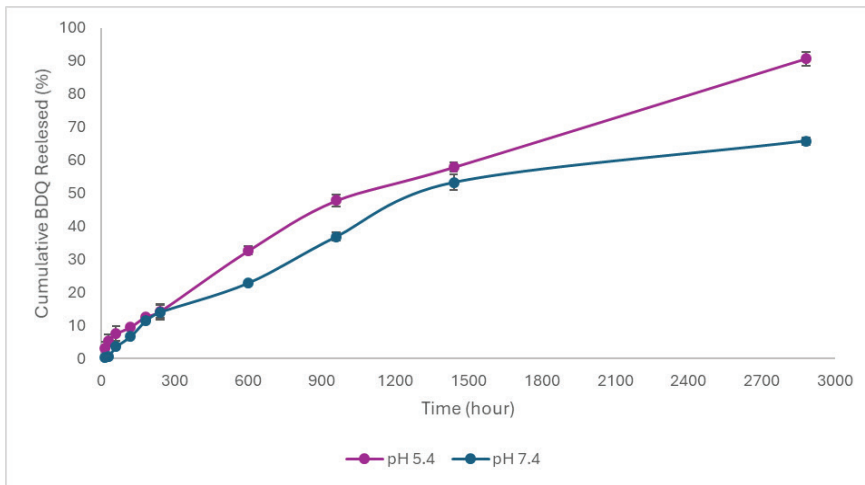


Figure 6. In vitro release profile of Bedaquiline (BDQ) from optimized nanostructured lipid carriers (NLCs) in two different pH media over 2880 minutes. The cumulative drug release (%) is plotted against time (minutes). Data are presented as mean ± SD (n = 3).

Table 5. Kinetic model parameters for BDQ release from NLCs

pH	Zero-Order (R^2)	First-Order (R^2)	Higuchi (R^2)	Korsmeyer-Peppas (R^2)
7.4	0.9169	0.4924	0.9747	0.9843
5.4	0.9379	0.7264	0.9706	0.9802

Stability study

The stability assessment evaluates the optimal BDQ-NLCs formulation by examining parameters such as particle size, encapsulation efficiency, and drug loading over 30 days at storage temperatures of 4, 25, and 40°C, with findings presented in Figure 7. The optimal BDQ-NLC formulation demonstrated no significant increase in particle size (P-value > 0.05) at day 30 (172.5 ± 11.9 nm) compared to the initial measurement at day 0 (153.5 ± 2.3 nm) when stored at 4°C. Significant increases in particle size (P-value < 0.05) were observed at both 25°C and 40°C. The BDQ-NLCs stored at 25°C exhibited an increase in particle size starting on day 30 (164.8 ± 8.7 nm), while at 40°C, the increase was observed from day 28 (174.8 ± 7.2 nm) compared to the initial size. The optimal BDQ-NLC formulation showed no significant changes in PDI or encapsulation efficiency (EE) over 30 days at 4°C, 25°C, and 40°C. PDI values remained below 0.5, indicating stable particle size distribution, while EE consistently ranged from 90-95%, confirming effective BDQ retention in the NLC matrix throughout storage. The significant increase in particle size at 25°C and 40°C suggests that the formulation is susceptible to aggregation under ambient and accelerated conditions. Therefore, refrigerated storage (4°C) is recommended to maintain colloidal stability during storage. Stability at 4°C is attributed to strong electrostatic forces and reduced kinetic energy, while elevated temperatures increase kinetic energy, promoting particle collisions and aggregation, leading to instability.

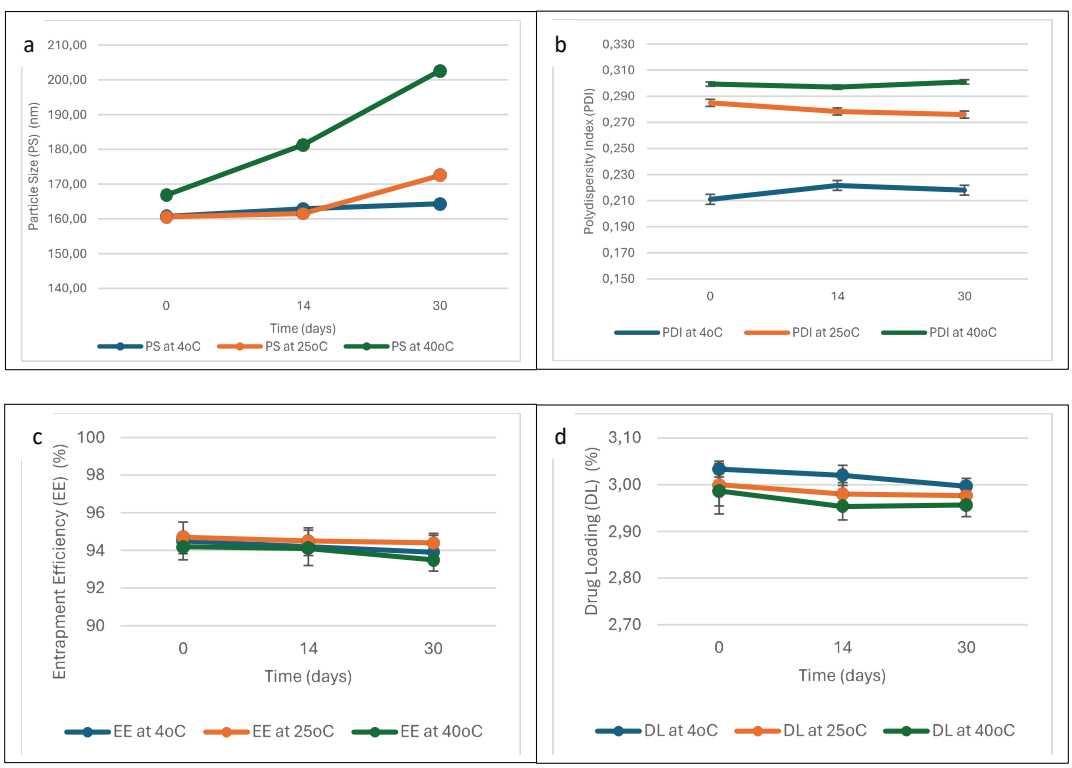


Figure 7. Stability assessment over a period of 30 days, focusing on (a) particle size; (b) PDI; (c) encapsulation efficiency; and (d) drug loading. The data, presented as mean ± standard deviation (n=3), demonstrate significant changes (*P < 0.05) compared to the initial measurements.

CONCLUSIONS

BDQ-NLCs were optimized using a Taguchi design followed by a central composite design, integrating DoE to identify critical factors and predict optimal conditions. Key factors influencing NLC quality included the solid-liquid binary mixture, surfactant concentration, and sonication time. BDQ was successfully incorporated into NLCs via hot homogenization-ultrasonication, enhancing its physicochemical properties. The optimized BDQ-NLC formulation consisted of a solid-to-liquid lipid ratio of 71.5:29.5, a surfactant concentration of 4.2% (w/v), and a sonication time of 5.4 minutes. This formulation yielded an optimal NLC system with a particle size of 153.5 ± 2.3 nm, PDI of 0.31 ± 0.04, an encapsulation efficiency of 94.46 ± 0.09%, and a drug loading capacity of 3.04 ± 0.02%. Further characterization of the optimized BDQ-NLCs revealed a zeta potential of -47.75 ± 3.21 mV and a spherical or oval particle morphology, as confirmed by TEM analysis. DSC analysis indicated an endothermic event between 45.94°C and 54.60°C, with a peak at 51.93°C. The in vitro release profile demonstrated a sustained and pH-dependent controlled release, governed by a diffusion-driven mechanism. The stability assessment was conducted over 30 days under controlled conditions. Long-term stability studies under varied storage environments would be valuable to further establish the shelf-life of the formulation. Future work should include biological assays such as MIC determination and cytotoxicity evaluation to assess therapeutic potential.

ACKNOWLEDGEMENTS

The authors gratefully acknowledge the financial support provided by the Overseas Research Grant from The Asahi Glass Foundation (Contract No: 1835/IT1.B07.1/TA.00/2025) for this research endeavor.

AUTHOR CONTRIBUTION STATEMENT

Concept (AR, RM), Design (AR, RM), Supervision (RM, ST, NFK), Resources (AR, RM), Materials (AR, RM), Data Collection and/or Processing (RM, AR), Analysis and/ or Interpretation (RM, ST, NFK), Literature Search (RM, AR), Writing (RM, AR), Critical Reviews (RM, ST, NFK).

CONFLICT OF INTEREST

The authors declare that there is no conflict of interest.

REFERENCES

Abraham, Y., Assefa, D. G., Hailemariam, T., Gebrie, D., Debela, D. T., Geleta, S. T., … Manyazewal, T. (2024). Efficacy and safety of shorter multidrug-resistant or rifampicin-resistant tuberculosis regimens: a network meta-analysis. *BMC Infectious Diseases*, *24*(1), 1087. https://doi.org/10.1186/s12879-024-09960-3

Beloqui, A., Solinís, M. Á., Rodríguez-Gascón, A., Almeida, A. J., & Préat, V. (2016). Nanostructured lipid carriers: Promising drug delivery systems for future clinics. *Nanomedicine: Nanotechnology, Biology, and Medicine*, *12*(1), 143–161. https://doi.org/10.1016/j.nano.2015.09.004

Bussi, C., & Gutierrez, M. G. (2019). Mycobacterium tuberculosis infection of host cells in space and time. *FEMS Microbiology Reviews*, *43*(4), 341–361. https://doi.org/10.1093/femsre/fuz006

Carnero Canales, C. S., Marquez Cazorla, J. I., Marquez Cazorla, R. M., Roque-Borda, C. A., Polinário, G., Figueroa Banda, R. A., & Pavan, F. R. (2024). Breaking barriers: The potential of nanosystems in antituberculosis therapy. *Bioactive Materials*, *39*(May), 106–134. https://doi.org/10.1016/j.bioactmat.2024.05.013

Chae, J., Choi, Y., Tanaka, M., & Choi, J. (2021). Inhalable nanoparticles delivery targeting alveolar macrophages for the treatment of pulmonary tuberculosis. *Journal of Bioscience and Bioengineering*, *132*(6), 543–551. https://doi.org/10.1016/j.jbiosc.2021.08.009

Costabile, G., Conte, G., Brusco, S., Savadi, P., Miro, A., Quaglia, F., … Ungaro, F. (2024). State-of-the-Art Review on Inhalable Lipid and Polymer Nanocarriers: Design and Development Perspectives. *Pharmaceutics*, *16*(3). https://doi.org/10.3390/pharmaceutics16030347

De Matteis, L., Jary, D., Lucía, A., García-Embid, S., Serrano-Sevilla, I., Pérez, D., … M. de la Fuente, J. (2018). New active formulations against M. tuberculosis: Bedaquiline encapsulation in lipid nanoparticles and chitosan nanocapsules. *Chemical Engineering Journal*, *340*, 181–191. https://doi.org/10.1016/j.cej.2017.12.110

Gavras, N., & Schluger, N. W. (2024). QT Prolongation Associated with Administration of Bedaquiline, a Novel Anti-Tuberculosis Drug. *Cardiology in Review*, *XXX*(00), 1–5. https://doi.org/10.1097/CRD.0000000000000790

Gordillo-Galeano, A., Ospina-Giraldo, L. F., & Mora-Huertas, C. E. (2021). Lipid nanoparticles with improved biopharmaceutical attributes for tuberculosis treatment. *International Journal of Pharmaceutics*, *596*, 120321. https://doi.org/10.1016/j.ijpharm.2021.120321

Guglielmetti, L., Jaspard, M., Le Dû, D., Lachâtre, M., Marigot-Outtandy, D., Bernard, C., … Fréchet-Jachym, M. (2017). Long-term outcome and safety of prolonged bedaquiline treatment for multidrug-resistant tuberculosis. *European Respiratory Journal*, *49*(3). https://doi.org/10.1183/13993003.01799-2016

Jia, B., He, J., Zhang, Y., Dang, W., Xing, B., Yang, M., … Liu, Z. (2024). Pulmonary delivery of magnolol-loaded nanostructured lipid carriers for COPD treatment. *International Journal of Pharmaceutics*, *662*, 124495. https://doi.org/10.1016/j.ijpharm.2024.124495

Keck, C. M., Kovačević, A., Müller, R. H., Savić, S., Vuleta, G., & Milić, J. (2014). Formulation of solid lipid nanoparticles (SLN): The value of different alkyl polyglucoside surfactants. *International Journal of Pharmaceutics*, *474*(1–2), 33–41. https://doi.org/10.1016/j.ijpharm.2014.08.008

Khan, S., Sharma, A., & Jain, V. (2023). An overview of nanostructured lipid carriers and its application in drug delivery through different routes. *Advanced Pharmaceutical Bulletin*, *13*(3), 446–460. https://doi.org/10.34172/apb.2023.056

Khosa, A., Reddi, S., & Saha, R. N. (2018). Nanostructured lipid carriers for site-specific drug delivery. *Biomedicine and Pharmacotherapy*, *103*, 598–613. https://doi.org/10.1016/j.biopha.2018.04.055

Kovačević, A. B., Müller, R. H., & Keck, C. M. (2020). Formulation development of lipid nanoparticles: Improved lipid screening and development of tacrolimus-loaded nanostructured lipid carriers (NLC). *International Journal of Pharmaceutics*, *576*, 118918. https://doi.org/10.1016/j.ijpharm.2019.118918

Kumar, M., Virmani, T., Kumar, G., Deshmukh, R., Sharma, A., Duarte, S., … Fonte, P. (2023). Nanocarriers in Tuberculosis Treatment: Challenges and Delivery Strategies. *Pharmaceuticals*, *16*(10), 1–38. https://doi.org/10.3390/ph16101360

Luo, M., Zhou, W., Patel, H., Srivastava, A. P., Symersky, J., Bonar, M. M., … Mueller, D. M. (2020). Bedaquiline inhibits the yeast and human mitochondrial ATP synthases. *Communications Biology*, *3*(1), 1–10. https://doi.org/10.1038/s42003-020-01173-z

Ma, J., Guan, R., Chen, X., Wang, Y., Hao, Y., Ye, X., & Liu, M. (2014). Response surface methodology for the optimization of beta-lactoglobulin nano-liposomes. *Food and Function*, *5*(4), 748–754. https://doi.org/10.1039/c3fo60476d

Marques, A. C., da Costa, P. C., Gonçalves, H., Catita, J., Velho, S., & Amaral, M. H. (2025). Development, optimization, and characterization of docetaxel-loaded nanostructured lipid carriers for gastric cancer treatment. *Journal of Drug Delivery Science and Technology, 114*. https://doi.org/10.1016/j.jddst.2025.107571

Mauludin, R., Garmana, A. N., & Fauzian, F. (2024). Physicochemical Improvement of Carvacrol-Loaded Nanostructured Lipid Carrier (NLC). *Biointerface Research in Applied Chemistry*, *14*(5). https://doi.org/10.33263/BRIAC145.107

Millington, K. A., White, R. G., Lipman, M., McQuaid,

C. F., Hauser, J., Wooding, V., … Wingfield, T. (2024). The 2023 UN high-level meeting on tuberculosis: renewing hope, momentum, and commitment to end tuberculosis. *The Lancet Respiratory Medicine*, *12*(1), 10–13. https://doi.org/10.1016/S2213-2600(23)00409-5

Müller, R. H., Radtke, M., & Wissing, S. A. (2002a). Nanostructured lipid matrices for improved microencapsulation of drugs. *International Journal of Pharmaceutics*, *242*(1–2), 121–128. https://doi.org/10.1016/S0378-5173(02)00180-1

Müller, R. H., Radtke, M., & Wissing, S. A. (2002b). Nanostructured lipid matrices for improved microencapsulation of drugs. *International Journal of Pharmaceutics*, *242*(1–2), 121–128. https://doi.org/10.1016/S0378-5173(02)00180-1

Patil, S. M., Sawant, S. S., & Kunda, N. K. (2021). Inhalable bedaquiline-loaded cubosomes for the treatment of non-small cell lung cancer (NSCLC). *International Journal of Pharmaceutics*, *607*, 121046. https://doi.org/10.1016/j.ijpharm.2021.121046

Pornputtapitak, W., Thiangjit, Y., & Tantirungrotechai, Y. (2024). Effect of Functional Groups in Lipid Molecules on the Stability of Nanostructured Lipid Carriers: Experimental and Computational Investigations. *ACS Omega*, *9*(9), 11012–11024. https://doi.org/10.1021/acsomega.4c00685

Rajendhiran, N., & Bhattacharyya, S. (2024). Preparation and Evaluation of Nanolipid Carriers of Bedaquiline: In vitro Evaluation and in silico Prediction. *Jordan Journal of Pharmaceutical Sciences*, *17*(3), 450–467. https://doi.org/10.35516/jjps.v17i3.1970

Rajyalakshmi, K., & Boggarapu, N. R. (2019). Expected range of the output response for the optimum input parameters utilizing the modified Taguchi approach. *Multidiscipline Modeling in Materials and Structures*, *15*(2), 508–522. https://doi.org/10.1108/MMMS-05-2018-0088

Sabour, M. R., & Amiri, A. (2017). Comparative study of ANN and RSM for simultaneous optimization of multiple targets in Fenton treatment of landfill leachate. *Waste Management*, *65*, 54–62. https://doi.org/10.1016/j.wasman.2017.03.048

Sathish, T., Giri, J., Rathinasamy, S., & Kanan, M. (2024). Optimization of docetaxel-loaded cholesterol nanostructured lipid carriers for improving cancer treatment using Taguchi experimental design. *Results in Engineering*, *24*, 103263. https://doi.org/10.1016/j.rineng.2024.103263

Satrialdi, Putri, P. A., & Lumintang, Y. A. (2023). Pengembangan Formula Nanostructured Lipid. *Majalah Farmasi Farmakologi*, *27*(2), 32–38. https://doi.org/10.20956/mff.v27i2.27395

Sułek, M. W., Ogorzałek, M., Wasilewski, T., & Klimaszewska, E. (2013). Alkyl polyglucosides as components of water-based lubricants. *Journal of Surfactants and Detergents*, *16*(3), 369–375. https://doi.org/10.1007/s11743-012-1428-y

Viegas, C., Patrício, A. B., Prata, J. M., Nadhman, A., Chintamaneni, P. K., & Fonte, P. (2023). Solid Lipid Nanoparticles vs. Nanostructured Lipid Carriers: A Comparative Review. *Pharmaceutics*, *15*(6). https://doi.org/10.3390/pharmaceutics15061593

Wei, S., He, C., Xie, X., Zhang, A., Tang, S., Li, S., & He, Y. (2024). Which fluoroquinolone is safer when combined with bedaquiline for tuberculosis treatment: evidence from the FDA Adverse Event Reporting System database from 2013 to 2024. *Frontiers in Pharmacology*, *15*. https://doi.org/10.3389/fphar.2024.1491921

Yadav, S., Rawal, G., & Baxi, M. (2016). Bedaquiline: A novel antitubercular agent for the treatment of multidrug-resistant tuberculosis. *Journal of Clinical and Diagnostic Research*, *10*(8), FM01–FM02. https://doi.org/10.7860/JCDR/2016/19052.8286

FABAD J. Pharm. Sci., 51, 1, 257-274, 2026
Doi: 10.55262/fabadeczacilik.1792099
RESEARCH ARTICLE

Anti-Aging Activity of Ethanol Extract of the Oil Palm Mesocarp (Elaeis guineensis Jacq.): *In Vitro* and *In Silico* Studies

Retno WIDYOWATI[*°], Anisa Yustikka PUTRI[**], SUKARDIMAN[***], Irawati SHOLOKHAH[****], Rosita HANDAYANI[*****], Katsuyoshi MATSUNAMI[******], Hsin-I CHANG[*******]

Anti-Aging Activity of Ethanol Extract of the Oil Palm Mesocarp (Elaeis guineensis Jacq.): In Vitro and In Silico Studies

SUMMARY

Aging constitutes a natural biological process and represents a major global health concern. In tropical regions such as Indonesia, elevated ultraviolet (UV) exposure accelerates cutaneous aging through mechanisms involving DNA damage and mitochondrial dysfunction. Although numerous chemical-based anti-aging products are commercially available, their frequent adverse effects, including irritation and itching, necessitate the exploration of safer alternatives. Natural ingredients are therefore of increasing interest, with palm oil (Elaeis guineensis Jacq.) recognized as a potential candidate due to its empirical use in wound healing and tissue regeneration. The present study investigated the anti-aging potential of secondary metabolites from the ethanol extract of oil palm mesocarp (EEOPM) through in vitro enzymatic assays and in silico molecular docking. In vitro evaluation was conducted against mushroom tyrosinase and collagenase from Clostridium histolyticum. Molecular docking simulations were performed to analyze binding interactions with tyrosinase (PDB: 5M8P) and collagenase (PDB: 2D1N). The enzymatic assays demonstrated dose-dependent inhibitory activity, with IC_{50} values of 218.42 µg/mL for tyrosinase and 22.44 µg/mL for collagenase. These inhibitory effects were lower in potency compared with standard agents, kojic acid (IC_{50} = 46.42 µg/mL) and ascorbic acid (IC_{50} = 5.58 µg/mL). Docking analysis further revealed that α-tocotrienol exhibited the strongest affinity toward tyrosinase (-7.33 kcal/mol), while β-carotene displayed the highest affinity toward collagenase (-12.71 kcal/mol). Collectively, these findings suggest that EEOPM contains bioactive secondary metabolites capable of inhibiting tyrosinase and collagenase, thereby demonstrating anti-aging potential. Although its activity is lower than that of standard inhibitors, this study provides the first combined in vitro and in silico evidence supporting EEOPM as a prospective natural alternative for the development of safer anti-aging agents.

Keywords: *Anti-aging, Elaeis guineensis Jacq., human & health, in vitro, in silico.*

Etanol Ekstresi Palm Yağı Mezokarpının (Elaeis guineensis Jacq.) Yaşlanma Karşıtı Etkisi: In Vitro ve In Silico Çalışmaları

ÖZ

Yaşlanma doğal bir biyolojik süreçtir ve küresel çapta önemli bir sağlık sorunu teşkil eder. Endonezya gibi tropikal bölgelerde, yüksek ultraviyole (UV) maruziyeti, DNA hasarı ve mitokondriyal işlev bozukluğunu içeren mekanizmalar aracılığıyla cilt yaşlanmasını hızlandırır. Çok sayıda kimyasal bazlı yaşlanma karşıtı ürün ticari olarak mevcut olsa da, tahriş ve kaşıntı gibi sık görülen yan etkileri, daha güvenli alternatiflerin araştırılmasını gerektirmektedir. Bu nedenle doğal içeriklere olan ilgi giderek artmaktadır ve yara iyileşmesi ve doku rejenerasyonundaki deneysel kullanımı nedeniyle palmiye yağı (Elaeis guineensis Jacq.) potansiyel bir aday olarak kabul edilmektedir. Bu çalışmada, in vitro enzimatik deneyler ve in silico moleküler yerleştirme yoluyla yağ palmiyesi mezokarpının etanol özütü (YPMEO) elde edilen sekonder metabolitlerin yaşlanma karşıtı potansiyeli araştırılmıştır. İn vitro değerlendirme, Clostridium histolyticum'dan elde edilen mantar tirozinaz ve kolajenaz enzimlerine karşı gerçekleştirilmiştir. Bağlanma etkileşimlerini tirozinaz (PDB: 5M8P) ve kolajenaz (PDB: 2D1N) ile analiz etmek için moleküler yerleştirme simülasyonları gerçekleştirildi. Enzimatik analizler, tirozinaz için 218,42 µg/mL ve kolajenaz için 22,44 µg/mL IC_{50} değerleriyle doza bağlı inhibitör aktivite gösterdi. Bu inhibitör etkiler, standart ajanlar olan kojik asit (IC_{50} = 46,42 µg/mL) ve askorbik asit (IC_{50} = 5,58 µg/mL) ile karşılaştırıldığında daha düşük etkiliydi. Yerleştirme analizi ayrıca, α-tocotrienol ün tirozinaza karşı en güçlü afiniteyi (-7,33 kcal/mol) gösterdiğini, β-karotenin ise kolajenaza karşı en yüksek afiniteyi (-12,71 kcal/mol) gösterdiğini ortaya koydu. Bu bulgular topluca değerlendirildiğinde, YPMEO'un tirozinaz ve kolajenazı inhibe edebilen biyoaktif sekonder metabolitler içerdiği ve dolayısıyla yaşlanma karşıtı potansiyele sahip olduğu ortaya çıkmaktadır. Etkinliği standart inhibitörlerden daha düşük olsa da, bu çalışma, YPMEO'un daha güvenli yaşlanma karşıtı ajanların geliştirilmesinde potansiyel bir doğal alternatif olduğunu destekleyen ilk birleşik in vitro ve in silico kanıtı sunmaktadır.

Anahtar Kelimeler: *Yaşlanma karşıtı, Elaeis guineensis Jacq., insan ve sağlık, in vitro, in silico.*

Recieved: 27.09.2025
Revised: 13.02.2026
Accepted: 26.02.2026

[*] ORCID: 0000-0002-6166-1289, Department of Pharmaceutical Sciences, Faculty of Pharmacy, Universitas Airlangga, Nanizar Zaman Joenoes Building, Campus C, Mulyorejo, Surabaya 60115, East Java, Indonesia
[**] ORCID: 0009-0001-0549-4850, Master Program of Pharmaceutical Sciences, Faculty of Pharmacy, Universitas Airlangga. Jl. Dr. Ir. H. Soekarno, Surabaya 60115, East Java, Indonesia
[***] ORCID: 0000-0001-9689-5088, Department of Pharmaceutical Sciences, Faculty of Pharmacy, Universitas Airlangga, Nanizar Zaman Joenoes Building, Campus C, Mulyorejo, Surabaya 60115, East Java, Indonesia
[****] ORCID: 0000-0002-0124-8302, Department of Pharmaceutical Sciences, Faculty of Pharmacy, Universitas Airlangga, Nanizar Zaman Joenoes Building, Campus C, Mulyorejo, Surabaya 60115, East Java, Indonesia
[*****] ORCID: 0000-0002-3304-3328, Department of Pharmaceutical Sciences, Faculty of Pharmacy, Universitas Airlangga, Nanizar Zaman Joenoes Building, Campus C, Mulyorejo, Surabaya 60115, East Java, Indonesia
[******] ORCID: 0000-0002-8034-0253, Biomedical & Health Sciences, Hiroshima University, Japan 734-8853
[*******] ORCID: 0009-0009-7373-3882, Department of Biochemical Science and Technology, National Chiayi University, Chiayi, Taiwan

[°] Corresponding Author; Retno Widyowati
E-mail: rr-retno-w@ff.unair.ac.id

INTRODUCTION

Aging is a natural biological process and has become a significant concern in the global population. In tropical countries like Indonesia, where exposure to ultraviolet (UV) radiation is high, the issue of skin aging is growing rapidly each year. According to the Badan Pusat Statistik (2023), the elderly population reached 11.75% and is projected to increase to 15.77% by 2035. Skin aging is characterized by reduced skin function, resulting in sagging skin, wrinkles, dark spots, and dryness, which ultimately reduce skin elasticity and collagen synthesis, accelerating skin tissue degradation (Brzezinski et al., 2017).

Skin aging is closely linked to DNA damage and mitochondrial dysfunction. In addition to extrinsic factors such as pollution, oxidative stress, and UV exposure, this process is impacted by internal factors, including age, hormonal changes, and heredity (Anwar et al., 2022). Both intrinsic and extrinsic factors contribute to macromolecular damage and the overall decline of skin structure and function. As awareness of skin health increases, the global demand for anti-aging products continous to grow, with a compound annual growth rate (CAGR) of 8.61% predicted between 2022 and 2030 (Facts & Factors, 2023).

However, many synthetic anti-aging products, such as isotretinoin and retinoids, often cause side effects including dryness, redness, irritation, and other skin complications (Brzezinski et al., 2017). This emphasizes the need for anti-aging medications that are safer and more efficient, especially those that address oxidative stress and inhibit the degradation of the extracellular matrix through antioxidant, collagenase, and tyrosinase inhibition mechanisms.

The development of natural-based cosmetics is becoming increasingly popular due to their perceived safety, environmental friendliness, and minimal side effects. One promising natural source is the oil palm (*Elaeis guineensis* Jacq.), a member of the Arecaceae family widely cultivated in Asia and predicted to reach a global demand of 240 million tons by 2050. Traditionally, palm oil has been used to promote wound healing and enhance tissue regeneration (Wondi et al., 2024). Palm mesocarp oil accounts for approximately 45–55% of the total oil yield and contains key bioactive compounds such as unsaturated fatty acids, vitamin E (tocopherols and tocotrienols), carotenoids, phytosterols, and coenzyme Q10, which are known for their strong antioxidant properties (Okpe, 2022).

Previous research has shown that tocopherols and tocotrienols from palm oil possess antioxidant properties with low toxicity, making them promising candidates for anti-aging applications. However, further studies are needed to investigate the potential of palm oil extracts as inhibitors of the enzymes tyrosinase and collagenase, which are involved in the skin aging process.

The use of 96% ethanol for extraction is considered effective for isolating bioactive compounds such as vitamin E and β-carotene without altering their chemical structures (Lee et al., 2024). Bioactive compounds were identified using LC-MS, which offers high precision in molecular detection and structural analysis (Alanazi, 2025). In addition, *in silico* studies such as molecular docking are valuable tools for predicting compound interactions with target proteins related to aging (Forli et al., 2016). The results are further validated through *in vitro* assays, including tyrosinase and collagenase inhibition tests. Therefore, this study aims to analyze potential anti-aging compounds from the mesocarp extract of oil palm using *in silico* methods and to evaluate their enzyme inhibition activity through *in vitro* experiments.

MATERIALS AND METHODS

Plant material

The plant material used in this study was palm oil from plantations of *Elais guineensis* Jacq. located in Bukit Makmur Village, Menthobi Raya District, Lamandau Regency, Central Kalimantan in February 2025. Then, plant determination was carried out at

the UPT Laboratorium Herbal Materia Medica Batu, Malang.

Extraction materials

The materials used were mesocarp oil palm simplicia and 96% technical ethanol. The instruments used were maceration equipment, oven, microwave, glassware, grinder (Fomag FCT-Z200), vacuum pump, rotary evaporator (Buchi Heating Bath B-490 and Buchi Rotavapor R-200), and analytical balance (OHAUSS PX224/E).

***In vitro* assay materials**

Mushroom Tyrosinase 250 U/mL, 0.1 M PBS pH 6.8 dan 5 mM DOPA (3,4-dihydroxy-L-phenylalanine) were used. BODIPY and Gelatin (Type B) served as fluorogenic substrates. Collagenase Assay Buffer XXXVIII, active collagenase, and the inhibitor (1,10)-phenanthroline (400 mM) were employed, along with distilled water and ethanol. 3T3 fibroblast cells were obtained from National Chiayi University, Taiwan, and cultured in Dulbecco's Modified Eagle's Medium (DMEM) supplemented with 10% fetal bovine serum (FBS). Additional reagents included 3-(4,5-dimethylthiazol-2-yl)-2,5 diphenyltetra-zolium bromide (MTT; Sigma Aldrich, USA), trypsin-EDTA, trypan blue (Sigma), bidistilled water and 70% alcohol. The MTT stock solution (5mg/mL PBS; 50 mg MTT dissolved in 10 mL PBS, pH 7.4) was prepared fresh. Stopper reagents consisted of 10% (w/v) sodium dodecyl sulphate (SDS; Merck-Schuchardt, Germany) in 0.01 N HCl (Merck, Darmstadt, Germany) protected from light with aluminum foil.

Equipment and consumables included an ELISA reader (Biochrom EZ Read 2000), Collagenase Inhibitor Screening Kit (Fluorometric; ab211108), tyrosinase kit, biological safety cabinet (BSC; EXCO SC2-4S1), reservoirs, 96-well plates (Biologix), CO_2 incubator (New Brunswick Galaxy 170R), beakers, vortex mixer (Thermo Scientific), centrifuge, analytical balance (Shimadzu), autoclave (Hiryama), hemocytometer (Neubauer), hand tally counter, inverted microscope (Zeiss MC 80), tissue culture dishes (IWAKI), conical tube (IWAKI), micropipette (2-20 µL; 20-200 µL; 100-1000 µL), disposable plastic gel casting cassettes, sterile yellow and blue pipette tips, (Eppendorf), OPF pen marker, label stickers, shelf, aluminum foil, and a camera (Oppo Reno 5F).

***In silico* materials**

Secondary metabolite compounds identified through LC-MS in the ethanol extracts of oil palm mesocarp were used in this investigation. Fatty acids, β-carotene, and vitamin E were the primary substances under study. The chemical structure of these compounds was obtained from the PubChem database (https://pubchem.ncbi.nlm.nih.gov/). Crystal structure of human tyrosinase-related protein 1 complexed with tyrosine (PDB ID: 5M8P) was shown in (Figure 1.), and Collagenase-3 (MMP-13) complexed with a hydroxamic acid inhibitor (PDB ID: 2D1N) was shown in (Figure 2.) were retrieved from the Protein Data Bank (https://www.rcsb.org/), both with their ligands bound. The resolutions of proteins 5M8P and 2D1N are 2.80 Å and 2.37 Å, respectively. Kojic acid and ascorbic acid, obtained from PubChem, were used as comparator compounds for molecular docking with tyrosinase and collagenase, respectively.

AutoDockTools are used for molecular docking simulation, which facilitates the preparation of macromolecules and the execution of tethering protocols. Grid creation and binding operations used autogrid4.exe and autodock4.exe. To minimize ligand energy before binding, Avogadro software was used. Visualization and analysis of ligand-receptor interactions used BIOVIA Discovery Studio Visualizer 2024 v.24.1.0.23298. All computational work was performed on the ASUS VivoBook laptop with 4.00 GB of RAM, running Windows 11 on an x64-based processor.



Figure 1. *Tyrosinase* (PDB ID: 5M8P)

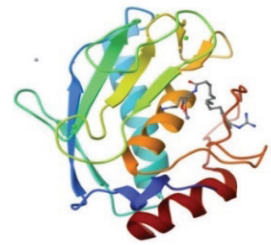


Figure 2. *Collagenase* (PDB ID: 2D1N)

Research method

This study is an experimental laboratory study with a post-test only control group design. Data collection for this study was carried out through experimental studies. Laboratory studies for in vitro work were carried out using tyrosinase inhibitor activity tests and collagenase inhibitor assays to analyze their IC_{50} values. The data collection method involved using a molecular database for in silico with protein preparation, ligand preparation, method validation, and molecular docking, followed by analysis of binding free energy, inhibition constants of binding interactions, and amino acid residues.

Procedures

Simplicia processing and extraction method

The samples were cleaned of dirt and then wet-sorted, washed under running water, the mesocarp was separated, and weighed to determine wet weight, reduced in size, air-dried without exposure to direct sunlight, dry-sorted, and finally weighed. Furthermore, the simplicia was ground using a grinder. Extraction was carried out on the mesocarp of oil palm with the MAE method using 96% ethanol solvent (1:10) at a frequency of 2450 MHz and a maximum power of 1000 W. Approximately 800 grams of mesocarp sample was reduced in size using a grinder, then extracted in a microwave using 96% ethanol 8000 mL for 3 minutes in stages. The mixture was filtered using a Buchner funnel, and the filtrate was evaporated with a rotating evaporator to produce a viscous extract from the oil palm mesocarp. After that, the filtrate was evaporated in an oven at 45°C for 24 hours to a constant weight, yielding the extract (Furi et al., 2022).

The extract yield was calculated using the following equation: $\% \; yield = \frac{weight \; of \; extract}{weight \; of \; simplicia} \times 100$ (1)

***In vitro* assay**

Tyrosinase inhibitor test

Tyrosinase inhibitory activity was measured using mushroom tyrosinase as an enzyme, L-DOPA as a substrate, phosphate buffer as a color control, DMSO solution as a blank, and kojic acid as a positive control (Widyowati et al., 2016). Mushroom tyrosinase reagent (250 U/mL) was prepared in cold conditions and protected from light. PBS pH 6.9 reagent (A) was made up in 50 mL of water. Then, 1 M phosphate dibasic (B) was prepared in 50 mL of water. Solution A, 4.97 mL, and solution B, 5.03 mL were mixed, and 100 mL of water was added. Reagent L-DOPA (5 mM) was made up in 50 mL of water. A standard kojic acid solution of 1000 mg/mL was prepared, and a standard kojic acid series solution was made into a 1.5 mL microtube, dilution series was carried out using 0.1 M PBS pH 6.8. The sample stock solution was prepared at a concentration of 100,000 mg/mL using 1 mL of DMSO, and homogenized. A series of six different sample concentrations was prepared in 1.5-mL microtubes, then 0.1 M PBS pH 6.8 was added according to the calculated volume, and homogenized. The first working step was to add 40 µL of L-DOPA solution to

a 96-well plate that had been made into a map plate, then add 40 µL of EEOPM sample solution, then add 160 µL of PBS 0.1 M pH 6.8 to the sample, and finally add 40 µL of mushroom tyrosinase 250 Units/mL. The second step was to cover the well-plate with aluminum foil and incubate for 15 minutes at 37°C. The results could be seen in the color change to brown or black due to oxidation to dopamine or melanin, and the amount of dopachrome was determined by measuring the absorbance at λ475 nm with an ELISA Reader. Analysis of IC_{50} values was performed (Nurrochmad et al., 2018).

The data obtained was in the form of absorbance, and then the inhibition percentage was calculated using the following equation:

$$\%Inhibition = \left(\frac{enzyme\ control\ absorbance - (sampale\ absorbance - buffer\ absorbance)}{enzyme\ control\ absorbance} \right) \times 100 \quad (2)$$

Collagenase inhibitor test

Collagenase inhibition test using active collagenase enzyme from *Clostridium histolyticum*, with gelatin substrate solution (BODIPY) and ascorbic acid as a positive control. A stock sample concentration of 10 mg/mL was prepared by weighing 10 mg of dry extract, then placing it in a microtube, and then adding 1 mL of DMSO, vortexing vigorously until homogeneous. 1 uL of the dissolved sample extract was added to a 96-well plate, then 5 µg/mL collagenase enzyme and 44 µL buffer XXXVIII were added to the 96-well microplate, and then preincubated for 15 minutes at 37°C. Then, a substrate solution (10 µM concentration) was added to initiate the reaction. Fluorescence results were measured at λ490/λ520 nm on excitation and emission after 0 and 30 minutes of incubation, using a fluorescence plate reader. The results were in the form of fluorescence values, and IC_{50} values were analyzed (Widyowati et al., 2016). The data obtained is in the form of absorbance, and then the inhibition percentage is calculated using the equation:

$$\%Inhibition = \left(\frac{enzyme\ control\ absorbance - (sample\ absorbance - buffer\ absorbance)}{enzyme\ control\ absorbance} \right) \times 100 \quad (3)$$

***In silico* test (Molecular docking)**

Proteins preparation

AutoDockTools was used to prepare the collagenase and tyrosinase protein structures for the ensuing molecular docking simulations. Tyrosinase-related protein 1 (TYRP1), complexed with chain A of 5,6-dihydroxyindole-2-carboxylic acid oxidase, was solved at an atomic resolution of 2.80 Å for the tyrosinase preparation. Meanwhile, collagenase with a protein resolution of 2.37 Å was prepared using chain A of collagenase-3 (MMP-13) complexed with a hydroxamic acid inhibitor. Before docking, all water molecules and nonstandard residues were meticulously eliminated from protein structures. In addition, hydrogen atoms and Kollman charges were added to guarantee accurate chemical representation. The processed protein structures were then saved in the.pdbqt format for use in molecular docking.

Ligand preparation

In a different examination in our study, certain chemicals from EEOPM were discovered using prior LC-MS/MS-QToF profiles. These identified compounds include α-tocotrienol, β-sitosterol, *3-(1,3-Benzodioxol-5-yl)-3-({[(2-methyl-2propanyl)oxy]carbonyl} amino)propanoic acid,* tocopherol, squalene, apigenin 6,8-diglucoside, β-carotene, Coenzym Q10, oleic acid, myristic acid and palmitic acid. For molecular docking simulations, the 3D structures of these chemicals were obtained in *.sdf format from PubChem. The "Optimize Geometry" feature in Avogadro software was used to minimize the energy of each compound in order to guarantee the most stable conformation for docking. The *.pdb format was used to store the optimized structures. AutoDockTools was used to continue the docking preparation.

Method validation

The technique validation approach guarantees the precision and dependability of molecular docking simulations. In this procedure, the native ligand was re-docked to the active site of each target protein. A grid box, usually 40 x 40 x 40 points, was defined using AutoDockTools and was centered on the native ligand's known location inside the protein's binding pocket. For the 5M8P protein, re-docking was carried out using a grid box centered at coordinates x: 30.088, y: 136.057, and z: 216.68 with a grid spacing of 0.142 Å. The grid box for the 2D1N protein had a grid spacing of 0.375 Å and was centered at x: -44.048, y: 25.846, and z: -19.485. The RMSD value is a crucial measure for successful validation. The ability of the docking method to precisely reproduce the ideal ligand binding position is confirmed when the re-docked ligand posture is sufficiently near to the native conformation as determined by experiment, as indicated by an RMSD value of less than 2.0 Å. Tyrosinase (tyrosine) and collagenase (hydroxamic acid), the native ligands of each protein, were re-docked to verify this accuracy. Their corresponding RMSD values were confirmed to be below the 2.0 Å threshold.

Molecular docking

Using AutoDockTools, molecular docking simulations were conducted to assess the molecular interactions and binding affinity of mesocarp oil palm mesocarp molecules with 5M8P and 2D1N receptors. The binding energies were given in kcal/mol. To guarantee the accuracy and consistency of the docking data, the grid box size and coordinates for every receptor were kept constant throughout the validation procedure.

Data analysis

Every experiment was conducted three times, and the mean (n=3) ± SD was used to assess the results. The data obtained from the tests were analyzed statistically using parametric methods in IBM SPSS Statistics 27 software, so that the significance of the previously quantified data could be concluded. Normally distributed and homogeneous data were subjected to parametric analysis using the 95% confidence level with a one-way Analysis of Variance (ANOVA) test. Tyrosinase and collagenase assay concentration variations were ascertained using the one-way ANOVA approach against each test, as seen in the significance number. If the assumptions were met, the Post Hoc test was continued using the Tukey HSD test to evaluate significant differences in data between treatment groups using a confidence level of $p<0.05$.

RESULTS AND DISCUSSION

Plant identification

Plant identification results indicated that the palm oil (*Elaeis guineensis* Jacq.) is a species from the Aracaceae (areca nut) family.

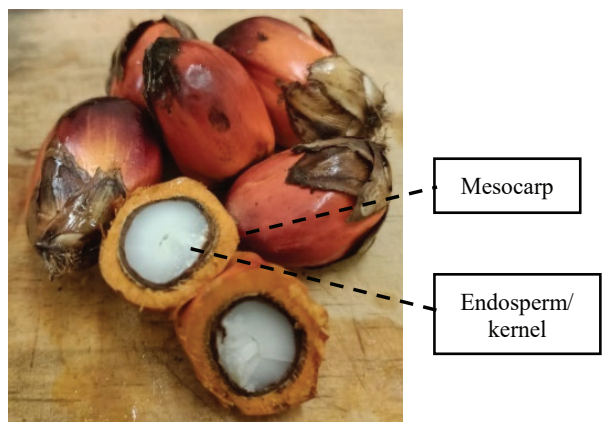


Figure 3. Samples of palm oil fruit after harvesting

Preparation and extraction of simplicia



Figure 4. Simplicia of oil palm mesocarp



Figure 5. Ethanol extract of oil palm mesocarp

The yield results from the extraction and organoleptic observation were listed in (Tables 1 and 2.).

Table 1. Yield of 96% ethanol extract of oil palm mesocarp

Simplicia	Simplicia weight (g)	Ethanol 96% volume (ml)	Extract weight (g)	Yield (%)	MC (%)
Mesocarp	800	8000	575	71.8	9.0

Table 2. Organoleptic observation of ethanol extract of oil palm mesocarp

Organoleptic observation	Result
Form	Condensed extract
Color	Brownish orange
Odor	Typical sweet caramel palm

The drying process for the mesocarp of oil palm was carried out using the air-drying method at room temperature, avoiding exposure to sunlight. The drying time was approximately 7 days. Careful monitoring of the drying process was crucial to ensure the preservation of desired secondary metabolites and the quality of the dried of oil palm mesocarp. In this study, the extraction method used was MAE with 96% ethanol, a polar solvent that can dissolve a variety of substances, such as polar, semipolar, and nonpolar active ingredients. Its low boiling point and inert nature make it suitable for extraction and evaporation without the need for high temperatures. The 71.8% yield in this study is thought to be due to the effect of the extraction time, which was 30 seconds in increments with six repetitions, maximizing the extraction process. The yield percentage is a measure of the efficiency of the extraction process and indicates the amount of active compounds contained in the extract. A higher yield percentage indicates that more active compounds are extracted from oil palm mesocarp, which are useful for various applications, such as pharmaceuticals and cosmetics, where these compounds are used for various health benefits. The results of the moisture content test (MC) for the EEOPM were 9.0%. This result is in accordance with the standard extract water content of <10% (BPOM, 2017). This means that the EEOPM in this study meets the stan-

dard. Too high water content can become a medium for the growth of fungi and bacteria and can cause a decrease in the stability of the active compounds in the extract (Krismayadi et al., 2024). The purpose of conducting an organoleptic test of extracts (Table 2.) is to introduce a simple start as objectively as possible (BPOM RI, 2017). The results of the EEOPM organoleptic test showed a thick liquid form because the use of 96% ethanol as a solvent accelerated the evaporation process during the evaporation stage, resulting in a concentrated extract. The extract had a brownish orange color, attributed to the reddish orange pulp used, which is rich in carotene compounds that are easily dissolved and will be carried into the extract (Riansyah et al., 2021). It had a distinctive odor, resembling the typical sweet smell of palm caramel.

***In vitro* assay using enzymatic test**

Tyrosinase inhibition test

The enzyme mushroom tyrosinase, the lubstrate l-1,4-dihydroxyphenylalanine (L-dopa), the positive control kojic acid, and the color control phosphate buffer were used to assess the tyrosinase inhibitory activity (Widyowati et al., 2016). Moreover, various concentrations of sample extracts were dissolved in DMSO, yielding concentrations of 6,250; 12,500; 25,000; 50,000, and 100,000 ppm. And the concentration for kojic acid was 2.34; 4.69; 9.38; 18.75; 37.50; 75.00; 150.00 ppm. Tyrosinase inhibitor activity with IC_{50} values for kojic acid and extract of mesocarp oil palm is shown in Table 3.

Table 3. IC_{50} value of the tyrosinase inhibitory properties of oil palm mesocarp extract and kojic acid

Sample	Concentration (µg/mL)	Inhibition(%)±SD	IC_{50} Value (µg/mL)	Category
Kojic acid (Control +)	2.34	8.36±0.66	46.42	Strong
	4.69	13.12±0.23		
	9.38	14.73±1.72		
	18.75	26.11±0.47		
	37.50	43.98±1.05		
	75.00	63.47±1.58		
	150.00	76.95±0.32		
Ethanol extract of Mesocarp	6.250	18.31±0.62	nd	nd
	12.500	21.24±0.46		
	25.000	26.61±0.67		
	50.000	32.32±1.44		
	100.000	42.81±0.21		

Fit (Sigmoidal, 4 parameters logistic, X is Concentration); nd (not defined)

The percentage of tyrosinase enzyme inhibition increased dose-dependently across all concentrations, within the activity test range of 6.25-100 µg/mL, with inhibition percentages ranging from 18-42% (Table 3.). From these results, the IC_{50} value was calculated based on the percentage of tyrosinase inhibition against the concentration of oil palm mesocarp extract using a non-linear regression model (curve fit) (Figure 6B.). The analysis yielded an IC_{50} value of 218.42 µg/mL for the oil palm mesocarp extract with an R-squared of 0.978. This IC_{50} value is an extrapolated estimate and does not define within the test concentration range. The extract showed no inhibitory activity against tyrosinase at the test concentration under these test conditions.

The anti-tyrosinase activity test against the reference compound kojic acid showed a profile similar to that of the oil palm mesocarp extract, with increased activity at low doses and stable activity at high doses (Figure 6A.). The percentage of kojic acid inhibition

in the concentration range of 1-20 µg/mL increased from 8% to 76% (Table 3.), indicating that increasing kojic acid concentration is directly proportional to the increase in inhibitory activity. From these results, the IC_{50} value of kojic acid was obtained, namely 46.42 µg/mL with an R-squared of 0.990. These results indicate that kojic acid has higher tyrosinase inhibitory activity than oil palm mesocarp extract.

The higher IC_{50} value observed in this study compared to previous reports, such as those Suzana et al. (2009), may be due to differences in extraction methods, phytochemical composition, and testing conditions. In that study, a tocotrienol-rich fraction (TRF) was used as a melanin synthesis inhibitor by inhibiting tyrosinase activity and reducing TYRP2 gene expression. Ethanol extracts of oil palm mesocarp are predominantly rich in lipophilic compounds, which are known to exhibit weaker tyrosinase inhibition than phenolic compounds, which are typically enriched in polar extracts. Furthermore, variations in enzyme source, substrate type, and assay parameters can substantially affect IC_{50} values.

The graph showing the relationship between concentration and percentage of inhibition of tyrosinase enzyme by kojic acid and oil palm mesocarp is shown in Figure 6.

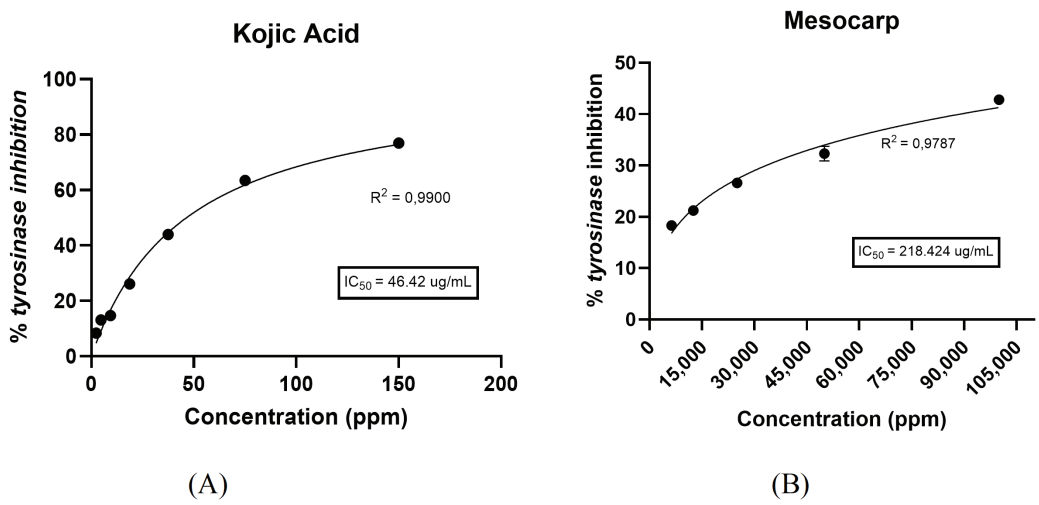


Figure 6. Regression graph of the relationship between concentration and percentage inhibition of (A) kojic acid and (B) oil palm mesocarp.

Based on the extrapolation results using GraphPad, the IC_{50} value was obtained at 218.42 µg/ml, where the results of the EEOPM reaction test on tyrosinase inhibition showed moderate activity potential based on the enzymatic inhibition test parameters. This means that a dose of 218 µg/ml can inhibit 50% of tyrosinase activity in the melanogenesis reaction. When compared with other plants, namely *Magnolia officinalis* essential oil, which was reported to have a tyrosinase IC_{50} test result of 61.9 µg/ml and is classified as a strong tyrosinase inhibitor (IC_{50} 50 - 200 µg/ml); moderate activity (IC_{50} 201-500 µg/ml) (You et al., 2022). The findings of a study conducted by Plyduang et al. (2022), palm oil contains several fatty acids, including palmitic acid (44%), oleic acid (39%), and lauric acid (48%), which have antioxidant properties and protect the skin from water loss. The anti-tyrosinase potential of a single composite isolate showed superior inhibitory potential. A study by Yusof et al. (2016) evaluated the potential application of oil palm (*elaeis guineensis*) leaf extract (ople) as a skin lightening agent and topical sunscreen. Ople also inhibited

fungal tyrosinase with an IC_{50} of 254.88 µg ml-1, significantly different from kojic acid, a more potent inhibitor with the lowest IC_{50} of 4.46 µg/ml. GTE (green tea extract) showed a comparable IC_{50} value to ople, namely 240.50 µg ml-1. The catechin group, which prevents melanin synthesis in B16 melanoma cells, is likely responsible for the tyrosinase-inhibiting effect on ople and GTE. The gallic acid content in ople likely adds anti-tyrosinase properties in addition to the catechin group. Tyrosinase activity and melanin formation are significantly inhibited by gallic acid (Yusof et al., 2016). These results indicate that the fatty acid and vitamin E compounds from EEPOM have tyrosinase-inhibiting potential.

Collagenase inhibition test

In vitro collagenase inhibition was determined using the Collagenase Assay Kit (Abcam). Collagenase activity testing aims to determine the ability of a material to inhibit collagenase, an enzyme involved in the skin aging process. Collagenase inhibitory activity was measured using active collagenase from *Clostridium histolyticum* as the enzyme and BODIPY-Gelatin as the substrate, which fluoresces when the gelatin breaks into fragments, and BODIPY is released. Collagenase and gelatin substrate were prepared by adding assay buffer at a ratio consistent with the Kit Protocol. Ascorbic acid served as a positive control, phosphate buffer saline XXXVIII as a color control, and various concentrations of sample extracts were dissolved separately in DMSO. The test was conducted by reacting the extract sample (80 mL) at concentrations of 10, 25, 50, 100, and 200 µg/mL with buffer and active collagenase (100 mL) in a 96-well plate, then incubated for 15 minutes, protected from light and at room temperature, and added with gelatin substrate solution (20 mL). The results were read using a fluorescence microplate reader (Spectramax M5, Molecular Devices, Sunnyvale, CA) with an excitation/emission wavelength of 490/520 nm. The ability to inhibit gelatinase/collagenase was calculated as follows:

$$\%ihibition = \left(\frac{A_{enzymecontrol} - (A_{sampel} - A_{buffer})}{A_{enzymecontrol}} \right) \times 100 \quad (4)$$

The results of collagenase inhibition are shown in (Table 4). The test extracts inhibited collagenase in a dose-dependent manner. The test extracts showed a very strong collagenase inhibitory effect, although still below the positive control, namely ascorbic acid. Regarding the anti-collagenase activity of mesocarp and ascorbic acid, they had comparable effects with IC_{50} values of 22.44 µg/mL and 5.58 µg/mL, respectively.

Table 4. IC_{50} value of collagenase inhibitor activity of ascorbic acid and mesocarp extract of oil palm

Sample	Concentration (µg/mL)	Inhibition(%)±SD	IC_{50} value (µg/mL)	Category
Ascorbic acid (Control +)	1	19.31±1.00	5.58	Very strong
	2.5	31.16±2.13		
	5	46.59±5.12		
	10	65.21±4.12		
	20	74.62±4.44		
Ethanol extract of Mesocarp	10	43.59±6.15	22.44	Very strong
	25	50.63±0.46		
	50	56.04±3.28		
	100	62.43±1.49		
	200	77.24±1.02		

The results of the collagenase activity test demonstrated a dose-dependent rise in enzyme inhibition percentage across the concentration range of 10-50 µg/mL, with an inhibition percentage of 43-56% (Table 4.). Collagenase inhibition activity showed no increase at concentrations of 100 µg/mL and 200 µg/mL.

At doubled and quadrupled concentrations, enzyme inhibition did not increase linearly with increasing dose, but only by 62-77%. From these results, the IC_{50} value was calculated based on the percentage of collagenase activity inhibition against the log concentration of oil palm mesocarp extract using a non-linear regression model (curve fit) (Figure 7B). The analysis yielded an IC_{50} value of 22.44 µg/mL for oil palm mesocarp extract with an R-square of 0.925, which is considered very strong.

The anti-collagenase activity test against the ascorbic acid reference compound showed a similar profile to that of oil palm mesocarp extract, namely increased activity at low doses and stable activity at high doses (Figure 7A.). The percentage of ascorbic acid inhibition in the concentration range of 1 - 20 µg/mL increased from 19% to 74% (Table 4.), indicating that the increase in ascorbic acid concentration was proportional to the increase in inhibitory activity. From these results, the IC_{50} value of ascorbic acid was also obtained, which was 5.58 µg/mL with an R squared of 0.993. These results indicate that the collagenase inhibition activity of ascorbic acid was higher than that of oil palm mesocarp extract.

The graph of the relationship between the concentration and percentage of inhibition of ascorbic acid and mesocarp oil palm against the collagenase enzyme is shown in Figure 7.

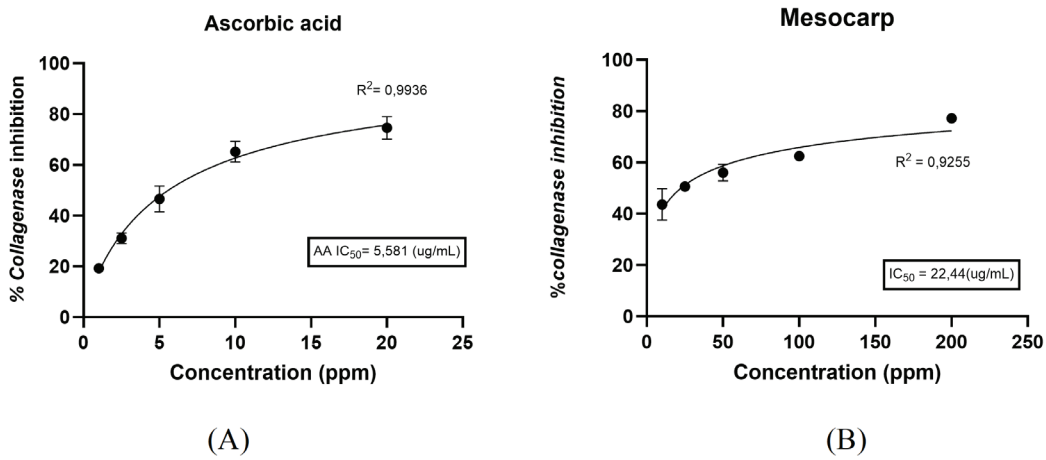


Figure 7. Regression graph of the relationship between concentration and percentage of inhibition of (A) ascorbic acid and (B) mesocarp oil palm

With an IC_{50} value of 22.44 µg/mL, the collagenase inhibition activity test findings demonstrated that the potential of EEOPM was active. Similar to the tyrosinase test, the phytochemical profile of the EEOPM sample was associated with the amount of vitamin E and fatty acid molecules in the collagenase test. A prior study by Aldrin et al. (2016) supported the findings of this investigation. Chemical testing of the extract revealed that it contained tocopherol (5.34±3.22 g/100 g) and tocotrienol (4.23±0.15 g/100 g) determined using HPLC-PDA and β-carotene (21.89±0.23 g/100 g) determined using HPLC-UV, various types of fatty acids, such as caprylic acid (2.18±0.12 g/100 g), capric acid (0.45±0.01 g/100 g), lauric acid (8.65±0.14 g/100 g), myristic acid (3.33±0.21 g/100 g), palmitic acid (74.53±0.68 g/100 g), and stearic acid (6.48±0.76 g/100 g) determined using gas chromatography (GC) analysis revealed that oil palm mesocarp extract accumulates significant vitamin E content, with 1300 µg/g total tocopherols, with γ-tocotrienol as the primary tocopherol, followed by α-tocopherol, α-tocotrienol, and α-tocomonoenol (Su et al., 2013). No results have been found to investigate anti-collagenase activity in oil palm mesocarp extract. However, similar results were demonstrated in a study of the anti-tyrosinase, anti-collagenase, anti-elastase, and anti-hyaluronidase activities of a *Stenocarpus sin-*

uatus leaf extract (Younis et al., 2022). In this study, the volatile components of the hexane-soluble fraction of the methanolic extract of *Stenocarpus sinuatus* (Proteaceae) leaves (SSHF) were identified. An amount of 52.59% of the extract was made up of vitamin E (α-tocopherol), which was followed by γ-sitosterol (8.65%), neophytadiene (8.19%), and β-tocopherol (6.07%). With IC_{50} values of 60.03, 177.5, 67.5, and 38.8 μg/mL, respectively, in vitro enzymatic assays demonstrated significant inhibition of collagenase, elastase, tyrosinase, and hyaluronidase by SSHF. These values were comparable to the positive controls, kojic acid (for tyrosinase) and epigallocatechin gallate (for collagenase, elastase, and hyaluronidase). Thus, in addition to the combined effects of other volatile ingredients, the high vitamin E content of SSHF may be responsible for its anti-aging properties. In vitro enzymatic testing results indicate that EEOPM can inhibit the activity of tyrosinase and collagenase enzymes, thus supporting the potential of EEOPM as an inhibitor of enzymes involved in premature skin aging.

***In silico* test using molecular docking**

The RMSD (Root Mean Square Deviation) value was less than 2Å, indicating that the docking process is valid. The position of the cocrystal ligand as the binding site determines how the grid box coordinates are arranged. Table 5 displays the validation results of the docking method. The validation results obtained an RMSD value of 1.004 for the tyrosinase receptor and 1.375 for the collagenase receptor.

Table 5. Validation results and RMSD values

Target Receptor	PDB ID	Grid Center			Docking area (x;y;z)	ΔG (Kcal/mol)	RMSD (Å)
		X	Y	Z			
Tyrosinase	5M8P	30.088	136.057	216.68	40 x 40 x 40	-5.81	1.004
Collagenase	2D1N	-44.048	25.846	-19.485	40 x 40 x 40	-7.87	1.375

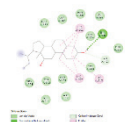
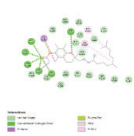
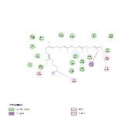
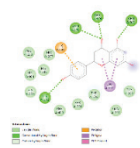
The results of molecular docking of 12 compounds obtained from LC-MS/MS-QToF of EEOPM against 5M8P and 2D1N can be observed in Table 5.

Table 6. Molecular docking results of EEOPM compounds identified by LC-MS/MS-QToF against 5M8P and 2D1N (Mean ± SD)

Ligands	5M8P		2D1N	
	Docking score (ΔG; kcal/mol)	Inhibition constant (Ki; μM)	Docking score (ΔG; kcal/mol)	Inhibition constant (Ki; μM)
α-Tocotrienol	**-7.33 ± 0.24**	4.56 ± 1.87	**-10.11 ± 0.38**	0.04 ± 27.07
β-sitosterol	**-7.20 ± 0.02**	5.28 ± 0.89	**-11.49 ± 0.09**	3.79 ± 12.09
3-(1,3-Benzodioxol-5-yl)-3-({[(2-methyl-2propanyl)oxy]carbonyl}amino)propanoic acid	**-7.12 ± 1.11**	28.79 ± 2.21	-8.80 ± 0.38	428.02 ± 7.21
Tocopherol	-6.36 ± 0.29	24.58 ± 12.76	-10.03 ± 0.29	0.05 ± 26.09
Squalene	-6.25 ± 0.29	29.88 ± 16.09	-8.66 ± 0.08	0.45 ± 58.62
Apigenin 6,8-diglucoside	-6.19 ± 0.00	28.68 ± 6.15	-9.21 ± 0.00	0.87 ± 5.76
β-carotene	-5.65 ± 0.01	372.30 ± 50.42	**-12.71 ± 0.24**	0.00 ± 21.29
Coenzym Q10	-5.23 ± 0.19	154.29 ± 48.48	-6.95 ± 0.02	8.01 ± 0.36
Oleic acid	-4.52 ± 0.33	571.29 ± 33.26	-6.18 ± 0.34	33.79 ± 15.97
Myristic acid	-4.37 ± 0.05	620.64 ± 48.33	-5.26 ± 0.18	143.56 ± 38.05
Palmitic acid	-4.23 ± 0.21	959.30 ± 39.11	-5.58 ± 0.08	81.21 ± 11.15
Kojic acid (+ control)	-4.60 ± 0.00	424.47 ± 8.71	-	-
Ascorbic acid (+ control)	-	-	-4.36 ± 0.17	669.84 ± 20.62

Based on the molecular docking data shown in Table 6 with the target 5M8P, the test compound with the lowest binding free energy (ΔG) value, namely α-tocotrienol (-7.33 kcal/mol), β-sitosterol (-7.20 kcal/mol), 3-(1,3-benzodioxol-5-yl)-3-({[(2-methyl-2propanyl)oxy]carbonyl} amino)propanoic acid (-7.12 kcal/mol), tocopherol (-6.36 kcal/mol), squalene (-6.25 kcal/mol), and Apigenin 6,8-diglucoside (-6.19 kcal/mol). Meanwhile, the native ligand compound 5M8P that has a binding free energy value of -5.81 kcal/mol can be seen in Table 5. On the other hand, the molecular docking data shown in Table 6 with the 2D1N target shows that the test compounds with the lowest binding free energy (ΔG) values are β-carotene (-12.71 kcal/mol), β-sitosterol (-11.49 kcal/mol), α-tocotrienol (-10.11 kcal/mol), tocopherol (-10.03 kcal/mol), Apigenin 6,8-diglucoside (-9.21 kcal/mol), and 3-(1,3-benzodioxol-5-yl)-3-({[(2-methyl-2propanyl)oxy]carbonyl} amino)propanoic acid (-8.80 kcal/mol). Meanwhile, the native ligand compound 2D1N that has a free binding energy value of -7.87 kcal/mol can be seen in Table 6.

Table 7. Interaction of amino acid compounds from EEOPM with tyrosinase receptor (5M8P)

Parameter	Native ligand (TYR)	α-tocotrienol	β-sitosterol	Propanoic acid	Tocopherol	Squalene	Apigenin 6,8-diglucoside
Chromophore group							
Amino acid residue	Asn378A[a]	-	-		-	-	Asn378A[a]
	Ser394A[a]	-	-	-	-	-	-
	Arg374A[a]	-	-	-	-	-	Arg374A[a]
	His192A[a]	-	-	His192A[a]	His192A[a]	His192A[d]	His192A[a]
	Thr391A[c]	-	-	Thr391A[a]	-	-	-
	Tyr513A[e]	-	-	-	-	-	-
	His381A[e]	His381A[c]	-	His381A[c]	His381A[d]	His381A[d]	His381A[e]
	Arg321A[f]	-	-	-	-	-	Arg321A[a]
		Asp212A[a]	His215A[c]	His377A[c]	His377A[a]	Lys198A[c]	Leu382A[d]
		His377A[c]	His377A[a]	His215A[c]	His224A[a]	His392A[c]	
		His215A[c]	Leu382A[c]	His192A[b]	His404A[a]	His215A[c]	
			Glu360A[a]		His215A[a]		
					Tyr362A[a]		
					His392A[c]		
					Val196A[c]		
Resemblance of amino acid with native ligand (%)		12.50	00.00	37.50	25.00	25.00	62.50
Resemblance of interaction with the native ligand (%)		00.00	00.00	25.00	12.50	00.00	50.00
Resemblance in ligand-receptor interaction (%)*		12.50	00.00	31.25	18.75	12.50	56.25
Interaction :		$a_{Hydrogen\ bond/Conventional\ hydrogen\ bond}$, $b_{Van\ der\ Waals}$, $c_{Alkyl/pi\text{-}alkyl}$, $d_{Pi\text{-}sigma}$, $e_{Pi\text{-}cation}$, $f_{Attractive\ Charge}$, $g_{Amide\text{-}Pi\ Stacked}$					

Further analysis of the interaction of the lowest binding free energy (ΔG) value with 5M8P (Table 7.) shows a high amino acid similarity score in the Apigenin 6,8-diglucoside compound is 62.50% with Asn378A, His192A, Arg374A, Arg321, and His381A. This indicates the presence of the same binding residues as the original ligand, the similarity score of the interaction between Apigenin 6,8-diglucoside and the original ligand is 50.00%. The high amino acid similarity score in propanoic acid compound is 37.50% with His192A, Thr391A, and His381A. This signals the presence of the same critical binding residues as the original ligand, the similarity score of the interaction between propanoic acid and the original ligand is 25.00%. Interestingly, Apigenin 6,8-diglucoside forms more hydrogen bonds at the 4 sites (Asn378A, His192A, Arg374A, Arg321) of the 5M8P binding site than at the other ligands tested. However, the higher docking score results were between α-tocotrienol and β-sitosterol. Fig.8 illustrates the complex relationship between the tyrosinase receptor and the highest docking score results of α-tocotrienol, β-sitosterol and 3-(1,3-benzodioxol-5-yl)-3-({[(2-methyl-2propanyl) oxy]carbonyl} amino)propanoic acid.

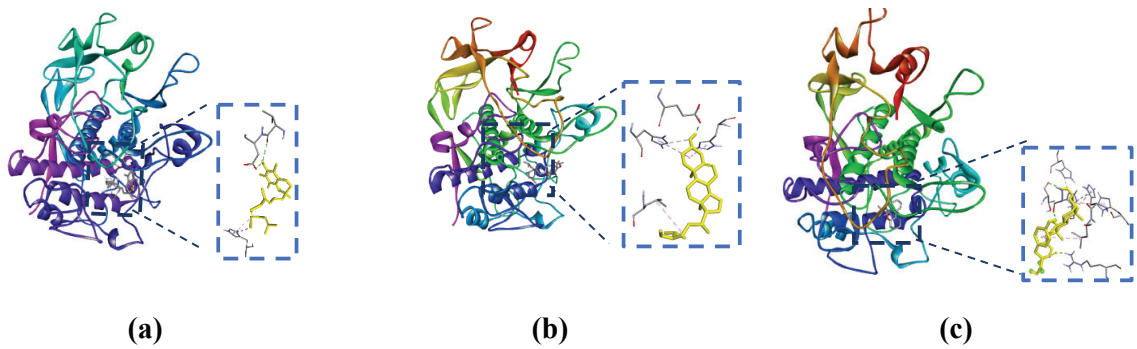
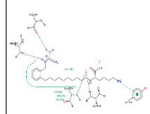
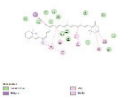
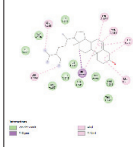
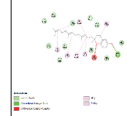
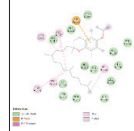
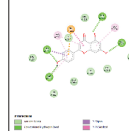
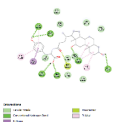
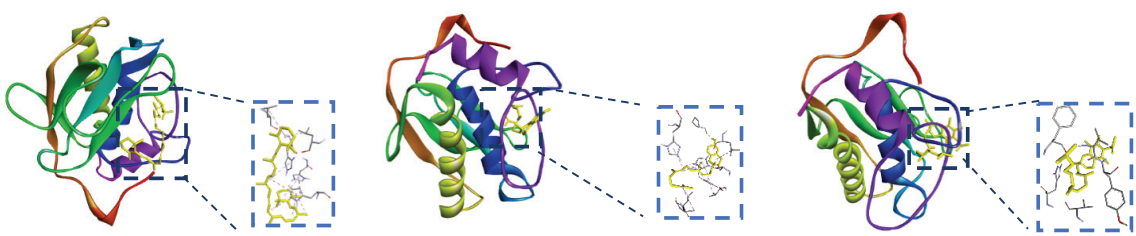


Figure 8. Compounds with the highest docking scores interacting with the 5M8P receptor: (a) α-tocotrienol; (b) β-sitosterol and (c) 3-(1,3-benzodioxol-5-yl)-3-({[(2-methyl-2propanyl)oxy]carbonyl} amino)propanoic acid

In the collagenase receptor (2D1N), such as Apigenin 6,8-diglucoside in 5M8P, propanoic acid has a binding site with an amino acid similarity score of 72.72% with the native ligand 2D1N, namely Val219A, His222A, His226, His232, Glu223, Pro242, Ile243 and Ala186A (Table 8.). The interaction profile of propanoic acid shows a similarity of 27.27%, which results in hydrogen bonds at His222A, His232A, Glu223A, Pro242A, Ile234A, and Ala186A with the native ligand at the 2D1N binding site, thus forming the highest hydrogen bond among all ligands tested. The superior docking score of propanoic acid is weakened by this large hydrogen bond network, which is comparable to that shown in Figure 8, while the highest docking score values interacting with the collagenase receptor are β-carotene, β-sitosterol and α-tocotrienol presented visually in Figure 9.

Table 8. Interaction of amino acid compounds from EEOPM with collagenase receptor (2D1N)

Parameter	Native ligand (FA4)	β-carotene	β-sitosterol	α-tocotrienol	Tocopherol	Apigenin 6,8-digluco-side	Propanoic acid
Chromophore group							
Amino acid residue	Ala188A[a] His187A[a] Val219A[a] His222A[a] His226A[a] His232A[a] Glu223A[a] Leu184A[c] Pro242A[c] Ile243A[g] Ala186A[h]	- Val219A[c] His222A[c] His226A[c] His232A[c] - - Pro242A[c] - - Leu218A[c] Leu259A[c]	- Val219A[c] His222A[d] - - - Leu184A[c] - - - Leu185A[c] Tyr244A[c] Leu218A[c] Leu239A[c]	- - Val219A[c] His222A[c] - His232A[c] - - Pro242A[a] Ile243A[h] - Leu185A[c] Tyr244A[c] Pro236A[a] Leu239A[c]	- - Val219A[c] His222A[c] - His232A[e] - - - - - Leu185A[c] Leu239A[c] Tyr244A[c]	- - - His222A[e] - - - - - - Ala186A[a] Leu185A[a] Ala238A[a] Thr245A[a] Val219A[c] Leu239A[c]	- - Val219A[d] His222A[a] His226A[c] His232A[a] Glu223A[a] - Pro242A[a] Ile243A[a] Ala186A[a] Thr245A[a] Asp231A[a] Leu185A[c]
Resemblance of amino acid with native ligand (%)		45.45	27.27	45.45	27.27	18.18	72.72
Resemblance of interaction with the native ligand (%)		9.09	9.09	00.00	00.00	00.00	27.27
Resemblance in ligand-receptor interaction (%)*		27.27	18.18	22.73	13.64	9.09	49.99
Interaction:		$a_{Hydogen\ bond/Conventional\ hydrogen\ bond}$, $b_{Van\ der\ Waals}$, $c_{Alkyl/pi\text{-}alkyl}$, $d_{Pi\text{-}sigma}$, $e_{Pi\text{-}cation}$, $f_{Attractive\ Charge}$, $g_{Amide\text{-}Pi\ Stacked}$, $h_{Unfavorable\ Positive\text{-}Positive}$, $i_{pi\text{-}lonepair}$					



(a) **(b)** **(c)**

Figure 9. Compounds with the highest docking scores interacting with the 2D1N receptor: (a) β-carotene, (b) β-sitosterol and (c) α-tocotrienol

Not every molecule in plant extracts contributes equally to pharmacological activity because they are complex combinations of metabolites. Nonetheless, a large number are categorized as bioactive substances that can have antagonistic, additive, or synergistic effects. The intricate makeup of extracts, which usually

include hundreds of metabolites, makes it difficult to identify specific activities for each compound, thus classifying plant extracts as multitarget interacting agents (Vaou et al., 2022). Tyrosinase and collagenase activity can be markedly increased by elevated quantities of free radicals, which come from both internal metabolic processes and external environmental influences. Consequently, the extracellular matrix, which is mainly made up of essential structural proteins as collagen, elastin, and hyaluronic acid, degrades (Abdelfattah et al. 2022). β-carotene, tocotrienols, and tocopherols are prominent compounds identified in ethanolic extracts of oil palm mesocarp, widely recognized as the main active components of the oil palm plant, contributing to its proven antioxidant properties. The anti-aging effects of β-carotene, tocotrienol, and tocopherol have been attributed to their capacity to reduce oxidative stress and wound healing. In several animal models, it has been demonstrated that β-carotene, tocotrienol, and tocopherol raise glutathione (GSH) levels and the activity of key antioxidant enzymes such as glutathione peroxidase (GPX), catalase (CAT), and superoxide dismutase (SOD) (Ayustaningwarno et al., 2024). Both mmp-13 and mmp-12 are significant macromolecular targets belonging to the mmp family. These enzymes are essential for the breakdown of the collagen matrix, which has a direct impact on the strength, flexibility, and suppleness of the skin. In particular, different forms of collagen (i, ii, iii, and iv) and elastin are broken down by MMP-13 and MMP-12, respectively (Alipour et al., 2016). Numerous studies have shown that β-carotene, tocotrienol, and tocopherol have anti-collagenase and anti-tyrosinase properties. In a human fibroblast cell culture, for instance, it has been demonstrated that oil palm, which is high in β-carotene and vitamin E, inhibits the activity of several MMPs, such as MMP-1, MMP-3, and MMP-13 (Hwang et al., 2017). Given that MMPs play a crucial role in aging-related tissue degradation, one important tactic for reducing the effects of systemic aging and for the creation of cosmetic goods is their inhibition.

CONCLUSION

The 96% ethanol extract of oil palm mesocarp (*Elaeis guineensis* Jacq.) showed a dose-dependent inhibition of the tyrosinase enzyme with a moderate IC_{50} value under the positive control of kojic acid and a dose-dependent inhibition of the collagenase enzyme with a very strong IC_{50} value but still below the positive control of ascorbic acid. Confirmed in an in silico study, α-tocotrienol compounds showed the strongest binding affinity to tyrosinase, and β-carotene compounds showed the highest affinity to collagenase. Thus, it can be concluded that secondary metabolites in EEOPM have potential as anti-aging agents by inhibiting aging-causing enzymes, namely tyrosinase and collagenase.

ACKNOWLEDGeMENTS

This study was supported by Airlangga Research Fund (ARF) 2025 under the subject International Research Collaboration (IRC) Top Over #300, 2025 with contract number 1735/B/UN3. LPPM/PT.01.03/2025 and also the author would like to thank for the support given from the Master Program of Pharmaceutical Sciences Faculty of Pharmacy, Universitas Airlangga.

AUTHOR CONTRIBUTION STATEMENT

Study concept and design, control of research activities, critical revision of the manuscript for important intellectual content, contribution to manuscript completion, obtaining funding, study supervision (RW), Literature search, data collection, raw material preparation, data extraction, analysis, and interpretation, manuscript preparation, statistical analysis, contribution to manuscript completion, molecular docking assay for protein docking, and enzymatic reaction assays of tyrosinase and collagenase (AYP), Contributed to the molecular docking assay for protein docking, critical revision of the manuscript, technical and administrative support and contributed to the completion of the manuscript (S), Technical and material support, study supervision, contributed to manuscript completion (IS), Technical and material support and study supervision (RH), Technical and material support and study supervision (KM), Technical and material support and study supervision (HC).

CONFLICT OF INTEREST

The authors declare that there is no conflict of interest.

REFERENCES

Abdelfattah, M. A. O., Dmirieh, M., Ben Bakrim, W., Mouhtady, O., Ghareeb, M. A., Wink, M., & Sobeh, M. (2022). Antioxidant and anti-aging effects of *Warburgia salutaris* bark aqueous extract: Evidence from in silico, in vitro, and in vivo studies. *Journal of Ethnopharmacology*, *292*. https://doi.org/10.1016/j.jep.2022.115187

Alanazi, S. (2025). Recent Advances in Liquid Chromatography–Mass Spectrometry (LC–MS) Applications in Biological and Applied Sciences. *Analytical Science Advances,* *6*(1). https://doi.org/10.1002/ansa.70024

Aldrin, A. H, Azizul Hasan, Z., Yusof, N. Z., Gani, S. S. A., Siddiqui, Y., & Mokhtar, N. F. M. (2016). Potential Uses Of Oil Palm (Elaeis Guineensis) Leaf Extract In Topical Application. *Journal Of Oil Palm Research, 28*(4). https://doi.org/10.21894/jopr.2016.2804.13

Alipour, H., Raz, A., Zakeri, S., & Dinparast Djadid, N. (2016). Therapeutic applications of collagenase (metalloproteases): A review. In *Asian Pacific Journal of Tropical Biomedicine, 6*(11), 975–981. Hainan Medical University. https://doi.org/10.1016/j.apjtb.2016.07.017

Anwar, S. S., Smith, S. D., Pongprutthipan, M., Kim, J. Y., Yuan, C., & van Steensel, M. (2022). Preaging of the skin among Asian populations. *JEADV Clinical Practice, 1.2*, 88–95. https://doi.org/10.1002/jvc2.22

Ayustaningwarno, F., Anjani, G., Ayu, A. M., & Fogliano, V. A. (2024). Critical review of Ginger's (*Zingiber officinale*) antioxidant, anti-inflammatory, and immunomodulatory activities. *Front Nutr, 11*, 1364836. https://doi.org/10.3389/fnut.2024.1364836

Badan Pengawas Obat dan Makanan Republik Indonesia (BPOM RI) (2017). *Farmakope Herbal Indonesia* (Edisi II). Jakarta: BPOM RI.

Badan Pusat Statistik. (2023). *Statistik Indonesia 2023*. ISSN/ISBN 0126-2912

Brzezinski, P., Borowska, K., Chiriac, A., & Smigielski, J. (2017). Adverse effects of isotretinoin: A large, retrospective review. *Dermatologic Therapy*, *30*(4). https://doi.org/10.1111/dth.12483

Facts & Factors. (2023). Revolutionary anti-aging market expected to reach USD 422.81 billion valuation by 2030, with a striking CAGR of 8.61%. PR Newswire, 24 July. Retrieved from https://www.prnewswire.com/news-releases/revolutionary-anti-aging-market-expected-to-reach-usd-422-81-billion-valuation-by-2030-with-a-striking-cagr-of-8-61-301882052.html?utm_source=chatgpt.com (Accessed: 17 November 2025).

Forli, S., Huey, R., Pique, M. E., Sanner, M. F., Goodsell, D. S., & Olson, A. J. (2016). Computational protein-ligand docking and virtual drug screening with the AutoDock suite. *Nature Protocols*, *11*(5), 905–919. https://doi.org/10.1038/nprot.2016.051

Furi, M., Dona, R., & Tristan, V. (2022). Penetapan Kadar Vitamin E dalam Ekstrak n-Heksan Buah Kelapa Sawit (Elaeis guineensis Jacq) dan CPO (Crude Palm Oil) dengan Metode KCKT (Determination of Vitamin E Levels in n-Hexane Extract of Palm Fruits (Elaeis guineensis Jacq) and CPO (Crude Palm Oil) using HPLC Method). *Jurnal Ilmu Kefarmasian Indonesia*, *20*(1), 49–54. doi:10.35814/jifi.v20i1.915

Hwang, J. H., Jung, H. W., Oh, S. Y., Kang, J. S., Kim, J. P., Park, Y. K. (2017). Effects of Zingiber officinale extract on collagen-induced arthritis in mice and IL-1β-induced inflammation in human synovial fibroblasts. *European Journal of Inflammation, 15*(3):168–78. doi: 10.1177/1721727X17727997

Krismayadi, K., Halimatushadyah, E., Apriani, D., & Cahyani, M. F. (2024). Standarisasi Mutu Simplisia dan Ekstrak Etanol Daun Kemangi (Ocimum x africanum Lour.). *Pharmacy Genius, 03*(02), 67-81. https://doi.org/10.56359/pharmgen.v3i2.333

Lee, J. E., Jayakody, J. T. M., Kim, J. II, Jeong, J. W., Choi, K. M., Kim, T. S., … Ryu, B. M. (2024). The Influence of Solvent Choice on the Extraction of Bioactive Compounds from Asteraceae: A Comparative Review. *Foods, 13*(19). https://doi.org/10.3390/foods13193151

Nurrochmad, A., Wirasti, Dirman, A., Lukitaningsih, E., Rahmawati, A., & Fakhrudin, N. (2018). Effects of antioxidant, anti-collagenase, anti-elastase, and anti-tyrosinase of the extract and fraction from *Turbinaria decurrens* Bory. *Indonesian Journal of Pharmacy*, *29*(4), 188–199. https://doi.org/10.14499/indonesianjpharm29iss4pp188

Okpe, A. (2022). A Comparative Study of Chemical Analysis of Locally Made and Refined Palm Endosperm Oil (Elaeis guineensis). *ScienceOpen*. https://doi.org/10.14293/S2199-1006.1.SOR-.PP8VWDQ.v1

Plyduang, T., Atipairin, A., Yoon, A. S., Sermkaew, N., Sakdiset, P., & Sawatdee, S. (2022). Formula development of red palm (*Elaeis guineensis*) fruit extract loaded with solid lipid nanoparticles containing creams and its anti-aging efficacy in healthy volunteers. *Cosmetics*, *9*(1). https://doi.org/10.3390/cosmetics9010003

Riansyah, H., Maharani, D. M., & Nugroho. A. (2021). Intensitas Dan Stabilitas Warna Ekstrak Daun Pandan, Suji, Katuk, Dan Kelor Sebagai Sumber Pewarna Hijau Alami. *Journal Riset Teknologi Industri, 15*(1), 103. doi: 10.26578/jrti.v15i1.6637

Su, T. R., Lin, J. J., Tsai, C. C., Huang, T. K., Yang, Z. Y., Wu, M. O., … Wu, Y. J. (2013). Inhibition of melanogenesis by gallic acid: possible involvement of the PI3K/Akt, MEK/ERK and Wnt/β-catenin signalling pathways in B16F10 cells. *International Journal of Molecular Sciences., 14*(10): 20443-20458. doi: 10.3390/ijms141020443

Suzana, M., Nadia, N. M. A., Zahariah, I., Chua, K. H., Anum, Y. M. Y., & Zurinah, W. W. N. (2009). Melanogenesis Inhibition by Palm Tocotrienol Rich Fraction in Cellular Ageing. Med *&* *Health, 4*(1), 25-34. Retrieved from https://mail.medicineandhealthukm.com/sites/default/files/article/2012/7-Page%2025-34%20%28MS%20079%29.pdf

Vaou, N., Stavropoulou, E., Voidarou, C. C., Tsakris, Z., Rozos, G., Tsigalou, C., & Bezirtzoglou, E. (2022). Interactions between Medical Plant-Derived Bioactive Compounds: Focus on Antimicrobial Combination Effects. *Antibiotics, 11*(8), 1014. https://doi.org/10.3390/antibiotics11081014

Widyowati, R., Sugimoto, S., Yamano, Y., Otsuka, H., & Matsunami, K. (2016). New Isolinariins C, D and E, Flavonoid Glycosides from Linaria japonica. *Chem. Pharm. Bull, 64*(5). doi: 10.1248/cpb.c16-00073

Wondi, M. H., Haris, N. I. N., Shamsudin, R., Yunus, R., Mohd Ali, M., & Iswardi, A. H. (2024). Development and testing of an oil palm (*Elaeis guineensis* Jacq.) fruit digester process for endosperm-free in crude palm oil production. *Industrial Crops and Products*, *208*. https://doi.org/10.1016/j.indcrop.2023.117755

You, Z., Li, Y., Chen, M., Wong, V. K. W., Zhang, K., Zheng, X., & Liu, W. (2022). Inhibition of plant essential oils and their interaction in binary combinations against tyrosinase. *Food and Nutrition Research*, *66*. https://doi.org/10.29219/fnr.v66.8466

Younis, M. M., Ayoub, I. M., Mostafa, N. M., el Hassab, M. A., Eldehna, W. M., Al-Rashood, S. T., & Eldahshan, O. A. (2022). GC/MS Profiling, Anti-Collagenase, Anti-Elastase, Anti-Tyrosinase, and Anti-Hyaluronidase Activities of a Stenocarpus sinuatus Leaf Extract. *Plants*, *11*(7). https://doi.org/10.3390/plants11070918

Yusof, N. Z., Gani, S. S. A., Siddiqui, Y., Mokhtar, N. F. M., & Hasan, Z. A. A. (2016). Potential uses of oil palm (Elaeis guineensis) leaf extract in topical application. *Journal of Oil Palm Research*, *28*(4), 520–530. https://doi.org/10.21894/jopr.2016.2804.13

FABAD J. Pharm. Sci., 51, 1, 275-290, 2026
Doi: 10.55262/fabadeczacilik.1752400
RESEARCH ARTICLE

Total Phenolic and Flavonoid Contents of Ethanol Extract of *Manilkara kauki* Leaves and Antibiofilm Activity Test Against Biofilms of *Pseudomonas aeruginosa*

Lilik FARKHIYAH[*], Tukiran TUKIRAN[**°]

Total Phenolic and Flavonoid Contents of Ethanol Extract of Manilkara kauki Leaves and Antibiofilm Activity Test Against Biofilms of Pseudomonas aeruginosa

SUMMARY

One of the infectious bacteria that can cause high morbidity and mortality is Pseudomonas aeruginosa. P. aeruginosa is a difficult pathogen to treat and often causes resistance to antibiotics. One of the causes of antibiotic resistance is the formation of biofilm. Manilkara kauki is one of the plants that has potential as an antibiofilm. The absence of publications related to information on total phenolic and flavonoid contents and the use of M. kauki leaves as antibiofilm makes this research important and necessary. This study aims to determine the total phenolic and flavonoid contents in the ethanol extract of M. kauki leaves and antibiofilm activity tests, which include optimization of biofilm formation time, inhibition activity test, and biofilm destruction using the Microtiter Plate Assay method with positive control of ciprofloxacin. According to the LC-MS results, the flavonoid content was relatively high at 46.15%, while the non-flavonoid phenolic content in the ethanol extract of small sapodilla leaves was 23.08%. Meanwhile, the total phenolic and flavonoid content tests yielded similar results, namely 48.9830 mg/g GAE and 21.3270 mg/g QE, respectively. The results of the antibiofilm activity test showed that P. aeruginosa is a strong biofilm-forming bacterium with an optimum formation time of 48 hours and an OD value of 0.5298. Meanwhile, the highest percentage of biofilm inhibition and destruction was observed at a concentration of 1000 ppm, with IC50 values of 134 and 108.4 µg/mL, respectively.

Keywords: *Antibiofilm, flavonoid, phenolic, Pseudomonas aeruginosa, Manilkara kauki.*

Manilkara kauki Yapraklarının Etanol Ekstraktının Toplam Fenolik ve Flavonoid İçeriği ve Pseudomonas aeruginosa Biyofilmlerine Karşı Antibiyofilm Etkinlik Testi

ÖZ

Yüksek morbidite ve mortaliteye neden olabilen enfeksiyöz bakterilerden biri Pseudomonas aeruginosa'dır. P. aeruginosa tedavisi zor bir patojendir ve sıklıkla antibiyotiklere karşı direnç geliştirir. Antibiyotik direncinin nedenlerinden biri biyofilm oluşumudur. Manilkara kauki, antibiyofilm potansiyeline sahip bitkilerden biridir. M. kauki yapraklarının toplam fenolik ve flavonoid içerikleri ile antibiyofilm olarak kullanımıyla ilgili yayınların bulunmaması, bu araştırmayı önemli ve gerekli kılmaktadır. Bu çalışmanın amacı, M. kauki yapraklarının etanol ekstraktındaki toplam fenolik ve flavonoid içeriklerini belirlemek ve antibiyofilm aktivitesini incelemektir. Antibiyofilm testleri, biyofilm oluşum süresinin optimizasyonu, inhibisyon aktivitesi testi ve biyofilm yıkımı testlerini kapsamakta olup, pozitif kontrol olarak siprofloksasin kullanılmıştır. Tüm testler Microtiter Plate Assay yöntemi ile gerçekleştirilmiştir. LC-MS sonuçlarına göre, flavonoid içeriği %46,15 ile nispeten yüksek bulunurken, küçük sapodilla (M. kauki) yapraklarının etanol ekstraktındaki flavonoid olmayan fenolik bileşiklerin oranı %23,08 olarak belirlenmiştir. Buna karşılık, toplam fenolik ve flavonoid içerik analizleri sırasıyla 48,9830 mg/g GAE ve 21,3270 mg/g QE değerlerini vermiştir. Antibiyofilm aktivite testi sonuçları, P. aeruginosa'nın güçlü bir biyofilm oluşturan bakteri olduğunu, optimum biyofilm oluşum süresinin 48 saat olduğunu ve OD değerinin 0,5298'e ulaştığını göstermiştir. Bu arada, biyofilm inhibisyonu ve yıkımının en yüksek yüzdesi 1000 ppm konsantrasyonda gözlemlenmiş olup, IC50 değerleri sırasıyla 134 ve 108,4 µg/mL'dir.

Anahtar Kelimeler: *Antibiyofilm, fenolik, flavonoid, Pseudomonas aeruginosa, Manilkara kauki.*

Recieved: 28.07.2025
Revised: 23.02.2026
Accepted: 27.02.2026

[*] ORCID: 0009-0007-8205-9864, Department of Chemistry, Faculty of Mathematics and Natural Science, Universitas Negeri Surabaya, Surabaya, Indonesia
[**] ORCID: 0000-0001-6613-128X, Department of Chemistry, Faculty of Mathematics and Natural Science, Universitas Negeri Surabaya, Surabaya, Indonesia

° Corresponding Author; Tukiran Tukiran
E-mail: tukiran@unesa.ac.id

INTRODUCTION

Infectious diseases are often experienced by developed and developing countries, including Indonesia (Santoso et al., 2020). Infection is a disease caused by pathogenic microbes such as bacteria (Konoralma, 2019). According to the National Institute of Health, microbial biofilms are responsible for about 65% of nosocomial infections and 80% of all microbial infections and chronic diseases (Singh et al., 2024). The effectiveness of antibiotics as antimicrobial agents is decreasing as the prevalence of drug resistance among microorganisms increases (Muteeb et al., 2023).

One of the bacteria that causes serious infections is *Pseudomonas aeruginosa* (Chen et al., 2024). This bacterium is capable of causing infections in the urinary tract and bloodstream (Qin et al., 2022) and is the dominant pathogen causing pulmonary infections in cystic fibrosis patients (Pang et al., 2019). This bacterium can cause a mortality rate as high as 50%, depending on the nature of the infection (Purnama et al., 2024). *P. aeruginosa* is a bacterium resistant to multiple drugs, making treatment challenging and frequently linked to high mortality rates (Hirsch & Tam, 2010).

The development of biofilms is one of the factors contributing to antibiotic resistance (Pamudi et al., 2024). The Centers for Disease Control and Prevention (CDC) in 2007 reported that approximately 1.7 million infections in hospitals were caused by biofilm formation (Goel et al., 2021). Biofilms consist of a community of bacterial cells that can produce a polymer matrix composed of exopolysaccharides, thereby inhibiting antibiotic penetration and resulting in chronic infection (Jayadi et al., 2023; Maghfirah et al., 2017). Until now, no drug specifically functions as an antibiofilm, so the development of antibiofilm agents is very necessary (Purnama et al., 2024).

Bacterial resistance to many drugs directs the search for new strategies, one of which is by utilizing natural materials (Prianggawe & Hajrin, 2024). The content of natural materials such as phenolics and flavonoids is considered to have potential as a natural antibiofilm that has the ability to damage bacterial polysaccharides (Rosyada et al., 2023). One of the plants that is predicted to be potentially useful as an antibiofilm is *Manilkara kauki.* (L.) Dubard. *M. kauki* (Indonesian people called as sawo kecik) is a fruit-producing tree from the Sapotaceae family and the Manilkara genus (Susilawati et al., 2023). The genus Manilkara comprises approximately 70–80 species widely distributed in tropical and subtropical regions, particularly in Southeast Asia, South Asia, Africa, and Central America. In Indonesia itself, *M. Kauki* can be found on the islands of Karimun, Kangean, Bali, Nusa Tenggara, Buton, Sulawesi, Maluku, and Papua (Pratiwi et al., 2021). *M. Kauki* is widely used in traditional medicine. Several parts of the plant have reported ethnomedical uses, where the bark and roots are used as astringents and to treat diarrhea in children, the seeds are used as antipyretics, anthelmintics, and antileprosy agents, while the leaves are used as compresses for tumors (Hegde et al., 2025). Although *M. kauki* leaves have long been used in traditional medicine, research on their antibiofilm activity has not yet been reported.

Previous studies have shown that *M. kauki* has various biological activities, including antibacterial activity against *Escherichia coli* and *Staphylococcus aureus*, as well as antidiabetic activity through lowering blood glucose levels in diabetic rats (Pratiwi et al., 2021; Prayudhani et al., 2013; Purba et al., 2023). These findings show similar activity to that reported in other Manilkara species, such as *Manilkara zapota* (L.) van Royen, reported by Kaneria et al. (2009), which showed that *M. zapota* methanol extract has antibacterial activity against *Bacillus subtilis*, *Staphylococcus aureus*, *Pseudomonas aeruginosa*, *Salmonella typhimurium*, and *Enterobacter aerogenes* bacteria, with an average activity value of 12.4.

According to research by Srisupap and Chaicharoenpong (2021), water extracts from small *M. kauki* leaves have the highest phenolic content compared to extracts from the fruit, seeds, stems, and roots. In addition, the flavonoid content in small *M. kauki* leaves for methanol extracts is also higher than that in extracts from the fruit, seeds, and stems. Therefore, leaves were used in this study. Referring to the background previously described, the researcher is interested in researching the ethanol extract of *M. kauki* leaves, which contain total phenolic and flavonoid compounds, as determined using UV-Vis Spectrophotometry. While the previous study focused on antibacterial activity against planktonic cells, this study specifically evaluated antibiofilm activity, which better represents chronic infection conditions. Then it is necessary to carry out a series of activities, including optimization of biofilm formation time, inhibitory activity test, and biofilm destruction to determine the antibiofilm potential of *M. kauki* leaf ethanol extract against *P. aeruginosa* bacterial biofilm. This approach allows for quantitative assessment of biofilm inhibition and destruction activities. The results of this study provide preliminary information on the potential antibiofilm activity of *M. Kauki* leaves. The absence of publications related to the information on *M. kauki* leaves as antibiofilm makes this research important to do.

MATERIALS AND METHODS

Materials

The materials used in this study included *M. kauki* leaves, ethanol 96%, quercetin (Merck), 10% (b/v) aluminum chloride ($AlCl_3$), filter paper, sodium acetate, distilled water, sodium carbonate (Na_2CO_3), acetic acid, barium chloride ($BaCl_2$), Folin–Ciocalteu reagent (Merck), and a pure culture of the bacterium *P. aeruginosa* (ATCC 27853), nutrient agar (NA) medium (Merck), physiological saline, peptone (Oxoid), dipotassium hydrogen phosphate (K_2HPO_4), glucose (Merck), sodium chloride (NaCl), tryptone (Merck), and crystal violet (Merck).

Instrumental

Equipment and instruments used in this study are incubator (Memmert IN55), volumetric flask (Herma), beakers (Iwaki), laminar air flow (Thermo Scientific 1300-Series A2), UV-Vis spectrophotometer (Shimadzu UV-1800), micropipettes, test tubes (Iwaki), inoculating loop, autoclave (HICLAVE HVE-50), 96-well plates, blue tips, ELISA microplate reader (BK-EL10A), and rotary evaporator (R-215, Buchi).

Characterization methods

M. kauki leaf collection and extraction process

The *M. Kauki* leaf plant used in this study was identified and verified botanically by Heri Santoso, Department of Botan on November 19th, 2024. The specimen is stored under the number BT-112495 at the Herbarium of Yayasan Generasi Biologi Indonesia. The plant material was collected from Tropodo, Sidoarjo Regency, East Java Province, Indonesia, on September 4th, 2024, with coordinates -7.360310, 112.764195. A total of 1.3 kg of the collected leaves was dried under sunlight for three days with occasional flipping. After drying, the leaves were pulverized with a grinder until they became powder and were weighed. 750 g of dry powder was obtained. The *M. kauki* leaf powder was extracted using ethanol as the solvent at a ratio of 1:2 within 24 hours. Maceration was repeated 3 times with occasional stirring. After that, filtering was carried out with a Buchner funnel assisted by a vacuum pump, and an ethanol filtrate was obtained. The ethanol filtrate was concentrated through evaporation to yield a thick extract, and weighed to obtain a thick extract of 169 grams. As much as approximately 0.5 mg of the extract was tested for phytochemicals using the LC-MS test. In this study, *M. kauki* leaf extract was prepared using ethanol, which is a polar solvent, because the test target was *Pseudomonas aeruginosa*, a Gram-negative bacterium. Previous research on the species *M. zapota* showed that extraction with polar solvents, such as acetone, produced broader antimicrobial activity compared to non-polar solvents, with effects on all

test bacteria (Kaneria & Chanda, 2012). Maceration is used because it is a simple method that does not involve heating, allowing for the extraction of compounds without damaging heat-sensitive natural ingredients (Riasari et al., 2022).

Total phenolic content

The procedure for this test follows the method described by Saputri et al. (2021). The total phenolic content in the ethanol extract of *M. kauki* leaves was measured using the Folin-Ciocalteu method. Gallic acid was used as the standard at concentrations of 10, 20, 30, 40, and 50 ppm. Each extract and standard solution was taken 0.4 mL, and then 2 mL of Folin-Ciocalteu reagent was added. Then, 1.6 mL of 1M Na_2CO_3 was homogenized and incubated at room temperature for 30 minutes in the absence of light, and then measured using a UV-Vis spectrophotometer at a wavelength of 743 nm.

Total flavonoid content

Total flavonoid content using quercetin as a control with concentrations of 20, 40, 60, 80, and 100 ppm. Extract and standard solutions were each taken 0.5 mL and then 0.1 mL of 10% (b/v) $AlCl_3$ solution, 0.1 mL of 1 M potassium acetate, and 2.8 mL of distilled water, then shaken until homogeneous. The solution was subsequently incubated at 37°C for 30 minutes and measured using a UV-Vis spectrophotometer at a wavelength of 424.6 nm.

Identification of the chemical content of the ethanol extract of *M. kauki* leaves using LC-MS

The LC-MS testing was performed according to the method described by Martha et al. (2023) with modifications. The ethanol extract of *M. kauki* leaves was analyzed to identify its secondary metabolites using a Shimadzu LC-MS instrument, model 8040. Before analysis, the crude ethanol extract was filtered through a 0.22 µm membrane filter to remove particulate matter. The concentrated extract was prepared as a stock solution by dissolving it in 95% ethanol with a concentration of 1 mg/mL. The stock solution was sonicated for 10 minutes to ensure complete dissolution and homogeneity. A 1 µL sample was injected into the system with a capillary voltage of 3.0 kV. Compound separation was carried out using a Shimadzu Shim-Pack FC-ODS column (2 mm × 150 mm, 3 µm particle size), maintained at a temperature of 35°C. An isocratic elution system was applied with 95% ethanol as the mobile phase at a flow rate of 0.5 mL/min, over a total run time of 60 minutes. Detection utilized Electrospray Ionization (ESI) in positive ion mode [M]+, with mass spectra recorded across an m/z range of 10–1500 and a scan time of 0.6 seconds per scan. Nitrogen gas was used as the desolvation gas during ionization. The resulting data were interpreted based on molecular ion peaks and fragmentation patterns. Compound identification analysis was carried out using the NIST database by comparing retention times and molecular mass spectra from the chromatograms. The analysis was performed in a single run for qualitative profiling of secondary metabolites. LC–MS analysis in this study aimed to qualitatively identify and determine the relative composition of compounds in ethanol extracts of *M. kauki* leaves. The data obtained were peak area percentages representing the relative abundance of each compound.

Optimization of biofilm formation time of *P. aeruginosa*

This optimisation aims to obtain the optimal incubation time for forming biofilm. The variations used were 24, 48, and 72 hours. Optimisation of biofilm formation time refers to the method used by Besan et al. (2023) with some modifications. A total of 200 µL of bacterial suspension was put into the well plate. Then, incubated for 24, 48, and 72 hours at 37°C. Following the incubation period, the microplate was rinsed three times using running water. Then, 200 µL of 1% crystal violet was added and incubated at room temperature for 15 minutes. Subsequently, it was rinsed three times with running water, followed by the addition of 200 µL of 96% ethanol to each well

and incubation at room temperature for 15 minutes. Then, the biofilm growth was read with an absorbance of 630 nm. The negative control used is growth media without bacteria. The average OD value that has been obtained is compared with the OD-cut value determined using the formula:

OD-cut (ODc) = Mean OD value of negative control + (3 × Deviation standard of negative control)

Biofilm inhibition activity test

The biofilm inhibition assay was conducted based on the method described by Kining et al. (2017), with slight modifications. A total of 80 µL of extract (concentrations of 62.5, 125, 250, 500, and 1000 ppm), 80 µL of HTR media, and 40 µL of bacterial suspension were placed in a microplate. Then, incubated at 37°C for the optimum time previously determined. The microplate was thoroughly washed three times using distilled water. A volume of 200 µL of 1% crystal violet solution was added to each well, followed by incubation at room temperature for 15 minutes. Then, washed with running water 3 times, and added 96% ethanol, as much as 200 µL, was added to each well and incubated at room temperature for 15 minutes. Next, the biofilm inhibition was read with an absorbance of 630 nm. The positive control used ciprofloxacin with a concentration of 0.625, 1.25, 2.5, 5, and 10 mg/mL.

%Biofilm inhibition = × 100%

Biofilm degradation activity test

The biofilm destruction test refers to the method used by Tobi et al. (2022) with modifications. The biofilm degradation assay was performed by adding 80 µL of HTR medium and 40 µL of a bacterial suspension standardized to 1.5×10^6 CFU/mL into each well, followed by incubation at 37°C for the predetermined optimal duration. After the incubation period, the contents of the wells were washed using water, and then the ethanol extract of *M. kauki* leaves at concentrations of 62.5, 125, 250, 500, and 1000 ppm was added as much as 80 µL, then the microplate was again incubated at 37°C for 90 minutes. The microplate was rinsed three times with sterile distilled water to remove non-adherent cells. A total of 200 µL of 1% crystal violet was put into the wells, then incubated at room temperature for 15 minutes. Then washed with running water 3 times, and added 96% ethanol was added to each well, up to 200 µL, and incubated at room temperature for 15 minutes. Next, the biofilm growth was read with an absorbance of 630 nm.

% Biofilm degradation = × 100%

Statistical analysis

The research results are presented in the form of OD values for each stage of biofilm formation, inhibition, and destruction. Statistical analysis was performed using SPSS version 25 (2017). The statistical test results can be seen in supporting file 2. A one-way ANOVA test was conducted to evaluate the differences between groups. Differences were considered significant if $p < 0.05$. Differences between groups were further analyzed using Tukey's post hoc test. A $p < 0.05$ indicated a significant difference in effect between treatments. The relationship between the concentration of the extract or control and the OD value was analyzed using Pearson's correlation test. $P < 0.05$ indicates a correlation between the concentration of the extract and control used and the level of biofilm inhibition or destruction.

RESULTS AND DISCUSSION

Total phenolic content of ethanol extract of *M. kauki* leaves

The determination of total phenolic content using the Folin-Ciocalteu reagent method. Folin-Ciocalteu reagent is common and often used because it is simple, sensitive, consistent, relatively accurate results, and does not require specific and sophisticated equipment (Agustin et al., 2022). The principle of this method is a reduction-oxidation reaction in which the phenolic compound acts as a reductant by donating electrons, while the Folin-Ciocalteu reagent acts as an oxidizer (Pérez et al., 2023). In this test, the standard used is

gallic acid. The absorbance measurement results of the standard solution concentration series obtained were then made into a calibration curve. According to the linear regression analysis of the gallic acid standard solution concentrations and their corresponding absorbance values, a regression equation of y = 0.0098x + 0.2303 was obtained, with a coefficient of determination (R^2) of 0.9976. Furthermore, the absorbance of the sample of ethanol extract of *M. kauki* leaves was substituted into the linear regression equation, resulting in a total phenolic content of 48.983 ± 0.059 mg GAE/g extract. This value is higher when compared to the research of Zakri et al. (2025) on the butanol fraction of 39.94 ± 4.01 mg GAE/g.

Total flavonoid content of the ethanol extract of *M. Kauki* leaves

The total flavonoid content was determined using a colorimetric assay involving the addition of aluminum chloride ($AlCl_3$). Where Al(III) is used as a complexing agent and does not require specific and sophisticated equipment (Agustin et al., 2022). This method is based on the principle of complex formation between aluminum chloride and the keto and hydroxyl groups located at the C4 and C5 positions of the flavonoid structure (Widyasari & Sari, 2021). The absorbance measurement results of the standard solution concentration series obtained were then made into a calibration curve. According to the results of linear regression analysis between the concentration of the gallic acid standard solution and its corresponding absorbance values, a regression equation of y = 0.005x - 0.0113 was obtained, with an R^2 value of 0.9997. By substituting the absorbance value of the *M. kauki* leaf ethanol extract into the equation, the total flavonoid content was calculated to be 21.260 ± 0.306 mg QE/g extract. This result is much greater when compared to the flavonoids in *M. zapota* extract, which is only 2.51 mg QE/g.

Identification of the chemical content of ethanol extract of *M. kauki* leaves using LC-MS

The results of LC-MS analysis showed that ethanol extracts of *M. kauki* leaves contained various compounds with varying relative compositions. The percentage of compounds was determined based on the peak area of the chromatogram, reflecting relative abundance rather than absolute content. According to LC-MS analysis, it can be identified that the content of chemical constituents present in the ethanol extract of *M. kauki* leaves includes phenolics, flavonoids, terpenoids, alkaloids, tannins, carbohydrates, steroids, vitamin C, and aromatic groups.

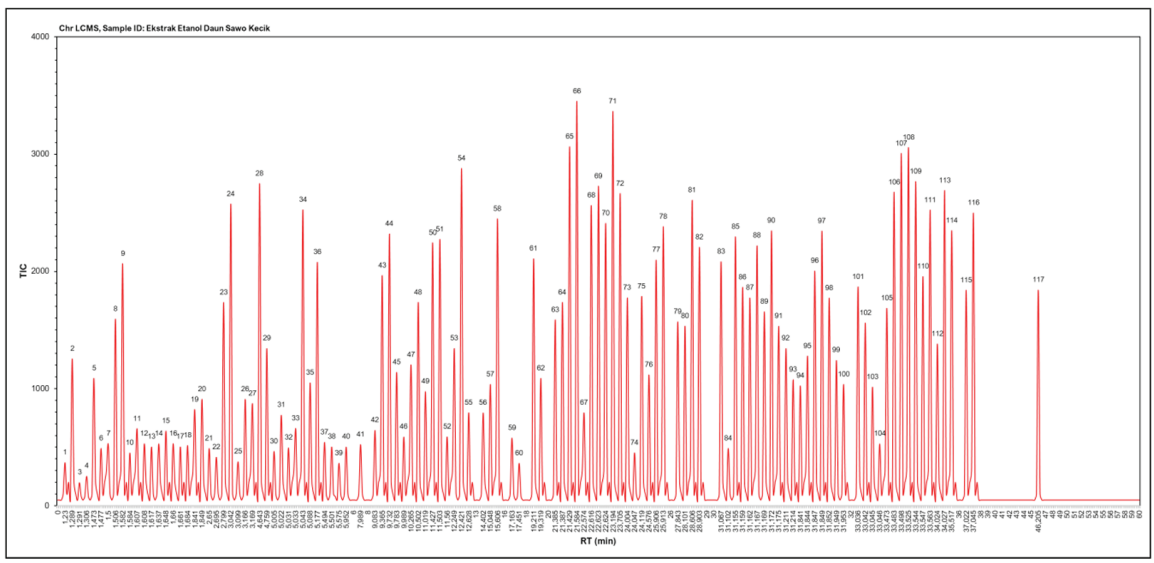


Figure 1. LC-MS chromatogram of the ethanol extract of *M. kauki* leaves

The identification results showed 117 compounds indicated by the LC-MS chromatogram in Figure 1. The phenolic composition of the ethanolic extract of *M. kauki* leaves is high, as much as 23.08%, while flavonoids are 46.15%, and other groups are 30.77%. This value is higher than the results of the total phenolic and flavonoid content tests that have been carried out. This is due to differences in measurement methods. Measurement of total phenolic and flavonoid contents using colorimetric methods with Folin–Ciocalteu and $AlCl_3$ reagents cannot always detect all phenolic and flavonoid compounds completely, so the results may be lower than the actual. Meanwhile, LC-MS has a more sensitive and selective ability, so it can detect and quantify more types of compounds, including compounds that are sometimes not detected by colorimetric methods. Furthermore, colorimetric assays provide cumulative values expressed as equivalents (mg GAE/g or mg QE/g), whereas LC–MS profiling is based on the detection of individual compounds and their relative abundance, which can lead to apparently higher values. Therefore, discrepancies between the two methods are expected and reflect fundamental differences in analytical principles rather than inconsistencies in the results.

The compounds identified by LC-MS (see supplementary file 1) are dominated by phenolic groups, especially flavonoids. The identified flavonoids can be classified based on their basic framework, such as flavone, flavan-3-ol, and flavanol. Flavonoids with a flavone basic framework include apigenin, luteolin, chryseriol, vitexin, and isovitexin. Compounds that belong to the flavan-3-ol group include epigallocatechin and its derivatives, namely epigallocatechin-3-*O*-coumarate, epicatechin-3-*O*-*p*-hydroxybenzoate, epigallocatechin-3-*O*-cinnamate, and epigallocatechin gallate, epiafzelechin, and its derivative, epiafzelechin-3-*O*-gallate. Epigallocatechin and epiafzelechin derivatives undergo esterification, where the -OH group at the C3 position reacts with phenolic acid to form an ester. Flavonoid compounds with flavonol basic skeletons include kaempferol-7-*O*-*β*-*D*-glucoside, kaempferol-3-*O*-*D*-glucoside, kaempferol-3-*O*-rhamnoside, kaempferitrin, quercetin, quercetin-3-*O*-rhamnoside, myricetin-3-glucoside, myricetin-3-*O*-*β*-*D*-galactopyranoside, and quercetin-3-*O*-rutinoside. These compounds, except quercetin, undergo glycosylation, where there is the addition of sugar groups to the flavonol hydroxyl group through glycosidic bonds.

In addition to flavonoids, there are non-flavonoid phenolic compounds identified in the ethanol extract of *M. kauki* leaves, such as phenolic acid. Compounds that include phenolic acids include gallic acid, cinnamic acid, syringic acid, benzoic acid, vanillic acid, ferulic acid, salicylic acid, and caffeic acid. This group of compounds is polar, so that it can be extracted by ethanol solvent.

The compounds identified by LC-MS were also found in other species of the Manilkara genus. In the *Manilkara zapota* species, caffeic acid, gallic acid, and epigallocatechin compounds were found (Baky et al., 2016). The extract also contained various other constituents, including salicylic acid, vanillic acid, ferulic acid, and quercetin, which were also identified in *Manilkara hexandra* (Roxb.) Dubard (Parikh & Patel, 2017b). This finding is in line with the concept of chemotaxonomy, which indicates that plant species with close taxonomic relationships may share similar chemical constituents (Uckele et al., 2021).

Optimization of *P. aeruginosa* biofilm formation

Optimization of biofilm formation was carried out to determine the time required for *P. aeruginosa* bacteria to form the best biofilm so that it can be used as an optimum condition for biofilm inhibition and destruction testing. In the incubation process, 3 variations of incubation time were carried out, namely 24, 48, and 72 hours. The *P. aeruginosa* bacterial suspension in this test was grown in liquid media. Media can encourage the growth and development of a microbe. Liquid culture media make it easier for bacteria to access nutrients (Bonnet et al., 2020).

The media used in this study is HTR media because it provides nutrients that support the optimal growth of heterotrophic bacteria, so that biofilm can form well on the surface of the microplate. The results of biofilm formation on the microplate were followed by measurement of the OD value. Measurement of OD value in this study was carried out to determine the strength of bacterial biofilm formation (Wang et al., 2024). An increase in OD value indicates an increase in suspension turbidity, which means that the number of microbial cells has increased. If used to measure the growth of biofilm formation, the higher the OD value, the more biofilm is formed on the surface (Turhan & Koca, 2024). OD value data of biofilm formation optimization results are presented in Figure 2.

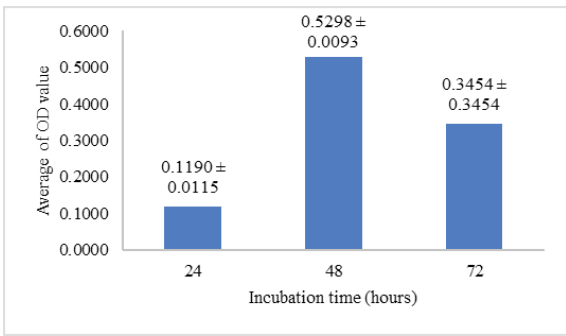


Figure 2. Average OD value on biofilm formation

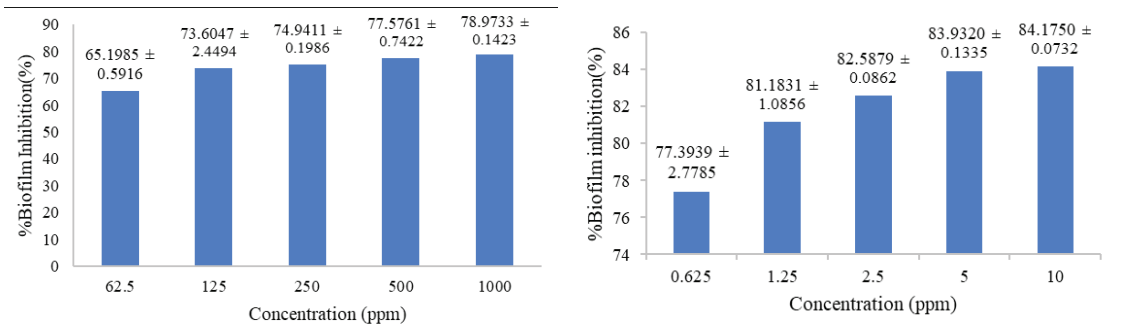
According to Figure 2, on the 24-hour mark, the average OD value of biofilm was 0.1190, on the 48-hour mark, an increase in the average OD of 0.5298, and on the 72-hour mark, a decrease in the average OD value of 0.3454. Thus, it is known that the incubation time of 48 hours showed the best formation and growth of *P. aeruginosa* biofilm with an OD value of 0.5298. This average was then compared with the ODCut value to determine the strength of biofilm formation. The ODcut value obtained was 0.0462. Therefore, the ability of the test bacteria to form biofilms is classified as strong, as it fulfills the criterion of 4×ODcut < OD isolate. This finding is consistent with the study conducted by Azimzadeh et al. (2025). that *P. aeruginosa* is a strong biofilm former with OD values meeting 4×ODcut < OD isolate.

Incubation for 48 hours had the highest OD value compared to 24 and 72 hours. Biofilm formation increased at 48 hours and a decrease on 72 hours. The increase in biofilm formation after 48 hours occurred because the bacteria were in the phase of active growth and biofilm maturation, where the bacteria multiplied, produced extracellular matrix, and formed a mature biofilm structure. After 72 hours, it began to decrease due to the dispersion phase, where some bacteria began to break away from the biofilm to find a new environment, or due to nutrient limitation and accumulation of waste products that inhibited further growth. At the beginning of biofilm formation, nutrients in the growth medium are abundant, supporting bacterial growth and multiplication. However, over time, these nutrients can be depleted, causing bacterial growth to slow or stop, so that the biofilm biomass no longer increases as quickly as before (Azizah et al., 2023). This cycle is a natural part of biofilm dynamics, where, after reaching maximum density, the biofilm will experience a decrease in biomass due to cell release, so that at that stage, the number of colonies attached to the well wall decreases. This is in accordance with the research of Chimi et al. (2024) that the best time for *P. aeruginosa* biofilm formation is 48 hours, where biofilm formation increases with incubation time up to 48 hours and decreases after 72 hours. Thus, it can be concluded that the time required for *P. aeruginosa* to be able to form the best biofilm for testing is 48 hours.

Biofilm formation inhibition activity

The biofilm inhibition assay was carried out to evaluate the ability of the ethanolic extract of *M. kauki* leaves to prevent biofilm formation by *Pseudomonas aeruginosa* during the initial phase of development. An inhibition test was conducted on several concentrations of extracts with a positive control of ciprofloxacin using the microtiter plate biofilm assay method. On the other hand, the negative control used is a suspension with media and solvent without the

addition of extracts. The OD value of the negative control was 0.4390. The OD value of the negative control illustrates the maximum amount of biofilm formed in the absence of extract treatment, so it is used as a reference in calculating the effectiveness of inhibition.



(a) (b)

Figure 3. (a) Percentage (%) inhibition of biofilm formation by (a) the ethanol extract of *M. kauki* leaves and (b) ciprofloxacin

Figure 3 shows the % inhibition of biofilm formation in the ethanol extract of *M. kauki* leaves and the ciprofloxacin control. The %inhibition value of biofilm formation continues to increase from low to high concentrations. This indicates that increasing the concentration of both the extract and the control results in a greater percentage of biofilm formation inhibition. This is because the higher the percentage of extracts and controls, the more antibiofilm substances they contain, so that they can prevent biofilm attachment better.

The highest percentage inhibition of ethanol extract is at a concentration of 1000 ppm, which is higher than the control at a concentration of 0.625 ppm. While the lowest % inhibition was at a concentration of 62.5 ppm. For the ciprofloxacin control, the highest biofilm inhibition was observed at 10 ppm, while the lowest was observed at 0.625 ppm. The biofilm inhibition percentages obtained from each concentration were subsequently used to calculate the IC_{50} value through non-linear dose–response regression curve analysis. The IC_{50} values of the ethanol extract of *M. kauki* leaves and ciprofloxacin are shown in Table 1.

Table 1. IC_{50} value of biofilm formation inhibition of ethanolic extract of *M. kauki* leaves and ciprofloxacin

Sample	IC_{50} (µg/mL)	Category
Ethanol extract of *M. kauki* leaves	134	Moderate
Ciprofloxacin	1.63	Very strong

The ethanol extract of *M. kauki* leaves has an IC_{50} of 134 µg/mL, indicating moderate antibiofilm activity. Ciprofloxacin showed significant antibiofilm activity with an IC_{50} value of 1.63 µg/mL, which is included in the very strong category. According to Souhoka et al. (2019), IC_{50} values <50 µg/mL are classified as very strong, 50–100 µg/mL as strong, 100–150 µg/mL as moderate, and 151–200 µg/mL as weak. The IC_{50} value is often used for biofilm formation inhibition tests; a lower IC_{50} value indicates greater effectiveness of the sample in inhibiting biofilm formation (Besan et al., 2023).

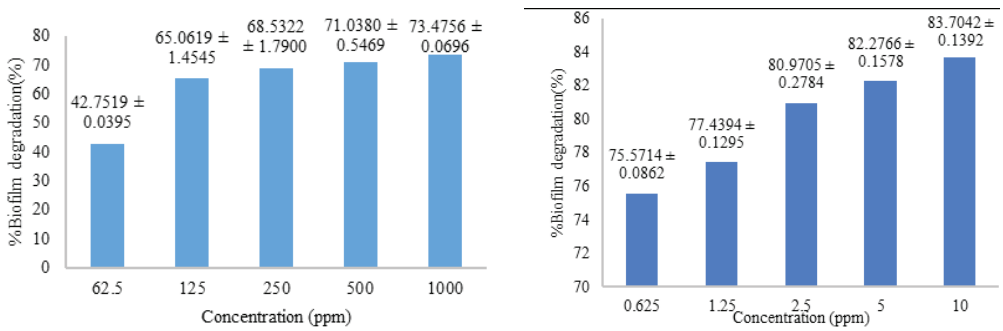
According to the LC-MS results on *M. Kauki* leaves, there is a fairly high concentration of epigallocatechin gallate (EGCG) at 1.549%. Referring to the results of research by Hao et al. (2021), it is

known that epigallocatechin gallate inhibits the formation of *P. aeruginosa* biofilm by more than 70% at a concentration of 256 µg/mL. This inhibitory effect increases with increasing EGCG concentration. EGCG inhibits the formation of *P. aeruginosa* biofilm through a mechanism in the QS system. Epigallocatechin gallate significantly reduces the production of C4-HSL and 3-oxo-C12-HSL, which are two major AHL molecules that activate the las and rhl regulatory systems. This decrease in AHL levels causes suppression of the transcription of important QS genes, including lasI, lasR, rhlI, rhlR, pqsA, and pqsR, which respectively encode QS synthase enzymes or transcription regulators. This directly impacts the reduced expression of other virulence genes, including lasB (encoding elastase), phzA, and phzM (involved in the biosynthesis of the toxic pigment pyocyanin). Additionally, EGCG significantly inhibits swimming and swarming motility, which are important initial stages for bacteria to spread and attach to the substrate surfaces before forming stable three-dimensional biofilms (Hao et al., 2021).

In the inhibition of biofilm formation, the ANOVA results for the extract and control showed p = 0.000, indicating a significant difference. The post hoc test showed that each OD value at the concentration of small *M. kauki* leaf ethanol extract and ciprofloxacin control was <0.05. The Pearson correlation test produced p = 0.000, indicating a significant correlation between the increase in concentration and the level of biofilm inhibition and destruction.

Biofilm degradation activity test

Biofilm degradation test was carried out by putting bacterial suspension and HTR media into a microplate and incubating for 48 hours. Then the solution in the plate was discarded and washed. Next, the extract and positive control were treated with various concentrations.



(a) (b)

Figure 4. Percentage of biofilm degradation (a) ethanol extract of *M. kauki* leaves and (b) ciprofloxacin

Figure 4 shows the % inhibition of biofilm formation in the ethanol extract of *M. kauki* leaves and the ciprofloxacin control. According to Figure 4, it is known that the % of biofilm destruction continues to increase from low to high concentrations. This indicated that increasing the concentration of both the extract and the control leads to a higher percentage of biofilm degradation. The higher the percentage of extracts and controls, the more antibiofilm substance content in it, so that it can destroy biofilm better.

The highest percentage of destruction of ethanol extract is at a concentration of 1000 ppm, which is higher than the control at a concentration of 0.625 ppm. While the lowest % destruction was at a concentration of 62.5 ppm. Meanwhile, for the ciprofloxacin control, the greatest level of biofilm destruction was observed at a concentration of 10 ppm, while the lowest occurred at 0.625 ppm.

In general, eliminating established biofilms using extracts is more challenging. Several studies have also

reported that preventing initial cell attachment is easier than disrupting already formed biofilms. These findings are consistent with the study conducted by Tobi et al. (2022), who conducted antibiofilm testing against *Staphylococcus aureus* bacteria, where the inhibition value was higher than destruction, namely 71.17% and 54%. This supports the notion that pathogens exhibit greater resistance to antimicrobial agents when embedded within biofilms, allowing infections to persist on various biotic and abiotic surfaces (Famuyide et al., 2019).

The biofilm formation inhibition percentage data were subsequently used to determine the IC_{50} value, which was calculated from the inhibition percentages at each concentration using non-linear dose–response regression curve analysis. Table 2 presents the IC_{50} values of the ethanolic extract of *M. kauki* leaves and ciprofloxacin.

Table 2. IC_{50} value of biofilm degradation inhibition of ethanolic extract from the leaves of *M. kauki* leaves and ciprofloxacin

Sample	IC_{50} (µg/mL)	Category
Ethanol extract of *M. kauki* leaves	108.40	Moderate
Ciprofloxacin	2.04	Very strong

According to Table 2, the ethanol extract of *M. kauki* leaves has an IC_{50} value of 108.40 µg/mL, which is included in the category of moderate antibiofilm activity. Meanwhile, ciprofloxacin showed significant antibiofilm activity with an IC_{50} value of 2.04 µg/mL, which is included in the very strong category. The IC_{50} value is often used for biofilm formation inhibition tests; a lower IC_{50} value indicates a higher efficacy of the sample in inhibiting biofilm formation.

Compounds present in the ethanol extract of *M. kauki* are capable of inhibiting and destroying biofilms through mechanisms such as degradation of the biofilm matrix, membrane leakage, and cell death (Besan et al., 2023). LC–MS analysis of *M. kauki* leaves revealed the presence of chlorogenic acid at a relatively high concentration of 1.674%. Chlorogenic acid has been reported by Wang et al. (2024) to exhibit biofilm-disrupting activity against *Pseudomonas putida*, achieving up to 70% biofilm destruction at a concentration of 25.4 mM. This biofilm-disrupting effect increased in a concentration-dependent manner. Chlorogenic acid disrupts biofilms by interfering with the physical structure of the extracellular polymeric substance (EPS) matrix, which consists of eDNA, exopolysaccharides, and proteins (Liu et al., 2025). Chlorogenic acid can bind and form hydrogen bonds with hydroxyl (–OH) and carboxylate ($–COO^-$) groups of polysaccharides or proteins within the EPS (Diniyah & Lee, 2020). This interaction leads to protein denaturation and disintegration of the EPS structure. Damage to the EPS compromises its ability to retain water and nutrients, protect against antibiotics, and maintain biofilm structural stability. The weakening of the biofilm may result in membrane disruption and leakage, as the compound inserts into the lipid layer, increasing membrane permeability. Increased membrane permeability can cause leakage of cytoplasmic contents, leading to the loss of essential components required for protein synthesis, DNA/RNA synthesis, and energy production, thereby disrupting fundamental cellular functions (Campos et al., 2025).

In the inhibition of biofilm destruction, the ANOVA results for the extract and control showed $p = 0.000$, indicating a significant difference. The post hoc test showed that each OD value at the concentration of small *M. kauki* leaf ethanol extract and ciprofloxacin control was <0.05. The Pearson correlation test produced $p = 0.000$, indicating a significant correlation between the increase in concentration and the level of biofilm inhibition and destruction.

CONCLUSION

This study concludes that the total phenolic and flavonoid contents in the ethanol extract of *M. kauki* leaves were 48.9830 mg GAE/g and 21.327 mg QE/g, respectively. *Pseudomonas aeruginosa* was identified as a strong biofilm-forming bacterium, with an

optimum formation time of 48 hours and an OD value of 0.5298. The ethanol extract of *M. kauki* leaves demonstrated inhibitory and disruptive activities against *P. aeruginosa* biofilms, with the highest inhibition and destruction percentages observed at a concentration of 1000 ppm, reaching 78.9733% and 73.4756%, respectively, and IC_{50} values of 134 µg/mL and 108.4 µg/mL.

ACKNOWLEDGEMENTS

No funding or other financial support was received for the study.

AUTHOR CONTRIBUTION STATEMENT

Writing original draft, experiment of TPC and TFC contents, antibiofilm experiment, analysis of data (LF). Writing review & Editing, Resources, Data curation, Supervision (TT).

CONFLICT OF INTEREST

The authors declare that there is no conflict of interest.

REFERENCES

Agustin, A., Widayanti, E., Ikayanti, R., & Kesuma, S. (2022). Penetapan kadar fenol total ekstrak etanol berbagai biji buah salak bali (*Salacca zalanca* var. Ambonensis) menggunakan metode Folin Ciocalteu. *Journal of Nutrition*, *1*(3), 19–25. https://doi.org/10.31290/nj.v1i3.3705

Azimzadeh, M., Greco, G., Farmani, A., Nourian, A., Pourhajibagher, M., Taherkhani, A.,…Bahador, A. (2025). Biofilm inhibition of multidrug-resistant *Pseudomonas aeruginosa* using green-synthesized silver nanoparticles and colistin. *Scientific Reports*, *15*(1), 1–15. https://doi.org/10.1038/s41598-025-00005-6

Azizah, M., Madona, A. A., Munarsih, E., Tinggi, S., Farmasi, I., & Palembang, B. P. (2023). Uji aktivitas antibakteri ekstrak etanol pelepah pisang ambon (*Musa paradisiaca* L.) terhadap tiga bakteri penyebab diare. *Jurnal 'Aisyiyah Medika*, *8*(2), 187-193. https://doi.org/10.36729/jam.v8i2.1100

Baky, M. H., Elgindi, M. R., Haggag, E. G., Baky, M. H., Kamal, A. M., & Mohamed Elgindi, C. R. (2016). A review of phenolic compounds from the family Sapotaceae. *Journal of Pharmacognosy and Phytochemistry*, *5*(2), 280–287. https://www.researchgate.net/publication/331249920

Besan, E. J., Rahmawati, I., & Saptarini, O. (2023). Aktivitas antibiofilm ekstrak dan fraksi-fraksi bunga telang (*Clitoria ternatea* L.) terhadap *Staphylococcus aureus*. *PHARMACY: Jurnal Farmasi Indonesia (Pharmaceutical Journal of Indonesia)*, *20*(1), 1–11. https://doi.org/10.30595/pharmacy.v0i0.14437

Bonnet, M., Lagier, J. C., Raoult, D., & Khelaifia, S. (2020). Bacterial culture through selective and non-selective conditions: the evolution of culture media in clinical microbiology. *New Microbes and New Infections*, *34*(C), 1-11. https://doi.org/10.1016/j.nmni.2019.100622

Campos, J. V., de Pontes, J. T. C., Canales, C. S. C., Roque-Borda, C. A., & Pavan, F. R. (2025). Advancing nanotechnology: targeting biofilm-forming bacteria with antimicrobial peptides. *BME Frontiers*, *6*, 1–22. https://doi.org/10.34133/bmef.0104

Chen, J., Huang, H., Liu, C., & Fu, Y. (2024). Risk factors for mortality in *Pseudomonas aeruginosa* bacteremia in children. *Pediatrics and Neonatology*, *65*(1), 31–37. https://doi.org/10.1016/j.pedneo.2023.03.012

Chimi, L. Y., Noubom, M., Bisso, B. N., Singor Njateng, G. S., & Dzoyem, J. P. (2024). Biofilm formation, pyocyanin production, and antibiotic resistance profile of *Pseudomonas aeruginosa* isolates from Wounds. *International Journal of Microbiology*, *2024*, 1-10. https://doi.org/10.1155/2024/1207536

Diniyah, N., & Lee, S.-H. (2020). Komposisi senyawa fenol dan potensi antioksidan dari kacang-kacangan: review. *Jurnal Agroteknologi, 14*(01), 91. https://doi.org/10.19184/j-agt.v14i01.17965

Famuyide, I. M., Aro, A. O., Fasina, F. O., Eloff, J. N., & McGaw, L. J. (2019). Antibacterial and antibiofilm activity of acetone leaf extracts of nine under-investigated South African *Eugenia* and *Syzygium* (Myrtaceae) species and their selectivity indices. *BMC Complementary and Alternative Medicine*, *19*(1), 1–13. https://doi.org/10.1186/s12906-019-2547-z

Goel, N., Fatima, S. W., Kumar, S., Sinha, R., & Khare, S. K. (2021). Antimicrobial resistance in biofilms: exploring marine actinobacteria as a potential source of antibiotics and biofilm inhibitors. *Biotechnology Reports*, *30*(2021), 1-10. https://doi.org/10.1016/j.btre.2021.e00613

Hao, S., Yang, D., Zhao, L., Shi, F., Ye, G., Fu, H.,… Tang, H. (2021). EGCG-mediated potential inhibition of biofilm development and quorum sensing in *Pseudomonas aeruginosa*. *International Journal of Molecular Sciences*, *22*(9), 11–19. https://doi.org/10.3390/ijms22094946

Hegde, M. M., Lakshman, K., & Handral, M. (2025). Integrative investigation of *Manilkara kaukiphyto* extract: elucidating multifaceted antineoplastic mechanisms from cellular viability modulation to in vivo tumor regression. *Journal of Microbiology, Biotechnology and Food Science, 14*(4), 1–7. https://doi.org/10.55251/jmbfs.11663

Hirsch, E. B., & Tam, V. H. (2010). Impact of multidrug-resistant *Pseudomonas aeruginosa* infection on patient outcomes. *Expert Review of Pharmacoeconomics and Outcomes Research*, *10*(4), 441–451. https://doi.org/10.1586/erp.10.49

Jayadi, N. E. A., Huda, C., & Fatimah, F. (2023). Aktivitas antibakteri fraksinasi daun sirih merah (*Pipper crocatum*) terhadap bakteri *Staphylococus aureus* secara *in vitro*. *Pharmasipha : Pharmaceutical Journal of Islamic Pharmacy*, *7*(1), 34–43. https://doi.org/10.21111/pharmasipha.v7i1.8960

Kaneria, M., Baravalia, Y., Vaghasiya, Y., & Chanda, S. (2009). Determination of antibacterial and antioxidant potential of some medicinal plants from Saurashtra Region, India. *Indian Journal of Pharmaceutical Sciences, 71*(4), 406-412. https://doi.org/10.4103/0250-474X.57289

Kaneria, M., & Chanda, S. (2012). Evaluation of antioxidant and antimicrobial properties of *Manilkara zapota* leaves by the sequential soxhlet extraction method. *Asian Pacific Journal of Tropical Biomedicine, 2*(3), 1526–1533. https://doi.org/10.1016/S2221-1691(12)60448-1

Kining, E., Falah, S., & Nurhidayat, N. (2017). The in vitro antibiofilm activity of water leaf extract of papaya (*Carica papaya* L.) against *Pseudomonas aeruginosa*. *Current Biochemistry, 2*(3), 150–163. https://doi.org/10.29244/cb.2.3.150-163

Konoralma, K. (2019). Identifikasi bakteri penyebab infeksi nosokomial di Rumah Sakit Umum Gmim Pancaran Kasih Manado. *Jurnal KESMAS*, *8*(1), 23–35.https://ejournal.unsrat.ac.id/index.php/kesmas/article/view/23949

Liu, Q., Wu, Q., Liu, J., Xu, T., Liu, J., Wu, Q.,… Zhang, Z. (2025). New insights into the mediation of biofilm formation by three core extracellular polysaccharide biosynthesis pathways in *Pseudomonas aeruginosa*. *International Journal of Molecular Sciences*, *26*(8), 1–20. https://doi.org/10.3390/ijms26083780

Maghfirah, F., Saputri, D., & Basri. (2017). Aktivitas pembentukan biofilm *Streptococcus mutans* dan *Candida albicans* setelah dipapar dengan cigarette smoke condensate dan minuman probiotik. *Journal Caninus Denstistry*, *2*(1), 12-19.

Martha, R. D., Fatimah, Danar, & Parbuntari, H. (2023). Identification of flavonoid compounds in ethanol extract of majapahit plant (*Crescentia cujete)* leaves and their potential as anticancer. *CHEESA: Chemical Engineering Research Articles*, *8757*(1), 34–48. https://doi.org/ 10.25273/cheesa.v6i1.14056.34-48.

Muteeb, G., Rehman, M. T., Shahwan, M., & Aatif, M. (2023). Origin of antibiotics and antibiotic resistance, and their impacts on drug development: a narrative review. *Pharmaceuticals*, *16*(11), 1–54. https://doi.org/10.3390/ph16111615

Pamudi, B. F., Munira, M., & Nasir, M. (2024). Uji aktivitas anti biofilm ekstrak daun kirinyuh (*Chromolaena odorata* I.) dari kawasan Geotermal le Seum terhadap *Staphylococcus aureus*. *SAGO : Gizi Dan Kesehatan*, *5*(3), 788–794. https://doi.org/10.30867/gikes.v5i3A.1844

Pang, Z., Raudonis, R., Glick, B. R., Lin, T. J., & Cheng, Z. (2019). Antibiotic resistance in *Pseudomonas aeruginosa*: mechanisms and alternative therapeutic strategies. *Biotechnology Advances*, *37*(1), 177–192. https://doi.org/10.1016/j.biotechadv.2018.11.013

Parikh, B., & Patel, V. H. (2017). Quantification of phenolic compounds and antioxidant capacity of an underutilized Indian fruit: Rayan [*Manilkara hexandra* (Roxb.) Dubard]. *Food Science and Human Wellness*, *6*(1), 10–19. https://doi.org/10.1016/j.fshw.2016.11.002

Pérez, M., Domínguez-López, I., & Lamuela-Raventós, R. M. (2023). The chemistry behind the Folin-Ciocalteu method for the estimation of (poly)phenol content in food: total phenolic intake in a Mediterranean dietary pattern. *Journal of Agricultural and Food Chemistry*, *71*(46), 17543–17553. https://doi.org/10.1021/acs.jafc.3c04022

Pratiwi, N., Retnosari, R., & Prabaningtyas, S. (2021). Preliminary study on antibacterial activity of sawo kecik (*Manilkara kauki* (L.) dubard) roots extract. *Jurnal Biodjati, 6*(1), 146–152. https://doi.org/10.15575/biodjati.v6i1.7708

Prayudhani, M. F., Hastuti, U. S., & Suarsini, E. (2013). Daya antibakteri ekstrak etanol daun dan kulit batang sawo kecik (*Manilkara kauki* (L) Dubard) terhadap bakteri *Escherichia coli*. *Seminar Nasional X Pendidikan Biologi FKIP UNS*, *10*(2), 1–7. https://jurnal.uns.ac.id/prosbi/article/view/6598.

Prianggawe, & Hajrin, W. (2024). Literature review: aktivitas antioksidan sediaan gel di berbagai tanaman menggunakan metode DPPH. *Jurnal Kesehatan Tambusai*, *5*(3), 7573–7582. https://doi.org/10.31004/jkt.v5i3.33161

Purba, N., Harahap, U., & Hasibuan, P. A. Z. (2023). Phytochemical screening and antidiabetic test of ethanol extract of sapodilla kecik leaves (*Manilkara kauki* (L.) dubard) on decreasing blood glucose of diabetic rats. *International Journal of Science, Technology & Management, 4*(4), 902–908. https://doi.org/10.46729/ijstm.v4i4.869

Purnama, F. M., Afifah, R., Hestiyani, N., & Karunia, A. P. (2024). Aktivitas antibiofilm propolis lebah madu terhadap bakteri *Pseudomonas aeruginosa*. *Mandala of Health*, *17*(2), 308–317. https://doi.org/10.20884/1.mandala.2024.17.2.9585

Qin, S., Xiao, W., Zhou, C., Pu, Q., Deng, X., Lan, L.,…Wu, M. (2022). *Pseudomonas aeruginosa*: pathogenesis, virulence factors, antibiotic resistance, interaction with host, technology advances, and emerging therapeutics. *Signal Transduction and Targeted Therapy*, *7*(1), 1–27. https://doi.org/10.1038/s41392-022-01056-1

Riasari, H., Fitriansyah, S. N., & Hoeriah, I. S. (2022). Perbandingan metode fermentasi, ekstraksi, dan kepolaran pelarut terhadap kadar total flavonoid dan steroid pada daun sukun (*Artocarpus altilis* (Parkinson) Fosberg). *Jurnal Sains dan Teknologi Farmasi Indonesia*, *11*(1), 1. https://doi.org/10.58327/jstfi.v11i1.165

Rosyada, A. G., Prihastuti, C. C., Sari, D. N. I., Setiawati, S., Ichsyani, M., Laksitasari, A.,… Kurniawan, A. A. (2023). Aktivitas antibiofilm ekstrak etanol kulit bawang merah (*Allium cepa* L.) dalam menghambat pembentukan biofilm *Staphylococcus aureus* ATCC 25923. *Jurnal Kedokteran Gigi Universitas Padjadjaran*, *35*(1), 34-40. https://doi.org/10.24198/jkg.v35i1.42451

Santoso, U., Utari, M., & Marpaung, M. P. (2020). Aktivitas antibakteri dan antijamur ekstrak batang akar kuning (*Fibraurea chloroleuca* Miers) terhadap *Escherichia coli*, *Staphylococcus aureus* dan *Candida albicans*. *Jurnal Kesehatan Bakti Tunas Husada: Jurnal Ilmu-Ilmu Keperawatan, Analis Kesehatan dan Farmasi*, *20*(2), 194-208. https://doi.org/10.36465/jkbth.v20i2.611

Saputri, N. E., Dhayan, R., Harsanti, B. R., Putri, D. M., & Fadly, D. (2021). Total fenol dan aktivitas anti-inflamasi jamur sawit (*Volvariella* sp). *Poltekita : Jurnal Ilmu Kesehatan*, *15*(3), 295–300. https://doi.org/10.33860/jik.v15i3.637

Singh, B., Mehta, S., Asare-Amoah, J., Appiah, P. O., Chauhan, S., & Amponash, R. D. (2024). Biofilm-associated multidrug-resistant bacteria among burn wound infections: a cross-sectional study. *Mediterranean Journal of Infection Microbes and Antimicrobials*. *13*, 24179.15. https://doi.org/10.4274/mjima.galenos.2024.24179.15

Souhoka, F. A., Hattu, N., & Huliselan, M. (2019). Uji aktivitas antioksidan ekstrak metanol biji kesumba keling (*Bixa orellana* (L)). *Indonesian Journal of Chemistry Research*, *7*(1), 25–31. https://doi.org/10.30598//ijcr.2019.7-fas

Srisupap, S., & Chaicharoenpong, C. (2021). In vitro antioxidant and antityrosinase activities of *Manilkara kauki*. *Acta Pharmaceutica*, *71*(1), 153–162. https://doi.org/10.2478/acph-2021-0009

Susilawati, L., Sari, P. A., Maulana, S., & Purnomo, E. (2023). Kajian anatomi, histokimia, dan karakteristik epidermal daun sawo kecik (*Manilkara kauki* (L.) Dubard - Sapotaceae). *Jurnal Biologi Udayana, 27*(1), 14. https://doi.org/10.24843/JBIOUNUD.2023.v27.i01.p02

Turhan, E. U., & Koca, E. E. (2024). Predictive modeling for inactivation of *Escherichia coli* biofilm with combined treatment of thermosonication and organic acid on polystyrene surface. *Foods*, 13, 1-16. https://doi.org/10.3390/foods13244002

Tobi, C. H. B., Saptarini, O., & Rahmawati, I. (2022). Aktivitas antibiofilm ekstrak dan fraksi-fraksi biji pinang (*Areca catechu* L.) terhadap *Staphylococcus aureus* ATCC 25923. *JPSCR: Journal of Pharmaceutical Science and Clinical Research*, *7*(1), 56. https://doi.org/10.20961/jpscr.v7i1.43698

Uckele, K. A., Jahner, J. P., Tepe, E. J., Richards, L. A., Dyer, L. A., Ochsenrider, K. M.,…Parchman, T. L. (2021). Phytochemistry reflects different evolutionary histories in traditional classes versus specialized structural motifs. *Scientific Reports*, *11*(1), 1–14. https://doi.org/10.1038/s41598-021-96431-3

Wang, H., Gu, C. M., Xu, S., Wang, H., Zhao, X., & Gu, L. (2024). Measurement of optical density of microbes by the multi-light path transmission method. *MLife*, *3*(4), 565–572. https://doi.org/10.1002/mlf2.12147

Widyasari, R., & Sari, D. Y. (2021). Penetapan kadar flavonoid total ekstrak etanol kulit batang sawo (*Manilkara zapota* (L.)) secara spektrofotometri UV-Visibel. *Jurnal Insan Farmasi Indonesia*, *4*(2), 237–244. https://doi.org/10.36387/jifi.v4i2.828

Zakri, D. F., Putri, D. H., Handayani, D., & Angelina, M. (2025). Activity of ethanol extract and fraction products leaves *Manilkara kauki* as inhibitors tyrosinase enzyme. *Jurnal Biologi Tropis*, *25*(1), 960–966. https://doi.org/10.29303/jbt.v25i1.8295

FABAD J. Pharm. Sci., 51, 1, 291-304, 2026
Doi: 10.55262/fabadeczacilik.1800540
REVIEW ARTCILE

Cimicifuga racemosa (L.) Nutt.: Pharmacological Effects, Using Areas and Current Clinical Data

Ecenur BAYIR[*°], Gözde ELGİN CEBE[**]

***Cimicifuga racemosa* (L.) Nutt.: Pharmacological Effects, Using Areas and Current Clinical Data**

SUMMARY

Cimicifuga racemosa (L.) Nutt., also known as "black cohosh", is a perennial herbaceous plant that has been widely used, particularly for its effects on physiological and neuroendocrine processes. This review aims to present a comprehensive evaluation of the pharmacological properties, active constituents, and current clinical data related to C. racemosa extracts. Bioactive components such as triterpene glycosides, phenolic acids, and flavonoids found in the plant contribute to its anti-inflammatory, antioxidant, and neuroregulatory effects. Studies have reported its potential to alleviate symptoms such as vasomotor disturbances, mood alterations, and sleep disorders. Although promising, the exact mechanisms of action remain under investigation, and further well-designed randomized clinical studies are needed to clarify its therapeutic role and ensure long-term safety.

Keywords: *Cimicifuga racemosa, medicinal plants, pharmacological profile, clinical efficacy.*

***Cimicifuga racemosa* (L.) Nutt.: Farmakolojik Etkileri, Kullanım Alanları ve Güncel Klinik Veriler**

ÖZ

"Kara kohoş" olarak da bilinen Cimicifuga racemosa (L.) Nutt., özellikle fizyolojik ve nöroendokrin süreçler üzerindeki etkileri nedeniyle yaygın olarak kullanılan çok yıllık otsu bir bitkidir. Bu derleme, C. racemosa'nın farmakolojik özellikleri, aktif bileşenleri ve mevcut klinik verileri hakkında kapsamlı bir değerlendirme sunmayı amaçlamaktadır. Bitkide bulunan triterpen glikozitler, fenolik asitler ve flavonoitler gibi biyoaktif bileşenler, bitkinin antienflamatuar, antioksidan ve nöroregülatör etkilerine katkıda bulunur. Çalışmalar, bitkinin vazomotor bozukluklar, ruh hali değişiklikleri ve uyku bozuklukları gibi semptomları hafifletme potansiyelini ortaya koymuştur. Bu sonuçlar umut verici olmasına rağmen, bitkinin kesin etki mekanizmaları halen araştırılmaktadır. Ayrıca bitkinin terapötik rolünü açıklığa kavuşturmak ve uzun vadeli güvenliğini sağlamak için iyi tasarlanmış randomize klinik çalışmaların yapılması gerekmektedir.

Anahtar Kelimeler: *Cimicifuga racemosa, tıbbi bitkiler, farmakolojik profil, klinik etkinlik.*

Recieved: 10.10.2025
Revised: 7.12.2025
Accepted: 18.12.2025

[*] ORCID: 0000-0003-4480-4417, Department of Pharmaceutical Botany, Faculty of Pharmacy, Ege University İzmir, Türkiye
[**] ORCID: 0000-0002-7253-3864, Department of Pharmaceutical Botany Faculty of Pharmacy, Ege University İzmir, Türkiye

° Corresponding Author; Ecenur BAYIR
E-mail: bayirecenur@gmail.com

INTRODUCTION

Black cohosh, also known as *Cimicifuga racemosa* (L.) Nutt. (syn. *Actaea racemosa* L.), has traditionally been used in North American ethnomedicine for gynaecological disorders, musculoskeletal pain, and inflammatory conditions. Phytochemical analyses demonstrate a complex profile of metabolites, including triterpene glycosides (e.g., actein, 27-deoxyactein), phenolic derivatives, flavonoids, tannins, and minor volatile constituents (Burdette et al., 2002), suggesting multiple pharmacodynamic targets. Preclinical findings indicate anti-inflammatory, antioxidant, and neuromodulatory activities, alongside possible oestrogen-modulating effects (Liske et al., 2002). Clinical studies suggest benefits for vasomotor symptoms, mood, anxiety, and sleep, but methodological heterogeneity limits interpretation of results (Mahady et al., 2005). Extracted materials differ significantly, leading to inconsistent pharmacological profiles. This hinders comparative effectiveness and the establishment of dose–response relationships. Safety concerns necessitate a critical appraisal of existing data. Although not definitively causal, conflicting findings highlight the need for more integrated evaluation (Naser et al., 2011a). A comprehensive review is required on black cohosh in complementary medicine due to its growing global use, since existing reviews focus on menopausal symptoms, and mechanistic aspects are often overlooked. The present review integrates preclinical and clinical evidence to clarify knowledge gaps and identify priority areas for future research for a robust *C. racemosa* evidence-based framework.

Botanical features

C. racemosa is a perennial, herbaceous, and rhizome plant belonging to the Ranunculaceae family (Flora of North America Editorial Committee, 2009). Although the height of the plant varies between 1.5 and 2.5 meters on average, it can grow taller under suitable ecological conditions (Foster & Duke, 2000). Underground organs, especially thick, irregularly branched, and fibrous rhizomes, constitute the most valuable parts of this plant from a medical point of view. Its rhizomes contain high levels of triterpene glycosides and some other phytochemical compounds (Jiang et al., 2008). The stem of the plant is erect, hollow, and often fragile, which is interpreted as part of the plant's adaptation to humid and shady forest environments (Moerman, 1998).

The leaves are arranged in a spiral shape on the upper parts of the plant, compound in structure, and usually divided into palmate or pinnate. The leaf margins are distinctly dentate, and the leaf surface is often hairy (Flora of North America Editorial Committee, 2009). In summer, the plant forms flowers of the frequent racemose type, white in color, with a characteristic appearance (Foster & Duke, 2000). As an important morphological feature, petals are absent in flowers; instead, the bright white color and transparent staminodes give the flower a distinctive appearance.

C. racemosa reproduces vegetatively, mostly through rhizomes, and rarely reproduces by seed. It usually takes several years for its seeds to germinate and for the plant to reach full maturity, revealing that the species has a slow-growing biological profile (Moerman, 1998). For this reason, rhizomes form a rich nutrient store for the survival of the plant, especially in competitive habitat conditions in the natural environment (Flora of North America Editorial Committee, 2009).



Figure 1. General appearance of *C. racemosa* (U.S. Forest Service, 2019)



Figure 2. Appearance of *C. racemosa* flowers (Wagner & Kessler, 2010)

National Center for Complementary and Integrative Health. (2024, January 5). Black cohosh. U.S. Department of Health and Human Services. https://www.nccih.nih.gov/health/black-cohosh



Figure 3. Appearance of *C. racemosa* fruits (Kaiser, 1997)

Board of Trustees of the Royal Botanic Gardens, Kew. (n.d.). Actaea racemosa: Images & distribution. Plants of the World Online. Retrieved February 18, 2026, from https://powo.science.kew.org/taxon/urn:lsid:ipni.org:names:316204-2/images

Distribution area and ecological characteristics

C. racemosa is a plant that is widely distributed in North America and especially in the eastern and southeastern regions of the United States (Foster et al., 2000). It is also distributed in moist, shady, and densely forested ecosystems along the Appalachian Mountain range (U.S. Forest Service, 2019). The plant prefers humus-rich, well-drained soils with high organic matter, often thrives in underforest vegetation, in the shade of trees, and grows more efficiently in cool, humid microclimates (Moerman, 1998). However, due to increased medical and commercial demand, regressions due to overgathering have been observed in some local populations, which have negatively affected the conservation status of the species (Wagner et al., 2010). In this regard, *C. racemosa* is among the "species at risk" in some regional nature conservation programs, with emphasis on sustainable harvesting practices (Kaiser, 1997). In recent years, controlled cultivation practices have increasingly been adopted to reduce pressure on natural populations of *C.*

racemosa, alongside growing efforts to preserve ecological balance. (Zhang et al., 2024; Upton, 2011). These practices both ensure the continuity of the plant in terms of biodiversity and reduce the environmental impact of commercial demand.

Phytochemical components and effects

The therapeutic efficacy of *C. racemosa* is based specifically on the components present in the rhizome and roots of the plant. The most notable of these components is the high content of triterpene glycosides. The main ones are structures such as actein, 27-deoxyactein, cimigenol, cimiracemosides A and B (Zhang et al., 2024). Triterpene glycosides have been implicated in alleviating menopausal symptoms by exhibiting anti-inflammatory, analgesic, and neuroregulatory effects. In addition, phenolic compounds also have an important place in the plant, and hydroxybenzoic acid derivatives such as ferulic acid and isoferulic acid attract attention with their antioxidant properties (Wagner et al., 2011). Isoflavones from the flavonoid class, particularly formononetin, have also been identified, contributing to the herb's hormonal balance-promoting properties with mild estrogen-like effects (Bolzan et al., 2014). In addition, tannins and caffeic acid derivatives are also present in the rhizomes of *C. racemosa*. These compounds are known for their anti-inflammatory and antimicrobial effects (Wilson et al., 2014). The essential oil content of the plant is relatively low and is not considered a major contributor to its pharmacological activity (European Medicines Agency, 2010). Although its alkaloid content is low, these compounds are thought to contribute to the complex pharmacodynamic profile of the plant (Wagner et al., 2011).

Indications and clinical uses

It is known that it has been used for various medicinal purposes for centuries by the indigenous peoples of North America. Its traditional uses include relieving headaches, rheumatism, postpartum uterine contractions, first aid against snakebites, and treating disorders related to the reproductive system in women (Beer et al., 2013; Burdette et al., 2002; Chen et al., 2017). The plant, which has an important place especially in the field of women's health, has also been evaluated as a regulator of uterine tone in the postpartum period (Burdette et al., 2002; Chen et al., 2017).

In modern applications, C. *racemosa* is most commonly used in the management of menopausal symptoms. Its efficacy has been investigated in relation to vasomotor symptoms (hot flashes, night sweats, and sudden bouts of sweating), menopause-related insomnia, anxiety, dysmenorrhea, and premenstrual syndrome (PMS) (Moerman, 1998). In addition, some clinical studies suggest that the plant has positive effects on mood disorders and symptoms of mild depression (Wuttke et al., 2003b). Since the phytoestrogenic effects of *C. racemosa*, which is considered an alternative to hormonal therapies (especially hormone replacement therapy), are based on selective estrogen receptor modulator (SERM)-like mechanisms, it is accepted to offer a safer profile compared to classical estrogen treatments (Wagner et al., 2011). This feature makes its use particularly important in women at risk of breast and endometrial cancer (Burdette et al., 2002; Chen et al., 2017). In evaluations by the European Medicines Agency (EMA) and the World Health Organization (WHO), it has been stated that short-term (usually 3-6 months) use of *C. racemosa* is safe, but it has been emphasized that the current scientific evidence for long-term use is insufficient and more extensive clinical studies are needed (Zhang et al., 2024). Therefore, careful consideration before use is recommended, especially in patients with chronic diseases or a history of hormonal cancers (European Medicines Agency, 2010).

Contraindications and warnings

The use of *C. racemosa* in specific patient groups needs to be carefully evaluated. It is emphasized that the use of this herb is contraindicated due to its

phytoestrogenic potential, especially in individuals with a history of estrogen-sensitive malignancies (e.g., breast cancer, endometrial cancer, or ovarian cancer) (National Center for Complementary and Integrative Health, 2024). Although the herb has a SERM-like effect, there is insufficient clinical data to completely rule out possible risks in these patients (Chen et al., 2017). Regarding pregnancy and lactation periods, clinical studies on the safety of *C. racemosa* are very limited. Therefore, its use is not recommended in women during pregnancy and lactation (Huntley & Ernst, 2003). Since the hormonal activity of the plant may have possible adverse effects on the fetus or infant, it should be used with caution (European Medicines Agency, 2010).

While potential hepatotoxic effects on liver function have been reported, this association has not been conclusively proven. Patients with a history of liver disease should consult a healthcare professional before using this herb (Wagner et al., 2011). Case reports and some clinical investigations have reported idiopathic hepatitis and elevation of liver enzymes after the use of *C. racemosa*; however, in most reports, it has been observed that other hepatotoxic agents are used simultaneously (Coon & Ernst, 2004). Still, regular monitoring of liver function tests is recommended during the use of this herb in individuals with liver disease (European Medicines Agency, 2010). In addition, attention should be paid to the interaction potential of *C. racemosa;* especially when used in combination with hormonal therapies, hepatotoxic drugs, or anticoagulants, side effects or changes in drug efficacy may occur (Wagner et al., 2011).

Side effects and safety profile

In general, *C. racemosa* is considered safe for short-term use (between 3-6 months), and there are mild, temporary side effects (Naser et al., 2011a). The most common adverse effects reported in clinical trials included headache, nausea, dizziness, breast tenderness, mild hypotension, and myalgia (Chen et al., 2017). These side effects have generally been observed to regress with dose adjustment or discontinuation of use (Ulrich et al., 2020). However, although rare, idiopathic hepatitis, elevated liver enzymes, and even liver failure associated with the use of *C. racemosa* have been reported in some case reports (Wuttke et al., 2003a, 2003b). The risk of hepatotoxicity is still controversial due to the simultaneous use of other hepatotoxic drugs in most of these cases (Naser et al. 2011a; Teschke et al., 2011). Regular monitoring of liver function tests is recommended, especially in patients with a history of liver disease and in cases of long-term use (European Medicines Agency, 2010). However, it is considered that the toxic dose of *C. racemosa* is quite high, and the risk of serious side effects is low in the general population. Further randomised controlled trials are needed to clarify safety and long-term use (Naser et al., 2011a).

Herb-drug interactions

C. racemosa has the potential to act on hormonal balance due to its phytoestrogenic and other bioactive compounds. This increases the risk of interactions, especially when used together with estrogen-containing drugs (oral contraceptives, hormone replacement therapies) (Wagner et al., 2011). In addition, pharmacodynamic and pharmacokinetic interactions may occur when used together with drugs such as tamoxifen in the SERM group. Therefore, caution should be exercised in combined therapies (Chen et al., 2017). In addition, due to the hepatotoxicity potential of *C. racemosa* and its effects on the liver, adverse effects on liver function can be seen when used together with hepatotoxic drugs. In simultaneous use with antihypertensive drugs, it is recommended that patients with high blood be careful in these combinations, as there may be a risk of excessive decrease in blood pressure due to the hypotensive effect of the plant (European Medicines Agency, 2010).

From a pharmacokinetic point of view, although

some of the components contained in *C. racemosa* are thought to have effects on the cytochrome P450 (CYP450) enzyme system, these effects, and in particular the potential mechanisms of interaction on the CYP3A4 isoenzyme, have not yet been fully clarified (Gonzalez et al., 2018). Therefore, there is a potential for a theoretical interaction with drugs metabolized via CYP3A4, and caution is advised in clinical use. In summary, close follow-up and dose adjustments are recommended in terms of drug-food interactions in patients using *C. racemosa,* especially when used in combination with hormonal therapies, hepatotoxic agents, and antihypertensive drugs (Fritz et al., 2014; Gurley et al., 2005).

MATERIALS AND METHODS

This review was developed through a literature search. It captures the full breadth of scientific evidence on the phytochemistry, pharmacological activities, clinical efficacy, and safety considerations of *C. racemosa*. A multi-stage search procedure was applied to major scientific databases (PubMed, Scopus, Web of Science, ScienceDirect, and Google Scholar) to identify peer-reviewed publications released between 2000 and 2024. To minimise publication bias and ensure comprehensive coverage, reference lists of key review papers, authoritative monographs, and regulatory assessments (EMA, WHO, NCCIH) were also examined manually.

The search strategy used a combination of controlled vocabulary and free-text terms, including: "*Cimicifuga racemosa* L.", "*Actaea racemosa* L.", "black cohosh", "triterpene glycosides", "phytochemical profile", "SERM-like activity", "clinical trial", "menopausal symptoms", "premenstrual syndrome", "safety" and "hepatotoxicity".

Studies on *C. racemosa* had to be of a certain quality and scope. They had to focus on the herb itself, either as a whole extract or as specific compounds from its rhizome. Included were studies on how it works, tested in models of cells or whole organisms, as well as clinical trials and observational studies reporting treatment outcomes. Also included were review articles and analytical papers on how to prepare extracts, their safety, and pharmacological characteristics. Excluded were publications assessing multi-herbal formulations, which lacked the detail and scientific quality needed, or were not available in English or Turkish.

For each study, data were collected on population, preparation, dosage, duration, outcomes, and any adverse effects. This was to identify inconsistencies in the extraction and solvent, and their influence on bioactive compounds and pharmacological interpretation. This approach allowed current evidence to be synthesised, as well as the existing literature's methodological heterogeneity to be critically evaluated.

Table 1. Studies on *Cimicifuga racemosa* (L.) Nutt.

Year	Authors	Study Type	Sample/Model	Extract/Component Used	Dose and Duration	Parameters Examined	Conclusions / Findings	Notes / Suggestions
2002	Liske et al.	*In vitro*	Cell culture	Triterpene glycosides	Not reported	Estrogen receptor binding	No direct estrogen receptor binding observed; neuroregulatory effects suggested *in vitro*	SERM-like mechanism
2003a	Wuttke et al.	Clinical study	Patients with premenstrual syndrome (n=90)	Standardized *C. racemosa* root extract	40 mg/day (standardized BNO 1055 extract)	PMS symptoms	Significant improvement in PMS symptom scores compared to baseline; well-tolerated	Clinically supported
2003b	Wuttke et al.	Clinical study	Menopausal women (n=100)	Standardized *C. racemosa* root extract (40% isopropanol)	40 mg/day, 12 weeks	Vasomotor symptoms	Significant reduction in frequency and severity of hot flashes and night sweats over 12 weeks; well-tolerated	Safe and effective
2003	Huntley & Ernst	Systematic review	Randomized controlled clinical trial	Standardized *C. racemosa* root extract	Not reported	Menopausal symptoms	Evidence suggests superior improvement in menopausal symptoms compared to placebo; long-term efficacy data are insufficient	Long-term data inadequacy
2004	Coon & Ernst	Review	Clinical studies	Standardize *C. racemosa* root extract	Not reported	Psychological symptoms	Positive effects observed on anxiety and depressive symptoms in women; evidence from multiple small studies	Supporting data
2006	Mahady	Review	Not reported	Phytochemical analyses	Not reported	Pharmacology, safety	Triterpene glycosides and other compounds exhibit anti-inflammatory and SERM-like effects; clinical safety is generally acceptable	More clinical trials are needed
2007	Green et al.	*In vivo*	Rat models	Standardized *C. racemosa* root extract (58–60% ethanol)	30 mg/kg, 3 weeks	Antioxidative gene expression changes capacity	Significant reduction of free radicals in treated mice; improved antioxidant status	Preclinical support

Year	Authors	Study Type	Sample/Model	Extract/Component Used	Dose and Duration	Parameters Examined	Conclusions / Findings	Notes / Suggestions
2007	Henz et al.	Clinical study	Menopausal women (n=120)	Standardized *C. racemosa* root extract	40 mg/day, 16 weeks	Psychological symptoms	Significant reduction in anxiety and depressive symptoms; treatment was well-tolerated	More clinical trials are needed
2008	Borrelli et al.	Meta-analysis	Menopausal women	Various *C. racemosa* preparations	Not reported	Phytoestrogenic effect, safety	Improvement in menopausal symptoms observed across studies; positive safety profile; long-term data limited	More long-term work is needed
2009	Schmid et al.	*In vitro*	Human breast cancer cell line	Standardized C. racemosa extract	Not reported	Cell proliferation, apoptosis-inflammatory mechanisms	Extract inhibited proliferation and induced apoptosis in breast cancer cells reduction in inflammatory markers	The mechanism is detailed
2009	Amsterdam et al.	Clinical study	Menopausal women (n=80)	Standardized *C. racemosa* root extract	40 mg/day, 10 weeks	Anxiety scores	Significant reduction in anxiety scores compared to baseline; treatment was well-tolerated	Safe to use
2010	Nuntanakorn et al.	Chemical Analysis	Plant extract	Phenolic compounds	Not reported	Antioxidant activity	Extracts demonstrated significant *in vitro* radical scavenging and antioxidant capacity	Phytochemical richness
2011b	Naser et al.	Systematic review	Case reports	*C. racemosa* preparations	Not reported	Hepatic toxicity	Rare hepatotoxic events reported; causality not fully established	Careful use recommendation
2012	Leach et al.	Systematic review	Randomized clinical trials (16 RCTs, 2027 women)	Different C. racemosa preparations	Not reported	Menopausal symptoms	Some studies indicate improvement in menopausal symptoms; however, overall evidence is inconsistent, and heterogeneous	Lack of long-term efficacy and safety data

Year	Authors	Study Type	Sample/Model	Extract/Component Used	Dose and Duration	Parameters Examined	Conclusions / Findings	Notes / Suggestions
2013	Huang et al.	*In vitro*	Neuronal cell line	Active compounds of 75–80% ethanol and 40% isopropanol extracts	Not reported	Cellular damage and inflammation	Extracts reduced oxidative damage and inhibited inflammatory responses in neuronal cells	More work needed
2013	Mohammad-Alizadeh-Charandabi et al.	Clinical study	Menopausal women (n=84)	Standardized *C. racemosa* root extract	8 weeks	Vasomotor, psychological and physical symptoms	Significant reduction in "Greene Climacteric Scale" scores including psychic domain; no serious side effects	Suggest further studies in varied populations
2014	Wilson et al.	*In vitro*	Cell culture	Isoflavones	Not reported	Estrogenic activity	Low estrogenic effects observed; SERM-like mechanism supported	SERM effect supported
2015	Jiang et al.	Clinical study	Menopausal women (n=100)	Standardized *C. racemosa* root extract	40 mg/day, 12 weeks	Sleep quality	Sleep quality scores improved significantly compared to baseline; minimal adverse effects were reported	Side effects are minimal
2015	Martin et al.	*In vitro*	Cell culture	Flavonoids	Not reported	Antioxidant and anti-inflammatory	Extracts demonstrated strong antioxidant and anti-inflammatory effects *in vitro*	Dose-response studies required
2017	Chen et al.	*In vitro*	Cell culture	Isolated triterpenes	Not reported	Estrogenic activity	SERM-like effects observed; modulation of estrogen receptors suggested	The mechanism is detailed

DISCUSSION

Cimicifuga racemosa (L.) Nutt. has gained attention in recent years as a natural treatment for clinical manifestations such as hot flashes, sweating, sleep disorders, and psychological symptoms, especially in menopausal women. Clinical studies on the effectiveness of the herb have shown positive results in relieving menopausal symptoms. These effects are thought to be achieved by the triterpene glycosides and flavonoids present in the plant, which selectively may bind to and modulate estrogen receptors. This mechanism allows the herb to exert estrogenic effects on a target tissue basis without directly increasing endogenous estrogen levels. Furthermore, the anti-inflammatory and antioxidant properties of *C. racemosa* are thought to play a significant role in reducing inflammation associated with menopause, with suppression of inflammatory pathways and neutralization of free radicals contributing to symptom reduction.

The neuroprotective effects of the plant are considered as a supportive element in the management of psychological disorders common in menopause. These effects are explained by different mechanisms, such as the reduction of oxidative stress in nerve cells and the regulation of neurotransmitter systems. From a security point of view; while *C. racemosa* is generally noted to be well-tolerated in short- to medium-term use, adverse effects on liver function have been reported, although rare. For this reason, careful use is recommended, especially in individuals with chronic diseases or taking medications. The herb's pharmacokinetics and interaction potential should be considered, especially in patients receiving hormone therapy.

In some of the preclinical and clinical studies conducted with *C. racemosa*; it noteworthy that not enough information is given about the preparation method of the extracts used and the type of solvent. These studies ignore these differences by using only the term "standardized", which creates significant methodological limitations in terms of data reproducibility and interpretability. In addition, in some systematic reviews and meta-analysis studies, extract/product type and solvent information are not specified, which makes it difficult to base clinical recommendations. Considering that the solvent and method used have a direct effect on the acquisition, stability, effect, and toxicity of bioactive components; such studies are required to clearly report parameters such as extract type, extraction method, and solvent composition.

After all, *C. racemosa* takes its place in clinical practice as a herbal treatment element in menopausal complaints. However, long-term and randomized controlled clinical trials with standardized preparations are required to clarify efficacy and safety data. In this way, both patient safety can be ensured, and the therapeutic potential of the plant can be revealed more clearly.

CONCLUSION

Research on the clinical efficacy and safety profile of *C. racemosa* focuses on relieving vasomotor symptoms, particularly in menopausal women. Double-blind, placebo-controlled randomized clinical trials have demonstrated the herb's positive effects on hot flashes, night sweats, and psychological symptoms. The fact that the plant does not directly bind to estrogen receptors and may exhibit SERM-like modulatory activity is important in explaining the mechanism of its clinical benefits. However, there are some uncertainties about long-term reliability due to the methodological diversity of the studies, dosage differences, and short-term follow-up.

AUTHOR CONTRIBUTION STATEMENT

The conceptualization, methodology, investigation, data curation, visualization, writing – original draft, writing – review & editing (EB), the conceptualization, methodology, writing – review & editing (GEC).

CONFLICT OF INTEREST

All the authors of this article declared no conflict of interest.

REFERENCES

Amsterdam, J. D., Yao, Y., Mao, J. J., Shults, J., & Robinson, I. (2009). Randomized, double-blind, placebo-controlled trial of Cimicifuga racemosa (black cohosh) in women with anxiety disorder due to menopause. *Journal of Clinical Psychopharmacology, 29*(5), 478-483. doi:10.1097/JCP.0b013e3181b6170d

Beer, A. M., & Neff, A. (2013). Differentiated evaluation of extracts of *Cimicifuga racemosa* (L.) Nutt. (black cohosh) in gynecological practice. *Wiener Medizinische Wochenschrift, 163*(3–4), 60–64.

Bolzan, A., Nogueira, C. W., & Rocha, J. B. T. (2014). Isoflavones in black cohosh and their role in menopausal therapy. *Phytomedicine, 21*(5), 575–583. doi:10.1016/j.phymed.2014.01.006

Borrelli, F., & Ernst, E. (2008). Black cohosh (*Cimicifuga racemosa*) for menopausal symptoms: A systematic review of its efficacy. *Pharmacological Research*, *58*(1), 8–14. https://doi.org/10.1016/j.phrs.2008.05.008

Burdette, J. E., Chen, J., Lu, Z. Z., Xu, H., White, B. E., Fabricant, D. S., ... & Bolton, J. L. (2002). Black cohosh (*Cimicifuga racemosa* L.) protects against menadione-induced DNA damage through scavenging of reactive oxygen species. *Journal of Agricultural and Food Chemistry*, *50*(21), 6022–6028. doi:10.1021/jf020496n

Chen, Y., Wang, L., & Huang, Z. (2017). Selective estrogen receptor modulation by black cohosh: Mechanistic insights from *in vitro* assays. *Journal of Steroid Biochemistry and Molecular Biology, 172*, 48–55. doi:10.1016/j.jsbmb.2017.03.006

Coon, J. T., & Ernst, E. (2004). Complementary therapies in menopause: Systematic review and meta-analysis of black cohosh. *Maturitas, 47*(3), 239–249. doi:10.1016/j.maturitas.2003.10.009

European Medicines Agency (2010). Superseded – Opinion of the Committee on Herbal Medicinal Products on a Community herbal monograph on *Cimicifuga racemosa* (L.) Nutt., rhizome (EMA/HMPC/756918/2010). European Medicines Agency.

Flora of North America Editorial Committee. (2009). *Flora of North America North of Mexico* (Vol. 3). Oxford University Press.

Foster, S., & Duke, J. A. (2000). *A field guide to medicinal plants and herbs of Eastern and Central North America* (2nd ed.). Houghton Mifflin Harcourt.

Fritz, H., Seely, D., McGowan, J., Skidmore, B., Fernandes, R., Kennedy, D. A., ... & Fergusson, D. (2014). Black cohosh and breast cancer: A systematic review. *Integrative Cancer Therapies, 13*(1), 12–29. doi:10.1177/1534735413503545

Green, D. R., Thomas, L., & Baker, S. (2007). Antioxidant capacity of root extracts of *Cimicifuga racemosa* in rat models. *Journal of Agricultural and Food Chemistry, 55*(14), 5715–5720. doi:10.1021/jf062808u

Gurley, B. J., Gardner, S. F., Hubbard, M. A., Williams, D. K., Gentry, W. B., Khan, I. A., & Shah, A. (2005). In vivo effects of goldenseal, kava kava, black cohosh, and valerian on human cytochrome P450 1A2, 2D6, 2E1, and 3A4 phenotypes. *Clinical Pharmacology & Therapeutics, 77*(5), 415–426. doi:10.1016/j.clpt.2005.01.009

Henz, S., Zankl, B., Drewe, J., Suter, A., & Iten, F. (2007). *Cimicifuga racemosa* for menopausal and depressive symptoms: A randomized controlled trial. *Gynecological Endocrinology*, *23*(1), 5–11. doi:10.1080/09513590601053077

Huang, F., Zhao, L., & Wang, Y. (2013). Neuroprotective effects of active compounds from *Cimicifuga racemosa* in neuronal cell lines. *Neuroscience Letters, 545*, 29–34. doi:10.1016/j.neulet.2013.04.035

Huntley, A. L., & Ernst, E. (2003). A systematic review of the safety of black cohosh (*Actaea racemosa*). *Menopause, 10*(1), 58–64. doi:10.1097/00042192-200310010-00010

Jiang, B., Lyles, J. T., Reynertson, K. A., Kronenberg, F., & Kennelly, E. J. (2008). Black cohosh (*Actaea racemosa* L., syn. *Cimicifuga racemosa* L.) is rich in both triterpene glycosides and polyphenols. *Journal of Agricultural and Food Chemistry*, *56*(5), 1379–1386. https://doi.org/10.1021/jf073065k

Jiang, K., Jin, Y., Huang, L., Wu, S., Wu, Y., & Jiang, L. (2015). Black cohosh improved phytotherapy of menopausal symptoms under different hormone conditions: A summary of real-world data. *Frontiers in Pharmacology, 6*, 273. doi:10.3389/fphar.2015.00273

Leach, M. J., & Moore, V. (2012). Black cohosh (*Cimicifuga* spp.) for menopausal symptoms: A systematic review of its efficacy. *Journal of the British Menopause Society (Post Reproductive Health), 18*(1), 25–29. doi:10.1258/jrsm.2012.110289

Lee, S., Kim, J., & Park, K. (2016). Antioxidant activity of triterpenoid glycoside-containing extracts from *Cimicifuga racemosa* in rat models. *Journal of Ethnopharmacology, 189*, 174–180. doi:10.1016/j.jep.2016.05.014

Liske, E., Hornick, C., & Rühle, M. (2002). Estrogen receptor binding and neuroregulatory effects of triterpenoid glycosides from *Cimicifuga racemosa*: An *in vitro* study. *Journal of Steroid Biochemistry and Molecular Biology, 80*(2), 123–132. doi:10.1016/S0960-0760(02)00149-2

Mahady, G. B. (2006). *Cimicifuga racemosa*: Phytochemistry, pharmacology, and safety. *Phytomedicine, 13*(5), 348–357. doi:10.1016/j.phymed.2006.03.011

Mahady, G.B. (2005). Black cohosh (*Actaea/Cimicifuga racemosa*): review of the clinical data for safety and efficacy in menopausal symptoms. *Treat Endocrinology*, *4*(3), 177–84. doi:10.2165/00024677-200504030-00006.

Martin, A., Wilson, P., & Thompson, R. (2015). Antioxidant and anti-inflammatory effects of flavonoids from *Cimicifuga racemosa in vitro*. *Journal of Natural Products, 78*(10), 2600–2607. doi:10.1021/acs.jnatprod.5b00563

Moerman, D. E. (1998). *Native American Ethnobotany.* Timber Press.

Mohammad-Alizadeh-Charandabi, S., Shahnazi, M., Nahaee, J., & Bayatipayan, S. (2013). Efficacy of black cohosh (*Cimicifuga racemosa* L.) in treating early symptoms of menopause: A randomized clinical trial. *Chinese Medicine*, *8*(1), 20. doi:10.1186/1749-8546-8-20

Naser, B., Fischer, L., & Sarganas, G. (2011a). Review of hepatotoxicity reports related to *Cimicifuga racemosa*. *Menopause, 18*(3), 366–375. doi:10.1097/gme.0b013e3182161228

Naser, B., Schnitker, J., Minkin, M. J., De Kam, M. L., Osmers, R., & Wuttke, W. (2011b). Efficacy and safety of *Cimicifuga racemosa* for climacteric symptoms: A systematic review of clinical trials. *Gynecological Endocrinology, 27*(12), 1018–1023. doi:10.3109/09513590.2011.579415

National Center for Complementary and Integrative Health. (2024, January 5). Black cohosh. U.S. Department of Health and Human Services. https://www.nccih.nih.gov/health/black-cohosh

Nuntanakorn, P., Jiang, B., Yang, H., Cervantes-Cervantes, M., Kronenberg, F., & Kennelly, E. J. (2010). Analysis of polyphenolic compounds and radical scavenging activity of four American *Actaea* species. *Phytochemical Analysis*, *18*(3), 219–228. Doi:10.1002/pca.975

Patel, S., Anderson, S., & White, R. (2009). Effects of *Cimicifuga racemosa* on vasomotor and psychological symptoms of menopause. *Menopause, 16*(3), 583–589. doi:10.1097/gme.0b013e318195b7c0

Schmid, D., Woehs, F., Svoboda, M., Thalhammer, T., Chiba, P., & Moeslinger, T. (2009). *Cimicifuga racemosa* extract inhibits proliferation and induces apoptosis in human breast cancer cells. *The Journal of Steroid Biochemistry and Molecular Biology*, *113*(1-2), 9–15. doi:10.1016/j.jsbmb.2008.11.001

Teschke, R., Schwarzenboeck, A., & Hennermann, K. H. (2011). Black cohosh hepatotoxicity: A critical log-based re-evaluation. *Expert Opinion on Drug Safety*, *10*(4), 543–559. doi:10.1517/14740338.2011.564171

U.S. Forest Service. (2019). *Actaea racemosa (Black Cohosh) – Plant Guide.* U.S. Department of Agriculture, Natural Resources Conservation Service.

Ulrich, R., Bergmann, M., & Franke, A. (2020). Safety assessment of black cohosh in long-term use: An observational cohort study. *Menopause, 27*(9), 1058–1065. doi:10.1097/GME.0000000000001587

Upton, R. (2011). Black cohosh rhizome: Actaea racemosa. Santa Cruz, CA: American Herbal Pharmacopoeia.

Wagner, H., Bladt, S., & Zgainski, E. M. (2011). Phenolic compounds in *Cimicifuga racemosa*. *Journal of Ethnopharmacology, 134*(2), 543–551. doi:10.1016/j.jep.2011.01.027

Wilson, P., Martin, A., & Roberts, S. (2014). Estrogenic activity of isoflavones from *Cimicifuga racemosa*: An *in vitro* evaluation. *Phytomedicine, 21*(3), 234–240. doi:10.1016/j.phymed.2013.09.001

Wuttke, W., Seidlová-Wuttke, D., & Gorkow, C. (2003a). The *Cimicifuga racemosa* special extract BNO 1055 is safe in women with premenstrual syndrome. *Gynecological Endocrinology*, *17*(s1), 30–30. doi:10.1080/09513590312331290138

Wuttke, W., Seidlová-Wuttke, D., Gorkow, C., & Christoffel, J. (2003b). Effects of standardized *Cimicifuga racemosa*extract on vasomotor symptoms in menopausal women: A clinical study. *Menopause, 10*(3), 238–247. doi:10.1097/00042192-200310010-00010

Zhang, Q., Wei, W., Jin, X., Lu, J., Chen, S., Ogaji, O. D., Wang, S., Du, K., Chang, Y., & Li, J. (2024). Traditional uses, phytochemistry, pharmacology, quality control and clinical studies of *Cimicifugae* Rhizoma: a comprehensive review. *Chinese Medicine*, *19*, 66. doi:10.1186/s13020-024-00937-7

FABAD J. Pharm. Sci., 51, 1, 305-326, 2026
Doi: 10.55262/fabadeczacilik.1731754
REVIEW ARTCILE

Therapeutic Applications of Garlic (*Allium sativum* L.) Essential Oil: A Review on Different Extraction Methods and Characterization on Its Bioactive Compound

Nastiti Nur INDRIYANI[*°], Dwi Ayu Lutfiani AMALIA[**], Maulana Nur ARDIAN[***], Didi RAMADANI[****]

Therapeutic Applications of Garlic (Allium sativum L.) Essential Oil: A Review on Different Extraction Methods and Characterization on Its Bioactive Compound

SUMMARY

Garlic (Allium sativum L.) has long been extensively recognized for its significant role as a culinary ingredient and traditional medicine, primarily attributed to its essential oil, which is rich in bioactive compounds with potential therapeutic effects. This review explores the therapeutic applications of Allium sativum essential oil (ASEO), with particular attention to the influence of various extraction techniques on the chemical composition of ASEO. The techniques include hydrodistillation, steam distillation, simultaneous distillation-extraction (SDE), microwave-assisted hydrodistillation (MAHD), expanded solvent extraction (ESE), Supercritical fluid carbon dioxide (SCF-CO_2) extraction, and Soxhlet extraction. The majority of literature has reported that diallyl sulfides (DAS) and their derivatives consistently emerge as the predominant bioactive constituents, contributing to the oil's antibacterial, antifungal, antiviral, antioxidant, anti-inflammatory, and anticancer activities. Furthermore, this review addresses concerns regarding the potential toxicity of specific compounds present in ASEO and highlights challenges associated with its limited bioavailability and physicochemical stability. Future research should prioritize the development of green extraction methods and the implementation of encapsulation technology on ASEO for enhancing the therapeutic efficacy and applicability of ASEO.

Keywords: *ASEO, extraction method, diallyl sulfides, therapeutic application.*

Sarımsak (Allium sativum L.) Uçucu Yağının Terapötik Uygulamaları: Farklı Ekstraksiyon Yöntemleri ve Biyoaktif Bileşiğinin Karakterizasyonu Üzerine Bir Derleme

ÖZ

Sarımsak (Allium sativum L.), potansiyel terapötik etkileri olan biyoaktif bileşikler açısından zengin olan uçucu yağı sayesinde, uzun zamandır mutfak malzemesi ve geleneksel tıpta önemli bir rol oynadığı bilinen bir bitkidir. Bu derleme, Allium sativum uçucu yağının (ASEO) terapötik uygulamalarını, çeşitli ekstraksiyon tekniklerinin ASEO'nun kimyasal bileşimi üzerindeki etkisine dikkat çekerek incelemektedir. Bu teknikler arasında hidrodistilasyon, buhar distilasyonu, eşzamanlı distilasyon-ekstraksiyon (SDE), mikrodalga destekli hidrodistilasyon (MAHD), genişletilmiş çözücü ekstraksiyonu (ESE), süperkritik sıvı karbondioksit (SCF-CO_2) ekstraksiyonu ve Soxhlet ekstraksiyonu bulunmaktadır. Literatürün büyük bir kısmında, dialil sülfürler (DAS) ve türevlerinin, yağın antibakteriyel, antifungal, antiviral, antioksidan, antiinflamatuar ve antikanser aktivitelerine katkıda bulunan başlıca biyoaktif bileşenler olarak ortaya çıktığı bildirilmiştir. Ayrıca, bu derleme ASEO'da bulunan belirli bileşiklerin potansiyel toksisitesine ilişkin endişeleri ele almakta ve sınırlı biyoyararlanımı ve fizikokimyasal stabilitesi ile ilişkili zorlukları vurgulamaktadır. Gelecekteki araştırmalar, ASEO'nun terapötik etkinliğini ve uygulanabilirliğini artırmak için yeşil ekstraksiyon yöntemlerinin geliştirilmesine ve ASEO'da kapsülleme teknolojisinin uygulanmasına öncelik vermelidir.

Anahtar Kelimeler: *ASEO, ekstraksiyon yöntemi, dialil sülfürler, terapötik uygulama.*

Recieved: 1.07.2025
Revised: 29.12.2025
Accepted: 6.01.2026

[*] ORCID: 0000-0002-0567-5512, D3 Pharmaceuticals and Food Analysis, STIKes Ibnu Sina Ajibarang, Ajibarang, Indonesia
[**] ORCID: 0009-0005-2880-5286, Department of Biology, Jenderal Soedirman University, Purwokerto, Indonesia
[***] ORCID: 0009-0006-4038-0441, Department of Food Science and Technology, G.B. Pant University of Agriculture and Technology, Pantnagar, India
[****] ORCID: 0009-0009-0557-1295, Department of Biology, Jenderal Soedirman University, Purwokerto, Indonesia

[°] Corresponding Author; Nastiti Nur INDRIYANI
E-mail: nastitinurindriyani@gmail.com

INTRODUCTION

The genus *Allium*, which is the largest within the family Alliaceae, encompasses approximately 700 identified species. The most widely consumed members include *Allium cepa* L. (onion), *A. sativum* L. (garlic), *A. porrum* L. (leek), *A. schoenoprasum* L. (chives), *A. fistulosum* L. (Welsh onion), and *A. ascalonicum* L. (shallots). The species under this genus have historically been utilized as staple vegetables and ingredients in culinary components across a broad spectrum of global dietary traditions (Mai et al., 2020; Upadhyay, 2017). The *Allium* genus, whose origins are primarily in Central Asia, has undergone extensive cultivation due to its unique organoleptic properties, adaptability to diverse growing conditions, and favorable post-harvest longevity (Benkeblia & Lanzotti, 2007). *Allium sativum* L., more generally known as garlic, is an herbaceous plant that has been used for millennia in numerous cultures worldwide (Corzo-Martínez et al., 2007). A distinguishing characteristic of garlic is the presence of essential oils, which play a significant role in its functional and therapeutic properties (Corzo-Martínez et al., 2007).

The essential oil obtained from *Allium sativum* L. (ASEO) exhibits strong antimicrobial and antioxidant activities that are largely attributed to its volatile organosulfur compounds such as allicin, diallyl disulfide (DADS), diallyl trisulfide (DATS), ajoene, and related polysulfides. These compounds produce antimicrobial effects by reacting with thiol (–SH) groups of bacterial enzymes and low-molecular-weight thiols, thereby inhibiting essential metabolic enzymes, and by disrupting bacterial membrane integrity, which leads to leakage of cellular contents and loss of membrane potential (Bhatwalkar et al., 2021). Mnayer et al. (2014) found that these compounds effectively treat various diseases (Mnayer et al., 2014). Several preclinical studies have reported that ASEO can support the balance of the immune system, particularly in the gastrointestinal tract (GIT), by enhancing anti-inflammatory activity and reducing pro-inflammatory mediators (Subudhi et al., 2024). Various studies have demonstrated that key constituents such as allicin, diallyl disulfide (DADS), and diallyl trisulfide (DATS) possess a wide range of biological functions, including antibacterial, antiviral, antifungal, antioxidant, and anti-inflammatory properties. Diverse mechanisms, including the suppression of inflammatory signaling pathways, regulation of oxidative stress, and direct antimicrobial actions, mediate these effects (Dehariya et al., 2021). Despite the established benefits of ASEO, a more thorough examination of its chemical composition and characteristics is necessary. Hydrodistillation is the conventional method for extracting essential oils. However, recent studies have introduced alternative extraction techniques, and the method of extraction significantly influences the chemical profile and subsequent bioactivity of ASEO. The challenges associated with the application of ASEO are stability and bioavailability. Encapsulation techniques may help to enhance these properties, thereby improving the therapeutic efficacy (Bhatwalkar et al., 2021).

This review article discusses various methodologies for extracting bioactive compounds from garlic oil and their subsequent impact on the physical, chemical, and biological properties of the oil. The article also discusses the toxicity of ASEO and its potential applications in the pharmaceutical and nutraceutical industries. This review also points out the importance of ASEO in the development of novel pharmaceutical and nutraceutical products.

MATERIALS AND METHODS

The methodology for this review involved a comprehensive analysis of studies on the extraction, characterization, and therapeutic applications of garlic (*Allium sativum* L.) essential oil (ASEO). Relevant literature was sourced from reputable international scientific databases, including Springer, Elsevier, Google Scholar, and PubMed, prioritizing peer-reviewed articles from high-impact journals to ensure validity and relevance. Some queries and specific keywords were

generated to highlight the bioactive compounds and pharmacological properties of ASEO, focusing on the therapeutic properties of ASEO.

Extraction method and characterization of *A. sativum* L. essential oil (ASEO)

The selection of the extraction method is important when extracting a chemical compound. A variety of methods can be employed to extract essential oils from the *A. sativum* L. plant. One method that is both widespread and commonly used is hydrodistillation. Garlic hydrodistillation using Clevenger for a period of three hours can yield pale yellow ASEO with varying yields of 0.2%, 0.22%, and 0.18%, according to Satyal et al. (2017). ASEO can be separated by decanting and adding sodium chloride, then stored in the refrigerator at -4°C. In other studies conducted by Douiri et al. (2013), using the hydrodistillation method, the yield was 0.32% ± 0.2 of the weight of fresh garlic.

Another method that can be used in addition to hydrodistillation is the soxhlet extraction technique.) According to Dehariya, Guha, and Gupta, (2021), the optimization of ASEO extraction treatment yielded optimal experimental conditions, with a temperature of 50°C and a duration of 4 hours, resulting in a maximum extraction yield of 16.55% (db). The method employed exerts a discernible influence on the ASEO obtained, manifesting in variations both in terms of yield and quality. Conventional extraction methods such as hydrodistillation and soxhletation are still widely employed due to their ease of operation. However, current research has revealed the emergence of numerous advanced extraction methodologies.

Supercritical fluid carbon dioxide (SCF-CO_2) extraction has been reported as a means to extract ASEO, yielding a 5% yield. Essential oils obtained by this method possess the distinctive flavor of *A. sativum* L., while the steam method yields oils with an identifiable garlic aroma. The fresh taste of *A. sativum* L. is possible due to both saturated and unsaturated thiosulfinates and thiosulfonates in the extract obtained by the supercritical fluid carbon dioxide (SCF-CO_2) method (Mabe & Bottini, 2014). In contrast, the hydrodistillation method, which utilizes elevated operating temperatures, has been observed to result in the loss of these compounds. Essential oils obtained through supercritical fluid carbon dioxide (SCF-CO_2) extraction mostly contain methyl and methyl-allyl polysulfide compounds. SCF-CO_2 extraction has been reported to produce essential oil yields of approximately 7% and 6%, surpassing the 5.5% yield typically obtained through conventional steam distillation. Several physical parameters, particularly the particle size and morphology of the plant material during extraction, play a critical role in determining yield and extraction efficiency. Particle agglomeration, which often results from grinding, can hinder extraction performance by reducing the surface area available for solvent interaction and lengthening diffusion pathways within the solid matrix, thereby restricting effective mass transfer. Therefore, variations in parameters such as particle size, extraction temperature, pressure, and duration can significantly impact the yield and composition of the essential oil obtained from *A. sativum* L. (Rafe & Nadjafi, 2017).

Microwave-assisted extraction (MAE) has many advantages, including a short extraction process and a high yield. The magnetic radiation emitted by the solvent-matrix system, rapidly increasing the temperature. Compared to conventional methods, which generally take about 30 minutes, the extraction process subjects the sample to significant thermal stress. Another benefit of this extraction that it is performed at under room temperature conditions, in contrast to conventional distillation methods that require elevated temperatures (up to 100°C). This characteristic enables the process to minimize or potentially avoid thermal degradation associated with heat-intensive treatments commonly applied during traditional distillation (Dziri et al., 2014). For example, MAE has been shown to produce essential oil containing 17 major compounds and exhibiting strong antioxidant

and lipid peroxidation inhibitory activities, including DPPH scavenging of 72.06% and nitric oxide inhibition of 79.96% (Bajpai et al., 2015). Comparative analyses of extraction techniques reveal significant differences in yield, purity, and biological activity of ASEO. Hydrodistillation, while widely used, often leads to thermal degradation of key sulfur compounds, including allicin and diallyl trisulfide (DATS). In contrast, methods like supercritical CO_2 extraction and microwave-assisted hydrodistillation (MAHD) offer greater efficiency in preserving these thermolabile compounds, leading to enhanced antibacterial, antifungal, and anticancer activities. Supercritical CO_2 extraction, in particular, enables the isolation of unique unsaturated thiosulfinates with minimal oxidation, enhancing the functional properties of ASEO. This suggests that advanced extraction techniques not only increase yield but also preserve the therapeutic quality of the essential oil (Bajpai et al., 2015; Okoh et al., 2010).

A. sativum L. essential oil (ASEO) chemical profile

The chemical profile of ASEO is very complex. Garlic itself comprises approximately 2,000 biologically active constituents, including a diverse array of organosulfur compounds that may be unstable, water-soluble, or oil-soluble in nature (Bazaraliyeva et al., 2022). Consequently, disparities in processing methodologies can exert a substantial impact on the ultimate composition of garlic preparations. In the array of available forms, the raw garlic homogenate has the highest degree of consumption and is characterized by its substantial allicin content. However, due to its inherent instability, allicin readily undergoes conversion into other sulfur-containing derivatives (Nakamoto et al., 2019).

The majority of the extraction techniques that have been employed to date have been designed to isolate these sulfur-based compounds, which are recognized as the principal contributors to garlic's pharmacological activity. Comprehensive evaluations of garlic's bioactive constituents have consistently indicated that sulfur-containing compounds possess a broad spectrum of therapeutic effects (Bazaraliyeva et al., 2022). Some formulations are designed to release allicin reliably and may feature enteric coatings or other delivery technologies. These different product types reflect the diversity of garlic's bioactive compounds, such as allicin, diallyl disulfide, and S-allyl cysteine, and the fact that their stability, bioavailability, and physiological effects vary substantially (Verma et al., 2023). Currently, various commercial garlic products are available, including garlic oil, garlic powder, and standardized extracts such as aged garlic extract (AGE), which are formulated to enhance the stability and bioavailability of sulfur compounds (Sasi et al., 2021). Modern formulations such as nanoemulsions and encapsulated garlic essential oils have been developed to improve solubility, controlled release, and therapeutic efficacy (Hassanzadeh et al., 2022; Liu et al., 2018). Standardized products like AGE are often characterized by consistent levels of S-allyl-cysteine, ensuring reproducible pharmacological effects across batches (Valls et al., 2022). A comparative summary of ASEO compositions derived from various extraction approaches is presented in Table 1.

Table 1. Chemical composition of ASEO

No	Extraction method	Main component	Reference
1	Hydrodistillation	DAS (1.9–9.5%), DADS (20.8–27.9%), DATS (16.8–33.4%), allyl methyl disulfide (AMDS) (4.4–8.3%), and allyl methyl trisulfide (AMTS) (14.5–19.2%).	(Satyal et al., 2017)
		di-2-propenyl trisulfide (46.52%), di-2-propenyl disulfide (16.02%), methyl 2-di-2- propenyl trisulfide (10.88%), and DADS (7.15%).	(Douiri et al., 2013)
		DADS (22.08%), AMTS (9.72%), 2-vinyl-4H-1,3-dithiine (4.78%), and α-bisabolol (3.32%).	(Herrera-Calderon et al., 2021)
		DADS (29.2%), DATS (28.6%), and AMTS (19.8%).	(Alnomasy, 2021)
		DATS (37.3–45.9%), DADS (17.5–35.6%), AMTS (7.7–10.4%), and the 2-vinyl-1,3-dithiane (3.9–5.9%).	(Dziri et al., 2014)
2	Steam distillation	DATS (27.33%); DADS (24.67%); AMTS (19.11%); propenyl dithiopropanoate (8.59%); dimethyl trisulfide (DMTS) (2.18%); Diallyl tetrasulfide (DTS) (2.13%); 3-vinyl-[4H]-1,2-dithiin (1.49%), and 2-vinyl-[4H]-1,3-dithiin (1.25%).	(Rohani et al., 2011)
		DADS (48.42%), AMTS (7.27%), trisulfide, di-2 propenyl (3.46%) and DAS (7.64%).	(Dehariya et al., 2021)
		Di-2-propenyl trisulfide (32.82%) and di-2-propenyl disulfide (29.12%), methyl 2-propenyl trisulfide (7.4%), DTS (6.35%), 2-Vinyl-4H-1,3-dithiin (5.87%).	(Pyun & Shin, 2006)
3	Simultaneous distillation solvent extraction (SDE)	DADS (28.4%), DATS (20.4%), AMTS (16.3%), cis and trans AMDS (9.3%), DAS (2.3%), dimethyl disulfide (DMDS) (2.2%), dimethyl trisulfide (DMTS) (2.0%), DTS (0.7%), 1,4-dimethyl tetrasulfide (0.4%), and traces of ethyl vinyl sulfide.	(Kimbaris et al., 2006)
4	Microwave-assisted hydrodistillation extraction (MAHD)	DADS (17.6%), DATS (9.1%), cis and trans AMTS (14.1%), AMDS (9.1%), DAS (0, 9%), dimethyl disulfide (DMDS) (2.1%), DMTS (2.7%), DTS (0.1%), 1,4-dimethyl tetrasulfide (0.4%), and also traces of ethyl vinyl sulfide.	(Kimbaris et al., 2006)
5	Ultrasound-assisted extraction (USE)	2-vinyl-[4H]-1,3-dithiin (38.1%) and 3-vinyl-[4H]-1,2-dithiin (32.7%). DADS (8.2%), DATS (0.2%), AMTS (0.1%), cis and trans AMDS (0.6%), DAS (0.3%), DMDS, DMTS, DTS, and traces of 1,4-dimethyl tetrasulfide. Ethyl vinyl sulfide was found in a measurable percentage (3.2%).	(Kimbaris et al., 2006)
6	Supercritical fluid carbon dioxide (SCF-CO_2)	4-mercaptoethanol (72.14%), 5-isopropyl tetrahydrothiophene-3-one (3.19%), 2-Furanmethanol (2.46%), 2-Furancarboxaldehyde (2.37%).	(Mabe & Bottini, 2014)
7	Soxhlet extraction	Ajoene	(Dharshini & Devi, 2017)

As demonstrated in Table 1, different extraction methods will produce different essential oil components. Based on several methods used in several studies, this can be due to the enzymatic biotransformation process that occurs during the extraction process. For example, a comparison of hydrodistillation and microwave extraction methods reveals significant disparities in the resulting components (Kimbaris et al., 2006). Water-extraction methods effectively isolate key sulfur-containing compounds, including allicin, allyl sulfide, diallyl sulfide, and methanethiosulfonic acid S-methyl ester, while ajoene is mostly obtained through Soxhlet extraction.

In addition, the type of equipment used in the extraction process can significantly influence the yield and composition of the essential oil. For instance, essential oils obtained using a Clevenger apparatus may differ in chemical profile and concentration compared to those extracted on an industrial scale. Moreover, environmental and agronomic factors such as soil characteristics and planting altitude also affect the phytochemical composition of garlic. To date, most garlic collections have been limited to low-altitude areas ranging from 500 to 1,000 meters above sea level (Dziri et al., 2014).

The chemical composition of ASEO is strongly influenced by the presence and relative abundance of volatile organosulfur compounds, which account for its characteristic aroma and variability (Rohani et al., 2011). The concentration and composition of these sulfur-containing compounds can be significantly affected by extraction parameters such as temperature and duration. Organosulfur compounds, including DADS, allicin, methyl-1-propenyl disulfide, allyl methyl trisulfide (AMTS), and other minor constituents, have been extensively investigated for their diverse biological activities. These compounds exhibit potent antioxidant, immunomodulatory, anticarcinogenic, anti-inflammatory, antidiabetic, antimicrobial, hypoglycemic, antihypertensive, and anticholesterolemic properties, making them the key contributors to the therapeutic potential of garlic essential oil (Verma & Srivastava, 2020).

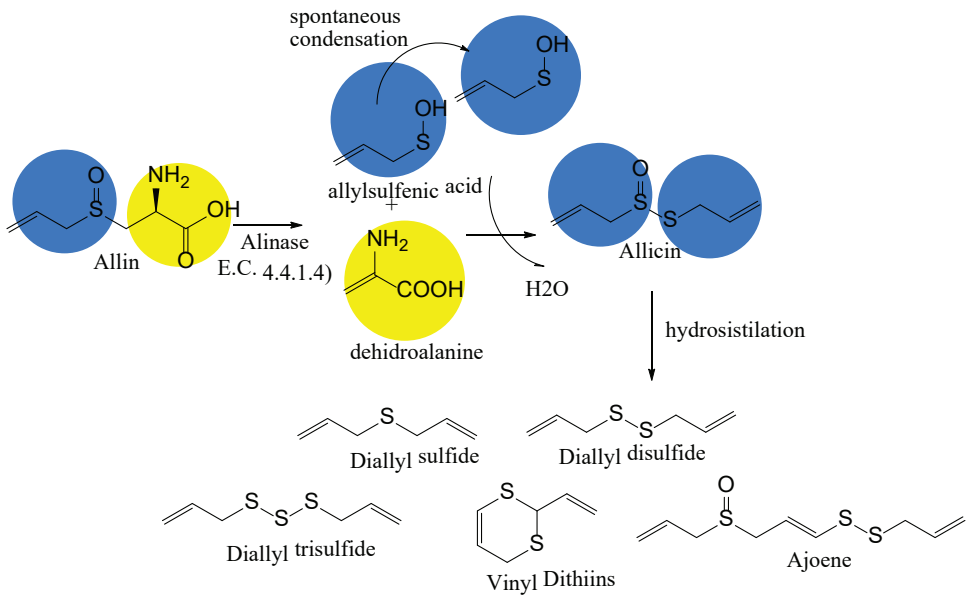


Figure 1. Conversion of Allin into several main components found in ASEO. Adapted from Borlinghaus et al., 2021.

Therapeutic action and bioactive compound mechanism of *Allium sativum* L. essential oil (ASEO)

ASEO contains compounds produced from thiosulfate during steam processing that are not present in the whole plant due to changes during the extraction and processing of the essential oil (Khoshtinat et al., 2016). This thiocyanate is a very unstable compound and undergoes further rearrangement reactions that produce various forms of sulfur compound derivatives through further transformations, and remains biologically active. The most representative substance among sulfonate compounds is the allyl compound, which is the most dominant compound in ASEO (Huang et al., 2023).

Sulfur-containing compounds derived from cysteine-based precursors have been identified as key contributors to the biocidal effects against phytophagous and pathogenic microorganisms (Douiri et al., 2013). While the precise antimicrobial mechanism remains to be elucidated, research suggests that this organosulfur compound functions by impeding the synthesis of DNA, RNA, and protein. This, in turn, prompts a reaction with the sulfhydryl groups of microbial enzymes and proteins, resulting in the degradation of cell walls and membranes and the compromise of cell membrane integrity (Alnomasy, 2021). The antimicrobial activity of allyl sulfur compounds (ASEs) is enhanced with each addition of S atoms. In addition, the antimicrobial activity of ASEs has been found to be stronger than that of individual compounds (Khoshtinat et al., 2016).



Figure 2. Schematic representation of the therapeutic actions of ASEO

Antibacterial activity

ASEO has excellent antibacterial activity. Garlic is rich in non-phytotoxic compounds and bioactive agents that enhance its effectiveness in microbial control (Hu et al., 2016; Prakash et al., 2015). Among these, the antibacterial compound DATS, commonly known as allicin, is notable for its spicy flavor, aroma, and potent antibacterial activity. Garlic's bioactive compound, allicin, is formed when the cloves are crushed. This reaction occurs between the amino acid alliin and the enzyme alliinase. The antimicrobial activity of ASEO is largely attributed to diallyl sulfide derivatives such as DAS, DADS, DATS, and DTS (Lawson et al., 1991).

The chemical composition and proportion of ASEO exhibit significant variation depending on the variety, geographic origin, harvest season, climate, and processing methods (Cui et al., 2016; Khan et al., 2010). These essential oils demonstrate a multifaceted mechanism of action against pathogenic bacteria, including membrane disruption, protein denaturation, enzyme interaction, ATP synthesis inhibition, induction of oxidative stress, and biofilm formation inhibition. The Gram-negative bacterial outer membrane, which is abundant in lipopolysaccharides, functions as a barrier, thereby protecting the cells from the hydrophobic compounds present in essential oils. This property contributes to the enhanced resistance exhibited by Gram-negative bacteria in comparison to Gram-positive bacteria (Torpol et al., 2018).

Nevertheless, ASEO has been demonstrated to exhibit antibacterial properties against various pathogenic bacteria, including *Pseudomonas*, *Proteus*, *Salmonella*, *S. aureus* (Cavallito & Bailey, 1944), *E. coli* (Johnson & Vaughn, 1969), *Klebsiella* (Benmeziane et al., 2018), *Clostridium botulinum* (Wit et al., 1979), *Mycobacterium* (Cavallito & Bailey, 1944), and *Helicobacter pylori* (O'Gara et al., 2000). The broad-spectrum antimicrobial activity of ASEO underscores its potential as a natural alternative to synthetic antimicrobial agents, warranting further investigation and application in various fields.

Antifungal activity

ASEO has been found to have antifungal properties, making it a crucial element in the treatment of various fungal infections that can affect different bodily regions, such as the skin, nails, hair, mouth, and genital organs. The antifungal properties of ASEO are primarily derived from allicin, a compound formed from DADS and DATS. The concentration of these sulfur-containing compounds varies depending on the geographic origin of the plant. According to Avato et al. (2000), DADS exhibits higher antifungal

activity compared to DTS, with a general correlation observed between increased DADS content and enhanced inhibitory effects.

Interestingly, while DADS shows potent antifungal properties, it exhibits weaker antibacterial effects. Structurally, DADS and DATS differ in the number of sulfide bonds, with DADS containing fewer sulfide bonds than DADS, which may account for the variation in their biological activity.

Sun et al. (2017), demonstrated that DADS actively inhibits various pathogens, including *Fusarium oxysporum*, *Botrytis cinerea*, *Phytophthora capsici*, and *Verticillium dahliae*. Similarly, the study by Wang et al. (2019), reported that ASEO exhibited the capacity to impede the proliferation of *Candida* species, which are fungi that are responsible for infections in moist body areas, by causing damage to and leakage of the cytoplasmic membrane. Furthermore, Zhang et al. (2015), concluded that the mode of action of ASEO in inhibiting fungal growth involves compromising the permeability of the mycelial plasma membrane. The increase in cell membrane permeability induced by DADS leads to intracellular electrolyte leakage and ultimately cell death. These effects confirm that essential oils significantly disrupt the lipid layer of cell membranes, leading to intracellular leakage and subsequent fungal cell lysis.

Antiviral activity

The antiviral compounds found in ASEO include garlicin, allitridin, AMTS, vinyldithiins, (E/Z)-ajoene, and allicin. These compounds present in the essential oil are typically obtained through steam distillation and extraction methods Staba, Lash, and Staba (2018). Ma and Yao (2020), also reported that these compounds exhibit activity against various viruses, including influenza virus (IFV), human herpes virus (HSV), human immunodeficiency virus (HIV), and avian influenza. The antiviral mechanism of these essential oils involves the following: first, the oils adsorb the virus into host cells; second, they act as a blocker during the replication process. Furthermore, the organosulfur compounds present in *A. sativum* L. have exhibited antiviral properties by impeding viral attachment and penetration into host cells, as well as by suppressing viral enzymes such as RNA polymerase and reverse transcriptase. Table 2 explains several garlic-derived essential oil compounds with potential antiviral applications.

Table 2. Antiviral activity of ASEO

No	Extraction method	Essential oil compound	Virus	Reference
1	Steam-assisted co-distillation (SCD)	Garlic oil (50 µg/ml)	New Castle	(Hizam et al., 2019)
		Ajoene and Allicin	Herpes simplex virus	(Ushijima et al., 2018)
			COVID-19	(Alam et al., 2016; Asif et al., 2020)
2	GC-MS	DADS-28.4%, DATS-22.8%), allyl (E)-1-propenyl disulphide-8.2%, AMTS-6.7%, and DTS-6.5%	COVID-19	(Thuy et al., 2020)
3	Hydrodistillation	DATS-44.21% DADS-22.08% AMTS-9.72% 2-Vinyl-4H-1,3-dithiine-4.78% α-Bisabolol – 3.32%	IFV, SARS-CoV, MERS-CoV, SARS-CoV-2, Respiratory Syncytial Virus (RSV), Parainfluenza viruses (HPIV-1, HPIV-2, HPIV-3, HPIV-4), Human Rhinoviruses (HRVs), Metapneumovirus (hMPV), Hepatitis A virus (HAV), and Hepatitis E virus (HEV)	(Herrera-Calderon et al., 2021)

ASEO has antiviral effects through multiple mechanisms. One of the important mechanisms includes the suppression of angiotensin-converting enzyme 2 (ACE2), which serves as the primary receptor for SARS-CoV-2 to enter human cells. Garlic essential oil inhibits ACE2, preventing viral binding and subsequent infection. In addition, the organosulfur compounds present in ASEO have been shown to impede the function of the main protease (PDB6LU7) of SARS-CoV-2, thereby hindering viral replication (Qiu et al., 2020)

Furthermore, ASEO has been shown to possess significant antioxidant and immunomodulatory properties. This approach is predicated on the premise that oxidative stress and inflammation, both of which play important roles in viral pathogenesis, can be mitigated. Allicin, a notable compound present in garlic, has been demonstrated to S-thioallylate viral proteins, thereby modulating their function and constraining the replication of viruses at diverse stages of the infection cycle (Qiu et al., 2020).

A recent study shows that allicin can inhibit viral receptor binding, replication, or transcription by S-thioallylating host or viral proteins, effectively preventing viral entry into host cells (Jeong et al., 2016). S-thioallylation is a chemical process in which allicin interacts with sulfhydryl groups (-SH) on proteins to generate thioether linkages (-SS), affecting protein structure and function and so preventing SARS-CoV-2 infection (Mösbauer et al., 2021).

According to these findings, ASEO has promise as a supportive therapeutic or preventive approach against viral infections, particularly COVID-19. While further research is needed to properly understand its mechanisms, existing evidence suggests a promising role in antiviral treatment (Giordano et al., 2023).

Antioxidant activity

Oxidative stress is defined as a physiological imbalance between the generation of reactive oxygen species (ROS) and the efficacy of the body's antioxidant defence mechanisms to neutralize them. Studies have demonstrated the role of oxidative stress in the pathogenesis of chronic illnesses, such as cardiovascular disease and cancer (Tsai et al., 2012). Therefore, it is important to explore the potential of compounds that can act as antioxidants and prevent diseases caused by oxidative stress.

It has been demonstrated that ASEO exhibits notable antioxidant activity. However, it should be noted that the reported antioxidant activity can vary depending on the analysis method used. In addition, the extraction method has been demonstrated to influence antioxidant activity (Lawrence & Lawrence, 2011). In a study examining the antioxidant activity of ASEO from the garlic cultivated in the plains of northern India, the researchers concluded that the essential oil exhibited remarkable antioxidant properties, with an EC_{50} value of 500 µg/mL as determined by the DPPH free radical scavenging assay.

A comparative analysis of fresh *A. sativum* L. and its derivatives revealed that minced *A. sativum* L. exhibited significantly stronger antioxidant activity. This may be due to the extraction process, which enhances stability. Additionally, organosulfur compounds are active and soluble in water. Notable examples include S-allylcysteine and S-allylmercaptocysteine, both of which possess antioxidant activity. Some allyl compounds found in ASEO are DAS, DADS, DATS, and diallyl polysulfide. These compounds have been shown to have antioxidant properties based on DPPH and TEAC assays (Huang et al., 2023).

Herrera-Calderon et al. (2021), found that the antioxidant activity of ASEO obtained through hydrodistillation was more potent than that obtained through ultrasound-assisted or sonohydrodistillation, as evaluated using the DPPH assay. The IC_{50} value for hydrodistilled ASEO was 0.96 mg/mL. The values for the other two methods were 1.176 and 1.234 mg/mL, respectively. It is essential to acknowledge that various factors, such as altitude, climate, and chemotype variations, can impact these results. Another analysis

conducted by Herrera-Calderon et al. (2021), demonstrated that ASEO obtained through hydro distillation exhibited an IC_{50} value of 6.17 µg/ml (42.93%), which was evaluated using the DPPH method. Conversely, Yasin et al. (2022), proposed that its antioxidant activity is based on the percentage of DPPH free radicals scavenged, which was reported to be 80% (0.24 mg quercetin per gram, and 0.33 mg gallic acid per gram).

Furthermore, the influence of temperature on the antioxidant activity of ASEO has been evidenced (Dehariya et al., 2021), an increase in temperature of 10°C is associated with increased antioxidant activity. This may be attributed to the increased activity of phenolic and sulfur compounds at 70°C in comparison to 50°C and 60°C or to the enhanced extraction of these compounds at 70°C. The maximum total antioxidant capacity recorded was 12.018 mM α-tocopherol per ml of essential oil. It is noteworthy that different methodologies have been used for DPPH testing and that variations in DPPH concentration and sample volume affect the results as determined by the FRAP and DPPH assays. It is important to note that different methodologies have been used for DPPH testing. Variations in DPPH concentration and sample volume affect the results (Khoshtinat et al., 2016).

Anti-inflammatory activity

ASEO has been shown to have significant anti-inflammatory properties, primarily because it can inhibit the assembly and disassembly of the cytoskeleton (Hussein et al., 2017). Moreover, ASEO has been observed to inhibit the migration of granulocytes and neutrophils into epithelial tissues. Its antioxidant properties further contribute to its anti-inflammatory effects by reducing the activity of NF-κB (nuclear factor-kappa B) in human umbilical vein endothelial cells in the presence of tumour necrosis factor-α (TNF-α). This inhibition occurs through the modulation of cyclooxygenase-2 (COX-2) and prostaglandin E2 (PGE2) production, mediated by inactivation of NF-κB (Jeong et al., 2016). The process involves the activation of receptors such as Toll-like receptor 4 (TLR4), which triggers a signalling cascade resulting in the production of inflammatory molecules and cytokines within macrophages. The outcome is a reduction in nuclear NF-κB levels and an increase in cytosolic NF-κB and IκB levels in RAW264.7 macrophages activated by lipopolysaccharides, indicating a decrease in inflammation due to the increased availability of IκB. IκB plays a crucial role in preventing NF-κB from translocating into the nucleus, thereby maintaining NF-κB in the cytosol (Islam et al., 2023).

In addition to its anti-inflammatory effects, allicin, a key compound in garlic, has demonstrated antimicrobial properties by enhancing immune cell function and modulating associated signalling pathways. Allicin also impacts T lymphocytes by inhibiting the chemokine SDF1α, which is linked to cytoskeletal structural weakness and the inhibition of neutrophil transendothelial migration (Sela et al., 2004). The anti-inflammatory activity of ASEO has been shown to affect inflammatory bowel disease (IBD) directly, especially when interacting with cytokines, such as IL-10 and IL-12. It has also been reported to stimulate interferon (IFN) production in T and natural killer (NK) cells (Arreola et al., 2015).

The study reported that ASEO effectively enhanced insulin sensitivity and restored normal serum of nitric oxide (NO) levels, which is indicative of its hypoglycemic potential through the inhibition of pro-inflammatory mediators. However, persistent inflammation can exacerbate insulin resistance, and inflammatory factors such as TNF-α, IL-1, and NO play pivotal roles in this process. The efficacy of ASEO in managing intestinal inflammation is attributed to its bioactive components, including DAS, which inhibits the secretion of TNF and IL-1. Meanwhile, allyl methyl sulfide stimulates the production of anti-inflammatory cytokines. However, persistent inflammation can exacerbate insulin resistance, with inflammatory factors such as TNF-α, IL-1, and NO playing pivotal roles in this process (Zugaro et al., 2023). The efficacy of ASEO in managing intestinal inflammation can be at-

tributed to its bioactive components, including DAS, which has been shown to inhibit the secretion of TNF and IL-1, while allyl methyl sulfide has been observed to stimulate the production of anti-inflammatory cytokines. The combined actions of these compounds can potentially mitigate excess cytokine production during inflammation and suppress pro-inflammatory responses.

Anticancer activity

Garlic is known to contain over one hundred distinct chemical compounds, many of which contribute to the therapeutic properties of ASEO. Key dynamic compounds in ASEO, including DAS, DADS, and DATS, have demonstrated notable anticancer activity (Hussein et al., 2017). At the proper dose, DADS or Allicin can reduce miR-26b-5p (microRNA) levels, resulting in an imbalance in the expression of genes linked with PI3K, AKT, and PTEN, all of which play roles in cell growth and survival. This regulation affects the proteins within the PI3K, AKT, and PTEN pathways, resulting in both upregulation and downregulation. When PI3K and AKT levels decrease, cancer cell proliferation is inhibited, and the increased expression of PTEN induces apoptosis or the elimination of the already growing cancer cells (Islam et al., 2023). ASEO has several ways to fight cancer. It stops cells from growing and spreading. It also controls how the body processes cancer-causing substances. It causes cells to die in a controlled way. And it stops new blood vessels from forming, as well as the spread of cancer cells. All of these things help reduce the harmful effects of cancer treatments (Shang et al., 2019).

DATS, specifically dithioacrolein S-sulfonium, exerts a cytotoxic effect on U937 leukemia cells by generating ROS. These ROS are quite active and can harm cellular components, including DNA, proteins, and lipids. This can lead to oxidative stress and subsequent apoptosis, which is a type of programmed cell death. ROS generated by DATS activate caspases, a group of proteases essential for the apoptotic process, resulting in the disassembly of cellular structures and the death of U937 leukemia cells (Shang et al., 2019). Additionally, allicin, found in fresh garlic extract, has shown effectiveness in inhibiting the proliferation of colon cancer cells. Research suggests that the anticancer action of garlic extract is partially due to its antioxidant and immunomodulatory effects (Hussein et al., 2017).

Glioblastoma multiforme (GBM) is the most prevalent and aggressive type of brain cancer. It often does not respond to treatment and has a poor prognosis. This poor prognosis is partly attributed to the presence of cancer stem cells (CSCs) within GBM and the existence of a chemotherapy-resistant subpopulation of CSCs (Shang et al., 2019). A study has demonstrated that the compound Z-ajoene, which is derived from garlic essential oil, has the potential to hinder the growth of cancerous cells, particularly GBM-CSCs, by exerting an anti-proliferative effect. Remarkably, this inhibition occurred at non-cytotoxic concentrations, indicating that Z-ajoene levels were therapeutically appropriate. Additionally, Z-ajoene has been demonstrated to block the proliferation of human breast cancer cells by inducing apoptosis through increased peroxide production and the activation of caspase-3 and caspase-8 (Zhang et al., 2015).

ASEO toxicity

The United States Food and Drug Administration (FDA) has classified *Allium sativum* L. as generally safe to be consumed by humans. However, adverse effects still exist, particularly when ingested in large quantities or by individuals with heightened sensitivity (Rana et al., 2018). Consuming large amounts, especially when consumed in a fasting state, may disrupt intestinal flora, leading to gastrointestinal issues such as flatulence and other disorders.

Allicin is recognized for its ability to permeate cellular membranes. At a concentration of 200 mg/mL, allicin has been shown to cause significant damage to isolated rat liver cells. Excessive ASEO intake has also been associated with chronic conditions including gastroesophageal reflux disease, kidney hematoma,

and an increased risk of pemphigus, an autoimmune disorder (Yogeswari et al., 2020). Oil-soluble allicin is noted to be toxic at higher concentrations than its water-soluble counterpart. However, research by Hizam et al. (2019), found that a dose of 50 µg/mL of ASEO did not induce toxicity or pathological effects when administered to chicken embryos. This was supported by the absence of viral presence in the allantoic fluid of all treated groups.

To assess the toxicity of ASEO, various studies have employed the Brine Shrimp Lethality Test (BSLT). These studies indicate that the toxicity of ASEO depends on factors such as the extraction method, concentration, and garlic source (Waghulde et al., 2019). The LC_{50} is the concentration of essential oil required to kill 50% of brine shrimp larvae within 24 hours. Waghulde et al. (2019), reported LC_{50} values of 10,840 mg/mL for the alcohol extract and 8,180 mg/mL for *A. sativum* L. bulbs. The toxicity of these compounds was tested at concentrations of 1, 10, 100, and 1,000 ppm in a 10 mL seawater solution with 1% (v/v) DMSO. The findings demonstrated that *A. sativum* L. bulbs possess cytotoxic activity against brine shrimp, as evidenced by an LC_{50} value of less than 1,000 ppm or µg/mL, indicating the presence of potent active components.

Strengths and weaknesses of *A. sativum* L. essential oil (ASEO) in bioactivity research

Allium sativum L., widely recognized as a traditional medicinal ingredient, has been used across many cultures and healing systems worldwide (Mugao et al., 2020). Its therapeutic properties are primarily attributed to allicin, a sulfur-containing compound known for its strong antimicrobial effects against a broad spectrum of microorganisms, making garlic a potential natural remedy for various infectious diseases. The antimicrobial efficacy of allicin is linked to its reactive thiosulfinate group, which can interact with thiol-containing enzymes and proteins in microbial cells, leading to the inhibition of vital metabolic functions (Yasin et al., 2022).

ASEO is recognized for its beneficial properties, including antioxidant and anticancer effects (Tanrıkulu et al., 2017). Additionally, ASEO is extensively used in the food industry to enhance flavour and aroma and as a preservative. Despite promising bioactivities, the commercial application of ASEO faces several challenges. One major issue is the variability in chemical composition due to cultivar differences, climatic factors, and extraction procedures. Furthermore, its strong pungent odor and volatility can limit its acceptability in food and pharmaceutical formulations. Therefore, standardization protocols and formulation strategies, such as microencapsulation, nano-emulsion, and solid-lipid nanoparticles, are essential to enhance stability, solubility, and sensory compatibility. The active components of ASEO are highly susceptible to degradation when exposed to light, oxygen, heat, and humidity, which can diminish its dietary and medicinal value (Ezeorba et al., 2022).

ASEO exhibits low solubility in water, which can limit its efficacy in certain applications (Sallam et al., 2004). While ASEO offers numerous benefits, excessively high concentrations can produce a strong and pungent odour and taste, which may negatively impact its sensory qualities in food products. This poses a challenge in optimizing the use of ASEO to maintain its beneficial properties without compromising the taste and overall appeal of food products (Li et al., 2023).

Potential applications of ASEO in the pharmaceutical and nutraceutical industry

The encapsulation technique has been shown to offer a promising solution to the limitations of ASEO, particularly with regard to its solubility and stability. One promising approach involves the use of β-cyclodextrin (β-CD), whose hydrophobic cavity can protect and encapsulate the hydrophobic active components of ASEO, while its hydrophilic outer surface enhances the oil's solubility in water (Khoshtinat et al., 2016). This method significantly improves the utilization and stability of garlic essential oil.

Kumar et al. (2024), reported that encapsulating

ASEO extends its antibacterial effect for up to 265 days at room temperature without loss or decrease in efficacy. This finding underscores the potential of encapsulation to expand the applications of ASEO in various fields, including food preservation and therapeutic interventions targeting a wide range of microorganisms. Furthermore, ASEO contains beneficial compounds, such as DADS and DATS, which have demonstrated potent anticancer properties. However, their limited solubility and stability in aqueous environments pose challenges for their application (Tesfaye, 2021).

To address these challenges, the encapsulation of DADS and DATS within nanocapsules derived from hyaluronic acid derivatives has been investigated. This strategy has been shown to protect DADS and DATS from oxidative damage and adverse interactions with blood and digestive components. It also reduces red blood cell membrane lysis and enhances the stability of these compounds while preserving their biological function and anticancer activity (Souto et al., 2020). The nanoformulation has also demonstrated the ability to inhibit the migration of neoplastic cells, highlighting its potential therapeutic benefits. Improving the stability, delivery, and therapeutic efficacy of DADS and DATS. This encapsulation approach represents a promising advancement in cancer treatment (Yeung et al., 2020).

Research by Hazuka et al. (2021), employed nuclear magnetic resonance (^{1}H-NMR) to monitor the oxidation process of these compounds. The proposed nanocapsule delivery system could achieve higher blood concentrations, prolong circulation time, and enhance therapeutic outcomes. In conclusion, this study emphasizes the transformative potential of nanocapsulation in enhancing the therapeutic applications of DADS and DATS for cancer treatment.

Insight into bioactive compounds

Sulfur-containing compounds such as DATS, AMTS, and DADS are also found abundantly in *A. Sativum* L. essential oil, and it is has reported to exert inhibitory effects on acetylcholinesterase and possess strong antioxidant and antithrombotic properties (Mitra et al., 2022). These compounds are also prevalent in *A. sativum* L., supporting their critical role in the therapeutic mechanisms of ASEO.

The therapeutic efficacy of ASEO is largely attributed to its organosulfur compounds. Allicin, a major bioactive compound, exerts antimicrobial effects by reacting with thiol groups in microbial enzymes, leading to S-thioallylation and subsequent enzyme inactivation. This mechanism disrupts bacterial metabolism and membrane integrity. Similarly, DADS and DATS function through ROS generation and mitochondrial dysfunction, particularly in cancer cells, promoting apoptosis. Understanding these mechanisms is critical for advancing the clinical application of ASEO (Paiva et al., 2014).

Green extraction and future perspectives

In recent years, there has been a shift from classical, solvent-intensive approaches (e.g., long refluxes, hydrodistillation with large solvent/energy footprints) toward greener, more selective techniques for recovering ASEO and sulfur-rich compounds. The concept of "green extraction" is predicated on the principles of reducing solvent toxicity and volume, minimizing energy consumption, and enhancing extract quality by preserving labile molecules. These principles are summarized in foundational reviews of the field (Chemat et al., 2012).

Several particular technologies have demonstrated potential for ASEO and related bioactives. Enzyme-assisted pretreatments, which include cell-wall-degrading enzymes such as cellulases and pectinases, have been shown to enhance the release of oil and volatile sulfur compounds. When employed in conjunction with conventional distillation or steam treatments, these pretreatments often result in a twofold increase in yield. This phenomenon can be attributed to the enhanced disruption of tissue and the subsequent liberation of intracellular alliin/alliinase systems (Sowbhagya et al., 2009). The United Arab Emirates (UAE)

utilizes the process of cavitation to achieve several objectives, including the reduction of extraction time, the decrease of temperatures, and the enhancement of the recovery of thermolabile constituents such as allicin and other sulfur volatiles. Numerous optimization studies for garlic have reported higher allicin yields and faster processing times in comparison to maceration or simple solvent extraction methods (Mathialagan et al., 2017).

Natural deep eutectic solvents (NADES) and other green solvents have emerged as flexible media for extracting polar and semi-polar phytochemicals. These solvents are characterized by low toxicity and frequently exhibit biodegradability. NADES can be tuned (choice of hydrogen bond donors/acceptors) to selectively solubilize target compounds, and, when paired with UAE or enzyme treatment, have produced synergistic improvements in yield and bioactivity in recent experimental work. Preliminary studies and reviews suggest that NADES enhance extraction efficiency and stabilize sensitive metabolites during processing (Liu et al., 2018).

Beyond isolated method improvements, hybrid and intensified processes hold particular promise for industrial translation. Examples of such methods include combinations of ultrasound-NADES, enzyme-assisted hydrodistillation, and pressurized or SCF-CO2 extraction for non-polar fractions. The objective of these integrated workflows is to maximize the recovery of specific sulfur species (allicin, ajoene, DATS/DADS) while minimizing thermal degradation and off-odors (Ye et al., 2025). These integrated approaches have demonstrated the potential for enhanced extraction efficiency and reduced environmental impact (Bar et al., 2022). Life-cycle thinking and techno-economic assessments in green extraction literature underscore the necessity of substantiating environmental benefits on a large scale. Key variables in this regard include energy and solvent recycling, solvent toxicity, and downstream purification costs (Ye et al., 2025).

Consequently, future research endeavors aimed at sustainable ASEO production should prioritize the following areas: The first objective is to undertake systematic, head-to-head comparisons of green methods (UAE, enzyme-assisted, NADES, supercritical fluids) using standardized garlic feedstocks and analytical endpoints (profile and stability of sulfur species, bioactivity assays). The second objective is to optimize solvent formulations (NADES components, water content) that both extract and stabilize target volatiles. The third objective is to conduct scale-up studies with solvent recovery and energy balances to validate real-world sustainability claims. The fourth objective is to perform regulatory and toxicology screening of new solvent systems and residuals to ensure food/pharma compatibility. Addressing these areas will facilitate the translation of promising lab-scale gains into reliable, low-impact commercial ASEO products (Bar et al., 2022).

In short, green extraction offers multiple routes to improve yield, selectivity, and environmental footprint in garlic essential oil production-but the most impactful next steps are comparative, quantitative studies that link extraction conditions to the chemical identity and bioactivity of sulfur constituents, and to real-world metrics of sustainability (Chemat et al., 2012).

CONCLUSION

This review provides an integrative and up-to-date synthesis of the therapeutic potential, mechanistic pathways, and technological advancements related to ASEO. The originality of this review lies in its combined focus on bioactivity–mechanism relationships and green technological innovations for ASEO extraction and formulation. *A. sativum* L. Essential Oil (ASEO) has exhibited a range of potentially efficacious therapeutic activities, including anticancer, antibacterial, anti-inflammatory, antifungal, antiviral, and antioxidant properties. A review of the extant research reveals the potential for ASEO to serve as a pharmaceutical agent for a range of medical indications. The mechanisms of action of ASEO include its capacity to scavenge free radicals, thereby reducing oxidative

stress, and its effectiveness in disrupting microbial cell membranes, which contributes to its antibacterial and antifungal properties. Furthermore, ASEO has been shown to modulate inflammatory pathways and induce apoptosis in cancer cells, underscoring its potential as an anticancer agent. However, the development of faster and more efficient extraction methods is crucial to ensure the production of specific constituents. Additionally, further exploration is necessary to investigate the nutraceutical bioactivity of ASEO, encompassing its bioavailability and toxicity. In the future, the implementation of green extraction methods and encapsulation technologies offers a sustainable path to enhancing the therapeutic efficacy and industrial applicability of ASEO.

ACKNOWLEDGEMENTS

The authors would like to express their sincere gratitude to the Research and Community Service Unit (UPPM) of STIKes Ibnu Sina Ajibarang and the Indonesia Endowment Fund for Education (LPDP) for their financial and administrative support provided for this study. The authors also acknowledge G.B. Pant University of Agriculture and Technology, Pantnagar, India, for providing research facilities and technical assistance.

AUTHOR CONTRIBUTION STATEMENT

DALA and NNI design and concept the study, including methodology and analysis, design and editing MNA, writing and editing manuscript by NNI, DALA, MNA, DR. All authors have reviewed and approved the final version of the manuscript.

CONFLICT OF INTEREST

The authors declare that there is no conflict of interest.

REFERENCES

Alam, K., Hoq, O., & Uddin, S. (2016). Medicinal plant *Allium sativum*=A Review. *Journal of Medicinal Plants Studies*, *4*(6), 72–79. https://www.plantsjournal.com/archives/2016/vol4issue6/PartB/4-5-43-447.pdf

Alnomasy, S. F. (2021). *Allium sativum* Essential Oil Against Toxoplasma In vitro and in vivo Anti-Toxoplasma Effects of A*llium sativum* Essential Oil Against *Toxoplasma gondii* RH Strain. *Infection and Drug Resistance*, *14*, 5057–5068. https://doi.org/10.2147/IDR.S337905

Arreola, R., Quintero-Fabián, S., López-Roa, R. I., Flores-Gutiérrez, E. O., Reyes-Grajeda, J. P., Carrera-Quintanar, L., & Ortuño-Sahagún, D. (2015). Immunomodulation and Anti-Inflammatory Effects of Garlic Compounds. *Hindawi*, *2015*. https://doi.org/10.1155/2015/401630

Asif, M., Saleem, M., Saadullah, M., Sidra, H., Raghdaa, Y., & Zarzour, A. (2020). COVID - 19 and Therapy with Essential Oils having antiviral, Anti-inflammatory, and Immunomodulatory properties. *Inflammopharmacology*, *28*(5), 1153–1161. https://doi.org/10.1007/s10787-020-00744-0

Avato, P., Tursi, F., Vitali, C., Miccolis, V., Candido, V. (2000). Allylsulfide constituents of garlic volatile oil as antimicrobial agents. *Phytomedicine*, *7*(3), 239–243. https://doi.org/10.1016/S0944-7113(00)80010-0

Bajpai, V. K., Sharma, A., Kim, S. H., & Baek, K. H. (2015). Chemical composition, antioxidant, lipid peroxidation inhibition and free radical scavenging activities of microwave extracted essential oil from *Allium sativum*. *Journal of Essential Oil-Bearing Plants*, *18*(2), 300–313. https://doi.org/10.1080/0972060X.2013.764215

Bar, M., Binduga, U. E., & Szychowski, K. A. (2022). Methods of Isolation of Active Substances from Garlic (*Allium sativum* L.) and Its Impact on the Composition and Biological Properties of Garlic Extracts. *Antioxidants*, *11*(7). https://doi.org/10.3390/antiox11071345

Bazaraliyeva, A., Moldashov, D., Turgumbayeva, A., Kartbayeva, E., Kalykova, A., Sarsenova, L., & Issayeva, R. (2022). Chemical and biological properties of bioactive compounds from garlic (*Allium sativum*). *Pharmacia*, *69*(4), 955–964. https://doi.org/10.3897/pharmacia.93.e93604

Benkeblia, N., & Lanzotti, V. (2007). Allium Thiosulfinates : Chemistry , Biological Properties and their Potential Utilization in Food Preservation. *Food*, *1*(2).

Benmeziane, F., Djermoune-Arkoub, L., Adamou Hassan K., & Zaghad, H. (2018). Evaluation of antibacterial activity of aqueous extract and essential oil from garlic against some pathogenic bacteria. *International Food Research Journal*, *25*(2), 561-564.

Bhatwalkar, S. B., Mondal, R., Babu, S., Krishna, N., Adam, J. K., Govender, P., & Anupam, R. (2021). Antibacterial Properties of Organosulfur Compounds of Garlic (*Allium sativum*). *Frontiers in Microbiology*, *12*, 1–20. https://doi.org/10.3389/fmicb.2021.613077

Borlinghaus, J., Foerster, J., Kappler, U., Antelmann, H., Noll, U., Gruhlke, M. C. H., & Slusarenko, A. J. (2021). Allicin, the Odor of Freshly Crushed Garlic: A Review of Recent Progress in Understanding Allicin's Effects on Cells. *Molecules*, *26*(6), 1505. https://doi.org/10.3390/molecules26061505

Cavallito, C. J., & Bailey, J. H. (1944). Allicin, the Antibacterial Principle of *Allium sativum*. L. Isolation, Physical Properties and Antibacterial Action. *Research Laboratories of Winthrop Chemical*, *66*(11), 1950-1951. https://doi.org/10.1021/ja01239a048

Chemat, F., Vian, M. A., & Cravotto, G. (2012). Green extraction of natural products: Concept and principles. *International Journal of Molecular Sciences*, *13*(7), 8615–8627. https://doi.org/10.3390/ijms13078615

Corzo-Martínez, M., Corzo, N., & Villamiel, M. (2007). Biological properties of onions and garlic. *Trends in Food Science & Technology*, *18*(12), 609–625. https://doi.org/10.1016/j.tifs.2007.07.011

Cui, H., Yuan, L., Li, W., & Lin, L. (2016). Edible film incorporated with chitosan and *Artemisia annua* oil nanoliposomes for inactivation of *Escherichia coli* O157 : H7 on cherry tomato. *International Journal of Food Science and Technology*, *52*(3), 687-698. https://doi.org/10.1111/ijfs.13322

Dehariya, N., Guha, P., & Gupta, R. K. (2021). Extraction and characterization of essential oil of garlic (*Allium sativa* L.). *International Journal of Characterization of Essential Oil of Garlic (Allium Sativa L)*, *9*(1), 1455–1959. https://doi.org/10.22271/chemi.2021.v9.i1u.11426

Dharshini, H. P., & Devi, A. (2017). A Study on Extraction of Ajoene from *Allium sativum* And Its Applications. *Journal of Medicinal Plants Studies*, *5*(5), 111–116.

Douiri, L., Boughdad, A., Assobhei, O., & Moumni, M. (2013). Chemical composition and biological activity of *Allium sativum* essential oils against *Callosobruchus maculatus*. *IOSR Journal of Environmental Science, Toxicology, and Food Technology*, *3*(1), 30–36. https://doi.org/https://doi.org/10.9790/2402-0313036

Dziri, S., Casabianca, H., Hanchi, B., & Hosni, K. (2014). Composition of garlic essential oil (*Allium sativum* L.) as influenced by drying method. *Journal of Essential Oil Research*, *26*(2), 37–41. https://doi.org/10.1080/10412905.2013.868329

Ezeorba, T. P. C., Chukwudozie, K. I., Ezema, C. A., Anaduaka, E. G., Nweze, E. J., & Okeke, E. S. (2022). Potentials for health and therapeutic benefits of garlic essential oils: Recent findings and future prospects. *Pharmacological Research - Modern Chinese Medicine*, *3*. https://doi.org/10.1016/j.prmcm.2022.100075

Giordano, D., Facchiano, A., & Carbone, V. (2023). Food Plant Secondary Metabolites Antiviral Activity and Their Possible Roles in SARS-CoV-2 Treatment: An Overview. *Molecules, 28*(6), 2470. https://doi.org/10.3390/molecules28062470

Hassanzadeh, H., Alizadeh, M., Hassanzadeh, R., & Ghanbarzadeh, B. (2022). Garlic essential oil-based nanoemulsion carrier : Release and stability kinetics of volatile components. *Food Science and Nutrition*, *10*(5), 1613-1625. https://doi.org/10.1002/fsn3.2784

Hazuka, M. J., Kaminski, K., Kaczor-Kaminska, M., Szafraniec-Szczesny, J., Kmak, A., Kassassir, H.,… Zapotoczny, S. (2021). Hyaluronic Acid-Based Nanocapsules as Efficient Delivery Systems of Garlic Oil Active Components with Anticancer Activity. *Nanomaterials*, *11*(5), 1354. https://doi.org/10.3390/nano11051354

Herrera-Calderon, O., Chacaltana-Ramos, L. J., Carmen, I., Algarni, M. A., Alqarni, M., & Batiha, G. E. (2021). Chemical Constituents, In Vitro Antioxidant Activity and In Silico Study on NADPH Oxidase of *Allium sativum* L. (Garlic) Essential Oil. *Antioxidants*, *10*(11), 1844. https://doi.org/https://doi.org/10.3390/antiox10111844

Hizam, M. M., Al-Mubarak, F. T. M., & Al-Masoudi, W. A. (2019). Antiviral Efficacy of Garlic Oil Against Newcastle disease Virus. *Bas.J.Vet.Res*, *18*(2), 234–247.

Hu, Q., Gerhard, H., Upadhyaya, I., Venkitanarayanan, K., & Luo, Y. (2016). Antimicrobial eugenol nanoemulsion prepared by gum arabic and lecithin and evaluation of drying technologies. *International Journal of Biological Macromolecules*, *87*, 130-140. https://doi.org/10.1016/j.ijbiomac.2016.02.051

Huang, L., Liu, Z., Wang, J., Fu, J., Jia, Y., Ji, L., & Wang, T. (2023). Bioactivity and health effects of garlic essential oil: A review. *Food Science and Nutrition*, *11*(6), 2450–2470. https://doi.org/10.1002/fsn3.3253

Hussein, H. J., Hameed, I. H., & Hadi, M. Y. (2017). A Review : Anti-microbial , Anti-inflammatory effect and Cardiovascular effects of Garlic : *Allium sativum* A Review : Anti-microbial , Anti-inflammatory effect and Cardiovascular effects of Garlic : Allium sativum. *Research J. Pharm and Tech*, *10*(11), 4069-4078. https://doi.org/10.5958/0974-360X.2017.00738.7

Islam, F., Nath, N., Zehravi, M., Khan, J., Jashim, S. B. T., Charde, M. S.,…Wilairatana, P. (2023). Exploring the role of natural bioactive molecules in genitourinary cancers: how far has research progressed? *Natural Products and Bioprospecting*, *13*(1), 39. https://doi.org/10.1007/s13659-023-00400-4

Jeong, Y. Y., Ryu, J. H., Shin, J., Kang, M. J., & Kang, J. R. (2016). Comparison of Anti-Oxidant and Anti-Inflammatory Effects between Fresh and Aged Black Garlic Extracts. *Molecules*, *21*(4), 430. https://doi.org/10.3390/molecules21040430

Johnson, M. G., & Vaughn, R. H. (1969). Death of Salmonella typhimurium and Escherichia coli in the Presence of Freshly Reconstituted Dehydrated Garlic and Onion. *Applied Microbiology*, *17*(6), 903–905.

Khan, A., Ahmad, A., Akhtar, F., Yousuf, S., Xess, I., Khan, L. A., & Manzoor, N. (2010). Ocimum sanctum essential oil and its active principles exert their antifungal activity by disrupting ergosterol biosynthesis and membrane integrity. *Research in Microbiologoy*, *161*(10), 816–823. https://doi.org/10.1016/j.resmic.2010.09.008

Khoshtinat, K., Barzegar, M., Sahari, M. A., & Hamidi, Z. (2016). Comparison of antioxidant and antibacterial activities of free and encapsulated Garlic oil with beta-cyclodextrin. *Applied Food Biotechnology*, *3*(4), 254–268. https://doi.org/10.22037/afb.v3i4.12631

Kimbaris, A. C., Siatis, N. G., Daferera, D. J., Tarantilis, P. A., Pappas, C. S., & Polissiou, M. G. (2006). Comparison of distillation and ultrasound-assisted extraction methods for the isolation of sensitive aroma compounds from garlic (*Allium sativum*). *Ultrasonic Conochemistry*, *13*, 54–60. https://doi.org/10.1016/j.ultsonch.2004.12.003

Kumar, A., Singh, B. R., Prakash SN, J., Kumar, S., Bhagirathi, Ahuja, D.,…Singh, P. (2024). Study of antimicrobial efficacy of garlic oil loaded ethosome against clinical microbial isolates of diverse origin. *Journal of Herbal Medicine*, *43*, 100824. https://doi.org/10.1016/j.hermed.2023.100824

Lawrence, R., & Lawrence, K. (2011). Antioxidant activity of garlic essential oil (*Allium Sativum*) grown in north Indian plains. *Asian Pacific Journal of Tropical Biomedicine*, *1*(1), S51-S54. https://doi.org/10.1016/S2221-1691(11)60122-6

Lawson, L., Wang, Z., & Hughes, G. (1991). Identification and HPLC Quantitation of the Sulfides and Dialk (en) yl Thiosulfinates in Commercial Garlic Products. *Planta Med*, *57*(57), 363–370.

Li, S., Chen, J., Liu, Y., Qiu, H., Gao, W., Che, K.,…Hu, W. (2023). Characterization of garlic oil/β-cyclodextrin inclusion complexes and application. *Frontiers in Nutrition*, *10*, 1–12. https://doi.org/10.3389/fnut.2023.1308787

Liu, Y., Friesen, J. B., McAlpine, J. B., Lankin, D. C., Chen, S.-N., & Pauli, G. F. (2018). Natural Deep Eutectic Solvents: Properties, Applications, and Perspectives. *Journal of Natural Products*, *81*(3), 679–690. https://doi.org/10.1021/acs.jnatprod.7b00945

Ma, L., & Yao, L. (2020). Antiviral Effects of Plant - Derived Essential Oils and Their Components : An Updated Review. *Molecules*, *25*(11), 2627. https://doi.org/10.3390/molecules25112627

Mabe, G., & Bottini, S. (2014). Extraction of Garlic Oil With Quasi-Critical Solvents Extraction of Garlic Oil With Quasi-Critical Solvents. *Mercosur Congress on Chemical Enggineering*, 1–9.

Mai, N. T., Dung, D. T., Nga, T. T., Xuan, V. T., Doan, V. V., Tai, B. H.,…Kim, S. H. (2020). Triterpenoid glycosides from the rhizomes of *Allium ascalonicum* and their anoctamin-1 inhibitory activity Triterpenoid glycosides from the rhizomes of *Allium ascalonicum* and their anoctamin-1 inhibitory activity. *Natural Product Research*, *35*(22), *4338-4346.* https://doi.org/10.1080/14786419.2020.1713122

Mathialagan, R., Mansor, N., Shamsuddin, M. R., Uemura, Y., & Majeed, Z. (2017). Optimisation of Ultrasonic-Assisted Extraction (UAE) of Allicin from Garlic (*Allium sativum* L.). *Chemical Engineering Transactions*, *56*(2017), 1747–1752. https://doi.org/10.3303/CET1756292

Mitra, S., Das, R., Emran, T. B., Labib, R. K., Tabassum, N. E., Islam, F.,…Wilairatana, P. (2022). Diallyl Disulfide : A Bioactive Garlic Compound with Anticancer Potential. *Frontiers in Pharmacology*, *13*, 1–21. https://doi.org/10.3389/fphar.2022.943967

Mösbauer, K., Fritsch, V. N., Adrian, L., Bernhardt, J., Gruhlke, M. C. H., Slusarenko, A. J.,…Antelmann, H. (2021). The Effect of Allicin on the Proteome of SARS-CoV-2 Infected Calu-3 Cells. *Frontiers in Microbiology*, *12*. https://doi.org/10.3389/fmicb.2021.746795

Mnayer, D., Fabiano-Tixier, A.-S., Petitcolas, E., Hamieh, T., Nehme, N., Ferrant, C., Fernandez, X., & Chemat, F. (2014). Chemical Composition, Antibacterial and Antioxidant Activities of Six Essentials Oils from the Alliaceae Family. *Moleculs*, *19*(12), 20034–20053. https://doi.org/10.3390/molecules191220034

Mugao, L. G., Gichimu, B. M., Muturi, P. W., & Mukono, S. T. (2020). Characterization of the Volatile Components of Essential Oils of Selected Plants in Kenya. *Biochemistry Research International, 2020*(1). https://doi.org/10.1155/2020/8861798

Nakamoto, M., Kunimura, K., Suzuki, J., & Kodera, Y. (2019). Antimicrobial properties of hydrophobic compounds in garlic: Allicin, vinyldithiin, ajoene and diallyl polysulfides (Review). *Experimental and Therapeutic Medicine*, *19*(2), 1550–1553. https://doi.org/10.3892/etm.2019.8388

O'Gara, E. A. O., Hill, D. J., Maslin, D.J. (2000). Activities of Garlic Oil , Garlic Powder , and Their Diallyl Constituents against Helicobacter pylori. *Applied and Envieromental Microiology*, *66*(5), 2269–2273. https://doi.org/https://doi.org/10.1128/aem.66.5.2269-2273.2000

Okoh, O. O., Sadimenko, A. P., & Afolayan, A. J. (2010). Comparative evaluation of the antibacterial activities of the essential oils of *Rosmarinus officinalis* L. obtained by hydrodistillation and solvent free microwave extraction methods. *Food Chemistry*, *120*(1), 308–312. https://doi.org/10.1016/j.foodchem.2009.09.084

Paiva, A., Craveiro, R., Aroso, I., Martins, M., Reis, R. L., & Duarte, A. R. C. (2014). Natural deep eutectic solvents - Solvents for the 21st century. *ACS Sustainable Chemistry and Engineering*, *2*(5), 1063–1071. https://doi.org/10.1021/sc500096j

Prakash, B., Kedia, A., Mishra, P. K., Dwivedy, A. K., & Dubey, N. K. (2015). Assessment of chemically characterised *Rosmarinus officinalis* L . essential oil and its major compounds as plant-based preservative in food system based on their efficacy against food-borne moulds anf aflatoxin secretion and as antioxidant. *International Journal of Food Science and Technology*, *50*(8), 1792–1798. https://doi.org/10.1111/ijfs.12822

Pyun, M. -S., & Shin, S. (2006). Antifungal effects of the volatile oils from Allium plants against Trichophyton species and synergism of the oils with ketoconazole. *Phytomedicine*, *13*(6), 394–400. https://doi.org/10.1016/j.phymed.2005.03.011

Qiu, Y., Chen, X., & Shi, W. (2020). Impacts of social and economic factors on the transmission of coronavirus disease 2019 (COVID-19) in China. *Journal of Population Economics*, *33*(4), 1127–1172. https://doi.org/10.1007/s00148-020-00778-2

Rafe, A., & Nadjafi, M. S. (2017). Physicochemical Characteristics of Garlic (*Allium sativum L.*) Oil : Effect of extraction procedure. *International Journal of Nutrition and Food Sciences*, *3*(6-1), 1–5. https://doi.org/10.11648/j.ijnfs.s.2014030601.11

Rana, S. V, Pal, R., Vaiphei, K., Sharma, S. K., & Ola, R. P. (2018). Garlic in health and disease Nutrition Research Reviews. *Nutrition Research Revieus*, *24*(1), 60–71. https://doi.org/10.1017/S0954422410000338

Rohani, S. M. R., Moradi, M., Mehdizadeh, T., Saei-Dehkordi, S. S., & Griffiths, M. W. (2011). LWT - Food Science and Technology The effect of nisin and garlic (*Allium sativum* L.) essential oil separately and in combination on the growth of Listeria monocytogenes. *LWT - Food Science and Technology*, *44*(10), 2260–2265. https://doi.org/10.1016/j.lwt.2011.07.020

Sallam, K. I., Ishioroshi, M., & Samejima, K. (2004). Antioxidant and antimicrobial effects of garlic in chicken sausage. *Lwt*, *37*(8), 849–855. https://doi.org/10.1016/j.lwt.2004.04.001

Sasi, M., Kumar, S., Kumar, M., Thapa, S., Prajapati, U., Tak, Y.,…Mekhemar, M. (2021). Garlic (*Allium sativum* L.) Bioactives and Its Role in Alleviating Oral Pathologies. *Antioxidants*. *10*(11), 1847 https://doi.org/https://doi.org/10.3390/antiox10111847

Satyal, P., Craft, J. D., Dosoky, N. S., & Setzer, W. N. (2017). The Chemical Compositions of the Volatile Oils of Garlic (*Allium sativum*) and Wild Garlic (*Allium vineale*). *Foods*, *6*(8), 63. https://doi.org/10.3390/foods6080063

Sela, U. R. I., Ganor, S., Hecht, I., Brill, A., Miron, T., Rabinkov, A.,…Hershkoviz, R. (2004). Allicin inhibits SDF-1α-induced T cell interactions with fibronectin and endothelial cells by down-regulating cytoskeleton rearrangement, Pyk-2 phosphorylation and VLA-4 expression. *Immunology*, *111*(4), 391–399. doi: 10.1111/j.0019-2805.2004.01841.x

Shang, A., Cao, S.-Y., Xu, X.-Y., Gan, R.-Y., Tang, G.-Y., Corke, H., Mavumengwana, V., & Li, H.-B. (2019). Bioactive Compounds and Biological Functions of Garlic (*Allium sativum* L.). *Foods*, *8*(7), 246. https://doi.org/https://doi.org/10.3390/foods8070246

Souto, E. B., Silva, G. F., Dias-Ferreira, J., Zielinska, A., Ventura, F., Durazzo, A.,…Santini, A. (2020). Nanopharmaceutics : Part II — Production Scales and Clinically Compliant Production Methods. *Nanomaterials*, *10*(3), 455. https://doi.org/https://doi.org/10.3390/nano10030455

Sowbhagya, H. B., Purnima, K. T., Florence, S. P., Appu Rao, A. G., & Srinivas, P. (2009). Evaluation of enzyme-assisted extraction on quality of garlic volatile oil. *Food Chemistry*, *113*(4), 1234–1238. https://doi.org/10.1016/j.foodchem.2008.08.011

Staba, E. J., Lash, L., & Staba, J. E. (2018). A Commentary on the Effects of Garlic Extraction and Formulation on Production Composition. *The Journal of Nutrition, 131*(3), 1118S-1119S. https://doi.org/https://doi.org/10.1093/jn/131.3.1118S

Subudhi, R. N., Poonia, N., Singh, D., & Arora, V. (2024). Natural approaches for the management of ulcerative colitis: evidence of preclinical and clinical investigations. *Natural Products and Bioprospecting*, *14*(1). https://doi.org/10.1007/s13659-024-00463-x

Sun, Y., Wang, Y., Han, L. R., Zhang, X., & Feng, J. T. (2017). Antifungal Activity and Action Mode of Cuminic Acid from the Seeds of *Cuminium cyminum* L. against *Fusarium oxysporum* f . sp. Niveum (FON) Causing Fusarium Wilt on Watermelon. *Molecule*, *22*(12), 2053. https://doi.org/10.3390/molecules22122053

Tanrıkulu, C. Ş., Tanrikulu, Y., Kılınç, F., Bahadır, B., Can, M., & Köktürk, F. (2017). Beneficial effects of garlic (*Allium sativum*) oil in experimental corrosive esophageal burns effects of garlic oil in esophageal burns. *Ulusal Travma ve Acil Cerrahi Dergisi*, *23*(3), 181–187. https://doi.org/10.5505/tjtes.2016.64509

Tesfaye, A. (2021). Revealing the Therapeutic Uses of Garlic (*Allium sativum*) and Its Potential for Drug Discovery. *Hindawi*, *2021*(1). https://doi.org/10.1155/2021/8817288

Thuy, B. T. P., My, T. T. A., Hai, N. T. T., Hieu, L. T., Hoa, T. T., Loan, H. T. P.,…Nhung, N. T. A. (2020). Investigation into SARS-CoV-2 Resistance of Compounds in Garlic Essential Oil. *ACS Omega*, *5*(14), 8312-8320.

Torpol, K., Wiriyacharee, P., Sriwattana, S., Sangsuwan, J., & Prinyawiwatkul, W. (2018). Antimicrobial activity of garlic (*Allium sativum* L.) and holy basil (*Ocimum sanctum* L.) essential oils applied by liquid vs vapour phases. *International Journal of Food Science and Technology*, *53*(9), 2119–2128. https://doi.org/10.1111/ijfs.13799

Tsai, C. W., Chen, H. W., Sheen, L. Y., & Lii, C. K. (2012). Garlic: Health benefits and actions. *BioMedicine (Netherlands)*, *2*(1), 17–29. https://doi.org/10.1016/j.biomed.2011.12.002

Upadhyay, R. K. (2017). Nutritional and Therapeutic Potential of Allium Vegetables. *Journal of Nutritional Therapeutics*, *6*(1), 18–37. https://doi.org/10.6000/1929-5634.2017.06.01.3

Ushijima, M., Takashima, M., Kunimura, K., Kodera, Y., Morihara, N., & Tamura, K. (2018). Effects of S-1-propenylcysteine, a sulfur compound in aged garlic extract, on blood pressure and peripheral circulation in spontaneously hypertensive rats. *Journal of Pharmacy and Pharmacology*, *70*(4), 559–565. https://doi.org/10.1111/jphp.12865

Valls, R. M., Companys, J., Calderón-Pérez, L., Salamanca, P., Pla-Pagà, L.,…Solà, R. (2022). Effects of an Optimized Aged Garlic Extract on Cardiovascular Disease Risk Factors in Moderate Hypercholesterolemic Subjects: A Randomized, Crossover, Double-Blind, Sustainedand Controlled Study. *Nutrients*, *14*(3), 405. https://doi.org/https://doi.org/10.3390/nu14030405

Verma, K., & Srivastava, M. (2020). Antibacterial finishing of cotton fabric with clove oil microcapsules. *Asian J. Home Sci., 15*(2), 330–335. https://doi.org/10.15740/HAS/AJHS/15.2/330-335

Verma, T., Aggarwal, A., Dey, P., Chauhan, A. K., Rashid, S., Chen, K. T., & Sharma, R. (2023). Medicinal and therapeutic properties of garlic, garlic essential oil, and garlic-based snack food: An updated review. *Frontiers in Nutrition*, *10*, 1–16. https://doi.org/10.3389/fnut.2023.1120377

Waghulde, S., Bhoir, A., Gholap, J., Patil, V., Kale, M. K., & Patil, V. R. (2019). Cumulative Effect of the Aqueous and Ethanolic Extracts of Annona Reticulate and *Allium Sativumon* Brine Shrimp Lethality Assay. *Proceedings*, *41*(1), 36. https://doi.org/10.3390/ecsoc-23-06698

Wang, Y., Wei, K., Han, X., Zhao, D., Zheng, Y., Chao, J.,…Zhang, C. -S. (2019). The Antifungal Effect of Garlic Essential Oil on *Phytophthora nicotianae* and the Inhibitory Component Involved. *Biomolecul*, *9*(10), 632. https://doi.org/https://doi.org/10.3390/biom9100632

Wit, J. C. D. E., Notermans, S., Gorin, N., & Kampelmacheri, E. H. (1979). Effect of Garlic Oil or Onion Oil on Toxin Production by *Clostridium botulinum* in Meat Slurry. *Journal of Food Protection*, *42*(3), 222–224. https://doi.org/10.4315/0362-028X-42.3.222

Yasin, G., Jasim, S. A., Mahmudiono, T., Al-Shawi, S. G., Shichiyakh, R. A., Shoukat, S.,…Fenjan, M. (2022). Investigating the effect of garlic (*Allium sativum*) essential oil on foodborne pathogenic microorganisms. *Food Science and Technology (Brazil)*, *42*, 1–6. https://doi.org/10.1590/FST.03822

Ye, L., Wan, H., Lu, Y., Yang, J., He, Y., Wan, H., & Li, C. (2025). Natural deep eutectic solvent-ultrasonic-enzyme combination assisted extraction: Establishment of an integrated method and application on Astragalus polysaccharides. *Sustainable Chemistry and Pharmacy*, *46*, 102049. https://doi.org/https://doi.org/10.1016/j.scp.2025.102049

Yeung, A. W. K., Souto, E., Durazzo, A., Lucarini, M., Novellino, E., Tewari, D.,…Santini, A. (2020). Big Impact of Nanoparticles: Analysis of The Most Cited Nanopharmaceuticals and Nanonutraceuticals Research. *Current Research in Biotechnology*, *2*, 53-63. https://doi.org/10.1016/j.crbiot.2020.04.002

Yogeswari, S., Bindu, K. H., Kamalraj, S., Ashokkumar, V., & Jayabaskaran, C. (2020). Antidiabetic, Antithrombin and Cytotoxic bioactive compounds in five cultivars of *Piper betle* L. *Environmental Technology and Innovation*, *20*, 101140. https://doi.org/10.1016/j.eti.2020.101140

Zhang, X., Zhu, Y., Duan, W. E. I., Feng, C., & He, X. (2015). Allicin induces apoptosis of the MGC-803 human gastric carcinoma cell line through the signaling pathway. *Molecular Medicine Reports*, *11*(4), 2755–2760. https://doi.org/10.3892/mmr.2014.3109

Zugaro, S., Benedetti, E., & Caioni, G. (2023). Garlic (*Allium sativum* L.) as an Ally in the Treatment of Inflammatory Bowel Diseases. *Current Issues in Molecular Biology*, *45*(1), 685–698. https://doi.org/https://doi.org/10.3390/cimb45010046

FABAD J. Pharm. Sci., 51, 1, 327-350, 2026
Doi: 10.55262/fabadeczacilik.1729218
REVIEW ARTICLE

Tailored Polymers in Therapeutics: Bridging Drug Delivery and Biomedical Engineering

Manjeet KAUR[*], Lakhvir KAUR[**°], Gurjeet SINGH[***], Lovepreet SINGH[****], RK DHAWAN[*****], Navdeep KAUR[******], Manbir KAUR[*******], Peeyush SHARMA[********]

Tailored Polymers in Therapeutics: Bridging Drug Delivery and Biomedical Engineering

SUMMARY

Polymers have revolutionized the pharmaceutical and biomedical landscape by serving as adaptable and multifunctional materials in advanced drug delivery systems, tissue engineering, implants, and regenerative medicine. Their chemical versatility and tunable physicochemical properties enable precise control over drug release profiles, targeting, and biocompatibility, significantly enhancing therapeutic efficacy and patient compliance. Initially used as inert excipients, polymers have evolved into dynamic carriers that address formulation challenges such as poor solubility, instability, and non-specific biodistribution. Notably, polymer-based nanoparticles and hydrogels offer site-specific, controlled drug delivery with reduced systemic toxicity. Biodegradable polymers, particularly in injectable and implantable systems, eliminate the need for removal procedures, thereby improving patient safety. Innovations such as polymer-drug conjugates, programmable microdevices, and 3D-printed scaffolds are pushing the boundaries of precision therapeutics. Synthetic polymers offer consistency and thermal stability, while natural polymers provide superior biocompatibility and biodegradability, making their combined use highly effective. Despite the promising advancements, challenges remain in scalability, cost-efficiency, and long-term safety. Continued interdisciplinary research is crucial for addressing these hurdles. Looking forward, polymers are poised to play a pivotal role in the development of sustainable and smart drug delivery platforms, aligning with the goals of precision and personalized medicine. This review highlights the transformative role of polymers in current pharmaceutical innovations and future applications, underscoring their potential to reshape therapeutic strategies.

Keywords: *Smart polymers, hydrogels, tissue engineering, controlled release, 3d printed implants, regenerative medicine*

Terapötiklerde Özelleştirilmiş Polimerler: İlaç Taşıma ve Biyomedikal Mühendisliği Arasındaki Köprü

ÖZ

Polimerler, ilaç ve biyomedikal alanında ileri düzey ilaç taşıma sistemleri, doku mühendisliği, implantlar ve rejeneratif tıpta çok yönlü ve uyarlanabilir malzemeler olarak devrim yaratmıştır. Kimyasal çeşitlilikleri ve ayarlanabilir fizikokimyasal özellikleri sayesinde ilaç salım profilleri, hedefleme ve biyouyumluluk üzerinde hassas kontrol sağlanarak terapötik etkinlik ve hasta uyumu büyük ölçüde artırılmıştır. Başlangıçta inert yardımcı maddeler olarak kullanılan polimerler, kötü çözünürlük, kimyasal dengesizlik ve özgül olmayan biyodağılım gibi formülasyon zorluklarını aşabilen dinamik taşıyıcılara dönüşmüştür. Özellikle polimer bazlı nanoparçacıklar ve hidrojeller, sistemik toksisiteyi azaltırken hedefe yönelik ve kontrollü ilaç salımı sunar. Özellikle enjekte edilebilir ve implante edilebilir sistemlerde kullanılan biyobozunur polimerler, çıkarılma ihtiyacını ortadan kaldırarak hasta güvenliğini artırır. Polimer-ilaç konjugatları, programlanabilir mikrocihazlar ve 3B yazıcıyla üretilmiş iskeletler ve sürdürülebilir polimer yaklaşımları, hassas tedavi yaklaşımlarının sınırlarını zorlamaktadır. Sentetik polimerler tutarlılık ve ısıl stabilite sunarken, doğal polimerler üstün biyouyumluluk ve biyobozunurluk özellikleriyle dikkat çeker; bu nedenle birlikte kullanımları oldukça etkilidir. Tüm bu umut verici gelişmelere rağmen, üretim ölçeklenebilirliği, maliyet etkinliği ve uzun vadeli güvenlik konularında bazı zorluklar devam etmektedir. Bu engellerin aşılması için disiplinlerarası araştırmaların sürdürülmesi gereklidir. Geleceğe bakıldığında, polimerler sürdürülebilir ve akıllı ilaç taşıma platformlarının geliştirilmesinde kritik bir rol oynamaya adaydır ve bu durum hassas ve kişiselleştirilmiş tıbbın hedefleriyle örtüşmektedir. Bu derleme, polimerlerin güncel farmasötik yeniliklerdeki dönüştürücü rolünü ve gelecekteki uygulamalarını vurgulayarak, tedavi stratejilerini yeniden şekillendirme potansiyelini ortaya koymaktadır.

Anahtar Kelimeler: *Akıllı polimerler, hidrojeller, doku mühendisliği, kontrollü salım, 3B baskılı implantlar, rejeneratif tıp*

Recieved: 30.06.2025
Revised: 11.01.2026
Accepted: 29.01.2026

[*] ORCID: 0000-0001-8977-398X, Department of Pharmaceutics, Khalsa College of Pharmacy, Amritsar, 143001
[**] ORCID: 0000-0001-8091-2365, School of Pharmaceutical Sciences, CT University, Ludhiana, Punjab, 142024
[***] ORCID: 0000-0003-4399-4693, Department of Pharmaceutics, ASBASJSM College of Pharmacy, Ropar, Punjab, 140111
[****] ORCID: 0000-0003-3217-9431, Department of Pharmaceutics, Khalsa College of Pharmacy, Amritsar, 143001
[*****] ORCID: 0000-0002-8587-6807, Department of Pharmacology, Khalsa College of Pharmacy, Amritsar, 143001
[******] ORCID: 0000-0002-6213-4640, Department of Chemistry, Khalsa College, Amritsar, Punjab, 143001
[*******] ORCID: 0009-0007-3851-6335, Department of Pharmaceutics, Khalsa College of Pharmacy, Amritsar, 143001
[********] ORCID: 0000-0002-1025-830X, Department of Pharmachemistry, Khalsa College of Pharmacy, Amritsar, 143001

[°] Corresponding Author; Dr. Lakhvir Kaur
E-mail: lakhvir86@gmail.com

INTRODUCTION

Polymers have emerged as cornerstone materials in biomedical and pharmaceutical advancements, underpinning innovations in drug delivery, tissue engineering, ophthalmic systems, implants, prosthetics, and regenerative medicine (El-Tanani et al., 2025; Lu, Cai, & Hu, 2024). Their remarkable chemical versatility and structural diversity enable the development of sophisticated delivery systems that prioritize therapeutic efficacy and patient well-being. The integration of polymer science with pharmaceutical research has reshaped formulation strategies, fostering precision in therapeutic interventions and elevating patient outcomes (Bharathy & Thanikachalam, 2024; Shergujri et al., 2025).

Despite the broad adoption of polymeric materials, a clear knowledge gap remains.While extensive reviews catalogue polymer platforms, fewer articulate how emerging polymeric systems are converging with digital design, smart implants, and next-generation manufacturing to address unmet therapeutic needs (Yue et al., 2025). In particular, the rapid advances in polymeric microneedles for transdermal and long-acting delivery (Chen et al., 2025; Mahajan et al., 2021; Meng et al., 2024), bioresorbable polymeric implants for tissue repair (Dobrzyńska-Mizera et al., 2024; Yu et al., 2023), and computer-assisted polymer design (Chou et al., 2025; Gao et al., 2024; Singh et al., 2020; Yue et al., 2025; Zhou et al., 2025) remain underreview in an integrated manner. Hence, this review aims to critically map and synthesize the state-of-the-art in advanced polymer platforms,focusing on how tailored polymeric materials, smart manufacturing, and multifunctional system design are enabling the next frontier of therapeutic delivery and regenerative medicine (Long et al., 2025; Nosrati & Nosrati, 2023; Son et al., 2024). By doing so, the review contributes to existing literature by delineating emerging trends, comparing traditional versus modern polymer approaches, and identifying future directions for translational research.

These macromolecules can be tailored to exhibit a spectrum of physicochemical properties by adjusting chain length, functional groups, and molecular interactions. Such adaptability allows precise control over surface and bulk characteristics to meet specific delivery goals (Chemban et al., 2022; Singh et al., 2022). Polymers serve diverse functions, including forming films, modulating rheology, enabling pH-dependent solubility, enhancing solubility, supporting sustained-release gelling, enhancing adhesion, and creating protective barriers—all of which optimize drug kinetics, stability, and safety (Alavi et al., 2024; Al-Sahlawi et al., 2024; Long et al., 2025; Nunziata et al., 2025).

Originally employed as inert excipients, polymers have evolved into dynamic carriers that address critical formulation challenges such as poor aqueous solubility, chemical instability, and non-specific biodistribution (Geszke-Moritz & Moritz, 2024; Singh et al., 2023). Their capacity to encapsulate fragile compounds and direct them to specific sites has transformed therapeutic approaches.

Notably, polymer-based nanoparticles and hydrogels have shown exceptional promise for targeted and controlled drug release, reducing systemic exposure while enhancing treatment accuracy. Bioresponsive polymers, which respond to physiological cues like pH, temperature, or enzymatic activity, mark a significant advance toward intelligent, patient-specific delivery systems (El-Tanani et al., 2025; Quader et al., 2022). Biodegradable polymers stand out for their ability to provide sustained release while being naturally metabolized or excreted, minimizing risks associated with long-term residue accumulation (Bachhav et al., 2025; Farjaminejad et al., 2024; Kurowiak et al., 2023; Ogay et al., 2020). These materials are particularly valuable in injectable and implantable systems, where durability and biocompatibility are paramount (Lu et al., 2025; Quader et al., 2022; Sharma et al., 2024).

Emerging developments now extend into polymeric microneedle systems for long-acting delivery and wearable diagnostics; recent reviews highlight the mechanisms, materials, and clinical applications of polymeric microneedles (Chen et al., 2025; Meng et al., 2024). Computer-assisted polymer design, leveraging artificial intelligence and machine learning, is accelerating the formulation of high-performance polymeric materials with tailored properties (Gao et al., 2024; Yue et al., 2025). In parallel, smart bioresorbable polymer implants enable structural repair combined with drug release and sensor integration, creating multifunctional therapeutic platforms (Dobrzyńska-Mizera et al., 2024; Heidari et al., 2024; Yu et al., 2023). These innovations reflect a paradigm shift—from traditional polymer use toward integrated, data-driven, and responsive polymer-therapeutic systems.

Synthetic and natural polymers each offer unique strengths. Synthetic variants are prized for their thermal stability, reproducibility, and processability, while natural polymers excel in biocompatibility and degradability (González et al., 2023; Meng et al., 2024). Together, they enable functions such as improving drug solubility and bioavailability through hydrogels and microparticles, refining drug distribution via nanoparticle carriers, delivering biomolecules to targeted sites, solubilizing hydrophobic drugs through micelle formation, enabling stimuli-responsive release, masking unpleasant tastes, and creating mechanically robust nanocomposites. Despite these advances, challenges persist, including scalability, production costs, regulatory hurdles, and potential long-term toxicity. Overcoming these hurdles will demand interdisciplinary collaboration, standardized data systems, and sustained innovation (Mukherjee et al., 2023; Nanda et al., 2022).

Looking ahead, polymers will remain pivotal in shaping the future of pharmaceuticals. Their evolving capabilities hold promise for advancing personalized therapeutics, sustainable drug delivery platforms, and integrated biotechnological systems, aligning with the growing needs of precision medicine (Dallaev, 2025; Huang et al., 2019; Rezaei et al., 2021).

HISTORICAL EVOLUTION OF POLYMERS IN BIOMEDICAL APPLICATIONS

The use of polymers in medicine dates back millennia, with natural polymers integral to traditional herbal remedies. Modern pharmacognosy has since advanced our understanding of these natural macromolecules, elucidating their mechanisms and therapeutic potential (Bhatia, 2016). This historical foundation has paved the way for the sophisticated integration of polymers into contemporary biomedical and pharmaceutical applications.

Emergence of synthetic polymers

The advent of synthetic polymers marked a transformative era in medical science, aligning with the birth of polymer science in the early 20th century. Hermann Staudinger's pioneering work in the 1920s established polymers as macromolecules, demonstrating their high molecular weight through physicochemical studies of rubber (Staudinger, 1920). His insights laid the intellectual groundwork for polymer science, earning him the Nobel Prize in 1953, a year that also saw the elucidation of DNA's structure, underscoring the broader significance of macromolecular science (Staudinger, 1953; Watson & Crick, 1953). Concurrently, Wallace Carothers' experiments in 1929 leveraged organic chemistry to synthesize polymers, further solidifying the field's foundations (Carothers, 1929). These milestones catalyzed the development of synthetic, water-soluble polymers as both therapeutic agents and components of drug delivery systems.

Polymer applications in wartime and beyond

The utility of synthetic polymers became particularly evident during World War II, with materials like polyvinylpyrrolidone finding widespread use in healthcare. This period also marked the introduction of polymer-drug conjugates, heralding the era of biologically active polymers. By the 1960s, efforts

to explore polymers as anticancer agents gained momentum, though early trials were hindered by toxicity concerns (Duncan et al., 2005). Despite these challenges, the groundwork laid during this time proved instrumental for subsequent innovations.

Foundations of modern polymer therapeutics

The 1970s ushered in a focused effort to design polymer-based therapeutics with tailored chemical and biological properties. This era saw the development of polymer-protein and polymer-drug conjugates, which have since become central to therapeutic strategies. A significant milestone came in 1994 with the introduction of the first synthetic polymer-drug conjugate for cancer therapy, combining hydroxypropyl methacrylate (HPMA) with doxorubicin (Duncan et al., 2005). The early 2000s marked further progress, with regulatory approvals for polymer-protein conjugates like PEG-interferon-α for chronic hepatitis and PEG-GCSF as a colony-stimulating agent. Additionally, polymer-based nanoparticles, such as paclitaxel-loaded systems, gained approval for treating metastatic breast cancer, highlighting the growing impact of polymers in precision therapeutics (Gandhi et al., 2012; Wang & Chang, 2023).

This historical progression—from ancient natural remedies to cutting-edge synthetic polymer conjugates—illustrates the dynamic evolution of polymers in medical science. This development embodies a synergy between scientific discovery and clinical innovation, laying a strong foundation for future advancements in polymer-based therapeutics.

RECENT ADVANCES IN BIOMEDICAL POLYMER APPLICATIONS

Polymers have become indispensable in modern biomedical applications, driving innovations in drug delivery, tissue engineering, and nanomedicine. Their chemical and structural versatility enables the design of tailored systems that improve therapeutic precision and patient outcomes across multiple delivery routes and clinical use cases. Recent work emphasizes not only novel materials but also manufacturing strategies such as 3D printing, electrospinning, and microfluidics, alongside design paradigms like stimuli-responsiveness, multi-functionality, and materials informatics, which together elevate polymer platforms from passive carriers to active, adaptive therapeutic systems (Clegg et al., 2024; Lu, Cai, & Hu, 2024).

Advanced polymeric drug delivery systems

Advanced polymeric drug delivery systems encompass far more than gastrointestinal targeting; they represent a platform technology for transporting therapeutic agents to a wide array of anatomical sites using tailored polymer architectures (Waqar et al., 2024; Zhang & Tian et al., 2024). Natural polymers like chitosan, alginate, pectin, xanthan, and guar gum have long been central to gastroretentive and mucoadhesive systems due to their inherent biocompatibility, ability to adhere to biological tissues, and safety profile (Harun-Or-Rashid et al., 2023; Turac et al., 2024). However, recent advances highlight the shift toward multifunctional systems, combining natural and synthetic polymers with nanomaterials, to address diverse therapeutic needs far beyond the gastric environment (Bachhav et al., 2025). Hybrid polymer matrices often integrating biodegradable synthetic elements like PLGA, polycaprolactone, and nanofibers are engineered for enhanced mechanical strength, controlled and responsive release, and compatibility with a variety of delivery routes, including transdermal, pulmonary, and ocular applications (Geszke-Moritz & Moritz, 2024; Shergujri et al., 2025). For example, polymeric microneedle arrays and patches, often made with smart blends of synthetic and natural polymers, now enable minimally invasive transdermal delivery of proteins, vaccines, and long-acting small molecules (Meng et al., 2024; Wang et al., 2022). In pulmonary delivery, polymeric nanoparticles and microparticles provide extended airway residence and targeted lung transport, with engineered release profiles and minimal toxicity (Mukherjee et al., 2023). In ocular and intranasal formulations, mucoadhesive

polymer-based hydrogels prolong drug retention time on mucosal surfaces and enhance therapeutic efficacy in eye and central nervous system diseases (Lu et al., 2024; Shergujri et al., 2025). For tumor and tissue targeting, polymers are tailored for stealth coating and ligand-mediated active targeting, exemplified by polymer-drug conjugates and nanocarriers loaded with chemotherapeutics or gene-editing agents (Geszke-Moritz & Moritz, 2024). Gene delivery is rapidly evolving through polymeric vectors, which protect nucleic acids from enzymatic degradation and facilitate cellular uptake, often utilizing biodegradable and stimuli-responsive carriers for enhanced safety and efficacy (Dallaev, 2025) (Figure 1.).

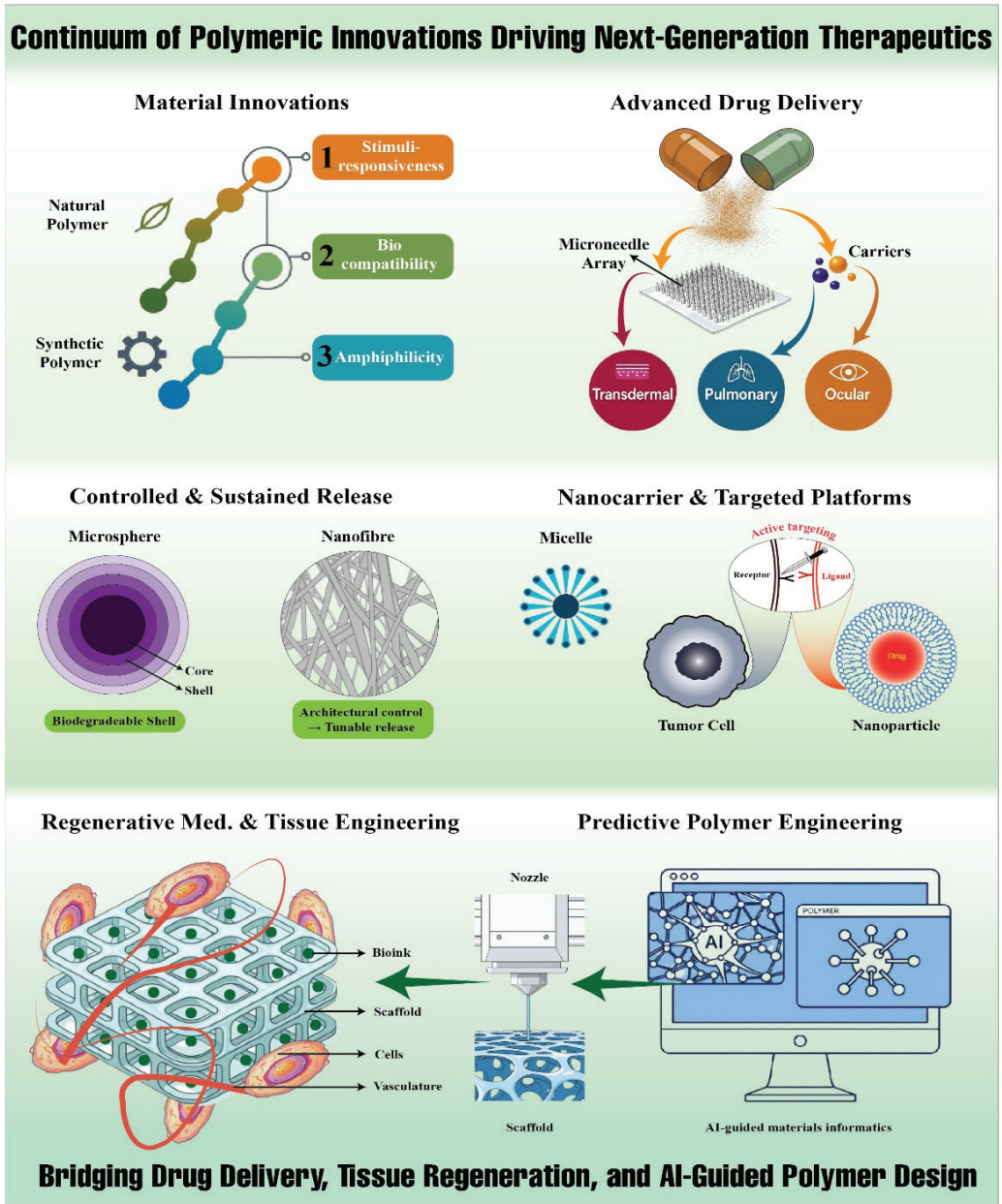


Figure 1. Advancements in polymeric drug delivery systems

Across all modalities, advances in computer-assisted design and machine learning have accelerated the development of intelligent polymer systems, enabling modular carriers that respond to physiological pH, temperature, or enzyme presence (Yue et al., 2025). These strategies are particularly prominent in the design of injectable hydrogels and nanocomposite scaffolds for localized, sustained delivery, regenerative medicine, and tissue engineering (Lu et al., 2024; Shergujri et al., 2025). The transition to composite and multifunctional polymer systems incorporating smart materials and bioresponsive mechanisms marks a major transformation in how drugs, biologics, and genetic therapies are transported within the body. Comparative studies now recommend hybrid designs that blend natural and synthetic polymers when both biofunctionality and structural robustness are critical, while also addressing manufacturing complexity and regulatory hurdles (Turac et al., 2024).

Innovations in controlled and sustained release

Modern controlled-release systems emphasize architectural design including core shell particles, layered films, and porous nano fibres and stimuli responsive chemistries that enable predictable long-term release and on-demand activation (Gaydhane et al., 2023). Electrospun nano fibres composed of PLGA, PCL, and PEG blends are especially valuable for local delivery in bone regeneration or wound healing, providing high surface area, tunable porosity, and controllable drug loading heterogeneity. These systems allow rapid adjustment of release kinetics via fiber diameter, porosity, and multilayer configurations (Fei et al., 2008; Wildy & Lu, 2023). However, scale-up and batch variability remain practical limitations compared with established microsphere technologies. PLGA hydrogels and depot systems have gained renewed attention for long-acting systemic delivery. Engineered PLGA based depots and hydrogel composites mitigate initial burst release and provide weeks tomonths release with predictable degradation, rivaling polymeric microspheres for sustained dosing (Cordovez et al., 2011; Marquina et al., 2023; Visan &Negut, 2024; Wan, Bao, & Burgess, 2022). Major limitations include burst control, polymer-acidification effects on labile drugs, and sterilization-related degradationissues that can be addressed through polymer blending, buffering excipients, or coreshell architectures (Gaydhane et al., 2023; Visan &Negut, 2024).

Nanocarriers, micelles, and targeted platforms

Polymeric nanoparticles, micelles, and polymer-lipid hybrids have matured significantly. Polymeric micelles enhance solubilization and tumor targeting via the enhanced permeability and retention (EPR) effect, and modern designs now incorporate ligands and stimuli cleavable linkers to achieve site-specific release (Beach et al., 2024; Harun-Or-Rashid et al., 2023). These platforms are promising for poorly water-soluble anticancer agents, though their clinical translation depends on circulatory stability and manufacturing reproducibility (Mahajan et al., 2023; Marquina et al., 2023). Recent reviews identify micelles demonstrating both *in vivo* stability and ligand integrity as the most promising for clinical success (Beach et al., 2024).

Comparative performance (nanocarriers vs microspheres). Nanocarriers excel at systemic targeting and intracellular delivery (for nucleic acids or small molecules), whereas microspheres and depots are preferred for localized, long-duration release (Marquina et al., 2023; Wan, Bao, & Burgess, 2022). The selection depends on therapeutic goals, drug stability, and regulatory considerations;nanoparticles demand extensive biodistribution studies, while depots follow clearer device-based regulatory pathways (Marquina et al., 2023).

Polymers in tissue engineering and regenerative medicine

Tissue engineering scaffolds now integrate multiple functionalities: mechanical support, cell instructive cues, controlled release of bioactive agents, and,

increasingly, biosensing. Natural polymers such as collagen, gelatin, and chitosan provide biocompatible cell matrices, whereas synthetic polymers like PCL, poly(lactic-co-glycolic acid) (PLGA), and PEG derivatives offer tunable mechanical properties and degradation rates. Current advances focus on functionally graded scaffolds, bioinks for 3D printing, and nanocomposite hydrogels, enhancing vascularization and tissue integration (Clegg et al., 2024; Lu, Cai, & Hu, 2024; Mahajan et al., 2023). Smart and stimuli-responsive scaffolds. Hydrogels responsive to pH, enzymes, temperature, or redox conditions enable on-demand drug release synchronized with the body's healing phases. Such responsiveness reduces dosing frequency and promotes localized therapeutic activity, though material design must prevent premature activation or degradation (Lu et al., 2024). Recent preclinical and early-clinical evidence supports several hydrogel classes for wound and tissue repair (Clegg et al., 2024).

Comparative assessment

To strengthen scientific rigor, the selection and optimization of polymeric systems should be guided by comparative performance metrics that ensure therapeutic reliability and clinical applicability. These include the reproducibility of the release profile (burst versus sustained), mechanical matching with the target tissue, stability of the incorporated drug during processing and *in vivo* conditions, nature of biodegradation byproducts, and the scalability and robustness of sterilization methods. For instance, PLGA microspheres provide predictable degradation kinetics but may create acidic microenvironments that compromise the stability of protein-based drugs, while electrospun fibers offer high drug loading efficiency yet encounter significant challenges during scale-up manufacturing (Gaydhane et al., 2023; Visan &Negut, 2024). Similarly, polymeric micelles are highly effective for delivering hydrophobic molecules; however, their stability and pharmacokinetic behavior often necessitate additional modifications such as PEGylation or crosslinking to ensure prolonged systemic circulation and controlled release (Beach et al., 2024; Harun-Or-Rashid et al., 2023). Therefore, system selection must balance pharmacokinetics, biocompatibility, degradation behavior, and manufacturability to achieve optimal clinical outcomes (Marquina et al., 2023).

Predictive polymer engineering

A defining trend in polymer research is the integration of AI-driven materials informatics and additive manufacturing to accelerate polymer discovery and predict *in vivo* behavior (Lu et al., 2024). This data-driven paradigm enables rational selection of polymer chemistries and scaffold architectures tailored for therapeutic use, minimizing trial-and-error and facilitating regulatory acceptance. Future progress will depend on interdisciplinary collaboration across materials science, biomedical engineering, and regulatory sciences to deliver clinically impactful polymer systems (Clegg, 2024; Lu et al., 2024).

POLYMERIC PLATFORMS IN DRUG DELIVERY

Overarching design principles and tailored therapeutic approaches

The diverse polymeric platforms in drug delivery, spanning film coatings, capsules, vesicles, micelles, microspheres, nanoparticles, hydrogels, and gene vectors, collectively embody a unified, tailored polymeric approach to therapeutics (Figure 2.) built upon several overarching design principles (Kurul et al., 2025; Zhang et al., 2025a). At their core, these systems harness structure-function relationships that govern their therapeutic performance: biocompatibility and biodegradability for safe *in vivo* application and predictable clearance (Bachhav et al., 2025), amphiphilicity and self-assembly for organizing both hydrophilic and hydrophobic agents (Krishnan et al., 2022), stimuli-responsiveness for spatiotemporal control in response to pH, temperature, enzymes, or redox gradients (Rosario & Ma, 2024), and surface functionalization for selective targeting via passive or ligand-mediated routes

(Shanahan et al., 2025). These shared design principles create a modular framework where polymer selection, architecture, and function are rationally engineered for specific therapies, transforming conventional delivery into precision nanomedicine (Rodriguez-Cruz et al., 2025; Zhang et al., 2022). This progression from basic coatings to multi-responsive nanocarriers reflects the field's conceptual maturation (Balcerak-Woźniak et al., 2024). Diverse polymeric systems represent context-specific applications of these strategies, enabling protection from the GI tract environment, in situ depot formation, or targeted cytosolic release. Such conceptual linkage, transcending single-platform descriptions, is now central to advanced polymer-based therapeutics (Kurul et al., 2025).

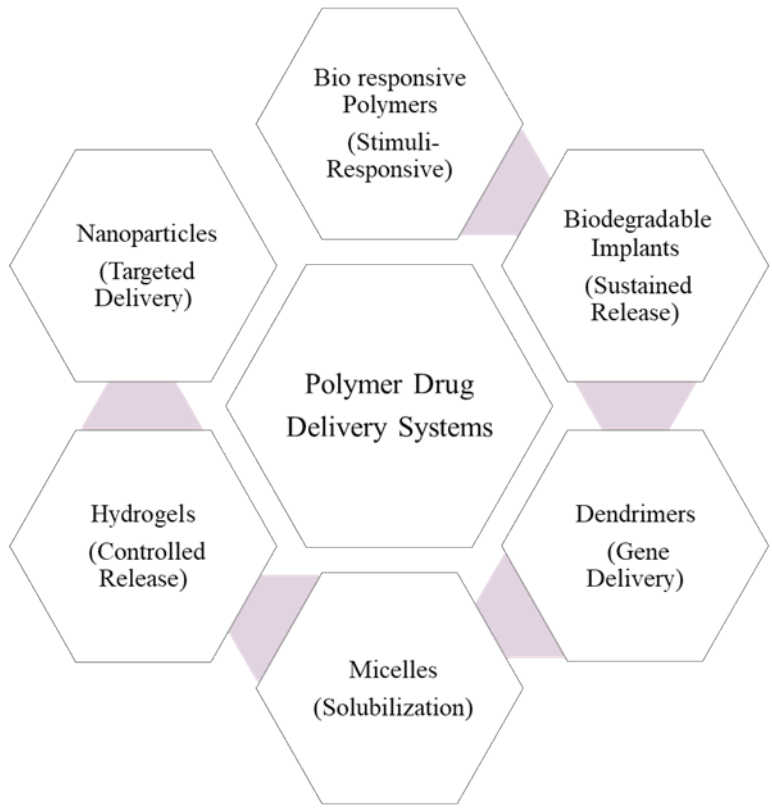


Figure 2. Polymeric platforms in drug delivery

Film coatings

Film coatings enhance both the mechanical integrity and release control of dosage forms (Rosario & Ma, 2024). Common polymer choices (shellac, zein, cellulose acetate phthalate, glyceryl stearate, Eudragit®) function as either rapid-release films or diffusion-controlling barriers (Rosario & Ma, 2024). More recent variants—such as pH-sensitive and nanocomposite coatings enable on-demand, location-specific drug release (Xu et al., 2025a). These innovations expand applications to transdermal, implantable, and ocular platforms, exemplifying how surface and stimuli-responsive engineering guide modern coating utility (Rosario & Ma, 2024; Xu et al., 2025b).

Capsules and encapsulation systems

Traditionally, both hard-shell and soft-shell capsules are made of gelatin and are used for various drugs requiring rapid release. Hydroxypropyl methylcellulose (HPMC) capsules, favored for plant-based and stability advantages, have gained wide acceptance (Al-Tabakha, 2010; Zhang et al., 2025a). Latest strategies feature ultra-thin polymer shells, hybrid encapsulation, and biodegradable nano-/micro-capsules for

targeted and delayed delivery (Zhang et al., 2025b). These advances in capsule materials and architectures illustrate modular polymer adaptation for modern pharmaceutical demands.

Polymer vesicles (polymersomes)

Polymersomes are self-assembled vesicles from amphiphilic block copolymers or graft copolymers, offering high stability and tunable permeability for targeted or triggered release. Smart vesicles offer co-delivery, imaging, and sequential release via multi-compartmental structures (Krishnan et al., 2022; Yetisgin et al., 2025), highlighting the design flexibility that distinguishes polymersomes from liposomes.

Polymeric micelles

Micelles self-assembled from amphiphilic copolymers enable solubilization and targeting of poorly water-soluble drugs in a stable core–shell structure (Kehrein et al., 2024; Krishnan et al., 2022). Recent variations include actively targeted micelles, enzyme or pH-responsive versions, and scalable microfluidic manufacturing aimed at translation to clinical use (Kehrein et al., 2024; Li et al., 2025a). The synergy of self-assembly, ligand targeting, and stimuli-responsiveness positions micelles as dynamic platforms for next-generation therapies.

Polymeric microspheres and microcapsules

Microspheres and microcapsules encapsulate both hydrophilic and hydrophobic agents, releasing drugs via engineered core–shell structures (Shendge et al., 2024; Sumathi, 2025). Modern approaches, such as multi-layering, in situ forming capsules, and ligand-functionalization, advance the targeting and dynamic release control (Shendge et al., 2024; Wan, Bao, & Burgess, 2022). Such developments demonstrate how design principles like biodegradability and functionalization extend microspheres to multifunctional therapeutic carriers.

Polymeric nanoparticles

Nanoparticles below 1 μm allow precise release kinetics, improved stability, and effective targeting when constructed from biodegradable polymers (e.g., PLGA) (Geszke-Moritz & Moritz, 2024; Islam et al., 2025). Newly engineered versions with ligand conjugation, hybrid systems, and multimodal properties have matured to preclinical and clinical application, uniting targeting, imaging, and on-demand release (Kaur et al., 2023; Kurul et al., 2025; Mahajan et al., 2022; Shanahan et al., 2025).

Polymeric hydrogels

Hydrogels of hydrophilic polymer networks excel for local/systemic delivery, wound healing, and tissue applications, thanks to tunable porosity and compatibility (Lohani et al., 2025; Shergujri et al., 2025). Stimuli-responsive, nanoparticle-loaded, and 3D-printed hydrogels now enable targeted, sustained, and tissue-integrated therapies (Delgado-Pujol et al., 2025; Karchoubi et al., 2024; Lohani et al., 2025).

Polymeric vectors for gene delivery

Polymeric vectors shield nucleic acids from degradation and facilitate cell uptake in RNA-based therapies. Recent breakthroughs include polymer-lipid hybrid nanoparticles and CRISPR delivery scaffolds, improving transfection and control (Gameiro et al., 2024; Hou et al., 2021; Maeki et al., 2024; Ullah et al., 2025). The design of these systems demonstrates functional integration across platforms from classic drug to advanced gene delivery.

Innovations in controlled and sustained release

Polymers form the foundation of controlled-release technology, leveraging biodegradable building blocks (PLGA, PCL, PEG) for tailored kinetics (Bachhav et al., 2025; Senthilkumar et al., 2025). Electrospun nanofibers, microneedles, and 3D-printed depots deliver localized, precise dosing (CeCe et al., 2024; Meng et al., 2024; Razzaghi, 2025). Integration of smart polymers, hybrid structures, and digital fabrication opens new frontiers for truly personalized, responsive therapy (Bernatoniene et al., 2025; Panchpuri et al., 2025).

SMART AND STIMULI-RESPONSIVE POLYMER GELS FOR PRECISION MEDICINE

Hydrogels have emerged as versatile platforms for advanced drug delivery, leveraging their water-absorbent, biocompatible nature to encapsulate diverse therapeutics. Their design, guided by polymer composition, crosslinking density, and responsiveness to environmental cues like pH or temperature, enables precise control over drug release, aligning with the demands of precision medicine (van der Meel et al., 2019).

Responsive hydrogel

pH-sensitive hydrogels, such as those based on poly(acrylic acid) (PAA) or chitosan, tailor drug release to specific physiological environments. For instance, PAA hydrogels achieved 80% methotrexate release within 48 hours at pH 5.5, mimicking tumor microenvironments, while limiting release at physiological pH (Jiang et al., 2019). Liu et al. (2017) developed an injectable thermoresponsive hydrogel based on alginate-graft-PNIPAM that effectively released ~70% of doxorubicin within 24 hours at 37 °C, demonstrating potential for localized, tumor-targeted chemotherapy.

Nanoparticle-infused gel matrices

Integrating nanoparticles into hydrogels improves drug stability and release kinetics. Alginate hydrogels embedded with PLGA nanoparticles sustained curcumin release over seven days, achieving 85% cumulative release and accelerating wound healing (Kass & Nguyen, 2022). Similarly, liposome-encapsulated gels protect drugs from degradation, while polymeric nanoparticles enhance tissue penetration and bioavailability (Abbas et al., 2022; Mou et al., 2022). Magnetic nanoparticles within gels enable site-specific delivery via external magnetic fields, offering promise for localized cancer therapies (Liu et al., 2020; Wang & Chang, 2023).

Biodegradable and dual-responsive gel platforms

Biodegradable hydrogels, crafted from natural polymers like chitosan, alginate, or hyaluronic acid, or synthetic polymers like PLGA and PEG, degrade into non-toxic byproducts, eliminating the need for surgical removal (Yuan et al., 2023). Dual-responsive hydrogels, sensitive to combined stimuli such as pH and temperature or electric fields, provide unparalleled precision. For example, pH- and temperature-sensitive gels target acidic tumor environments, while electro-responsive systems enable on-demand release (Naik et al., 2020; Yadav et al., 2021).

Targeted and nanocomposite gels

Functionalized hydrogels with ligands, such as antibodies or peptides, direct drugs to specific cells, enhancing therapeutic specificity for conditions like cancer (Deng et al., 2022; van der Meel et al., 2019; Wang & Chang, 2023). Nanocomposite gels incorporating carbon nanotubes, graphene, or silica nanoparticles bolster mechanical strength and drug-loading capacity, enabling sustained release and improved tissue penetration (Rao et al., 2022; Sun et al., 2021).

SMART POLYMERS FOR STIMULI-RESPONSIVE DRUG DELIVERY

Recent advances in polymer engineering have led to the development of smart polymers—materials capable of altering their physicochemical behavior in response to specific environmental stimuli. These stimuli can be physical (e.g., temperature, light, ultrasound, mechanical force), chemical (e.g., pH, ionic strength), or biological (e.g., enzymes, biomolecules), enabling highly controlled and site-specific drug release.Smart polymeric systems are designed to either passively target pathological tissues—leveraging the Enhanced Permeability and Retention (EPR) effect—or to actively engage in triggered delivery. Biochemical targeting, in contrast, involves conjugating specific ligands (e.g., antibodies, peptides) to polymer carriers for precise cellular interactions. In triggered systems,

drug release is activated by external or internal cues, aligning with the core principles of precision medicine, which further refines delivery specificity, ensuring drugs are released only under designated conditions (Kaur et al., 2014; van der Meel et al., 2019). Smart polymers thus offer innovative solutions for personalized, responsive therapeutics.

3D-PRINTED POLYMERIC SCAFFOLDS IN REGENERATIVE MEDICINE

Three-dimensional (3D) printing of polymeric scaffolds is revolutionizing the landscape of precision medicine and regenerative therapies by enabling the fabrication of patient-specific structures with complex anatomical geometries and tailored mechanical properties. This technology integrates biocompatible polymers with digital design, facilitating the creation of scaffolds that closely mimic native tissues, guide cellular behavior, and support controlled drug delivery (Anand et al., 2020a, 2020b; Qi et al., 2025). The following sections outline innovations across bone, nerve, and spinal tissue engineering, highlighting how materials, architecture, and multifunctionality converge to push the boundaries of polymer-based scaffold design.

Biomimetic bone scaffolds

Oladapo et al. (2023) developed 3D printed composite scaffolds designed to replicate the hierarchical structure and mechanical strength of natural bone. By combining polyetheretherketone (PEEK) with bioceramic fillers, they achieved implants that not only possess stiffness compatible with cancellous bone but also promote bone cell proliferation. The team demonstrated that tunable porosity and pore geometry, optimized through computational modeling and additive manufacturing, can strike a balance between mechanical integrity and nutrient diffusion. Surface modifications, including nano-roughening and tailored wettability, further enhanced osteointegration by creating favorable microenvironments for osteoblast adhesion (Oladapo et al., 2021). Recent advances in PEEK-based scaffolds highlight immunomodulation and angiogenesis as additional functional dimensions. Zhao et al. (2025) fabricated a multifunctional astragalus polysaccharide (APS)-coated, strontium-doped bioactive glass (SrBG)-reinforced PEEK scaffold (APS/PSBPK) that promotes M2 macrophage polarization, reduces inflammation, and enhances vascularization alongside osteogenic differentiation. This scaffold demonstrated superior in vivo bone regeneration through synergistic immune regulation and growth factor signaling (Zhao et al., 2025). Similarly, Mi et al. (2024) showed that nano-hydroxyapatite (nHA) and carbon fiber (CF)-reinforced PEEK scaffolds fabricated by fused deposition modeling (FDM) exhibit enhanced bioactivity and mechanical properties suitable for load-bearing bone defects, with significant improvements in osteoblast adhesion and proliferation (Mi et al., 2024). Furthermore, Qi et al. (2025) demonstrated that 3D-printed bioceramic scaffolds can modulate immune microenvironments and counteract bone aging by delivering anti-osteoporosis drugs, providing a therapeutic strategy for osteoporotic bone defects (Qi et al., 2025). These findings collectively underscore how biomimetic scaffold design integrates structural, immunomodulatory, and bioactive features to optimize bone regeneration.

Natural polymer-based hydrogels: Alginate and Carrageenan

Biopolymers such as alginate and κ-carrageenan have gained attention for their intrinsic biocompatibility and gel-forming ability, rendering them ideal for scaffold fabrication via extrusion-based 3D printing. Stavarache et al. (2024a) successfully printed hydrogel scaffolds composed of sodium alginate and κ-carrageenan, demonstrating their suitability for cell culture and tissue regeneration applications. These scaffolds exhibited rapid gelation upon crosslinking and maintained structural fidelity, with high porosity and interconnectivity—attributes essential for vascularization and cell migration (Stavarache et al., 2024a). In a subsequent study, Stavarache et al. (2024b) introduced carboxymethyl cellulose (CMC)

to the alginate/κ-carrageenan blend, improving printability, mechanical strength, and moisture retention. These composite scaffolds retained high cytocompatibility and mechanical resilience, exhibiting resistance to collapse during handling. Such enhancements underline the adaptability of natural polysaccharide blends for replicating soft tissue architectures with precise dimensional control (Stavarache et al., 2024b). Additional studies further validate the versatility of alginate-based systems. Jahani et al. (2024) demonstrated that alginate-chitosan composite hydrogels with controlled rheological properties and crosslinking behavior yield scaffolds with enhanced mechanical strength and cellular integration for cartilage tissue engineering (Jahani et al., 2024). Chowdhury et al. (2025) incorporated nano-hydroxyapatite (nHAP) into alginate-gelatin formulations, tuning mechanical, rheological, and osteogenic properties for bone regeneration applications (Chowdhury et al., 2025). These findings collectively emphasize how strategic polymer blending and nanocomposite integration advance natural hydrogel scaffolds from simple matrices to mechanically robust, bioactive platforms.

Self-sensing and smart nanocomposite scaffolds

Schneider et al. (2024) introduced an advanced scaffold platform using 3D-printed PEEK reinforced with conductive nanofillers to create self-sensing smart nanocomposites. Incorporating carbon nanotubes and graphene nanosheets endowed the scaffold with piezoresistive sensing capabilities, enabling detection of micro-deformations—mimicking the self-monitoring behavior of native bone. These scaffolds demonstrated high compressive strength (≥ 80 MPa) combined with strain-monitoring resolutions below 0.1%, proving suitable for load-bearing orthopedic applications. Cytocompatibility assays confirmed that their conductive properties can support osteogenic differentiation, indicating potential for "smart implants" capable of real-time monitoring of bone healing (Schneider et al., 2024).Building on this paradigm, Zaszczyńska et al. (2024) reviewed piezoelectric polymers and ceramics for bone tissue engineering, emphasizing how piezoelectric scaffolds—particularly those based on polyvinylidene fluoride (PVDF), poly-L-lactic acid (PLLA), and barium titanate (BTO)—generate electrical signals in response to mechanical stress, promoting osteoblast activity and mineralization (Zaszczyńska et al., 2024). Li et al. (2025b) recently fabricated BTO/β-tricalcium phosphate (β-TCP) piezoelectric composite scaffolds using digital light processing (DLP) 3D printing; under ultrasound stimulation, these scaffolds exhibited significantly enhanced alkaline phosphatase activity and osteogenic gene expression, validating the therapeutic potential of piezoelectric biomaterials (Li et al., 2025b). The integration of sensing, actuation, and bioelectric stimulation into 3D-printed scaffolds reflects a transformative shift toward intelligent, responsive regenerative platforms.

Scaffold design for spinal cord regeneration

Khaledian et al. (2024) reviewed the latest developments in 3D-printed scaffolds aimed at repairing spinal cord injuries. Polymers such as poly(lactic-co-glycolic acid) (PLGA), PEEK, and polycaprolactone (PCL) were designed into anisotropic structures that aligned neural growth and accommodated gradient release of growth factors and chemokines. The 3D architecture incorporated microchannels to guide axonal extension, while polymer blends enabled sequential degradation, optimizing the timing of therapeutic release. *In vivo* studies in animal models showed that neuro-conductive scaffolds with VEGF-loaded microspheres supported neovascularization and improved functional recovery (Khaledian et al., 2024). These findings underscore the crucial role of polymer engineering not only in structural healing but also in precision-controlled biochemical signaling—vital for functional tissue regeneration.Further supporting this direction, Zhu et al. (2025) highlighted integrated 3D-printed BDNF/collagen/chitosan scaffolds that accelerate neural regeneration following spinal cord injury by providing structural support, biochemical cues, and controlled neurotrophic factor release (Zhu et al., 2025). Chen et al. (2024) reviewed biomaterial-based strategies for spinal cord repair, emphasizing that conductive polymer hydrogels (e.g., polypyrrole)

combined with electrical stimulation enhance axonal guidance and remyelination (Chen et al., 2024). Ma and Li (2025) demonstrated that 3D-printed scaffolds incorporating neural progenitor cells and growth factors using microscale continuous projection printing can promote host axonal extension and exogenous cell integration at injury sites (Ma & Li, 2025). Harley-Troxell et al. (2025) developed PLGA/graphene oxide nerve guidance conduits via 3D printing, showing improved biocompatibility and enhanced neural differentiation (Harley-Troxell et al., 2025). Collectively, these studies demonstrate that advanced 3D printing strategies, when coupled with multifunctional polymer composites, provide spatiotemporal control over neural regeneration and functional recovery.

POLYMER SYSTEMS IN THERAPEUTICS

Polymer-based therapeutic platforms have evolved from laboratory innovations into clinically relevant systems (Bai & Tirella, 2022; Tewari et al., 2022; Wang et al., 2023; Yusuf et al., 2023). These systems, incorporating widely approved polymers such as PEG, PLGA, and PCL, offer significant improvements in drug solubility, stability, targeting, and release kinetics, representing a cornerstone of modern pharmaceutical science (Desai et al., 2025; Önel, 2022; Palma, 2025; Thapa & Kim, 2023).

Recent years have seen rapid progress, particularly in oncology and anti-infective applications, driven by regulatory approvals and robust late-stage clinical trials (Abdullah et al., 2025; Alam, 2023; Jia et al., 2023; Nirmala et al., 2023). With more than 50 FDA- and EMA-approved polymer therapeutics as of 2025, the translational landscape is robust, yet faces challenges around scalability, immunogenicity, and complex-generic regulatory pathways (Gultepe et al., 2026; Patil et al., 2024; Scott et al., 2023). Recent and ongoing clinical investigations (Table 1.) and recent FDA/EMA approvals are summarized (Table 2.), with outcomes and status validated.

Table 1. Recent and ongoing clinical investigations of polymeric therapeutics (Phases 1–3, 2023–2025)

Trial Name/ID	Polymer System	Therapeutic Agent/ Indication	Status/ Completion	Key Outcomes/ Notes	Sponsor	Reference
SHIELD II (NCT02468778)	PLEX hydrogel (PolyPid)	Doxycycline / SSI prevention (colorectal surgery)	Completed (June 2025), NDA in 2026	38% SSI/mortality reduction, positive topline results	PolyPid Ltd.	PolyPid, 2025; ClinicalTrials.gov, 2025
OTX-TKI (NCT05695417)	Elutyx hydrogel insert	TKI/ Diabetic retinopathy	Ongoing, completes Q2 2026	Sustained retinal delivery; Phase 2 showed good tolerability	Ocular Therapeutix	ClinicalTrials.gov, 2025
STELLAR-303 (NCT05613124)	Polymeric nanoparticle (albumin)	Zanzalintinib /Renal cell carcinoma	Ongoing, completes Q4 2025	Tumor microenvironment modulation, FDA app. 2025	Exelixis	Exelixis, 2025; ClinicalTrials.gov, 2025
Explore-CKD (NCT05182840)	PLGA microsphere	Lorundrostat /CKD with hypertension	Ongoing, interim Q4 2025	Long-acting release; ASN presentation 2025	Mineralys	MineralysTherapeutics, 2025; ClinicalTrials.gov, 2025
ORIGIN 3 (NCT04716231)	PEGylated conjugate	Investigational biologic/ Myasthenia gravis	Ongoing, update Nov 2025	Immunomodulation, all enrollment is complete	Vera Therapeutics	VeraTherapeutics, 2025; ClinicalTrials.gov, 2025
HRS9531 Obesity (NCT05991598)	Polymeric LAI depot	GLP-1 agonist/ Obesity	Ongoing, Phase 3 at ObesityWeek 2025	3-month sustained release; weight management	Hengrui/ Kailera	Hengrui Pharma, 2025; ClinicalTrials.gov

Table 2. Recent FDA/EMA polymer drug approvals

Product Name	Polymer System	Agent / Indication	Approval Date	Notes / Sponsor	Reference
Inlexzo	Intravesical polymeric system	Gemcitabine/ BCG-unresponsive bladder CA	Sep 2025	Bladder gel, 1st for instillation/ PolyPid	FDA, 2025; EMA, 2025; PolyPid, 2025
Bondlido	Polymeric patch hydrogel	Lidocaine/ Postherpetic neuralgia	Sep 2025	Transdermal hydrogel/ Medherant/BioPharma	FDA, 2025; EMA, 2025; MedherantLtd, 2025
Dextenza*	Elutyx hydrogel insert	Dexamethasone/ Ocular (conjunctivitis, expansion)	2021, 2025 (Pediatric)	>24 hydrogel approvals, 30-day release	FDA, 2025; Ocular Therapeutix, 2025
Neulasta Onpro	PEG conjugate, on-body	Pegfilgrastim/ Neutropenia (biosimilar wave)	2024	2002 original; biosimilars 2022-24	FDA, 2025; AmgenInc, 2024
Lupron Depot	PLGA microspheres	Leuprolide/ Prostate cancer, endometriosis	Expansions 2023–24	Biodegradable, pediatric/ oncology doses	FDA, 2024; AbbottLaboratories, 2024
Nubeqa (EU)	Polymeric nanoparticle (albumin)	Darolutamide/ Prostate cancer (HRR+)	Q2 2025 (EMA)	Dual US/EU; expanded indication	EMA, 2025; Bayer AG, 2025
Trodelvy	Hydrophilic polymer conjugate	Sacituzumab govitecan / TNBC	Q3 2023 (EMA)	First-in-class ADC	EMA, 2023; GileadSciences, 2023
Columvi	PEG-bispecific antibody	Glofitamab/ DLBCL	Q2 2023 (EMA)	T-cell engager, polymer stabilized	EMA, 2023; Roche, 2023
Inaqovi	Oral polymeric combo	Decitabine/ cedazuridine/ AML	EMA 2023	Polymer for oral bioavailability	EMA, 2023; TaihoOncology, 2023
Voranigo	Poly-enabled small molecule	Vorasidenib/ CNS glioma	Sep 2025 (EMA)	First approved CNS penetrant	EMA, 2025; Servier, 2025

*Expansion or additional indication approvals.

FUTURE PERSPECTIVES AND EMERGING TRENDS

The future of polymer-based biomedical applications lies in the convergence of material science, biotechnology, and data-driven design. As personalized medicine gains momentum, polymers will play a critical role in tailoring drug delivery systems to individual patient profiles. The integration of AI and machine learning in polymer engineering is expected to revolutionize formulation optimization, enabling predictive modeling of polymer-drug interactions, release kinetics, and therapeutic outcomes.

A significant trend involves the development of multi-functional, stimuli-responsive polymers capable of responding to multiple physiological cues—such as pH, temperature, redox potential, and enzymatic activity—allowing on-demand, site-specific drug release with minimal off-target effects. These smart systems are being increasingly adapted for cancer therapy, gene delivery, and implantable biosensors.

Biodegradable and bioresorbable polymers will continue to be at the forefront, especially in the design of implantable devices, 3D-printed scaffolds, and injectable hydrogels for tissue engineering and regenerative medicine. Innovations in natural-synthetic hybrid systems are expected to harness the biocompatibility of natural polymers and the tunable functionality of synthetics, creating next-generation platforms with enhanced mechanical strength and biological performance.

Additionally, green polymer chemistry is gaining importance, driven by sustainability concerns. The shift toward eco-conscious, renewable, and non-toxic polymeric systems will be vital for aligning pharmaceutical development with global environmental goals.

Finally, regulatory harmonization and translational scalability remain critical challenges. Bridging the gap between laboratory-scale innovation and clinical-grade production will require robust manufacturing practices, interdisciplinary partnerships, and advances in polymer characterization and standardization.

In conclusion, polymer science stands at a transformative juncture. By embracing cross-disciplinary innovation and sustainability, future polymeric systems are poised to drive next-generation therapeutics—precise, responsive, patient-friendly, and globally accessible.

ACKNOWLEDGEMENTS

The author acknowledges the cooperation of all those who have contributed in one sense or another to this review.

AUTHOR CONTRIBUTION STATEMENT

M. K., L. K., G. S., L. S.: Idea of Manuscript; M. K., L. S., M. K.: Literature Search; M. K., L. S., N. K., P. S.: Writing-Original Draft; M. K., L. S., N. K.: Critical Review and Editing; L. K., G. Singh, R. K. D.: Supervision

CONFLICT OF INTEREST

The authors declare that there is no conflict of interest.

REFERENCES

Abbas, M. N., Khan, S. A., Sadozai, S. K., Khalil, I. A., Anter, A., Fouly, M. E., ... Kazi, M. (2022). Nanoparticles loaded thermoresponsive in situ gel for ocular antibiotic delivery against bacterial keratitis. *Polymers, 14*(6), 1135. doi:10.3390/polym14061135

Abdullah, K. M., Sharma, G., Singh, A. P., & Siddiqui, J. A. (2025). Nanomedicine in cancer therapeutics: Current perspectives from bench to bedside. *Molecular Cancer, 24*(1), 169.

Abbott Laboratories. (2024). *Lupron Depot (leuprolide) updated label and regulatory expansion*.

Alam, M. K. (2023). Nanocarrier-based drug delivery systems using microfluidic-assisted techniques. *Advanced NanoBiomed Research, 3*(11), 2300041.

Alavi, S. E., Alharthi, S., Alavi, S. Z., Raza, A., &Shahmabadi, H. E. (2024). Bioresponsive drug delivery systems. *Drug Discovery Today, 29*(1), 103849.

Al-Sahlawi, F., Alabdali, A. Y. M., Chinnappan, S., Al-Samydai, A., & Maki, M. A. A. (2024). Polymer-based nanoparticles in targeted cancer therapy: A review. *Journal of Applied Pharmaceutical Science, 14*(9), 057-068.

Al-Tabakha, M. M. (2010). HPMC capsules: Current status and future prospects. *Journal of Pharmacy & Pharmaceutical Sciences, 13*(3), 428-442.

Amgen Inc. (2024). *Neulasta Onpro (pegfilgrastim) biosimilar regulatory filings*.

Anand, N., Singh, D., Singh, G., Kaur, L., Dhawan, R. K., & Kaur, N. (2020a). 3D printing technology in pharmaceutical delivery system: Recent advancement in innovative approach. *FABAD Journal of Pharmaceutical Sciences, 45*(3), 253–268.

Anand, S., Sahu, A. K., & Sinha, M. K. (2020b). 3D printing of polymeric scaffolds for tissue engineering applications: A review. *Journal of Materials Science, 55*(12), 5175-5193.

Bachhav, R., Bachhav, P., Deore, R., Sonawane, G., Surana, K., & Mahajan, S. (2025). Biodegradable polymers in drug delivery: A detailed review. *Asian Journal of Pharmaceutical Research, 15*(2), 153-158.

Bai, X., & Tirella, A. (2022). Injectable multifunctional natural polymer-based hydrogels for the local delivery of therapeutic agents. *International Journal of Drug Discovery and Pharmacology*, 10-10.

Balcerak-Woźniak, A., Dzwonkowska-Zarzycka, M., &Kabatc-Borcz, J. (2024). A comprehensive review of stimuli-responsive smart polymer materials-recent advances and future perspectives. *Materials (Basel, Switzerland), 17*(17), 4255. https://doi.org/10.3390/ma17174255

Bayer AG. (2025). *Nubeqa (darolutamide) regulatory submission updates*. Bayer Annual Report.

Beach, M. A., Nayanathara, U., Gao, Y., Zhang, C., Xiong, Y., Wang, Y., & Such, G. K. (2024). Polymeric nanoparticles for drug delivery. *Chemical Reviews, 124*(9), 5505-5616. doi:10.1021/acs.chemrev.3c00705

Bernatoniene, J., Stabrauskiene, J., Kazlauskaite, J. A., Bernatonyte, U., &Kopustinskiene, D. M. (2025). The future of medicine: How 3D printing is transforming pharmaceuticals. *Pharmaceutics, 17*(3), 390.

Bharathy, P., & Thanikachalam, P. V. (2024). Recent advances and future prospects in polymer-mediated drug delivery systems: A comprehensive review. *Int. J. Drug Deliv. Technol., 14*(3), 1896-1907.

Bhatia, S. (2016). Nanoparticles types, classification, characterization, fabrication methods and drug delivery applications. In *Natural polymer drug delivery systems: Nanoparticles, plants, and algae* (pp. 33–93). Cham, Switzerland: Springer International Publishing.

Carothers, W. H. (1929). Studies on polymerization and ring formation: I. An introduction to the general theory of condensation polymers. *Journal of the American Chemical Society, 51*(8), 2548–2559.

CeCe, R., Jining, L., Islam, M., Korvink, J. G., & Sharma, B. (2024). An overview of the electrospinning of polymeric nanofibers for biomedical applications related to drug delivery. *Advanced Engineering Materials, 26*(1), 2301297.

Chemban, S. A., Kaur, L., Singh, G., Dhawan, R. K., & Kaur, A. (2022). Competency of lyophilization and spray drying techniques to improve the solubility of bosentan monohydrate: A comparative study. *FABAD Journal of Pharmaceutical Sciences, 47*(2), 129–150.

Chen, K., Yu, W., Zheng, G., Xu, Z., Yang, C., Wang, Y., ... Chen, H. (2024). Biomaterial-based regenerative therapeutic strategies for spinal cord injury. *NPG Asia Materials, 16*(1), 5.

Chen, K., Sun, X., Liu, Y., Li, S., & Meng, D. (2025). Advances in clinical applications of microneedle. *Frontiers in Pharmacology, 16*, 1607210.

Chou, W. C., Canchola, A., Zhang, F., & Lin, Z. (2025). Machine learning and artificial intelligence in nanomedicine. *Wiley Interdisciplinary Reviews: Nanomedicine and Nanobiotechnology, 17*(4), e70027.

Chowdhury, S. R., Dey, K., & Basu, B. (2025). 3D extrusion-printed alginate–gelatin hydrogel modified with nanoscale hydroxyapatite: A comprehensive understanding of process science and evaluation of the antimicrobial property. ACS Omega, *10*(18), 18428-18443.

Clegg, J. R., Adebowale, K., Zhao, Z., & Mitragotri, S. (2024). Hydrogels in the clinic: An update. *Bioengineering & Translational Medicine, 9*(6), e10680. doi:10.1002/btm2.10680

ClinicalTrials.gov. (2025). Status of registered polymer-based phase 3 clinical trials. Retrieved from https://clinicaltrials.gov/

Cordovez, B., Chung, A. J., Mak, M., & Erickson, D. (2011). A novel polymer microneedle fabrication process for active fluidic delivery. *Microfluidics and Nanofluidics, 10*(4), 785–791.

Dallaev, R. (2025). Smart and biodegradable polymers in tissue engineering and interventional devices: A brief review. *Polymers, 17*(14), 1976.

Delgado-Pujol, E. J., Martínez, G., Casado-Jurado, D., Vázquez, J., León-Barberena, J., Rodríguez-Lucena, D., ... Begines, B. (2025). Hydrogels and nanogels: Pioneering the future of advanced drug delivery systems. *Pharmaceutics, 17*(2), 215.

Deng, Z., Guo, Y., Zhao, X., Du, T., Zhu, J., Xie, Y., ... Guan, M. (2022). Poly(N-isopropylacrylamide) based electrically conductive hydrogels and their applications. *Gels, 8*(5), 280. doi:10.3390/gels8050280

Desai, N., Rana, D., Patel, M., Bajwa, N., Prasad, R., & Vora, L. K. (2025). Nanoparticle therapeutics in clinical perspective: Classification, marketed products, and regulatory landscape. *Small*, 2502315.

Dobrzyńska-Mizera, M., Dodda, J. M., Liu, X., Knitter, M., Oosterbeek, R. N., Salinas, P., ... Sadiku, E. R. (2024). Engineering of bioresorbable polymers for tissue engineering and drug delivery applications. *Advanced Healthcare Materials, 13*(30), 2401674.

Duncan, R., Vicent, M. J., Greco, F., & Nicholson, R. I. (2005). Polymer–drug conjugates: Towards a novel approach for the treatment of endocrine-related cancer. *Endocrine-Related Cancer, 12*(Suppl. 1), S189–S199. doi:10.1677/erc.1.01045

El-Tanani, M., Mahmud, H., & Serrano-Aroca, Á. (2025). Revolutionizing drug delivery: The impact of advanced polymeric systems on precision medicine. *Pharmaceutics, 17*(3), 412.

EMA. (2025). Human medicines highlights. European Medicines Agency. Retrieved October 24, 2025, from https://www.ema.europa.eu/en/human-regulatory/medicines

Exelixis. (2025). *STELLAR-303 trial status for zanzalintinib*. Exelixis IR Update.

Farjaminejad, S., Farjaminejad, R., Hasani, M., Garcia-Godoy, F., Abdouss, M., Marya, A., ... Jamilian, A. (2024). Advances and challenges in polymer-based scaffolds for bone tissue engineering: A path towards personalized regenerative medicine. *Polymers, 16*(23), 3303.

FDA. (2025). Novel drug approvals. Retrieved October 24, 2025, from https://www.fda.gov/drugs/new-drugs-fda-cders-new-molecular-entities-and-new-therapeutic-biological-products/novel-drug-approvals

FDA. (2024). *Lupron Depot (leuprolide acetate for depot suspension) prescribing information*. Retrieved October 24, 2025

Fei, Z., Hu, Y., Wu, D., Bai, J., & Song, H. (2008). Preparation and property of a novel bone graft composite consisting of rhBMP-2 loaded PLGA microspheres and calcium phosphate cement. *Journal of Materials Science: Materials in Medicine, 19*(3), 1109–1116. doi:10.1007/s10856-007-3050-5

Gameiro, M., Mano, J. F., & Gaspar, V. M. (2024). Emerging lipid–polymer hybrid nanoparticles for genome editing. *Polymer Chemistry, 15*(34), 3436-3468.

Gandhi, K. J., Deshmane, S. V., & Biyani, K. R. (2012). Polymers in pharmaceutical drug delivery system: A review. *International Journal of Pharmaceutical Sciences Review and Research, 14*(2), 57–66.

Gao, L., Lin, J., Wang, L., & Du, L. (2024). Machine learning-assisted design of advanced polymeric materials. *Accounts of Materials Research, 5*(5), 571-584.

Gaydhane, M. K., Sharma, C. S., & Majumdar, S. (2023). Electrospunnanofibres in drug delivery: Advances in controlled release strategies. *RSC Advances, 13*(11), 7312-7328. doi:10.1039/D2RA06023J

Geszke-Moritz, M., & Moritz, M. (2024). Biodegradable polymeric nanoparticle-based drug delivery systems: Comprehensive overview, perspectives and challenges. *Polymers, 16*(17), 2536.

Gilead Sciences. (2023). *Trodelvy (sacituzumabgovitecan) SmPC and EMA assessment report*.

González, Z., Ferrandez-Montero, A., & Domínguez-Robles, J. (2023). Recent advances in polymers as matrices for drug delivery applications. *Pharmaceuticals, 16*(12), 1674.

Gultepe, E., Valluru, R., Brown, N. B., & Sridhar, S. (2026). The landscape of nanomedical clinical trials. *Nano Today, 66*, 102898.

Harley-Troxell, M. E., Pedersen, A. P., Newby, S. D., Christoph, E., Stephenson, S., Masi, T. J., ... & Dhar, M. (2025). 3D-printed poly (lactic-co-glycolic acid) and graphene oxide nerve guidance conduit with mesenchymal stem cells for effective axon regeneration in a rat sciatic nerve defect model. *International Journal of Nanomedicine*, 3201-3217.

Harun-Or-Rashid, M., Aktar, N., Hossain, M. S., Sarkar, N., Islam, M. R., Arafat, M. E., … Yusa, S. (2023). Recent advances in micro- and nano-drug delivery systems based on natural and synthetic biomaterials. *Polymers, 15*(23), 4563. doi:10.3390/polym15234563

Heidari, B. S., Dodda, J. M., El-Khordagui, L. K., Focarete, M. L., Maroti, P., Toth, L., ... Zheng, M. (2024). Emerging materials and technologies for advancing bioresorbable surgical meshes. *Acta Biomaterialia, 184*, 1-21.

Hengrui Pharma. (2025). *Announcement of HRS9531 obesity trial status*. Company Press Release.

Hou, X., Zaks, T., Langer, R., & Dong, Y. (2021). Lipid nanoparticles for mRNA delivery. *Nature Reviews Materials, 6*(12), 1078-1094.

Huang, H. J., Tsai, Y. L., Lin, S. H., & Hsu, S. H. (2019). Smart polymers for cell therapy and precision medicine. *Journal of Biomedical Science, 26*(1), 73.

Islam, S., Ahmed, M. M. S., Islam, M. A., Hossain, N., & Chowdhury, M. A. (2025). Advances in nanoparticles in targeted drug delivery-A review. *Results in Surfaces and Interfaces*, 100529.

Jahani, A., Nourbakhsh, M. S., Ebrahimzadeh, M. H., Mohammadi, M., Yari, D., & Moradi, A. (2024). Biomolecules-loading of 3D-printed alginate-based scaffolds for cartilage tissue engineering applications: A review on current status and future prospective. *Archives of Bone and Joint Surgery, 12*(2), 92.

Jiang, B., Yan, L. J., & Wu, Q. (2019). ABCB1 (C1236T) polymorphism affects P-glycoprotein-mediated transport of methotrexate, doxorubicin, actinomycin D, and etoposide. *DNA and Cell Biology, 38*(5), 485–490. doi:10.1089/dna.2018.4583

Jia, Y., Jiang, Y., He, Y., Zhang, W., Zou, J., Magar, K. T., … He, W. (2023). Approved nanomedicine against diseases. *Pharmaceutics, 15*(3), 774. https://doi.org/10.3390/pharmaceutics15030774

Karchoubi, F., Ghotli, R. A., Pahlevani, H., & Salehi, M. B. (2024). New insights into nanocomposite hydrogels; a review on recent advances in characteristics and applications. *Advanced Industrial and Engineering Polymer Research, 7*(1), 54-78.

Kass, L. E., & Nguyen, J. (2022). Nanocarrier-hydrogel composite delivery systems for precision drug release. *Wiley Interdisciplinary Reviews: Nanomedicine and Nanobiotechnology, 14*(2), e1756. doi:10.1002/wnan.1756

Kaur, M., Kaur, L., Singh, G., Singh, L., Kaur, A., & Dhawan, R. K. (2023). Recent advancements in biomimetic drug delivery system of single-chain fatty acids as ufasomes and ufosomes: A comprehensive review. *Current Nanoscience, 19*(3), 362–371.

Kaur, R., & Kaur, S. (2014). Role of polymers in drug delivery. *Journal of Drug Delivery and Therapeutics, 4*(3), 32–36. Retrieved from https://jddtonline.info/index.php/jddt/article/view/826

Kehrein, J., Bunker, A., &Luxenhofer, R. (2024). POxload: Machine learning estimates drug loadings of polymeric micelles. *Molecular Pharmaceutics, 21*(7), 3356-3374.

Khaledian, S., Mohammadi, G., Abdoli, M., Fatahian, A., Fatahian, A., &Fatahian, R. (2024). Recent advances in implantable 3D-printed scaffolds for repair of spinal cord injury. *Advanced Pharmaceutical Bulletin, 14*, 331–345.

Khaledian, S., Rezaei, M., & Khosravi, A. (2024). 3D-printed scaffolds for spinal cord injury repair: Recent advances and future perspectives. *Biomaterials Science, 12*(6), 1455-1478.

Krishnan, A., Roy, S., & Menon, S. (2022). Amphiphilic block copolymers: From synthesis including living polymerization methods to applications in drug delivery. *European Polymer Journal, 172*, 111224.

Kurul, F., Turkmen, H., Cetin, A. E., &Topkaya, S. N. (2025). Nanomedicine: How nanomaterials are transforming drug delivery, bio-imaging, and diagnosis. *Next Nanotechnology, 7*, 100129.

Kurowiak, J., Klekiel, T., &Będziński, R. (2023). Biodegradable polymers in biomedical applications: A review—developments, perspectives and future challenges. *International Journal of Molecular Sciences, 24*(23), 16952. https://doi.org/10.3390/ijms242316952

Li, H., Wen, H., Zhang, H., Li, J., Cao, X., Zhang, J., ... Cai, X. (2025a). Polymeric micelle-hydrogel composites design for biomedical applications. *Chinese Chemical Letters, 36*(5), 110072.

Li, S., Shan, Y., Chen, J., Su, R., Zhao, L., He, R., & Li, Y. (2025b). Piezoelectricity promotes 3D-printed BTO/β-TCP composite scaffolds with excellent osteogenic performance. *ACS Applied Bio Materials, 8*(3), 2204-2214.

Liu, M., Song, X., Wen, Y., Zhu, J.-L., & Li, J. (2017). Injectable thermoresponsive hydrogel formed by alginate-g-poly(N-isopropylacrylamide) that releases doxorubicin encapsulated micelles as a smart drug delivery system. *ACS Applied Materials & Interfaces, 9*(42), 35673–35682. doi:10.1021/acsami.7b12849

Liu, Z., Liu, J., Cui, X., Wang, X., Zhang, L., & Tang, P. (2020). Recent advances on magnetic sensitive hydrogels in tissue engineering. *Frontiers in Chemistry, 8*, 124. doi:10.3389/fchem.2020.00124

Lohani, A., Saxena, R., Duarte, J. G., Khan, S., Figueiras, A., & Mascarenhas-Melo, F. (2025). Tailored polymeric hydrogels for regenerative medicine and drug delivery: From material design to clinical applications. *International Journal of Pharmaceutics, 681*, 125818. https://doi.org/10.1016/j.ijpharm.2025.125818

Long, T., Pang, Q., Deng, Y., Pang, X., Zhang, Y., Yang, R., & Zhou, C. (2025). Recent progress of artificial intelligence application in polymer materials. *Polymers, 17*(12), 1667.

Lu, H., Cai, Z., & Hu, P. (2024). Recent advances in polymeric delivery vehicles for controlled and sustained drug release. *Pharmaceutics, 16*(9), 1184.

Lu, P., Ruan, D., Huang, M., Tian, M., Zhu, K., Gan, Z., & Xiao, Z. (2024). Harnessing the potential of hydrogels for advanced therapeutic applications: Current achievements and future directions. *Signal Transduction and Targeted Therapy, 9*(1), 166. doi:10.1038/s41392-024-01852-x

Lu, Y., Essadki-Aittaji, I., Gao, J., Abraham, A. M., Anjani, Q. K., Cobo-González, A. B., ... Domínguez-Robles, J. (2025). Implantable and injectable drug delivery systems for pain management. *Expert Opinion on Drug Delivery*, 1-24.

Ma, W., & Li, X. (2025). Spinal cord injury repair based on drug and cell delivery: From remodeling microenvironment to relay connection formation. *Materials Today Bio, 31*, 101556.

Maeki, M., Uno, S., Sugiura, K., Sato, Y., Fujioka, Y., Ishida, A., … Tokeshi, M. (2024). Development of polymer-lipid hybrid nanoparticles for large-sized plasmid DNA transfection. *ACS Applied Materials & Interfaces, 16*(2), 2110–2119. https://doi.org/10.1021/acsami.3c14714

Mahajan, A., Kaur, L., Singh, G., Dhawan, R. K., & Singh, L. (2021). Multipotentiality of luliconazole against various fungal strains: Novel topical formulations and patent review. *Recent Advances in Anti-Infective Drug Discovery, 16*(3), 182–195.

Mahajan, A., Kaur, L., Singh, G., Dhawan, R. K., Singh, L., & Kaur, A. (2022). COVID-19 vaccines: Fabrication techniques and current status. *Coronaviruses, 3*(1), 42–48.

Mahajan, A., Singh, L., Singh, G., Dhawan, R. K., Kaur, M., Malhi, P. K., ... Kaur, L. (2023). An evidence-based review on bexarotene. *Tumor Discovery, 2*(2), 0436.

Marquina, S., Ozgul, M., Robertson-Brown, K., & Kenney, M. C. (2023). A review on PLGA particles as a sustained drug-delivery system and its effect on the retina. *Experimental Eye Research, 235*, 109626. doi:10.1016/j.exer.2023.109626

Medherant Ltd. (2025). *Bondlido patch EMA and FDA press releases*.

Meng, F., Qiao, X., Xin, C., Ju, X., & He, M. (2024). Recent progress of polymeric microneedle-assisted long-acting transdermal drug delivery. *Journal of Pharmacy & Pharmaceutical Sciences, 27*, 12434.

Mi, L., Li, F., Xu, D., Liu, J., Li, J., Zhong, L., ... Bai, N. (2024). Performance of 3D printed porous polyetheretherketone composite scaffolds combined with nano-hydroxyapatite/carbon fiber in bone tissue engineering: A biological evaluation. *Frontiers in Bioengineering and Biotechnology, 12*, 1343294.

Mineralys Therapeutics. (2025). *Company clinical trial disclosures and press reports*.

Mou, Y., Zhang, P., Lai, W. F., & Zhang, D. (2022). Design and applications of liposome-in-gel as carriers for cancer therapy. *Drug Delivery, 29*(1), 3245–3255.

Mukherjee, C., Varghese, D., Krishna, J. S., Boominathan, T., Rakeshkumar, R., Dineshkumar, S., ... Sivaramakrishna, A. (2023). Recent advances in biodegradable polymers–properties, applications and future prospects. *European Polymer Journal, 192*, 112068.

Naik, S., Krishna, T. V., Nayak, A., Joshi, M., & Pai, K. G. (2020). Hydrogels for cancer drug delivery. *Research Journal of Pharmacy and Technology, 13*(8), 4023–4027.

Nanda, H. S., Yang, L., Hu, J., Mao, H., & Jiang, S. (2022). Biodegradable polymers for biomedical applications. *Frontiers in Materials, 9*, 944755.

Nirmala, M. J., Kizhuveetil, U., Johnson, A., G, B., Nagarajan, R., & Muthuvijayan, V. (2023). Cancer nanomedicine: A review of nano-therapeutics and challenges ahead. *RSC Advances, 13*(13), 8606–8629. https://doi.org/10.1039/d2ra07863e

Nosrati, H., & Nosrati, M. (2023). Artificial intelligence in regenerative medicine: Applications and implications. *Biomimetics, 8*(5), 442.

Nunziata, G., Pollonio, D., Lacroce, E., & Rossi, F. (2025). Smart pH-responsive polymers in biomedical applications: Nanoparticles, hydrogels, and emerging hybrid platforms. *Materials Today Chemistry, 49*, 103063.

Ocular Therapeutix. (2025). *OTX-TKI and Dextenza clinical and regulatory updates*. Company Newsroom.

Ogay, V., Mun, E. A., Kudaibergen, G., Baidarbekov, M., Kassymbek, K., Zharkinbekov, Z., & Saparov, A. (2020). Progress and prospects of polymer-based drug delivery systems for bone tissue regeneration. *Polymers, 12*(12), 2881.

Oladapo, B. I., Zahedi, A., Ismail, S. O., Fernando, W., &Ikumapayi, O. M. (2023). 3D printed biomimetic bone implant polymeric composite scaffolds. *The International Journal of Advanced Manufacturing Technology, 126*, 4259–4267.

Oladapo, B. I., Zahedi, S. A., Ismail, S. O., Adeoye, A. O. M., & Muhammad, M. A. (2021). 3D printing of PEEK–cHAp scaffold for medical bone implant. *Bio-Design and Manufacturing, 4*(1), 44–59.

Önel, G. T. (2022). Poly (lactic-co-glycolic acid): FDA and EMA-approved biodegradable elastomeric copolymer. *Recent Approaches in, 9*.

Palma, S. I. (2025). Clinically approved nanotherapeutics. In *Nanotherapeutics for infectious diseases* (pp. 43-91). Jenny Stanford Publishing.

Panchpuri, M., Painuli, R., & Kumar, C. (2025). Artificial intelligence in smart drug delivery systems: A step toward personalized medicine. *RSC Pharmaceutics, 2*(5), 882-914. https://doi.org/10.1039/d5pm00089k .

Patil, S., Kumar, S., Rao, D. M., &Rewatkar, K. (2024). Current regulatory framework and challenges for the approval of complex generics in the US and the EU. *Current Indian Science, 2*(1), E2210299X269535.

PolyPid Ltd. (2025). *PLEX hydrogel clinical update and NDA filing plan*. PolyPid Press Release, June 2025.

Qi, H., Zhang, B., & Lian, F. (2025). 3D-printed bioceramic scaffolds for bone defect repair: Bone aging and immune regulation. *Frontiers in Bioengineering and Biotechnology, 13*, 1557203.

Quader, S., & Van Guyse, J. F. R. (2022). Bioresponsive polymers for nanomedicine-expectations and reality!.*Polymers, 14*(17), 3659. https://doi.org/10.3390/polym14173659

Rao, Z., Lan, M., Zhu, D., Jiang, L., Wang, Z., Wan, H., … Liu, H. (2022). Synergistically promoted proton conduction of proton exchange membrane by phosphoric acid functionalized carbon nanotubes and graphene oxide. *Journal of Membrane Science, 659*, 120810. doi:10.1016/j.memsci.2022.120810

Razzaghi, M. (2025). Polymeric 3D-printed microneedle arrays for non-transdermal drug delivery and diagnostics. *Polymers, 17*(14), 1982.

Rezaei, N., Akbarzadeh, I., Kazemi, S., Montazeri, L., Zarkesh, I., Hossein-Khannazer, N., ... &Vosough, M. (2021). Smart materials in regenerative medicine. *Modern Medical Laboratory Journal, 4*(1), 39-51.

Roche. (2023). *Columvi (glofitamab) EMA approval notification*. Roche News.

Rodriguez-Cruz, J. J., Chapa-Villarreal, F. A., Duggal, I., & Peppas, N. A. (2025). Advanced rational design of polymeric nanoparticles for the controlled delivery of biologics. *Journal of Controlled Release: Official Journal of the Controlled Release Society, 384*, 113940. https://doi.org/10.1016/j.jconrel.2025.113940

Rosario, A. J., & Ma, B. (2024). Stimuli-responsive polymer networks: Application, design, and computational exploration. *ACS Applied Polymer Materials, 6*(23), 14204-14228.

Schneider, J., Basak, S., Hou, Y., Koo, J. H., Wardle, B. L., Gadegaard, N., & Kumar, S. (2024). 3D printed polyetheretherketone smart polymer nanocomposite scaffolds: Mechanical, self-sensing, and biological attributes. *Advanced Engineering Materials, 26*(4), 2301659.

Schneider, J., et al. (2024). Self-sensing smart nanocomposite scaffolds based on 3D-printed PEEK for bone tissue engineering. *Advanced Healthcare Materials, 13*(8), 2302145.

Scott, E. C., Baines, A. C., Gong, Y., Moore Jr, R., Pamuk, G. E., Saber, H., ... Beaver, J. A. (2023). Trends in the approval of cancer therapies by the FDA in the twenty-first century. *Nature Reviews Drug Discovery, 22*(8), 625-640.

Senthilkumar, D., Don, T. M., Liao, Y. J., & Kuo, C. Y. (2025). The art of biodegradable polymer design for the treatments against osteomyelitis. *International Journal of Biological Macromolecules, 285*, 138347.

Servier. (2025). *Voranigo (vorasidenib) EMA approval press release*.

Shanahan, K., Coen, D., &Nafo, W. (2025). Polymer-based nanoparticles for cancer theranostics: Advances, challenges, and future perspectives. *Exploration of BioMat-X, 2,* 101342 DOI: https://doi.org/10.37349/ebmx.2025.101342

Sharma, S. J., Gupta, R., & Gupta, M. (2024). Advanced testing and biocompatibility strategies for sustainable biomaterials. *Biotechnology for Sustainable Materials, 1*(1), 18.

Shendge, R. S., Zalte, T. S., & Khade, S. B. (2024). Polymeric microspheres redefining the landscape of colon-targeted delivery: A contemporary update. *European Journal of Medicinal Chemistry Reports, 11*, 100156.

Shergujri, D. A., Khanday, M. A., Noor, A., Adnan, M., Arif, I., Raza, S. N., ... Khan, N. A. (2025). Next-generation biopolymer gels: Innovations in drug delivery and theranostics. *Journal of Materials Chemistry B, 13,* 3222-3244. DOI: 10.1039/D4TB02068E .

Singh, A. V., Rosenkranz, D., Ansari, M. H. D., Singh, R., Kanase, A., Singh, S. P., ... Luch, A. (2020). Artificial intelligence and machine learning empower advanced biomedical material design to toxicity prediction. *Advanced Intelligent Systems, 2*(12), 2000084. https://doi.org/10.1002/aisy.202000084

Singh, L., Kaur, L., Singh, G., Kaur, M., Dhawan, R. K., Kaur, N., … Singh, P. (2022). Determination of alteration in micromeritic properties of a solid dispersion: Brunauer-Emmett-Teller based adsorption and other structured approaches. *AAPS PharmSciTech, 23*(6), 209.

Singh, L., Kaur, L., Singh, G., Dhawan, R. K., Kaur, M., Kaur, N., … Singh, S. (2023). Impact of molecular building blocks on dynamic nature of novel biomimetic drug delivery systems as ufasomes and ufosomes: Modification in structure and surface charge. *Current Nanomedicine, 13*(2), 91–101.

Son, A., Park, J., Kim, W., Yoon, Y., Lee, S., Park, Y., & Kim, H. (2024). Revolutionizing molecular design for innovative therapeutic applications through artificial intelligence. *Molecules, 29*(19), 4626.

Staudinger, H. (1920). ÜberPolymerisation. *Berichte der DeutschenChemischen Gesellschaft, 53*(6), 1073–1085. doi:10.1002/cber.19200530627

Staudinger, H. (1953). *Nobel lecture: Macromolecular chemistry*. NobelPrize.org. Retrieved from https://www.nobelprize.org/uploads/2018/06/staudinger-lecture.pdf

Stavarache, C., et al. (2024). Enhanced 3D-printed alginate/carrageenan/carboxymethyl cellulose hydrogel scaffolds for tissue engineering. *Carbohydrate Polymers, 328*, 121710.

Stavarache, C., Gârea, S. A., Serafim, A., Olăreț, E., Vlăsceanu, G. M., Marin, M. M., & Iovu, H. (2024). Three-dimensional printed sodium alginate and κ-carrageenan based scaffolds with potential biomedical applications. *Polymers, 16*(3), 305. doi:10.3390/polym16030305

Stavarache, C., Ghebaur, A., Serafim, A., Vlăsceanu, G. M., Vasile, E., Gârea, S. A., & Iovu, H. (2024). Fabrication of k-carrageenan/alginate/carboxymethyl cellulose based scaffolds via 3D printing for potential biomedical applications. *Polymers, 16*(11), 1592. doi:10.3390/polym16111592

Sumathi, S. (2025). A review of electrospun polymeric fibers as potential drug delivery systems for tunable release kinetics. *Journal of Science: Advanced Materials and Devices*, 100933.

Sun, X., Yu, X., Cheng, F., & He, W. (2021). Cationic polymeric template-mediated preparation of silica nanocomposites. *Soft Matter, 17*(40), 8995–9007. doi:10.1039/D1SM00773D

Taiho Oncology. (2023). *Inaqovi (decitabine/cedazuridine) EU SmPC and approval history*.

Tewari, A. K., Upadhyay, S. C., Kumar, M., Pathak, K., Kaushik, D., Verma, R., …Cavalu, S. (2022). Insights on development aspects of polymeric nanocarriers: The translation from bench to clinic. *Polymers, 14*(17), 3545. https://doi.org/10.3390/polym14173545

Thapa, R. K., & Kim, J. O. (2023). Nanomedicine-based commercial formulations: Current developments and future prospects. *Journal of Pharmaceutical Investigation, 53*(1), 19-33.

Turac, I.-R., Porfire, A., Iurian, S., Crișan, A. G., Casian, T., Iovanov, R., &Tomuță, I. (2024). Expanding the manufacturing approaches for gastroretentive drug delivery systems with 3D printing technology. *Pharmaceutics, 16*(6), 790. doi:10.3390/pharmaceutics16060790

Ullah, A., Khan, M., Zhang, Y., Shafiq, M., Ullah, M., Abbas, A., … Diao, Y. (2025). Advancing therapeutic strategies with polymeric drug conjugates for nucleic acid delivery and treatment. *International Journal of Nanomedicine, 20*, 25–52. https://doi.org/10.2147/IJN.S429279

van der Meel, R., Sulheim, E., Shi, Y., Kiessling, F., Mulder, W. J., & Lammers, T. (2019). Smart cancer nanomedicine. *Nature Nanotechnology, 14*(11), 1007-1017.

Vera Therapeutics. (2025). *ORIGIN phase 3 program update*. Corporate Presentation.

Visan, A. I., &Negut, I. (2024). Development and applications of PLGA hydrogels for sustained delivery of therapeutic agents. *Gels, 10*(8), 497. doi:10.3390/gels10080497

Wan, B., Bao, Q., & Burgess, D. J. (2022). In vitro-in vivo correlation of PLGA microspheres: Effect of polymer source variation and temperature. *Journal of Controlled Release, 347*, 347-355. doi:10.1016/j.jconrel.2022.05.014

Wang, G., Zhang, X. A., Kapilevich, L., & Hu, M. (2023). Recent advances in polymeric microparticle-based drug delivery systems for knee osteoarthritis treatment. *Frontiers in Bioengineering and Biotechnology, 11*, 1290870.

Wang, R., Jiang, G., Aharodnikau, U. E., Yunusov, K., Sun, Y., Liu, T., &Solomevich, S. O. (2022). Recent advances in polymer microneedles for drug transdermal delivery: Design strategies and applications. *Macromolecular Rapid Communications, 43*(8), 2200037.

Wang, T., & Chang, T. M. S. (2023). Superparamagnetic artificial cells PLGA Fe_3O_4 micro/nanocapsules for cancer targeted delivery. *Cancers, 15*(24), 5807. doi:10.3390/cancers15245807

Waqar, M. A., Mubarak, N., Khan, A. M., Khan, R., Shaheen, F., & Shabbir, A. (2024). Advanced polymers and recent advancements on gastroretentive drug delivery system; A comprehensive review. *Journal of Drug Targeting, 32*(6), 655-671.

Watson, J. D., & Crick, F. H. C. (1953). Molecular structure of nucleic acids: A structure for deoxyribose nucleic acid. *Nature, 171*(4356), 737–738. doi:10.1038/171737a0

Wildy, M., & Lu, P. (2023). Electrospun nanofibers: Shaping the future of controlled and responsive drug delivery. *Materials, 16*(22), 7062. doi:10.3390/ma16227062

Xu, Y., Chen, J., Ding, J., Sun, J., Song, W., Tang, Z., ... & Chen, X. (2025a). Synthetic polymers for drug, gene, and vaccine delivery. *Polymer Science & Technology, 1*(3), 171-220.

Xu, Z., Deng, J., Gao, D., Du, Y., Zhang, Y., & Lai, Y. (2025b). Stimuli-responsive biomedical polymeric films for tissue regeneration. *Microstructures, 5*(3), N-A.

Yadav, P., Jain, J., &Sherje, A. P. (2021). Recent advances in nanocarriers-based drug delivery for cancer therapeutics: A review. *Reactive and Functional Polymers, 165*, 104970. doi:10.1016/j.reactfunctpolym.2021.104970

Yetisgin, A. A., Malliappan, S. P., &Cetinel, S. (2025). Current state and potential of polymersomes as ocular drug delivery systems. *Nanoscale, 17*, 14458-14476.

Yu, H., Liu, H., Shen, Y., & Ao, Q. (2023). Synthetic biodegradable polymer materials in the repair of tumor-associated bone defects. *Frontiers in Bioengineering and Biotechnology, 11*, 1096525. https://doi.org/10.3389/fbioe.2023.1096525

Yuan, N., Shao, K., Huang, S., & Chen, C. (2023). Chitosan, alginate, hyaluronic acid and other novel multifunctional hydrogel dressings for wound healing: A review. *International Journal of Biological Macromolecules, 240*, 124321. doi:10.1016/j.ijbiomac.2023.124321

Yue, T., He, J., & Li, Y. (2025). Machine-learning-assisted molecular design of innovative polymers. *Accounts of Materials Research, 6*(8), 1033-1045.

Yusuf, A., Almotairy, A. R. Z., Henidi, H., Alshehri, O. Y., &Aldughaim, M. S. (2023). Nanoparticles as drug delivery systems: A review of the implication of nanoparticles' physicochemical properties on responses in biological systems. *Polymers, 15*(7), 1596.

Zaszczyńska, A., Zabielski, K., Gradys, A., Kowalczyk, T., &Sajkiewicz, P. (2024). Piezoelectric scaffolds as smart materials for bone tissue engineering. *Polymers, 16*(19), 2797.

Zhang, F., Guo, J., Zhang, Z., Duan, M., Wang, G., Qian, Y., ... Jiang, X. (2022). Application of engineered extracellular vesicles for targeted tumor therapy. *Journal of Biomedical Science, 29*(1), 14.

Zhang, H., Chen, H., Hu, X., Muhammad, W., Liu, C., & Liu, W. (2025a). Inflammation-modulating polymeric nanoparticles: Design strategies, mechanisms, and therapeutic applications. *EBioMedicine, 118*, 105837. https://doi.org/10.1016/j.ebiom.2025.105837

Zhang, J., Yang, X., Chang, Z., Zhu, W., Ma, Y., & He, H. (2025b). Polymeric nanocarriers for gene delivery. *Asian Journal of Pharmaceutical Sciences*, 101015.

Zhang, Y., & Tian, J. (2024). Strategies, challenges, and prospects of nanoparticles in gynecological malignancies. *ACS Omega, 9*(36), 37459-37504.

Zhao, M., Yang, H., Yang, Q., Zhang, C., Liu, J., Wu, Z., ... Liu, W. (2025). A multifunctional PEEK composite scaffold with immunomodulatory, angiogenic, and osteogenic properties for enhanced bone regeneration. *Polymers, 17*(9), 1206.

Zhou, B., Li, X., Pan, Y., He, B., & Gao, B. (2025). Artificial intelligence-assisted next-generation biomaterials: From design and preparation to medical applications. *Colloids and Surfaces B: Biointerfaces*, 114970.

Zhu, S., Diao, S., Liu, X., Zhang, Z., Liu, F., Chen, W., ... Chen, J. (2025). Biomaterial-based strategies: A new era in spinal cord injury treatment. *Neural Regeneration Research, 20*(12), 3476-3500.

FABAD J. Pharm. Sci., 51, 1, 351-382, 2026
Doi: 10.55262/fabadeczacilik.1757782
REVIEW ARTICLE

Medicinal Chemistry Approaches for Combatting SARS-CoV-2 and COVID-19 Therapeutics

Neelottama KUSHWAHA[*°], Swatantra K.S. KUSHWAHA[**], Anmol KUMAR[***]

Medicinal Chemistry Approaches for Combating SARS-CoV-2 and COVID-19 Therapeutics

SUMMARY

The COVID-19 pandemic has underscored the need for innovative and adaptable solutions in medicinal chemistry to address the growing global health challenges. New strategies, including structure-based drug design, AI-driven drug discovery, and drug repurposing, have shown promising advancements in accelerating the creation of treatments. Significant strides have been made in focusing on crucial viral proteins, particularly the main protease (Mpro) and RNA-dependent RNA polymerase (RdRp), which have created new opportunities for small-molecule inhibitors. Additionally, advancements in peptide-based therapies, monoclonal antibodies, and nanotechnology-enhanced drug delivery systems have expanded the tools available against SARS-CoV-2. However, significant challenges persist, such as addressing viral mutations, improving access to medications, and ensuring rapid scalability of treatments. Ongoing investment in interdisciplinary collaborations, enhanced screening technologies, and real-time genetic monitoring will be essential for refining these strategies. By adopting a proactive approach, medicinal chemistry can respond to the current pandemic and lay the groundwork for effectively tackling future viral threats with greater precision and efficiency.

Keywords: *SARS-CoV-2, antiviral agents, viral protein, drug repurposing, ligand-based drug design, structure-based drug design.*

SARS-CoV-2 ve COVID-19 Tedavilerinde Tıbbi Kimya Yaklaşımları

ÖZ

COVID-19 pandemisi, artan küresel sağlık sorunlarıyla mücadele etmek için tıbbi kimyada yenilikçi ve uyarlanabilir çözümlere olan acil ilgiyi artırdı. Yapıya dayalı ilaç tasarımı, yapay zekâ destekli ilaç keşfi ve ilaçların yeniden kullanımı gibi yeni stratejiler, tedavilerin geliştirilmesini hızlandırma potansiyelini ortaya koydu. Proteaz (Mpro) ve RNA bağımlı RNA polimeraz (RdRp) gibi temel viral proteinleri hedeflemedeki ilerleme, küçük moleküllü inhibitörler için yeni fırsatlar yarattı. Ayrıca, peptit bazlı tedaviler, monoklonal antikorlar ve nanoteknoloji destekli ilaç salım sistemlerindeki gelişmeler, SARS-CoV-2'ye karşı mevcut araçları genişletti. Bununla birlikte, viral mutasyonların ele alınması, ilaçlara erişimin iyileştirilmesi ve tedavilerin hızlı ölçeklenebilirliğinin sağlanması gibi önemli zorluklar devam etmektedir. Disiplinlerarası iş birliklerine, gelişmiş tarama teknolojilerine ve gerçek zamanlı genetik izlemeye devam eden yatırımlar, bu stratejilerin geliştirilmesi için hayati önem taşıyacaktır. Tıbbi kimya, proaktif bir yaklaşım benimseyerek mevcut pandemiye yanıt verebilir ve gelecekteki viral tehditlerle daha fazla hassasiyet ve verimlilikle etkili bir şekilde mücadele etmek için zemin hazırlayabilir.

Anahtar Kelimeler: *SARS-CoV-2, antiviral ajanlar, viral protein, ilaçların yeniden kullanımı, ligand tabanlı ilaç tasarımı, yapı temelli ilaç tasarımı.*

Recieved: 4.08.2025
Revised: 29.01.2026
Accepted: 14.02.2026

[*] ORCID: 0000-0001-9653-1313, Krishna Institute of Pharmacy & Sciences, Kanpur-208017, India
[**] ORCID: 0000-0002-1004-6323, Krishna Institute of Pharmacy & Sciences, Kanpur-208017, India
[***] ORCID: 0009-0009-1566-4874, Krishna Institute of Pharmacy & Sciences, Kanpur-208017, India

° Corresponding Author; Prof. Dr. Neelottama Kushwaha
E-mail: neelottama@gmail.com

INTRODUCTION

The coronavirus is a type of virus characterised by a single RNA strand that ranges from 27 to 32 kilobases in length (Batool et al., 2025; Nagu et al., 2024). It is part of the Coronaviridae family, which includes various types such as alpha, beta, delta, and gamma coronaviruses. When viewed under an electron microscope, the spherical-shaped virus is adorned with viral surface spike proteins, giving it a unique crown-like appearance (Rut et al., 2020; Zhang et al., 2025). This virus can infect many animals, including humans, mammals, and birds, leading to various symptoms that can impact the respiratory, digestive, and genital systems. The most prevalent coronaviruses that affect humans include 229E, NL63, OC43, and HKU1. These viruses are responsible for a range of respiratory conditions, varying from mild cold-like symptoms to more serious illnesses such as Middle East Respiratory Syndrome (MERS) and Severe Acute Respiratory Syndrome (SARS) (Han et al., 2024).

Structure of SARS-CoV-2

The virus has three main components: a genome composed of single-stranded RNA, accompanied by a lipid bilayer of viral membrane, and surface proteins (Mondal et al., 2023). The RNA genome consists of approximately 30,000 nucleotides and is responsible for encoding four key structural proteins: nucleocapsid (N), membrane (M), envelope (E), and spike (S). In addition to these structural components, the genome also produces various non-structural proteins (nsps), contributing to its overall functionality (Figure 1.).

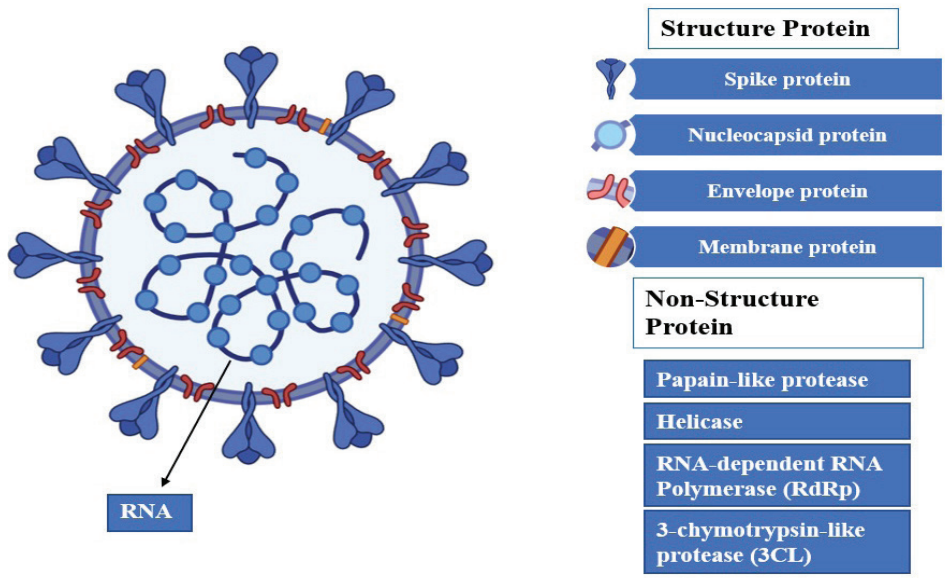


Figure 1. The virus SARS-CoV-2 and its molecular target proteins

The protein called Nucleocapsid (N) is essential for the construction of the nucleocapsid, which serves as a protective shield for the virus's genome. The genome of specific viral RNA is enclosed within a ribonucleoprotein complex, creating the nucleocapsid. The most abundant **M-protein** is a surface protein of the virus that facilitates viral assembly by inducing membrane curvature. The E-protein, the smallest of the membrane proteins, consists of 76 to 109 amino acid residues. It plays a vital role in several processes, including virus assembly, envelope formation, the permeability of host cell membranes, and overall pathogenicity. In contrast, the S protein, which ranges from 1,200 to 1,400 amino acid residues, serves as an essential structural transmembrane protein on the virus's outer envelope. This protein is critical for the virus to invade host cells, as it interacts with specific receptors located on the surface of human cells (Jain et al., 2022; Woo et al., 2023).

VIRAL TARGETS FOR ANTI-VIRAL AGENTS

Anti-coronavirus agents are categorised into various groups based on their site of action (Enjuanes et al., 2022; Niknamian, 2021).

1. **Targets of the drug on the Spike Protein or the entry of the virus:** Amiodarone
2. **ACE Inhibitors and ATR Blockers:** Losartan (Tikhomirova et al., 2024)
3. **TMPRSS2 Inhibitors:** Namafostat, Camostat, Upamostat
4. **Protease Inhibitors of the Virus:** Lopinavir, Ritonavir, Nirmatrelvir
5. **The Virus RNA Polymerase inhibitors:** Remdesivir (Eltayeb et al., 2024; GBD 2019 Meningitis Antimicrobial Resistance Collaborators, 2023).

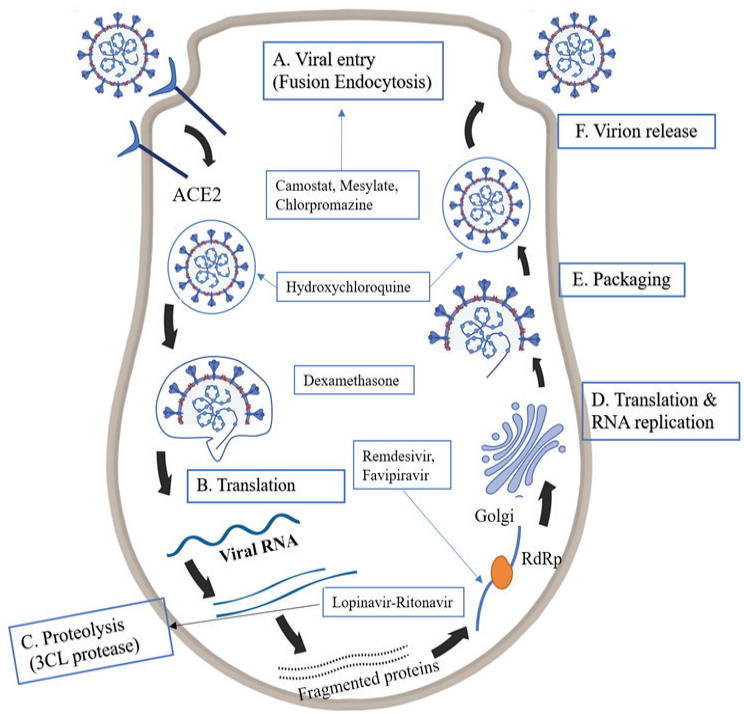


Figure 2. Various Drugs targeted at different viral target sites

DRUGS TARGETING THE SPIKE PROTEIN OR THE PROCESS OF VIRAL ENTRY

Infectious viruses bind to a crucial receptor on the surface of host cells called angiotensin-converting enzyme. After the first interaction, a serine protease called TMPRSS2 (transmembrane serine protease 2) helps fuse the membranes of the virus and the host cell (Cervantes et al., 2023). This allows the virus to enter the cell through a mechanism called endocytosis. Once inside, the virus begins its replication process. Several proteins play critical roles in this viral life cycle, including the spike protein of SARS-CoV-2, the ACE-2 receptor, and the TMPRSS2 protease. These components represent viable targets for developing antiviral treatments (Yaro et al., 2024)

THE RECEPTOR ACE INHIBITORS AND ATR BLOCKERS

Since ACE acts as the type of cell receptor for the specific spike protein of the virus, it has been specifically explored as a potential target for the specific treatment of COVID-19. Research has indicated that certain antihypertensive medications can enhance the production of the ACE-2 enzyme, which acts as the doorway for SARS-CoV-2 to enter cells. Consequently, at the onset of the COVID-19 pandemic, there was optimism that this category of drugs, including losartan, might assist in managing the infection. This optimism

was based on early mechanistic insights into the role of the renin–angiotensin–aldosterone system (RAAS) in SARS-CoV-2 pathogenesis. The virus was found to utilise angiotensin-converting enzyme 2 (ACE-2) as its cellular entry receptor, and ARBs were known to modulate the angiotensin-converting enzyme 2 (ACE2) expression and activity (Zipeto et al., 2020).

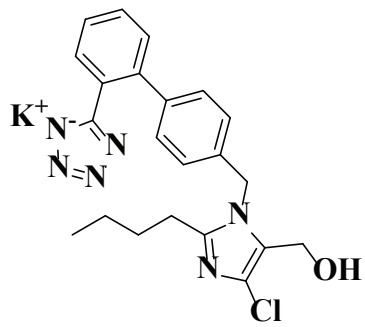


Figure 3. Losartan potassium (LOS-K)

Losartan potassium (LOS-K) is a synthetic antihypertensive agent known as an angiotensin II receptor antagonist. Its chemical structure is defined as a specific compound 2-*n*-butyl-4-chloro-5-hydroxymethyl-1-((2-(1*H*-tetrazol-5-yl) (biphenyl-4-4-yl) methyl) imidazole (Magrone et al., 2020; Mostafa-Hedeab, 2020).

TMPRSS2 BLOCKERS

TMPRSS-2, a specific serine protease, is a possible and specific target for the COVID-19 treatment. In the beginning stage of the pandemic, nafamostat, a serine protease inhibitor that acts on TMPRSS-2, was investigated for its efficacy in treating COVID-19 pneumonia among elder patients who need oxygen therapy. Other similar compounds include Nafamostat, Camostat, and Upamostat (Gunathilaka, 2023; Zhang et al., 2024).

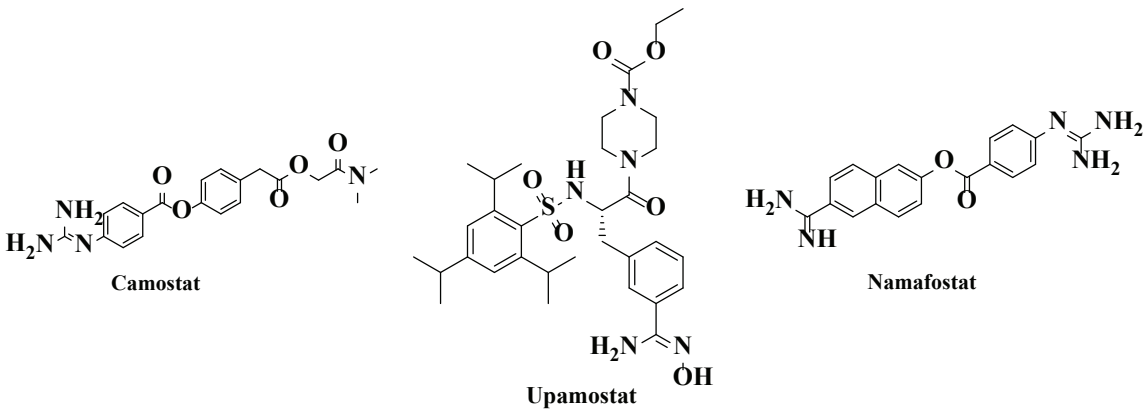


Figure 4. Structures of TMPRSS2 Inhibitors

THE VIRAL PROTEASE INHIBITORS

After the virus releases its genetic material into the host cell, the host's ribosomes translate it into a long polyprotein chain. However, this polyprotein must be broken down into smaller, functional viral proteins—including the essential RNA-dependent RNA polymerase (RdRp). To facilitate this cleavage, the virus relies on two key proteases: 3CLpro (also known as the main protease) and PLpro (papain-like protease). These enzymes systematically process the polyprotein, enabling the production of mature viral proteins necessary for replication and infection. Lopinavir was originally formulated as a therapeutic agent for HIV, specifically targeting the 3C-like protease (Figure 5.) (Sarkar et al., 2024). This enzyme is classified within the cysteine protease family and the medication functions by imitating the transition state of the hydrolysis reaction. Because of its low metabolic stability, lopinavir is often used in combination with ritonavir (Figure 6.). The combination of lopinavir and ritonavir was commonly used during the early phase of the COVID-19 pandemic. Consequent clinical trials demonstrated that incorporating it into standard care does not provide any benefits for patients (Keller et al., 2022; Singh et al., 2020).

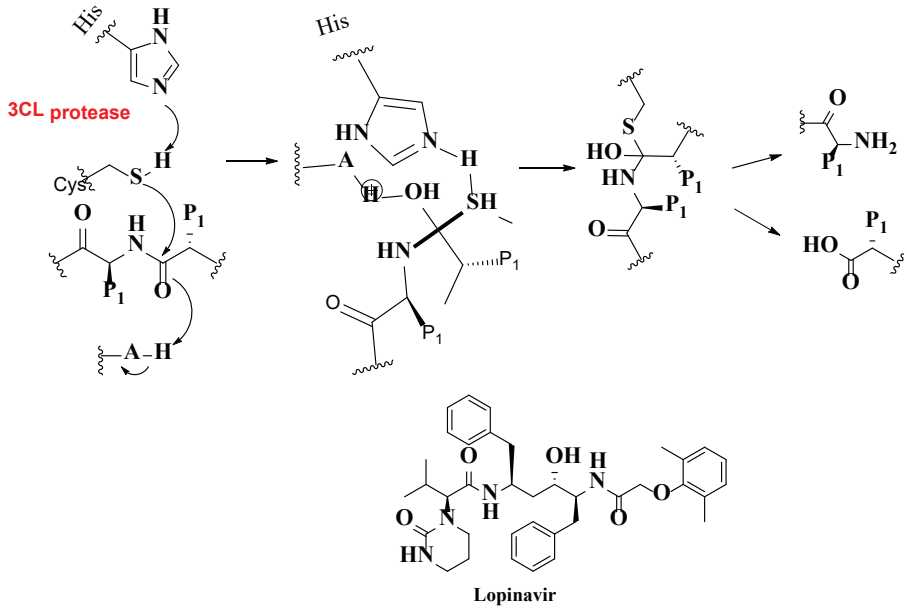


Figure 5. The Chemical representation of the mechanism of action of Lopinavir

The combination of nirmatrelvir and ritonavir shows great promise, as it is about 88% effective in preventing hospital admission or mortality in adult outpatients when administered within a specific 5 days following the appearance of the virus COVID-19 symptoms (Figure 7.). However, the cytochrome inhibitor ritonavir has the specific potential to cause significant interactions with other specific medications, which need to be carefully evaluated.

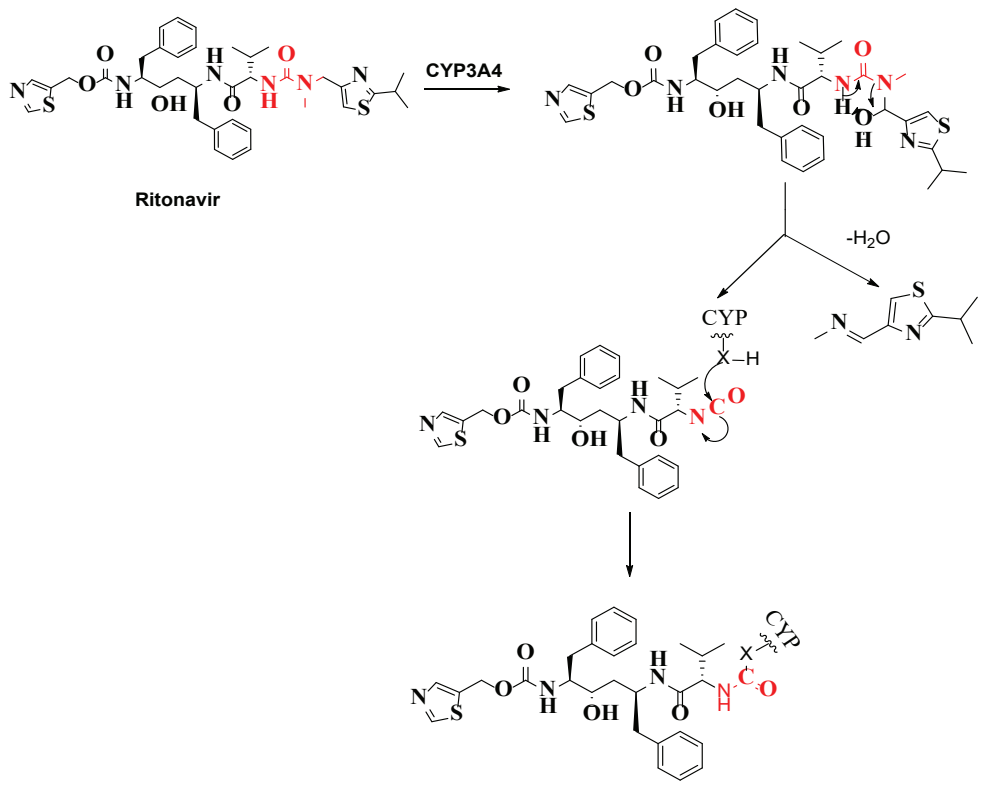


Figure 6. Ritonavir serves as a pharmacokinetic enhancer for Lopinavir

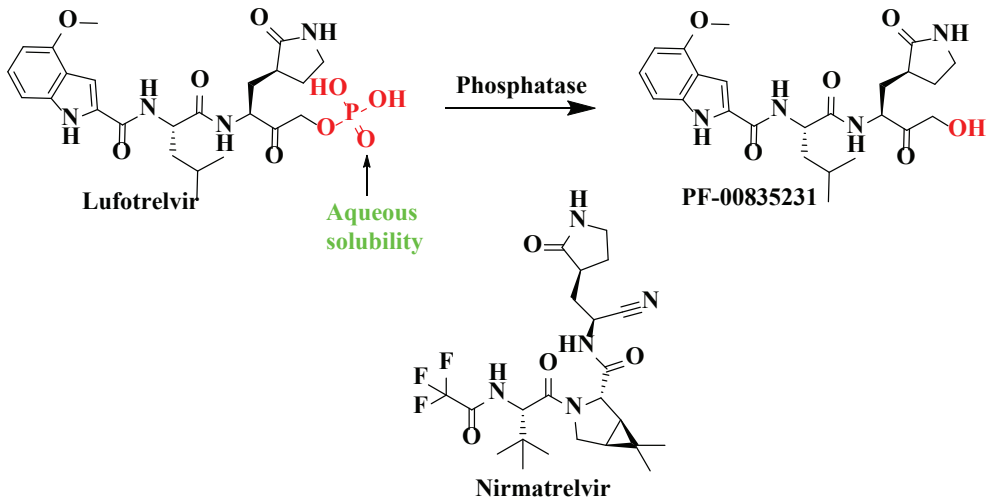


Figure 7. The molecular structures of Lufotrelvir, PF-00835231, and Nirmatrelvir

RNA POLYMERASE INHIBITORS

In the search for antiviral drugs, one common method is to inhibit RNA polymerase. Inhibitors of this enzyme are often addressed using modified nucleosides with altered ribose configurations (Kalkanli et al., 2021). Following tri-phosphorylation by kinases, these changed nucleosides can be recognised by RNA polymerase and used as substrates, resulting in their incorporation into the elongation of the RNA chain. However, these structural changes prevent the addition of further nucleotides, effectively terminating the elongation of the RNA chain (Figure 8.) (Patel et al., 2021a).

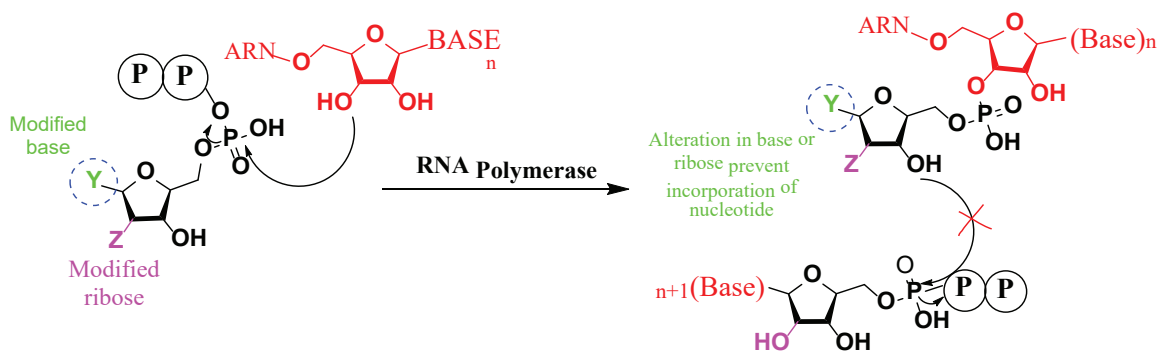


Figure 8. The fundamental mechanism by which nucleoside-type RNA polymerase inhibitors operate

Remdesivir, developed by Gilead Sciences, was the inaugural drug for COVID-19 to receive approval from the FDA. Following phosphorylation, this molecule can be regarded as an ATP analogue, which serves as a specific medium, like a substrate for RNA-dependent RNA polymerase. Remdesivir exhibits certain structural anomalies (Figure 9.). Its adenine component undergoes modification and C-C bond linkage to ribose, making it a C-nucleoside. The occurrence of the chemical cyano group at the anomeric carbon is rare, leading to decreased activity on mammalian RNA polymerases. As a prodrug, the phosphorus atom in Remdesivir is integral to the phosphoramidate group that must undergo hydrolysis to produce the corresponding phosphate.

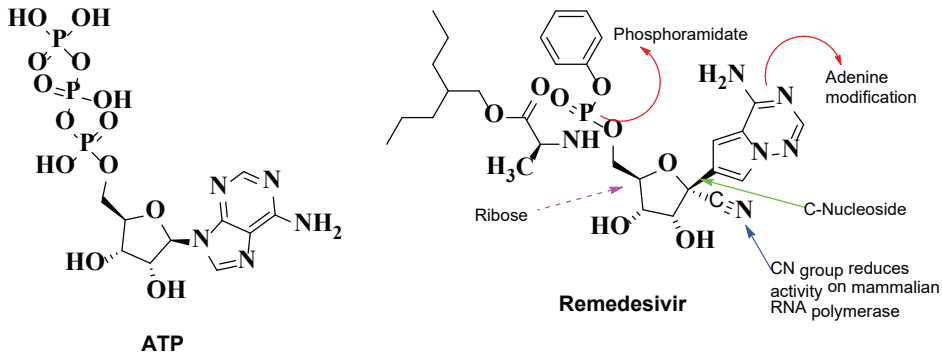


Figure 9. Structural comparison of Remedesivir with ATP

Another ProTide pro-drug, initially developed for hepatitis C treatment, is bemnifosbuvir (AT-527), which is orally available (Good et al., 2025) Atea Pharmaceuticals developed the product, which was subsequently licensed to Roche for markets outside the USA, identified by the research code RO7496998. The drug was subjected to bioactivation via the previously mentioned process, resulting in an adenosine fluoro analog (Figure 10.). After triphosphorylation, this medication inhibits and block the RNA polymerase enzyme of the virus SARS-CoV-2.

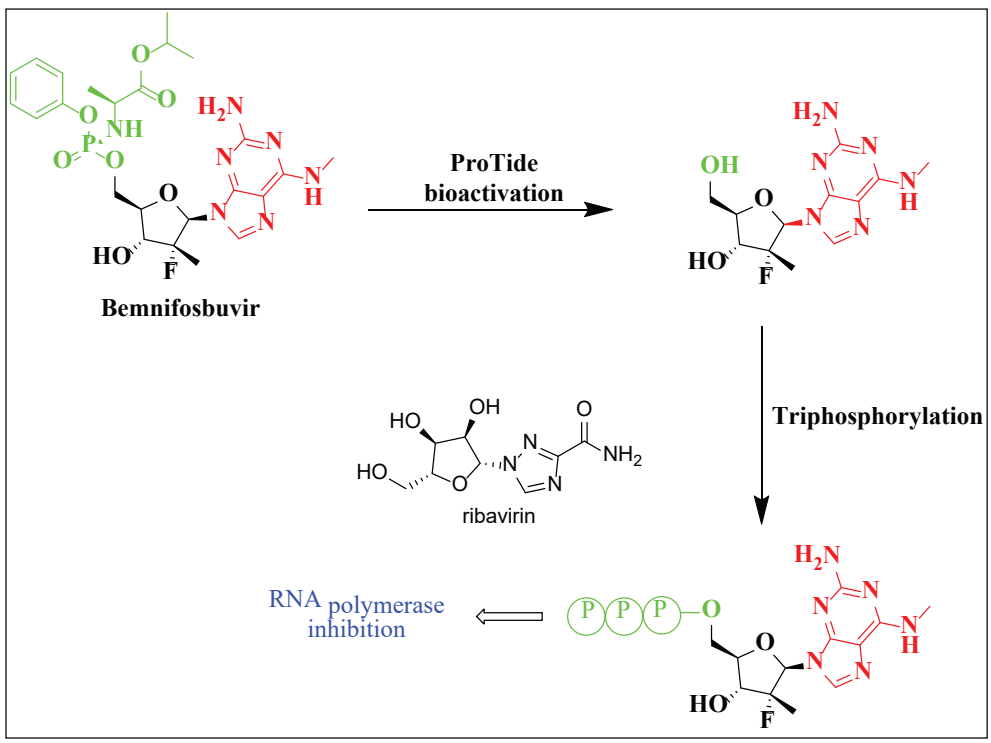


Figure 10. Bioactivation and mechanism of action of Bemnifosbuvir

STRATEGIES IN MEDICINAL CHEMISTRY SEEKING SPECIFIC, EFFECTIVE INHIBITORS OF THE SARS-COV-2 VIRUS

Identifying the specific lead compounds is an important step in researching and developing new medications. Insights gained from discovering and developing inhibitors for SARS-CoV can inform some standard medicinal chemistry methods to help find candidate drugs for SARS-CoV-2 in these urgent circumstances. A variety of strategies are employed in

the pursuit of new therapeutics. These methods encompass drug repurposing, comprehensive screening techniques that can involve either computational (*in silico*) or laboratory-based (*in vitro*) approaches, and the use of target-oriented rational drug design. Additionally, the integration of natural products, including elements from traditional Chinese medicine, plays a significant role in this research landscape (Cao et al., 2020; Sigfrid et al., 2019).

Repurposing of the drug / drug reposition

Drug repurposing is an interesting technique to identify new applications for existing drugs or substances. This strategy enables the rapid identification of new therapeutic alternatives that are either presently available for clinical use or may be expedited for approval to address a variety of diseases and disorders. Since the SARS-CoV-1 pandemic, there has been a concerted effort to repurpose approved drugs (Figure 11.). Additionally, we provide several examples of potential SARS-CoV-2 treatments identified through this strategy, as represented in the figure (Gordon et al., 2020; Zhang et al., 2023).

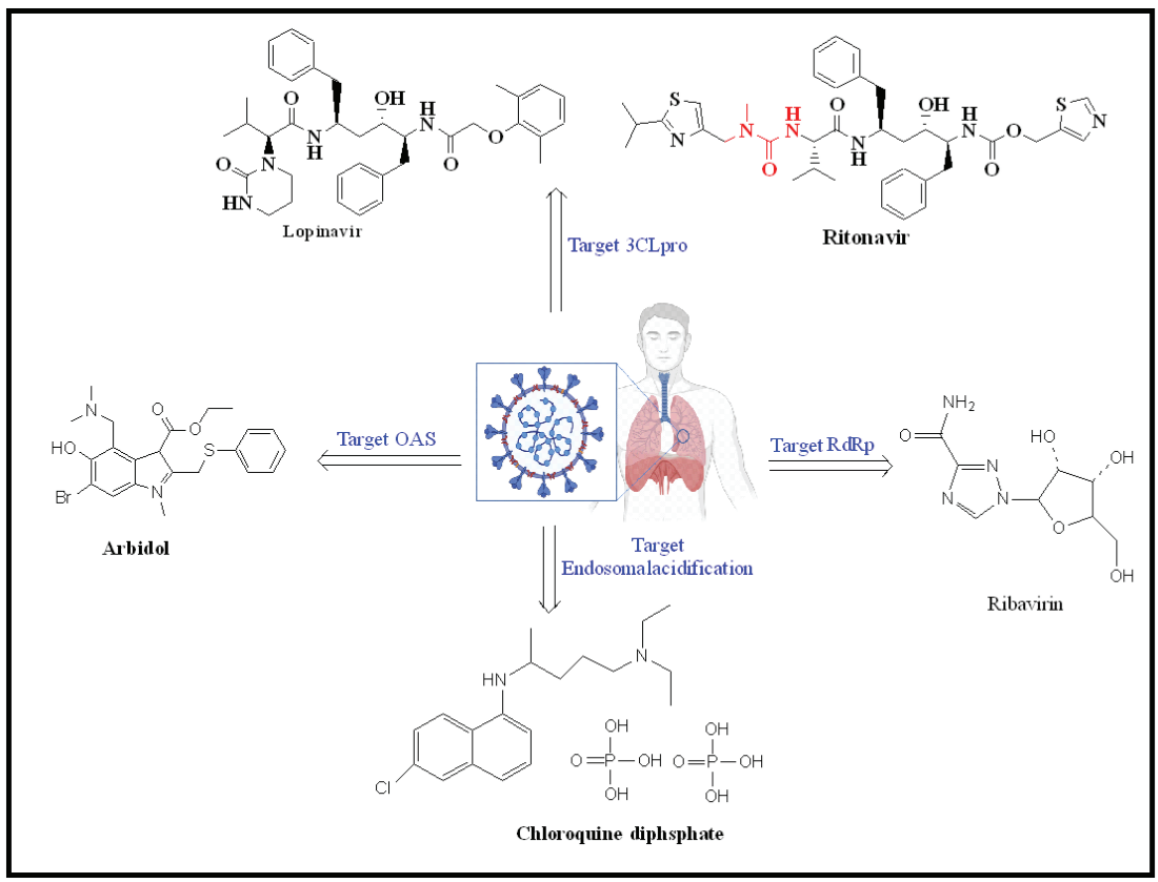


Figure 11. Schematic presentation of Repurposing of existing Anti-viral agents as possible inhibitors of SARS-CoV-2 (RdRp RNA RNA-dependent RNA polymerase, 3CLpro= 3 Chymotrypsin-like protease, OAS=Oligoadenylate synthetase)

Reposition of current extended-spectrum antiviral drugs

A promising way to identify and specify the potent treatments against the COVID-19 virus, SARS-CoV-2, is by repurposing existing broad-spectrum antiviral drugs. Several traditional methods can be considered to develop or evaluate new and specific broad-spectrum coronavirus inhibitors (Figure 12.).

One approach involves repurposing nucleoside analogues to inhibit and block the SARS-CoV-2 RNA-dependent RNA polymerase (RdRp), an enzyme that is conserved among various coronavirus families and is significant for the life cycle of the virus (Duflos et al., 2023). RdRp serves as an excellent target for broad-spectrum antiviral treatments. Inside the cell, kinases convert these nucleoside analogues into their active triphosphate forms, which are then involved and change into the expanding RNA chain, subsequent in the cessation of the replication process and contributing to their antiviral effects. However, some nucleoside analogues, like ribavirin, are ineffective against coronaviruses to probe the function of the 3'-5' exoribonuclease (ExoN). Remdesivir is an inhibitor of RdRp that has a wide range of activity against coronaviruses (Fearns & Deval, 2016; Wu et al., 2020).

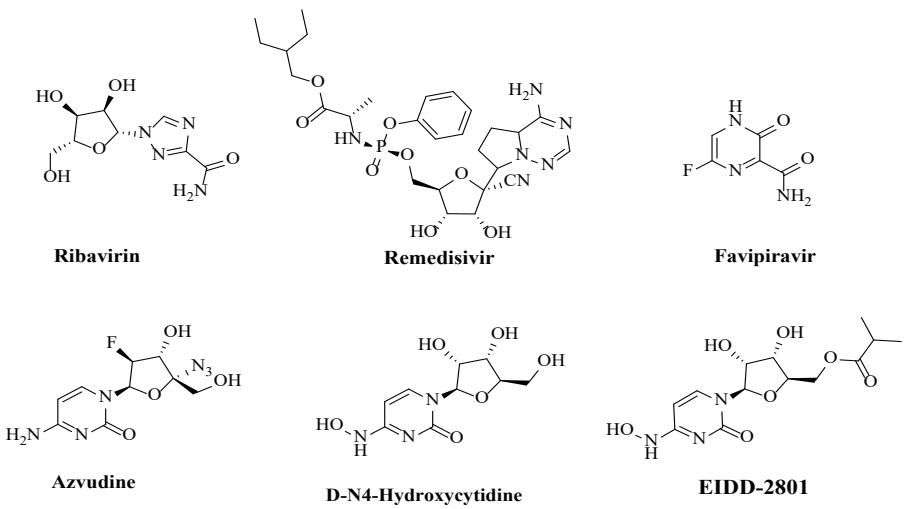


Figure 12. The chemical structure of Ribavirin, Remdesivir, Favipiravir, FNC, NHC, and EIDD-2801

Nitazoxanide is an antiparasitic agent with an extended spectrum activity that can suppress SARS-CoV-2 and exhibit an EC50 of 2.12 μM in Vero E6 cells. This drug, which induces interferon, is currently under investigation for its specific potential to treat a v variety of medical conditions. Niclosamide, ciclesonide, and nelfinavir exemplify antiparasitic or host-targeted agents with extended-spectrum activity, capable of suppressing SARS-CoV-2 through multifactorial mechanisms—including inhibition of viral entry, replication, protease activity, and host inflammatory pathways. Their study during the pandemic highlighted the strategic importance of drug repurposing, particularly for rapidly addressing emerging viral infections when specific antivirals are limited (Figure 13.).

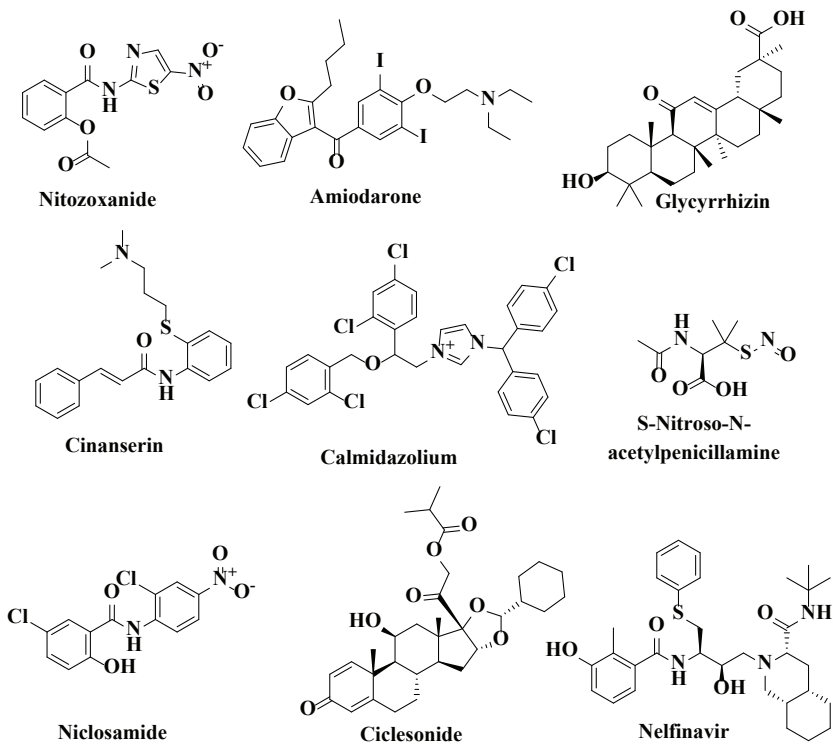


Figure 13. Selected drug structures suitable for repositioning in the treatment and prevention of SARS-CoV-1 & SARS-CoV-2, the viruses responsible for the more severe acute respiratory syndrome coronavirus

The antiarrhythmic medication amiodarone diminished the step of replication of SARS-CoV-1 in infected Vero cells (Hamilton et al., 2020). It seems to interfere with the endocytotic pathway, blocking the entry of the virus into endosomes (Stadler et al., 2008) **Glycyrrhizin** demonstrated the ability to inhibit viral replication in Vero cells, showing an EC50 of 300 mg/L, and may also help prevent the entry of the virus (Zhou et al., 2020). S-nitroso-N-acetylpenicillamine has emerged as a noteworthy nitric oxide donor with potential antiviral properties (Goudie et al., 2016) Research indicates that it can significantly reduce the replication of SARS-CoV-1 in a dose-dependent manner. In a thorough investigation of a library consisting of 8,000 approved drugs, cinanserin—acting as a serotonin antagonist—was identified as a promising inhibitor of SARS-CoV-1 (Rukthong et al., 2020). Its mechanism targets the virus's main protease (Mpro), showcasing an IC50 value of 4.0 μM. Additionally, the calmodulin antagonist calmidazolium has been demonstrated to inhibit SARS-CoV-1 Mpro with a Ki value of 61 μM, following virtual screening and molecular docking studies. virus (Han et al., 2023). Furthermore, compounds like cycloheximide and anisomycin, which are known to obstruct protein processing, have shown remarkable efficacy against both coronaviruses (Bustos-Hamdan et al., 2024). Lopinavir, an HIV protease inhibitor, demonstrated greater and specific efficacy against SARS-CoV-1 and the Middle East respiratory syndrome coronavirus. Loperamide, an antidiarrheal medication, demonstrated moderate inhibitory effects against both coronaviruses. Emetine, an alkaloid known for its anti-protozoal and emetic properties, has shown considerable antiviral effectiveness in combating MERS-CoV. The antiparasitic medications such as chloroquine, hydroxychloroquine, and mefloquine exhibited moderate efficacy against both coronaviruses (Figure 14.). Additionally, E-64-D, a cathepsin inhibitor, was effective in suppressing bothcoronaviruses (Luong et al., 2025).

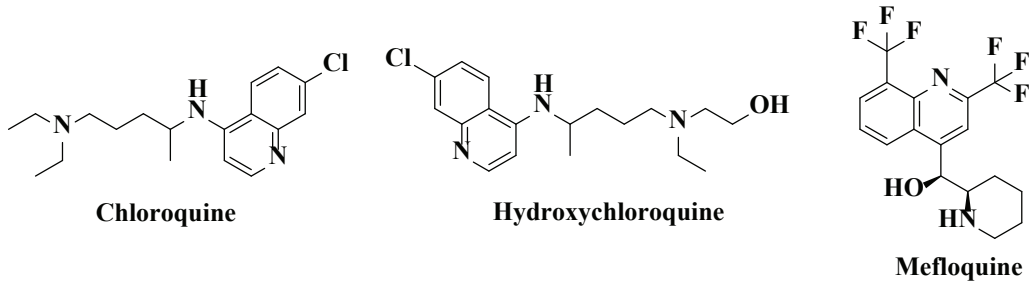


Figure 14. Structures of anti-protozoal agents effective against MERS-CoV

Azvudine, which was originally designed for HIV, a nucleoside-based inhibitor, is safe and highly effective for SARS-CoV-2 RdRp, demonstrating the potential use in the treatment of COVID-19. **β-D-N4-Hydroxycytidine** is an N-hydrolysed analogue of cytidine. Originally used to induce genetic mutations in bacteria, it has shown a wide range of effectiveness against specific and various RNA viruses, including SARS-CoV and HCoV-NL63 (Leger et al., 2022; Pinzi et al., 2021).

The second method of approach focuses on creating drugs for SARS-CoV-2 that disrupt key metabolic processes in the host's cell. The virus relies on the chemicals, enzymes, and organelles these cells supply to facilitate its replication. A prominent illustration of this strategy is the suppression of dihydroorotate dehydrogenase (DHODH), an enzyme involved in the de novo production of pyrimidine nucleotides. These nucleotides are vital for the formation of viral genomic RNA or DNA. Consequently, DHODH presents a promising target for developing inhibitors to halt coronavirus replication. Teriflunomide is the active metabolite derived from leflunomide (Figure 15.), is one such DHODH inhibitor that is used in clinical practice to treat immune diseases (Zhu et al., 2022).

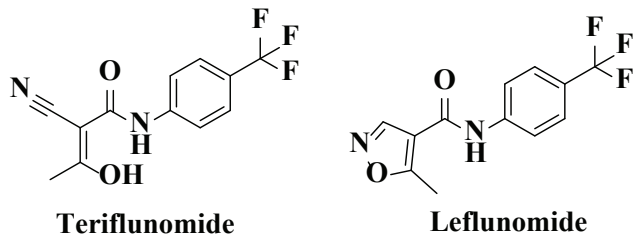


Figure 15. Structures of dihydroorotate dehydrogenase inhibitors

Ivermectin (Figure 16.) is a commercially available anti-parasitic medication that has been recognised for its specific broad-spectrum antiviral activity, showing a significant suppressive impact on SARS-CoV-2 in laboratory conditions. When Vero-hSLAM cells were disease-ridden with SARS-CoV-2 and treated with ivermectin, a reduction of the RNA of the virus by approximately 5000 times was observed after 48 hours (Parihar et al., 2022; Petty & Malani, 2022). Ranitidine has drawn scientific attention for its unexpected anti-parasitic and antiviral potential, including a significant suppressive impact on SARS-CoV-2, beyond its conventional role as an H_2-receptor antagonist. This interest emerged from drug-repurposing and *in silico* screening studies, which suggested that ranitidine may interfere with key molecular processes involved in viral survival and replication. Mechanistically, ranitidine is thought to modulate host cell pathways rather than directly targeting the virus, including alteration of endosomal pH, lysosomal function, and cellular protease activity, which are crucial for viral entry, uncoating, and replication.

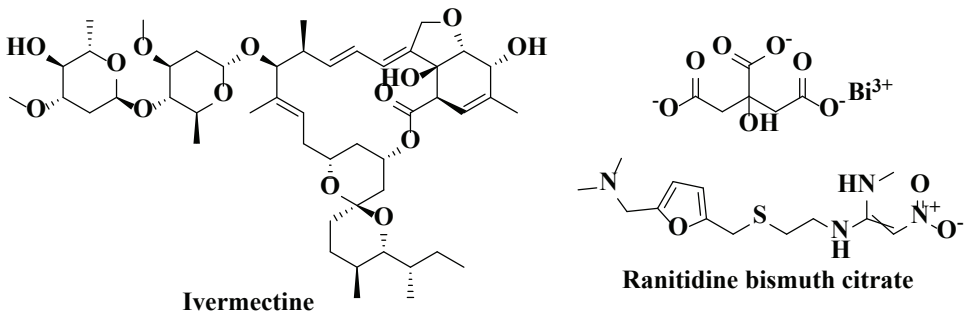


Figure 16. Structures of anti-parasitic agents having SARS-CoV-2 inhibitory activity

EXTENSIVE SCREENING CONDUCTED THROUGH *SPECIFIC IN SILICO* OR *IN VITRO* APPROACHES

Advancements in the bioscience and the utilisation of computer-assisted drug design (CADD), virtual screening has emerged as an important addition to the specific high-throughput screening in the quest for new anti-coronavirus treatments: A. Ligand-oriented virtual screening. B. Target-oriented virtual screening.

A. LIGAND-ORIENTED VIRTUAL SCREENING

A widely used method in CADD is ligand-oriented drug design, instrumental in the specific absence of the 3D structure of the target receptor. By analysing a collection of active agents that interact with a specific receptor target, researchers can uncover the physicochemical and structural characteristics that contribute to the observed biological activity, as similar structures often lead to similar biological effects. Various methods utilised in virtual screening ligand-based drug design include pharmacophore modelling, quantitative structure-activity relationships, and artificial intelligence.

Pharmacophore modeling

A pharmacophoric model illustrates how the chemical features of the ligands are spatially arranged, which is crucial for their binding with the target receptor. Pharmacophore modelling relies on several crucial chemical features that play a vital role in understanding molecular interactions. These features include hydrogen bond donors and acceptors, the presence of aromatic rings, regions that are hydrophobic, as well as entities that are positively or negatively charged and can be ionised. By analysing these characteristics, researchers can better predict how different compounds will interact within biological systems (Chen et al., 2023). By utilising pharmacophore-oriented virtual screening, one can discover ligands that possess distinct scaffolds while maintaining comparable spatial configurations of critical interacting functional groups. Some of the most widely used applications for automatically generating pharmacophore models incorporate Catalyst, PHASE, LigandScout, GALAHAD, and PharmMapper (Table 1.) (Williams et al., 2021; Yu & Chang, 2020).

Table 1. Tools for automatically generating pharmacophore models

S. N.	Tool	Description
1.	**Catalyst**	The Catalyst program employs an algorithm designed to recognise the 3D- structures of chemical properties that are prevalent among a group of ligands. Each configuration is assessed for its estimated rarity and its degree of similarity to the provided input set (Zaidi & Dehgani-Mobaraki, 2021).
2.	**LigandScout**	LigandScout functions as an automated tool designed to create pharmacophoric models that identify and classify interactions between proteins and ligands, such as hydrogen bonds, charge transfers, and lipophilic portions. These models serve as the basis for efficient virtual high-throughput screening (Gurung et al., 2021).
3.	**DISCO**	An automated pharmacophore approach is DISCO, which evaluates data to identify all appropriate pharmacophore hypotheses, serving as a complementary tool for 3D QSAR (Chang et al., 2022).
4.	**PharmaGist**	PharmaGist is a free online tool that creates ligand-based pharmacophore models using a collection of drug-like compounds (up to 32 specific molecules) that exhibit a binding affinity for the target protein (Hosseini, et al., 2021).
5.	**PharmMapper**	PharmMapper is a complementary online service frequently employed to determine possible receptor targets for a specific small molecule through the pharmacophore mapping method (Chang, et al., 2022).
6.	**Pharmer**	Pharmer is an innovative program designed for pharmacophore modelling that adeptly organises molecular data using the unique Pharmer KDB-tree and bloom fingerprints. This approach enables the swift assessment of millions of compounds in a timely and efficient manner, streamlining the evaluation process for researchers and scientists. With its advanced capabilities, Pharmer significantly enhances the speed and accuracy of pharmacophore analysis (Seidel et al., 2020).
7.	**PHASE**	PHASE is a tool for advanced pharmacophore-based methods that utilises an innovative, unique tree-based partitioning approach to delineate the shared spatial functional group configuration in a collection of bioactive ligands (Giordano et al., 2022).
8	**ZINCPharmer**	ZINCPharmer is an accessible web server that allows users to screen small compounds from the database of ZINC utilized by the search tool, i.e. Pharmer pharmacophore. You can create an initial pharmacophore hypothesis by using PDB structures or by importing pharmacophore models created with various third-party software (Qing et al., 2014).
9.	**e-Pharmacophore**	The e-pharmacophore method offers an innovative approach to pharmacophore modelling by focusing on energetically optimised, structure-based techniques. This advanced methodology efficiently screens a large array of chemical compounds while assessing the interactions between proteins and ligands. Utilising the Glide XP scoring function, it proves to be highly effective for database screening, providing a robust framework for identifying potential drug candidates (Riziotis et al., 2023).
10.	**GASP**	The GASP program utilises a genetic algorithm (GA) to overlay a collection of flexible ligands. It begins by selecting the ligand with the least complex chemical characteristics as a template, which is then used to effectively position the other molecules in the series. This method allows for a more optimised fit of the ligands, enhancing the overall molecular alignment (Jiang et al., 2020; Vuorinen et al., 2014).
11.	**GALAHAD**	GALAHAD functions as a pharmacophore program designed to flexibly align with specific small molecules that engage with a specific target protein, focusing on those that exhibit similar patterns and shapes in their interactions (Wang et al., 2017).

The quantitative structure-activity relationships (QSARs) studies of bioactive substances

QSAR research is based on the idea that differences in the bioactivity of drugs might be linked to changes in their molecular structures. These methods are frequently used in drug development, especially during hit-to-lead identification and optimisation (Liu et al., 2010). These correlation studies create a statistical model that can assess the biological efficacy of novel compounds (Table 2.). To generate a reliable QSAR model, several key requirements must be met: (a) an adequate quantity of data featuring biological activities derived from standardized experimental procedures, (b) careful screening of compounds for both training and test, and (c) ensuring there is no specific autocorrelation amongst the physicochemical specific properties of the ligands, as such a condition may result in data overfitting, and (d) The final model's applicability and predictability must be validated both internally and externally. Based on chemometric methodologies, QSAR techniques are classed as linear or nonlinear (Alzain et al., 2024; Koes & Camacho,

2011). The linear methodology involves a range of analytical techniques, including partial least squares (PLS), linear regression (LR), multiple linear regression (MLR), principal component analysis (PCA), and principal component regression (PCR). These methods are typically utilised for their straightforward approach to modelling relationships between variables.

On the other hand, nonlinear QSAR methodologies embrace more complex techniques such as k-nearest neighbours (kNN) and artificial neural networks (ANN), including Bayesian neural networks. These methods are designed to capture intricate patterns and relationships in data that linear models might overlook (Gaurav & Gautam, 2014; Song et al., 2009).

Table 2. Various software tools are available to compute molecular descriptors essential for developing QSAR models.

S. N.	Tool	Description
1.	**ADMET Predictor**	It predicts more than 140 attributes, including solubility, logP, pKa, Ames mutagenicity, and CYP metabolism sites (Salam et al., 2009).
2.	**ChemAxon**	The tool offers a comprehensive range of chemical calculations, including important metrics such as molecular weight, elemental composition, logP, pKa, logD, logS, and counts of hydrogen bond donors and acceptors (HBDA). Additionally, it provides both 2D topological and 3D geometric descriptors, enabling a thorough analysis of chemical properties (Creevey et al., 2023; Schneidman-Duhovny et al., 2008).
3.	**PaDEL-Descriptor**	PaDEL-Descriptor is an independent software tool designed to calculate molecular descriptors and fingerprints. It features a total of 797 descriptors, which include the specific 663 1D and 2D descriptors, along with 134 3D descriptors, as well as ten specific different types of fingerprints (Neves et al., 2018).
4.	**E-DRAGON**	E-DRAGON serves as the digital counterpart to the previously discussed software, DRAGON. This application is capable of calculating more than 1,600 molecular descriptors, which play a crucial role in examining the relationships between molecular structure and its corresponding activities or properties (Vilar & Costanzi, 2012).
5.	**CODESSA PRO**	CODESSA PRO is a powerful software tool designed for analysing quantitative structure-activity and structure-property relationships (QSAR/QSPR). It enables users to calculate a wide range of molecular descriptors derived from both two-dimensional and three-dimensional molecular geometries, as well as from quantum-chemical wave functions of small molecules. This program is particularly valuable for researchers looking to explore the relationships between molecular structure and biological activity or other properties in a detailed and computationally efficient manner (Serafim, et al., 2023; Megantara et al., 2022).
6.	**Pre-ADMET**	PreADMET is a web-based tool designed to evaluate a range of drug-like physicochemical characteristics. It analyses important factors such as molecular weight, lipophilicity (logP), water solubility, and polar surface area. This tool is essential for researchers and developers in the pharmaceutical industry, as it aids in assessing the potential of compounds during the early stages of drug discovery. By providing valuable insights into these properties, PreADMET helps streamline the process of identifying viable drug candidates (Patel et al., 2021b).

The impression of artificial intelligence on the discovery of novel anti-coronavirus therapeutics

The new technology, Artificial Intelligence (AI), refers to the capability of machines to learn from data. The application of various computational modelling techniques has been utilised to anticipate the biological outcomes and toxic effects of pharmaceutical compounds (Ashraf et al., 2023). AI significantly contributes to the process of drug discovery, with applications like predicting protein folding, analysing protein-protein interactions, conducting virtual screenings, performing QSAR assessments, evaluating ADMET properties, and creating new drugs from scratch. Two key technologies frequently utilised in the field of rational drug design are machine learning (ML) and deep learning. These advanced methods

have transformed the way researchers approach drug development, enabling them to analyse vast datasets and predict how different compounds will interact with biological targets. By leveraging these techniques, scientists can streamline the drug discovery process, making it more efficient and targeted (Tallei et al., 2021).

B. RATIONAL DRUG DESIGN WITH TARGET-ORIENTED METHOD

Recent advancements in high-resolution cocrystal structures have confirmed the mechanisms of action and provided valuable insights into the structural elements that influence binding interactions. In the field of drug development, target-based rational drug design focuses on identifying promising drug candidates with therapeutic relevance by analysing the interactions between ligands and their specific targets. This approach highlights the importance of understanding these relationships to enhance the efficacy of novel treatments (Ruusmann et al., 2014). Molecular docking serves as a robust method for exploring essential biological questions at the specific atomic level. The main pharmaceutical targets within the replication cycle of the virus SARS-CoV-2 include Mpro, PLpro, RdRp, Spike protein, and ACE2 (Murugavel et al., 2022).

Mpro as the target

The virus SARS-CoV-2 Mpro represents a compelling aim for COVID-19 treatment because of its unique structure. This enzyme protease is crucial for the replication cycle of all coronaviruses. It functions as a homodimer composed of two promoters, A and B, which, after dimerization and activation, achieve the correct shape for catalytic activity. The active site of the enzyme comprises four pockets (S1', S1, S2, and S3), with the S10 pocket containing a catalytic dyad. This dyad, made up of the Cys145 and His41 residues, is situated between domains I and II. Small-molecule inhibitors are capable of efficiently displacing two specific water molecules at the binding site, leading to a significant boost in efficacy. Mpro cleaves viral polyproteins at the unique Leu-Gln (Ser, Ala, Gly) sequence found in all coronaviruses (Figure 17.). The human host cell proteases are unable to perform this cleavage (Lionta et al., 2014; Zhang et al., 2025). Consequently, peptidomimetics and small-molecule Mpro inhibitors are anticipated to be highly selective. The catalytic dyad consists of Cys145 and His41, with the thiol (-SH) group of cysteine playing a crucial role in the hydrolysis reaction (Citarella et al., 2021). His41 creates the necessary pH conditions to activate the -SH group, leading to a nucleophilic attack on the substrate. Figure 4 illustrates the complete process of Mpro, which can be divided into four stages: (1) His41 deprotonates the -SH group of Cys145, creating the activated thiolated ion; (2) this ion then carries out a nucleophilic attack on the carbonyl carbon of the substrate, results in the creation of a tetrahedral adduct; (3) the component peptide hydrolysis product is released, resulting in a free N-terminus, while His41 is restored; and (4) thioester hydrolysis takes place, releasing the specific residual peptide fragment possessing a free C-terminus (Jin et al., 2020; Joshi et al., 2021).

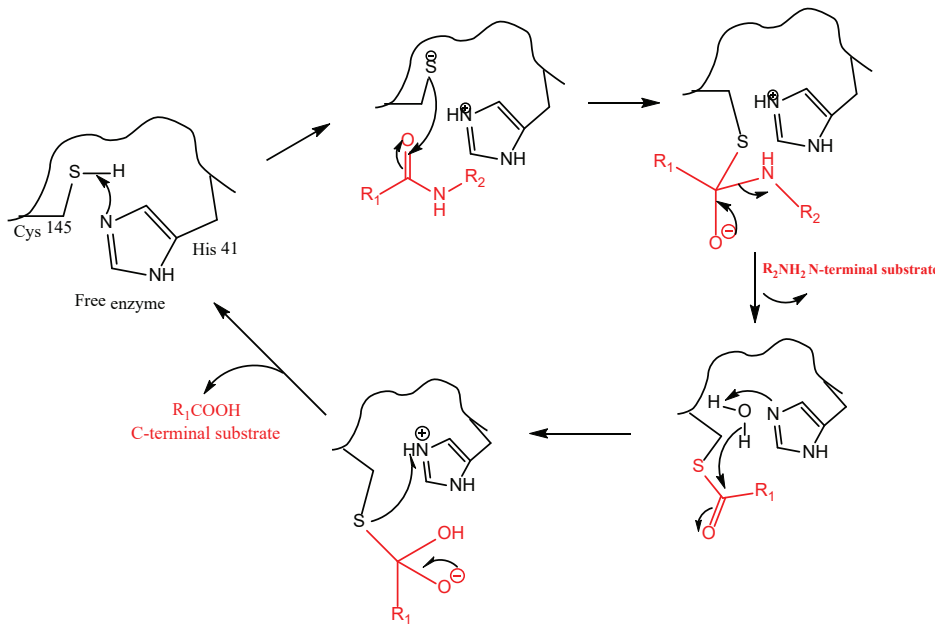


Figure 17. Understanding the Hydrolysis Mechanism of SARS-CoV-2 Mpro The hydrolysis mechanism of SARS-CoV-2 Mpro features the amino acids of the catalytic dyad highlighted in blue, while the substrate is represented in red.

SARS-CoV PLpro is an important target and is categorised as part of the CA Clan within the peptidase family. The enzyme features a precisely arranged catalytic triad made up of three key amino acids: Cys112, His273, and Asp287. These residues situate themselves at the junction of the thumb and palm subdomains, playing a critical role in the enzyme's function.

The proposed mechanism through which SARS-CoV PLpro operates is comparable to a hypothesised catalytic cycle typical of cysteine proteases. In this context, Cys112 serves as the nucleophile, while His273 functions as a versatile acid-base catalyst. Additionally, Asp287 collaborates closely with histidine to ensure proper alignment and facilitate the deprotonation of Cys112, thereby enhancing the catalytic efficiency of the enzyme (Figure 18.) (Shin et al., 2020; Zhang et al., 2020). In its unliganded form, ''E", the catalytic residues of SARS-CoV PLpro are situated in proximity sufficient to establish hydrogen bonds. This suggests that the protonation state of Cys112 may be in equilibrium with that of His273. This state of equilibrium shifts toward the reactive thiolate upon substrate binding (Figure 18, step a). Cys112 may undergo deprotonation upon binding with the substrate, leading to the formation of an enzyme-substrate (ES) complex. This complex then transitions through an addition-elimination mechanism, where the thiolate group of Cysteine112 attacks the carbonyl carbon of the peptide bond. This process results in a tetrahedral intermediate that is initially negatively charged and referred to as "TI-1" or "FP" (Figure 18, step b). The negative charge on the oxyanion within this tetrahedral intermediate is stabilised by an oxyanion hole situated near the active site of the PLpro enzyme. Notably, this oxyanion hole includes a vital tryptophan residue (Trp107), which plays a significant role in the enzymatic activity of PLpro, as demonstrated through site-directed mutagenesis studies (Gao et al., 2020; Osipiuk et al., 2021).

In its unliganded state, referred to as "E," the catalytic residues of SARS-CoV PLpro are positioned closely enough to facilitate hydrogen bonding between them. This proximity suggests that the protonation state of Cysteine112 may exist in a state of equilibrium

with that of His273. When a substrate binds, it appears to shift this equilibrium towards a more reactive thiolate form (Figure 18, step a). Another possibility is that the binding of the substrate induces the deprotonation of Cys112, resulting in the establishment of the "ES" complex. In its unliganded state, referred to as "E," the catalytic residues of SARS-CoV PLpro are positioned closely enough to facilitate hydrogen bonding between them. This proximity suggests that the protonation state of Cysteine112 may exist in a state of equilibrium with that of His273. When a substrate binds, it appears to shift this equilibrium towards a more reactive thiolate form (Figure 18, step a). Another possibility is that the binding of the substrate induces the deprotonation of Cys112, resulting in the establishment of the "ES" complex (Rut et al., 2020). An addition-elimination sequence follows, where Cys112 thiolate attacks the carbon of the carbonyl group within the peptide bond, resulting in the initial negatively charged tetrahedral intermediate, referred to as ''TI-1" or ''FP" (Figure 18, step b). The oxyanion formed during the tetrahedral intermediate is stabilised by an oxyanion hole situated near the active site of the PLpro enzyme. This crucial region includes a tryptophan residue (Trp107), which is vital for the enzymatic function of PLpro, as noted by (Baez-Santos et al. 2014). Additionally, an asparagine residue (Asn110) is highly conserved across coronaviral PLP2s and likely contributes significantly to the stability of the oxyanion hole, as it is positioned above the catalytic cysteine. When the amine group located at the C-terminal end of the substrate is removed, this results in the cleavage of the peptide bond, thereby leading to the production of the thioester precursor identified as "F (Figure 18, step c). Following this step, a sequence of addition and elimination occurs where water functions as a nucleophile, adding to the carbonyl carbon of the thioester. This reaction produces a second tetrahedral intermediate, designated as "TI-2" or "FQ" (Figure 18, step d). The negative charge on the oxyanion of this intermediate is stabilised by the oxyanion hole located within the PLpro active site (Liu et al., 2014). As the tetrahedral intermediate undergoes deconstruction, the cysteine is released, resulting in the formation of an N-terminal carboxylic acid known as "EQ." This acid may briefly be stabilized within the PLpro active site through a hydrogen bond that forms between its carbonyl carbon and the nitrogen of the indole ring in Trp107 (Figure 18, step e). The final step of this catalytic cycle involves the separation of the cleaved N-terminus from the peptide substrate, leading to the release of the end product "Q" from the active site and restoring the enzyme to its free form, referred to as "E" (Figure 18, step f) (Henderson et al., 2020).

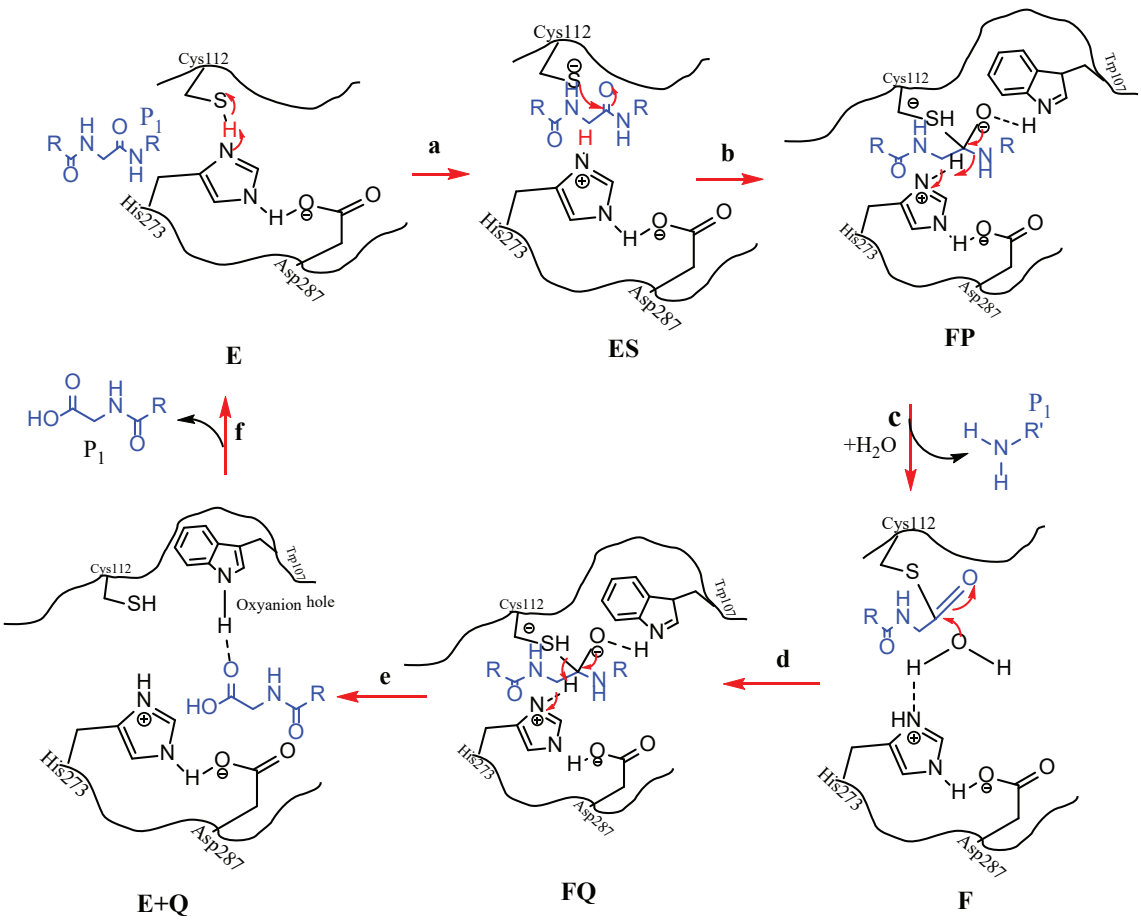


Figure 18. The catalytic mechanism of the SARS-CoV PLpro reaction is depicted in detail. Central to this process is the catalytic triad composed of cysteine (Cys112), histidine (His273), and aspartate (Asp287). The residue Trp107, which plays a critical role in forming the oxyanion hole, is also highlighted. In this illustration, the peptide substrate is shown in blue, while a water molecule involved in the catalysis is represented in black. This visual representation provides a clearer understanding of the enzyme's function and the molecular interactions at play.

The engagement of SARS-CoV PLpro inhibitors with Cys112 involves cysteine proteases that can interact with various electrophilic or "warhead" groups found in covalent inhibitors. Typically, these inhibitors begin by forming a noncovalent interaction complex within the active site of the cysteine protease, which helps position the warhead group near the reactive cysteine nucleophile (Narayanan et al., 2022). The process starts when the thiolate performs a nucleophilic attack on the electrophilic carbon of the warhead, leading to the formation of a covalently modified enzyme-inhibitor complex. This modification ultimately results in the inactivation of the enzyme.

A variety of reactive warhead groups have been recognised for their ability to inhibit cysteine proteases. These include aldehydes, epoxy-ketones, alkynes, Michael acceptors, alkyl halides, vinyl sulfones, activated esters, activated ketones, acrylamides, and nitriles (Lu et al., 2024; Machitani et al., 2020).

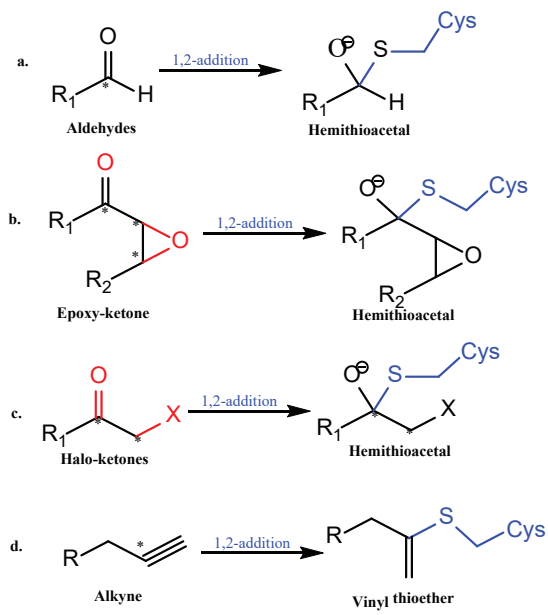


Figure 19. Several examples of cysteine protease inhibitors containing covalent "warheads" are shown here. The reactive electrophilic groups are highlighted in red, with the key electrophilic carbon—marked by an asterisk—serving as the critical site of interaction. The resulting covalent bonds between the inhibitor and the cysteine residue are depicted with arrows, while the cysteine components of the adducts are coloured in blue for clarity.

The virus SARS-CoV-2 PLpro enzyme was co-crystallised with a semisynthetic form of ubiquitin, which had its C-terminus altered to include an aldehyde functional group (Ubal).

RdRp as the target

RNA-dependent RNA polymerase (RdRp) is a viral enzyme present in nearly all RNA virus families, excluding Retroviridae, and belongs to the transferase class. Its primary function is to synthesise a complementary RNA strand by sequentially adding ribonucleotides to the growing 3′-hydroxyl end, ensuring elongation in the 5′→3′ direction. For this process, RdRp requires an RNA template, ribonucleotide triphosphates (ATP, GTP, UTP, and CTP) as substrates, and two Mg^{2+} ions within its active site to catalyse phosphodiester bond formation. Beyond its catalytic core, the enzyme also binds Zn^{2+} through tetrahedral coordination at a secondary site, where these ions help stabilise its three-dimensional structure (Vijay et al., 2024; Yi et al., 2024). Structurally, RdRp contains two distinct channels that converge at the active site: one accommodates the template RNA strand, while the other facilitates the entry of incoming nucleotide triphosphates (NTPs) (Figure 20.).

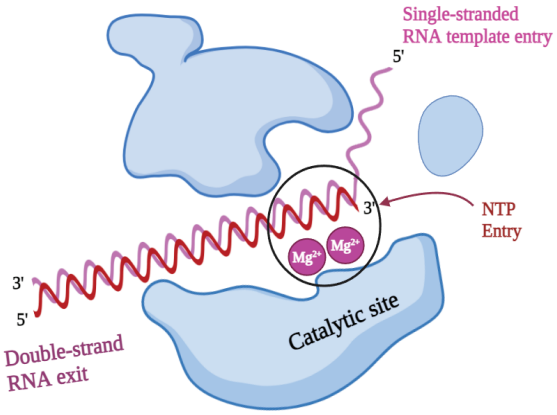


Figure 20. The Graphical depiction of the RdRp illustrates the RNA template as a blue line while the newly synthesised RNA is depicted as a red line. Mg^{2+} ions are shown in purple spheres.

The incoming nucleotide triphosphates (NTPs) are incorporated into the newly synthesised RNA strand following Watson-Crick base pairing rules: uracil (U) pairs with adenine (A) from the template strand, while guanine (G) pairs with cytosine (C). During catalysis, the 3'-hydroxyl group at the growing end of the RNA strand acts as a nucleophile, attacking the α-phosphate of the incoming NTP. This reaction results in the formation of a phosphodiester bond and the release of pyrophosphate (PPi) as a by-product (Figure 21.)

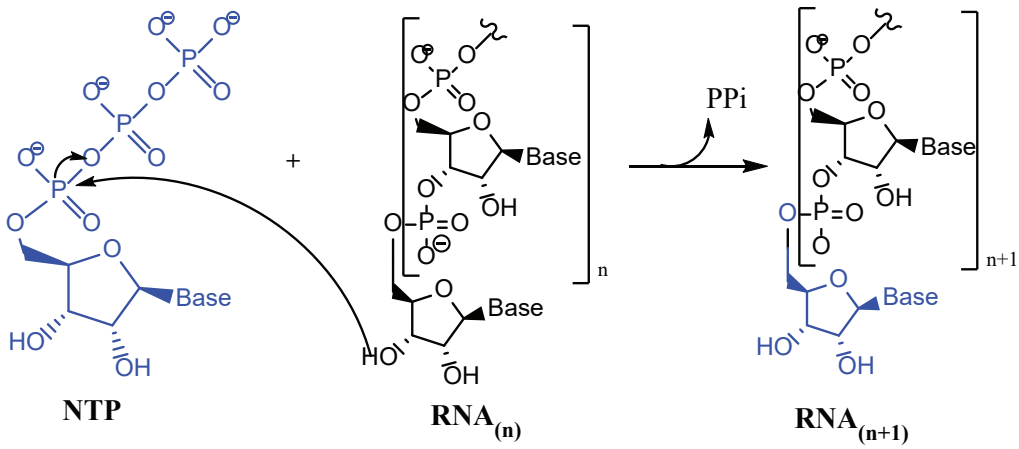


Figure 21. RdRp catalyses the RNA synthesis reaction

The facilitation of this procedure is achieved through the coordination of Mg^{2+} ions, which are arranged in an octahedral configuration via the phosphate of incoming NTP, along with three aspartate residues that exhibit a high degree of conservation across various viral RNA-dependent RNA polymerases (Figure 22.). One Mg^{2+} ion engages the specific nucleophilic attack of the 3'-hydroxyl group of the elongating RNA on the α-phosphate of the incoming nucleotide triphosphate (NTP). In contrast, another Mg^{2+} ion assists in the release of the PPi molecule. This catalytic mechanism, referred to as and is known as "two metal ions catalysis", is universally observed in all RdRps (Schimunek et al., 2024). Strategies for developing small-molecule RdRp inhibitors targeting RNA viruses have resulted in the creation of different categories of inhibitors, each acting through unique mechanisms of action: (i) nucleotide analogues (NIs), (ii) non-nucleotide analogues (NNIs), (iii) inhibitors of protein-protein interactions, and (iv) targeted covalent inhibitors (TCIs) (Godwin et al., 2024).

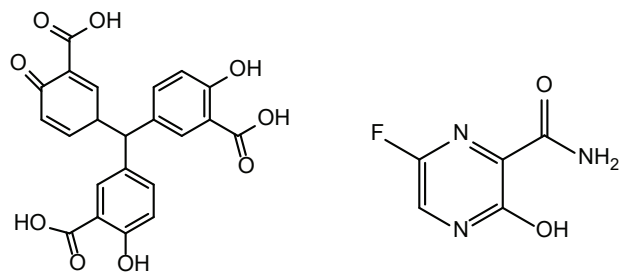


Figure 22. Small-molecule inhibitors targeting coronavirus RNA-dependent RNA polymerase (RdRp)

Nucleotide analogues (NIs) are synthetic compounds that mimic natural nucleotides and competitively bind to the RdRp active site, where their incorporation is mediated by metal ions and catalytic residues. These inhibitors compete with natural nucleotide triphosphates (NTPs) for incorporation into the elongating RNA strand, leading to either delayed or immediate chain termination depending on their specific chemical properties. A major pharmacological challenge with NIs is their intracellular delivery in the active triphosphate form. Under normal physiological conditions, the negatively charged phosphate groups significantly reduce cell membrane permeability. To overcome this limitation, researchers commonly employ prodrug strategies to improve drug absorption and bioavailability. A prominent example

is sofosbuvir (Figure 23.), an effective RdRp inhibitor pro-drug. After metabolic activation, its bioactive form (2'-deoxy-2'-fluoro-β-C-methyluridine-5'-triphosphate) functions as a potent chain terminator, effectively halting viral RNA replication (Huang et al., 2024; Molaei et al., 2024).

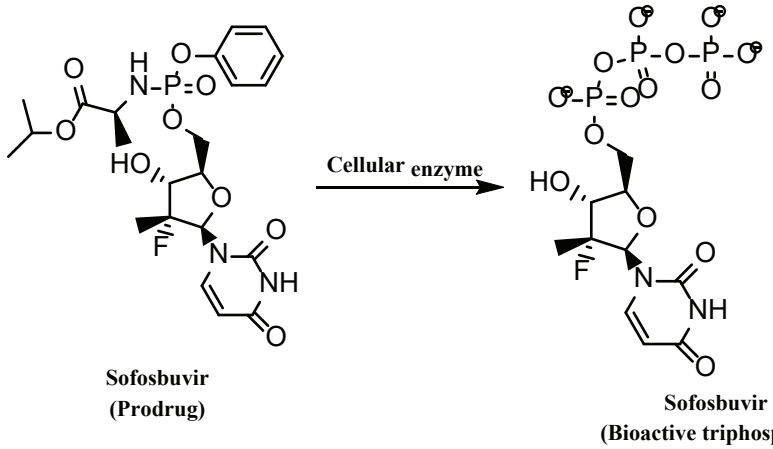


Figure 23. Schematic illustration of the enzyme-catalysed conversion of sofosbuvir prodrug into its biologically active form

Remdesivir was initially created as a therapeutic for hepatitis C but was later assessed from a collection of around 1,000 compounds for its potential against Ebola and Marburg viruses during the 2014 emergence of an epidemic in West Africa. It showed broad-spectrum antiviral properties, leading to its testing against MERS-CoV in laboratory cell-based studies. Remdesivir is a specific prodrug of an adenine derivative that belongs to the class of phosphoramidate, known for its wide-ranging antiviral effects and its role as a delayed chain terminator (Figure 24.) (Yang et al., 2024).

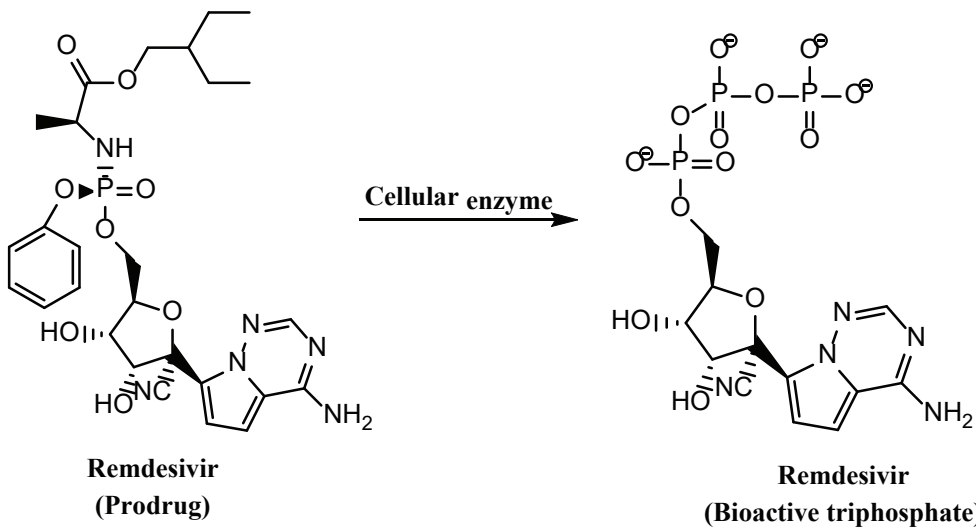


Figure 24. Schematic illustration of the specific enzymatic conversion of Remdesivir prodrug into its active biological form

Favipiravir is a prodrug that is metabolically converted into a specific favipiravir triphosphate, which is its bioactive form (Figure 25.).

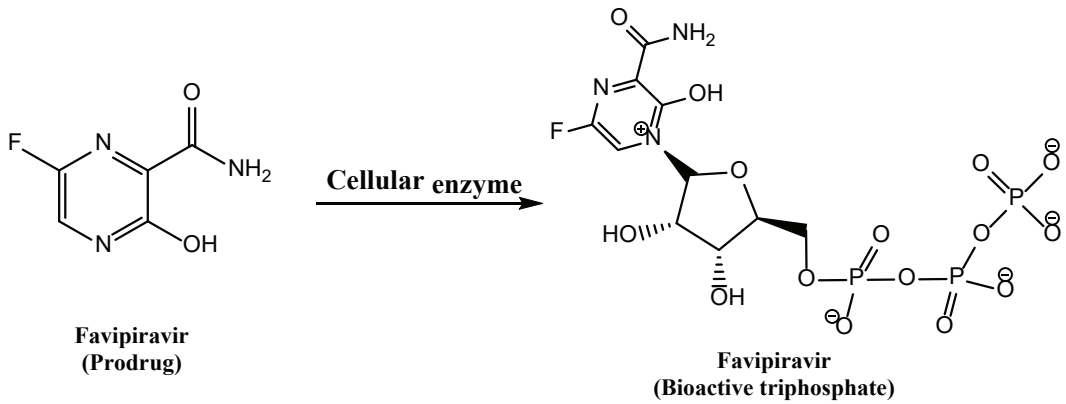


Figure 25. Metabolic activation of favipiravir from prodrug to bioactive form

Non-nucleoside inhibitors (NNIs) exert their antiviral effects through allosteric inhibition, binding to distinct pockets surrounding the polymerase active site. These include thumb domains I and II (T1/T2), palm regions I, II, and β (P1/P2/Pβ). By occupying these regulatory sites, NNIs prevent the conformational changes required for proper polymerase function. The inhibitory mechanism varies depending on the specific binding location and the polymerase's conformational state. For instance, NNIs targeting the T1 and T2 pockets primarily interfere with the initiation phase of RNA synthesis. They disrupt the critical interaction between the palm and thumb subdomains, preventing formation of a functional RdRp-RNA complex and reducing the enzyme's affinity for its RNA template (Lu et al., 2020).

Emerging as a promising new class of antiviral agents, protein-protein interaction (PPI) inhibitors target the critical interfaces between RNA-dependent RNA polymerase (RdRp) and its associated non-structural proteins. By disrupting these essential interactions, PPI inhibitors prevent proper assembly of the viral replication complex multi-protein machinery required for genome replication. One particularly compelling example involves the targeted disruption of the NS5 (RdRp)-NS3 (protease) interaction in dengue virus (DENV), which has been shown to effectively block viral replication (Goyal et al., 2020).

Targeted covalent inhibitors: reversible vs. irreversible mechanisms

Targeted covalent inhibitors (TCIs) represent another innovative strategy, incorporating specialised functional groups designed to form specific bonds with key amino acid residues on the target protein. These inhibitors fall into two distinct categories:

Reversible TCIs: These compounds establish transient interactions with their target, maintaining a dynamic equilibrium between bound and unbound states. The protein's activity can be restored upon inhibitor dissociation.

Irreversible TCIs: Characterised by their ability to form permanent covalent bonds, these inhibitors lead to sustained inactivation of the target protein (Luo et al., 2024).

Targeting host ACE2 in antiviral therapy

The initial step of coronavirus infection involves the virus attaching to specific receptors on the surface of host cells. Among these, ACE2 has been identified as a key receptor facilitating SARS-CoV-2 entry. As a result, therapeutic strategies have emerged that aim to modulate or inhibit ACE2 to block viral access. ACE2 is a zinc-dependent metalloprotease consisting of 805 amino acids, structurally divided into two primary domains: the amino-terminal catalytic domain and the carboxy-terminal domain (Lazou et al., 2024). Functionally, ACE2 plays a vital role in downregulat-

ing the renin-angiotensin system (RAS) by converting angiotensin II (Ang II) into the vasodilatory peptide angiotensin 1–7 (Ang 1–7). This enzyme is predominantly expressed in epithelial cells lining the lungs, liver, and testes. Notably, unlike the classical ACE enzyme, ACE2 is positioned on the apical surface of respiratory epithelial cells, which may enhance the likelihood of viral attachment and entry. Inhibiting the interaction between the viral spike protein and ACE2—through small molecules that disrupt critical protein-protein interactions—has been proposed as a possible intervention. Given the association of ACE2 with cardiac injury in COVID-19, therapeutic agents such as ACE inhibitors or angiotensin receptor blockers (ARBs) have been explored for their potential to mitigate heart-related complications. Among them, telmisartan has shown promise as a candidate for managing SARS-CoV-2 infection. Additionally, administering soluble recombinant ACE2 has garnered attention as a therapeutic approach. This form of ACE2 can act as a decoy receptor, binding to the viral spike protein and thereby preventing the virus from attaching to membrane-bound ACE2 on host cells. By doing so, it may help preserve endogenous ACE2 levels, which the virus tends to downregulate during infection.

CONCLUSION

The COVID-19 pandemic has triggered an extraordinary global response, placing pharmaceutical chemistry at the centre of efforts to combat the effects of SARS-CoV-2. Researchers have rapidly developed innovative methods for detecting, creating, and refining treatments for this growing threat through creative approaches and interdisciplinary collaboration. Structure-based drug design has effectively pinpointed small molecules that target essential viral components, including the main specific protease (Mpro), spike protein, and RNA-dependent RNA polymerase (RdRp). These targets have formed the basis for developing inhibitors that are both highly specific and effective, while computational modelling and molecular docking studies have significantly reduced the time needed for initial drug discovery. AI and ML have become transformative tools in drug discovery, helping to identify potential therapeutic options and repurpose existing medications. The integration of AI with medicinal chemistry has enabled the screening of extensive chemical libraries, the optimisation of pharmacokinetic properties, and the forecasting of drug resistance patterns. A significant strategy in this field is drug repurposing, which offers a cost-effective and efficient approach to finding FDA-approved drugs with antiviral effects. For instance, remdesivir and molnupiravir, originally developed for other RNA viruses, have shown effectiveness against SARS-CoV-2, leading to the creation of new formulations. In addition to small molecules, recent advancements in peptide-based therapies, monoclonal antibodies, and nanotechnology have significantly expanded the range of treatment options available. Monoclonal antibodies targeting the spike protein have been essential in preventing severe illness among high-risk groups, while nanoparticle delivery systems have enhanced the absorption and targeting of antiviral medications. Moreover, the creation of multifunctional materials that can simultaneously deliver drugs and immune modulators has opened up new avenues for combination therapies. Nevertheless, there are still significant challenges to overcome. The rise of viral variants that are more transmissible and can evade immune responses highlights the need for flexible and adaptable approaches in developing therapies. Tackling global disparities in the distribution of medical treatments and ensuring that new therapies remain affordable are also critical priorities. Finding a balance between quick medication development and thorough safety and efficacy evaluations continues to be a challenge. Moving forward, the insights gained from the COVID-19 pandemic highlight the importance of ongoing investment in medicinal chemistry

research, especially in areas like high-throughput screening, real-time genomic monitoring, and modular drug design platforms. Collaboration among academic institutions, industry, and regulatory agencies will be essential to accelerate the journey from discovery to clinical use.

The use of current technologies, teamwork, and a focus on translational research has tremendously aided our efforts to combat COVID-19. These measures not only provide hope for conquering the present pandemic, but also lay the framework for addressing future infectious disease epidemics with greater resilience and effectiveness.

ACKNOWLEDGMENT

All authors are thankful to Krishna Institute of Pharmacy and Sciences, Kanpur, for continuous support during the manuscript preparation.

AUTHOR CONTRIBUTION STATEMENT

Study conception and design: NK; data collection: NK, SKSK; draft manuscript: NK, AK. All authors reviewed the results and approved the final version of the manuscript.

CONFLICT OF INTEREST

The authors declare that there is no conflict of interest.

REFERENCES

Alzain, A. A., Elbadwi, F. A., Shoaib, T. H., Sherif, A. E., Osman, W., Ashour, A.,…Hassan, A. H. E. (2024). Integrating computational methods guided the discovery of phytochemicals as potential Pin1 inhibitors for cancer: pharmacophore modeling, molecular docking, MM-GBSA calculations, and molecular dynamics studies. *Frontiers in Chemistry 12*, 1339891. doi 10.3389/fchem.2024.1339891

Ashraf, F. B., Akter, S., Mumu, S. H., Islam, M. U., & Uddin, J. (2023). Bio-activity prediction of drug candidate compounds targeting SARS-Cov-2 using machine learning approaches, *PLoS One. 18*(9), 1-19. doi.org/10.1371/journal.pone.0288053

Baez-Santos, Y. M., John, S. E., & Mesecar, A. D. (2014). The SARS-coronavirus papain-like protease: Structure, function and inhibition by designed antiviral compounds. *Antiviral Research, 115*, 21-38. doi: 10.1016/j.antiviral.2014.12.015

Batool, S., Chokkakula, S., Jeong, J. H., Baek, Y. H., & Song, M. S. (2025). SARS-CoV-2 drug resistance and therapeutic approaches. *Heliyon, 11*, 1-25, e41980. doi.org/10.1016/j.heliyon.2025.e41980

Bustos-Hamdan, A., Bracho-Gallardo, J. I., Hamdan-Partida, A., & Bustos-Martínez, J. (2024). Repositioning of Antibiotics in the Treatment of Viral Infections. *Current Microbiology, 81*(12), 427-444. doi.org/10.1007/s00284-024-03948-7

Cao, B., Wang, Y., Wen, D., Liu, W., Wang, J., Fan, G.,… Wang, C. (2020). A Trial of Lopinavir–Ritonavir in Adults Hospitalized with Severe Covid-19. *New England Journal of Medicine (NEJM), 382*(19), 1787–1799. doi.org/10.1056/NEJMoa2001282

Cervantes, M., Hess, T., Morbioli, G. G., Sengar, A., & Kasson, P. (2023). The ACE2 receptor accelerates, but is not biochemically required for SARS-CoV-2 membrane fusion. *Chemical Science, 2023*(14), 6997-7004.

Chang, Y., Hawkins, B. A., Du, J. J., Groundwater, P. W., Hibbs, D. E., & Lai, F. (2022). A Guide to In Silico Drug Design. *Pharmaceutics, 15*(1), 49. doi:10.3390/pharmaceutics15010049

Chen, Z., & Tian, F. (2023). Efficacy and safety of azvudine in patients with COVID-19: A systematic review and meta-analysis. *Heliyon, 9*(9), e20153. doi:10.1016/j.heliyon.2023.e20153

Citarella, A., Scala, A., Piperno, A., & Micale, N. (2021). SARS-CoV-2 mpro: A potential target for peptidomimetics and small-molecule inhibitors. *Biomolecules, 11*(4), 607-641. doi: 10.3390/biom11040607

Creevey, F. M., Hill, C. D., & Hollenberg, L. C. L. (2023). *GASP -- A Genetic Algorithm for State Preparation, 2023*(13), 11956. doi.org/10.1038/s41598-023-37767-w

Duflos, C., & Michiels, T. (2023). Regulation of viral RNA-dependent RNA polymerases by phosphorylation. *Frontiers in Virology, 3*, 1176840. doi:10.3389/fviro.2023.1176840

Eltayeb, A., Al-Sarraj, F., Alharbi, M., Albiheyri, R., Mattar, E., Abu Zeid, I. M.,…Redwan, E. M. (2024). Overview of the SARS-CoV-2 nucleocapsid protein. *International Journal of Biological Macromolecules, 260*(Pt 2), 129523. doi: 10.1016/j.ijbiomac.2024.129523

Enjuanes, L., Sola, I., Zuniga, S., Honrubia, J. M., Bello-Pérez, M., Sanz-Bravo, A.,…Ripoll-Gómez, J. (2022). Nature of viruses and pandemics: Coronaviruses. *Current Research in Immunology, 2022*(3), 151-158. doi:10.1016/j.crimmu.2022.08.003

Fearns, R., & Deval, J. (2016). New antiviral approaches for respiratory syncytial virus and other mononegaviruses: Inhibiting the RNA polymerase. *Antiviral Research, 134*, 63-76.

Gao, X., Qin, B., Chen, P., Zhu, K., Hou, P., Wojdyla, J. A.,…Cui, S. (2020). Crystal structure of SARS- CoV-2 papain-like protease. *Acta Pharmaceutica Sinica B;11*(1), 237-245. doi:10.1016/j.apsb.2020.08.014

Gaurav, A., & Gautam, V. (2014). Structure-based three-dimensional pharmacophores as an alternative to traditional methodologies. *Journal of Receptor, Ligand and Channel Research 2014*(7), 27-38. doi.org/10.2147/JRLCR.S46845

GBD 2019 Meningitis Antimicrobial Resistance Collaborators. (2023). Global, regional, and national burden of meningitis and its aetiologies, 1990-2019: a systematic analysis for the Global Burden of Disease Study 2019. *Lancet Neurology, 22*(8), 685-711. doi:10.1016/S1474-4422(23)00195-3

Giordano, D., Biancaniello, C., Argenio, M.A., & Facchiano, A. (2022). Drug Design by Pharmacophore and Virtual Screening Approach. *Pharmaceuticals, 15* (5), 646. doi: 10.3390/ph15050646

Godwin, P. O., Polsonetti, B., Caron, M. F., & Oppelt, T. F. (2024). Remdesivir for the Treatment of COVID-19: A Narrative Review. *Infectious Diseases and Therapy, 13* (1), 1-19. doi: 10.1007/s40121-023-00900-3

Good, S. S., Luo, S., Lin, K., Vo, A., Nancy, Agrawal, N. G. B., & Sommadossi, J. –P. (2025). Bemnifosbuvir and Ruzasvir in combination exhibit potent synergistic antiviral activity *in vitro* while maintaining a favourable nonclinical safety profile *in vivo. Antiviral Research, 237*, 106137. doi.org/10.1016/j.antiviral.2025.106137

Gordon, C. J., Tchesnokov, E. P., Feng, J. Y., Porter, D. P., & Götte, M. (2020). The antiviral compound remdesivir potently inhibits RNA-dependent RNA polymerase from Middle East respiratory syndrome coronavirus. *Journal of Biological Chemistry, 295*(15), 4773-4779. doi:10.1074/jbc.AC120.013056

Goudie, M. J., Brisbois, E. J., Pant, J., Thompson, A., Potkay, J. A. & Handa, H. (2016) Characterisation of an S-nitroso-N-acetylpenicillamine-based nitric oxide releasing polymer from a translational perspective. *International Journal of Polymeric Materials and Polymeric Biomaterials. 65*(15), 769-778. doi: 10.1080/00914037.2016.1163570

Goyal, R. K., Majeed, J., Tonk, R., Dhobi, M., Patel, B., Sharma, K., & Apparsundaram, S. (2020). Current targets and drug candidates for the prevention and treatment of SARS-CoV-2 (COVID-19) infection. *Reviews in Cardiovascular Medicine, 21*(3), 365-384. doi: 10.31083/j.rcm.2020.03.118

Gunathilaka, M. D. T. L. (2023). Utilisation of Marine Seaweeds as a Promising Defence Against COVID-19: a Mini-review. *Marine Biotechnology, 25*, 415-427. doi.org/10.1007/s10126-023-10214-7

Gurung, A. B., Ali, M. A., Lee, J., Farah, M. A., Al-Anazi, K. M. (2021). An Updated Review of Computer-Aided Drug Design and Its Application to COVID-19. *BioMed Research International, 2021*, 8853056, 1-18. doi:10.1155/2021/8853056

Hamilton, D., Sr., Nandkeolyar, S., Lan, H., Desai, P., Evans, J., Hauschild, C.,…Hilliard, A. (2020). Amiodarone: A Comprehensive Guide for Clinicians. *American Journal of Cardiovascular Drugs, 20*(138), 1-10. doi:10.1007/s40256-020-00401-5

Han, J., Wang, Z., Han, F., Peng, B., Du, J, & Conggang, Z. (2024). Microtubule Disruption Synergizes with sting signalling to show potent and broad-spectrum antiviral activity. *PLOS Pathogens, 20*(2), e1012048. doi: 10.1371/journal.ppat.1012048

Han, Y., Bai, X., Wu, S., Luan, X., Ren, L., Wang, J.,... Du, G. (2023). In Silico Screening, in Vitro Mpro Inhibitory, and Adjunctive Therapy Value of Minocycline for the Treatment of COVID-19. *Journal of Clinical Pharmacy and Therapeutics, 2023*, 9955105, 1-12. doi.org/10.1155/2023/9955105

Henderson, J. A., Verma, N., & Shen, J. (2020). Assessment of Proton-Coupled Conformational Dynamics of SARS and MERS Coronavirus Papain-like Proteases: Implication for Designing Broad-Spectrum Antiviral Inhibitors. *The Journal of Chemical Physics, 153,* 115101. doi.org/10.1101/2020.06.30.181305

Hosseini, M., Chen, W., Xiao, D., & Wang, C. (2021). Computational molecular docking and virtual screening revealed promising SARS-CoV-2 drugs. *Precision Clinical Medicine, 4*(1), 1–16. doi:10.1093/pcmedi/pbab001

Huang, Y. B., Ng, C. J., Chiu, C. H., Chaou, C. H., Gao, S. Y., & Chen, S. Y. (2024). Safety and effectiveness of remdesivir for the treatment of COVID-19 patients with end-stage renal disease: A retrospective cohort study. Journal of Microbiology, *Immunology and Infection, 57*(1), 76-84. doi:10.1016/j.jmii.2023.12.003

Jain S, Rana M, & Jain P. (2022) Emergence, Evolution and Economics of Coronaviruses. *European Journal of Biology, 81*(2), 206–216. doi:10.26650/EurJBiol.2022.1113847

Jiang, S., Feher, M., Williams, C., Cole, B., Shaw, D. E. (2020). AutoPH4: An Automated Method for Generating Pharmacophore Models from Protein Binding Pockets. *J Chem Inf Model, 60*(9), 4326–4338. doi:10.1021/acs.jcim.0c00121

Jin, Z., Du, X., Xu, Y., Deng, Y., Liu, M., Zhao, Y.,… Yang, H. (2020). Structure of Mpro from SARS-CoV-2 and discovery of its inhibitors. *Nature, 582*(7811), 289-293. doi: 10.1038/s41586-020-2223-y

Joshi, R. S., Jagdale, S. S., Bansode, S. B., Shankar, S. S., Tellis, M. B., Pandya, V. K.,…Kulkarni, M. J. (2021). Discovery of potential multi-target-directed ligands by targeting host-specific SARS-CoV-2 structurally conserved main protease. *Journal of Biomolecular Structure and Dynamics, 39*(9), 3099-3114. doi: 10.1080/07391102.2020.1760137

Kalkanli, A., Kirkik, D., Bostanci, E., & Tas, S. K. (2021). The Important Role of TMPRSS2 Gene in COVID-19 and Prostate Cancer: In Silico Approach. *Brazilian Archives of Biology and Technology, 64*(8):e21200785. doi.org/10.1590/1678-4324-2021200785

Keller, C., Bottcher-Friebertshauser, E., & Lohoff, M. (2022). TMPRSS2, a novel host-directed drug target against SARS-CoV-2. *Signal Transduction and Targeted Therapy, 7*, 251. doi.org/10.1038/s41392-022-01084-x

Koes, D. R., & Camacho, C. J. (2011). Pharmer: Efficient and Exact Pharmacophore Search. *Journal of Chemical Information and Modelling, 51*(6), 1307-14. doi.org/10.1021/ci200097m

Lazou, M., Hutton, J. R., Chakravarty, A., & Joseph-McCarthy, D. (2024). Identification of a druggable site on GRP78 at the GRP78-SARS-CoV-2 interface and virtual screening of compounds to disrupt that interface. *Journal of Computer-Aided Molecular Design, 38*(1), 6. doi:10.1007/s10822-023-00546-w

Léger, C., Pitard, I., Sadi, M., Carvalho, N., Brier, S., Mechaly,…Chenal, A. (2022). Dynamics and structural changes of calmodulin upon interaction with the antagonist calmidazolium. *BMC Biology, 20*(1), 176. doi.org/10.1186/s12915-022-01381-5

Lionta, E., Spyrou, G., Vassilatis, D. K., & Cournia, Z. (2014). Structure-Based Virtual Screening for Drug Discovery: Principles, Applications and Recent Advances. *Current Topic in Medicinal Chemistry, 14*(16), 1923-38. doi:10.2174/1568026614666140929124445

Liu, J., Chakraborty, S., Hosseinzadeh, P., Yu, Y., Tian, S., Petrik, I.,...Lu, Y. (2014). Metalloproteins containing cytochrome, iron-sulfur, or copper redox centers. *Chemical Reviews, 114*(8), 4366-4669. doi:10.1021/cr400479b

Liu, X., Ouyang, S., Yu, B., Liu, Y., Huang, K., Gong, J.…Jiang, H. (2010). PharmMapper server: a web server for potential drug target identification using a pharmacophore mapping approach. *Nucleic Acids Research, 38*, W609-14. doi:10.1093/nar/gkq300

Lu, D., Yu, X., Lin, H., Cheng, R., Monroy, E. Y., Qi, X.,…Wang, J. (2022). Applications of Covalent Chemistry in Targeted Protein Degradation. *Chemical Society Reviews, 51*, 9243-9261. doi:10.1039/d2cs00362g

Lu, Y., Yang, Q., Ran, T., Zhang, G., Li, W., Zhou, P., & Shang, J. (2024). Discovery of orally bioavailable SARS-CoV-2 papain-like protease inhibitor as a potential treatment for COVID-19. *Nature Communications, 15*(1), 10169. doi:10.1038/s41467-024-54462-0

Luo, M., Jia, J., Wang, R., & Wang, L. (2024). Effect of antiviral drugs on Covid-19 treatment. *Discrete and Continuous Dynamical Systems - Series B, 29*(5), 2353-2367. doi: 10.3934/dcdsb.2023180

Luong, Q. X. T., Hoang, P. T., Ho, P. T., Ayun, R. Q., Lee, T. K, & Lee, S. (2025). Potential Broad-Spectrum Antiviral Agents: A Key Arsenal Against Newly Emerging and Reemerging Respiratory RNA Viruses. *International Journal of Molecular Sciences, 26*(4), 1481. doi: 10.3390/ijms26041481

Machitani, M., Yasukawa, M., Nakashima, J., Furuichi, Y., & Masutomi, K. (2020). RNA-dependent RNA polymerase, RdRP, a promising therapeutic target for cancer and potentially COVID-19. *Cancer Science, 111*(11), 3976-3984. doi:10.1111/cas.14618

Magrone, T., Magrone, M., & Jirillo, E. (2020). Focus on Receptors for Coronaviruses with Special Reference to Angiotensin-Converting Enzyme 2 as a Potential Drug Target - A Perspective. *Endocrine, Metabolic & Immune Disorders-Drug Targets. 20*(6), 807-811. doi:10.2174/1871530320666200427112902

Megantara, S., Musfiroh, I., Lestari, D. (2022). In-silico study of diterpenoid lactones from Andrographis paniculate to interleukin-6 (IL-6) protein target. *RASAYAN Journal of Chemistry, 15*(03), 2004-2009. doi:10.31788/RJC.2022.1536999

Molaei, E., Molaei, A., Hayes, A. W., & Karimi, G. (2024). Remdesivir: treatment of COVID-19 in special populations. *Naunyn-Schmiedeberg's Archives of Pharmacology, 397*(6), 3829-3855. doi:10.1007/s00210-023-02927-2

Mondal A, Maffe P, Wilson S. N., Ghalei, S., Palacio, R., Handa, H., & Brisbois, E. J. (2023). Catalytic effect of transition metal-doped medical-grade polymer on S-nitrosothiol decomposition and its biological response. *Materials Advances, 4*(15), 3197–206. doi: 10.1039/d3ma00191a

Mostafa-Hedeab, G. (2020). ACE2 as a drug target of COVID-19 virus treatment, simplified updated review. *Reports of Biochemistry and Molecular Biology, 9*(1), 97–105. doi:10.29252/rbmb.9.1.97

Murugavel, S., Vasudevan, P., Chandrasekaran, R. K., Archana, V., & Ponnuswamy, A. (2022). Synthesis, crystal structure elucidation, DFT analysis, drug-likeness and ADMET evaluation, and molecular docking studies of triazole derivatives: Binary inhibition of spike protein and ACE2 receptor protein of COVID-19. *Journal of the Chinese Chemical Society, 69*(6), 884-900. doi:10.1002/jccs.202200140

Nagu, P., Parashar, A., Sharma, P., & Mehta, V. (2024). Recent developments in the therapeutics of SARS-CoV-2 infection. *One health bulletin, 4*, 143-56. doi:10.4103/ohbl.ohbl_17_24

Narayanan, A., Narwal, M., Majowicz, S. A., Varricchio, C., Toner, S. A., Ballatore, C.,…Jose, J. (2022). Identification of SARS-CoV-2 inhibitors targeting Mpro and PLpro using in-cell-protease assay. *Communications Biology, 5*(1), 169. doi.org/10.1038/s42003-022-03090-9

Neves, B. J., Braga, R. C., Melo-Filho, C. C., Moreira-Filho, J. T., Muratov, E. N., & Andrade, C. H. (2018). QSAR-Based Virtual Screening: Advances and Applications in Drug Discovery. *Frontiers in Pharmacology*, *9*, 1-7. doi:10.3389/fphar.2018.01275

Niknamian, S. (2021). Brief Facts about Covid-19 (Sars-Cov-2). *Journal of Surgery Research and Practice, 2*(1), 1-9. doi.org/10.46889/JSRP.2021.2103

Osipiuk, J., Azizi, S. A., Dvorkin, S., Endres, M., Jedrzejczak, R., Jones, K. A.,…Joachimiak, A. (2021). Structure of papain-like protease from SARS-CoV-2 and its complexes with non-covalent inhibitors. *Nature Communications, 12*(1), 743-751. doi:10.1038/s41467-021-21060-3

Parihar, A., Zafar, T., Khandia, R., Parihar, D. S., Dhote, R., Mishra, Y., & Khan, R. (2022). In silico Analysis for the Repurposing of Broad-spectrum Antiviral Drugs against Multiple Targets from SARS-CoV-2: A Molecular Docking and ADMET Approach. *Archives of Proteomics and Bioinformatics, 3*(1), 3-14.

Patel, A. H., Patel, R. B., Memon, M. J., Patel, S. S., Desai, S. A., & Meshram, D. B. (2021a). Docking, Binding Free Energy Estimation, and MD Simulation of Newly Designed CQ and HCQ Analogues Against the Spike-ACE2 Complex of SARS-CoV-2. *International Journal of Quantitative Structure-Property Relationships, 6*(4), 77-89. doi:10.4018/IJQSPR.2021100105

Patel, T. K., Patel, P. B., Barvaliya, M., Saurabh, M. K., Bhalla, H. L., & Khosla, P. P. (2021b). Efficacy and safety of lopinavir-ritonavir in COVID-19: A systematic review of randomised controlled trials. *Journal of Infection and Public Health, 14*(6), 740–748. doi.org/10.1016/j.jiph.2021.03.015

Petty, L. A., & Malani, P. N. (2022). Oral Antiviral Medications for COVID-19. *Journal of the American Medical Association, 327*(24), 2464. doi:10.1001/jama.2022.6876

Pinzi, L., Tinivella, A., Caporuscio, F., & Rastelli, G. (2021). Drug Repurposing and Polypharmacology to Fight SARS-CoV-2 Through Inhibition of the Main Protease. *Frontiers in Pharmacology, 12*, 636989, 1-11. doi:10.3389/fphar.2021.636989

Qing, X., Lee, X. Y., De Raeymaeker, J., Tame, J. R., Zhang, K. Y., De Maeyer, M. & Voet, A. (2014). Pharmacophore modeling: advances, limitations, and current utility in drug discovery. *Journal of Receptor, Ligand and Channel Research, 2014*(7), 81–92. doi.org/10.2147/JRLCR.S46843

Riziotis, I. G., Ribeiro, A. J. M., Borkakoti, N., & Thornton, J. M. (2023). The 3D Modules of Enzyme Catalysis: Deconstructing Active Sites into Distinct Functional Entities. *Journal of Molecular Biology, 435*(20),168254. doi.org/10.1016/j.jmb.2023.168254

Rukthong, P., Sereesongsang, N., Kulsirirat, T., Boonnak, N., & Sathirakul, K. (2020). In vitro investigation of metabolic fate of α-mangostin and gartanin via skin permeation by LC-MS/MS and in silico evaluation of the metabolites by ADMET predictor™. *BMC Complementary Medicine and Therapies, 2*(1), 359. doi:10.1186/s12906-020-03144-7

Rut, W., Lv, Z., Zmudzinski, M., Patchett, S., Nayak, D., Snipas, S. J.,…Olsen, S. K. (2020). Activity profiling and crystal structures of inhibitor-bound SARS-CoV-2 papain-like protease: A framework for anti–COVID-19 drug design. *Science Advances, 6*(42), 1-12. doi: 10.1126/sciadv.abd4596

Ruusmann, V., Sild, S., & Maran, U. (2014). QSAR DataBank - an approach for the digital organisation and archiving of QSAR model information. *Journal of Cheminformatics, 6*, 25, 1-17. doi:http://www.jcheminf.com/content/6/1/25

Salam, N. K., Nuti, R., & Sherman, W. (2009). Novel method for generating structure-based pharmacophores using energetic analysis. *Journal of Chemical Information and Modelling, 49*, 2356-2368. doi:10.1021/ci900212v

Sarkar, B., Mandal, S., Sarkar, T., & Sarkar, S. (2024). A Research Work on Design, Development and In-Vitro Evaluation of Losartan Potassium-Loaded Pectinate Microspheres. *International Journal For Multidisciplinary Research, 6*(2), 1-23. doi.org/10.36948/ijfmr.2024.v06i02.15156

Schimunek, J., Seidl, P., Elez, K., Hempel, T., Le, T., Noe, F.,…Hermans, T. M. (2024). A community effort in SARS-CoV-2 drug discovery. *Molecular Informatics, 43*(1), e202300262. doi:10.1002/minf.202300262

Schneidman-Duhovny, D., Dror, O., Inbar, Y., Nussinov, R., & Wolfson, H. J. (2008). Deterministic Pharmacophore Detection via Multiple Flexible Alignments of Drug-Like Molecules. *Journal of Computational Biology, 15*(7), 737-54. doi:10.1089/cmb.2007.0130

Seidel, T., Wieder, O., Garon, A., & Langer, T. (2020). Applications of the Pharmacophore Concept in Natural Product-Inspired Drug Design. *Molecular Informatics, 39*(11), 2000059. doi.org/10.1002/minf.202000059

Serafim, M. S. M., Queiroz, P. S., Barbosa, S. E., McKerrow, J. H., Eduardo, F., Mota, B.,…Maltarollo, V. G. (2023). The importance of good practices and false hits for QSAR-driven virtual screening real application: a SARS-CoV-2 main protease (Mpro) case study. *Frontiers in Drug Discovery, 3*, 1237655, 1-18. doi:10.3389/fddsv.2023.1237655

Shin, D., Mukherjee, R., Grewe, D., Bojkova, D., Baek, K., Bhattacharya, A.,…Dikic, I. (2020). Papain-like protease regulates SARS-CoV-2 viral spread and innate immunity. *Nature, 587*, 657-662. doi.org/10.1038/s41586-020-2601-5

Sigfrid, L., Perfect, C., Rojek, A., Longuere, K. S., Lipworth, S., Harriss, E.,…Horby, P. (2019). A systematic review of clinical guidelines on the management of acute, community-acquired CNS infections. *BMC Medicine, 17*(1), 170. doi.org/10.1186/s12916-019-1387-5

Singh, M., Kaur, R., Rajput, R., Agarwal, S., Kumar, S., Sharma, M., & Sharma, A. (2020). Analysis of Process and Formulation Variables on Chitosan-based Losartan Potassium Nanoparticles: Preparation, Validation and *in vitro* Release Kinetics. *Recent Innovations in Chemical Engineering, 13*(1), 41-54. doi:10.2174/2405520412666190502161137

Song, C. M., Lim, S. J., & Tong, J. C. (2009). Recent advances in computer-aided drug design. *Briefings in Bioinformatics, 10*(5), 579-91. doi:10.1093/bib/bbp023

Stadler, K., Ha, H. R., Ciminale, V., Spirli, C., Saletti, G., Schiavon, M.,…Baritussio, A. (2008). Amiodarone alters late endosomes and inhibits SARS coronavirus infection at a post-endosomal level. *American Journal of Respiratory Cell and Molecular Biology, 39*(2), 142-9. doi:10.1165/rcmb.2007-0217OC

Tallei, T. E., Tumilaar, S. G., Lombogia, L.T., Adam, A. A., Sakib, S. A., Emran, T. B., & Idores, R. (2021). Potential of betacyanin as an inhibitor of SARS-CoV-2 revealed by molecular docking study. *IOP Conference Series: Earth and Environmental Science, 711*, 012028, 1-9. doi:10.1088/1755-1315/711/1/012028

Tikhomirova, M. A., Kuzmenko, O. L., Arifulin, E. A., Shirokova, O. M., Musinova, Y. R., & Sheval, E. V. (2024). The Nucleocapsid (N) Proteins of Different Human Coronaviruses Demonstrate a Variable Capacity to Induce the Formation of Cytoplasmic Condensates. *International Journal of Molecular Sciences, 25*(23), 13162, 1-22. doi.org/10.1101/2024.11.20.624003

Vijay, A., Adury, V. S. S., & Mukherjee, A. (2024). Targeting RdRp of SARS-CoV-2 with De Novo Molecule Generation. *ACS Applied Bio Materials, 7*(2), 609-616. doi: 10.1021/acsabm.3c00339

Vilar, S., & Costanzi, S. (2012). Predicting Biological Activities through QSAR Analysis and Docking-based Scoring. *Methods in Molecular Biology, 914*, 271-284. doi:10.1007/978-1-62703-023-6_16

Vuorinen, A., Engeli, R., Meyer, A., Bachmann, F., Griesser, U.J., Schuster, D., & Odermatt, A. (2014). Ligand-Based Pharmacophore Modelling and Virtual Screening for the Discovery of Novel 17β-Hydroxysteroid Dehydrogenase 2 Inhibitors. *Journal of Medicinal Chemistry, 57*(14), 5995-6007. doi:10.1021/jm5004914

Wang, X., Shen, Y., Wang, S., Li, S., Zhang, W., Liu, X.,…Li, H. (2017). PharmMapper 2017 update: a web server for potential drug target identification with a comprehensive target pharmacophore database. *Nucleic Acids Research, 45*(W1), W356-360. doi: 10.1093/nar/gkx374

Williams, C. G., Jureka, A. S., Silvas, J. A., Nicolini, A. M., Chvatal, S. A., Carlson-Stevermer, J.,… Basler, C. F. (2021). Inhibitors of VPS34 and fatty-acid metabolism suppress SARS-CoV-2 replication. *Cell Reports, 36*(5), 109479. doi:10.1016/j.celrep.2021.109479

Woo, P. C. Y., De Groot, R. J., Haagmans, B., Lau, S. K. P., Neuman, B. W., Perlman, S.,…Yeh, S. -H. (2023). ICTV Virus Taxonomy Profile: Coronaviridae. *Journal of General Virology, 104*(4), 001843. doi:10.1099/jgv.0.001843

Wu, C., Liu, Y., Yang, Y., Zhang, P., Zhong, W., Wang, Y.,…Li, H. (2020). Analysis of therapeutic targets for SARS-CoV-2 and discovery of potential drugs by computational methods. *Acta Pharmaceutica Sinica B, 10*(5), 766–88. doi:10.1016/j.apsb.2020.02.008

Yang, E., Choi, H. Z., Kim, S., Oh, D. H., Ahn, M. Y., Ham, S.,…Choi, J. –P. (2024). Propensity score matched analysis for the safety and effectiveness of remdesivir in COVID-19 patients with renal impairment. *BMC Infectious Diseases, 24*(1), 1-9. doi.org/10.1186/s12879-023-08859-9

Yaro, P. A., Ohanyido, D. F., & Rattan, A. (2024). Drug Resistance in four important human viruses: Updated review. *Microbes of Medical Importance*, 268-286. doi:10.58532/nbennurmmch11

Yi, S., Guk, K., Kim, H., Lee, K. S., Lim, E. K., Kang, T., & Jung, J. (2024). RdRp activity test using CRISPR/Cas13a enzyme (RACE) for screening of SARS-CoV-2 inhibitors. *Sensors Actuators B: Chemical, 399*, 134748, 1-8. doi:10.1016/j.snb.2023.134748

Yu, B., & Chang, J. (2020). Azvudine (FNC): a promising clinical candidate for COVID-19 treatment. *Signal Transduction and Targeted Therapy, 5*, 236. doi.org/10.1038/s41392-020-00351-z

Zaidi, A. K., & Dehgani-Mobaraki, P. (2021). The mechanisms of action of ivermectin against SARS-CoV-2: an extensive review. *Journal of Antibiotics, 75*(2), 60–71. doi: 10.1038/s41429-021-00491-6

Zhang, K., Yang, X., Wang, Y., Yu, Y., Huang, N., Li, G.,…Yang, S. (2025). Artificial intelligence in drug development. *Nature Medicine, 31*(1), 45–59. doi:10.1038/s41591-024-03434-4

Zhang, L., Lin, D., Sun, X., Curth, U., Drosten, C., Sauerhering, L.,…Hilgenfeld, R. (2020). Crystal structure of SARS-CoV-2 main protease provides a basis for design of improved a-ketoamide inhibitors. *Science, 368*(6489), 409-412. doi: 10.1126/science.abb3405

Zhang, P., Niemela, E., Lopez Cerda, S., Sorvisto, P., Virtanen, J., & Santos, H. A. (2024). Host-Directed Virus-Mimicking Particles Interacting with the ACE2 Receptor Competitively Block Coronavirus SARS-CoV-2 Entry. *Nano Letters, 24*(14), 4064-4071. doi: 10.1021/acs.nanolett.3c04430

Zhang, Y., Sun, Y., Xie, Y., Shang, W., Wang, Z., Jiang, H.,…Zhang, L. (2023). A viral RNA-dependent RNA polymerase inhibitor VV116, broadly inhibits human coronaviruses and has synergistic potency with 3CLpro inhibitor nirmatrelvir. *Signal Transduction and Targeted Therapy, 8*(1), 360. doi: 10.1038/s41392-023-01587-1.

Zhou, Y., Hou, Y., Shen, J., Huang, Y., Martin, W., & Cheng, F. (2020). Network-based drug repurposing for novel coronavirus 2019-nCoV/SARS-CoV-2. *Cell Discovery, 6*(14), 1-18. doi.org/10.1038/s41421-020-0153-3

Zhu, W., Chen, C. Z., Gorshkov, K., Xu, M., Lo, D. C., & Zheng, W. (2022). RNA-Dependent RNA Polymerase as a Target for COVID-19 Drug Discovery. *Advancing the Science of Drug Discovery, 25*(10), 1141-1151. doi:10.1177/2472555220942123

Zipeto, D., Palmeira, J. F., Argañaraz, G. A., & Argañaraz, E. R. (2020). ACE2/ADAM17/TMPRSS2 Interplay May Be the Main Risk Factor for COVID-19. *Front Immunology, 11*, 576745. doi: 10.3389/fimmu.2020.576745

FABAD J. Pharm. Sci., 51, 1, 383-402, 2026
Doi: 10.55262/fabadeczacilik.1774008
REVIEW ARTICLE

Repurposing Antidiabetic Agents as Potential Therapeutics in Neurodegenerative Diseases: Current Status and Future Perspectives

Ahmet Hüsamettin BARAN [*°]

Repurposing Antidiabetic Agents as Potential Therapeutics in Neurodegenerative Diseases: Current Status and Future Perspectives

SUMMARY

This review focuses on preclinical, clinical, and epidemiological studies that highlight the therapeutic potential of antidiabetic drugs for the prevention and treatment of neurodegenerative diseases. Neurodegenerative disorders represent a significant public health concern, with their global prevalence steadily increasing. These conditions are progressive and heterogeneous, substantially reducing quality of life and imposing a considerable burden on healthcare systems and society. The rising disability, morbidity, and mortality associated with these diseases coincide with the aging of the global population. Due to their complex etiology and progressive nature, neurodegenerative diseases pose considerable challenges for diagnosis and treatment. Current therapies are primarily limited to alleviating cognitive and/or motor symptoms and are generally insufficient to slow, halt, or prevent disease progression. Consequently, there is an urgent need for novel interventions that can enhance neuronal function and attenuate underlying disease mechanisms. Recent evidence from preclinical and clinical studies has revealed significant links between diabetes and neurodegenerative diseases. This review aims to guide future research by providing an up-to-date overview of the effects of antidiabetic agents on neurodegenerative disorders.

Keywords: *Neurodegenerative diseases, type 1 diabetes mellitus, type 2 diabetes mellitus, insulin resistance, antidiabetic drugs.*

Antidiyabetik İlaçların Nörodejeneratif Hastalıklarda Yeniden Konumlandırılması: Güncel Durum ve Gelecek Perspektifleri

ÖZ

Bu derleme, antidiyabetik ilaçların nörodejeneratif hastalıkların önlenmesi ve tedavisindeki terapötik potansiyelini ortaya koyan preklinik, klinik ve epidemiyolojik çalışmalara odaklanmaktadır. Nörodejeneratif hastalıklar dünyada her geçen gün artan prevalansa sahip, yaşam kalitesini önemli derecede bozan, ilerleyici ve heterojen yapılarıyla sağlık sistemleri ve sosyoekonomik yapı üzerinde ciddi yük oluşturan önemli halk sağlığı sorunlarıdır. Nörodejeneratif hastalıkların yol açtığı sakatlık, morbidite ve mortalite oranlarındaki artış dünya nüfusundaki yaşlanma hızına paralel artmaktadır. Nörodejeneratif hastalıklar karmaşık etyolojileri ve ilerleyici yapıları nedeniyle tanı ve tedavide önemli zorluklar ortaya çıkarmaktadır. Son yıllarda bu hastalıkların altında yatan temel mekanizmaları anlamak için büyük ilerlemeler kaydedilmiş olsa da mevcut tedaviler sadece bilişsel gerilemeyi ve/veya motor semptomları hafifletebilmekte, hastalığı yavaşlatma, durdurma veya önleme konusunda yetersiz kalmaktadır. Bu bağlamda nöronal işlevi iyileştirecek ve altta yatan hastalık süreçlerini yavaşlatacak güncel tedavilere acil ihtiyaç vardır. Son yıllarda gerçekleştirilen çalışmalardan elde edilen kanıtlar diyabet ve nörodejeneratif hastalıklar arasında önemli bağlantılar olduğunu ortaya koymuştur. Bu derlemenin temel amacı, bu alandaki araştırmacılara, antidiyabetik ajanların nörodejeneratif hastalıklardaki etkilerini değerlendirmeleri için güncel bir bakış açısı sunarak, gelecekteki bilimsel çalışmalara yön vermektir.

Anahtar Kelimeler: *Nörodejeneratif hastalıklar, tip 1 diabetes mellitus, tip 2 diabetes mellitus, insülin direnci, antidiyabetik ilaçlar.*

Recieved: 30.08.2025
Revised: 9.02.2026
Accepted: 14.02.2026

[*] ORCID: 0000-0003-0830-313X, Republic of Türkiye Ministry of Health, Türkiye Medicines and Medical Devices Agency, Ankara, Türkiye

[°] Corresponding Author; Ahmet Hüsamettin BARAN
E-mail: eczabaran@gmail.com

INTRODUCTION

Neurodegenerative diseases (NDs) comprise a heterogeneous group of progressive disorders that involve the accumulation of misfolded intracellular or extracellular proteins, which leads to synaptic dysfunction and ultimately neuronal death (Forrest & Kovacs, 2025). The most prevalent NDs, most prominently Alzheimer's disease (AD) and Parkinson's disease (PD), alongside other conditions like Huntington's disease (HD), multiple sclerosis (MS), and amyotrophic lateral sclerosis (ALS), collectively affect millions worldwide and impose a heavy burden on the functional independence of affected individuals. The prevalence of AD and PD, which are strongly age-associated, has risen sharply in parallel with the global increase in life expectancy (Lamptey et al., 2022). According to the World Health Organization (WHO) (2023), neurological disorders are currently the second leading cause of death globally, responsible for approximately 9 million deaths each year. Despite major advances, the precise pathophysiological mechanisms underlying most NDs remain incompletely understood. Shared molecular pathways include glutamate excitotoxicity, calcium dysregulation, proteotoxic stress, neuroinflammation, mitochondrial dysfunction, and oxidative stress (Jurcau, 2021). These complex etiologies, combined with their progressive nature, pose significant challenges for both diagnosis and therapy, and currently available treatments are limited to symptomatic relief. Hence, there is an urgent need for innovative interventions capable of restoring neuronal function and modifying the underlying disease course.

Developing novel pharmacological compounds is time-consuming, expensive, and often unsuccessful in clinical translation. Therefore, researchers have increasingly turned to drug repurposing, defined as the re-evaluation of approved medications for new therapeutic indications, as a promising and cost-effective strategy. Emerging evidence suggests a strong bidirectional relationship between diabetes mellitus (DM) and NDs, which has garnered growing scientific attention (Szablewski, 2025; Verdile et al., 2019).

DM is a chronic, progressive, and heterogeneous metabolic disorder affecting millions worldwide. As reported by the American Diabetes Association Professional Practice Committee (2024), DM is a metabolic condition marked by sustained elevations in blood glucose levels and impaired glucose regulation arising from defective insulin secretion, reduced tissue responsiveness to insulin, or both processes. Type 1 diabetes mellitus (T1DM) predominantly develops as a consequence of immune-mediated destruction of pancreatic β-cells, ultimately resulting in an absolute lack of endogenous insulin. By comparison, type 2 diabetes mellitus (T2DM), which constitutes nearly 90% of diagnosed cases, is associated with peripheral insulin resistance together with a progressive and relative decline in insulin secretory function (DeFronzo, 2015). Neurological complications such as peripheral neuropathy, retinal neurodegeneration, and diabetic encephalopathy underscore that diabetes extends beyond a metabolic disorder to affect the central nervous system. Indeed, pathophysiological parallels between T2DM and AD have led some researchers to describe AD as type 3 diabetes, highlighting the shared mechanisms of insulin resistance, cognitive decline, and neurodegeneration (Kandimalla et al., 2017).

Epidemiological and experimental studies have revealed that DM significantly influences the incidence and progression of NDs through shared mechanisms, including insulin resistance, impaired glucose metabolism, oxidative stress, mitochondrial dysfunction, and chronic inflammation (Akter et al., 2011; Butterfield et al., 2014; De La Monte, 2017; Li & Hölscher, 2007; Luchsinger et al., 2004). Our prior investigations and research provide a multi-faceted rationale for exploring shared pathways in neurodegeneration. Specifically, our review on Sestrin-2 highlights it as a critical therapeutic target for neuroprotection (Baran,

2022b), while our experimental research into pro-inflammatory cytokines (TNF-α and IL-6) emphasizes the importance of modulating systemic inflammation to mitigate acute toxicity and neuronal damage (Baran et al., 2024). Furthermore, our study on pharmacogenetic variability (Baran, 2022a) underscores that individual differences in drug response must be considered when repurposing antidiabetic agents for neurological indications. These findings collectively support the strategy of targeting metabolic and inflammatory axes to develop more personalized and effective neuroprotective therapies.

Given the biological and epidemiological connections between DM and NDs, the therapeutic repurposing of antidiabetic agents has emerged as a significant area of investigation. Currently approved pharmacotherapies for NDs provide primarily symptomatic relief and have a limited impact on disease progression. Considering the high global prevalence and economic burden of these disorders, the identification of effective and well-tolerated therapeutic alternatives is an urgent priority. Therefore, this review synthesizes current evidence on the pharmacological actions of antidiabetic agents in neurodegenerative disorders and highlights implications for future experimental and clinical investigations. To support this objective, a comprehensive literature search was performed across PubMed, ScienceDirect, Web of Science, and ClinicalTrials.gov to retrieve relevant interventional and translational studies. Data extraction, processing, and visualization were performed using Python-based computational workflows to systematically map research trends, drug classes, and mechanistic overlaps.

SHARED PATHOPHYSIOLOGICAL MECHANISMS LINKING T2DM AND NDs

T2DM and NDs share multiple convergent molecular and cellular mechanisms leading to impaired neuronal homeostasis and declining cognitive performance. The key interconnected pathways underlying this relationship are outlined below.

Brain insulin resistance and glucose metabolism impairment

Brain insulin resistance constitutes a pivotal pathophysiological intersection between NDs and T2DM. Insulin plays a crucial role in neuronal survival, synaptic plasticity, and glucose uptake by activating the PI3K/AKT and MAPK/ERK signaling cascades (Andrade et al., 2024; Carvalho & Moreira, 2023; Dai et al., 2023). Impaired insulin signaling diminishes AKT phosphorylation and activates GSK-3β, which in turn promotes β-amyloid (Aβ) accumulation and tau hyperphosphorylation (Andrade et al., 2024; Kciuk et al., 2024). In PD, reduced expression of GLUT3 and GLUT4 transporters within dopaminergic neurons limits glucose uptake, resulting in ATP depletion and α-synuclein aggregation (Dai et al., 2023; Sabari et al., 2023; Tanvir et al., 2024). Collectively, these alterations impair neuronal energy metabolism, exacerbate protein aggregation, and contribute to progressive synaptic loss and cognitive deterioration.

Mitochondrial dysfunction and energy metabolism deficits

Among the shared mechanisms between DM and NDs, mitochondrial impairment is increasingly recognized as a key driver of neuronal damage. Hyperglycemia and insulin resistance suppress mitochondrial respiratory chain complexes I and III, which leads to reduced ATP synthesis and increased reactive oxygen species (ROS) generation (Carvalho & Moreira, 2023; Veselov et al., 2023). This process leads to cytochrome c release and apoptotic signaling cascades. Dopaminergic neurons in PD are particularly vulnerable to mitochondrial stress and energy deficits, which promote neuronal death and α-synuclein aggregation (Dai et al., 2023; Sabari et al., 2023). Pharmacologically, metformin and several GLP-1 receptor agonists (GLP-1 RAs) promote AMPK signaling, support mitochondrial biogenesis, and enhance neuronal energy metabolism, thereby improving both glucose homeostasis and neuronal resilience (Mohammed & Kelemu, 2025; Reed et al., 2025).

Oxidative stress and redox imbalance

Chronic hyperglycemia and insulin resistance increase excessive ROS production from NADPH oxidases and mitochondrial sources, intensifying oxidative stress in neuronal tissue (Li et al., 2023; Veselov et al., 2023). This redox imbalance accelerates lipid peroxidation, protein carbonylation, and DNA damage while fostering Aβ and α-synuclein accumulation (Ghosh et al., 2023; Veselov et al., 2023). Antidiabetic agents such as GLP-1 RAs, DPP-4 inhibitors, and metformin counteract these effects by activating the Nrf2/ARE pathway, enhancing the transcription of endogenous antioxidant enzymes (SOD, CAT, GPx), and thereby exerting robust neuroprotective actions (Ghosh et al., 2023; Ibrahim et al., 2025; Mohammed & Kelemu, 2025; Reed et al., 2025).

Amyloid and protein aggregation

Insulin resistance and oxidative stress disrupt protein homeostasis, thereby accelerating neurodegenerative cascades. Dysregulated insulin signaling alters amyloid precursor protein (APP) processing, facilitating Aβ overproduction and tau hyperphosphorylation (Andrade et al., 2024; Kciuk et al., 2024). In PD, mitochondrial dysfunction and ROS accumulation foster α-synuclein misfolding and oligomerization (Dai et al., 2023; Sabari et al., 2023). GLP-1 RAs and DPP-4 inhibitors mitigate these effects by enhancing autophagy and proteasomal degradation, thereby reducing toxic protein aggregates (Ibrahim et al., 2025; Mohammed & Kelemu, 2025; Sulangi et al., 2024; Złotek et al., 2023).

Neuroinflammation and microglial activation

Prolonged hyperglycemic states stimulate inflammatory signaling pathways, increasing the release of cytokines, including TNF-α, IL-1β, and IL-6, and thereby facilitating microglial reactivity and neuroinflammatory cascades (Li et al., 2023; Yu et al., 2025). This sustained inflammatory milieu contributes to synaptic impairment and neuronal apoptosis. Metformin and GLP-1 RAs attenuate these processes by suppressing NF-κB and JNK signaling cascades, shifting microglial polarization toward an anti-inflammatory M2 phenotype, and ultimately conferring neuroprotection in both AD and PD models (Ibrahim et al., 2025; Mohammed & Kelemu, 2025; Reed et al., 2025).

Autophagy and proteostasis dysregulation

Defective autophagic clearance represents another critical mechanism linking T2DM and NDs. Hyperglycemia and insulin resistance impair autophagic flux, leading to the accumulation of misfolded Aβ and α-synuclein species. GLP-1 RAs and DPP-4 inhibitors restore autophagic function through modulation of AMPK and mTOR, enhancing lysosomal biogenesis and promoting neuronal proteostasis (Ibrahim et al., 2025; Luo et al., 2025; Złotek et al., 2023). These effects may slow cognitive decline and neuronal loss in diabetic and neurodegenerative contexts.

Glucose metabolism and neuronal energy imbalance

Disturbances in cerebral glucose metabolism lead to neuronal energy depletion and lactate accumulation (Dai et al., 2023; Dou et al., 2025; Kan et al., 2025). Reduced expression of GLUT1 and GLUT3 transporters diminishes glucose uptake and ATP production, impairing synaptic efficacy. GLP-1 RAs and SGLT2 inhibitors improve cerebral glucose utilization, stabilize energy metabolism, and ameliorate synaptic dysfunction (Dou et al., 2025; Ibrahim et al., 2025; Złotek et al., 2023).

Incretin system and neuroprotection

Beyond glycemic regulation, incretin-based therapies exhibit pleiotropic neuroprotective properties. GLP-1 RAs and DPP-4 inhibitors activate PI3K/AKT and AMPK pathways, enhance synaptic plasticity, attenuate oxidative stress, suppress NF-κB-driven inflammation, and promote autophagy (Ibrahim et al., 2025; Koshatwar et al., 2023; Nowell et al., 2023; Pandiyan et al., 2024; Sulangi et al., 2024). Consequently, these agents reduce Aβ and α-synuclein burden, preserve neuronal energy homeostasis, and mitigate cognitive decline in both AD and PD.

Taken together, these overlapping mechanisms highlight the multifaceted neuroprotective potential of antidiabetic agents. As summarized in table 1, these drugs target several interconnected neurodegenerative pathways, including insulin resistance, disruptions in mitochondrial homeostasis, increased oxidative burden, pathological protein misfolding, neuroimmune activation, impaired autophagy, and altered glucose metabolism. By modulating these mechanisms, antidiabetic agents may not only restore metabolic balance but also mitigate neuronal injury and cognitive decline, providing a promising avenue for therapeutic repurposing in neurodegenerative disorders.

Table 1. Shared pathophysiological mechanisms and the impact of antidiabetic agents

Primary Pathophysiological Category	Pathophysiological Mechanism	Key Molecular/Cellular Outcomes	Associated Antidiabetic Agents
Insulin and Glucose Regulation	Brain insulin resistance	Increased Aβ deposition, tau hyperphosphorylation and reduced bioenergetics	Metformin, GLP-1 RAs
Cellular Energy Metabolism	Mitochondrial dysfunction	Decreased ATP production, elevated ROS and enhanced apoptosis	Metformin, GLP-1 RAs
Oxidative Balance	Oxidative stress	Lipid peroxidation, protein carbonylation and DNA damage	GLP-1 RAs, DPP-4 inhibitors, Metformin
Protein Aggregation	Amyloid and protein aggregation	Accumulation of Aβ and α-synuclein	DPP-4 inhibitors, GLP-1 RAs
Proteostasis and Autophagy	Autophagy impairment	Accumulation of toxic proteins, disrupted homeostasis	GLP-1 RAs, DPP-4 inhibitors
Neuroinflammation	Microglial activation	Increased proinflammatory cytokines (TNF-α, IL-6, IL-1β)	Metformin, GLP-1 RAs
Glucose and Energy Metabolism	Glucose metabolism impairment	Reduced ATP synthesis and impaired synaptic function	GLP-1 RAs, SGLT2 inhibitors
Incretin-mediated Neuroprotection	Incretin signaling	Enhanced synaptic plasticity, decreased ROS, improved autophagy	GLP-1 RAs, DPP-4 inhibitors

REPURPOSING POTENTIAL OF ANTIDIABETIC DRUGS FOR THE MANAGEMENT OF NDs

Given the emerging overlap between T2DM and NDs, several antidiabetic drug classes have been evaluated for their neuroprotective potential. The following sections synthesize pivotal evidence regarding the repurposing potential of these agents, focusing on both mechanistic insights and clinical outcomes.

Biguanides

Biguanide agents, metformin being the main example, are widely prescribed for the treatment of T2DM. The presence of shared pathophysiological pathways between DM and NDs, including chronic hyperglycemia, insulin resistance, oxidative stress, and neuroinflammatory processes, supports the potential neurological repurposing of these agents. In a post-mortem cohort study conducted by Barthold et al. (2021), individuals with diabetes who had used metformin for at least five years exhibited a significant reduction in cortical Aβ1-42 levels, suggesting a possible protective effect against AD-specific pathology. However, analyses of established AD neuropathological parameters, including plaque load, tangle distribution, and CERAD classification, revealed no measurable differences. Mechanistically, Cai et al. (2020) demonstrated that metformin modulates unfolded protein response (UPR) pathways via AMPK/ERK1/2 signaling, contributing to proteostasis maintenance and regulating intracellular energy balance, mitochondrial function, and cell survival. Papini et

al. (2024) suggested that metformin may also exert effects through lysosome-dependent mechanisms, activating AMPK via lysosomal targets and modulating autophagy and lysosomal function. Additionally, Campagnoli et al. (2025) summarized the pleiotropic actions of metformin, highlighting its ability to influence neurodegenerative processes through both lysosomal/autophagy pathways and metabolic signaling. Collectively, these findings suggest that metformin has the potential to affect specific neurodegenerative biomarkers, particularly Aβ1-42, although its impact may not be consistent across to all AD pathological endpoints. Consequently, while the repurposing of metformin and related biguanides for AD and other neurodegenerative processes appears promising, further well-designed randomized controlled trials are required to establish optimal dosing, treatment duration, patient selection, and safety-efficacy profiles.

Thiazolidinediones (TZDs)

Thiazolidinediones (TZDs) are an oral antidiabetic drug class that enhances insulin sensitivity in T2DM management. The presence of shared pathophysiological pathways between DM and NDs (particularly insulin resistance, chronic inflammation, mitochondrial dysfunction, and oxidative stress) supports their potential neurological repurposing. A prospective observational study based on the U.S. Veterans Affairs database, including T2DM patients aged ≥60 years, reported that individuals receiving TZD monotherapy had approximately a 22% lower risk of all-cause dementia compared to those on metformin monotherapy. In contrast, sulfonylurea monotherapy was associated with an approximately 12% increased dementia risk relative to metformin (Tang et al., 2022). These findings suggest that TZDs may exert neuroprotective effects at the central nervous system level, beyond their glucose-lowering properties. Mechanistically, studies have shown that PPARγ agonists (e.g., glitazones) can modulate processes related to neurodegeneration, including mitochondrial redox balance, oxidative stress, neuroinflammation, proteasomal activity and pathological protein accumulation, as well as cellular energy metabolism (Durai et al., 2022). In particular, Alhowail et al. (2022) reviewed evidence indicating that pioglitazone can exert neuroprotective effects by regulating inflammatory cytokines (IL-1, IL-6, TNF-α) and NF-κB/p38 MAPK signaling pathways, while ameliorating oxidative stress and mitochondrial dysfunction. In an *in vitro* neuronal culture model, troglitazone was shown to enhance PPARγ activation and modulate autophagic flux, preventing neuronal cell death induced by prion peptides (Moon et al., 2021). Additionally, in a chronic repetitive mild traumatic brain injury model, PPARγ activation reduced microglial activation, prevented learning and memory deficits, and regulated signaling pathways including NLRP3 inflammasome, STAT3, and NF-κB (Pearson et al., 2024). Taken together, these findings from clinical observational, molecular mechanistic, and in vitro/preclinical studies highlight TZDs as a promising candidate for repurposing in the prevention or slowing of progression of neurodegenerative disorders such as AD and vascular dementia. However, because most of the available evidence is observational or preclinical, causal inferences are limited. Further clinical studies are needed.

GLP-1 receptor agonists (GLP-1 RAs)

GLP-1 RAs are widely used in the treatment of T2DM and are effective in both glycemic control and weight reduction. This class includes agents such as liraglutide, semaglutide, dulaglutide, and exenatide (Yao et al., 2024). The presence and functional significance of GLP-1 RAs in the human brain play a central role in the link between T2DM and NDs. Animal models have demonstrated that GLP-1 RAs are essential for learning and memory processes, with receptor deficiency leads to impairments in spatial memory and neuronal survival (During et al., 2003). Notably, GLP-1 receptors are primarily expressed in neurons but not in glial cells, suggesting that GLP-1 exerts its central nervous system effects directly at synaptic and neuronal levels (Hamilton & Hölscher, 2009).

Evidence from human studies indicates that GLP-1 receptors are expressed in several brain regions, including the parietal cortex, hypothalamus, and medulla. Moreover, liraglutide administration in individuals with T2DM has been associated with reduced neural responses to highly palatable food stimuli (Farr et al., 2016). Among neurodegenerative disorders, PD has received the most attention, as GLP-1 RAs have been shown to reduce dopaminergic neuronal loss, support mitochondrial function, and suppress oxidative stress and neuroinflammation (Kalinderi et al., 2024). These agents improve neuronal insulin signaling, reduce brain insulin resistance, enhance mitochondrial ATP production, decrease pro-inflammatory cytokines, promote synaptic growth, elevate neurotrophic factors (BDNF, GDNF), modulate protein aggregation (Aβ, tau), and maintain the stability of the blood–brain barrier and neurovascular unit (Kalinderi et al., 2024; Kopp et al., 2022). Meta-analyses indicate that GLP-1 RAs can improve motor function in PD, although effects vary and adverse effects are possible (Helal et al., 2025; Kopp et al., 2022). Conversely, in ALS mouse models, GLP-1 RAs such as liraglutide have not demonstrated a slowing of disease progression (Keerie et al., 2021). Collectively, these findings demonstrate that GLP-1 RAs not only regulate glucose homeostasis but also influence neurodegenerative processes through multiple mechanisms, including insulin signaling, mitochondrial function, oxidative stress, neuroinflammation, proteostasis, synaptic plasticity, and blood-brain barrier preservation.

Sodium-glucose cotransporter-2 (SGLT2) inhibitors

Emerging evidence indicates that SGLT2 inhibitors may help maintain cognitive performance by modulating oxidative stress-related processes within the central nervous system (e.g., activation of NADPH oxidase subunits, superoxide production, 8-hydroxydeoxyguanosine levels), suppressing neuroinflammation (e.g., glial cell reactivity accompanied by increased release of inflammatory mediators), maintaining blood-brain barrier integrity, preventing amyloid-β accumulation and tau hyperphosphorylation, ameliorating mitochondrial dysfunction (e.g., increased ROS, loss of membrane potential), enhancing synaptic plasticity and neurotrophic factor expression (e.g., BDNF), and improving cerebral glucose utilization (Mei et al., 2024; Shin et al., 2024). In a recent retrospective cohort study of patients with T2DM aged 60 years or over found that, those treated with SGLT2 inhibitors had a 20% lower incidence of dementia (Sarabhai et al., 2025). A meta-analysis of eight cohort studies involving 1,275,257 participants indicated that SGLT2 inhibitor use was associated with approximately 33% lower risk of all-cause dementia compared to DPP-4 inhibitors (Mei et al., 2024). Furthermore, a pharmacodynamic-based multicenter network meta-analysis evaluating the preventive potential of SGLT2 inhibitors and GLP-1 RAs against NDs reported that only dapagliflozin showed a significant protective effect against PD (OR = 0.28, 95% CI 0.09–0.93) (Tseng et al., 2025). This effect has been attributed to dapagliflozin's high SGLT2 selectivity and anti-inflammatory properties, which may reduce dopaminergic neuron loss and suppress neuroinflammation. Other SGLT2 inhibitors (e.g., empagliflozin, canagliflozin) and GLP-1 RAs (e.g., liraglutide, semaglutide) did not demonstrate significant effects, likely due to methodological and biological factors such as insufficient follow-up duration, lack of neurological endpoints, pharmacodynamic variability, and limited sample sizes (Tseng et al., 2025). Nevertheless, clinical evidence remains limited, and long-term safety profiles, efficacy in non-diabetic populations, and the role of combination therapies warrant further investigation.

Dipeptidyl peptidase-4 (DPP-4) inhibitors

DPP-4 inhibitors possess significant potential for reducing the risk of NDs, consciousness impairment, and cognitive dysfunction in individuals with T2DM. Clinical cohort analyses have demonstrated that treatment with DPP-4 inhibitors among diabetic

patients is associated with a significant reduction in neurological morbidity compared to other oral antidiabetic agents (Brauer et al., 2020; Lin et al., 2023). Moreover, a deep learning-based drug screening study combined with retrospective clinical analysis suggested that saxagliptin may have a beneficial effect in long-term cases of consciousness impairment. DPP-4 inhibition elevates endogenous GLP-1 and GIP levels, thereby reactivating neuronal insulin/IGF-1 signaling, suppressing neuroinflammation, oxidative stress, and tau/amyloid-β pathology, and supporting monoaminergic and GABAergic neurotransmission (Toker et al., 2025). Systematic review and meta-analysis data further indicate that DPP-4 inhibitors have a positive effects on the cognitive function of patients with T2DM, as evidenced by improvements in MMSE and IADL scores (Meng et al., 2023). Collectively, these findings increasingly suggest that DPP-4 inhibitors may serve as neuroprotective agents in modulating diabetes-associated cognitive dysfunction (Sulangi et al., 2024).

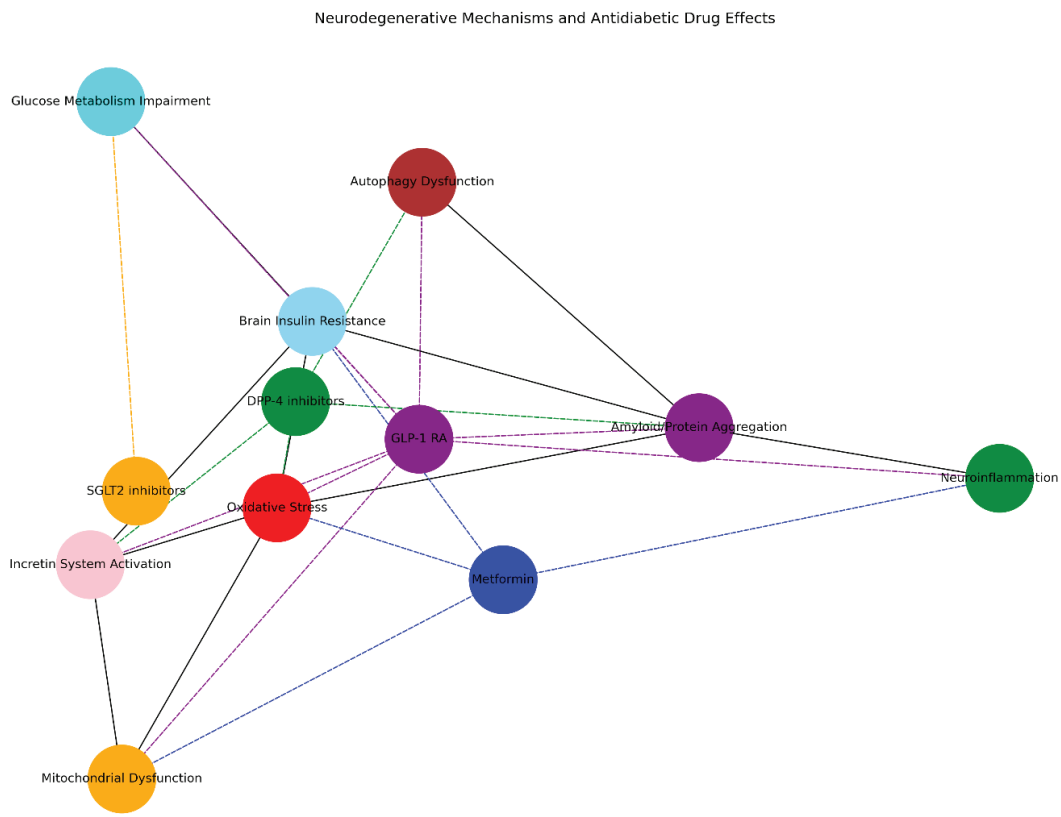


Figure 1. Pathways of neurodegeneration and the therapeutic targets of antidiabetic drugs

Figure 1 presents a color-coded network visualization of the pathways of neurodegeneration and the therapeutic targets of antidiabetic drugs. Solid black arrows represent established mechanistic interactions between pathological processes, while dashed colored lines indicate the modulatory effects of specific drug classes. Nodes are categorized by functional domain: brain insulin resistance (skyblue), glucose metabolism impairment (cyan), mitochondrial dysfunction (orange), oxidative stress (red), amyloid/protein aggregation (purple), neuroinflammation (dark green), autophagy dysfunction (brown), and incretin system activation (pink). Drug nodes (Metformin, GLP-1 RA, DPP-4 inhibitors, and SGLT2 inhibitors) are positioned centrally to demonstrate their pleiotropic impact across multiple neuroprotective axes.

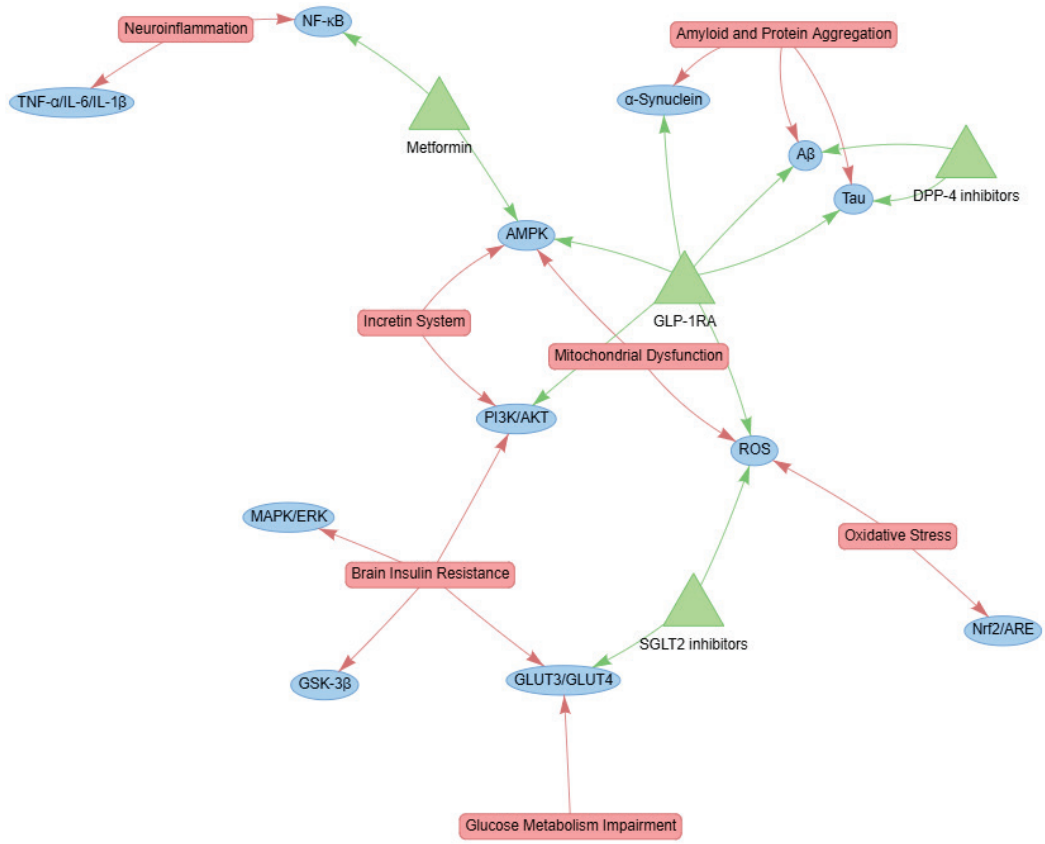


Figure 2. Therapeutic network of antidiabetic drugs targeting pathophysiological links between T2DM and NDs

Figure 2 illustrates a mechanistic network highlighting the key pathophysiological mechanisms linking T2DM with NDs. Nodes represent major processes -including brain insulin resistance, mitochondrial dysfunction, oxidative stress, neuroinflammation, glucose metabolism disturbance, and protein aggregation- as well as associated molecular pathways and proteins such as PI3K/AKT, MAPK/ERK, GSK-3β, GLUT3/GLUT4, AMPK, ROS, Nrf2/ARE, TNF-α/IL-6/IL-1β, NF-κB, Aβ, tau, and α-synuclein. Pharmacological agents (metformin, GLP-1 RAs, DPP-4 inhibitors, and SGLT2 inhibitors) are also represented. Edges indicate mechanistic or regulatory relationships, including activation, inhibition, upregulation, downregulation, hyperphosphorylation, or aggregation. The network demonstrates how insulin resistance activates GSK-3β and reduces GLUT3/GLUT4 expression, thereby promoting protein aggregation and impairing neuronal glucose uptake, while antidiabetic agents modulate these pathways to exert neuroprotective effects.

SUMMARY OF INTERVENTIONAL STUDIES ON ANTIDIABETIC AGENTS IN NEURODEGENERATIVE DISORDERS

A systematic search of the ClinicalTrials.gov database was conducted to identify interventional trials investigating the therapeutic potential of antidiabetic agents in NDs up to October 31, 2025.

The search strategy included the following keywords in the *Intervention/Treatment* field:

"metformin" OR "pioglitazone" OR "rosiglitazone" OR "liraglutide" OR "exenatide" OR "semaglutide" OR "lixisenatide" OR "dulaglutide" OR "sitagliptin" OR "vildagliptin" OR "empagliflozin" OR "dapagliflozin" OR "canagliflozin" OR "insulin".

Inclusion criteria encompassed interventional studies targeting AD, PD, ALS, HD, or other NDs, in which the aforementioned antidiabetic agents were used as primary or adjunctive interventions. Data extraction focused the study phase, status, target condition, intervention, and mechanistic information reported in the trial summaries. Frequencies of interventions and molecular pathways were tabulated to provide a quantitative overview of the current clinical landscape.

The analysis of 76 included trials reveals that the majority of trials are in early to intermediate phases (Phase I-II), with fewer progressing to late-phase studies (Phase III-IV) (Figure 3.). Disease distribution highlights a predominant focus on PD and AD, with other significant conditions including MS and trials focusing on (ALS) (Figure 5.), while examination of study status indicates that a substantial number of trials are still ongoing or recruiting, and that the largest proportion of trials has been completed (Figure 4.). From a pharmacological standpoint, the most frequently investigated interventions are GLP-1 RAs, DPP-4 inhibitors, SGLT2 inhibitors, and metformin (Figure 6.). Mechanistic information extracted directly from trial summaries includes modulation of insulin signaling, attenuation of neuroinflammation, reduction of oxidative stress, enhancement of mitochondrial function, and regulation of autophagy, with less frequently reported mechanisms include reduction of endoplasmic reticulum stress, neurotrophic signaling, and anti-apoptotic pathways. These findings provide direct evidence of the molecular targets actively pursued in clinical investigations of metabolic modulators for neurodegenerative disorders.

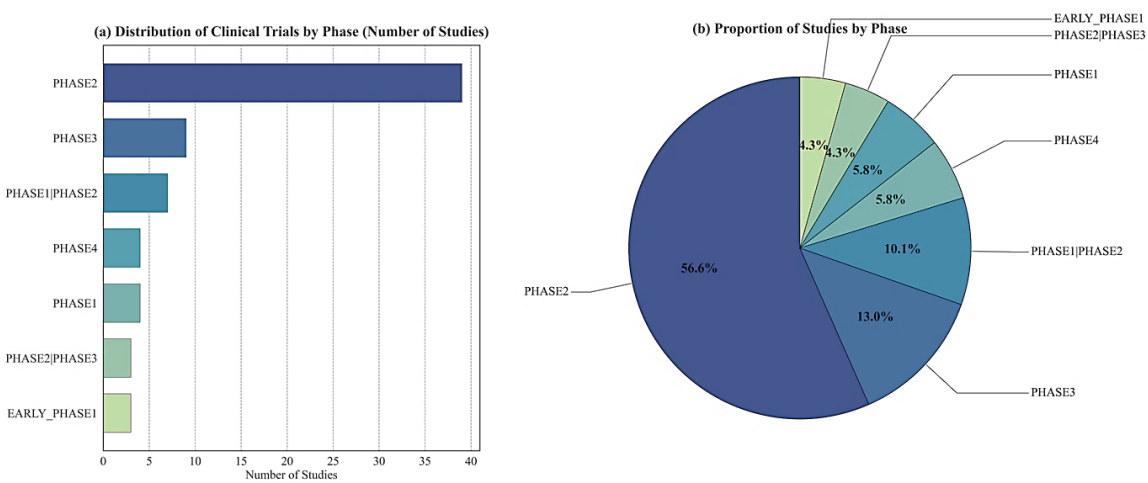


Figure 3. Numerical (a) and proportional (b) distribution of clinical trials by phase.

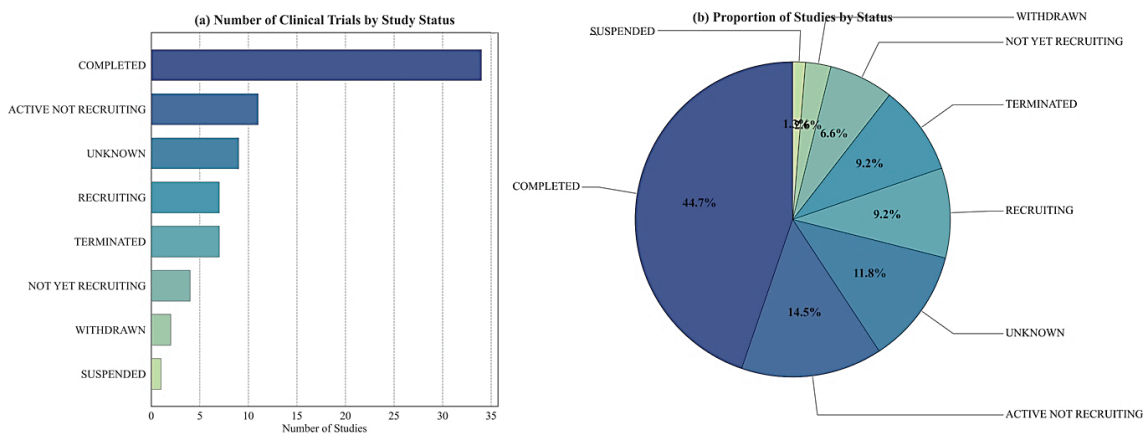


Figure 4. Numerical (a) and proportional (b) distribution of clinical trials by study status. (*COMPLETED*: study finished; *ACTIVE, NOT RECRUITING*: ongoing, no new enrollment; *UNKNOWN*: status not recently updated; *RECRUITING*: open for enrollment; *TERMINATED*: stopped early; *NOT YET RECRUITING*: registered but not started; *WITHDRAWN*: cancelled before enrollment; *SUSPENDED*: temporarily halted).

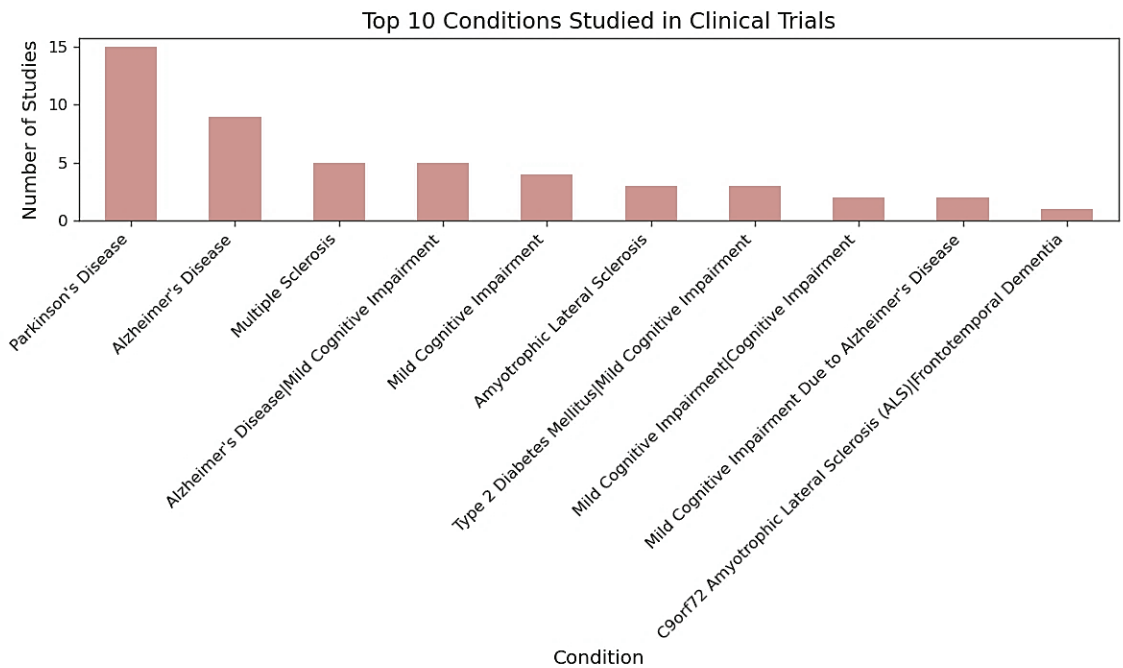


Figure 5. Top 10 conditions studied in clinical trials.

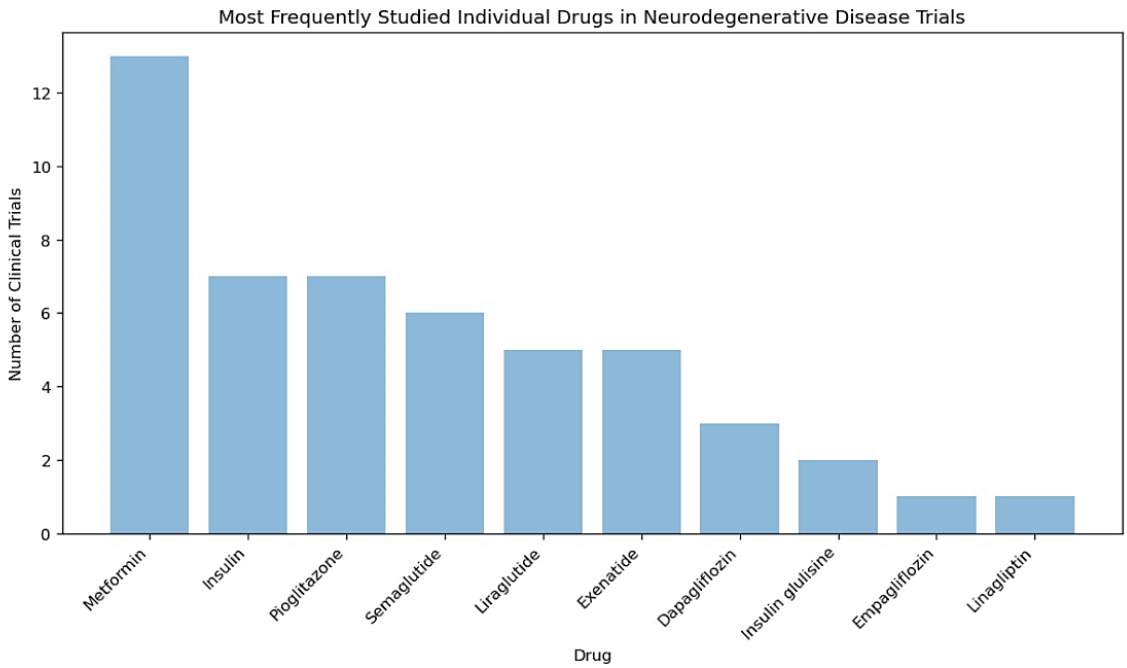


Figure 6. Most frequently studied antidiabetic drugs in NDs trials.

Antidiabetic and metabolically active agents evaluated in clinical trials for NDs demonstrate heterogeneous efficacy across drug classes and disease indications. To address the availability of outcome data from completed studies, the main clinical findings of eligible trials are summarized in table 2, providing a structured overview of reported efficacy and safety results. Although a substantial proportion of trials remain ongoing or in early phases, analysis of completed studies offers important insights into clinical outcomes. Several completed trials did not report publicly available outcomes, highlighting that trial completion alone does not necessarily indicate clinical benefit and should be interpreted cautiously (Santiago et al., 2023). Among agents with reported results, GLP-1 receptor agonists and related compounds showed the most consistent signals of potential benefit; exenatide improved off-medication motor scores in PD (Athauda et al., 2017) and lixisenatide reduced progression of motor disability (Meissner et al., 2024), while liraglutide prevented decline in cerebral glucose metabolism despite limited cognitive effects (Gejl et al., 2016). Intranasal insulin demonstrated improvements in verbal fluency, cognitive performance, and white matter hyperintensity progression in selected populations (Kellar et al., 2021; Novak et al., 2019), and multi-target metabolic interventions were associated with improvements in cognition and biomarker profiles (Erichsen et al., 2025). In contrast, several trials reported neutral or negative efficacy findings, including futility results for pioglitazone in early PD (NINDS Exploratory Trials in Parkinson Disease Investigators, 2015) and lack of significant clinical benefit with metformin or NLY01 in specific populations (Abdelgaied et al., 2026; McGarry et al., 2024). Mechanistic and biomarker-focused studies identified proteomic and metabolic alterations without clear short-term clinical improvement (Weinberg et al., 2024). Importantly, across studies, antidiabetic agents were generally well tolerated with acceptable safety profiles, supporting continued investigation despite variable efficacy outcomes (Athauda et al., 2017; Erichsen et al., 2025; McGarry et al., 2024; Meissner et al., 2024).

Table 2. Clinical outcomes and safety profiles of completed clinical trials evaluating antidiabetic and metabolically active agents in NDs

NCT	Disease	Intervention	Main Clinical Outcome	Overall Interpretation	Safety
NCT05081219 (Erichsen et al., 2025)	MCI and early AD	Combination therapy (intranasal insulin, empagliflozin)	Improved cognitive performance and modulated fluid biomarkers of neurodegeneration.	Positive signal	Well tolerated
NCT01965756 (Weinberg et al., 2024)	MCI related to AD	Metformin	Significant alterations in multiple plasma and cerebrospinal fluid protein levels.	Biomarker signal only	NR
NCT06812585 (Abdelgaied et al., 2026)	Relapse-remitting MS	Metformin (as an add-on therapy to IFNβ-1a)	No significant improvement in neurodegeneration biomarkers or clinical outcomes.	Neutral outcome	Well tolerated
NCT01971242 (Athauda et al., 2017)	PD	Exenatide	Significant improvement in off-medication motor scores sustained through the washout period.	Positive signal	Well tolerated
NCT01469351 (Gejl et al.,, 2016)	AD	Liraglutide	Prevented decline in cerebral glucose metabolism without altering amyloid or cognition.	Biomarker signal only	NR
NCT01767909 (Kellar et al., 2021)	MCI or AD	Intranasal insulin	Reduced white matter hyperintensity progression associated with improved cognitive function.	Positive signal	NR
NCT01280123 (NINDS Exploratory Trials in Parkinson Disease Investigators, 2015)	Early PD	Pioglitazone	No significant difference in motor score progression compared to placebo.	Negative or Futility	Well tolerated
NCT02064166 (Novak et al., 2019)	PD and MSA	Intranasal insulin	Functional improvement in verbal fluency and standardized motor performance scores.	Positive signal	Well tolerated
NCT04154072 (McGarry et al., 2024)	Early untreated PD	NLY01 (A brain-penetrant, pegylated, longer-lasting version of exenatide)	No significant improvement in motor or non-motor features versus placebo.	Neutral outcome	Well tolerated
NCT03439943 (Meissner et al., 2024)	Early PD	Lixisenatide	Significantly less progression of motor disbility compared to placebo.	Positive signal	Adverse events notable

NCT: National Clinical Trial identifier, NR: Not reported, MCI: Mild Cognitive Impairment, MSA: Multiple System Atrophy

CONCLUSIONS

The growing global burden of NDs, driven by population aging and increased life expectancy, continues to pose a major challenge to public health. Conventional therapeutic approaches have largely failed to halt or reverse neurodegenerative progression, underscoring the urgent need for novel, disease-modifying strategies. Within this context, the pharmacological

repurposing of antidiabetic agents has emerged as a promising and cost-effective approach. These compounds, characterized by well-established pharmacokinetic and safety profiles, offer the opportunity to bypass the prolonged and costly process of de novo drug development while providing mechanistic plausibility through their modulation of shared metabolic and neurodegenerative pathways.

Accumulating preclinical and clinical evidence suggests that antidiabetic agents, such as GLP-1 RAs, DPP-4 inhibitors, SGLT-2 inhibitors, metformin and insülin, have multifaceted neuroprotective actions. Their effects extend beyond glycemic regulation to include the modulation of central insulin signaling, attenuation of oxidative stress and mitochondrial dysfunction, suppression of neuroinflammatory and apoptotic cascades, and restoration of synaptic and autophagic homeostasis. By targeting convergent molecular networks implicated in both T2DM and NDs, these metabolic agents hold potential for disease-modifying efficacy rather than merely providing symptomatic relief. However, despite encouraging findings, substantial translational gaps persist. Clinical evidence remains fragmented, with inconsistent reporting of long-term cognitive and functional outcomes, and a lack of mechanistic biomarkers in clinical trial protocols. Furthermore, heterogeneity in study design, patient selection, and outcome measures continues to hinder comparative evaluation across drug classes.

Future research should prioritize biomarker-driven, mechanism-targeted clinical trials integrating neuroimaging, molecular, and electrophysiological endpoints to clarify therapeutic mechanisms. Harmonization of neurocognitive assessment tools and the inclusion of early-intervention paradigms -particularly at prodromal or preclinical stages- may further enhance translational validity. Moreover, multi-omics approaches and systems pharmacology modeling offer promising tools for delineating network-level drug effects and identifying novel metabolic targets within the neurodegenerative cascade. By systematically integrating mechanistic and clinical trial data, this review provides a unique translational framework for understanding how metabolic modulation may be leveraged in the prevention and treatment of NDs. Ultimately, incorporating metabolic therapeutics into the broader neuropharmacological framework may not only advance our understanding of the shared pathophysiology between DM and NDs but also pave the way toward accessible, mechanism-informed interventions capable of altering disease trajectories.

AUTHOR CONTRIBUTION STATEMENT

Concept (AHB), design (AHB), literature search (AHB), data processing (AHB), writing (AHB), interpretation (AHB), critical reviews (AHB).

CONFLICT OF INTEREST

The authors declare that there is no conflict of interest.

REFERENCES

Abdelgaied, M. Y., Abdelgawad, O., Rashad, M. H., Solayman, M. H., & El-Tayebi, H. M. (2026). Efficacy and tolerability of metformin as an adjuvant therapy in patients with relapse-remitting multiple sclerosis receiving interferon beta 1a: A randomized pilot trial. *Journal of Neuroimmunology*, *412,* 578852. https://doi.org/10.1016/j.jneuroim.2025.578852

Akter, K., Lanza, E. A., Martin, S. A., Myronyuk, N., Rua, M., & Raffa, R. B. (2011). Diabetes mellitus and Alzheimer's disease: Shared pathology and treatment? *British Journal of Clinical Pharmacology*, *71*(3), 365-376. https://doi.org/10.1111/j.1365-2125.2010.03830.x

Alhowail, A., Alsikhan, R., Alsaud, M., Aldubayan, M., & Rabbani, S. I. (2022). Protective effects of pioglitazone on cognitive ımpairment and the underlying mechanisms: A review of literature. *Drug Design, Development and Therapy, Volume 16*, 2919-2931. https://doi.org/10.2147/DDDT.S367229

American Diabetes Association Professional Practice Committee, ElSayed, N. A., Aleppo, G., Bannuru, R. R., Bruemmer, D., Collins, B. S., … Gabbay, R. A. (2024). 2. Diagnosis and classification of diabetes: Standards of care in diabetes-2024. *Diabetes Care*, *47*(Suppl. 1), S20-S42. https://doi.org/10.2337/dc24-S002

Andrade, L. J. D. O., Oliveira, L. M. D., Bittencourt, A. M. V., Lourenço, L. G. D. C., & Oliveira, G. C. M. D. (2024). Brain insulin resistance and Alzheimer's disease: A systematic review. *Dementia & Neuropsychologia*, *18*, e20230032. https://doi.org/10.1590/1980-5764-dn-2023-0032

Athauda, D., Maclagan, K., Skene, S. S., Joseph, M. B., Letchford, D., Chowdhury, K., ... Foltynie, T. (2017). Exenatide once weekly versus placebo in Parkinson's disease: a randomised, double-blind, placebo-controlled trial. *The Lancet*, *390*(10103), 1664-1675. https://doi.org/10.1016/S0140-6736(17)31585-4

Baran, A. H. (2022a). The role of pharmacogenetics in individual response to antiparkinsonian drugs. *Journal of Faculty of Pharmacy of Ankara University*, 523-536. https://doi.org/10.33483/jfpau.994367

Baran, A. H. (2022b). A promising therapeutic target in neurodegenerative diseases: Sestrin-2. *Health Academy Kastamonu*, *7*(2), 352-363. https://doi.org/10.25279/sak.991294

Baran, A. H., Berk, A., Uyumlu, A. B., Arslan Solmaz, Ö., & Yalım, G. (2024). Sildenafil decreased TNF-α and IL-6 levels in Cd-induced acute toxicity. *Journal of Faculty of Pharmacy of Ankara University*, *48*(3), 16-16. https://doi.org/10.33483/jfpau.1443799

Barthold, D., Gibbons, L. E., Marcum, Z. A., Gray, S. L., Dirk Keene, C., Grabowski, T. J., … Crane, P. K. (2021). Alzheimer's disease-related neuropathology among patients with medication treated type 2 diabetes in a community-based autopsy cohort. *Journal of Alzheimer's Disease*, *83*(3), 1303-1312. https://doi.org/10.3233/JAD-210059

Brauer, R., Wei, L., Ma, T., Athauda, D., Girges, C., Vijiaratnam, N., … Foltynie, T. (2020). Diabetes medications and risk of Parkinson's disease: A cohort study of patients with diabetes. *Brain*, *143*(10), 3067-3076. https://doi.org/10.1093/brain/awaa262

Butterfield, D. A., Di Domenico, F., & Barone, E. (2014). Elevated risk of type 2 diabetes for development of Alzheimer disease: A key role for oxidative stress in brain. *Biochimica et Biophysica Acta (BBA) - Molecular Basis of Disease*, *1842*(9), 1693-1706. https://doi.org/10.1016/j.bbadis.2014.06.010

Cai, H., Han, B., Hu, Y., Zhao, X., He, Z., Chen, X., … Kong, W. (2020). Metformin attenuates the D-galactose-induced aging process via the UPR through the AMPK/ERK1/2 signaling pathways. *International Journal of Molecular Medicine*, *45*(3), 715-730. https://doi.org/10.3892/ijmm.2020.4453

Campagnoli, L. I. M., Varesi, A., Fahmideh, F., Hakimizad, R., Petkovic, P., Barbieri, A., … Pascale, A. (2025). From diabetes to degenerative diseases: The multifaceted action of metformin. *International Journal of Molecular Sciences*, *26*(19), 9748. https://doi.org/10.3390/ijms26199748

Carvalho, C., & Moreira, P. I. (2023). Metabolic defects shared by Alzheimer's disease and diabetes: A focus on mitochondria. *Current Opinion in Neurobiology*, *79*, 102694. https://doi.org/10.1016/j.conb.2023.102694

Dai, C., Tan, C., Zhao, L., Liang, Y., Liu, G., Liu, H., … Chen, L. (2023). Glucose metabolism impairment in Parkinson's disease. *Brain Research Bulletin*, *199*, 110672. https://doi.org/10.1016/j.brainresbull.2023.110672

De La Monte, S. M. (2017). Insulin resistance and neurodegeneration: Progress towards the development of new therapeutics for Alzheimer's disease. *Drugs*, *77*(1), 47-65. https://doi.org/10.1007/s40265-016-0674-0

DeFronzo, R. A. (2015). Pathogenesis of type 2 diabetes mellitus. *International textbook of diabetes mellitus*, 371-400. https://doi.org/10.1002/9781118387658.ch25

Dou, X., Zhao, L., Li, J., & Jiang, Y. (2025). Effect and mechanism of GLP-1 on cognitive function in diabetes mellitus. *Frontiers in Neuroscience*, *19*, 1537898. https://doi.org/10.3389/fnins.2025.1537898

Durai, P., Beeraka, N. M., Ramachandrappa, H. V. P., Krishnan, P., Gudur, P., Raghavendra, N. M., & Ravanappa, P. K. B. (2022). Advances in PPARs molecular dynamics and glitazones as a repurposing therapeutic strategy through mitochondrial redox dynamics against neurodegeneration. *Current Neuropharmacology*, *20*(5), 893-915. https://doi.org/10.2174/1570159X19666211109141330

During, M. J., Cao, L., Zuzga, D. S., Francis, J. S., Fitzsimons, H. L., Jiao, X., … Haile, C. N. (2003). Glucagon-like peptide-1 receptor is involved in learning and neuroprotection. *Nature Medicine*, *9*(9), 1173-1179. https://doi.org/10.1038/nm919

Erichsen, J. M., Register, T. C., Sutphen, C., Ma, D., Gaussoin, S. A., Rudolph, M., ... Craft, S. (2025). A phase 2A/B randomized trial of metabolic modulators intranasal insulin and empagliflozin for MCI and early AD. *Alzheimer's & Dementia*, *21*(10), e70704. https://doi.org/10.1002/alz.70704

Farr, O. M., Sofopoulos, M., Tsoukas, M. A., Dincer, F., Thakkar, B., Sahin-Efe, A., … Mantzoros, C. S. (2016). GLP-1 receptors exist in the parietal cortex, hypothalamus and medulla of human brains and the GLP-1 analogue liraglutide alters brain activity related to highly desirable food cues in individuals with diabetes: A crossover, randomised, placebo-controlled trial. *Diabetologia*, *59*(5), 954-965. https://doi.org/10.1007/s00125-016-3874-y

Forrest, S. L., & Kovacs, G. G. (2025). Current concepts and molecular pathology of neurodegenerative diseases. *Pathology*, *57*(2), 178-190. https://doi.org/10.1016/j.pathol.2024.10.006

Gejl, M., Gjedde, A., Egefjord, L., Møller, A., Hansen, S. B., Vang, K., ... Rungby, J. (2016). In Alzheimer's disease, 6-month treatment with GLP-1 analog prevents decline of brain glucose metabolism: randomized, placebo-controlled, double-blind clinical trial. *Frontiers in Aging Neuroscience*, *8*, 108. https://doi.org/10.3389/fnagi.2016.00108

Ghosh, P., Fontanella, R. A., Scisciola, L., Pesapane, A., Taktaz, F., Franzese, M., … Barbieri, M. (2023). Targeting redox imbalance in neurodegeneration: Characterizing the role of GLP-1 receptor agonists. *Theranostics*, *13*(14), 4872-4884. https://doi.org/10.7150/thno.86831

Hamilton, A., & Hölscher, C. (2009). Receptors for the incretin glucagon-like peptide-1 are expressed on neurons in the central nervous system. *NeuroReport*, *20*(13), 1161-1166. https://doi.org/10.1097/WNR.0b013e32832fbf14

Helal, M. M., AbouShawareb, H., Abbas, O. H., Haddad, R., Zain, Y., Osman, A. S. A., & Hassan, A. K. (2025). GLP-1 receptor agonists in Parkinson's disease: An updated comprehensive systematic review with meta-analysis. *Diabetology & Metabolic Syndrome*, *17*(1), 352. https://doi.org/10.1186/s13098-025-01888-1

Ibrahim, R., Kambal, A., & Abdelmajeed, M. A. (2025). Glucagon-like peptide-1 receptor agonists in neurodegenerative diseases: A comprehensive review. *Cureus*, *17*(9), e92441. https://doi.org/10.7759/cureus.92441

Jurcau, A. (2021). Insights into the pathogenesis of neurodegenerative diseases: Focus on mitochondrial dysfunction and oxidative stress. *International Journal of Molecular Sciences*, *22*(21), 11847. https://doi.org/10.3390/ijms222111847

Kalinderi, K., Papaliagkas, V., & Fidani, L. (2024). GLP-1 receptor agonists: A new treatment in Parkinson's disease. *International Journal of Molecular Sciences*, *25*(7), 3812. https://doi.org/10.3390/ijms25073812

Kan, W., Qu, M., Wang, Y., Zhang, X., & Xu, L. (2025). A review of type 2 diabetes mellitus and cognitive impairment. *Frontiers in Endocrinology*, *16*, 1624472. https://doi.org/10.3389/fendo.2025.1624472

Kandimalla, R., Thirumala, V., & Reddy, P. H. (2017). Is Alzheimer's disease a type 3 diabetes? a critical appraisal. *Biochimica et Biophysica Acta (BBA) - Molecular Basis of Disease*, *1863*(5), 1078-1089. https://doi.org/10.1016/j.bbadis.2016.08.018

Kciuk, M., Kruczkowska, W., Gałęziewska, J., Wanke, K., Kałuzińska-Kołat, Ż., Aleksandrowicz, M., & Kontek, R. (2024). Alzheimer's disease as type 3 diabetes: understanding the link and implications. *International Journal of Molecular Sciences*, *25*(22), 11955. https://doi.org/10.3390/ijms252211955

Keerie, A., Brown-Wright, H., Kirkland, I., Grierson, A., Alix, J. J. P., Holscher, C., & Mead, R. J. (2021). The GLP-1 receptor agonist, liraglutide, fails to slow disease progression in SOD1G93A and TDP-43Q331K transgenic mouse models of ALS. *Scientific Reports*, *11*(1), 17027. https://doi.org/10.1038/s41598-021-96418-0

Kellar, D., Lockhart, S. N., Aisen, P., Raman, R., Rissman, R. A., Brewer, J., & Craft, S. (2021). Intranasal insulin reduces white matter hyperintensity progression in association with improvements in cognition and csf biomarker profiles in mild cognitive impairment and alzheimer's disease. *The Journal of Prevention of Alzheimer's Disease*, *8*(3), 240-248. https://doi.org/10.14283/jpad.2021.14

Kopp, K. O., Glotfelty, E. J., Li, Y., & Greig, N. H. (2022). Glucagon-like peptide-1 (GLP-1) receptor agonists and neuroinflammation: Implications for neurodegenerative disease treatment. *Pharmacological Research*, *186*, 106550. https://doi.org/10.1016/j.phrs.2022.106550

Koshatwar, M., Acharya, S., Prasad, R., Lohakare, T., Wanjari, M., & Taksande, A. B. (2023). Exploring the potential of antidiabetic agents as therapeutic approaches for Alzheimer's and Parkinson's diseases: A comprehensive review. *Cureus*, *15*(9), e44763. https://doi.org/10.7759/cureus.44763

Lamptey, R. N. L., Chaulagain, B., Trivedi, R., Gothwal, A., Layek, B., & Singh, J. (2022). A review of the common neurodegenerative disorders: current therapeutic approaches and the potential role of nanotherapeutics. *International Journal of Molecular Sciences*, *23*(3), 1851. https://doi.org/10.3390/ijms23031851

Li, H., Ren, J., Li, Y., Wu, Q., & Wei, J. (2023). Oxidative stress: The nexus of obesity and cognitive dysfunction in diabetes. *Frontiers in Endocrinology*, *14*, 1134025. https://doi.org/10.3389/fendo.2023.1134025

Li, L., & Hölscher, C. (2007). Common pathological processes in Alzheimer disease and type 2 diabetes: A review. *Brain Research Reviews*, *56*(2), 384-402. https://doi.org/10.1016/j.brainresrev.2007.09.001

Lin, Y.-H., Hsu, C.-C., Liu, J.-S., Chang, K.-C., & Huang, J.-A. (2023). Use of dipeptidyl peptidase-4 inhibitors was associated with a lower risk of Parkinson's disease in diabetic patients. *Scientific Reports*, *13*(1), 22489. https://doi.org/10.1038/s41598-023-49870-z

Luchsinger, J. A., Tang, M.-X., Shea, S., & Mayeux, R. (2004). Hyperinsulinemia and risk of Alzheimer disease. *Neurology*, *63*(7), 1187-1192. https://doi.org/10.1212/01.WNL.0000140292.04932.87

Luo, L., Que, M., Zeng, L., Wang, X., Sun, T., Zhou, Z., … Luo, A. (2025). Selective autophagy in type 2 diabetes-associated cognitive dysfunction: Insightful mechanisms and therapies. *Pharmacological Research*, *220*, 107947. https://doi.org/10.1016/j.phrs.2025.107947

McGarry, A., Rosanbalm, S., Leinonen, M., Olanow, C. W., To, D., Bell, A., ... Kieburtz, K. (2024). Safety, tolerability, and efficacy of NLY01 in early untreated Parkinson's disease: a randomised, double-blind, placebo-controlled trial. *The Lancet Neurology*, *23*(1), 37-45. https://doi.org/10.1016/S1474-4422(23)00378-2

Mei, J., Li, Y., Niu, L., Liang, R., Tang, M., Cai, Q., … Yu, P. (2024). SGLT2 inhibitors: A novel therapy for cognitive impairment via multifaceted effects on the nervous system. *Translational Neurodegeneration*, *13*(1), 41. https://doi.org/10.1186/s40035-024-00431-y

Meissner, W. G., Remy, P., Giordana, C., Maltête, D., Derkinderen, P., Houéto, J. L., ... Rascol, O. (2024). Trial of lixisenatide in early Parkinson's disease. *New England Journal of Medicine*, *390*(13), 1176-1185. https://doi.org/10.1056/NEJMoa2312323

Meng, J., Yan, R., Zhang, C., Bai, X., Yang, X., Yang, Y., … Liu, X. (2023). Dipeptidyl peptidase-4 inhibitors alleviate cognitive dysfunction in type 2 diabetes mellitus. *Lipids in Health and Disease*, *22*(1), 219. https://doi.org/10.1186/s12944-023-01985-y

Mohammed, O., & Kelemu, T. (2025). Incretin-based therapies in Alzheimer's and Parkinson's disease: Advancing neuroprotection with dual and triple agonists-a review. *Health Science Reports*, *8*(7), e71065. https://doi.org/10.1002/hsr2.71065

Moon, J.-H., Hong, J.-M., & Park, S.-Y. (2021). The antidiabetic drug troglitazone protects against PrP (106-126)-induced neurotoxicity via the PPARγ-autophagy pathway in neuronal cells. *Molecular Medicine Reports*, *23*(6), 430. https://doi.org/10.3892/mmr.2021.12069

NINDS Exploratory Trials in Parkinson Disease (NET-PD) FS-ZONE Investigators (2015). Pioglitazone in early Parkinson's disease: a phase 2, multicentre, double-blind, randomised trial. *The Lancet Neurology*, *14*(8), 795-803. https://doi.org/10.1016/S1474-4422(15)00144-1

Novak, P., Maldonado, D. A. P., & Novak, V. (2019). Safety and preliminary efficacy of intranasal insulin for cognitive impairment in Parkinson disease and multiple system atrophy: A double-blinded placebo-controlled pilot study. *PLoS One*, *14*(4), e0214364. https://doi.org/10.1371/journal.pone.0214364

Nowell, J., Blunt, E., Gupta, D., & Edison, P. (2023). Antidiabetic agents as a novel treatment for Alzheimer's and Parkinson's disease. *Ageing Research Reviews*, *89*, 101979. https://doi.org/10.1016/j.arr.2023.101979

Pandiyan, C. K., Manivannan, A. G., Jaishankar, N., & Vellapandian, C. (2024). From glucose to neuroprotection: exploring antidiabetic medications as a novel approach to Alzheimer's disease treatment. *Cureus*, *16*(10), e70710. https://doi.org/10.7759/cureus.70710

Papini, N., Giussani, P., & Tringali, C. (2024). Metformin lysosomal targeting: A novel aspect to be investigated for metformin repurposing in neurodegenerative diseases? *International Journal of Molecular Sciences*, *25*(16), 8884. https://doi.org/10.3390/ijms25168884

Pearson, A., Koprivica, M., Eisenbaum, M., Ortiz, C., Browning, M., Vincennie, T., … Ojo, J. (2024). PPARγ activation ameliorates cognitive impairment and chronic microglial activation in the aftermath of r-mTBI. *Journal of Neuroinflammation*, *21*(1), 194. https://doi.org/10.1186/s12974-024-03173-w

Reed, S., Taka, E., Darling-Reed, S., & Soliman, K. F. A. (2025). Neuroprotective effects of metformin through the modulation of neuroinflammation and oxidative stress. *Cells*, *14*(14), 1064. https://doi.org/10.3390/cells14141064

Sabari, S. S., Balasubramani, K., Iyer, M., Sureshbabu, H. W., Venkatesan, D., Gopalakrishnan, A. V., … Vellingiri, B. (2023). Type 2 diabetes (T2DM) and Parkinson's disease (PD): A mechanistic approach. *Molecular Neurobiology*, *60*(8), 4547-4573. https://doi.org/10.1007/s12035-023-03359-y

Santiago, J. A., Karthikeyan, M., Lackey, M., Villavicencio, D., & Potashkin, J. A. (2023). Diabetes: a tipping point in neurodegenerative diseases. *Trends in Molecular Medicine*, *29*(12), 1029-1044. https://doi.org/10.1016/j.molmed.2023.09.005

Sarabhai, T., Zingel, R., Bohlken, J., & Kostev, K. (2025). Association between SGLT2 inhibitor therapy and prolonged dementia-free survival in older adults with type 2 diabetes: A retrospective cohort study from Germany. *Diabetes Research and Clinical Practice*, *229*, 112430. https://doi.org/10.1016/j.diabres.2025.112430

Shin, A., Koo, B. K., Lee, J. Y., & Kang, E. H. (2024). Risk of dementia after initiation of sodium-glucose cotransporter-2 inhibitors versus dipeptidyl peptidase-4 inhibitors in adults aged 40-69 years with type 2 diabetes: Population based cohort study. *BMJ*, *386*, e079475. https://doi.org/10.1136/bmj-2024-079475

Sulangi, A. J., Lyons, S. E., Abdou, A. A., Patel, H., Nagliya, D., Joseph, E., … Parmar, M. S. (2024). Exploring the therapeutic potential of DPP4 inhibitors in Alzheimer's disease: Molecular insight and clinical outcome. *Cureus*, *16*(10), e72648. https://doi.org/10.7759/cureus.72648

Szablewski, L. (2025). Associations between diabetes mellitus and neurodegenerative diseases. *International Journal of Molecular Sciences*, *26*(2), 542. https://doi.org/10.3390/ijms26020542

Tang, X., Brinton, R. D., Chen, Z., Farland, L. V., Klimentidis, Y., Migrino, R., … Zhou, J. J. (2022). Use of oral diabetes medications and the risk of incident dementia in US veterans aged ≥60 years with type 2 diabetes. *BMJ Open Diabetes Research & Care*, *10*(5), e002894. https://doi.org/10.1136/bmjdrc-2022-002894

Tanvir, A., Jo, J., & Park, S. M. (2024). Targeting glucose metabolism: A novel therapeutic approach for Parkinson's disease. *Cells*, *13*(22), 1876. https://doi.org/10.3390/cells13221876

Toker, D., Chiang, J. N., Vespa, P. M., Schnakers, C., & Monti, M. M. (2025). The dipeptidyl peptidase-4 inhibitor saxagliptin as a candidate treatment for disorders of consciousness: A deep learning and retrospective clinical analysis. *Neurocritical Care*, *43*(1), 101-118. https://doi.org/10.1007/s12028-025-02217-0

Tseng, P.-T., Zeng, B.-Y., Hsu, C.-W., Hung, C.-M., Carvalho, A. F., Stubbs, B., … Liang, C.-S. (2025). The pharmacodynamics-based prophylactic benefits of GLP-1 receptor agonists and SGLT2 inhibitors on neurodegenerative diseases: Evidence from a network meta-analysis. *BMC Medicine*, *23*(1), 197. https://doi.org/10.1186/s12916-025-04018-w

U.S. National Library of Medicine (2000), National Institutes of Health. Retrieved from https://clinicaltrials.gov/ Access date: 31 October 2025

Verdile, G., Fraser, P. E., & Martins, R. N. (2019). The link between diabetes, glucose control, and Alzheimer's disease and neurodegenerative diseases. In R. N. Martins, C. S. Brennan, W. M. A. D. Binosha Fernando, M. A. Brennan, S. J. Fuller (Eds.), *Neurodegeneration and Alzheimer's Disease: The Role of Diabetes, Genetics, Hormones, and Lifestyle* (pp. 89-115). John Wiley & Sons Ltd

Veselov, I. M., Vinogradova, D. V., Maltsev, A. V., Shevtsov, P. N., Spirkova, E. A., Bachurin, S. O., & Shevtsova, E. F. (2023). Mitochondria and oxidative stress as a link between Alzheimer's disease and diabetes mellitus. *International Journal of Molecular Sciences*, *24*(19), 14450. https://doi.org/10.3390/ijms241914450

Weinberg, M. S., He, Y., Kivisäkk, P., Arnold, S. E., & Das, S. (2024). Effect of metformin on plasma and cerebrospinal fluid biomarkers in non-diabetic older adults with mild cognitive impairment related to Alzheimer's disease. *Journal of Alzheimer's Disease*, *99*(s2), S355-S365. https://doi.org/10.3233/JAD-230899

World Health Organization (WHO). (2023). New global action plan on epilepsy and other neurological disorders published. Retrieved from https://www.who.int/news/item/20-07-2023-new-global-action-plan-on-epilepsy-and-other-neurological-disorders-published Access date: 30 October 2025

Yao, H., Zhang, A., Li, D., Wu, Y., Wang, C.-Z., Wan, J.-Y., & Yuan, C.-S. (2024). Comparative effectiveness of GLP-1 receptor agonists on glycaemic control, body weight, and lipid profile for type 2 diabetes: Systematic review and network meta-analysis. *BMJ*, *384*, e076410. https://doi.org/10.1136/bmj-2023-076410

Yu, X., He, H., Wen, J., Xu, X., Ruan, Z., Hu, R., … Ju, H. (2025). Diabetes-related cognitive impairment: Mechanisms, symptoms, and treatments. *Open Medicine*, *20*(1), 20241091. https://doi.org/10.1515/med-2024-1091

Złotek, M., Kurowska, A., Herbet, M., & Piątkowska-Chmiel, I. (2023). GLP-1 Analogs, SGLT-2, and DPP-4 Inhibitors: A triad of hope for Alzheimer's disease therapy. *Biomedicines*, *11*(11), 3035. https://doi.org/10.3390/biomedicines11113035

FABAD J. Pharm. Sci., 51, 1, 403-418, 2026
Doi: 10.55262/fabadeczacilik.1812206
REVIEW ARTICLE

Asbestos Exposure in Occupational and Environmental Settings Following the 2023 Earthquake in Türkiye: A Focused Review

Hürü DİKEÇ[*], Aysun ÖKÇESİZ HACISEYİTOĞLU[**°]

Asbestos Exposure in Occupational and Environmental Settings Following the 2023 Earthquake in Türkiye: A Focused Review

SUMMARY

The earthquakes centred in Kahramanmaraş on 6 February 2023 caused the collapse of a large number of buildings in Türkiye and the generation of vast amounts of debris, thereby turning environmental and occupational asbestos exposure into a significant public health concern. During post-earthquake debris removal, demolition, and reconstruction activities, asbestos fibres released from the fragmentation of asbestos-containing building materials pose a serious exposure risk not only to search and rescue teams, debris workers, and construction workers, but also to the local population. This review aims to evaluate the potential public health impacts of increased exposure during post-disaster periods by focusing on scientific studies addressing environmental and occupational asbestos exposure following the 2023 earthquakes. In this context, the toxicological properties of asbestos associated with inhalation exposure, as well as asbestos-related diseases—primarily asbestosis, lung cancer, and malignant mesothelioma—are briefly summarized. The review also examines post-earthquake debris management, occupational exposure prevention, and regulatory frameworks to support effective risk management and disease prevention.

Keywords: *Asbestos, earthquakes, earthquake-related asbestos exposure, lung neoplasms, mesothelioma.*

Türkiye'de 2023 Depremi Sonrası Mesleki ve Çevresel Ortamlarda Asbest Maruziyeti: Odaklanmış Bir Derleme

ÖZ

6 Şubat 2023 tarihinde Kahramanmaraş merkezli meydana gelen depremler, Türkiye'de çok sayıda yapının yıkılmasına ve büyük miktarda enkazın açığa çıkmasına neden olarak, çevresel ve mesleki asbest maruziyetini önemli bir halk sağlığı sorunu haline getirmiştir. Deprem sonrası enkaz kaldırma, yıkım ve yeniden inşa süreçlerinde, asbest içeren yapı malzemelerinin parçalanması sonucunda ortaya çıkan lifler; başta arama-kurtarma ekipleri, enkaz işçileri ve inşaat çalışanları olmak üzere, bölge halkı için de ciddi bir maruziyet riski oluşturmaktadır. Bu derleme, 2023 depremleri sonrasında ortaya çıkan çevresel ve mesleki asbest maruziyetine odaklanan bilimsel çalışmaları temel alarak, afet sonrası süreçlerde artan maruziyetin halk sağlığı üzerindeki olası etkilerini değerlendirmeyi amaçlamaktadır. Bu bağlamda, asbestin solunum yoluyla maruziyette ortaya çıkan toksikolojik etkileri ve başta asbestozis, akciğer kanseri ve malign mezotelyoma olmak üzere neden olduğu hastalıklar kısaca özetlenmiştir. Bu derleme ayrıca deprem sonrası enkaz yönetimini, mesleki maruziyetin önlenmesini ve düzenleyici çerçeveleri, etkili risk yönetimi ve hastalıkların önlenmesini desteklemek amacıyla incelemektedir.

Anahtar Kelimeler: *Asbest, deprem, depremle ilişkili asbest maruziyeti, akciğer neoplazmaları, mezotelyoma.*

Recieved: 28.10.2025
Revised: 13.01.2026
Accepted: 19.02.2026

[*] ORCID: 0009-0002-4106-6025, Faculty of Pharmacy, Erciyes University, 38280, Kayseri, Türkiye
[**] ORCID: 0000-0001-9130-2853, Department of Pharmaceutical Toxicology, Faculty of Pharmacy, Erciyes University, 38280, Kayseri, Türkiye

[°] Corresponding Author; Aysun Ökçesiz Hacıseyitoğlu
E-mail: aysunokcesiz@erciyes.edu.tr

INTRODUCTION

Asbestos is a group of naturally occurring metamorphic minerals characterized by a fibrous crystalline structure. Owing to their distinctive physicochemical properties—such as resistance to fire and high temperatures, chemical stability, mechanical strength, and effective electrical insulation—asbestos minerals have historically been incorporated into a wide range of industrial and construction materials (Van Gosen, 2007).

The widespread use of asbestos-containing materials increased markedly during the early and mid-20th century, reaching its peak between the 1970s and 1980s. During this period, asbestos was extensively utilized in the construction sector, especially in asbestos–cement products used for roofing and wall systems, drywall and joint compounds, vinyl flooring and adhesives, panels, pipes, acoustic ceilings, fireproofing materials, thermal insulation, and heating, ventilation, and air conditioning systems (Curado et al., 2024). As a result, asbestos became an integral component of many residential and public buildings, particularly those constructed before regulatory restrictions were introduced.

Despite its advantageous material properties, asbestos poses significant risks to human health. The International Agency for Research on Cancer (IARC) has classified asbestos as "carcinogenic to humans," based on strong evidence linking exposure to severe and often fatal diseases (IARC, 2012; Sen, 2015). The primary route of asbestos exposure is inhalation, whereby airborne fibres are deposited in the respiratory tract. Once inhaled, these fibres can persist in lung tissue and pleural membranes for decades, leading to diseases such as asbestosis, lung cancer, and malignant mesothelioma. Ingestion may occur secondarily; however, inhalation remains the dominant and most critical exposure pathway. A defining characteristic of asbestos-related diseases is their long latency period, with clinical symptoms typically emerging 20 years or more after initial exposure (OSHA, 2002).

International organisations such as the World Health Organization (WHO) and the International Labour Organization (ILO) emphasize that the elimination of asbestos use is the most effective strategy for preventing asbestos-related diseases. Nevertheless, asbestos exposure remains a global public health concern. In recent years, asbestos mining and consumption have continued in several countries, and both occupational and environmental exposures still contribute substantially to disease burden worldwide. It is estimated that asbestos-related occupational exposure accounted for more than 222,000 deaths in 2016, and the incidence of asbestos-related diseases is expected to rise due to past and ongoing exposures combined with long latency periods (Lin et al., 2018).

Beyond occupational settings, the degradation of aging buildings and the disturbance of asbestos-containing materials during structural damage represent major sources of environmental exposure. Earthquakes, in particular, pose a critical risk by causing the collapse of older structures that contain asbestos, resulting in the release of asbestos fibres into the air. The subsequent debris removal and reconstruction processes can further amplify airborne fibre concentrations if appropriate control measures are not implemented. Following the February 2023 earthquakes in Türkiye, investigations conducted by the Turkish Medical Association (TMA) and the Right to Clean Air Platform detected asbestos fibres in dust samples collected from affected areas. These findings demonstrate that insufficient precautions during debris management expose both workers and local populations to serious health risks, underscoring the urgent need for effective regulations and protective strategies in post-disaster settings (Varol, 2023).

In this context, the present study aims to contribute to the development of strategies for preventing asbestos-related health problems, to identify measures that reduce environmental and occupational exposure—particularly in post-earthquake scenarios—and to increase awareness to protect public health.

History of asbestos

The history of asbestos use dates back to ancient civilizations (Gochfeld, 2005; Vallyathan et al., 1985). In Ancient Greece, it was preferred in the production of tablecloths and garments due to its fire-resistant properties, and its ability to be cleaned by exposure to fire was considered remarkable at the time (Laufer, 1915). In Rome, asbestos was mainly employed in fabrics used to wrap bodies during cremation, thereby contributing to the preservation of the ashes (Browne, 2003).

The areas of asbestos use have diversified and expanded over the centuries. Particularly during the Industrial Revolution, the growing demand for fire-resistant and heat-insulating materials significantly increased interest in this mineral (Kośny & Yarbrough, 2022). During this period, asbestos came to be widely used in roofing materials, cement-based products, vehicle braking systems, and various insulation materials. By the 20th century, its usage had reached its peak, being incorporated into numerous applications within residential and industrial buildings as well as public infrastructure (Erker, 2014). However, in the following years, it was recognized that inhalation of asbestos fibres posed serious health risks, which led to a decline in its use and stimulated the development of safer alternatives. Therefore, the historical trajectory of asbestos began with its widespread use due to its exceptional physical properties and was even referred to as a "miracle mineral" (Curado et al., 2024) in the past; however, as its associated health risks became increasingly evident, its use was significantly restricted and subjected to various bans (Bolan et al., 2023).

Types of asbestos

Two families of asbestos minerals are known: amphibole and serpentine group asbestos types. The amphibole group consists of five members: crocidolite, amosite, actinolite, anthophyllite, and tremolite. The serpentine group includes types such as chrysotile, lizardite, and antigorite (Frank, 2020; Frank & van Zandwijk, 2024). The classification scheme of asbestos types is presented in Figure 1. Chrysotile, which belongs to the serpentine group, is the most commonly used commercial form of asbestos. This mineral has flexible and curly fibres and is typically employed in roof shingles, curbs, and cladding materials (Kanarek, 2011). In contrast, asbestos types in the amphibole group possess straighter and more rigid fibres compared to chrysotile. Among them, crocidolite stands out for its high durability and strength, yet due to its fine fibres and ease of inhalation, it is considered the most hazardous type for human health (Kusiorowski et al., 2012). The fibres that pose the greatest threat to human health are those capable of penetrating the deep tissues of the respiratory system and resisting removal by natural elimination mechanisms. Such fibres are typically longer than 5 μm, thinner than 3 μm in diameter, and have a length-to-diameter ratio generally exceeding 3:1 (Zaremba et al., 2010).

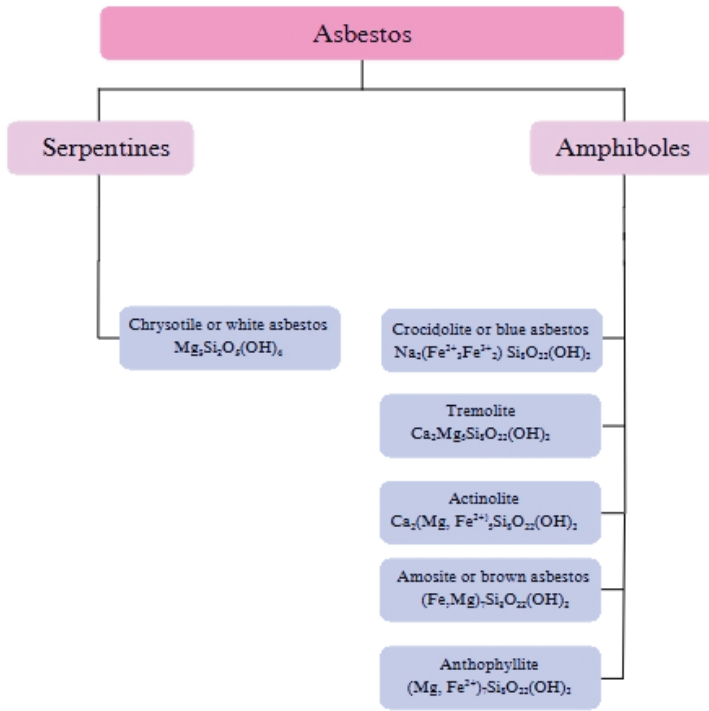


Figure 1. Classification scheme of asbestos main varieties (Virta, 2002)

Chrysotile (white asbestos), composed of fine, flexible, and silky fibres, exhibits high resistance to heat but is vulnerable to the effects of acids. More than 90% of the asbestos used today consists of chrysotile. Initially employed for fire protection and acoustic insulation, it has gradually found widespread applications in various industrial fields. To date, chrysotile has been identified in the composition of more than 5,000 products. It stands out as the most frequently used form in the construction sector (François & Michel, 2016; Rodríguez Elizalde, 2022).

Amphibole asbestos has a coarse, fibrous structure and is used less commercially compared to chrysotile. These fibres are of particular biological significance due to their chemical and crystallographic properties. The rigid and linear nature of the fibres increases the potential for the small subunits generated during fragmentation to cause harm to human tissue. Consequently, these structural characteristics play a critical role in assessing the potential health risks associated with amphibole asbestos (Craighead et al., 1980). Current evidence indicates that the genotoxic and carcinogenic properties of asbestos types vary, with amphibole fibres being most strongly associated with the development of mesothelioma (Virta, 2002).

Areas of asbestos use

Construction and building materials

In buildings constructed before 1980, it was commonly found in spray-applied coatings, cement-based boards (such as fibre cement), pipe and boiler insulation, ceiling and floor tiles, fire-resistant panels, gaskets, and chimney systems (Akboğa-Kale et al., 2017; IARC, 2023; Murgia et al., 2025). Types of asbestos, such as chrysotile and crocidolite, were specifically preferred in cement pipes, filler materials, and insulation products to provide resistance against heat and pressure (Akboğa-Kale et al., 2017). Common materials that may contain asbestos in industrial buildings are shown in Figure 2.

The areas of asbestos use have diversified over time, and it has gained significant prevalence in the construction sector. During this period, asbestos was employed in many building components, ranging from roof tiles to panels, from coating materials to asbestos–cement-based products. The 20th century witnessed a significant acceleration in asbestos production, driven both by the demands arising from the two World Wars and by the reconstruction activities that intensified in the post-war period. Particularly in developing countries, the rapidly expanding automotive industry and the surge in construction activities further supported this growth and led to the wider global prevalence of asbestos (Curado et al., 2024).

Industrial and occupational use

Asbestos minerals have been extensively employed across various industrial sectors due to their unique properties, including high heat resistance, thermal and acoustic insulation, and durability. The industrial potential of these minerals was recognized toward the end of the 19th century, initiating their commercial applications. In the early stages, their use was predominantly limited to serving as thermal insulation in steam engines and boilers (Frank & Joshi, 2014).

Asbestos was extensively used in many areas requiring insulation, primarily in the construction sector and the shipbuilding industry. On an industrial scale, its use expanded further, and asbestos was even employed in the filtration of beer, wine, and pharmaceutical products (Frank & Joshi, 2014).

Consumer products and other applications

Beyond the construction sector, it also became a preferred material in the production of brake pads, heat-resistant textile products, and various machinery and equipment parts. In addition to industrial applications, it was also present in various consumer products used in daily life. For instance, the internal components of toasters, hair dryers, and certain arts and crafts materials contained asbestos (Frank & Joshi, 2014).

Regulatory awareness and decline in use

From the second half of the 20th century onward, mounting scientific evidence regarding the adverse health impacts of asbestos revealed its strong association with severe diseases such as asbestosis, malignant mesothelioma, and lung cancer. Consequently, many countries introduced strict regulations and implemented bans on its use, import, and export (Curado et al., 2024; Damiran & Frank, 2018; Michaels, 2008).

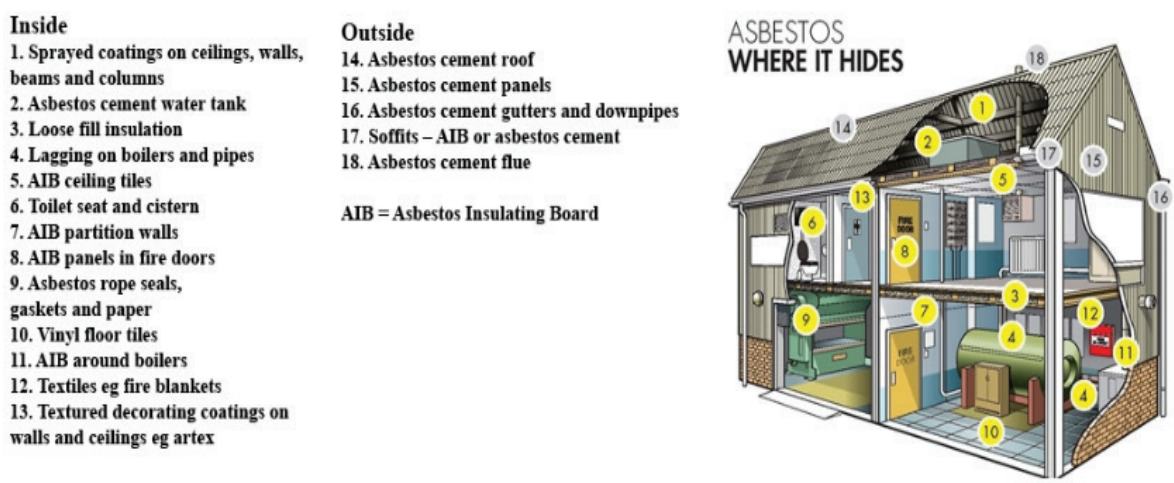


Figure 2. Common materials used in the ındustrial building where we can find asbestos (Rodríguez Elizalde, 2022)

Asbestos exposure

Asbestos exposure is a significant environmental and occupational risk factor that affects millions of people worldwide and leads to serious respiratory diseases, particularly mesothelioma and lung cancer (Altuntaş et al., 2009). Over the past fifty years, the majority of malignant mesothelioma cases diagnosed worldwide have been primarily associated with occupational exposure. However, a significant number of cases also result from para-occupational, domestic, and environmental exposures (Linton et al., 2012). From a public health perspective, construction-related asbestos exposure becomes particularly critical in earthquake-prone regions, where structural damage transforms previously contained materials into widespread environmental and occupational hazards. Today, one of the most concerning sources of exposure is debris generated after earthquakes. Asbestos fibres released into the air during the demolition of old buildings pose a serious health risk to search and rescue teams, residents, and debris removal workers. This situation highlights that asbestos is not merely a problem of the past but remains an active public health threat in post-disaster settings as well (Güneş et al., 2017).

Occupational asbestos exposure

Workers in the shipbuilding and repair sector face a high risk of asbestos exposure due to the widespread use of asbestos in insulation and thermal protection materials. Construction workers are also at risk, as they may encounter asbestos fibres during building demolition, renovation, and insulation activities. In the automotive industry, employees involved in the manufacturing and maintenance of brake pads and clutch components have historically been exposed to asbestos over extended periods. Additionally, the mining sector represents a significant risk for asbestos exposure, particularly during the extraction and processing of naturally occurring asbestos-containing rocks (Cruz et al., 2018; Kim et al., 2015; Noonan, 2017; Wu et al., 2015). While 125 million workers around the world continue to be exposed to asbestos, approximately 250,000 asbestos-related deaths are reported annually (Frank & van Zandwijk, 2024). Therefore, the protection of workers, proper training and education, and implementation of regular health screenings are of critical importance (Barbiero et al., 2018; Vicari et al., 2023). A summary of the potential pathways of asbestos exposure worldwide is presented in Figure 3.

Environmental and para-occupational exposure

Workers directly exposed to asbestos bear the highest health risks due to intense exposure; however, the risk is not limited to this group alone. Individuals working near asbestos-containing environments—such as in the construction and shipbuilding industries—may also be affected through indirect exposure. Furthermore, asbestos fibres carried home on workers' clothing can lead to diseases among spouses and children. Such domestic exposures have been documented since the 1960s, and early regulations recommended that workers clean themselves before returning home. Additionally, residing near asbestos-related facilities also poses a risk of environmental exposure, which has been reported in various countries (Frank & Joshi, 2014).

Earthquake-related asbestos exposure

The uncontrolled release of asbestos from debris following the February 6, 2023, Kahramanmaraş earthquakes has posed a serious public health threat in the affected regions (Turan & Alpaydın, 2024). Asbestos, which was commonly used in buildings constructed before the regulatory framework established after the 2010 asbestos ban and subsequent occupational safety regulations introduced in 2013, may become respirable in fibrous form during debris removal operations, posing a significant health risk for both workers and nearby residents (Hancı & Kepekli, 2022). Therefore, identifying asbestos-containing structures, ensuring their removal by specialized teams, and enforcing the use of Personal Protective Equipment (PPE) are of vital importance and must be carried out in accordance with Regulation No. 28539 (Hancı & Kepekli, 2022).

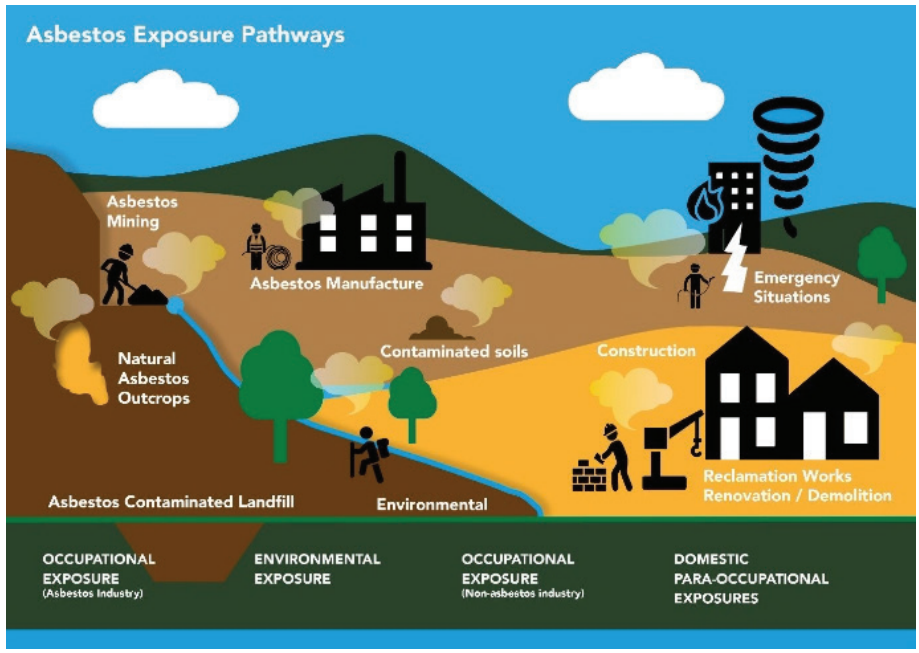


Figure 3. A summary of potential exposure pathways for asbestos exposure globally (Berry et al., 2022)

Health effects of asbestos

The respiratory system constitutes the primary pathway through which asbestos enters the human body (Berry et al., 2022). Due to their small size, fine structure, and fibrous morphology, asbestos fibres can remain airborne for prolonged periods, facilitating inhalation and deep penetration into lung tissues. Their resistance to biological degradation allows these fibres to persist in the body for many years, resulting in long-term biological effects (Bernstein & Pavlisko, 2017). After a long latent period, these fibers can lead to serious diseases, including mesothelioma, lung cancer, and asbestosis (Akboğa & Baradan, 2011; IARC, 2012). Classic epidemiological investigations have long established the carcinogenicity of asbestos, particularly with respect to mesothelioma and lung cancer (Frank & Joshi, 2014; Selikoff et al., 1968). Although most epidemiological data originate from occupational cohorts, these findings constitute the primary scientific foundation for evaluating environmental asbestos exposure, including scenarios involving widespread structural damage after earthquakes.

Population-based epidemiological studies consistently demonstrate a strong association between asbestos exposure and both mesothelioma and lung cancer, indicating that mesothelioma risk is largely independent of smoking, whereas lung cancer risk is modified by concurrent tobacco exposure (Offermans et al., 2014; Taeger et al., 2022).

A key determinant in the development of asbestos-related diseases is the latency period. Mesothelioma risk has been shown to increase primarily with time since first exposure, while lung cancer risk is more closely related to cumulative exposure over time (Pira et al., 2007). Population-based cohort evidence further supports an exposure duration–related increase in lung cancer risk following asbestos exposure (Barbiero et al., 2018). This long latency period is particularly important in post-earthquake settings, where environmental asbestos exposure following building collapse and debris removal may not result in immediately observable health effects.

Consistent with epidemiological findings from large cohort studies, IARC has classified asbestos as causally associated with lung, laryngeal, mesothelial (mesothelioma), and ovarian cancers (Camargo et al., 2011; IARC, 2023; Singh et al., 2023). Several biological mechanisms have been proposed to explain the epidemiologically observed association between asbestos exposure and cancer. The inability of phagocytic cells to eliminate the fibres enhances oxidative stress and free radical production, thereby increasing cellular damage and tumor formation risk (Pugnaloni et al., 2013). Moreover, numerous studies conducted in different biological systems have demonstrated that oxidative stress contributes significantly to the pathogenesis of many diseases (Ökçesiz & Bucurgat, 2021).

The carcinogenic effects of asbestos vary according to the structural properties of the fibres as well as individual susceptibility factors (Celsi et al., 2019; van Zandwijk et al., 2020). The process by which asbestos induces cancer involves a complex interplay of genetic mutations, oxidative stress, inflammation, and epigenetic alterations (Bogen, 2023). In addition to its carcinogenic effects, prolonged asbestos exposure has been associated with adverse psychological outcomes in environmentally contaminated settings, primarily due to persistent health-related uncertainty and concern (Yiğitalp & Saka, 2017). Figure 4 illustrates the structural differences between a healthy respiratory system and one severely affected by asbestos-related diseases.

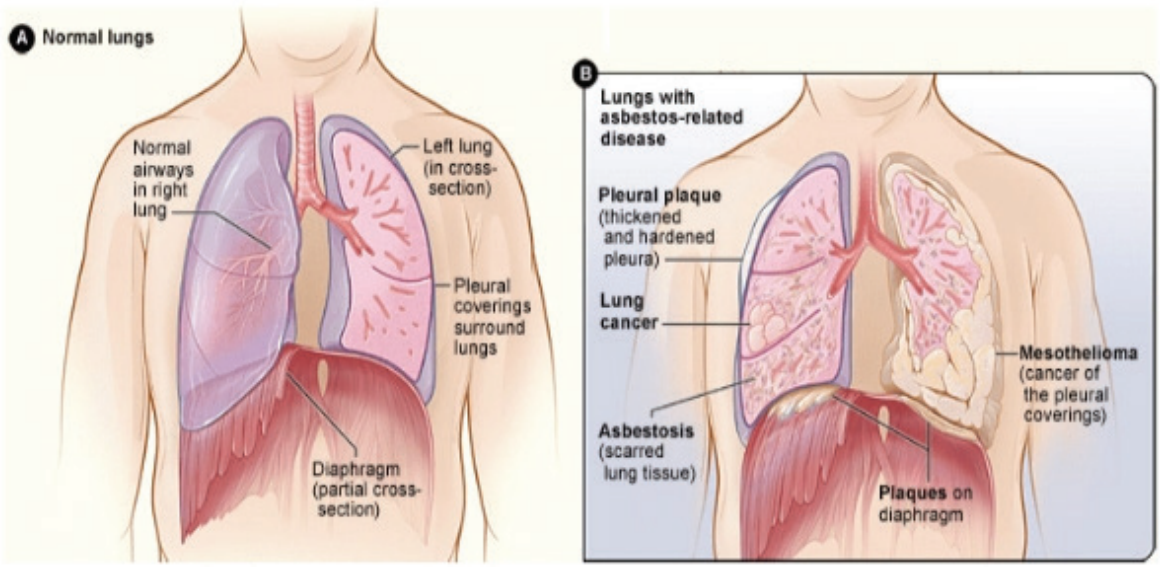


Figure 4. Normal, healthy respiratory system (left) and a respiratory system affected by severe asbestos-related diseases (right) (Rodríguez Elizalde, 2022)

Post-earthquake asbestos exposure: evidence from global studies and Türkiye

Earthquakes and large-scale disasters constitute critical scenarios for asbestos exposure due to the sudden collapse of buildings, extensive debris generation, and uncontrolled demolition activities. In regions where asbestos-containing materials were historically used in construction, seismic events can lead to the widespread release of asbestos fibres into the environment, posing serious occupational and environmental health risks. Evidence from different earthquakes worldwide consistently demonstrates that the magnitude of structural damage, the age and composition of buildings, and the effectiveness of post-disaster management practices are key determinants of asbestos exposure levels.

Comparative analyses of major seismic events reveal a consistent post-disaster pattern of increased airborne particulate matter and asbestos fibre release.

This pattern has been documented following the 1995 Great Hanshin (Kobe) earthquake in Japan, the 2009 L'Aquila earthquake in Italy, the 2011 Tohoku earthquake in Japan, the 2002 Sultandağı earthquake in Türkiye, and the 2023 Kahramanmaraş earthquakes.

In the aftermath of the Great Hanshin (Kobe) earthquake, approximately 18 million tons of debris were generated. Environmental measurements confirmed the presence of asbestos fibres in ambient air. Notably, asbestos removal accounted for a substantial proportion of total debris management costs, indicating both the scale of contamination and the economic burden associated with delayed preventive measures (Yavuz, 2024). Similar challenges were observed after the 2011 Tohoku earthquake, where elevated concentrations of respirable particles were reported, contributing to severe respiratory outcomes among exposed individuals (Balbay et al., 2024).

Across these international case studies, certain population groups consistently emerged as the most vulnerable to asbestos exposure. Demolition and debris removal workers, security personnel, and residents living in proximity to damaged structures were frequently exposed to airborne fibres under conditions of insufficient awareness and inadequate protective measures. Reports from L'Aquila and Tohoku highlighted that occupational exposure often exceeded recommended limits, largely due to the absence of systematic asbestos risk assessments and the lack of enforced use of personal protective equipment during emergency response and reconstruction phases.

In line with these observations, measurements conducted at demolition sites in post-disaster settings demonstrated that airborne asbestos fibre concentrations could exceed permissible occupational limits, reinforcing the critical need for continuous monitoring and preventive measures to protect worker health (Stevulova et al., 2020).

Evidence from Türkiye aligns closely with these international observations while providing original insights into post-earthquake asbestos exposure under local conditions. Field investigations conducted after the 2023 Kahramanmaraş earthquakes detected various types of asbestos fibres in debris and environmental samples collected from severely affected provinces such as Adıyaman, Kahramanmaraş, Elbistan, and Hatay (Varol, 2023). Similarly, post-earthquake assessments following the İzmir earthquake identified chrysotile asbestos in a considerable proportion of examined buildings, underscoring the persistence of asbestos-containing materials in the existing building stock (Tetik et al., 2024). These findings indicate that asbestos exposure following earthquakes in Türkiye is not incidental but represents a systematic risk associated with the characteristics of the built environment and post-disaster practices.

Further reinforcing this concern, a recent study assessing asbestos awareness among demolition workers, security staff, and nearby residents after the 2023 Kahramanmaraş earthquakes revealed critically low levels of knowledge regarding asbestos-related health risks and protective measures. The study also demonstrated that existing safety regulations were inadequately implemented during debris removal and demolition processes (Süzergöz & Doğan, 2025). These results suggest that regulatory frameworks alone are insufficient without effective field-level enforcement and targeted training programmes.

Taken together, international and national evidence highlights that asbestos risk is a recurrent yet often underestimated component of post-earthquake environments. The consistent identification of similar high-risk groups and exposure pathways across different disasters suggests the need to reconsider current disaster response planning strategies. Asbestos risk management should be systematically integrated into national disaster preparedness, emergency response, and debris management protocols. This integration should include pre-disaster identification of asbes-

tos-containing structures, mandatory asbestos risk assessments before demolition, strict enforcement of personal protective equipment use, and continuous training programmes for all personnel involved in post-disaster operations. Embedding asbestos control strategies into disaster management frameworks is essential to prevent avoidable long-term health consequences following future earthquakes.

Worldwide and Türkiye regulations on asbestos

Worldwide regulations on asbestos

Throughout the 20th century, asbestos was widely used worldwide due to its high heat resistance, thermal and acoustic insulation properties, and long-lasting durability. However, from the last quarter of the century onward, as scientific evidence increasingly demonstrated that exposure to this mineral is strongly associated with serious health issues, particularly lung diseases and cancer, many countries imposed restrictions on or completely banned its use (Murray, 1990). Although asbestos has been completely banned in many regions today, it is still being extracted and used in a limited manner under regulatory frameworks in certain countries (Ali et al., 2017; Lee et al., 2008).

The majority of European Union member states have completely banned the use of asbestos in accordance with European Commission Directive 1999/77/EC. This prohibition has been expanded to cover a wide range of asbestos-containing products throughout the Union (European Commission, 1999a). In the Fifty-eighth World Health Assembly held in 2005, Member States were urged to implement measures aimed at reducing cancer risks associated with chemical exposures in workplaces, households, and other living environments. Within this context, asbestos was particularly emphasized as the most significant carcinogen, being responsible for nearly half of occupational cancer deaths (WHO, 2005). This issue has also been examined in epidemiological studies investigating occupational cancer mortality associated with asbestos exposure (Curado et al., 2024; Nicholson, 1996). Member states were required to phase out the use of chrysotile asbestos by January 1, 2005, although a limited exemption was granted for its use in diaphragms until 2008 (European Commission, 1999b). Under Directive 2009/148/EC, as amended by Directive (EU) 2023/2668, the binding occupational exposure limit for asbestos was reduced to 0.01 fibres/cm^3 as an eight-hour time-weighted average (TWA) (European Parliament and the Council, 2023). The adequacy of this limit and the need for lower exposure thresholds and additional protective measures, particularly for asbestos present in existing buildings, have been examined in the scientific literature (Takala, 2022).

Regulations on asbestos in Türkiye

In Türkiye, the import, production, and use of asbestos were gradually restricted starting in 1993 (T.C. Resmî Gazete, 1993), and with the regulation published in 2010, the extraction, use in products, and sale of all types of asbestos, including chrysotile, were completely banned (T.C. Resmî Gazete, 2010). Regulations issued by the Ministry of Labour and Social Security in 2003 and 2013 established exposure limits and occupational safety measures, and in 2015, training for asbestos removal specialists was made mandatory (T.C. Resmî Gazete, 2003; T.C. 28539 sayılı Resmî Gazete, 2013). However, the presence of asbestos-containing materials in the existing building stock reveals a public health issue that cannot be addressed solely through legislation, but must also be supported by active field implementation and enforcement (Çil et al., 2021). Therefore, to reduce the public health risks of asbestos, there is a need not only for bans but also for comprehensive strategies that include the identification of high-risk structures, safe removal practices, and effective disposal processes.

In Türkiye, the legally defined TWA exposure limit for asbestos is 0.1 fibres/cm^3 (T.C. 28539 sayılı Resmî Gazete, 2013; T.C. 28812 sayılı Resmî Gazete, 2013). This value is substantially higher than the exposure levels recommended by international organisations such as the WHO, which propose limits ranging be-

tween 0.001 and 0.0001 fibres/cm³ (Peña-Castro et al., 2023). The discrepancy between national and international reference values indicates a markedly less stringent regulatory threshold in Türkiye. While such limits are defined for controlled occupational environments, their adequacy becomes particularly questionable in high-uncertainty settings, such as post-earthquake debris zones, where asbestos-containing materials may be extensively disturbed, and airborne fibre concentrations are difficult to monitor. In these contexts, reliance on comparatively higher legal exposure limits may underestimate actual health risks, potentially increasing uncontrolled exposure among workers, volunteers, and the general population involved in debris removal and recovery activities.

CONCLUSION

Occupational, environmental, and post-disaster asbestos exposure causes permanent and severe toxicological effects on human health. As strongly demonstrated in the literature, asbestos exposure is directly associated with fatal diseases such as asbestosis, malignant mesothelioma, and lung cancer (Markowitz, 2015; Türk Tabipleri Birliği, 2023). Specifically in Türkiye, the effects of approximately 500,000 tons of asbestos, which was extensively used in the past, still pose a significant risk today (Metintaş and Yılmaz Demirci, 2015). Although the use of asbestos was officially banned in 2010, inadequate enforcement in practice continues to threaten public health—particularly during urban transformation projects and post-disaster debris management processes (Allen, 2010; Yavuz, 2024). Indeed, asbestos fibres identified in the rubble following the February 6, 2023, Kahramanmaraş earthquakes have revealed serious shortcomings in safe waste management and occupational health measures (Türk Tabipleri Birliği, 2023; Yavuz, 2024). Minimizing asbestos-related health risks during post-earthquake debris removal requires the systematic identification of asbestos-contaminated structures before intervention, the engagement of trained professionals adhering to established asbestos removal protocols, the provision of appropriate personal protective equipment for workers, comprehensive education on asbestos-related hazards and safe work practices, and the implementation of continuous environmental and air quality monitoring to effectively control airborne fibre exposure (Koyunoğlu, 2024). In this context, the effective management of toxicological risks associated with asbestos should not be limited to the existence of legal regulations alone; it must also be supported by rigorous on-site enforcement, the development of a competent and certified workforce, and the promotion of public awareness and preventive health behaviours (Akgün, 2015). Furthermore, asbestos safety should be addressed as a specific component within disaster management processes, and logistical capacity should be strengthened for the provision of protective equipment, the implementation of safe removal techniques, and the proper disposal of asbestos waste. The coordinated and sustainable implementation of all these measures will play a critical role in reducing the incidence of asbestos-related diseases, both now and in the future (Metintaş & Yılmaz Demirci, 2015; Türk Tabipleri Birliği, 2023; Yavuz, 2024).

AUTHOR CONTRIBUTION STATEMENT

Determination of the subject, literature research, preparation of the manuscript (HD), Determination of the subject, literature research, reviewing the manuscript, and supervision (AÖH).

CONFLICT OF INTEREST

The authors declare that there is no conflict of interest.

REFERENCES

Akboğa, Ö., & Baradan, S. (2011). Asbestin inşaat sektöründeki yeri ve maruziyetin önlenmesi. *Türkiye Mühendislik Haberleri, 56*(469), 70.

Akboğa-Kale, Ö., Gürcanlı, G. E., & Baradan, S. (2017). Kentsel dönüşüm sürecinde asbest maruziyeti ve korunma yöntemleri. *Pamukkale Üniversitesi Mühendislik Bilimleri Dergisi, 23*(6), 694–706.

Akgün, M. (2015). Elimination of asbestos-related diseases in Turkey still has a long way to go. *Turkish Thoracic Journal, 16*(3), 105.

Ali, S. H., Giurco, D., Arndt, N., Nickless, E., Brown, G., Demetriades, A., ... Kinnaird, J. (2017). Mineral supply for sustainable development requires resource governance. *Nature, 543*, 367–372.

Allen, L. K. (2010). *Asbestos ban in Turkey!* Retrieved from https://ibasecretariat.org/lka_asb_ban_turkey.php

Altuntaş, H. D., Öztürk, F., Yılmaz, S. İ., & Eröz, R. (2009). Asbest ve erionite bağlı mezotelyomalı hastaların parafin bloklarında p53 tümör supressör ve ras onkogen mutasyonlarının araştırılması. *Erciyes Medical Journal, 31*(1), 1–8.

Balbay, E. G., Kayalar, Ö., Balbay, Ö., Dikensoy, Ö., Arbak, P., & Bayram, H. (2024). Impact of earthquakes on lung health. *Thoracic Research and Practice, 25*(2), 89.

Barbiero, F., Zanin, T., Pisa, F. E., Casetta, A., Rosolen, V., Giangreco, M., & Barbone, F. (2018). Cancer incidence in a cohort of asbestos-exposed workers undergoing health surveillance. *International Archives of Occupational and Environmental Health, 91*(7), 831–841.

Bernstein, D. M., & Pavlisko, E. N. (2017). Differential pathological response and pleural transport of mineral fibres. In A. F. Gualtieri (Ed.), *Mineral fibres: Crystal chemistry, chemical-physical properties, biological interaction and toxicity* (pp. 417–434). European Mineralogical Union and the Mineralogical Society of Great Britain and Ireland, London, UK.

Berry, T. A., Belluso, E., Vigliaturo, R., Gieré, R., Emmett, E. A., Testa, J. R., & Wallis, S. L. (2022). Asbestos and other hazardous fibrous minerals: Potential exposure pathways and associated health risks. *International Journal of Environmental Research and Public Health, 19*(7), 4031.

Bogen, K. T. (2023). Ultrasensitive dose-response for asbestos cancer risk implied by new inflammation-mutation model. *Environmental Research, 230*, 115047.

Bolan, S., Kempton, L., McCarthy, T., Wijesekara, H., Piyathilake, U., Jasemizad, T., ... Wang, H. (2023). Sustainable management of hazardous asbestos-containing materials: Containment, stabilization and inertization. *Science of the Total Environment, 881*, 163456.

Browne, C. (2003). Salamander's wool: The historical evidence for textiles woven with asbestos fibre. *Textile History, 34*, 64–73.

Celsi, F., Crovella, S., Moura, R. R., Schneider, M., Vita, F., Finotto, L., ... Borelli, V. (2019). Pleural mesothelioma and lung cancer: the role of asbestos exposure and genetic variants in selected iron metabolism and inflammation genes. *Journal of Toxicology and Environmental Health, Part A*, *82*(20), 1088-1102.

Camargo, M. C., Stayner, L. T., Straif, K., Reina, M., Al-Alem, U., Demers, P. A., & Landrigan, P. J. (2011). Occupational exposure to asbestos and ovarian cancer: a meta-analysis. *Environmental health perspectives*, *119*(9), 1211.

Craighead, J. E., Mossman, B. T., & Bradley, B. J. (1980). Comparative studies on the cytotoxicity of amphibole and serpentine asbestos. *Environmental Health Perspectives*, *34*, 37-46.

Cruz, M. J., Sampol, J., Pallero, M., Rodríguez, E., & Ferrer, J. (2018). Asbestos-related disease in upholsterers. *Archives of Environmental & Occupational Health*, *73*(3), 186-188.

Curado, A., Nunes, L. J., Carvalho, A., Abrantes, J., Lima, E., & Tomé, M. (2024). The use of asbestos and its consequences: an assessment of environmental impacts and public health risks. *Fibers*, *12*(12), 102.

Çil, B., Polat, M. R., & Kabak, M. (2021). Old Habits Die Hard–Asbestos Exposure. *Turkish Thoracic Journal*, *22*(5), 381.

Damiran, N., & Frank, A. (2018). Asbestos consumption in Mongolia: 1996–2014. *International journal of environmental research and public health*, *15*(1), 136.

Erker, P. (2014). A comparative perspective of asbestos as an industrial and environmental hazard. *Global Environment*, *7*(1), 72-105.

European Commission. (1999a). *Council Directive 1999/77/EC of 26 July 1999 on the approximation of the laws of the Member States relating to the use of asbestos and asbestos-containing products.* EUR-Lex. Retrieved from https://eur-lex.europa.eu/eli/dir/1999/77/oj

European Commission. (1999b). Commission extends ban on asbestos products in EU. Retrieved from https://cordis.europa.eu/article/id/13445-commission-extends-ban-on-asbestos-products-in-eu

European Parliament and the Council. (2023). Directive (EU) 2023/2668 of 22 November 2023 amending Directive 2009/148/EC on the protection of workers from the risks related to exposure to asbestos at work. EUR-Lex. Retrieved from https://eur-lex.europa.eu/eli/dir/2023/2668/oj/eng

François, B., & Michel, T. (2016). *Guide technique de l'amiante dans les bâtiments: Du dossier technique amiante aux travaux de retrait* (pp. 11–65). Antony, France: Editions Le Moniteur.

Frank, A. L., & Joshi, T. K. (2014). The global spread of asbestos. *Annals of global health*, *80*(4), 257-262.

Frank, A. L. (2020). Global use of asbestos: Legitimate and illegitimate issues. *Journal of Occupational Medicine and Toxicology, 15*(1), 16.

Frank, A. L., & van Zandwijk, N. (2024). Asbestos history and use. *Lung Cancer*, *193*, 107828.

Gochfeld, M. (2005). Chronological history of occupational medicine. *Journal of occupational and Environmental Medicine*, *47*(2), 96-114.

Güneş, M., Güneş, A., İlbeyli, N., & Kaya, B. (2017). Asbest maruziyeti ve etkileri. *Turkish Journal of Scientific Reviews*, *10*(1), 1-5.

Hancı, Ö., & Kepekli, T. A. (2022). Afet ve acil durum risklerinin belirlenmesi ve çözüm önerileri: Erzurum ili örneği. *3rd International Disaster Management Congress*. Tokat, Türkiye.

International Agency for Research on Cancer (IARC). (2012). *Arsenic, metals, fibres, and dusts* (IARC Monographs on the Evaluation of Carcinogenic Risks to Humans, Vol. 100, Pt. C). Lyon, France: Author

International Agency for Research on Cancer (IARC). (2023). *Occupational exposure as a firefighter* (IARC Monographs on the Evaluation of Carcinogenic Risks to Humans, Vol. 132, pp. 1–739). Lyon, France: Author.

Kanarek, M. S. (2011). Mesothelioma from chrysotile asbestos: update. *Annals of epidemiology*, *21*(9), 688-697.

Kim, Y., Myong, J. P., Lee, J. K., Kim, J. S., Kim, Y. K., & Jung, S. H. (2015). CT characteristics of pleural plaques related to occupational or environmental asbestos exposure from South Korean asbestos mines. *Korean Journal of Radiology*, *16*(5), 1142-1152.

Kośny, J., & Yarbrough, D. W. (2022). Short history of thermal insulation and radiation control technologies used in architecture. In *Thermal Insulation and Radiation Control Technologies for Buildings* (pp. 1–35). Cham: Springer International Publishing.

Koyunoğlu, C. (2024). Increased cancer risk from asbestos exposure during post-earthquake building cleanup. *Acta Scientific Biotechnology, 5*(4).

Kusiorowski, R., Zaremba, T., Piotrowski, J., & Adamek, J. (2012). Thermal decomposition of different types of asbestos. *Journal of thermal analysis and calorimetry*, *109*(2), 693-704.

Laufer, B. (1915). Asbestos and Salamander, an essay in Chinese and Hellenistic Folk-Lore. *T'oung Pao*, *16*(3), 299-373.

Lee, R. J., Strohmeier, B. R., Bunker, K. L., & Van Orden, D. R. (2008). Naturally occurring asbestos—A recurring public policy challenge. *Journal of Hazardous materials*, *153*(1-2), 1-21.

Lin, R. T., Soeberg, M. J., Chien, L. C., Fisher, S., Takala, J., Lemen, R., ... Takahashi, K. (2018). Bibliometric analysis of gaps in research on asbestos-related diseases: declining emphasis on public health over 26 years. *BMJ open*, *8*(7), e022806.

Linton, A., Vardy, J., Clarke, S., & van Zandwijk, N. (2012). The ticking time-bomb of asbestos: its insidious role in the development of malignant mesothelioma. *Critical reviews in oncology/hematology*, *84*(2), 200-212.

Markowitz, S. (2015). Asbestos-related lung cancer and malignant mesothelioma of the pleura: selected current issues. In *Seminars in respiratory and critical care medicine*, *36*(03), 334-346.

Metintaş, M., & Yılmaz Demirci, N. (2015). Turkish Mesothelioma Working Group, Turkey Asbestos Control Strategic Plan final report. *Turkish Thoracic Journal, 16*(2).

Michaels, D. (2008). *Doubt is their product: how industry's assault on science threatens your health*. Oxford University Press.

Murgia, N., Akgun, M., Blanc, P. D., Costa, J. T., Moitra, S., Muñoz, X., ... Ferreira, A. J. (2025). Issue 3—The occupational burden of respiratory diseases: an update. *Pulmonology*, *31*(1), 1-16, 2416808.

Murray, R. (1990). Asbestos: a chronology of its origins and health effects. *Occup. Environ. Med.*,47, 361–365.

Nicholson, W. J. (1996). Cancer risk in the work place, including asbestos. *European Journal of Cancer Prevention*, *5*(5), 393-396.

Noonan, C. W. (2017). Environmental asbestos exposure and risk of mesothelioma. *Annals of translational medicine*, *5*(11), 234.

Offermans, N. S., Vermeulen, R., Burdorf, A., Goldbohm, R. A., Kauppinen, T., Kromhout, H., & van den Brandt, P. A. (2014). Occupational asbestos exposure and risk of pleural mesothelioma, lung cancer, and laryngeal cancer in the prospective Netherlands cohort study. *Journal of occupational and environmental medicine*, *56*(1), 6-19.

Occupational Safety and Health Administration (OSHA). (2002). *Asbestos standard for the construction industry (OSHA 3096).* U.S. Department of Labor. Retrieved from https://www.osha.gov/sites/default/files/publications/osha3096.pdf

Ökçesiz, A., Bucurgat, Ü. Ü. (2021). Evaluation of the toxic effects of statins and their possible role in the treatment of cancer. *Istanbul Journal of Pharmacy*, *51*(1), 154-160.

Peña-Castro, M., Montero-Acosta, M., & Saba, M. (2023). A critical review of asbestos concentrations in water and air, according to exposure sources. *Heliyon*, *9*(5), e15730.

Pira, E., Pelucchi, C., Piolatto, P. G., Negri, E., Discalzi, G., & La Vecchia, C. (2007). First and subsequent asbestos exposures in relation to mesothelioma and lung cancer mortality. *British Journal of Cancer*, *97*(9), 1300-1304.

Pugnaloni, A., Giantomassi, F., Lucarini, G., Capella, S., Bloise, A., Di Primio, R., & Belluso, E. (2013). Cytotoxicity induced by exposure to natural and synthetic tremolite asbestos: an in vitro pilot study. *Acta Histochemica*, *115*(2), 100-112.

Rodríguez Elizalde, R. (2022). Asbestos presence in 20th century buildings. *Journal of Engineering and Applied Sciences Technology, 4*(3).

Selikoff, I. J., Hammond, E. C., & Churg, J. (1968). Asbestos exposure, smoking, and neoplasia. *Jama*, *204*(2), 106-112.

Sen, D. (2015). Working with asbestos and the possible health risks. *Occupational Medicine*, *65*(1), 6-14.

Singh, S., Pradhan, S. R., Yadav, A., & Singh, P. K. (2023). Banning asbestos in talcum powder: Time for action in India. *Dialogues in Health*, *3*, 1-4, 100158.

Stevulova, N., Estokova, A., Holub, M., Singovszka, E., & Csach, K. (2020). Characterization of demolition construction waste containing asbestos, and the release of fibrous dust particles. *Applied Sciences*, *10*(11), 4048.

Süzergöz, A., & Doğan, T. R. (2025). Statistical evaluation of asbestos exposure awareness that may arise from removal of building debris in the 2023 Kahramanmaraş earthquakes. *Afyon Kocatepe Üniversitesi Fen ve Mühendislik Bilimleri Dergisi, 25*(3), 565–575.

Taeger, D., Wichert, K., Lehnert, M., Casjens, S., Pesch, B., Weber, D. G., ... Behrens, T. (2022). Lung cancer and mesothelioma risks in a prospective cohort of workers with asbestos-related lung or pleural diseases. *American Journal of Industrial Medicine*, *65*(8), 652-659.

T.C. Resmî Gazete. (1993). 21634 sayılı Resmî Gazete. Retrieved from https://www.resmigazete.gov.tr/arsiv/21634.pdf

T.C. Resmî Gazete. (2003). 25328 sayılı Resmî Gazete. Retrieved from https://www.resmigazete.gov.tr/eskiler/2003/12/20031226.htm#6

T.C. Resmî Gazete. (2010). 27687 sayılı Resmî Gazete. Retrieved from https://www.resmigazete.gov.tr/eskiler/2010/08/20100829-3.htm

T.C. Resmî Gazete. (2013). 28539 sayılı Resmî Gazete. Retrieved from https://www.resmigazete.gov.tr/eskiler/2013/01/20130125-24.htm

T.C. Resmî Gazete. (2013). 28812 sayılı Resmî Gazete: Tozla Mücadele Yönetmeliği (EK-1: Özelliği olan kayaç veya mineraller maruziyet eşik sınır değerleri). Retrieved from https://www.resmigazete.gov.tr/eskiler/2013/11/20131105-9.htm

Takala, J. (2022). Global elimination of asbestos and asbestos-related diseases. *Safety and Health at Work*, *13*, S66.

Tetik, Y. Ö., Zümrüt, İ. B., Çamurcu, A. G., Kale, Ö. A., & Baradan, S. (2024). Measurement and removal of asbestos in residential dwellings to be demolished—urban transformation experience in Izmir, Turkey. *Environmental Science and Pollution Research*, *31*(6), 9857-9866.

Turan, H., & Alpaydın, Z. (2024). Deprem enkazının kaldırılması sürecinde asbest riskinin yönetimi. *The Journal of Academic Social Science, 142*(142), 155–178.

Türk Tabipleri Birliği. (2023). TTB ve THHP asbest raporunu açıkladı: Kahramanmaraş Merkez ve Elbistan ilçesi ile Adıyaman'da asbest tespit edildi. Retrieved from https://www.ttb.org.tr/haber_goster.php?Guid=640aeab6-74bd-11ee-9552-48095692dc98#:~:text=ikinci%20y%C3%BCzy%C4%B1l%C4%B1nda%20y%C3%BCzle%C5%9Femedi%C4%9Fimiz%20hakikatler%20e%C5%9Flik,yer%20alan%20ve%20koruyucu%20%C3%B6nlemlerden

Vallyathan, V., Green, F. H., & Abraham, J. L. (1985). The role of analytical techniques in the diagnosis of asbestos-associated disease. *CRC Critical reviews in clinical laboratory sciences*, *22*(1), 1-42.

Van Gosen, B. S. (2007). The geology of asbestos in the United States and its practical applications. *Environmental & Engineering Geoscience*, *13*(1), 55-68.

Van Zandwijk, N., Reid, G., & Frank, A. L. (2020). Asbestos-related cancers: the 'Hidden Killer'remains a global threat. *Expert review of anticancer therapy*, *20*(4), 271-278.

Varol, G. (2023). 2023 Şubat depremlerinde Türk Tabipleri Birliği ve Halk Sağlığı Kolu deneyimi. *Community & Physician / Toplum ve Hekim, 38*(6), 431–437.

Vicari, K., Ribeiro, I. M., Aguiar, B. F., Brey, C., Boller, S., & Miranda, F. M. D. A. (2023). Occupational characterization of workers exposed to asbestos: an integrative review. *Revista Brasileira de Medicina do Trabalho*, *20*(4), 650.

Virta R.L. (2002) Asbestos: Geology, Mineralogy, Mining, And Uses. From U.S. Geological Survey Publication 2002-149.

Virta, R. L. (2002). *Asbestos: Geology, mineralogy, mining, and uses* (p. 28). Washington, DC, USA: U.S. Department of the Interior, U.S. Geological Survey.

Yavuz, C. I. (2024). The additional burden of earthquakes: Asbestos risks rising in Türkiye. *Thoracic Research and Practice, 25*(3), 100.

Yiğitalp, G., & Saka, G. (2017). Çevresel asbeste maruz kalan erişkin bireylerde kaygı ve umutsuzluk düzeyleri. *Dicle Medical Journal*, *44*(4), 355-364.

Zaremba, T., Krząkała, A., Piotrowski, J., & Garczorz, D. (2010). Study on the thermal decomposition of chrysotile asbestos. *Journal of Thermal Analysis and Calorimetry*, *101*(2), 479-485.

World Health Organization (WHO). (2005). *Resolutions and decisions, annex*. In *Proceedings of the Fifty-Eighth World Health Assembly, Geneva, Switzerland, 16–25 May 2005* (p. 143). Geneva, Switzerland: World Health Organization.

Wu, W. T., Lin, Y. J., Li, C. Y., Tsai, P. J., Yang, C. Y., Liou, S. H., & Wu, T. N. (2015). Cancer attributable to asbestos exposure in shipbreaking workers: a matched-cohort study. *PloS one*, *10*(7), e0133128.

FABAD J. Pharm. Sci., 51, 1, 419-434, 2026
Doi: 10.55262/fabadeczacilik.1825544
REVIEW ARTICLE

The Role of Glucocorticoids in Hepatic Gluconeogenesis, Associated Pathologies, and Novel Therapeutic Approaches

Yusuf Anil AY[*], Elif CADIRCI[**°]

The Role of Glucocorticoids in Hepatic Gluconeogenesis, Associated Pathologies, and Novel Therapeutic Approaches

SUMMARY

Glucocorticoids are essential steroid hormones that play a pivotal role in regulating hepatic gluconeogenesis, thereby contributing to the maintenance of systemic glucose homeostasis. This review provides a comprehensive overview of the molecular mechanisms by which glucocorticoids modulate hepatic glucose production and explores their clinical implications in metabolic health and disease. Glucocorticoids exert their primary effects through genomic pathways, involving the translocation of activated glucocorticoid receptors (GRs) into the nucleus, where they bind to glucocorticoid response elements (GREs) on DNA. This interaction promotes the transcription of key gluconeogenic enzymes, notably phosphoenolpyruvate carboxykinase (PEPCK) and glucose-6-phosphatase (G6Pase). Additionally, glucocorticoids enhance the expression of these enzymes by synergizing with critical transcriptional regulators such as peroxisome proliferator-activated receptor gamma coactivator 1-alpha (PGC-1α), forkhead box protein O1 (FOXO1), and hepatocyte nuclear factor 4-alpha (HNF-4α). Beyond their hepatic effects, glucocorticoids influence systemic metabolism by stimulating proteolysis and lipolysis in peripheral tissues, thereby increasing the availability of substrates for gluconeogenesis. Furthermore, they antagonize insulin signaling, contributing to insulin resistance. The local activation of glucocorticoids via the enzyme 11β-hydroxysteroid dehydrogenase type 1 (11β-HSD1) adds another layer of regulation. Non-genomic effects through the cAMP/PKA/CREB signaling pathway allows for rapid metabolic responses. Chronic glucocorticoid excess, as observed in conditions like Cushing's syndrome, is linked to the development of type 2 diabetes. Emerging therapeutic strategies, including 11β-HSD1 inhibitors, selective GR modulators, and targeted inhibitors of gluconeogenic enzymes, present promising avenues for managing glucocorticoid-induced metabolic disorders.

Keywords: *Glucocorticoid, gluconeogenesis, glucose metabolism, hyperglycemia, diabetes.*

Glukokortikoidlerin Hepatik Glukoneogenezdeki Rolü, İlişkili Patolojiler ve Yeni Tedavi Yaklaşımları

ÖZ

Glukokortikoidler, hepatik glukoneogenezi düzenlemede önemli bir rol oynayan ve böylece sistemik glikoz homeostazının korunmasına katkıda bulunan temel steroid hormonlardır. Bu derleme, glukokortikoidlerin hepatik glikoz üretimini modüle ettiği moleküler mekanizmalara kapsamlı bir genel bakış sunmakta ve metabolik sağlık ve hastalıklar üzerindeki klinik etkilerini incelemektedir. Glukokortikoidler, aktive edilmiş glukokortikoid reseptörlerinin (GR) çekirdeğe taşınması ve burada DNA üzerindeki glukokortikoid yanıt elemanlarına (GRE) bağlanmasıyla genomik yolaklar aracılığıyla birincil etkilerini gösterir. Bu etkileşim, fosfoenolpiruvat karboksikinaz (PEPCK) ve glikoz-6-fosfataz (G6Pase) gibi önemli glukoneojenik enzimlerin transkripsiyonunu teşvik eder. Ek olarak, glukokortikoidler, peroksizom proliferatör ile aktive olan reseptör gama koaktivatörü 1-alfa (PGC-1α), forkhead box proteini O1 (FOXO1) ve hepatosit nükleer faktör 4-alfa (HNF-4α) gibi kritik transkripsiyon düzenleyicileri ile sinerji oluşturarak bu enzimlerin ekspresyonunu artırır. Karaciğer üzerindeki etkilerinin ötesinde, glukokortikoidler periferik dokularda proteoliz ve lipolizi uyararak sistemik metabolizmayı etkiler ve böylece glukoneogenez için substratların kullanılabilirliğini artırır. Ayrıca, insülin sinyalini antagonize ederek insülin direncine katkıda bulunurlar. 11β-hidroksisteroid dehidrojenaz tip 1 (11β-HSD1) enzimi aracılığıyla glukokortikoidlerin lokal aktivasyonu, düzenlemeye başka bir katman ekler. cAMP/PKA/CREB sinyal yoluyla genomik olmayan etkiler, hızlı metabolik yanıtlara olanak tanır. Cushing sendromu gibi durumlarda gözlenen kronik glukokortikoid fazlalığı, tip 2 diyabetin gelişimi ile bağlantılıdır. 11β-HSD1 inhibitörleri, seçici GR modülatörleri ve glukoneojenik enzimlerin hedefli inhibitörleri dahil olmak üzere ortaya çıkan terapötik stratejiler, glukokortikoid kaynaklı metabolik bozuklukların yönetimi için umut verici yollar sunmaktadır.

Anahtar Kelimeler: *Glukokortikoid, glukoneogenez, glikoz, hiperglisemi, diyabet.*

Recieved: 18.11.2025
Revised: 19.02.2026
Accepted: 5.03.2026

[*] ORCID: 0009-0002-6007-694X, Department of Biochemistry, Faculty of Pharmacy, Ataturk University, 25240, Erzurum, Türkiye
[**] ORCID: 0000-0003-0836-7205, Department of Pharmacology, Faculty of Medicine, Ataturk University, 25240, Erzurum, Türkiye

[°] Corresponding Author; Elif CADIRCI
E-mail: ecadirci@atauni.edu.tr

INTRODUCTION

Glucocorticoids (GCs), including endogenous cortisol and synthetic analogues (e.g., dexamethasone, prednisone), are one of the cornerstones of modern medicine due to their anti-inflammatory, immunosuppressive, and metabolic effects. These molecules, widely used in the treatment of rheumatoid arthritis, autoimmune diseases, allergic reactions, chronic obstructive pulmonary disease, and certain malignancies, exhibit complex and multifaceted effects on energy metabolism (De Guia, Rose, & Herzig, 2014). GCs play critical roles in the stress response and maintenance of homeostasis; they bind to glucocorticoid receptors (GR) with high affinity, regulating gene transcription and modulating key components of energy metabolism such as gluconeogenesis, fatty acid oxidation, and mitochondrial function (Vandewalle, Luypaert, De Bosscher, & Libert, 2018). These effects support energy mobilization in acute stress conditions but chronic exposure can lead to metabolic complications such as; insulin resistance, hyperglycemia, dyslipidemia, and mitochondrial dysfunction (Sharma & Singh, 2019). This review aims to comprehensively examine the biochemical effects of glucocorticoids on gluconeogenesis.

Gluconeogenesis is a fundamental metabolic pathway that synthesizes glucose from non-carbohydrate sources (lactate, glycerol, and glucogenic amino acids). It primarily supplies energy to glucose-dependent tissues such as the brain, erythrocytes, and renal medulla during conditions of increased glucose demand such as; fasting, stress, and intense exercise (Kuo, McQueen, Chen, & Wang, 2015). GCs stimulate this process by increasing the transcription of key enzymes of gluconeogenesis, such as phosphoenolpyruvate carboxylase (PEPCK) and glucose-6-phosphatase (G6Pase), in the liver and renal cortex (Shah & Wondisford, 2023). The transactivation of enzymes such as PEPCK and G6Pase occurs through the binding of the activated glucocorticoid receptor (GR) to glucocorticoid response elements (GREs) in DNA (Ratman et al., 2013). Chronic GC exposure increases the risk of insulin resistance and type 2 diabetes due to excessive stimulation of gluconeogenesis. This process is not only related to gluconeogenesis but also to the suppression of glucose transporter 4 (GLUT4) translocation (Sakoda et al., 2000). Additionally the use of amino acids for gluconeogenesis triggers protein catabolism and may leads to muscle mass loss (sarcopenia) (Oray, Abu Samra, Ebrahimiadib, Meese, & Foster, 2016). Considering these effects, GCs are beneficial for energy mobilization in acute conditions but cause metabolic disorders in chronic conditions and may exacerbate existing metabolic disorders.

Clinically, the effects of glucocorticoids on energy metabolism have both therapeutic and adverse outcomes. Their life-saving effects have been proven in acute inflammatory conditions and/or severe respiratory diseases such as COVID-19 (The RECOVERY Collaborative Group, 2021). However, chronic use is associated with serious side effects such as metabolic syndrome, type 2 diabetes, cardiovascular diseases, and osteoporosis (Noetzlin, Breville, Seebach, & Gastaldi, 2022; Oray et al., 2016; Saag, Furst, & Barnes, 2022). These side effects stem from a combination of excessive stimulation of gluconeogenesis, imbalances in fatty acid metabolism, and the intracellular effects of GR. While the current literature has significantly illuminated the molecular mechanisms of glucocorticoids, there is many unanswered questions regarding tissue-specific effects and long-term outcomes.

This review aims to provide new perspectives for basic science and clinical research by thoroughly examining the biochemical effects of glucocorticoids on gluconeogenesis in the light of current and high-impact studies.

Pharmacological Properties of Glucocorticoids

Glucocorticoids, both endogenous (cortisol, corticosterone) and synthetic (dexamethasone, prednisone, methylprednisolone), play an important role in clinical use due to their pharmacological anti-inflammatory, immunosuppressive, and metabolic effects.

These molecules exert critical functions in physiological processes such as; the regulation of the stress response, suppression of inflammatory processesand maintenance of energy homeostasis (Barnes, 2011; Becker, 2013; Şengül & Çadırcı, 2023). The pharmacological properties of glucocorticoids depend on their GR binding affinity, pharmacokinetic profiles, tissue-specific effects, and interactions with metabolic pathways. These properties enable the therapeutic use of glucocorticoids in conditions such as rheumatoid arthritis, systemic lupus erythematosus, allergic reactions, prevention of organ transplant rejection, and severe COVID-19 cases, while also potentially causing serious side effects such as insulin resistance, hyperglycemia, dyslipidemia, and osteoporosis (Alexaki & Henneicke, 2021; Barnes, 2011; Becker, 2013; Compston, 2018; Lim, Kohli, & Bloom, 2017; Morand, Fernandez-Ruiz, Blazer, & Niewold, 2023; Noetzlin et al., 2022; Oray et al., 2016; Youssef, Novosad, & Winthrop, 2016). In this section, we will summarize the pharmacological properties of GCs to shed light on their relationship with gluconeogenesis.

GCs bind to the inactive GR in the cell cytoplasm. GR is a member of the nuclear receptor superfamily. This receptor forms a multiprotein complex consisting of molecules such as heat shock proteins (HSP90, HSP70, HSP40, HSP56), immunophilins (FKBP51, FKBP52), p23, and Src, which maintain the inactive conformation of GR when no ligand is bound (Heitzer, Wolf, Sanchez, Witchel, & DeFranco, 2007; Oakley & Cidlowski, 2013; Pratt & Toft, 1997). Binding of the GC molecule to GR induces a conformational change in the receptor, which triggers the dissociation of the HSP complex and exposes GR's nuclear localization signals (NLS) (Vandevyver, Dejager, & Libert, 2012). Additionally, FKBP51 in the GR complex converts in FKBP52, facilitating GR interaction with the dynein molecular motor complex (Echeverria & Picard Didier, 2010; Storer, Dickey, Galigniana, Rein, & Cox, 2011; Vandevyver et al., 2012). Once activated, GR is transported along microtubules via dynein to the nuclear pore complex and translocated into the nucleus with the help of nuclear carrier proteins. This process is regulated by post-translational modifications such as sumoylation, ubiquitination, and phosphorylation (Duma, Jewell, & Cidlowski, 2006; Vandevyver et al., 2012). Within the nucleus, GR binds to GRE and activates the transcription of anti-inflammatory proteins (Clark & Belvisi, 2012; Surjit et al., 2011). Additionally, GR binds to negative GREs, directly suppressing the transcription of pro-inflammatory genes and playing a role in inhibiting cytokine and chemokine production (Surjit et al., 2011). Furthermore, GCs can suppress pro-inflammatory transcription factors, including nuclear factor kappa B (NF-κB), activator protein-1 (AP-1), cAMP response element-binding protein (CREB), nuclear factor of activated T cells (NFAT), signal transducer and activator of transcription proteins (STAT3 and STAT6), and interferon regulatory factor 3 (IRF3). This occurs through direct protein–protein interactions without binding directly to DNA, a mechanism known as transrepression (Ratman et al., 2013; Reichardt et al., 2001). In addition to these genomic anti-inflammatory effects, membrane-bound GR variants alter cellular signaling pathways through a non-genomic mechanism and exhibit acute anti-inflammatory and immunosuppressive effects that can occur within minutes (Boldizsar et al., 2010; Panettieri et al., 2019).

The pharmacological effects of glucocorticoids are not limited to the suppression of inflammation and regulation of the immune response, but also play a decisive role at various levels of energy metabolism (Vegiopoulos & Herzig, 2007). The genomic effects that arise following GR activation regulate the transcriptional levels of various metabolic genes. This results in the stimulation of pathways that increase energy production, such as gluconeogenesis, and the suppression of insulin signaling in peripheral tissues (Sacta, Chinenov, & Rogatsky, 2016). On the other hand, the non-genomic effects of GR also contribute to the rapid activation of processes such as hepatic glucose production and lipolysis by modulating intracellular signaling pathways (Kuo et al., 2015; Peckett, Wright,

& Riddell, 2011; Xu et al., 2009). These dual-action mechanisms explain why glucocorticoids play such a central role in physiological adaptations that redistribute energy substrates during the stress response. From this point of view, in addition to the regulatory effects of glucocorticoids on gluconeogenesis, a detailed examination of their metabolic implications on fatty acid oxidation is of great importance for better understanding the contribution of these hormones to energy homeostasis.

Glucocorticoids and Hepatic Gluconeogenesis

GCs are among the key regulators of gluconeogenesis in the liver. They play a critical role in maintaining blood glucose homeostasis, especially during fasting, stress, and inflammatory response. The regulatory effect of these steroid hormones on gluconeogenesis is mediated by several mechanisms.

GCs act by directly activating the expression of genes encoding key enzymes of gluconeogenesis (Rose & Herzig, 2013). This effect, mediated through the genomic pathway, is initiated by activated GR translocating into the nucleus and binding to GRE in the promoter regions of target genes (Ratman et al., 2013). The major gluconeogenic enzymes whose transcription is increased by GR include PEPCK and G6Pase (Imai, Miner, Mitchell, Yamamoto, & Granner, 1993; Pedersen et al., 2007; Vander Kooi et al., 2005). Increased expression of these enzymes, which catalyze rate-limiting steps of gluconeogenesis, results in accelerated glucose synthesis from gluconeogenic substrates such as pyruvate and lactate (Hers & Hue, 1983). The PEPCK gene (PCK1) is among the best characterized targets of GC regulation. GREs present in human and rodent PCK1 promoters markedly increase gene transcription in response to GCs (Friedman, 1994; Wang et al., 2004). The effect of GCs on gluconeogenesis is not limited to direct GRE binding but also involves interactions with other transcription factors and coactivators that regulate gluconeogenesis (Kuo et al., 2015). One of the most important interactions occurs between GR and Peroxisome Proliferator-Activated Receptor Gamma Coactivator 1-alpha (PGC-1α). PGC-1α is a transcription coactivator that plays a central role in the control of gluconeogenesis in the liver and is induced by GCs (Lin, Puigserver, Donovan, Tarr, & Spiegelman, 2002). Activated PGC-1α acts as a coactivator of transcription factors such as hepatic nuclear factor-4α (HNF-4α) and forkhead box O1 (FOXO1), further increasing the transcription of PEPCK and G6Pase genes (Puigserver et al., 2003). GkCs synergistically stimulate PGC-1α expression and indirectly regulate transcription factors such as HNF-4α and FOXO1 (Yoon et al., 2001). FOXO1, which is negatively regulated by insulin signaling, can be upregulated by GC administration and is a transcription factor that plays a key role in the regulation of gluconeogenesis (Kamagate et al., 2008; Lecker et al., 2004; Shi, Qiao, Mu, Zuo, & Yuan, 2017; Waddell et al., 2008). Furthermore, increased FOXO1 protein levels in chronic GC exposure contribute to insulin resistance (Beaupere, Liboz, Fève, Blondeau, & Guillemain, 2021).

GCs not only increase the expression of gluconeogenic enzymes but also enhance the efficiency of the metabolic pathway by increasing substrate availability for gluconeogenesis. This effect is mediated through stimulation of proteolysis and lipolysis in peripheral tissues (Finn & Dice, 2006; Magomedova & Cummins, 2015; Rose & Herzig, 2013). GCs increase protein degradation in skeletal muscle, allowing amino acids such as alanine, important precursors for gluconeogenesis, to reach the liver (Kuo et al., 2015). It also increases glycerol release by stimulating lipolysis in adipose tissue. Glycerol is used as a direct substrate for gluconeogenesis in the liver (Exton et al., 1972; Kuo et al., 2015; Xu et al., 2009). In a study, it was reported that dexamethasone administration increased amino acid transport to the liver but there was no increase in liver amino acid amount due to gluconeogenesis and the urea cycle (Okun et al., 2015).

The suppressive effect of insulin on gluconeogenesis and the stimulatory effect of GCs have an antag-

onistic relationship (Beaupere et al., 2021). Under normal conditions, insulin phosphorylates FOXO1 via phosphoinositide 3-kinase (PI3K)/protein kinase B (Akt) signaling pathway, translocates it from the nucleus to the cytoplasm, and suppresses gluconeogenic gene expression (Sin, Yung, & Siu, 2015). At the molecular level, GCs reduce the expression of insulin receptor substrate-1 (IRS-1) and IRS-2 and consequently suppress the insulin-activated PI3K/Akt signaling pathway (Hu, Wang, In, Du, & Mitch, 2009; Xie, Perry, Espinoza, Zhang, & Price, 2018).

In addition to genomic effects, GCs also have non-genomic effects that provide rapid metabolic adaptations that can occur within minutes. Some of these rapid effects are mediated by membrane-bound GR or the interaction of GR with other signaling molecules in the cytoplasm (Song & Buttgereit, 2006). For example, GR phosphorylates activated protein kinase A (PKA); increases cAMP levels resulting in cAMP response element binding protein (CREB) phpsphorilation, which can rapidly induce the expression of PEPCK and G6Pase genes (Choi et al., 2017). They also can activate stress kinases such as p38 mitogen-activated protein kinase (MAPK) (Liu et al., 2024).

The activity of GCs at the tissue level is also regulated by the expression and activity of 11β-hydroxysteroid dehydrogenase (11β-HSD) enzymes (Chapman, Holmes, & Seckl, 2013). 11β-HSD1 and 11β-HSD2 are the two main isoforms and regulate cortisol-cortisone conversion in tissues (Krozowski, 1999). 11β-HSD1 is highly expressed in the liver and potentiates hepatic GC signaling by converting inactive GCs to their active forms (Chapman et al., 2013). In transgenic mice overexpressing liver-specific 11β-HSD1, PEPCK expression was increased, and insulin sensitivity was enhanced (Paterson et al., 2004). Another study reported that 11β-HSD1 knockout mice were protected from glucose intolerance, supporting that 11β-HSD1 enhances gluconeogenesis (Morgan et al., 2014). In another study, decreased activity of direct gluconeogenesis enzymes was observed in 11β-HSD1 knockout mice (Yao et al., 2017). The genomic and non-genomic pathways described in this section are shown in Figure 1.

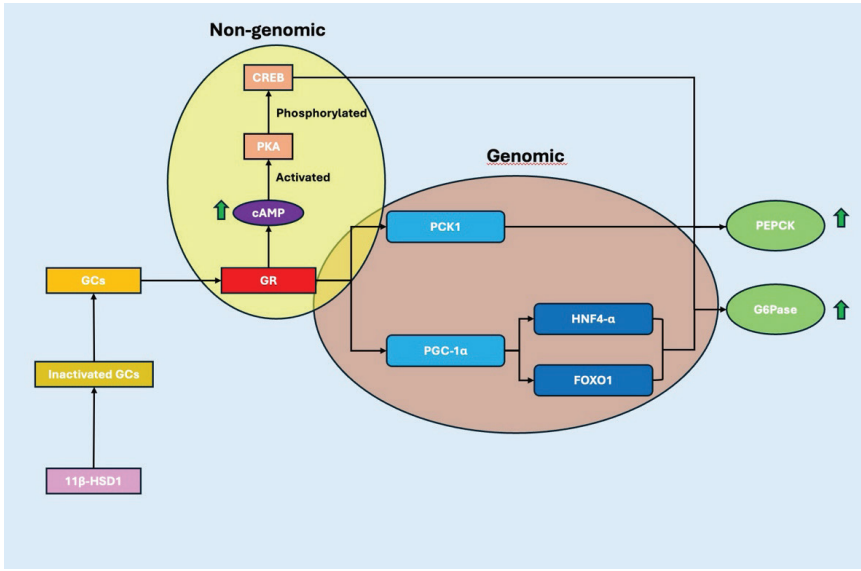


Figure 1. The effect of glucocorticoids on gluconeogenesis enzymes via genomic and non-genomic pathways. (GCs: Glucocorticoids, GR: Glucocorticoid Receptor, cAMP: cyclic Adenosine Monophosphate, CREB: cAMP Response Element-Binding protein, PKA: Protein Kinase A, PCK1: Phosphoenolpyruvate Carboxykinase 1, PGC-1α: Peroxisome Proliferator-activated receptor Gamma Coactivator 1-alpha, HNF4-α: Hepatocye Nuclear Factor 4-alpha, FOXO1: Forkhead box O transcription factor 1, 11β-HSD1: 11β-Hydroxysteroid Dehydrogenase type 1, PEPCK: Phosphoenolpyruvate Carboxykinase, G6Pase: Glucose-6-Phosphatase)

Overactivation of GCs on gluconeogenesis can be seen in a variety of pathological conditions and can exacerbate these pathological conditions, leading to metabolic imbalances. For example, in Cushing's syndrome, GCs excess increases glucose production by increasing the expression of gluconeogenesis enzymes in the liver, while suppressing insulin signaling in the liver and skeletal muscle, leading to insulin resistance (Pivonello et al., 2010). In addition, these metabolic changes can also lead to the development of type 2 diabetes over time (Di Dalmazi, Pagotto, Pasquali, & Vicennati, 2012). Therapeutic approaches targeting GC-mediated overactivation of gluconeogenesis include 11β-HSD1 inhibitors, GR antagonists, or selective inhibitors of gluconeogenic enzymes (Agius, 2007; Clark, 2008; Yuan et al., 2007). Clinical trials have shown that some 11β-HSD1 inhibitors improve insulin sensitivity and reduce hepatic glucose production (Anderson & Walker, 2013). Similarly, liver-specific G6Pase and fructose 1,6-bisphosphatase inhibitors are being investigated as potential targets for the treatment of diabetes (Agius, 2007). Recent technological advances enable more selective modulation of glucocorticoid signaling. Selective glucocorticoid receptor modulators (SGRMs) have the potential to reduce the stimulatory effects of glucocorticoids on gluconeogenesis and other potential side effects while preserving their anti-inflammatory effects (De Bosscher, Haegeman, & Elewaut, 2010). Preclinical studies suggest that these compounds may significantly reduce metabolic side effects (Sundahl, Bridelance, Libert, De Bosscher, & Beck, 2015).

GCs are complex and versatile regulators of the gluconeogenesis process in the liver, increasing glucose production both at the gene level and through cellular mechanisms. This regulation involves both the expression of gluconeogenic enzymes and the provision of substrates required for gluconeogenesis. However, the adverse effects of GCs on insulin signaling can lead to metabolic imbalances and insulin resistance, especially in long-term exposures. While local enzyme activities in the liver modulate the effects of these hormones, pathological conditions caused by excessive activation play an important role in the development of metabolic diseases. Therefore, selective modulation of glucocorticoid signaling and novel therapeutic strategies targeting this pathway are critical in the prevention and treatment of metabolic diseases.

Pathologies Associated with Glucocorticoid-Impaired Gluconeogenesis and Therapeutic Approaches

GCs induce hyperglycemia by increasing hepatic gluconeogenesis (upregulation of PEPCK and G6Pase expression), reducing insulin sensitivity in peripheral tissues and enhancing lipolysis and visceral adiposity in adipose tissue. These effects are dose- and duration-dependent and can emerge rapidly, within hours to days (Barker, Morrison, Llano, Sainsbury, & Jones, 2023). Clinical studies and guidelines report that the risk of hyperglycemia becomes particularly pronounced at doses exceeding the daily equivalent of 20 mg prednisolone, 50 mg hydrocortisone, or 4 mg dexamethasone; however, even low doses carry a risk for new-onset diabetes and metabolic dysregulation (Shah et al., 2022). In our previous study, we also demonstrated that serum glucose and vaspin levels increased in mice receiving prednisolone at doses of 5 mg/kg, 10 mg/kg and 20 mg/kg in a dose-dependent manner (Noyin, Akpinar, Cadirci, Cinar, & Aydin, 2018). Therefore, in patients with substantial steroid exposure (particularly those requiring inpatient care), early initiation of glucose monitoring and implementation of dose-specific glucose management algorithms—such as those described in the JBDS-IP guidelines—is recommended (Roberts et al., 2018). From the perspective of muscle tissue, GCs are known to cause proximal muscle weakness and myopathy when used at high doses (e.g., approximately 40 mg/day prednisolone or high-dose IV regimens) and/or over prolonged periods of weeks to months. Both clinical and preclinical evidence indicate that this effect is mechanistically linked to increased pro-

teolysis, inhibition of protein synthesis and activation of the ubiquitin–proteasome pathway (Wu, Michalski, Cortes, Rozenberg, & Mathur, 2022; Wu, Liu, & Sun, 2024). Consequently, metabolic adverse effects may further manifest as an impaired gluconeogenic response.

Strategies aimed at correcting GC-induced metabolic dysfunction largely focus on two major domains: first, pharmacological innovations (Selective glucocorticoid receptor modulators (SEGRAMs) and dissociative GR ligands, 11β-HSD1 inhibitors, tissue-targeted or nano-formulations) (Lesovaya et al., 2022; Othonos et al., 2023) and second, the implementation of steroid-sparing regimens in clinical practice (biologic agents, JAK inhibitors, etc.) alongside protocolized monitoring and prevention approaches (Hanberg & Miloslavsky, 2023; Kameda, 2023; Kubo, Nakayamada, & Tanaka, 2023).

Selective glucocorticoid receptor modulators (SEGRAMs) are designed to preferentially increase the GR-mediated transrepression of inflammatory transcription factors while decreasing the GRE-mediated transactivation of metabolic genes. Thus, they aim to separate anti-inflammatory effects from adverse metabolic consequences (Mao, Wei, & Chen, 2023). Among the earliest clinical examples of the SEGRAM approach, vamorolone has been evaluated at doses between 2–6 mg/kg/day in Duchenne muscular dystrophy and has shown the potential to provide a more favorable profile than conventional steroids regarding growth, bone health and metabolic adverse effects (Dang et al., 2024). Preclinical work with other selective GR modulators, such as the non-steroidal ligands Compound A and AL-438, has shown that selective GR binding profiles can skew signaling toward GR transrepression, supporting the potential for reduced glucocorticoid-induced side effects in inflammatory disease models (Doggrell, 2003; Drebert, Bracke, & Beck, 2015). GRM-01, another SEGRAM candidate, displays partial transactivation and robust anti-inflammatory efficacy with minimal effects on glucose regulation and bone metabolism in animal models, highlighting the feasibility of minimizing metabolic adverse effects via selective receptor modulation (Jakob, Hennen, Gautrois, Khalil, & Lockhart, 2025).

11β-HSD1 inhibitors aim to mitigate metabolic adverse effects by reducing the local peripheral activation of prednisolone and similar corticosteroids. Studies combining prednisolone with AZD4017 and related molecules have yielded data suggesting that these agents may attenuate prednisolone-associated metabolic disturbances (Othonos et al., 2023).

JAK inhibitors suppress JAK/STAT-mediated cytokine signaling by targeting JAK1, JAK2, JAK3, and TYK2 isoforms with distinct selectivity profiles (Kameda, 2023). The principal agents approved for the treatment of rheumatoid arthritis include the pan-JAK inhibitor tofacitinib, the JAK1/2 inhibitor baricitinib, the selective JAK1 inhibitors upadacitinib and filgotinib and the predominantly JAK3-targeting agent peficitinib (Kameda, 2023; Kubo et al., 2023). These agents inhibit the signaling of pro-inflammatory mediators, particularly interleukin-6 (IL-6) and interferons, thereby reducing inflammatory cell activation and cytokine production within the synovium. Moreover, JAK inhibitors are considered to possess steroid-sparing potential and may contribute to reducing long-term glucocorticoid exposure (Kubo et al., 2023).

Although nanotechnology-based GC delivery systems may enhance drug bioavailability in target tissues by overcoming physiological barriers while reducing systemic toxicity, challenges in manufacturing and risks of biological accumulation currently limit their translational applicability (Cui et al., 2025).

The main treatment strategies aimed at mitigating GC-related side effects are systematically summarized in Table 1.

Table 1. Overview of therapeutic strategies targeting glucocorticoid-related metabolic adverse effects.

Strategy Category	Mechanistic Target	Representative Agents	Advantages Compared with Conventional Glucocorticoids	References
Selective GR Modulators (SEGRAMs / Dissociative GR ligands)	Selective enhancement of GR-mediated transrepression of pro-inflammatory transcription factors while minimizing GRE-dependent transactivation of metabolic genes.	Vamorolone Compound A AL-438 GRM-01	Preserve anti-inflammatory efficacy while reducing GRE-driven transcription of gluconeogenic genes; improved growth and bone safety profile; attenuated metabolic adverse effects, including hyperglycemia	(Dang et al., 2024; Doggrell, 2003; Drebert et al., 2015; Jakob et al., 2025; Mao et al., 2023)
11β-HSD1 Inhibitors	Inhibition of peripheral cortisol/prednisolone activation	AZD4017	Reduce local hepatic activation of glucocorticoids, thereby attenuating prednisolone-associated dysglycemia and limiting excessive stimulation of hepatic gluconeogenesis.	(Othonos et al., 2023)
JAK Inhibitors (Steroid-sparing strategy)	JAK/STAT pathway inhibition (JAK1/2/3)	Tofacitinib Baricitinib Upadacitinib Filgotinib Peficitinib	Enable reduction of cumulative glucocorticoid exposure through steroid-sparing regimens and decrease cytokine-driven insulin resistance and systemic metabolic burden.	(Kameda, 2023; Kubo et al., 2023)
Nano- or Tissue-Targeted GC Delivery Systems	Targeted drug delivery and reduced systemic exposure	Various nano-formulations	Improve tissue-specific bioavailability while minimizing systemic toxicity and widespread metabolic adverse effects.	(Cui et al., 2025)

In conclusion, although GC therapy remains indispensable due to its clinical benefits, its dose- and duration-dependent spectrum of adverse effects necessitates careful patient selection, early monitoring, preventive strategies and rigorous assessment of emerging pharmacological approaches. Furthermore, innovations such as SEGRAMs, 11β-HSD1 inhibitors and tissue-targeted formulations require extensive long-term safety and efficacy studies across broader indications.

CONCLUSION

This review has comprehensively examined the complex and multifaceted regulatory mechanisms of glucocorticoids on hepatic gluconeogenesis. Our analysis demonstrates how GCs control hepatic glucose production through both genomic and non-genomic pathways. At the genomic level, activated GR directly stimulates gene expression of key enzymes such as PEPCK and G6Pase, constituting the fundamental regulatory mechanism of gluconeogenesis. Synergistic interactions with transcription factors and coactivators, including PGC-1α, FOXO1 and HNF-4α, amplify the regulatory effects of GCs, enhancing metabolic pathway efficiency.

The effects of GCs on gluconeogenesis extend beyond enzyme expression to encompass substrate mobilization from peripheral tissues. Stimulation of protein breakdown in skeletal muscle and lipolysis in adipose tissue ensures delivery of essential precursors to the liver, meeting the substrate requirements of the metabolic pathway. However, the antagonistic effects of GCs on insulin signaling can lead to metabolic imbalances, particularly during chronic exposure. Suppression of IRS-1 and IRS-2 expression and inhibition of the PI3K/Akt signaling pathway play critical roles in insulin resistance development.

The modulation of tissue-level GC activity by the 11β-HSD1 enzyme provides an important mechanism for local control of hepatic glucocorticoid signaling. While overexpression of this enzyme enhances gluconeogenesis, its inhibition improves metabolic parameters. The rapid metabolic adaptations provided by non-genomic effects through the cAMP/PKA/CREB pathway underscore the critical role of GCs in acute stress situations.

Metabolic complications resulting from excessive GC activation in pathological conditions highlight the necessity for tight control of these hormones. The

glucose intolerance and type 2 diabetes development observed in Cushing's syndrome demonstrate the serious consequences of glucocorticoid signaling imbalance. These findings emphasize the importance of close monitoring of metabolic side effects during long-term glucocorticoid therapy.

Importantly, chronic or high-dose GC exposure can also disturb peripheral insulin sensitivity, promote lipolysis-driven substrate overload and induce muscle proteolysis, collectively worsening hepatic gluconeogenic responses. These adverse metabolic outcomes have encouraged the development of clinical monitoring strategies and steroid-sparing regimens in parallel with pharmacological innovations designed to reduce GC-associated toxicity.

From a therapeutic perspective, novel approaches, including 11β-HSD1 inhibitors, selective glucocorticoid receptor modulators and gluconeogenic enzyme inhibitors, show promising results. These strategies hold potential for reducing metabolic side effects while preserving the anti-inflammatory properties of GCs. The development of selective GR modulators particularly suggests that safer glucocorticoid therapies may be possible in the future.

In conclusion, the central role of glucocorticoids in hepatic gluconeogenesis regulation demonstrates the physiological importance of these hormones while showing that excessive activation can lead to metabolic diseases. Future research should focus on more selective modulation of GC signaling, development of tissue-specific targeting strategies and personalized treatment approaches. The findings presented in this review provide an important foundation for developing therapeutic strategies targeting glucocorticoid signaling in the prevention and treatment of metabolic diseases.

AUTHOR CONTRIBUTION STATEMENT

Y.A.A.: Literature research, Conceptualization, Preparing the study text; E.C. Conceptualization, Reviewing the text

CONFLICT OF INTEREST

The authors declare that there is no conflict of interest.

REFERENCES

Agius, L. (2007). New hepatic targets for glycaemic control in diabetes. *Best Practice and Research in Clinical Endocrinology and Metabolism*, *21*(4), 587-605. doi:10.1016/j.beem.2007.09.001

Alexaki, V. I., & Henneicke, H. (2021). The Role of Glucocorticoids in the Management of COVID-19. *Hormone and Metabolic Research*, *53*(1), 9-15. doi:10.1055/a-1300-2550

Anderson, A., & Walker, B. R. (2013). 11β-HSD1 inhibitors for the treatment of type 2 diabetes and cardiovascular disease. *Drugs*, *73*(13). doi:10.1007/s40265-013-0112-5

Barker, H. L., Morrison, D., Llano, A., Sainsbury, C. A. R., & Jones, G. C. (2023). Practical Guide to Glucocorticoid Induced Hyperglycaemia and Diabetes. *Diabetes Therapy*, *14*(5), 937. doi:10.1007/S13300-023-01393-6

Barnes, P. J. (2011). Glucocorticosteroids: Current and future directions. *British Journal of Pharmacology*, *163*(1), 29-43. doi:10.1111/j.1476-5381.2010.01199.x

Beaupere, C., Liboz, A., Fève, B., Blondeau, B., & Guillemain, G. (2021). Molecular mechanisms of glucocorticoid-induced insulin resistance. *International Journal of Molecular Sciences*, *22*(2), 623. doi:10.3390/ijms22020623

Becker, D. E. (2013). Basic and clinical pharmacology of Glucocorticosteroids. *Anesthesia Progress*, *60*(1). doi:10.2344/0003-3006-60.1.25

Boldizsar, F., Talaber, G., Szabo, M., Bartis, D., Palinkas, L., Nemeth, P., & Berki, T. (2010). Emerging pathways of non-genomic glucocorticoid (GC) signalling in T cells. *Immunobiology*, *215*(7), 521-526. doi:10.1016/j.imbio.2009.10.003

Chapman, K., Holmes, M., & Seckl, J. (2013). 11β-hydroxysteroid dehydrogenases intracellular gate-keepers of tissue glucocorticoid action. *Physiological Reviews*, *93*(3). doi:10.1152/physrev.00020.2012

Choi, G. E., Lee, S. J., Lee, H. J., Ko, S. H., Chae, C. W., & Han, H. J. (2017). Membrane-associated effects of glucocorticoid on BACE1 upregulation and Aβ generation: Involvement of lipid raft-mediated CREB activation. *Journal of Neuroscience*, *37*(35). doi:10.1523/JNEUROSCI.0074-17.2017

Clark, A. R., & Belvisi, M. G. (2012). Maps and legends: The quest for dissociated ligands of the glucocorticoid receptor. *Pharmacology and Therapeutics*, *134*(1), 54-67. doi:10.1016/j.pharmthera.2011.12.004

Clark, R. (2008). Glucocorticoid Receptor Antagonists. *Current Topics in Medicinal Chemistry*, *8*(9). doi:10.2174/156802608784535011

Compston, J. (2018). Glucocorticoid-induced osteoporosis: an update. *Endocrine, 61*(1), 7-16. doi:10.1007/s12020-018-1588-2

Cui, L., Yang, Y., Hao, Y., Zhao, H., Zhang, Y., Wu, T., & Song, X. (2025). Nanotechnology-Based Therapeutics for Airway Inflammatory Diseases. *Clinical Reviews in Allergy & Immunology*, *68*(1). doi:10.1007/S12016-024-09019-W

Dang, U. J., Damsker, J. M., Guglieri, M., Clemens, P. R., Perlman, S. J., Smith, E. C., … Hoffman, E. P. (2024). Efficacy and Safety of Vamorolone Over 48 Weeks in Boys With Duchenne Muscular Dystrophy: A Randomized Controlled Trial. *Neurology*, *102*(5), e208112. doi:10.1212/WNL.0000000000208112/SUPPL_FILE/SUPPLEMENTARY_DATA1.PDF

De Bosscher, K., Haegeman, G., & Elewaut, D. (2010). Targeting inflammation using selective glucocorticoid receptor modulators. *Current Opinion in Pharmacology*, *10*(4), 497-504. doi:10.1016/j.coph.2010.04.007

De Guia, R. M., Rose, A. J., & Herzig, S. (2014). Glucocorticoid hormones and energy homeostasis. *Hormone Molecular Biology and Clinical Investigation*, *19*(2), 117-128. doi:10.1515/hmbci-2014-0021

The RECOVERY Collaborative Group. (2021). Dexamethasone in Hospitalized Patients with Covid-19. *New England Journal of Medicine*, *384*(8). doi:10.1056/nejmoa2021436

Di Dalmazi, G., Pagotto, U., Pasquali, R., & Vicennati, V. (2012). Glucocorticoids and type 2 diabetes: From physiology to pathology. *Journal of Nutrition and Metabolism*, *2012*. doi:10.1155/2012/525093

Doggrell, S. (2003). Is AL-438 likely to have fewer side effects than the glucocorticoids? *Expert Opinion on Investigational Drugs*, *12*(7), 1227–1229. doi:10.1517/13543784.12.7.1227

Drebert, Z., Bracke, M., & Beck, I. M. (2015). Glucocorticoids and the non-steroidal selective glucocorticoid receptor modulator, compound A, differentially affect colon cancer-derived myofibroblasts. *The Journal of Steroid Biochemistry and Molecular Biology*, *149*, 92–105. doi:10.1016/j.jsbmb.2015.02.002

Duma, D., Jewell, C. M., & Cidlowski, J. A. (2006). Multiple glucocorticoid receptor isoforms and mechanisms of post-translational modification. *Journal of Steroid Biochemistry and Molecular Biology*, *102*(1-5), 11-21. doi:10.1016/j.jsbmb.2006.09.009

Echeverria, P. C., & Picard Didier, D. (2010). Molecular chaperones, essential partners of steroid hormone receptors for activity and mobility. *Biochimica et Biophysica Acta - Molecular Cell Research*, *1803*(6), 641-649. doi:10.1016/j.bbamcr.2009.11.012

Exton, J. H., Friedmann, N., Wong, E. H., Brineaux, J. P., Corbin, J. D., & Park, C. R. (1972). Interaction of glucocorticoids with glucagon and epinephrine in the control of gluconeogenesis and glycogenolysis in liver and of lipolysis in adipose tissue. *Journal of Biological Chemistry*, *247*(11). doi:10.1016/s0021-9258(19)45180-6

Finn, P. F., & Dice, J. F. (2006). Proteolytic and lipolytic responses to starvation. *Nutrition*, *22*(7-8), 830-844. doi:10.1016/j.nut.2006.04.008

Friedman, J. E. (1994). Role of glucocorticoids in activation of hepatic PEPCK gene transcription during exercise. *American Journal of Physiology - Endocrinology and Metabolism*, *266*(4 Pt 1), E560-566. doi:10.1152/ajpendo.1994.266.4.e560

Hanberg, J. S., & Miloslavsky, E. M. (2023). Steroid sparing in vasculitis: Myth or reality? *Best Practice & Research. Clinical Rheumatology*, *37*(1). doi:10.1016/J.BERH.2023.101843

Heitzer, M. D., Wolf, I. M., Sanchez, E. R., Witchel, S. F., & DeFranco, D. B. (2007). Glucocorticoid receptor physiology. *Reviews in Endocrine and Metabolic Disorders*, *8*(4), 321-330. doi:10.1007/s11154-007-9059-8

Hers, H. G., & Hue, L. (1983). Gluconeogenesis and related aspects of glycolysis. *Annual Review of Biochemistry*, *52*. doi:10.1146/annurev.bi.52.070183.003153

Hu, Z., Wang, H., In, H. L., Du, J., & Mitch, W. E. (2009). Endogenous glucocorticoids and impaired insulin signaling are both required to stimulate muscle wasting under pathophysiological conditions in mice. *Journal of Clinical Investigation*, *119*(10). doi:10.1172/JCI38770

Imai, E., Miner, J. N., Mitchell, J. A., Yamamoto, K. R., & Granner, D. K. (1993). Glucocorticoid receptor-cAMP response element-binding protein interaction and the response of the phosphoenolpyruvate carboxykinase gene to glucocorticoids. *Journal of Biological Chemistry*, *268*(8). doi:10.1016/s0021-9258(18)53327-5

Jakob, F., Hennen, S., Gautrois, M., Khalil, F., & Lockhart, A. (2025). Novel selective glucocorticoid receptor modulator GRM-01 demonstrates dissociation of anti-inflammatory effects from adverse effects on glucose and bone metabolism. *Frontiers in Pharmacology*, *16*. doi:10.3389/fphar.2025.1542351

Kamagate, A., Qu, S., Perdomo, G., Su, D., Dae, H. K., Slusher, S., … Dong, H. H. (2008). FoxO1 mediates insulin-dependent regulation of hepatic VLDL production in mice. *Journal of Clinical Investigation*, *118*(6). doi:10.1172/JCI32914

Kameda, H. (2023). JAK inhibitors～overview～. *Immunological Medicine*, *46*(3), 108–111. doi:10.1080/25785826.2023.2183594

Krozowski, Z. (1999). The 11β-hydroxysteroid dehydrogenases: Functions and physiological effects. *Molecular and Cellular Endocrinology*, *151*(1–2). doi:10.1016/S0303-7207(98)00256-1

Kubo, S., Nakayamada, S., & Tanaka, Y. (2023). JAK inhibitors for rheumatoid arthritis. *Expert Opinion on Investigational Drugs*, *32*(4), 333–344. doi:10.1080/13543784.2023.2199919

Kuo, T., McQueen, A., Chen, T. C., & Wang, J. C. (2015). Regulation of glucose homeostasis by glucocorticoids. *Advances in Experimental Medicine and Biology*, *872*. doi:10.1007/978-1-4939-2895-8_5

Lecker, S. H., Jagoe, R. T., Gilbert, A., Gomes, M., Baracos, V., Bailey, J., … Goldberg, A. L. (2004). Multiple types of skeletal muscle atrophy involve a common program of changes in gene expression. *The FASEB Journal*, *18*(1). doi:10.1096/fj.03-0610com

Lesovaya, E. A., Chudakova, D., Baida, G., Zhidkova, E. M., Kirsanov, K. I., Yakubovskaya, M. G., & Budunova, I. V. (2022). The long winding road to the safer glucocorticoid receptor (GR) targeting therapies. *Oncotarget*, *13*(1), 408–424. doi:10.18632/ONCOTARGET.28191

Lim, M. A., Kohli, J., & Bloom, R. D. (2017). Immunosuppression for kidney transplantation: Where are we now and where are we going? *Transplantation Reviews*, *31*(1), 10-17. doi:10.1016/j.trre.2016.10.006

Lin, J., Puigserver, P., Donovan, J., Tarr, P., & Spiegelman, B. M. (2002). Peroxisome proliferator-activated receptor γ coactivator 1β (PGC-1β), a novel PGC-1-related transcription coactivator associated with host cell factor. *Journal of Biological Chemistry*, *277*(3). doi:10.1074/jbc.C100631200

Liu, H., Zhou, L., Wang, X., Zheng, Q., Zhan, F., Zhou, L., … Hua, F. (2024). Dexamethasone upregulates macrophage PIEZO1 via SGK1, suppressing inflammation and increasing ROS and apoptosis. *Biochemical Pharmacology*, *222*. doi:10.1016/j.bcp.2024.116050

Magomedova, L., & Cummins, C. L. (2015). Glucocorticoids and metabolic control. *Handbook of Experimental Pharmacology*, *233*. doi:10.1007/164_2015_1

Mao, L., Wei, W., & Chen, J. (2023). Biased regulation of glucocorticoid receptors signaling. *Biomedicine & Pharmacotherapy*, *165*, 115145. doi:10.1016/j.biopha.2023.115145

Morand, E. F., Fernandez-Ruiz, R., Blazer, A., & Niewold, T. B. (2023). Advances in the management of systemic lupus erythematosus. *BMJ*, *383*, e073980. doi:10.1136/bmj-2022-073980

Morgan, S. A., McCabe, E. L., Gathercole, L. L., Hassan-Smith, Z. K., Larner, D. P., Bujalska, I. J., … Lavery, G. G. (2014). 11β-HSD1 is the major regulator of the tissue-specific effects of circulating glucocorticoid excess. *Proceedings of the National Academy of Sciences of the United States of America*, *111*(24). doi:10.1073/pnas.1323681111

Noetzlin, S., Breville, G., Seebach, J. D., & Gastaldi, G. (2022). Short-term glucocorticoid-related side effects and adverse reactions: a narrative review and practical approach. *Swiss Medical Weekly*, *152*, w30088. doi:10.4414/smw.2022.w30088

Noyin, K., Akpinar, E., Cadirci, E., Cinar, I., & Aydin, P. (2018). THE EFFECTS OF VARIOUS DOSES OF PREDNISOLONE ADMINISTRATION ON SERUM VASPIN LEVELS IN RATS. *Acta Endocrinologica (Bucharest, Romania : 2005)*, *14*(3), 320–323. doi:10.4183/AEB.2018.320

Oakley, R. H., & Cidlowski, J. A. (2013). The biology of the glucocorticoid receptor: New signaling mechanisms in health and disease. *Journal of Allergy and Clinical Immunology*, *132*(5), 1033-44. doi:10.1016/j.jaci.2013.09.007

Okun, J. G., Conway, S., Schmidt, K. V., Schumacher, J., Wang, X., de Guia, R., … Rose, A. J. (2015). Molecular regulation of urea cycle function by the liver glucocorticoid receptor. *Molecular Metabolism*, *4*(10). doi:10.1016/j.molmet.2015.07.006

Oray, M., Abu Samra, K., Ebrahimiadib, N., Meese, H., & Foster, C. S. (2016). Long-term side effects of glucocorticoids. *Expert Opinion on Drug Safety*, *15*(4), 457-465. doi:10.1517/14740338.2016.1140743

Othonos, N., Pofi, R., Arvaniti, A., White, S., Bonaventura, I., Nikolaou, N., … Tomlinson, J. W. (2023). 11β-HSD1 inhibition in men mitigates prednisolone-induced adverse effects in a proof-of-concept randomised double-blind placebo-controlled trial. *Nature Communications, 14*(1), 1025. doi:10.1038/s41467-023-36541-w

Panettieri, R. A., Schaafsma, D., Amrani, Y., Koziol-White, C., Ostrom, R., & Tliba, O. (2019). Non-genomic Effects of Glucocorticoids: An Updated View. *Trends in Pharmacological Sciences*, *40*(1), 38-49. doi:10.1016/j.tips.2018.11.002

Paterson, J. M., Morton, N. M., Fievet, C., Kenyon, C. J., Holmes, M. C., Staels, B., … Mullins, J. J. (2004). Metabolic syndrome without obesity: Hepatic overexpression of 11β-hydroxysteroid dehydrogenase type 1 in transgenic mice. *Proceedings of the National Academy of Sciences of the United States of America*, *101*(18). doi:10.1073/pnas.0305524101

Peckett, A. J., Wright, D. C., & Riddell, M. C. (2011). The effects of glucocorticoids on adipose tissue lipid metabolism. *Metabolism: Clinical and Experimental*, *60*(11), 1500-1510. doi:10.1016/j.metabol.2011.06.012

Pedersen, K. B., Zhang, P., Doumen, C., Charbonnet, M., Lu, D., Newgard, C. B., … Scott, D. K. (2007). The promoter for the gene encoding the catalytic subunit of rat glucose-6-phosphatase contains two distinct glucose-responsive regions. *American Journal of Physiology - Endocrinology and Metabolism*, *292*(3). doi:10.1152/ajpendo.00510.2006

Pivonello, R., De Leo, M., Vitale, P., Cozzolino, A., Simeoli, C., De Martino, M. C., … Colao, A. (2010). Pathophysiology of diabetes mellitus in Cushing's syndrome. *Neuroendocrinology*, *92*(Suppl 1), 77-81. doi:10.1159/000314319

Pratt, W. B., & Toft, D. O. (1997). Steroid receptor interactions with heat shock protein and immunophilin chaperones. *Endocrine Reviews*, *18*(3), 306-360. doi:10.1210/er.18.3.306

Puigserver, P., Rhee, J., Donovan, J., Walkey, C. J., Yoon, J. C., Oriente, F., … Spiegelman, B. M. (2003). Insulin-regulated hepatic gluconeogenesis through FOXO1-PGC-1α interaction. *Nature*, *423*(6939). doi:10.1038/nature01667

Ratman, D., Vanden Berghe, W., Dejager, L., Libert, C., Tavernier, J., Beck, I. M., & De Bosscher, K. (2013). How glucocorticoid receptors modulate the activity of other transcription factors: A scope beyond tethering. *Molecular and Cellular Endocrinology*, *380*(1-2), 41-54. doi:10.1016/j.mce.2012.12.014

Reichardt, H. M., Tuckermann, J. P., Göttlicher, M., Vujic, M., Weih, F., Angel, P., … Schütz, G. (2001). Repression of inflammatory responses in the absence of DNA binding by the glucocorticoid receptor. *EMBO Journal*, *20*(24). doi:10.1093/emboj/20.24.7168

Roberts, A., James, J., Dhatariya, K., Agarwal, N., Brake, J., Brooks, C., … Winocour, P. (2018). Management of hyperglycaemia and steroid (glucocorticoid) therapy: a guideline from the Joint British Diabetes Societies (JBDS) for Inpatient Care group. *Diabetic Medicine : A Journal of the British Diabetic Association*, *35*(8), 1011–1017. doi:10.1111/DME.13675

Rose, A. J., & Herzig, S. (2013). Metabolic control through glucocorticoid hormones: An update. *Molecular and Cellular Endocrinology*, *380*(1–2). doi:10.1016/j.mce.2013.03.007

Saag, K. G., Furst, D. E., & Barnes, P. J. (2022). Major side effects of inhaled glucocorticoids. *UpToDate*.

Sacta, M. A., Chinenov, Y., & Rogatsky, I. (2016). Glucocorticoid Signaling: An Update from a Genomic Perspective. *Annual Review of Physiology*, *78*, 155-180. doi:10.1146/annurev-physiol-021115-105323

Sakoda, H., Ogihara, T., Anai, M., Funaki, M., Inukai, K., Katagiri, H., … Asano, T. (2000). Dexamethasone-induced insulin resistance in 3T3-L1 adipocytes is due to inhibition of glucose transport rather than insulin signal transduction. *Diabetes*, *49*(10). doi:10.2337/diabetes.49.10.1700

Şengül, E., & Çadirci, E. (2023). Kortikotropin salgılatıcı hormon ve kanser. In H. T. Akkoyun, M. Bayramoğlu Akkoyun, Ş. Melek (Eds.), *Sağlık Bilimleri Alanında Uluslararası Akademik Çalışmalar ve Teorik Bilgiler-I* (pp.15-28). Ankara: İKSAD Yayınevi.

Shah, A., & Wondisford, F. E. (2023). Gluconeogenesis Flux in Metabolic Disease. *Annual Review of Nutrition, 43*, 153-177. doi:10.1146/annurev-nutr-061121-091507

Shah, P., Kalra, S., Yadav, Y., Deka, N., Lathia, T., Jacob, J. J., … Das, S. (2022). Management of Glucocorticoid-Induced Hyperglycemia. *Diabetes, Metabolic Syndrome and Obesity: Targets and Therapy*, *15*, 1577. doi:10.2147/DMSO.S330253

Sharma, V. K., & Singh, T. G. (2019). Chronic Stress and Diabetes Mellitus: Interwoven Pathologies. *Current Diabetes Reviews*, *16*(6). doi:10.2174/1573399815666191111152248

Shi, Y., Qiao, J., Mu, B., Zuo, B., & Yuan, J. (2017). 3-(2-amino-ethyl)-5-[3-(4-butoxyl-phenyl)-propylidene]-thiazolidine-2,4-dione (K145) ameliorated dexamethasone induced hepatic gluconeogenesis through activation of Akt/FoxO1 pathway. *Biochemical and Biophysical Research Communications*, *493*(1). doi:10.1016/j.bbrc.2017.09.029

Sin, T. K., Yung, B. Y., & Siu, P. M. (2015). Modulation of SIRT1-foxo1 signaling axis by resveratrol: Implications in skeletal muscle aging and insulin resistance. *Cellular Physiology and Biochemistry*, *35*(2), 541-552. doi:10.1159/000369718

Song, I. H., & Buttgereit, F. (2006). Non-genomic glucocorticoid effects to provide the basis for new drug developments. *Molecular and Cellular Endocrinology*, *246*(1–2). doi:10.1016/j.mce.2005.11.012

Storer, C. L., Dickey, C. A., Galigniana, M. D., Rein, T., & Cox, M. B. (2011). FKBP51 and FKBP52 in signaling and disease. *Trends in Endocrinology and Metabolism*, *22*(12), 481-90. doi:10.1016/j.tem.2011.08.001

Sundahl, N., Bridelance, J., Libert, C., De Bosscher, K., & Beck, I. M. (2015). Selective glucocorticoid receptor modulation: New directions with non-steroidal scaffolds. *Pharmacology and Therapeutics*, *152*, 28-41. doi:10.1016/j.pharmthera.2015.05.001

Surjit, M., Ganti, K. P., Mukherji, A., Ye, T., Hua, G., Metzger, D., … Chambon, P. (2011). Widespread negative response elements mediate direct repression by agonist-liganded glucocorticoid receptor. *Cell*, *145*(2). doi:10.1016/j.cell.2011.03.027

Vander Kooi, B. T., Onuma, H., Oeser, J. K., Svitek, C. A., Allen, S. R., Vander Kooi, C. W., … O'Brien, R. M. (2005). The glucose-6-phosphatase catalytic subunit gene promoter contains both positive and negative glucocorticoid response elements. *Molecular Endocrinology*, *19*(12). doi:10.1210/me.2004-0497

Vandevyver, S., Dejager, L., & Libert, C. (2012). On the Trail of the Glucocorticoid Receptor: Into the Nucleus and Back. *Traffic*, *13*(3), 364-374. doi:10.1111/j.1600-0854.2011.01288.x

Vandewalle, J., Luypaert, A., De Bosscher, K., & Libert, C. (2018). Therapeutic Mechanisms of Glucocorticoids. *Trends in Endocrinology and Metabolism*, *29*(1), 42-54. doi:10.1016/j.tem.2017.10.010

Vegiopoulos, A., & Herzig, S. (2007). Glucocorticoids, metabolism and metabolic diseases. *Molecular and Cellular Endocrinology*, *275*(1-2), 43-61. doi:10.1016/j.mce.2007.05.015

Waddell, D. S., Baehr, L. M., Van Den Brandt, J., Johnsen, S. A., Reichardt, H. M., Furlow, J. D., & Bodine, S. C. (2008). The glucocorticoid receptor and FOXO1 synergistically activate the skeletal muscle atrophy-associated MuRF1 gene. *American Journal of Physiology - Endocrinology and Metabolism*, *295*(4). doi:10.1152/ajpendo.00646.2007

Wang, X. L., Herzog, B., Waltner-Law, M., Hall, R. K., Shiota, M., & Granner, D. K. (2004). The synergistic effect of dexamethasone and all-trans-retinoic acid on hepatic phosphoenolpyruvate carboxykinase gene expression involves the coactivator p300. *Journal of Biological Chemistry*, *279*(33). doi:10.1074/jbc.M403455200

Wu, K., Michalski, A., Cortes, D., Rozenberg, D., & Mathur, S. (2022). Glucocorticoid-induced myopathy in people with asthma: a systematic review. *Journal of Asthma*, *59*(7), 1396–1409. doi:10.1080/02770903.2021.1926488

Wu, M., Liu, C., & Sun, D. (2024). Glucocorticoid-Induced Myopathy: Typology, Pathogenesis, Diagnosis, and Treatment. *Hormone and Metabolic Research = Hormon- Und Stoffwechselforschung = Hormones et Metabolisme*, *56*(5), 341–349. doi:10.1055/A-2246-2900

Xie, Y., Perry, B. D., Espinoza, D., Zhang, P., & Price, S. R. (2018). Glucocorticoid-induced CREB activation and myostatin expression in C2C12 myotubes involves phosphodiesterase-3/4 signaling. *Biochemical and Biophysical Research Communications*, *503*(3). doi:10.1016/j.bbrc.2018.07.056

Xu, C., He, J., Jiang, H., Zu, L., Zhai, W., Pu, S., & Xu, G. (2009). Direct effect of glucocorticoids on lipolysis in adipocytes. *Molecular Endocrinology*, *23*(8). doi:10.1210/me.2008-0464

Yao, F., Chen, L., Fan, Z., Teng, F., Zhao, Y., Guan, F., … Liu, Y. (2017). Interplay between H6PDH and 11β-HSD1 implicated in the pathogenesis of type 2 diabetes mellitus. *Bioorganic and Medicinal Chemistry Letters*, *27*(17). doi:10.1016/j.bmcl.2017.07.043

Yoon, J. C., Puigserver, P., Chen, G., Donovan, J., Wu, Z., Rhee, J., … Spiegelman, B. M. (2001). Control of hepatic gluconeogenesis through the transcriptional coaotivator PGC-1. *Nature*, *413*(6852). doi:10.1038/35093050

Youssef, J., Novosad, S. A., & Winthrop, K. L. (2016). Infection Risk and Safety of Corticosteroid Use. *Rheumatic Disease Clinics of North America*, *42*(1), 157-176. doi:10.1016/j.rdc.2015.08.004

Yuan, C., St. Jean, D. J., Liu, Q., Cai, L., Li, A., Han, N., … Fotsch, C. (2007). The discovery of 2-anilinothiazolones as 11β-HSD1 inhibitors. *Bioorganic and Medicinal Chemistry Letters*, *17*(22). doi:10.1016/j.bmcl.2007.09.070

FABAD J. Pharm. Sci., 51, 1, s1-s2, 2026
Doi: 10.55262/fabadeczacilik.1340872
SUPPLEMENT ARTICLE

Supplementary Materials

Dornase Alfa as a Potential Treatment Option for SARS-CoV-2: In Vitro Insights

SUPPLEMENTARY TABLES

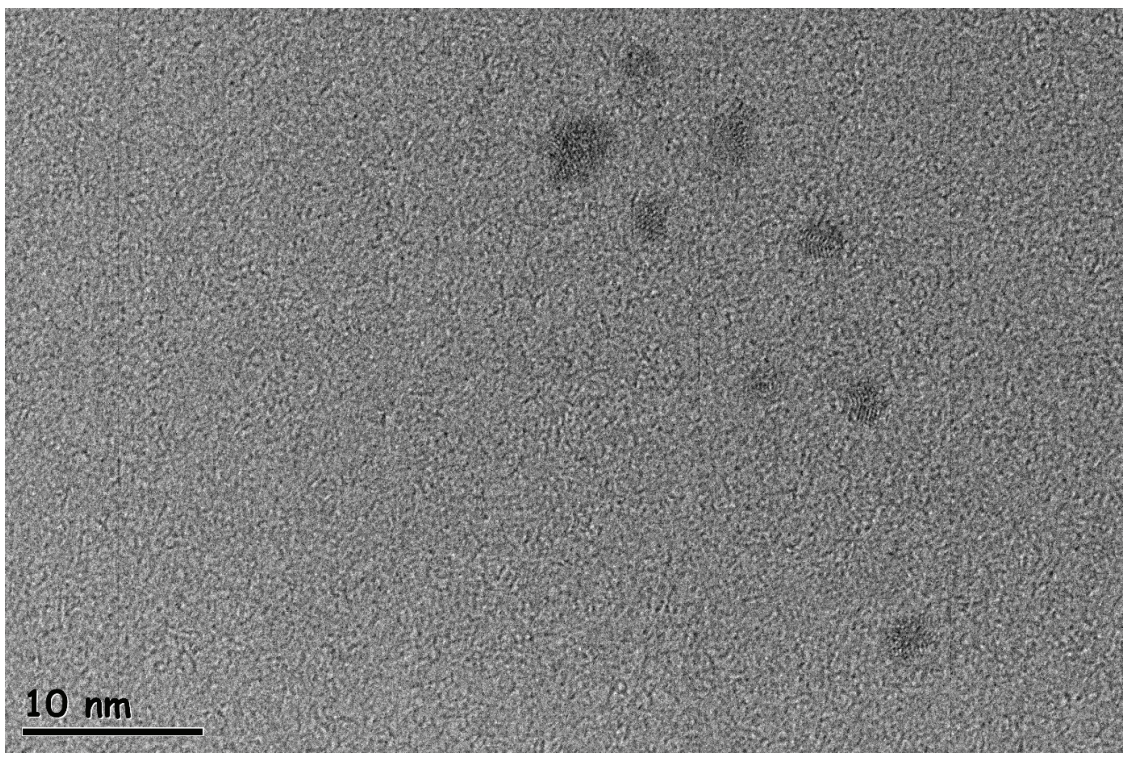
Supplementary Table 1. The formulation of Qdots-E3

Formulation	Hydrodinamic size	nm Numeric	% PDI	m^2/sn Difraction. ceoff.	Mv Zeta ∓	µmcm / VS Elektroforethic mobility	mS/cm conductance
E3	6,04	0,42	32,3	81,2			
	4,86	1,95	32,3	101,0	-4,30,6	-0,3339	8,421
	4,86	0,45	30,9	100,9			

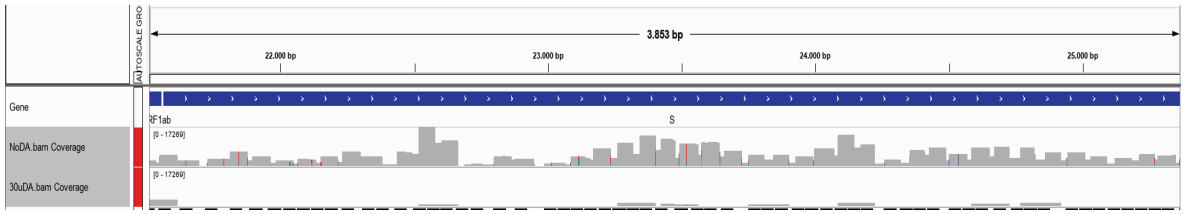
Supplementary Table 2. The immune response in PBMC cells treated with different concentration of dornase alfa and viral peptide mix was examined by CBA assay after 72h CBA was performed.

Deney Grupları	IL10 (pg/ml)	IL17 (pg/ml)	IL6 (pg/ml)	IFNg (pg/ml)	TNFa (pg/ml)
3U DA + Peptit + PBMC	120,046±117,77	36,969±8,34	455,121±145,23	261,429±193,89	144,339±192,74
10U DA + Peptit + PBMC	149,539±68,70	113,892±126,86	579,786±151,31	524,442±441,88	65,401±62,61
Peptit+PBMC	46,863±2,33	85,193±26,26	139,052±102,29	1044,948±869,66	120,689±143,08
Only PBMC	42,673±2,98	43,124±25,39	279,891±222,44	357,071±321,98	133,504±86,64

SUPPLEMENTARY FIGURES



Supplementary Figure 1. Transmission Electron Microscopy Imaging of QDots-E3



Supplementary Figure 2. Following treatment of 100X TCID50 SARS-CoV-2 with different concentration of dornase alfa, whole genome sequencing analysis of viral RNA was performed. The lines show the coverage profile after none or 30U dornase alfa incubation